A Nonconventional CO_2-EOR Target in the Illinois Basin: Oil Reservoirs of the Thick Cypress Sandstone

Final Report

Reporting Period Start Date: 10/01/2014

Reporting Period End Date: 4/30/2019

Principal Author: Nathan D. Webb, M.S. (PI), ndwebb2@illinois.edu

July 2019

Project Number DE-FE0024431

Board of Trustees of the University of Illinois

c/o Office of Sponsored Programs & Research Administration

1901 S. First Street, Suite A

Champaign, Illinois 61820

DISCLAIMER

ABSTRACT

The Illinois State Geological Survey (ISGS) identified and quantified nonconventional carbon dioxide (CO_2) enhanced oil recovery (EOR) target opportunities within the thick Cypress Sandstone in the Illinois Basin. Up to 60 m thick Cypress Sandstone bodies define a northeast-southwest fairway that is approximately 230 km long and 100 km wide across the central portion of the Illinois Basin. These sandstones commonly contain relatively thin oil reservoirs and were found to have associated underlying residual oil zones (ROZs). The presence of a thick brine aquifer underlying the ROZ and high vertical permeability results in characteristic low primary oil recovery caused by excessive brine production from the aquifer. Nonconventional CO_2-EOR in these oil reservoirs are expected to require more CO_2 to produce a unit of oil compared to conventional CO_2-EOR. Consequently, nonconventional CO_2-EOR will have a higher storage component and offer a unique storage opportunity.

An integrated approach of detailed site-specific geologic reservoir characterization, three-dimensional geocellular modeling, and reservoir simulation of multiple development cases at Noble Field was employed to determine development strategies for CO_2-EOR and storage. The findings of Noble Field research were leveraged to assess the regional CO_2-EOR and associated storage resource within the nonconventional reservoirs of the thick Cypress Sandstone in the Illinois Basin.

Regional characterization shows that thick, multistory fluvial facies of the Cypress Sandstone exhibits porosity from 15% to 21% and horizontal and vertical permeability up to approximately 0.98 μm^2 (1,000 mD). Oil saturation indicators screened from well records and well log analyses were used to map 27 brownfield and greenfield ROZ prospects with residual oil saturation (S_{OR}) values ranging from 14 to 35%. ROZ thickness varies from 2.7 to 21.6 m (9 to 71 ft).

The 27 Cypress Sandstone ROZ prospects have approximately 290.8 million m^3 (1.8 billion barrels) of oil in place. Specific CO_2-EOR development strategies depend on the goals of the project (prioritizing EOR performance vs. storage performance and NCNO) and geologic setting (brownfield vs greenfield), and company's business strategies (economic metrics). Nevertheless, applying two unique development strategies derived from reservoir simulation of the depleted main pay zone and ROZ in the Cypress Sandstone at Noble Field, 31.1 million m^3 (196 million barrels) of oil is estimated to be recoverable using the 80-acre blanket WAG development strategy (which favors EOR and economic metrics, but is carbon positive) whereas 21.3 million m^3 (144 million barrels) of oil is estimated to be recoverable using the 40-acre high CO_2 injection rate development strategy (which favors storage and economic metrics and results in net carbon negative oil production). Storage of CO_2 associated with EOR in these ROZ prospects alone, not accounting for associated main pay zones, underlying brine formation, or intervals adjacent to or between prospects, is estimated to be up to 10.4 billion tonnes using the latter development strategy.

TABLE OF CONTENTS

List of Figures

List of Tables

EXECUTIVE SUMMARY

Nonconventional oil reservoirs, including relatively thin main pay zones (MPZs) above thick aquifers and residual oil zones (ROZs), have traditionally been overlooked due to production difficulties(i.e. high water cuts via water coning), but ROZ development projects in the Permian Basin suggest that they can be economically produced via carbon dioxide enhanced oil recovery (CO_2-EOR). Such reservoirs are likely to exist in a range of lithologies in other basins and could represent a large bypassed oil resource and create an economic incentive to store anthropogenic CO_2 in the subsurface.

This research project increased the understanding of CO_2-EOR and associated storage of the nonconventional oil reservoirs within the thick Cypress Sandstone in the Illinois Basin. The project involved regional characterization of geology, identification and characterization of ROZs, a detailed site-specific study for simulating projected CO_2-EOR and storage performance and economics analyses, and a regional assessment of the Cypress Sandstone ROZ resource play.

Regional geologic characterization focused on understanding the depositional environments, diagenetic alteration and reservoir characteristics (porosity, permeability, heterogeneity and anisotropy). In addition to over 100 existing core and thousands of well logs, two new thick Cypress Sandstone cores were drilled and analyzed. Up to 60 m thick, multistory fluvial Cypress Sandstone bodies occur within a continuous fairway that is approximately 230 km long, up to 100 km wide, and trends northeast-southwest across the central portion of the Illinois Basin.

The site-specific study focused on Noble Oil Field, which has over 80 years of oil production from a MPZ above a thick aquifer in the Cypress Sandstone, but only approximately 25% OOIP oil recovery compared to 45% or more, the Illinois Basin average. Geophysical logs and core were used to develop a detailed geologic conceptual model. The Cypress Sandstone is interpreted to be composed of multistory fluvial sandstone deposited during lowstand and transgression with evidence of a change to estuarine conditions near the top. Multiple sandstone stories amalgamate at Noble, resulting in a thick, relatively widespread sandstone body that has characteristics favorable for CO_2 storage (such as high lateral and vertical permeability, limited compartmentalization, and large pore volumes).

Additional research was required to understand the distribution of oil saturation within the ROZ to assess the CO_2-EOR and storage performance. A well log analysis methodology was developed at Noble Field to identify the producing oil-water contact and the oil-water contact, which bound the top and base of a ROZ, respectively; this methodology uses a combination of established techniques (S_W, BVW, MHI, R_{WA}). At Noble Field, the methodology identified a ROZ (approximately 6.1 m thick interval of 25% residual oil saturation) beneath the MPZ (approximately 3-7 m thick initially at 55% oil saturation). The methodology was validated by comparing oil water contacts to newly collected pulsed neutron logs and historical information (such as oil shows and perforation depths).

The conceptual geologic model and well log analyses provided key parameters on which static and dynamic digital models were created and populated to represent geologic heterogeneity and fluid saturation distributions. The dynamic reservoir model of Noble Field was calibrated to 80 years of historical oil production data and used to simulate various CO_2-EOR cases to identify development strategies. Based on analyses of CO_2-EOR-storage and economic metrics, the elements of a development strategy for CO_2-EOR in the Noble Field (and presumably similar brownfield ROZs) are as follows:

- 80-acre injection pattern;
- MPZ and ROZ injection or MPZ only;
- High injection rates (leading to out-of-pattern CO_2);
- water-alternating-gas (WAG) if using low injection rates; and

- continuous injection if using high injection rates.

Specific development strategies depend on the goals of the project (prioritizing EOR performance vs. storage performance and NCNO) and geologic setting (brownfield vs greenfield), and company's business strategies (economic metrics). Changes in oil and/or CO_2 price would impact the choice to prioritize (or balance) EOR or storage in the development strategy.

The ROZ fairway was delineated by creating regional isopach and isoporosity maps of the Cypress Sandstone and overlaying well-based oil indicator data (oil shows, drill stem tests, core-indicated oil saturation). The well log analysis methodology developed at Noble was used to identify ROZ related fluid contacts in areas where oil indicators were mapped. ROZ thickness and saturation values derived from the well log analyses were used to calculate original oil in place (OOIP) for 27 potential ROZ prospects throughout the thick Cypress fairway. Based on that volumetric analysis, the Cypress Sandstone ROZ prospects contain approximately 290.8 million m^3 (1.8 billion barrels) of oil in place (using a median S_{OR} = 23%). Applying two unique CO_2-EOR development strategies derived from economic analyses of the results from reservoir simulation of the depleted main pay zone and ROZ in the Cypress Sandstone at Noble Field, 31.1 million m^3 (196 million barrels) of oil is estimated to be recoverable using the 80-acre blanket WAG development strategy (which favors EOR and economic metrics, but is carbon positive) whereas 21.3 million m^3 (144 million barrels) of oil is estimated to be recoverable using the 40-acre high CO_2 injection rate development strategy (which favors storage and economic metrics and results in net carbon negative oil production). Storage of CO_2 associated with EOR in these ROZ prospects alone, not accounting for associated main pay zones or underlying brine formation, is estimated to be up to 10.4 billion tonnes.

CONTRIBUTORS

The background on the geology of the Cypress Sandstone was written by Nathan Webb and Kalin Howell based on a thorough review of the literature. The site screening was done by Nathan Webb, Nate Grigsby, Bev Seyler, and John Grube.

The following people contributed to the geologic characterization:
Kalin Howell conducted the study of the sedimentology of the Cypress Sandstone within Dale Field, and regionally, completing a MS thesis under advisement of Nathan Webb, and Jim Best. Nathan Webb conducted the geologic characterization of Noble and Kenner West Fields. Donna Willette investigated the oil source rock for Noble Field. John Grube conducted the characterization of Loudon Field. Mingyue Yu and Leo Gianetta conducted the petrographic analysis of the Cypress sandstone under advisement from Jared Freiburg, and Nathan Webb. Yaghoob Lasemi and Zohreh Askari conducted an analysis of the stratigraphic variability and reservoir characteristics of the Cypress Formation in Clay City Consolidated Field. Nathan Webb, Kalin Howell, John Grube, and Jim Best all contributed to the development of the regional conceptual geologic model for the Cypress Sandstone.

Nathan Webb coordinated the effort to collect the two new cores and pulsed neutron logs in four existing wells for the project. Joe Devera scouted for and facilitated the collection of the Tripp #1 core on the Brenda and Marvin Tripp property. CountryMark Energy Resources, specifically Malcolm Booth (Production Engineer), facilitated the collection of the Long #2 core. Podolsky Oil Company, specifically Stephanie Storckman (Geologist) and Michael Podolsky (President) facilitated the collection of the pulsed neutron logs in Noble Field.

Nathan Grigsby was responsible for geocellular modeling. Nathan Grigsby and Scott Frailey developed the well log analysis methodology for determining the critical fluid contacts to identify ROZs. Nathan Grigsby applied the well log analysis methodology at Noble and Kenner West Fields and regionally.

Roland Okwen conducted the reservoir simulations with assistance from Fang Yang and guidance from Scott Frailey. Scott Frailey conducted the economic analysis of the simulation results.

Damon Garner provided database support.

Elizabeth Prete provided editing and formatting of the final report.

1. Introduction

Residual oil zones (ROZs) are volumes of rock of significant scale into which oil accumulated and, later, was naturally displaced, leaving behind a low, largely immobile remaining oil saturation (West, 2014). Oil saturation (S_O) in ROZs range from 20 to 40%, making them functionally like conventional reservoirs that have been depleted by decades of waterflooding; therefore, they are well suited for tertiary oil recovery processes like CO_2 flooding (Harouaka et al., 2013). ROZs are anticipated to substantially increase oil resource estimations due to increases in the thickness and lateral extent of the oil-bearing rock in many oil fields.

Generally, ROZs are not economic-producing reservoirs for primary or waterflood recovery due to their low to moderate oil saturation (Koperna and Kuuskraa, 2006). However, there is demonstrated success of production from ROZs in the Permian Basin of West Texas and New Mexico using tertiary carbon dioxide enhanced oil recovery (CO_2-EOR). ROZs undergoing CO_2-EOR in the Permian Basin are producing at a rate of at least 1,749 m^3 (11,000 bbl) of oil per day (Harouaka et al., 2013).

ROZs are commonly associated with relatively thin, mobile oil columns immediately above a somewhat thicker, mobile water-saturated formation. This reservoir configuration is common within Chesterian (Upper Mississippian) sandstones in the Illinois Basin (ILB) with the most extensive example being the thick portion of the Cypress Sandstone (**Figure 1.1**). In the analogous Chesterian Tygett Sandstone Member of the Clore Formation (**Figure 1.1**) at the Midwest Geological Sequestration Consortium (MGSC) Mumford Hills Pilot, a CO_2-EOR pilot injection succeeded in increasing oil production from reservoirs 3 to 7 m (10 to 23 ft) thick that overlie approximately 7 m (23 ft) of brine aquifer (Frailey et al., 2012a). From a CO_2 perspective, CO_2 utilization was high, while CO_2-EOR projections were typical (15–20%). Moreover, little of the nearly 8,000 tonnes of CO_2 was produced (<5%) during the pilot. Numerical modeling showed that most of the CO_2 remained trapped in the brine aquifer below the oil reservoir.

Relatively thin oil reservoirs underlain with strong, bottom-drive brine aquifers are nonconventional CO_2-EOR targets since injected CO_2 is likely to pass underneath the oil into the underlying brine due to the favorable relative permeability of the aquifer to CO_2 compared to the oil-saturated reservoir. Geologic formations in which absolute permeability increases with depth will further exacerbate this effect. Conventional CO_2-EOR would avoid underlying aquifers in order to minimize the expense of injected CO_2 passing underneath the oil into the underlying brine. Yet, this type of reservoir has significant CO_2 storage and CO_2-EOR potential that may not be harnessed without a storage option. This research project intends to contribute to the scientific understanding of nonconventional CO_2-EOR targets, including their storage potential. Research is needed to determine if CO_2 should be injected directly into the oil zone, the base of the aquifer, or the upper part of the aquifer near the oil-water contact. Likewise, the placement of injectors with respect to producers, such as regular patterns (e.g., a five-spot or line drive) or a peripheral flood near the edges of the oil-saturated part, is an important consideration for CO_2-EOR development for these fields. Research applications of horizontal and/or vertical injectors and producers are needed to determine the combination that leads to storage with enhanced oil recovery in oil reservoirs that have had, at best, only primary production attempts. Vital to all ROZ assessments is quantifying the volume and fate of injected CO_2; whether recycled as part of the EOR process or permanently stored within the formation, the utilized volume has implications for cost to purchase and/or tax credits for utilization and storage (i.e. 45Q). Consequently, the economics of nonconventional CO_2-EOR is an important aspect of this study.

Since 2008, the MGSC has included the portions of the ILB with thicker Cypress Sandstone in its saline storage portfolio. However, structural traps are present within these portions of the ILB where oil has accumulated above a thick, brine-saturated lower part of the Cypress. These relatively thin oil accumulations are common features in the ILB and other basins across the US, and they have potential for associated, thick ROZs. For decades, these oil accumulations have been known, but are considered a challenge to produce via primary production and waterflooding. The dilemma arises from excess water production, which occurs nearly at inception due to water coning upward into the oil-saturated part of the formation. This part of the Cypress is made up of thick fluvial deposits, with high vertical permeability and few to no flow barriers that would inhibit the vertical movement of water.

Attempts at different completion techniques have been made in production wells to reduce water production. Some operators have attempted drilling less than a meter (in some cases, only a few cm) into the formation, but because of the unfavorable distribution of permeability, the well begins producing water at high rates within a few days or weeks of production and often quickly becomes uneconomical. Due to the high saturation and mobility of the water naturally occurring in this formation, formal waterfloods are rarely attempted, except in wells further away from oil production wells; the technique was primarily attempted in the form of water disposal rather than pressure maintenance. In the past few decades, moderate success has been made to improve primary oil recovery by placing horizontal wells near the top of the thin oil zone in the Cypress Sandstone. These horizontal wells have produced oil with lower water rates for longer periods of time. Attempts have also been made to inject various polymer treatments either directly into the oil zone or into the water immediately below the oil zone to delay water production; however, these attempts have been unsuccessful. CO_2 injection into the underlying aquifers has the potential to be an effective water block by restricting the contact of the water with oil and has the added benefit of CO_2 storage via dissolution in brine. The injection of CO_2 into the Cypress Sandstone would be a novel approach to producing more incremental oil from thin oil zone and associated ROZs while also using the brine aquifer for its storage potential.

The water-saturated portion of the Cypress offers a great opportunity for CO_2 storage in the ILB while the thin, 3 to 10 m (9.8 to 32.8 ft) thick oil reservoirs in the top of the formation are excellent targets for nonconventional CO_2-EOR, especially if ROZs are present beneath these thin oil zones as suspected. Following CO_2 injection into the water-saturated base of the formation, the challenge will be keeping the majority of the CO_2 in the lower part of the formation in order to maximize storage, while another portion of the CO_2 simultaneously moves vertically upward to make contact with the oil and enhance oil recovery. Therefore, it is necessary to find operational solutions which increase the contact of CO_2 with oil to increase oil production.

While there has been established success in producing economic quantities of oil from nonconventional, thin oil zones, the need to shift the carbon balance from net positive to net negative necessarily requires storing a significant portion of CO_2 while producing as much oil per injected unit of CO_2 as possible; this goal could be met by optimizing sweep and storage efficiency. As such, it is important to consider storing in relatively thin oil reservoirs underlain by high-volume aquifers in order to maximize the storage potential of CO_2 and utilize methods – such as geocellular modeling and reservoir simulation based on rigorous reservoir characterization – to aid in the design of injection scenarios that could achieve such a goal.

Nonconventional CO_2-EOR targets such as ROZs are thought to have formed over geologic time through a natural waterflooding process in which oil was displaced by brine following tectonic events that changed the hydrodynamic flow direction within the basin (Melzer et al., 2006). Thin oil reservoirs in the

ILB may have similarly developed due to changes in the hydrodynamic setting of the Basin driven by tectonics, sweeping away the lower portion of the reservoir and creating a thin oil zone overlying a thicker ROZ. It is well established that the Late Permian to Early Mesozoic uplift of the Pascola Arch to the southwest enclosed the ILB (Kolata and Nelson, 1991), which previously had been a southward-opening embayment. This major reconfiguration of the Basin established a new hydrodynamic regime capable of initiating the natural waterflooding of many Chesterian (and other) sandstone units, and was responsible for the long-range migration of hydrocarbons from presumed Devonian source rocks to reservoirs (Bethke et al., 1991). As a result, thin oil reservoirs often occupy the upper portions of thick Chesterian sandstones, with a thick brine aquifer occupying much of the remaining deposit.

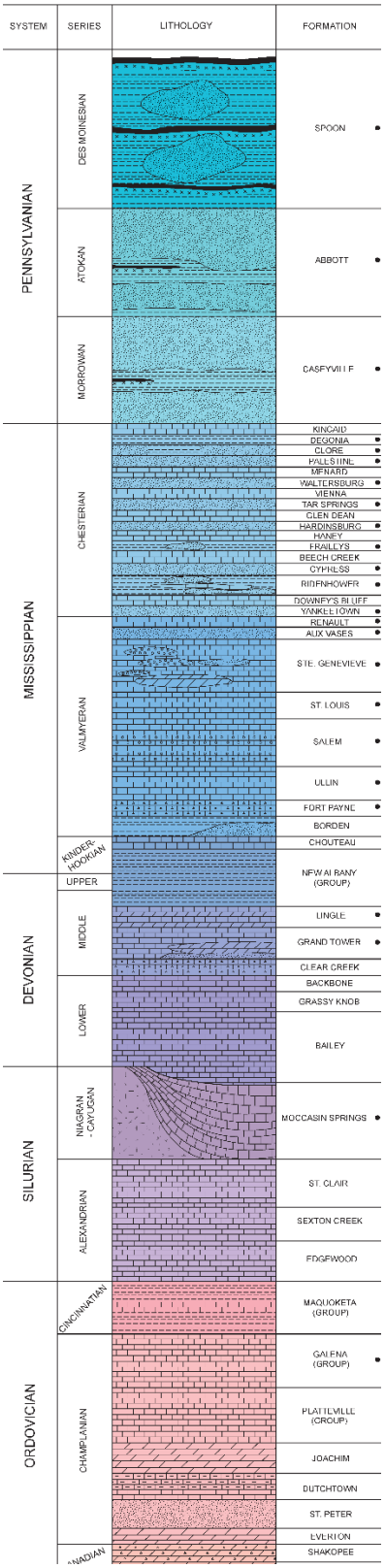

Figure 1.1. Simplified stratigraphic column of the ILB. Formations that are known to contain oil reservoirs are shown with a black dot.

It is possible that the change in hydrodynamic flow and the associated natural waterflooding may have created ROZs within these thick sandstones in certain regions. If these low-saturated zones underlie the thin, conventional reservoirs, they would be considered brownfield ROZs, which are associated with conventional, primary oil production reservoirs typically beneath main pay zones (MPZs). However, it is also possible that greenfield ROZs exist in other areas of the Basin where conventional reservoirs were naturally waterflooded out, as greenfield ROZs are associated with areas that have no historical primary production but may contain producible quantities of oil. Little research exists with respect to these possibilities in the ILB.

In the ILB, thin oil zones with potential ROZs are common among several Chesterian sandstone units. The Chesterian Series consists of a succession of cyclic deposits of sandstones, limestones, and shales. Many Chesterian sandstones, when deposited in a fluvial setting, reach thicknesses of 30 m or more and can be laterally continuous. Formations with thick sandstones and bypassed thin oil reservoirs that would be CO_2-EOR targets in the ILB include the Waltersburg Formation, Tar Springs Sandstone, Hardinsburg Sandstone, Cypress Sandstone, Bethel Sandstone, Yankeetown Sandstone, Aux Vases Sandstone, and Spar Mountain Sandstone (**Figure 1.1**). These sandstones are some of the most prolific oil-producing horizons in the ILB, having a combined production between 159 and 318 million m^3 (1 and 2 billion bbl) of oil in the state of Illinois alone, which accounts for well over 60% of the ILB's hydrocarbon production (Howard, 1991; Huff and Seyler, 2011). The position of the Chesterian sandstones, deposited between impermeable seal strata, has contributed to their highly productive character, making them good candidates for the geologic storage of CO_2.

The most obvious nonconventional target for CO_2-EOR in the ILB is the thick Cypress Sandstone. The Cypress Sandstone is a prolific Chesterian oil producer that has accounted for 159 million m^3 (1 billion bbl) of 668 million m^3 (4.2 billion bbl), or approximately 24 %, of the oil produced from the ILB. Much of the oil produced from the Cypress has come from highly compartmentalized, very fine-grained, stacked sandstone bars that formed in a low accommodation shelf setting where a high tidal range deposited sediments into elongated, shore-normal bars. However, another sandstone facies is also present in the Cypress, as intraformational sequence boundaries separate the bar facies from lithologically similar, yet genetically distinct, fluvial sandstone facies. Although these sandstones commonly contain a zone of oil as thick as 15 m (49.2 ft) in their top, they are generally overlooked. The thin oil reservoirs in the top of the Cypress Sandstone are in immediate contact with the underlying, relatively thick brine aquifer with possibly no measurable in-situ oil-water capillary transition zone. This characteristic makes completing a successful well in the formation difficult due to water coning.

The thick fluvial facies of the Cypress Sandstone occupy a continuous fairway that is approximately 230 km (143 mi) long, up to 100 km (62 mi) wide, and trends northeast-southwest across the central portion of the ILB (**Figure 1.2**). These sandstones can reach thickness of up to 60 m and can be incised into the underlying formations (Nelson et al., 2002). The fluvial facies of the Cypress deposits are classified as having medium potential for CO_2 storage (NETL, 2010). US Department of Energy (DOE) funded research by the Illinois State Geological Survey (ISGS) focusing on the CO_2 storage efficiency and storage potential of deposits from different depositional environments; this research has also confirmed that fluvial deposits are good candidates for CO_2 storage projects. In the Fairfield Basin, the central deep portion of the ILB where the Cypress occurs below a depth of 800 m (2,625 ft), the thick fluvial facies of the Cypress Sandstone is so extensive that it has the potential to store as much as 0.2 to 2.3 billion tonnes of CO_2 (US DOE, 2012).

These thick Cypress Sandstone reservoirs provide the promise of increased oil recovery in response to CO_2-EOR, with the potential to store significant volumes of CO_2. However, there are currently no operators conducting CO_2-EOR in the ILB. This is due to factors which include low operator interest, a lack of well-developed, economical CO_2 supply, infrastructure, local expertise, and low oil prices. By demonstrating the utility of CO_2 as an effective agent for producing oil from thin oil reservoirs in the ILB through modeling and development of a completion and injection methodology, this research will provide operators with a methodology that they can use to unlock a hitherto bypassed opportunity.

Given its thickness, extent, potential for oil recovery and carbon storage, its thin oil zones and potential for ROZs, the Cypress Sandstone is a prime candidate for research into completion and injection strategies that maximize both oil production and CO_2 storage. Lessons learned from study of the Cypress would be equally applicable to other Chesterian sandstone oil reservoirs in the ILB known for analogous lithology, texture, and thickness, as mentioned previously. Likewise, thick, coarser-textured sandstone belts with thin oil reservoirs and promising CO_2 storage potential are also known to occur, albeit at shallower depths, within the Caseyville and Tradewater Formations of the Lower and Middle Pennsylvanian (**Figure 1.1**). Additional, similar oil reservoirs with thick, underlying water zones exist in the Lower and Middle Mississippian and Lower Paleozoic, as well. All told, research conducted by the MGSC indicates that CO_2-EOR efforts have the potential to yield 127 to 207 million m^3 (0.8 to 1.3 billion bbl) in the ILB and, consequently, geologic CO_2 storage of 154 to 485 million tonnes (MGSC, 2005). Only through comprehensive geologic investigation integrated with engineering analyses of all reservoir parameters will CO_2 storage and production of nonconventional CO_2-EOR targets be viable in the ILB.

Figure 1.2. Map showing the distribution of facies within the Cypress Sandstone across the ILB. The thick fluvial facies of the Cypress Sandstone occupy a continuous northeast-southwest trending fairway in the central portion of the ILB.

2. Background

2.1 Residual Oil Zones

Melzer et al. (2006) define three types of naturally occurring ROZs that occur in nature (**Figure 2.1**). Type 1 ROZs occur in fields that have been subjected to a regional tilt over geologic time, allowing leakage of the original oil accumulation at a new spill point. Type 2 ROZs occur in fields with breached and repaired seals, which initially resulted in leakage of the original oil accumulation; such leakage was stemmed when the seal was repaired. Moreover, fields with breached seals usually have thick ROZs (Honarpour et al., 2010). Type 3 ROZs occur in fields where a change in hydrodynamic conditions has caused a portion of the original oil accumulation to be swept away. All three ROZ types exhibit characteristically low capillary numbers (i.e., low flow velocity), bottom and/or edge water drives from closed aquifers, or open aquifers recharged from the surface.

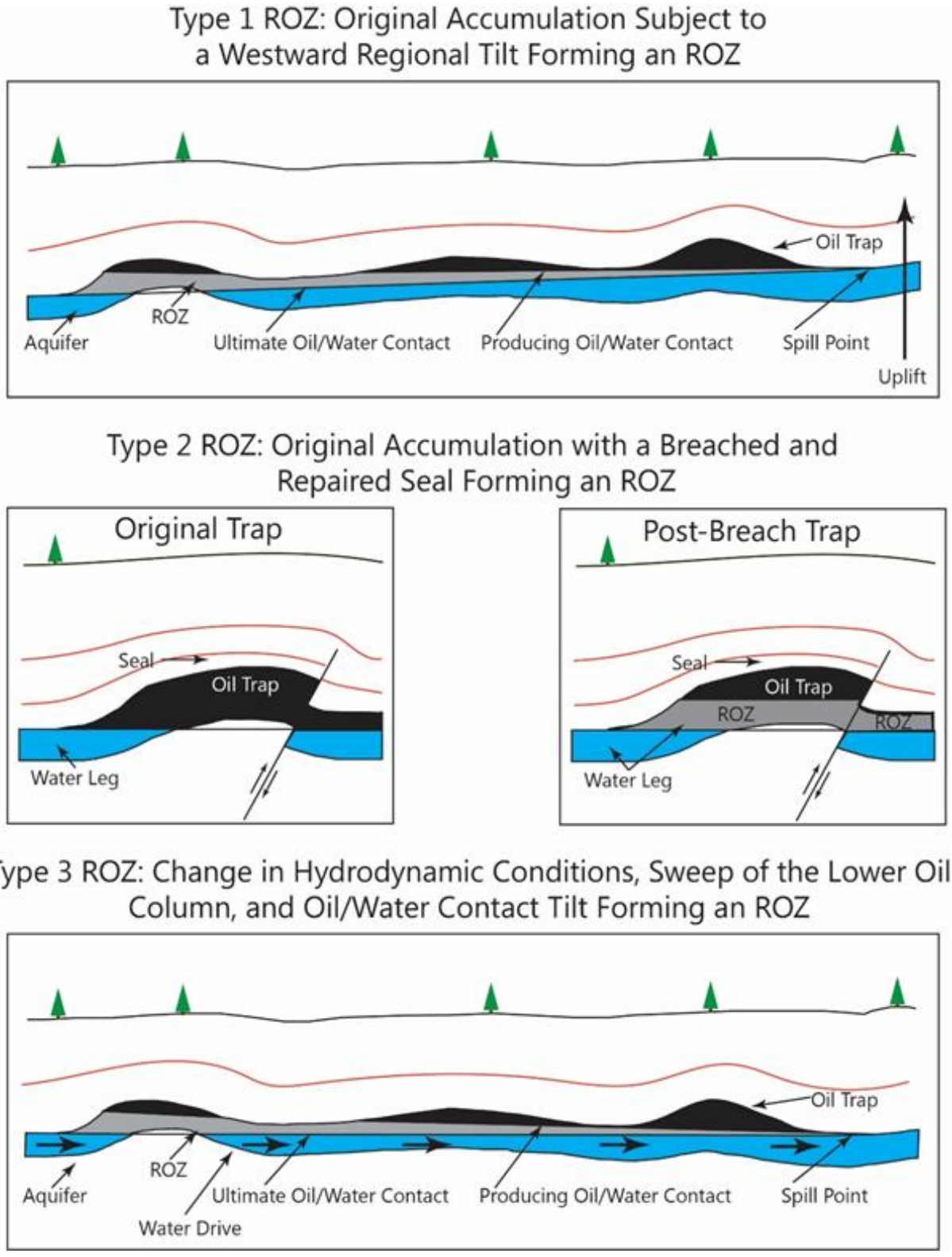

Figure 2.1. Graphical examples of the three types of ROZs, modified from Melzer et al. (2006).

ROZs may be thicker than the remaining MPZ occupying the oil trap. Most ROZs that have been identified to date are located beneath MPZs in mature oil fields and were detected via the deepening and coring of existing wells in those mature fields, but ROZs may also occur in areas where the entire MPZ has been swept away.

All three ROZ types result from natural waterflooding that occurs over geologic time (Harouaka et al., 2013). Analytical modeling results suggest that the water drive in natural waterfloods, which take place both during and after the formation of ROZs, can flow at rates as low as one foot per thousand years (Trentham, 2011; Hubbert, 1953). Trentham's (2011) analytical model assumes that ROZs have been flushed with about 20 pore volumes of water over geologic time and are immobile to water (e.g., at residual oil saturation to water [S_{ORW}]). The oil trapped within ROZs is, therefore, held in place by capillary forces, which is a key reason why they make suitable candidates for tertiary oil recovery operations like CO_2 flooding (Harouaka et al., 2013).

The prototypical example of a ROZ is that which occurs within the San Andres Dolomite in Seminole Field, Permian Basin, Texas, USA (e.g. Melzer at al., 2006). This field contains a thick ROZ beneath the MPZ that has been economically produced. The S_{ORW} of the ROZ, measured using centrifuge capillary pressure tests, ranges between 28 and 32%. Long core composites of lengths from six to twelve inches were used to conduct CO_2 injection core flood tests, which found the S_{ORM} to be approximately 12%. Laboratory results also show that the MMP of the oil within the ROZ at Seminole Field is less than the current reservoir pressure (of 13,790 kPa [2,000 PSI]); further, the dissolution of CO_2 caused the ROZ oil saturation value to increase by nearly 75% due to swelling (Honarpour et al., 2010). Rocks with low S_{or} largely consist of pores with large pore throats and, thus, exhibit high permeability, while small pore throats dominate the pore network of rocks which have high S_{or} (Honarpour et al., 2010).

In addition to the Permian Basin, ROZs exploration is occurring in other basins including the Williston Basin, Anadarko Basin, California Oil Basins, and Canadian Oil Basins. Many of the observed ROZs occur in carbonate formations; however, ROZs are expected to occur in any formation that exhibits properties favorable for the retention of residual oil, such as widespread, porous, and permeable fairways. As such, this study focuses on the evaluation of the Cypress Sandstone in the Illinois Basin (ILB) and its theoretical potential to contain ROZs. Specifically, this study focuses on areas where the thick, fluvial facies of the Cypress Sandstone is present, which commonly contains a thin MPZ at the top of the sandstone and may be underlain by a ROZ (**Figure 2.2**).

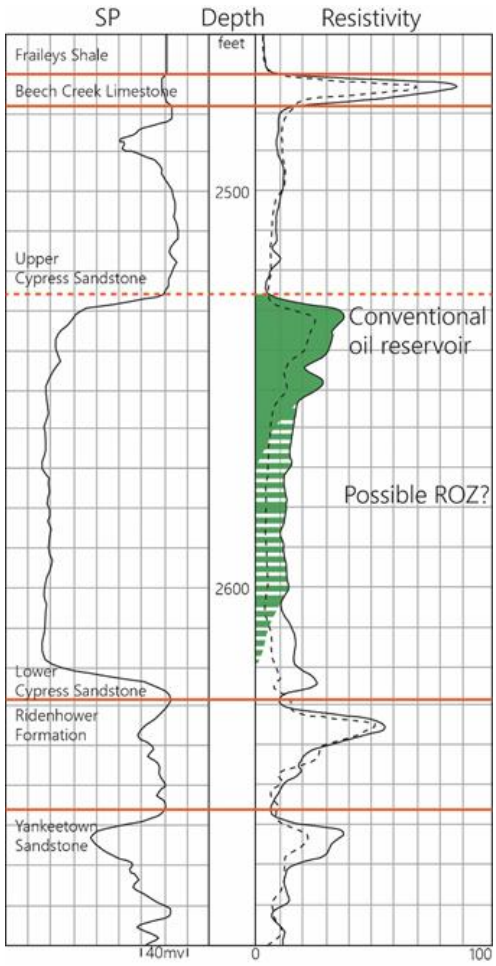

Figure 2.2. Geophysical well log showing typical character of the "thick" Cypress Sandstone with higher resistivity values in the upper ~20 feet, indicating MPZ oil saturation.

2.2 The Cypress Sandstone

2.2.1 Overview

The Cypress Sandstone was first described by Englemann (1863) who named it for outcrops along the Cypress Creek in Union County, Illinois. In Indiana, the Cypress Sandstone is commonly referred to as the Elwren Sandstone (Malott, 1919). Additional names for the Cypress Sandstone occur in records and literature and include units described and named in the outcrop belt by Illinois State Geological Survey (ISGS) researchers as well as locally applied petroleum industry terms (e.g., Weiler sand, Kirkwood sand), many of which predate regional correlation with the Cypress type locality. However, the name "Cypress Sandstone" takes priority and is used throughout this report.

The Cypress Sandstone (**Figure 2.3**), a dominantly siliciclastic, Chesterian-aged (Late Mississippian) unit in the ILB, contains significant oil reservoirs and has been studied for over a century. The Cypress Sandstone exhibits diverse lithological and sedimentological characteristics across the ILB which indicate deposition in a range of environments, from nearshore shallow-marine, tidally influenced deposits, to deltaic deposits, and incised valley-fill fluvial deposits. Similarly, a range of diagenetic

features have been observed, including porosity-destroying cements and porosity-creating dissolution, which reflect the large spatial extent and burial history of the unit.

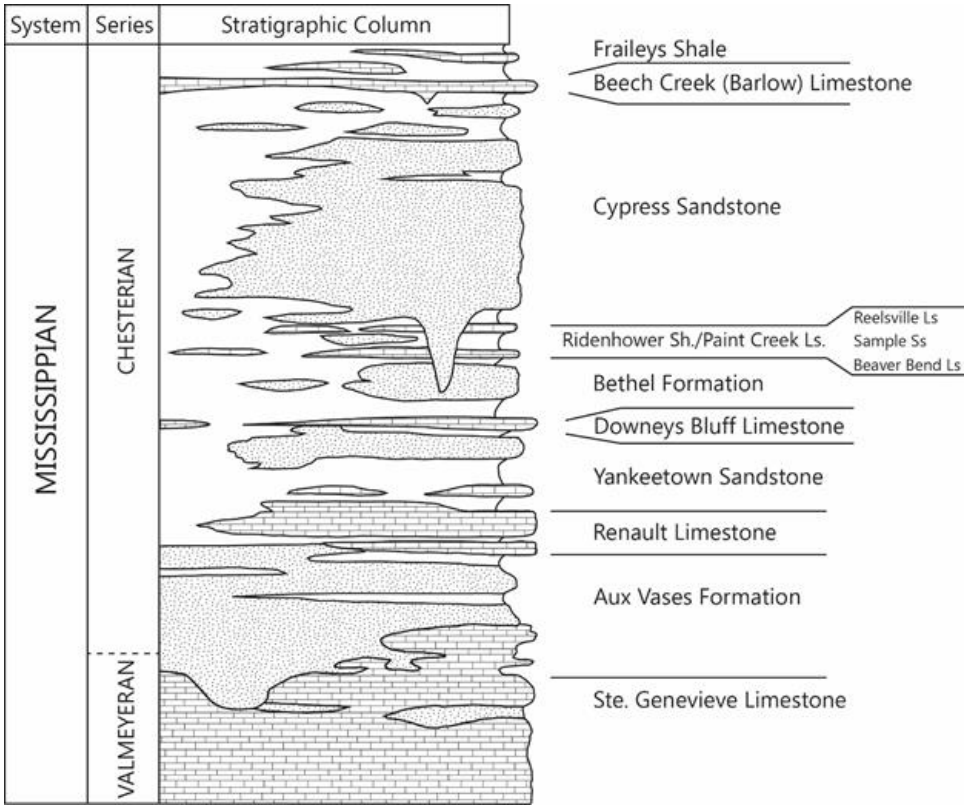

Figure 2.3. Generalized stratigraphic column displaying the location of the Cypress Sandstone within the Gasperian Stage of the Chesterian Series. Modified from Whitaker and Finley (1992) and Seyler et al. (2000).

In order to understand the geologic context of the Cypress Sandstone and the probability that it contains ROZs, a brief overview of the Chesterian Series in the ILB, including general geologic setting, structure, and sedimentology and stratigraphy is presented.

2.2.2 Geologic Setting

The ILB is a gently sloping, intracratonic basin covering an area of 110,000 mi^2 (285,000 km^2) over most of Illinois, Southwestern Indiana, and Western Kentucky (Nelson, 1995). Bounded by the Ozark Dome on the west, the Cincinnati Arch to the southeast, and the Wisconsin Arch on the north, the ILB was open to the south during the Mississippian and formed a portion of a carbonate ramp that spans from New Mexico to Virginia (Nelson et al., 2002). In late Mississippian time, the ILB experienced semi-arid and seasonal (wet-dry) tropical climates (Cecil, 1990) and had a tropical setting between 5˚ and 15˚ south of the equator (**Figure 2.4**; Craig & Conner, 1979; Scotese & McKerrow, 1990; Nelson et al., 2002).

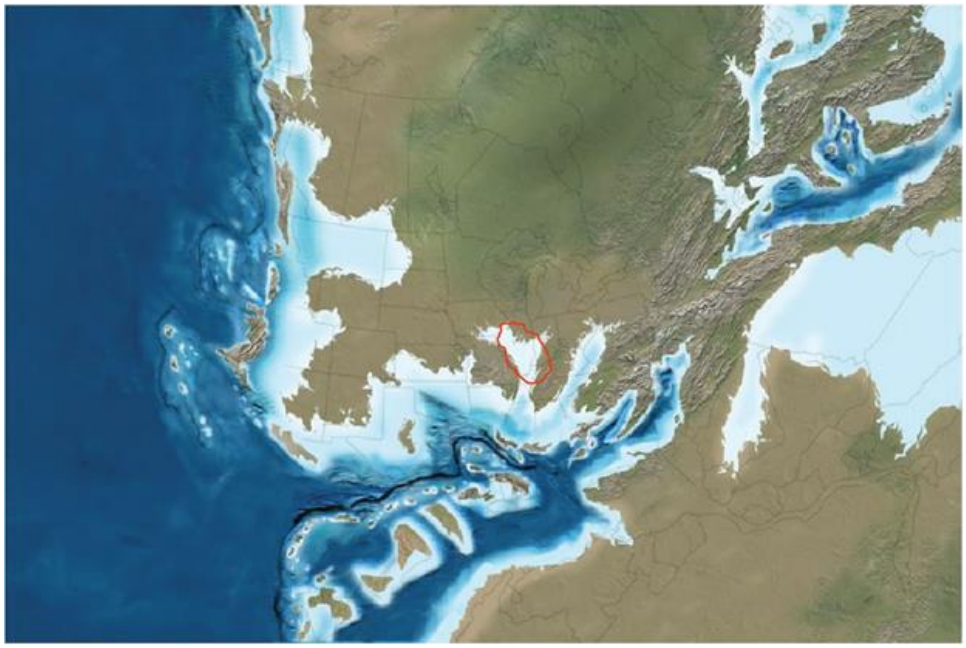

Figure 2.4. Paleogeographic time-slice map of North America during the Chesterian (~325 Ma) (modified from Blakey, 2013). The ILB (outlined in red) is represented during a sea level high-stand period with drainage systems entering into the basin from the north and northeast.

Structural History

The ILB has a complex structural history that begins in the Late Precambrian and continues through the Paleozoic. During the Late Precambrian (800–550 Ma), the supercontinent of Rodinia began to break up. A resulting failed rift zone south of Illinois, known as the New Madrid Rift Complex, constituted a zone of weakness in the lithosphere that eventually initiated subsidence in Southern Illinois, the southeastern margin of Indiana, and Northwestern Kentucky. Basement-seated normal faults within the rift complex propagated roughly perpendicular to the North American cratonic margin as the Iapetus Ocean opened during the breakup of Rodinia (Kolata & Nelson, 1990). Moreover, two of four rifts created as a result—the Reelfoot Rift and the Rough Creek Graben—within the New Madrid Rift Complex **(Figure 2.5**) are closely associated with the development of the ILB (Nelson, 1991).

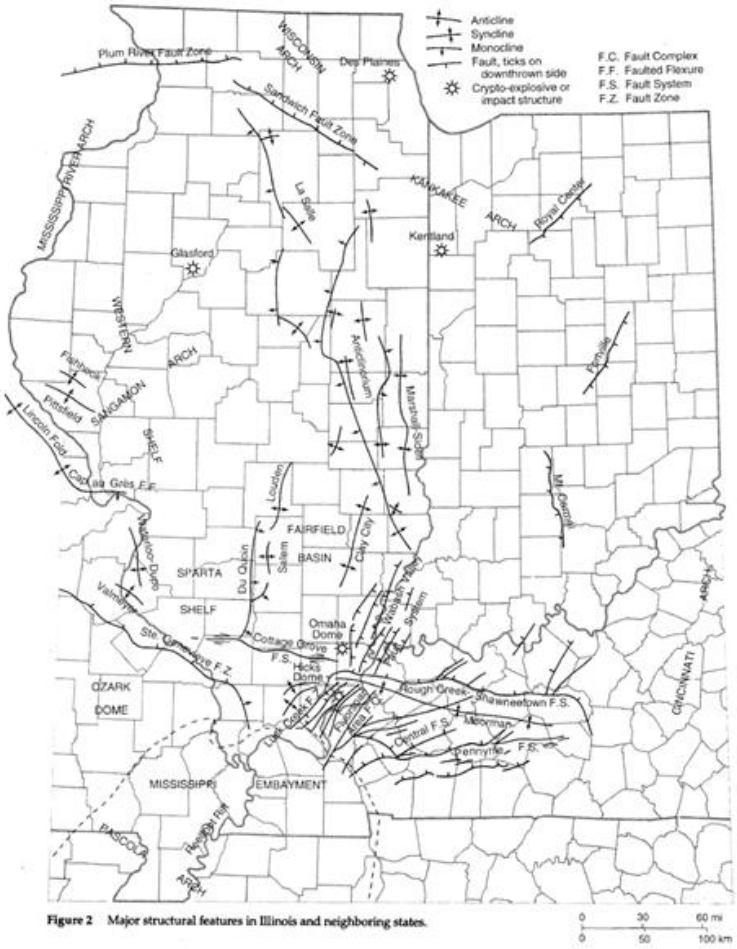

Figure 2.5. Map showing major structural features and the location of the Reelfoot Rift. Figure modified from Nelson (1995).

Gradually, the rift basin transitioned into a cratonic embayment complex which underwent episodic downwarping throughout the Paleozoic. Subsidence resulted from thermal contraction, isostatic adjustment, and sediment loading (Cole & Nelson, 1995). The proto-ILB, as a result, was defined throughout the Paleozoic as a southward-plunging trough similar to the Mississippi Embayment (Kolata & Nelson, 1990).

The subsidence rate of the ILB increased abruptly at the beginning of the Mississippian (Kolata & Nelson, 1991; Treworgy et al., 1989), but stabilized through the remainder of the period (Kolata & Nelson, 1990). Widespread deformation within the ILB began in the Late Mississippian (Chesterian), peaked in the Early Pennsylvanian (Morrowan to Atokan), and continued sporadically throughout the Pennsylvanian (Kolata & Nelson, 1990). During this time, basement-seated reverse faults reactivated due to stresses associated with the assembly of Pangaea. The results of the deformation include monoclines and asymmetrical anticlines composed of Paleozoic sediments (Braile et al., 1986; Kolata & Nelson, 1990). **Figure 2.5** shows the locations of these principal structural features of the ILB. Features formed within the central portion of the ILB during the Chesterian and Pennsylvanian deformations include the Loudon Anticline, La Salle Anticlinorium, and Du Quoin Monocline. Strata of the Chesterian

Series thins over the La Salle Anticlinorium, the Du Quoin Monocline and related Salem, the Loudon and Mattoon anticlines, the Sparta Shelf, the Clay City Anticline, and, possibly, the Wabash Valley Fault System, indicating structural movement concurrent with deposition (Kolata & Nelson, 1990).

Chesterian Sedimentology and Stratigraphy

The Chesterian Series (Worthen, 1860, p. 312-313; Swann, 1963, p. 20) is the uppermost series of the Mississippian System, extending from the major unconformity at the base of the Pennsylvanian System (sub-Absaroka unconformity) down to the base of the Ste. Genevieve Limestone. The Chesterian Series occurs over much of the southern half of Illinois. Chesterian strata are generally characterized by alternating siliciclastic and carbonate units that were deposited during a period of both fluctuating sea level (Swann, 1963; Seyler et al 2000; Smith and Read 2001; **Figure 2.6**) and changing rates of sediment influx into the ILB.

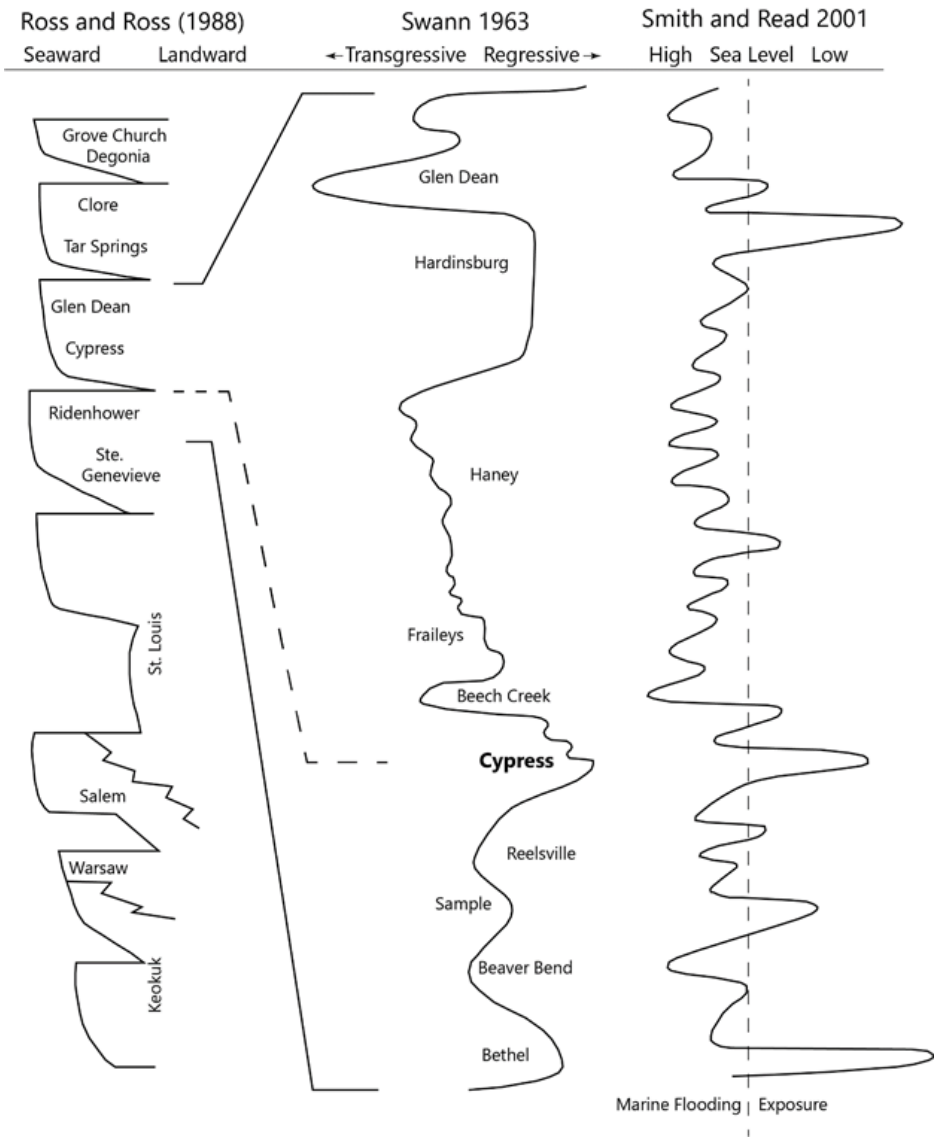

Figure 2.6. Figure showing broad global sea level changes reported by Ross and Ross (1988) and the smaller scale perturbations that affect the ILB, with alternative interpretations by Swann (1963) and Smith and Read (2001). Figure modified from Smith and Read 2001.

Beerbower (1964) defines cyclical sedimentation as having two drivers: autocyclic processes that are inherent to the depositional system (e.g., river/delta avulsion) and allocyclic processes that are controlled by external forces (e.g., tectonics, sea level, climate). Chesterian cyclical sedimentation was both a product of lateral shifts in the southwesterly course of the Michigan River (autocyclic) and sea level fluctuations (allocyclic) driven by glacial/interglacial cycles. These mechanisms caused the paleoshoreline to shift 100 to 600 mi (160.9 to 965.6 km) in a northeast-southwest direction (Pryor & Sable, 1974).

In the ILB, the Chesterian Series deposits reflect a transitional climatic period, whereas the underlying, dominantly-carbonate Valmeyeran Series indicates deposition in a semi-arid setting. The dominantly-clastic, overlying Lower Pennsylvanian Morrowan Series was deposited in a tropical

perhumid climate (Cecil, 1990; Siever, 1953). Twenty cyclical successions of siliciclastic-carbonate deposition are recorded (Devera et al., 2010; Nelson et al., 2002) within the Chesterian Series, which collectively spanned 5 to 10 million years (Swann, 1964). Nelson et al. (2002) identify eleven depositional sequences within the lower Chesterian succession (**Figure 2.7**). Since delta progradation likely occurred several times per million years, the frequency of Chesterian cyclicity is comparable to Pennsylvanian cyclicity in the ILB (Swann, 1964), although Chesterian strata contain volumetrically more limestone and less coal than Pennsylvanian strata (Cecil, 1990). However, coal beds overlying Chesterian sandstones, although thinner and less common than coals overlying Pennsylvanian sandstones, increase the resemblance of Chesterian cyclothems to Pennsylvanian cyclothems in the ILB (Siever, 1953; Smith and Read, 2001).

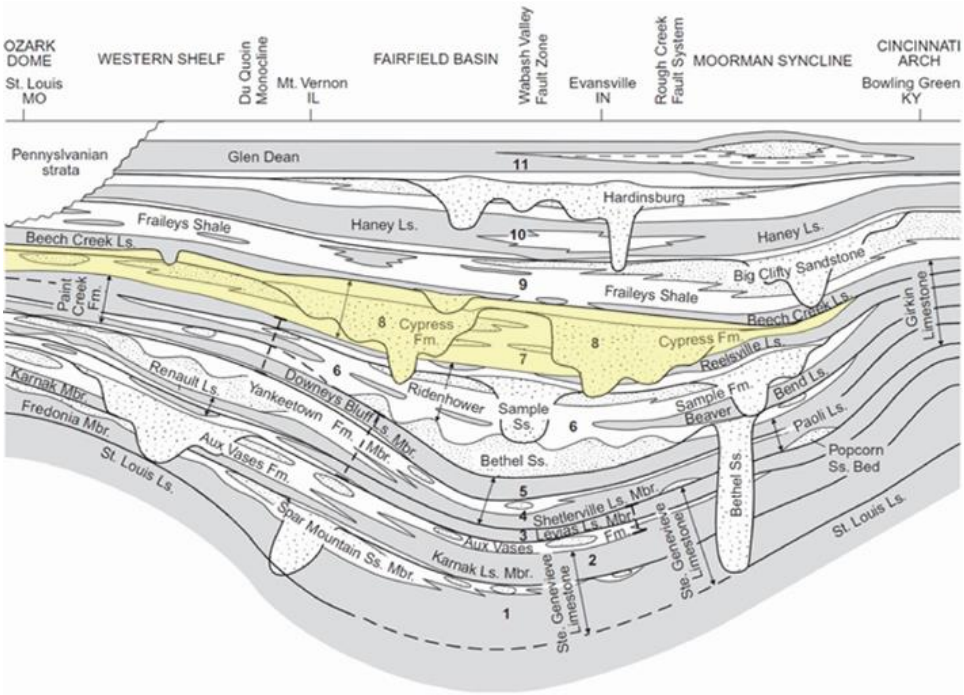

Figure 2.7. Generalized cross section of the lower Chesterian Series from the Ozark Dome to the Cincinnati Arch displaying the eleven depositional sequences of the lower Chesterian Series. The Cypress Sandstone (yellow) is comprised of three depositional sequences (Sequences 7, 8, and 9). Figure 2.8 shows the cross-section's orientation. Figure modified from Nelson et al. (2002).

The lower Chesterian Series, including the Cypress Sandstone, is confined to the southern half of Illinois and consists of the Hombergian and Gasperian stages, spanning from the bottom of the Ste. Genevieve Limestone to the top of the Glen Dean Limestone (Nelson et al., 2002; Devera et al., 2010; **Figure 2.3**). Since the Cypress Sandstone is part of the upper Gasperian Stage, selected formations from the Gasperian and overlying Hombergian Stage are of relevance to this review. However, Willman et al (1975) and Nelson et al (2002) provide detailed descriptions of the Chesterian stratigraphy relevant to a discussion of the Cypress Sandstone; as such, the related formations will not be discussed here.

2.2.3 Cypress Intraformational Stratigraphy

The Cypress Sandstone is lithologically variable, being composed of thick sandstone in some areas and being shale-interbedded with numerous lenticular, well-cemented sandstone bodies in others. The Cypress Sandstone is predominantly sublitharenitic and subarkosic in composition (Pitman et al. 1998). Two, mostly parallel, northeast-southwest trending clastic belts composed of generally thick sandstone bodies are found within the Cypress Sandstone (**Figure 2.8**). These two belts are referred to here as either the Western Belt or the thick Cypress Sandstone (located in Illinois) and the West Baden Trend (located in Southwestern Indiana and Northwestern Kentucky), respectively. Both the Western Belt and West Baden Trend are thought to represent incised valley-fill systems (Nelson et al. 2002). The part of the Cypress Sandstone that comprises the Western Belt is the focus of ROZ research in this study.

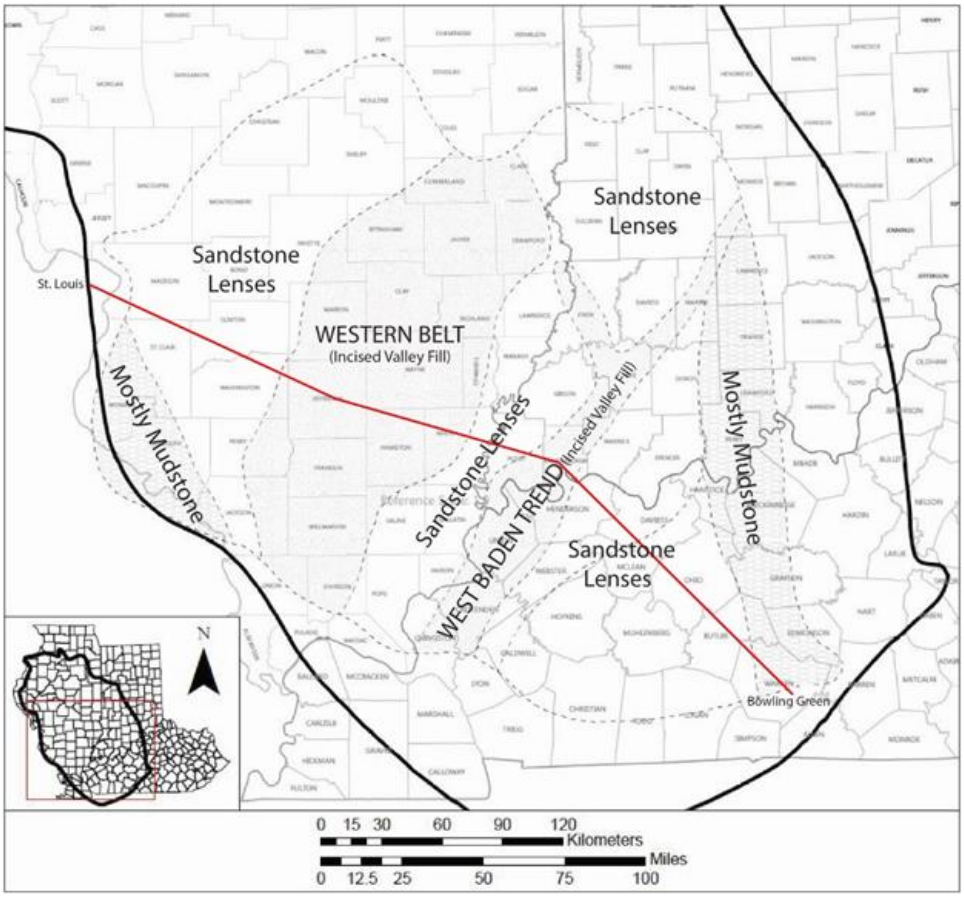

*Figure 2.8. Generalized facies map displaying the subcrop limit of the Cypress Sandstone and the dominant facies of the Cypress Sandstone across the ILB (black outline). The orientation of the cross section in **Figure 2.7** is shown (red line). Figure modified from Nelson et al. (2002).*

The Cypress Sandstone in the Western Belt (**Figure 2.8**) attains a thickness of between 100 and 200 ft (30.5–61 m) but thins and changes facies to the east and west (Willman et al. 1975). These sandstones in the Western Belt, sometimes referred to as the "massive," "main," or "lower" Cypress Sandstone in literature and drilling records, are commonly overlain by thin, lenticular sandstone bodies encased in shale (Fituri 1987). In the West Baden Trend (**Figure 2.8**), the Cypress Sandstone amalgamates with sandstones of the underlying Ridenhower and Bethel Formations (**Figure 2.3**), forming a linear, northeast-southwest trending tract (Sullivan 1972). The thick sandstones characteristic

of the Western Belt and the West Baden Trend constitute one of the two most common sandstone facies within the Cypress Sandstone; the second most common sandstone facies is sandstone lenses (**Figure 2.8**).

The thick Cypress Sandstone features generally fining-upward sequences, characteristic of their interpreted deposition as bar deposits in fine-grained channel belts and fluvial-dominated deltas. Permeability appears to increase with depth as a function of coarsening grain size within typical reservoir units. In outcrop, this facies exhibits stacked, imbricate sand bars (Cole and Nelson 1995). Coarse lag deposits of marine fossil hash in the bases of channels indicate a close proximity to marine/estuarine conditions (Seyler et al. 2000). However, since this facies has been largely overlooked as a viable oil reservoir, it has received relatively little study, and the presumed depositional environments and reservoir architecture may be more complex.

2.3 Historical Perspective – Cypress Sandstone Oil Fields and Oil-Producing Areas

Cypress Sandstone oil reservoirs were discovered in the first decade of the 1900s in the oil fields of southeastern Illinois (Blatchley 1913). Most of the known Cypress reservoirs have undergone decades of production and are depleted from a primary and waterflood production standpoint, though a significant amount of economically recoverable oil remains unswept (Grube & Frankie 1999). The thick Cypress Sandstones of the Western Belt, which formed as part of the incised valley-fill facies, are pervasive in the central part of the ILB (**Figure 2.8**). Production from thick sandstones within the Western Belt is relatively sparse (**Figure 2.9**), as most production comes from the tidal bar facies overlying the thick Cypress Sandstones. Although the thick Cypress Sandstones tend to exhibit higher porosities and permeabilities, they generally produce less oil due to the technical difficulties associated with high water production. Thick Cypress Sandstone reservoirs have low primary recovery due to the early onset of excessive water production, owing to the high vertical permeability of the Cypress, and are thus an underproduced oil resource in the ILB.

Lee (1939) first proposed that the Cypress Sandstone could be subdivided into three sandstone units: lower, middle, and upper. The thick sandstone portion of the Cypress Formation was informally called “Weiler” in order to differentiate it from the true top of the Cypress Sandstone. Lee described the Cypress Sandstone in general as a massive sandstone body ranging in thickness from 120 to 175 ft (36.6 to 53.3 m) that often grades laterally over short distances to shale and sandstone beds. The thick Cypress Sandstone is referred to as the “lower” Cypress because of its relative position below the sandstone lenses in the central part of the ILB. These prevalent lenticular sandstone lenses of the Cypress Sandstone have been interpreted as tidal bar deposits (Grube 1992; Xu and Huff 1999). Historically, these tidal bars have contained the most prolific Cypress Sandstone reservoirs and produce oil in some of the largest oil fields in the state, such as Loudon Field and Lawrence Field. The tidal bars are commonly composed of individual sandstone lenses, often less than 10 ft (3.3 m) thick, that are typically stacked and/or shingled within the formation and are productive in stratigraphic or structural traps associated with its anticlines (Grube 1992; Grube 2000).

Although the tidal bar facies’ high degree of both lateral and vertical lithologic variability leads to highly heterogeneous and compartmentalized reservoirs, the individual bar compartments can be individually recognized, and water flood programs can be designed to effectively sweep these reservoirs; empirically, such program designs have led to exceptional recovery efficiencies of at least 45% (Grube

and Frankie 1999). The most productive tidal bar facies by volume of oil produced is located in Lawrence Field in Lawrence County, Illinois, where the entire Cypress Sandstone is comprised of the tidal bar facies (**Figure 2.9**) (Seyler et al. 2000). On the West flank of the basin, where tidal bars persist and are ubiquitous, Cypress Sandstone oil fields are relatively rare and production is limited to the uppermost sandstones (Grube & Frankie 1999). The distribution of Cypress Sandstone oil fields is shown in **Figure 2.9**.

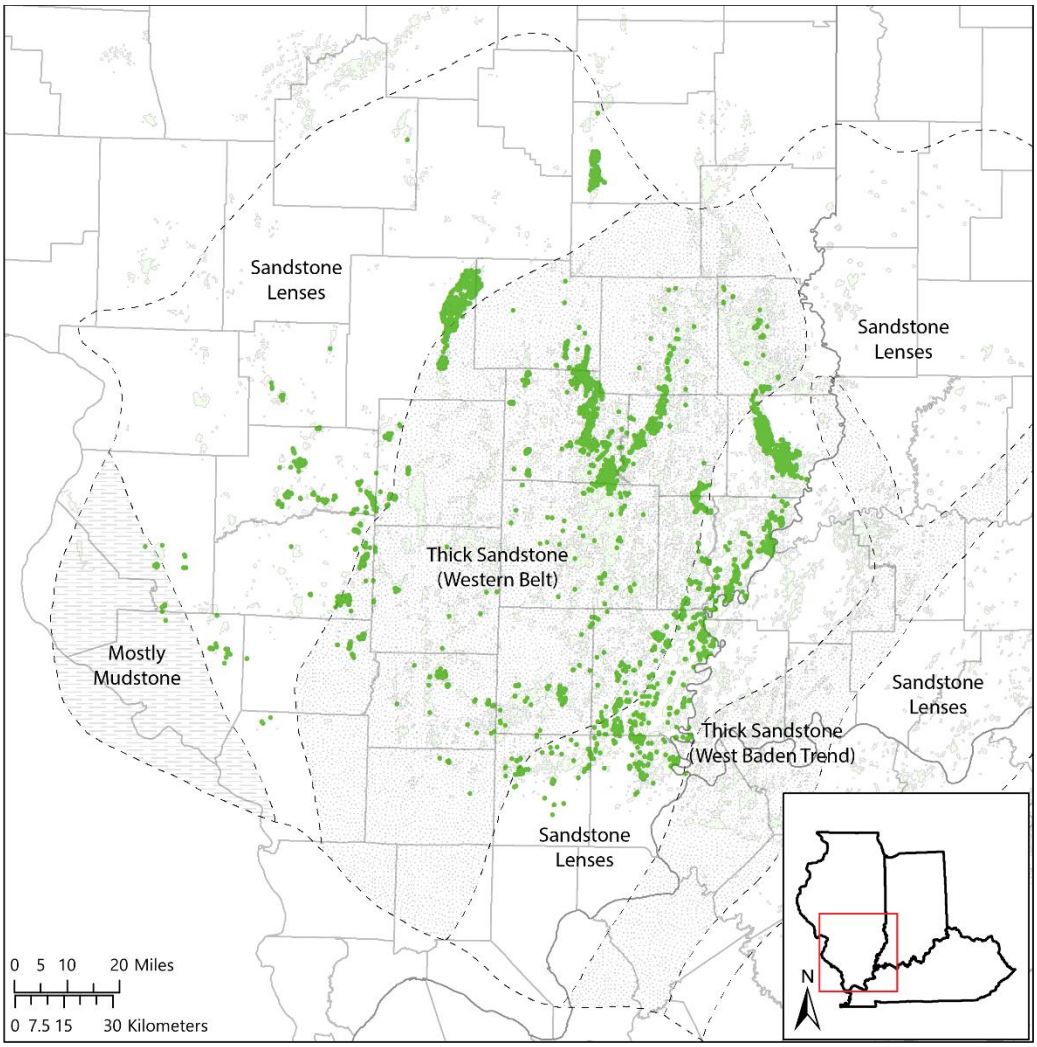

Figure 2.9. Map showing provinces of the Cypress Sandstone within the ILB (modified from Nelson et al. 2002). The boundaries of the thick sandstone where it contacts other Cypress facies are approximate. Green dots are locations of wells that have production from the Cypress Formation. These provinces are based on the subsurface work of Sullivan, (1972), Seyler et al., (2000), and Nelson et al., (2002).

2.4 Study Area Selection

2.4.1 Oil Field Screening and Selection

To begin the effort to identify ROZs and ultimately development of injection scenarios designed to maximize oil production and CO_2 storage, we needed to select a study area for detailed geologic reservoir characterization, geocellular modeling, and reservoir simulation representative of thick Cypress Sandstone reservoirs in the ILB. Identifying the study area was a two-step process. First, available data –

including well and geologic data – were compiled and analyzed at the basin-scale in order to narrow the search to eight candidate study areas; data was analyzed for each respective candidate. Secondly, a preliminary geologic assessment was conducted for each of the candidates. Data availability and geologic properties were paramount considerations during the identification process and were used to identify the candidate site with both the highest probability of containing a ROZ and the available data necessary for detailed study.

Criteria for Selecting Candidate Study Areas

A preliminary basin-scale evaluation to identify the candidate study areas was based on several criteria key to the success of the project. First, the study area must have documented production from the thick Cypress Sandstone; this requirement was imposed in order to ensure that the field contained oil in the thick Cypress Sandstone and to establish typical decline curves for the thick Cypress Sandstone. Second, the study area must contain abundant wells with available geophysical log data, which is a prerequisite for cross section correlation, isopach and structure mapping, and, ultimately, 3D geocellular modeling. Thirdly, the study area must be in an area of active drilling. Due to the empirical, relatively poor production from the thick Cypress Sandstone, these wells were typically drilled through to deeper, more productive horizons. The hope was that companies actively drilling to deeper horizons would be amenable to coring the Cypress interval with funds provided by this project. This core would provide a detailed look at the reservoir conditions of the study area.

Ideally, the optimal study area would occur at the intersection of these three criteria (**Figure 2.10**). However, due to the circumstances which arose from working with multiple data types in the old oil fields of the ILB as well as the interests of currently operating companies, it proved difficult to identify candidate areas where all three data types (i.e., reservoir data, production history, and data resulting from active drilling operations) existed concurrently. Therefore, it was necessary to include potential candidate sites that met only two of the data criteria. Acceptable combinations of available data types included either (a) reservoir data and production history or (b) reservoir data and active drilling.

The identification process was also affected by the recent decline in oil prices that has decreased drilling activity in the ILB as well as most areas in the United States. The decrease in drilling activity since 2014 has resulted in a subsequent decrease in drilling permits and has placed some field developments on hold. In either case, because reservoir data is critical for building geologic conceptual models and 3D geocellular models, choosing an area without reservoir data was deemed unacceptable for this project.

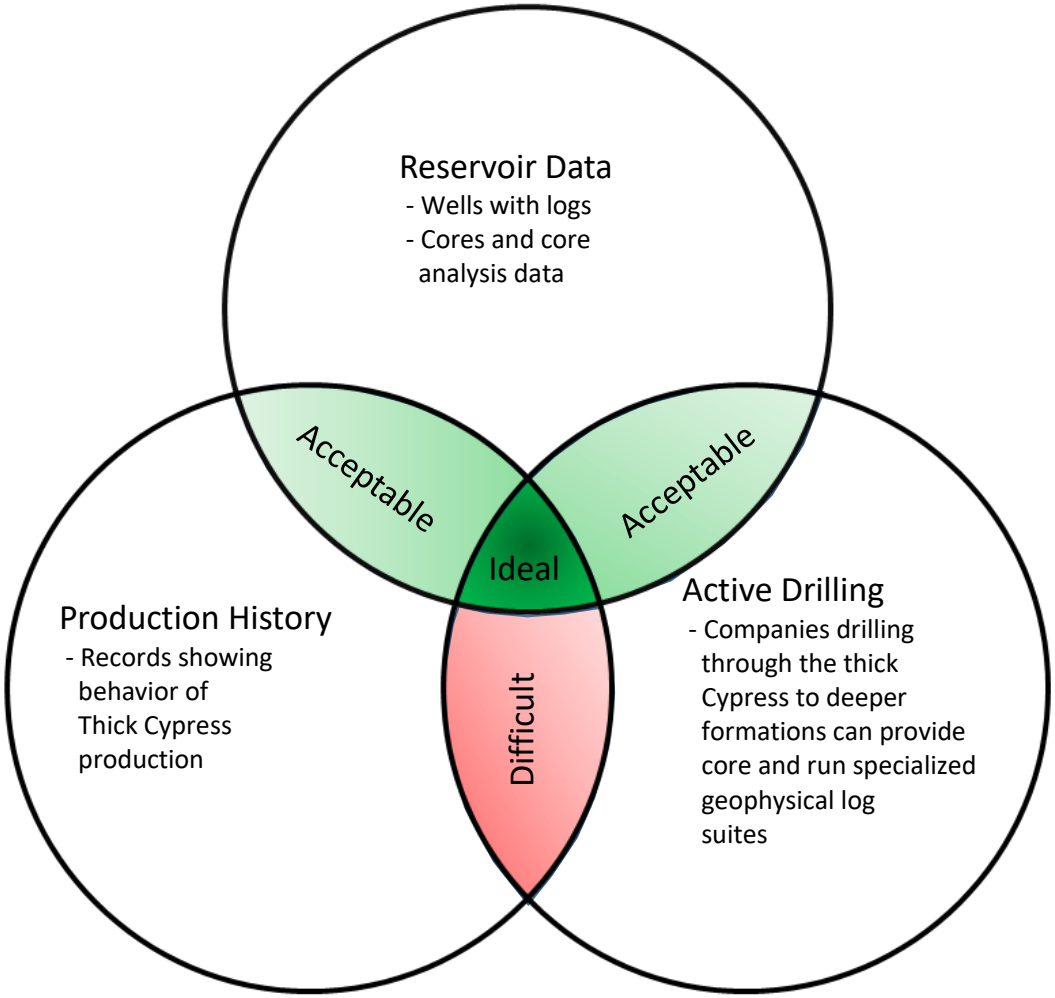

Figure 2.10. Diagram showing three main data types required for the study. First, the study area should have historical production data that documents production from the thick Cypress Sandstone in order to establish decline curves. Second, the study area should contain abundant wells with geophysical log data, which are prerequisites for cross-section correlation, isopach and structure mapping, and ultimately 3D geocellular modeling to be used in reservoir simulations. Building a comprehensive conceptual geologic model would be problematic without geophysical data. Third, the study area should be in an area of active drilling of the entire Cypress Sandstone. Active operating companies may be amenable to coring the Cypress interval with funds provided by this project. The core will provide data for a thorough reservoir analysis in the study area.

The first step in locating and identifying candidate study areas was completing a GIS-based assessment in order to define the distribution of available data types for areas within the ILB. By synthesizing all available data held in ISGS databases related to the Cypress Sandstone and then overlying them with one another on a map, a visual representation of the areas with the highest data density was created. The data queries performed in order to create the visual representation, the types of data queried, explanations of the data, and their significance to the success of the project are discussed below:

Presence of the thick Cypress Sandstone

Before beginning extensive database queries, many oil fields were eliminated based on previous mapping of the dominant facies of the Cypress Sandstone (**Figure 2.9**). Moreover, since this mapping of

the Cypress Sandstone provinces is generalized at the regional-scale and the boundaries of the thick Cypress Sandstone fairway are not perfectly defined, oil fields lying near the mapped boundaries of the fairway were included in the preliminary assessment.

Oil production from the Cypress Sandstone

The database was first queried in order to select wells with documented oil production within the thick Cypress Sandstone fairway (**Figure 2.9**). This query resulted in approximately 2,500 wells with available production data. A subset of these wells had data indicating from which zone within the Cypress Sandstone its production was derived. Next, wells were selected that had documented production from the lower Cypress. This query returned 33 wells scattered around the thick Cypress fairway. These wells, as well as the wells surrounding them, were checked for available geophysical logs that could be used in order to assess the character of the Cypress Sandstone. Through this process, it was established that thin oil zones are a common feature in the top of thick Cypress Sandstone deposits (**Figure 2.11**).

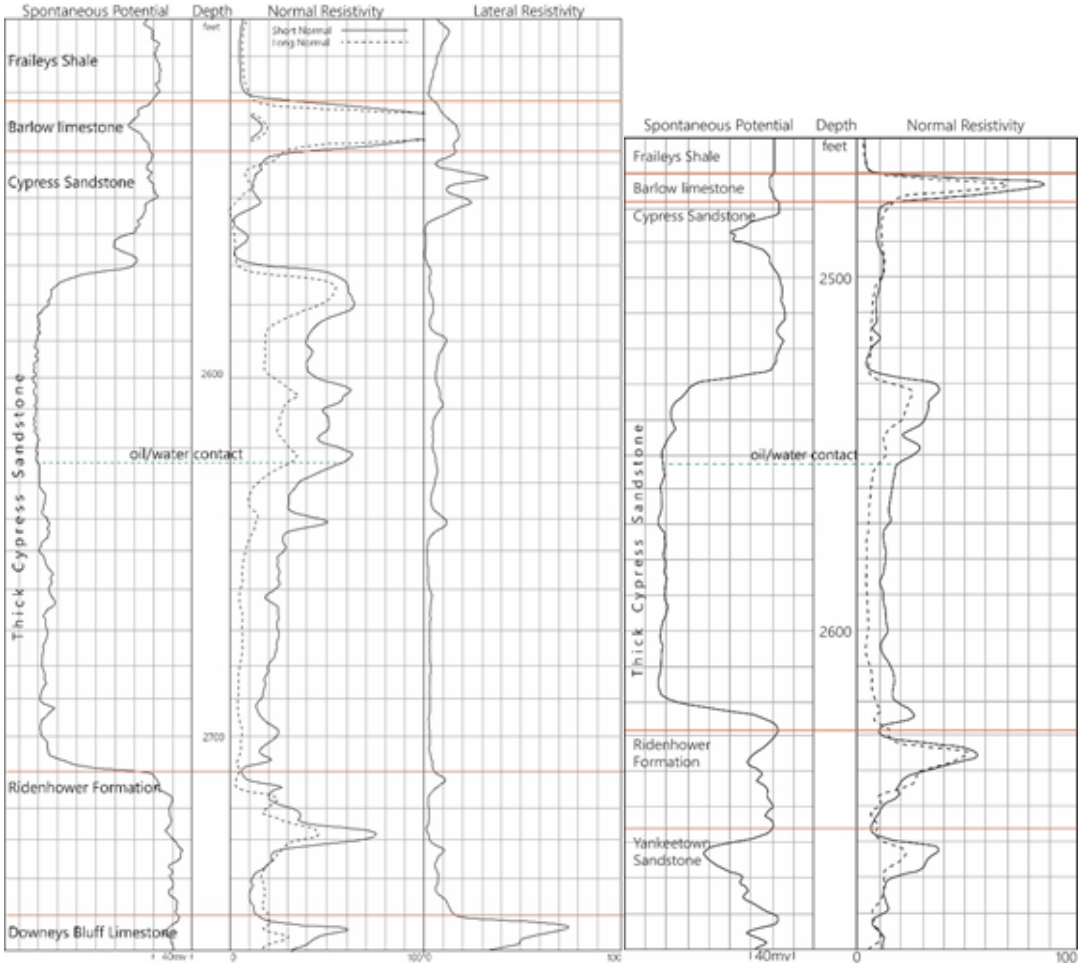

Figure 2.11. Example geophysical logs from Noble Field (left) and Bible Grove Field (right) showing the variation in thickness in the thick Cypress Sandstone as well as the presence of an oil zone developed in the top of the formation, as indicated by the higher resistivity values.

Recent drilling permits

The ISGS maintains a database of drilling permits which proved useful for highlighting areas of the ILB actively being drilled. These areas provide potential targets for operating companies interested in cutting a whole core through the thick Cypress Sandstone. Issued permits for the first nine months of 2014 (up to the most recent months that permit records were available at the time) were grouped by section and then plotted to produce a map of areas being actively drilled (**Figure 2.12**).

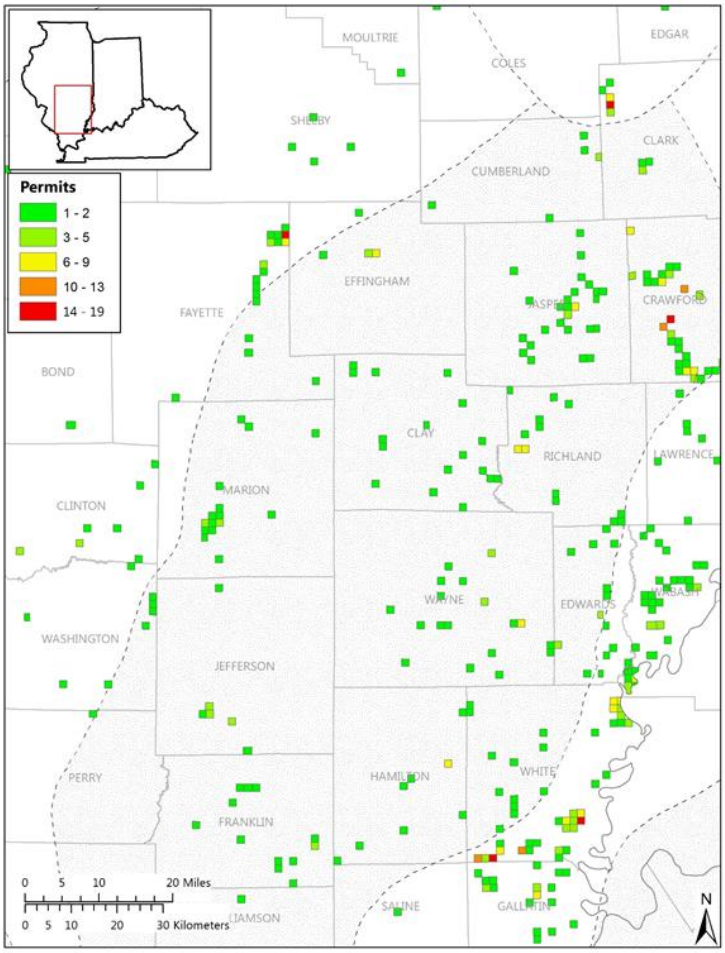

Figure 2.12: Map of sections that contain drilling permits issued in Illinois in 2014 (January through September). Map represents a proxy for actively drilled areas in the state and thus areas with the highest potential for collecting a core of the thick Cypress Sandstone.

Core analysis data availability

In addition to production data and data resulting from active drilling operations, the availability of core analysis data, including porosity and permeability requirements, was another consideration in selecting candidate study areas. Core analysis data is necessary in order to build comprehensive transforms for 3D geocellular modeling. The ISGS maintains a digital database of core analysis data derived from records supplied by operating companies. This database was queried to determine the availability and distribution of such data for each of the candidate study areas.

Oil field age

Finally, the overall age of the oil field was a consideration during the selection process, as age plays a role in both the quality and viability of reservoir data (**Figure 2.13**). All the evaluated fields were discovered during the time period between 1935 and 1945 and, since that time, have had distinct development histories. Some of the fields were nearly fully developed very early on in their history, whereas other fields have seen ongoing development throughout their lifespan.

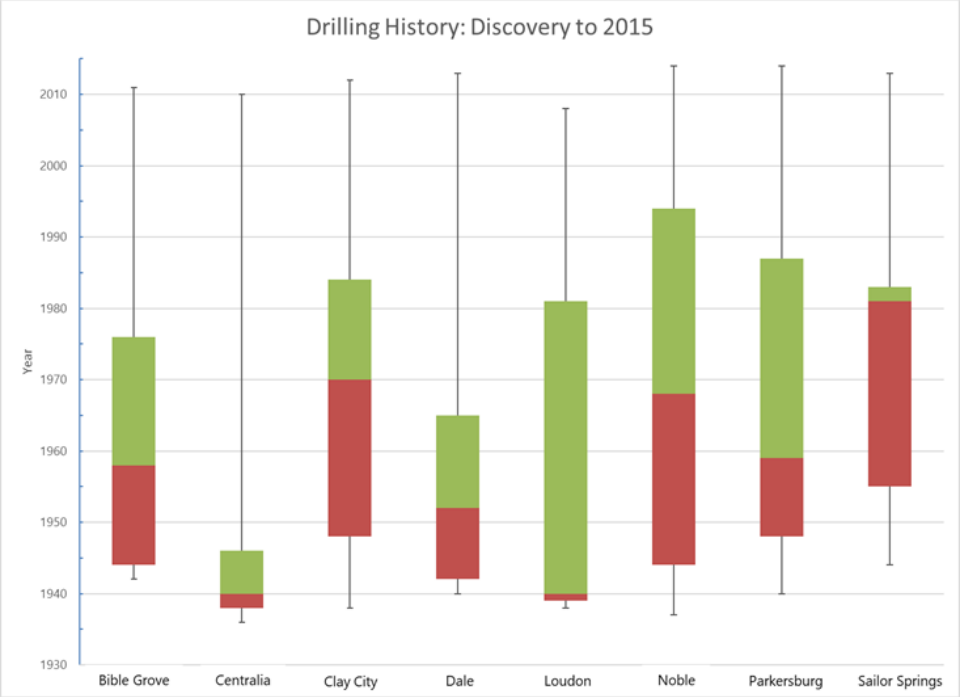

Figure 2.13: Box and whisker plot depicting the drilling activity for each of the candidate oil field study areas between 1930 and 2015. The complete drilling history of each field is divided into quartiles with the lower whisker representing the first quantile, the red box representing the second, the green box representing the third and the upper whisker representing the fourth. Centralia Field, for example, has 75% of its total drilling activity occurring between about 1937 and 1947 indicating the typical age of drilling records for the field will be quite old.

Candidate study area evaluation

After reviewing the quality, viability, and availability of the required data types on a basin-wide scale and for each candidate study area, eight candidates were chosen for a more thorough assessment. The eight candidates are summarized in **Table 2.1**. A number of these sites consist of portions of larger, often consolidated oil fields. The locations of these fields range from within the northern, southern, and central parts of the thick Cypress fairway, as well as along the flanks of the fairway (**Figure 2.14**).

Table 2.1. Location of candidate study areas. Some of the study areas fall within a larger, consolidated oil field and thus were given a name with the consolidated field listed in parenthesis.

Name of candidate study area	County	Location
Bible Grove Field	Clay	Sec 8, 9, 17, T5N, R7E
Centralia Field	Clinton	Sec 1, 12, T1N, R1W
Clay City (Clay City Consolidated)	Clay and Wayne	Sec 15, 16, 17, 20, 21, 22, T2N, R8E
East and Central Dale Consolidated Field	Hamilton	Sec 23, 24 T6S, R5E and Sec 18, T6S, R6E
Southeast Loudon Field	Fayette	Sec 20, 21, 28, 29, 31, T7N, R3E
Noble Field (Clay City Consolidated)	Richland	Sec 3, 4, 5, 8, 9, 10, T3N, R9E
Parkersburg Field	Richland and Edwards	Sec 30, 31, T2N, R11E
Sailor Springs Field	Clay	Sec 27, 28, 33, 34, T4N, R8E

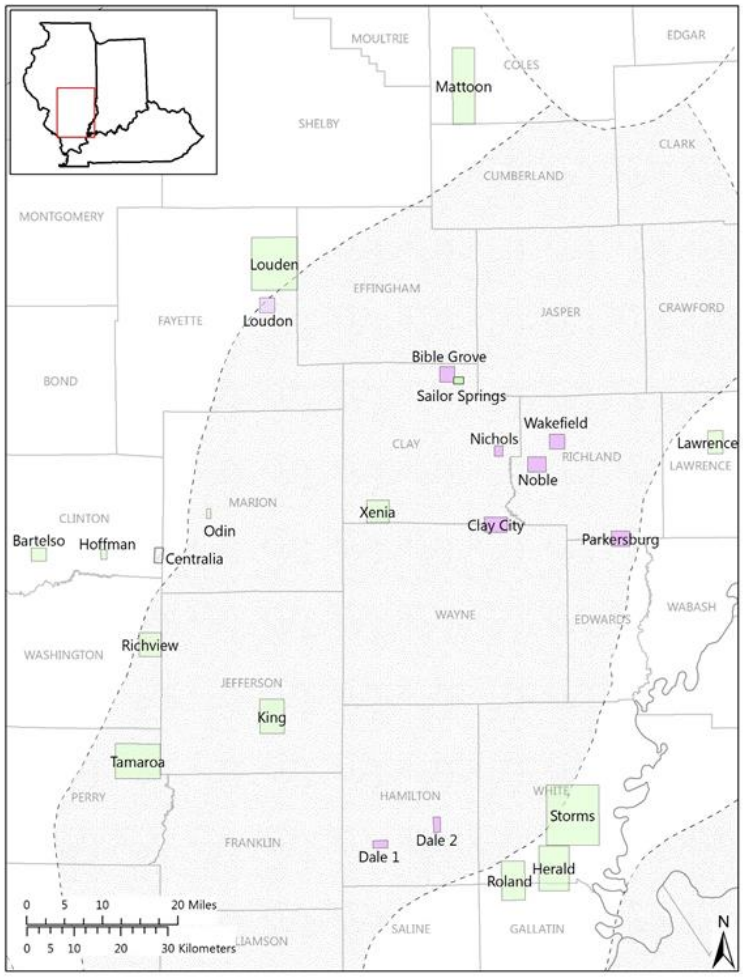

*Figure 2.14. Map showing eight candidate study areas (in purple; **Table 2.1**) within the fairway of the thick Cypress Sandstone (stippled) in Illinois. Each study area is being assessed for available data. Areas where the Cypress Sandstone has been studied in oil fields by the ISGS in the past are shown in green boxes. Centralia is shown as striped because it was previously studied, and it is being reviewed as a candidate study area.*

Each candidate study area was evaluated based on the following six criteria:

- the structural setting of the area
- the history of production and well completion data
- the geologic characteristics of the thick Cypress Sandstone (e.g., thickness, lateral continuity, internal heterogeneity)
- the relation of the thick Cypress Sandstone to the remainder of the Cypress Sandstone, such as being overlain by shale, overlain by sandstone lenses, or being located at a depth below the Barlow limestone (**Figure 2.3**)
- the reservoir properties of the thick Cypress Sandstone (e.g., porosity, permeability, thickness of oil column)
- the availability of the required data types

Data collected as a result of the assessment as to the attributes of each candidate study area are briefly summarized in **Table 2.2**.

Table 2.2. Geologic and data attributes of the thick Cypress Sandstone in eight candidate oil field study areas in the thick Cypress Sandstone fairway. Depths to and thicknesses of the thick Cypress Sandstone are representative for each oil field. The oil zone in the top of the thick Cypress Sandstone is identified by a high resistivity trend and possible suppression of the spontaneous potential curve on the electric log and records of oil production or oil shows. In places where the oil zone is indicated, its thickness is approximated from the resistivity curves. Reservoir data includes geophysical log data, cores, and core analysis (porosity and permeability) data. Production history includes reports of monthly and cumulative oil production, usually grouped by lease. Active drilling indicates that drilling permits were issued within the candidate study area location in calendar year 2014.

Oilfield Name	Average Cypress Depth (ft)	Average Cypress Thickness (ft)	Oil zone present? (thickness, ft)	Average Porosity (%)	Average Permeability (mD)	Reservoir Data	Production History in thick Cypress	Active Drilling (2014)
Bible Grove	2,500	100	Yes >10	20.0	240	Many electric logs, a few cores nearby, little core analysis data	Yes	No
Centralia	1,200	Transitioning to thinner stacked sandstones	No*	20.0	65	Many old electric logs with many that do not penetrate the entire Cypress, a few cores, some core analysis data	No	No
Clay City	2,700	90	Yes <10	No data	No data	Many electric logs and porosity logs, no cores, no core analysis data	Yes	No
Dale 1 & 2	2,700–2,900	70–90	Yes <10	13.5	55	Many electric logs, A few cores, no core analysis data	No	No
Loudon	1,500	70	Yes >10	20.7	135	Many electric logs and porosity logs, several cores, some core analysis data	Yes	Yes
Noble	2,600	150	Yes >10	17.0	439	Many electric logs and porosity logs, a few cores, abundant core analysis data	Yes	Yes
Parkersburg	2,800	Transitioning to thinner stacked sandstones	No*	No data	No data	Many electric logs and porosity logs, no cores, no core analysis data	No	Yes
Sailor Springs East	2,700	150	Yes >10	16.0	380	Many electric logs, no cores, little core analysis data	Yes	Yes

*The oil zone may be very thin, if present, and is difficult to detect because of the transitional nature of the Cypress Sandstone in the Centralia and Parkersburg areas. Additional examination of production records and advanced petrophysical analyses will be conducted to make final determinations.

Candidate Study Areas

Bible Grove

The Bible Grove area (**Figure 2.14**) is in Sailor Springs Field in the northeast corner of Clay County in Sections 16, 17, 8, and 9, 5N-7E. This study focuses mainly on Section 17, 5N, and 7E, since oil production records indicate verifiable production from the uppermost portion of the thick Cypress Sandstone. The Bible Grove area was selected for preliminary review because of its central location within the thick Cypress Sandstone fairway, its well-developed thick Cypress Sandstone with thin oil zones, and past verifiable, documented production from this reservoir. There are no known preexisting studies of the Bible Grove area.

The Bible Grove area is located on a small anticlinal nose that protrudes to the southeast out of the southeasterly plunging ramp between the Iola Anticline and the Bogota-Rinard Syncline (**Figure 2.15**). Its structure is nearly 6 km (4 mi) long and 3 km (2 mi) wide.

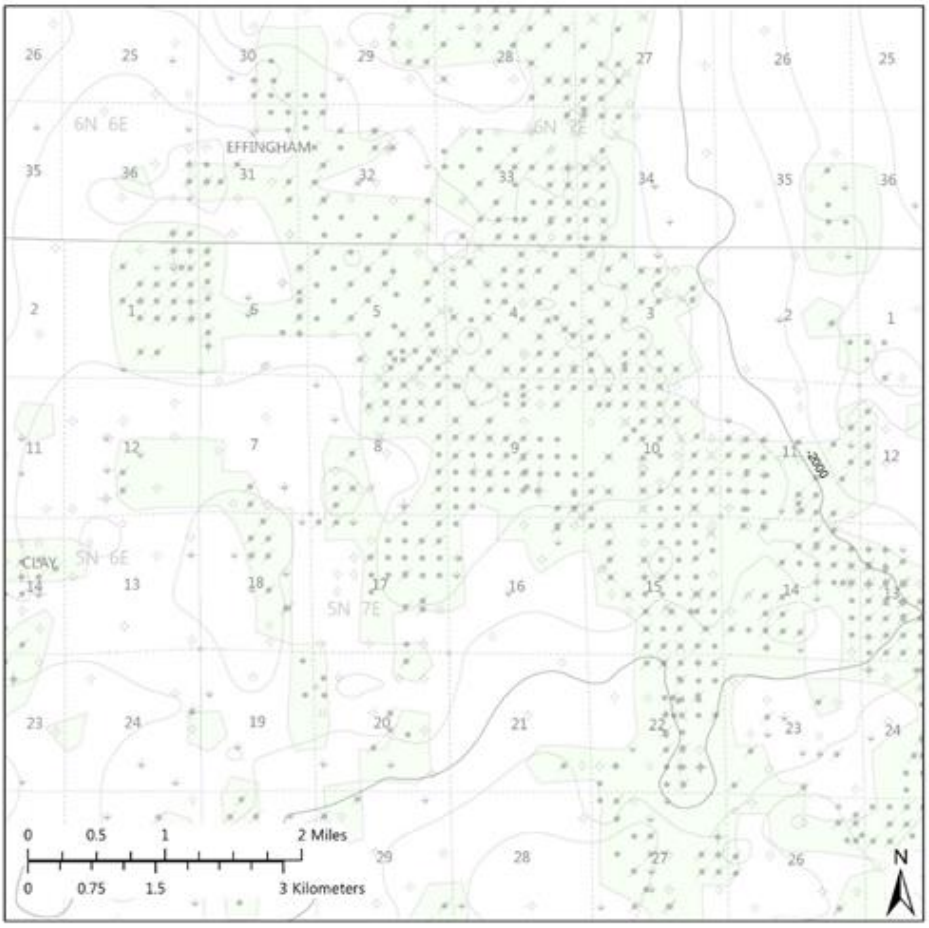

Figure 2.15. Structure on the base of the Barlow limestone showing southeasterly oriented anticlinal nose on which Bible Grove Field is developed. The base of the Barlow limestone is contoured on a 6.1-m (20-ft) interval with index contours and subsea elevations labeled every 30.5 m (100 ft). Oil field areas are highlighted in green.

The Bible Grove area has produced from several different formations, but the thick Cypress Sandstone is the area's most prolific producer. Previously drilled wells for which the thick Cypress Sandstone was the sole target generally reach their total depth in the upper part of the thick Cypress Sandstone in order to avoid the underlying water. Wells which penetrate the entire thick Cypress Sandstone have a sandstone body that typically ranges from 24 to 30.5 m (80 to 100 ft) thick and, in some places, exceeds 36.6 m (120 ft) thick (**Figure 2.16**). Some wells have a thin sandstone interval of 3 m (10 ft) or less that overlies the thick sandstone and is separated from it by a thin interval of shale. In some areas, a thin sandstone interval development directly underlies the Barlow limestone. The main sandstone body of the thick Cypress Sandstone typically lies about 15 m (50 ft) below the base of the Barlow limestone and occurs at a depth generally between 762 and 777 m (2,500 and 2,550 ft).

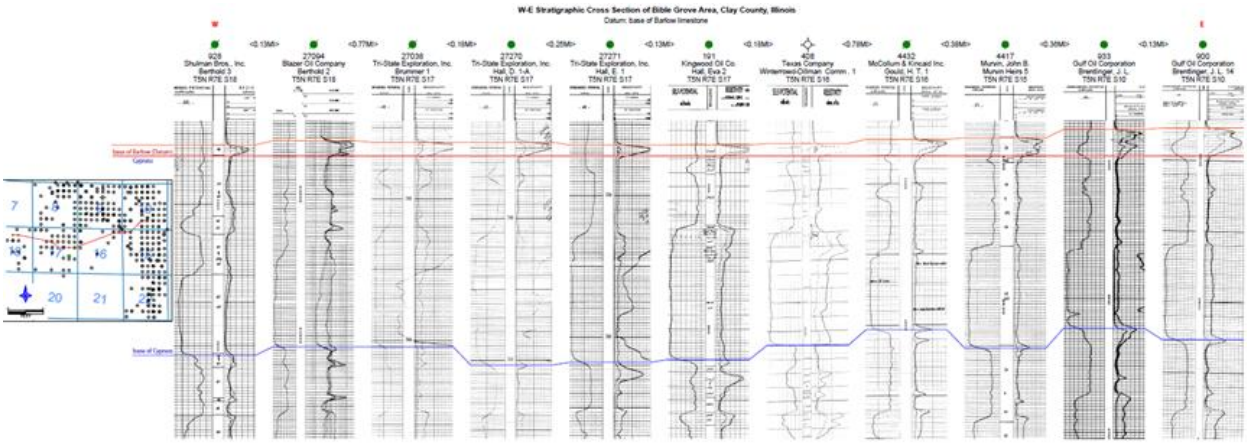

Figure 2.16. East-west cross section through Bible Grove Field showing the persistent thick Cypress Sandstone and the more discontinuous upper Cypress Sandstones.

The thick Cypress Sandstone has a blocky signature on spontaneous potential (SP) logs and some of its wells have a high-resistivity interval in their uppermost portion, which is indicative of oil saturation. The blocky, SP curve logs at the base of the thick Cypress Sandstone indicate an abrupt contact with underlying shale in the Ridenhower Formation (**Figure 2.3**). High-resistivity intervals within the thick Cypress sandstone may indicate sandstone containing carbonate cement. The SP logs in the thick Cypress sandstone in most wells appear to have breaks indicative of intervals of shale or silt. The oil zone within the top of the thick Cypress Sandstone can be over 6 m (20 ft) thick and appears to be best developed in the thickest areas of the Cypress Sandstone.

Core analysis data of the upper portion of the thick Cypress Sandstone are available for fifteen wells near Bible Grove. Most of the core analyses which yielded the available data were performed on wells drilled in 15, 5N, and 7E, but not all the data include core-measured porosity and permeability values. One well with available core analysis data recorded an average porosity around 20% and an average permeability of about 0.237 um^2 (240 mD). Whole core data is not available for the thick Cypress Sandstone of the Bible Grove area. However, there are likely four wells with core plugs suitable for thin section analysis within the upper portion of the thick Cypress Sandstone.

The data availability for the Bible Grove area is of adequate quality. Bible Grove has confirmed, documented production from a well-developed thick Cypress Sandstone that is approximately 30.5 m (100 ft) thick. Past coring operations in the area provide enough core porosity and permeability data. There are several vintages of geophysical logs available for the area, which begin in the 1940s and span through 2000. However, many previously drilled wells targeted the thick Cypress Sandstone and were only drilled in the upper portion in order to avoid the underlying water-saturated zone. Thus, many geophysical logs do not contain data on wells which penetrate the entire thickness of the Cypress Sandstone body. This deemed Bible Grove an unsuitable study area.

Centralia Field

The Centralia Oil Field is located primarily in Clinton County, Illinois, with its southeastern extent protruding slightly into the adjacent Marion County. Centralia Field is located along the western boundary of the thick Cypress Sandstone fairway (**Figure 2.14**). It was selected as a candidate site for comparison with fields more centrally located within the fairway and due to its history of production from the thick Cypress Sandstone. The field was discovered in 1937 and has produced mainly from the Benoist Sandstone (Bell 1939). Since its discovery, it has produced nearly 9.4 million m^3 (59 million BBL) of oil from the Pennsylvanian, Mississippian, Devonian, and Ordovician age strata.

The Centralia Oil Field lies along the northwest trending Centralia Anticline located on the upthrown western flank of the Du Quoin Monocline (Nelson 1995). The anticline exhibits more than 30.5 m (100 ft) of closure on the Barlow limestone and is 13 km (8 mi) long and 5.6 km (3.5 mi) wide (Brownfield 1954). The eastern end of the Centralia Anticline terminates in the Centralia Fault Zone.

The Cypress Sandstone in Centralia Field occurs at an average depth of 362.4 m (1,189 ft) and reaches an average thickness of about 33.5 m (110 ft). An isopach map of the net thickness of the Cypress Sandstone at Centralia Field (**Figure 2.17**) shows the northeast-southwest trend of thick sandstone that crosses the Centralia Anticline at an oblique angle. Cores in this trend of the Cypress Sandstone contain massive sandstones and a mud-clast conglomerate, both of which are features commonly found in an incised channel and fill. This channel within Centralia Field is 2,133 m (7,000 ft) long and 609.6 m (2,000 ft) wide. The thick Cypress Sandstone is not present to the northwest of this trend.

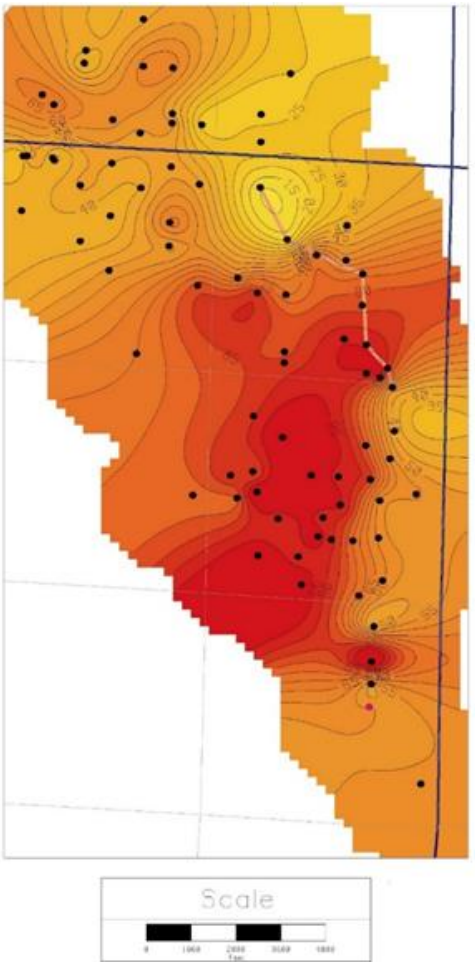

*Figure 2.17. Net isopach map of Cypress Sandstone at Centralia Field (from Cachine 2003). Contour interval is 2 m (5 ft). Line of cross section across the thickest portion of the Cypress Sandstone is shown (**Figure 2.18**).*

The top of the thick Cypress Sandstone occurs approximately 15 m (50 ft) below the base of the Barlow limestone and, often, thin sandstone lenses have developed within the interval. Wireline log correlation in Centralia Field shows that the thick Cypress Sandstone, though thick and blocky, is more broken-up relative to other fields investigated (**Figure 2.18**). The thickest of the individual sandstone intervals is approximately 12 m (40 ft) thick and is observed in Well #00842. The cross-section shows scouring of the underlying shale in the Ridenhower Formation by the thick Cypress Sandstone.

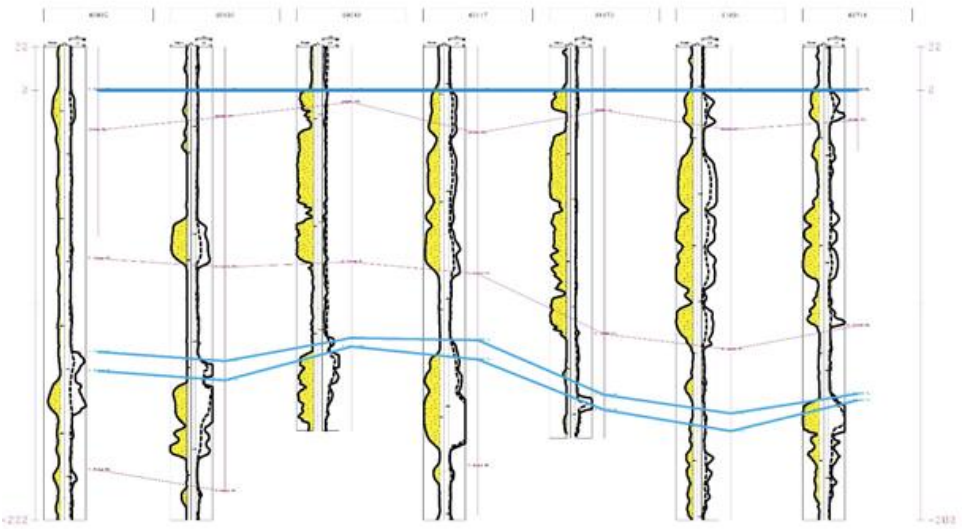

Figure 2.18. Cross section of Cypress Sandstone. The horizontal line in bold separates a smaller unit at the top of the Cypress from the rest of the unit and is used as a datum in this cross section (from Cachine 2003).

The discontinuous nature of the Cypress Sandstone at Centralia Field makes it difficult to determine the thickness or extent of the oil column that may be developed in the top of the thick sandstone. Yet, based on available core analysis data, it is known that one well has a reported average porosity of approximately 20% and an average permeability of about 0.06 um^2 (65 mD).

Overall, data availability for Centralia Field is mixed; adequate, quality physical core data are available, but available geophysical data necessary for mapping and 3D modeling are limited. Following its discovery, Centralia Field underwent rapid development, during which time drilling operations outpaced all other oil fields in the state (Bell 1939). As a result, most of the wells in Centralia Field are old; 94% of all wells were completed prior to 1970. Centralia Field has a long history of production; however, only the southeastern portion of its thick Cypress Sandstone is developed. Due in part to its age and its intense development prior to 1940 (**Figure 2.13**), many of the wells in Centralia Field have not been logged. The Cypress Sandstone reservoirs of Centralia Field were the subject of a characterization study by Cachine (2003), which reports that only about 96 logs in the field penetrate the Cypress Sandstone interval. Cores from the field are available for study but are generally taken from thin sandstone lenses within the upper Cypress Sandstone interval that overlies the thick Cypress Sandstone, although a few penetrate the thick Cypress. The lack of available geophysical data disqualified Centralia field from selection as a study area.

Clay City

Clay City Field is in Northeastern Wayne County. The pool was discovered in 1937 and, due to continuous development along the Clay City Anticline, was quickly incorporated as part of the Clay City Consolidated Field. This area was selected for investigation because of its central location within the thick Cypress Sandstone fairway.

The top of the thick Cypress Sandstone lies at approximately 21 m (70 ft) below the base of the Barlow limestone at a depth of approximately 823 m (2,700 ft). The shaley interval above the thick Cypress Sandstone in places contains two or more lenticular sandstone bodies which are oil-producing.

The thick Cypress Sandstone is present and partially well-developed in Clay City Field. The thickness of the sandstone body varies from 14 m (45 ft) to over 42.7 m (140 ft). In areas where the thick Cypress Sandstone reaches its maximum thickness, its top is roughly 12 m (40 ft) below the base of overlying Barlow limestone. The intervening interval consists of shale and thin, poorly developed sandstones. As the thick Cypress Sandstone thins, the intervening strata between the top of the sandstone and the base of the Barlow limestone increases to approximately 30.5 m (100 ft). The intervening strata contains both shale and more well-developed sandstones which are, individually, as much as 5 m (15 ft) thick. More often, however, these thin sandstones are thinner than 5 m (15 ft) and tend to be stacked (**Figure 2.19**).

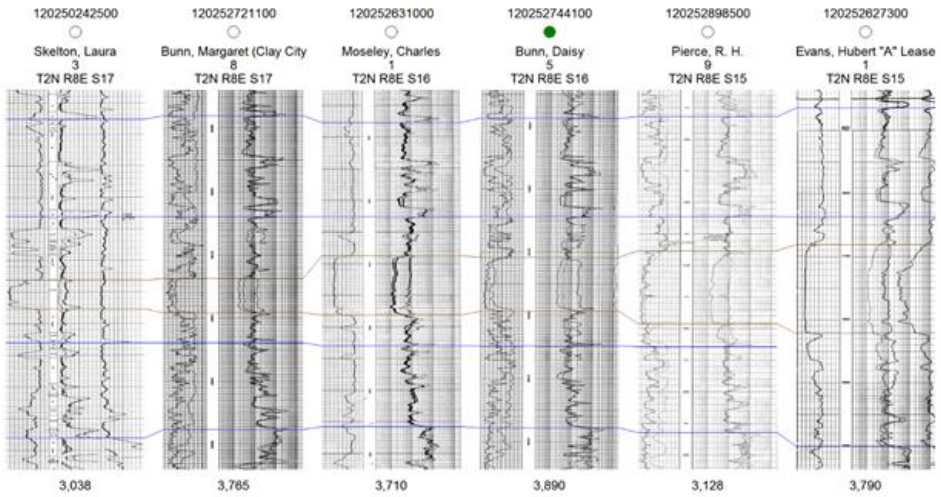

Figure 2.19. East-west Cross section flattened on the base of the Barlow limestone showing the change in thickness of the thick Cypress Sandstone, the characteristic upward thickening of the sandstone, and the relationship between the thick Cypress Sandstone and overlying lenticular Cypress Sandstone bodies. The thick Cypress Sandstone is bounded on the cross section by brown lines.

Clay City Field produces from several horizons, including the Cypress Sandstone. However, both geophysical logs and production records indicate that the thick Cypress Sandstone in this area does not contain an oil reservoir. Wells completed in the Cypress interval are usually perforated in one of the thin, lenticular sandstones overlying the thick Cypress Sandstone. Although the thick Cypress Sandstone in this area is believed to be largely an aquifer, resistivity logs do indicate a slightly upward increase in resistivity, especially where the sandstone thickens and occupies the stratigraphic position generally held by the thinner, lenticular sandstone bodies. In these completed wells, the zones of increased resistivity are at least 9.1 m (30 ft) thick. Petrophysical analysis of resistivity logs may indicate residual oil saturation within zones showing increased resistivity.

The Clay City area, being centrally located in an active oil field, has a wealth of geophysical log data of various vintages available for correlation and mapping purposes. However, the thick Cypress Sandstone in this area is not an oil reservoir, and neither relevant core analysis data nor whole cores are available. It was concluded that the Clay City Field would not be the best candidate for detailed study of the thick Cypress Sandstone.

Dale Field

The Dale Oil Field is in Hamilton County and is the southernmost of the evaluated fields, located about 80 km (50 mi) away from Centralia, Parkersburg, and Noble Fields. This preliminary assessment focused on two portions of what is a very large field: (1) the eastern portion (i.e., Sections 6, 7, and 18 of T6S, R7E) due to records which indicate past production from the Cypress Sandstone; (2) the middle portion of the field (i.e., Sections 7, 8, 9, 12, 17, and 18 of T6S, R6E) due to records indicating the availability of whole cores from the thick Cypress Sandstone.

Udegbunam et al. (1993) describe Dale Field as being situated along a regionally developed, yet unnamed anticline (**Figure 2.20**). The field itself consists of a series of domes which includes, from west to east, the Rural Hill Dome, the Hoodville Dome, and the Dale Dome; the series of domes may be representative the effect of differential compaction over buried Precambrian hills (Nelson 1995). The three domes follow a general west-southwest–east-southeast trend and form independent closures separated by structural saddles.

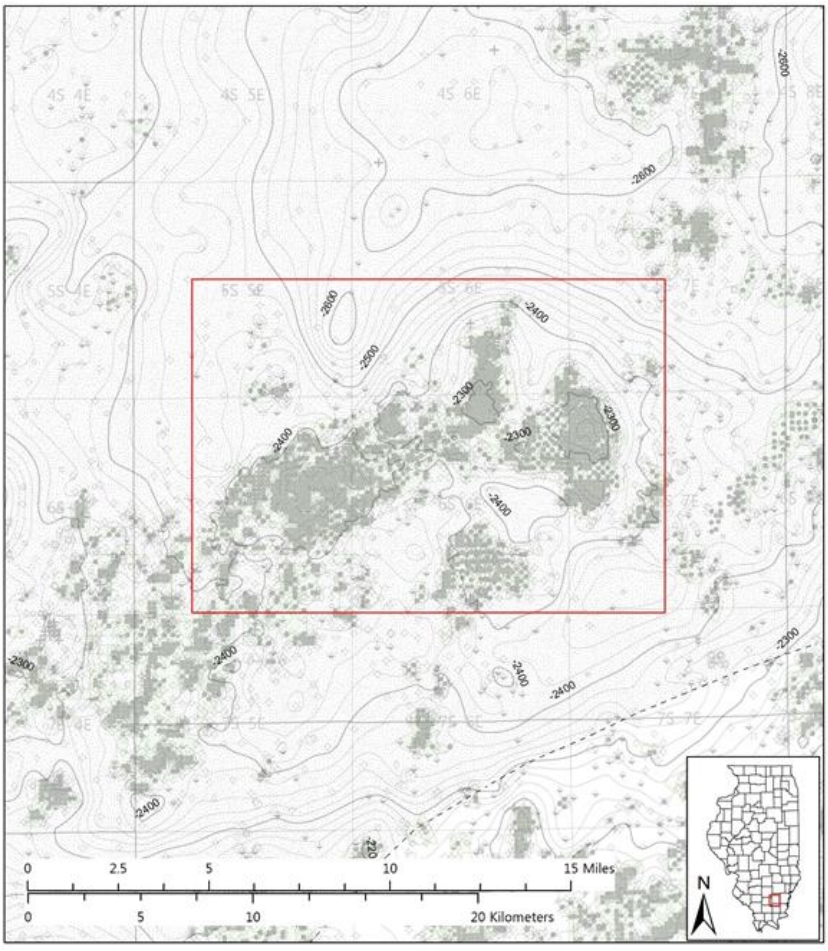

Figure 2.20. Regional structure map showing the location and three separate closures that comprise Dale Field. Dale Field is located in the red box. The base of the Barlow limestone is contoured on a 6.1-m (20-ft) interval with index contours and subsea elevations labeled every 30.5 m (100 ft). Oil field areas are highlighted in green. The eastern boundary of the thick Cypress Sandstone fairway is dashed, and the fairway area is stippled.

Oil production in Dale Field is largely from horizons other than the Cypress Sandstone; production originates primarily from other Chesterian sandstones including the Aux Vases, Bethel, and Tar Springs Sandstones. However, wells within the Cypress Sandstone at the eastern end of the field are, in fact, productive. These productive, completed wells are typically located in the upper Cypress Sandstone bars. Although the thick lower Cypress Sandstone is present in Dale Field, it appears to be entirely saturated with saltwater.

Most of the production from Dale Field originates from the Aux Vases Sandstone. Most of the wells in the field were drilled in the 1940s and 1950s. The eastern portion of the field (the Dale Dome) does, in fact, have wells producing oil from the Cypress Sandstone, but such production emanates from sandstone lenses perched on top of the thick zone. The eastern portion includes discontinuous sandstone bodies separated by shale breaks throughout. The thick Cypress Sandstone in the eastern part of the field comprises between 7.6 and 36.6 m (25 to 120 ft) of the sandstone's total thickness. The oil column is usually around 3 m (10 ft) thick and tends to be concentrated in the lenticular sandstones within the upper part of the thick Cypress Sandstone interval.

In the central portion of the field, the thick Cypress Sandstone is much more consistent, exhibits the characteristic blocky SP log response, and is much more widespread than in the field's eastern portion. The thick Cypress Sandstone has a typical thickness of between 15 and 30.5 m (50 to 100 ft). Geophysical logs indicate 2 m (5 ft) of oil column that is usually mixed with water, where present. The top of the thick Cypress Sandstone occurs in the central portion of the field at a depth of approximately 899.2 m (2,950 ft) and is roughly 9.1 m (30 ft) below the base of the Barlow limestone. The thick Cypress Sandstone is overlain by shale and discontinuous sandstone lenses throughout.

Although the thick Cypress Sandstone centrally located in Dale Field exhibits the characteristic blocky SP log response similarly as other areas of the basin, the thick Cypress Sandstone in Dale Field has a lower absolute resistivity. Core analysis data from two fairly complete thick Cypress Sandstone cores show porosity values averaging 13.5% and permeability values averaging approximately 0.05 um^2 (55 mD). Both the core porosity and permeability values are considerably lower than those values observed in the thick Cypress Sandstone almost anywhere else in the ILB. Moreover, the thick Cypress Sandstone interval is more complex than other areas in which the thick Cypress Sandstone exhibits more variability in thickness and spatial distribution. The reservoir properties of the thick Cypress Sandstone at Dale Field represent an anomaly and is not representative of other thick Cypress Sandstone reservoirs.

Data availability for Dale Field is adequate. Available geophysical logs are abundant, and several whole cores are available for detailed study. Data availability for Dale Field is more than enough to build a geological model, especially for the purposes of constructing a framework for understanding how the thick Cypress Sandstone relates to the more lenticular sandstone bodies. However, the anomalous core porosity and permeability data render Dale Field an outlier that would not be representative of all thick Cypress Sandstone reservoirs generally in a 3D model. Additionally, there is a shortage of relevant production data for Dale Field, as the thick Cypress Sandstone is, generally, not productive. Yet, Dale Field provides interesting contrast with other, more productive areas of the thick Cypress Sandstone, and detailed study of the field may provide insight into which factors control non-productive reservoirs within the thick Cypress Sandstone.

Loudon Field

The Loudon Oil Field is in Northeastern Fayette County, Illinois. Most of the field is located outside of the thick Cypress Sandstone fairway; however, the southern portion of Loudon Field, particularly in the southern half of T7N, R3E, falls within the its western boundary (**Figure 2.14**). Loudon Field is situated on the north-south trending yet sinuous Loudon Anticline (**Figure 2.21**). The anticline occurs nearly one-third of the way up the northwestern flank of the Fairfield Basin and has roughly 50.3 m (165 ft) of closure within the Cypress Sandstone interval (Adams, 1957b). The portion of the field evaluated for this study lies along the southward plunging nose of the anticline.

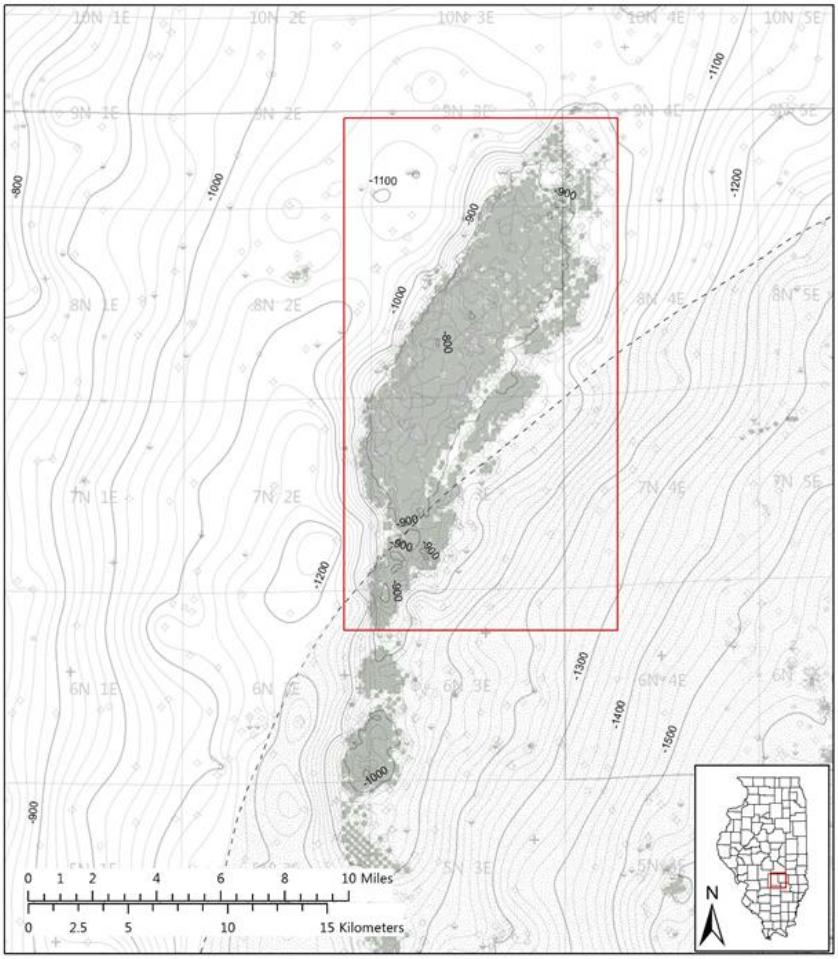

Figure 2.21. Structure map of Loudon Field along the western flank of the Fairfield Basin. Loudon Field is located in the red box. The base of the Barlow limestone is contoured on a 6.1-m (20-ft) interval with index contours and subsea elevations labeled every 30.5 m (100 ft). Oil field areas are highlighted in green. The western boundary of the thick Cypress sandstone fairway is dashed, and the fairway area is stippled.

Loudon Field was discovered in 1937 by Carter Oil. Primary production continued via solution gas drive until 1950, when waterflooding began (Fox 1957). In the 1980s, Exxon Corporation had two polymer pilot floods in the southern part of the field, targeting both the thick Cypress Sandstone and a tidal bar facies in the upper part of the Cypress (Bragg et al. 1982). These pilots were discontinued in the

1990s. In the mid-1990s, Petco Petroleum purchased the field and continued waterflood operations. Most of the Mississippian formations in Loudon Field have produced oil, including the Cypress Sandstone, Paint Creek sandstone, Bethel Sandstone, Aux Vases Sandstone, and the Carper Sandstone (Part of the Borden Siltstone) (**see Figure 1.1**). Originally, the Devonian formations were oil-producing, but are presently used by Kinder-Morgan for natural gas storage.

Although Loudon Field is quite large, only the southeastern part of the field contains thick Cypress Sandstone. The total thickness of the Cypress Sandstone ranges from 15–53.3 m (50–175 ft) and averages 23 m (75 ft) thick (Adams, 1957a). Here, the Cypress Sandstone is the field's most prolific reservoir, most often producing from the crest of the Loudon Anticline (Seyler and Cluff, 1990). The Cypress Sandstone has historically been most productive on the southeastern flank of the anticline, where two thick sandstone bodies which measure over 24 m (80 ft) thick pinch out and form a stratigraphic trap (Cluff and Lasemi, 1980).

Cross-sections of Loudon Field show that the Cypress Sandstone is highly variable and contains between one and three sandstone units which are separated by shale (Cluff and Lasemi, 1980). Adams (1957) divided the Cypress Sandstone at Loudon Field into lower, middle, and upper units. The upper unit comprises the first 9.1–12 m (30–40 ft) of the formation and consists mostly of shale with thin, scattered tidal sand bars measuring up to 1.6 km (1 mi) long. Below these upper bars are "middle" and "lower" sandstones, which appear to be comprised of stacked sandstone bodies and, individually, measure up to approximately 3 m (10 ft) in thickness but can stack to form amalgamated sandstone bodies measuring at least 9.1 m (30 ft) in thickness. The amalgamated sandstone bodies are believed to be stacked tidal bar-type sandstones similar to the upper Cypress Sandstone (Adams, 1957b). Their thickness varies from 0–45.7 m (150 ft) but generally includes the bottom 12 m (40 ft) of the formation. Shale, including laminations and interbeds up to 6.1 m (20 ft) thick, is common within the Cypress Sandstone. Laterally juxtaposed to the middle and lower units are characteristically blocky thick Cypress Sandstone reservoirs. The juxtaposition of these dissimilar facies in an area with the 4-hectare (10-acre) spaced well data density of Loudon Field provides a unique opportunity to understand the original depositional environment of the Cypress Sandstone's varied facies and determine their stratigraphic relationships. In most places, the Cypress Sandstone conformably overlies the Paint Creek Limestone; however, just beyond the southeastern edge of the field, near St. Elmo, incision is apparent where the thick Cypress ("Weiler") Sandstone is present (Adams, 1957a).

In the southeastern part of Loudon Field, an oil column is developed through the entire thickness of the Cypress Sandstone. Whole cores as well as core analysis data are available for this part of the field, as well. Most wells in Loudon Field have geophysical logs dating back to 1938. Available data from three cores indicate that the thick Cypress Sandstone in Loudon Field has an average core porosity value of 20.7% and an average permeability value of 0.133 um^2 (135 mD). Additional core analysis data as well as whole cores are also available for detailed study. Although core data are available, those from development wells tend to emphasize the "best" portions of the field's producing formations, and there are relatively few wells for which porosity logs are available. Yet, the position of Loudon Field along the edge of the thick Cypress Sandstone fairway provides an opportunity to develop a better understanding of the stratigraphic relationship between the thick Cypress Sandstone and the other Cypress Sandstone facies. As such, Louden Field was selected for a focused stratigraphic study.

Noble Field

The Noble Oil Field is in Northwestern Richland County, Illinois, in Sections 32, 33, and 34, T4N, R9E and Sections 3, 4, 5, 7, 8, 9, and 10, T3N, R9E. Today, Noble Field is part of the large Clay City Consolidated Field, a result of the continued development throughout the mid-1900s that caused the boundaries of Noble Field to merge with adjacent oil fields. Since other candidate study areas are also found in the Clay City Consolidated Field, this area will continue to be referred to as Noble Field to avoid confusion. Noble Field was identified as potential candidate study area for due to its central location within the thick Cypress Sandstone fairway (**Figure 2.14**) as well as its recorded history of production originating from the thin oil zone in the top of the thick Cypress Sandstone.

Phillips (1952) and Chapman (1952) both documented three subunits like Lee (1939) in the Clay and Richland County areas. A 6.1–9.1 m (20–30-ft) thick shale separates the base of the Barlow limestone from the thick Cypress Sandstone, which occurs at a depth of about 792.5 m (2,600 ft). Until 1939, oil shows were common in the thick Cypress Sandstone along the Clay City Anticline, but only North Noble Field was producing from the Cypress Sandstone. In some areas of Noble Field, the upper sandstone is not present, and the section is entirely comprised of shale.

Noble Field is located on the northeast-southwest trending Clay City Anticline, a long, sinuous, southward-plunging anticlinal nose that contains many small areas of closure (Nelson, 1995). One of these closures forms the trap that is Noble Field (**Figure 2.22**). Noble Field was discovered in July 1937 by the Pure Oil Company. Initial production in the field originated from the Ste. Genevieve (McClosky) oolitic limestone reservoirs, but oil sands were observed and noted in the “basal Chester” interval, including the Aux Vases and Cypress Sandstones. Most well completions in the thick Cypress Sandstone are open-hole, natural completions. Records indicate that perforations also became common in wells drilled after the 1950s. Initial daily production values from wells producing only from the thick Cypress Sandstone commonly show 15.9–47.7 m^3 (100–300 BBL) of oil with 0–47.7 m^3 (300 BBL) of water.

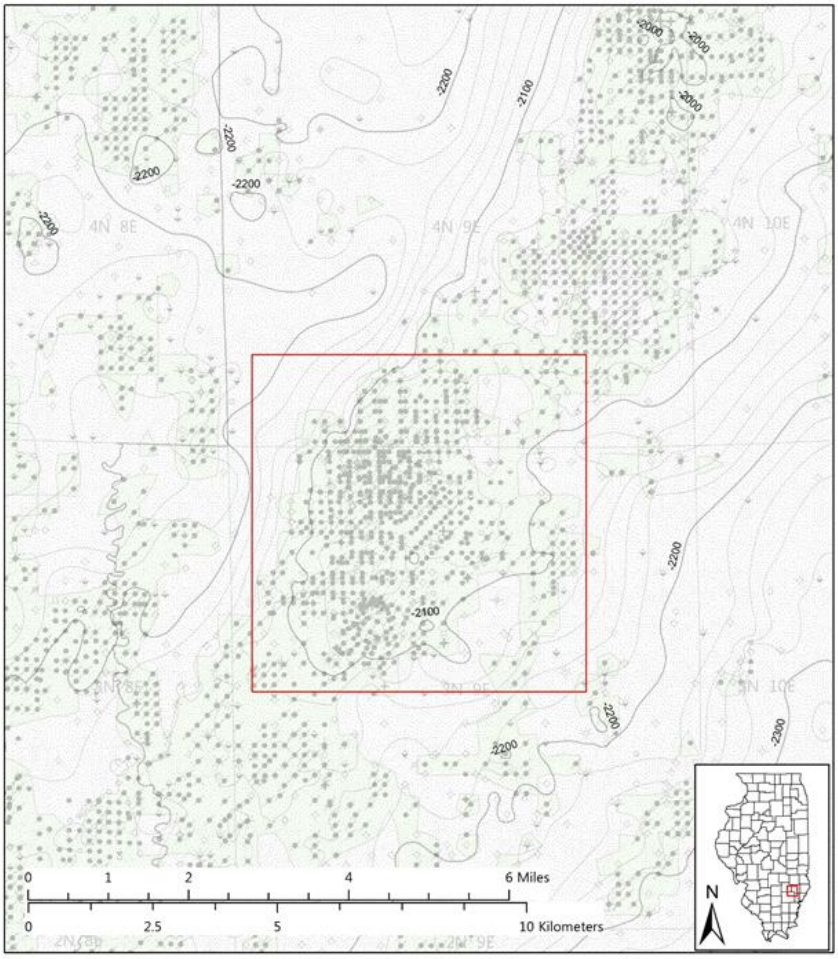

Figure 2.22. Structure map contoured on the base of the Barlow limestone showing the closure along the Clay City Anticline that forms Noble Field. Noble Field is located in the red box. The base of the Barlow limestone is contoured on a 6.1-m (20-ft) interval with index contours and subsea elevations labeled every 30.5 m (100 ft). Oil field areas are highlighted in green. Stippling indicates the entire vicinity of Noble Field is within the thick Cypress Sandstone fairway.

The thick Cypress Sandstone is well-developed in Noble Field, reaching a maximum thickness of more than 53.3 m (175 ft). The thick Cypress Sandstone shows excellent lateral continuity and is correlated with relative ease across the study area (**Figure 2.23**). Within the thick Cypress Sandstone, geophysical logs indicate the presence of thin shale or shaly sandstone beds, usually no more than one or two feet in thickness, which punctuate the thick sandstone (MGSC, 2005). These thin shale breaks are common and occur between 9.1 m and 12 m (30 to 40 ft) from the base of the sandstone. Thin zones of calcite cement also occur within the thick Cypress Sandstone, usually in the upper half of the sandstone body, and often coincide closely with the oil-water contact.

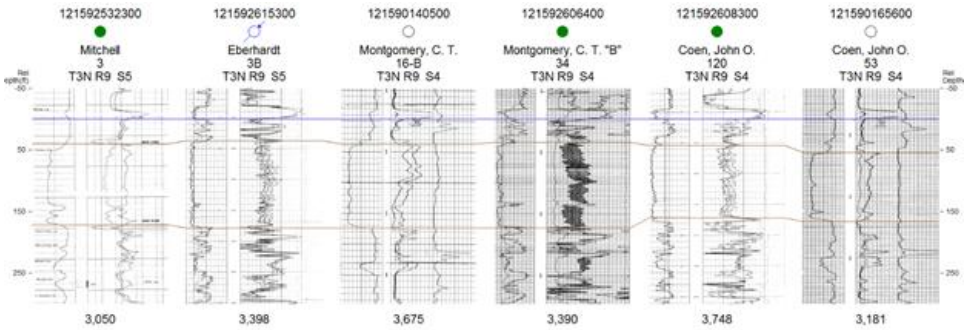

Figure 2.23. East-west cross section across Noble Field that shows the well-developed thick Cypress Sandstone with common shale breaks and calcite cemented zones.

A blocky log character is common for the thick Cypress Sandstone on both SP and gamma ray traces, with well-defined upper and lower boundaries. The most consistent breaks in the thick Cypress Sandstone occur within the upper and/or lower 9.1 m (30 ft) of the unit, as is seen in the example cross-section. In some places, the lower portion of the thick Cypress Sandstone can become separated from the main body by a considerably thick shale bed and the sandstone's log character can change from blocky to thin, individual, or stacked lenses (note the two end logs in the cross-section).

A previous study of North Noble Field, approximately 6 km (4 mi) to the northeast of Noble Field proper, concentrated on the upper portion of the Cypress Sandstone and found two discontinuous stringer sandstones lying within a mixed sand-shale interval at 9.1–12 m (30–40 ft) below the base of the Barlow limestone and above the more continuous thick Cypress Sandstone (MGSC, 2005).

Several cores were collected in and around the Noble Field area. The thick Cypress Sandstone at Noble Field exhibits an average core porosity value of 17% and an average permeability value of 0.433 um^2 (439 mD). The thick Cypress Sandstone at Noble Field is the most permeable of all the candidate areas reviewed, with permeability values that commonly exceeded 0.986 um^2 (1 Darcy). The oil column at Noble Field exhibits varied levels of thickness, ranging from approximately 3 m (10 ft) to over 17 m (55 ft) on the crest of the structure, and thus also has the thickest oil column of all the candidate fields.

Additionally, ample data are available for geologic assessment of Noble Field. The near continuous development of the field since 1937 supplies numerous geophysical logs of varying types and vintages, including many porosity logs for evaluation of the Cypress Sandstone interval. Moreover, whole cores are available for detailed study and abundant core analysis data are available. Overall, data resources for the thick Cypress Sandstone at Noble Field, including production history, indicate that Noble Field is the most appropriate of the candidate fields for an effective field study to research the prospect of nonconventional CO_2 enhanced oil recovery in the thin Cypress Sandstone reservoir and simultaneous CO_2 storage within the underlying thick sandstone.

Parkersburg Field

Parkersburg Field, discovered in 1941, is in Southeastern Richland and Northern Edwards Counties, with most of the field located within T2N, R14W, and T1N, R14W. The field was chosen for evaluation as a candidate study site due to its location along the eastern edge of the thick Cypress Sandstone fairway (**Figure 2.14**) as well as its considerable production history from the Cypress Sandstone. Parkersburg Field is in a structurally complex area along the western flank of the southern

extremity of the LaSalle Anticlinorium, and a short distance north of the Wabash Valley Fault System. A series of north-south oriented domes and anticlines in the vicinity of the candidate study area were originally mapped by Easton (1943). Easton named the largest of these structures the Parkersburg dome, after Parkersburg Field. A structural map of the base of the Barlow limestone shows considerable structural relief in the vicinity of Parkersburg Field (**Figure 2.24**).

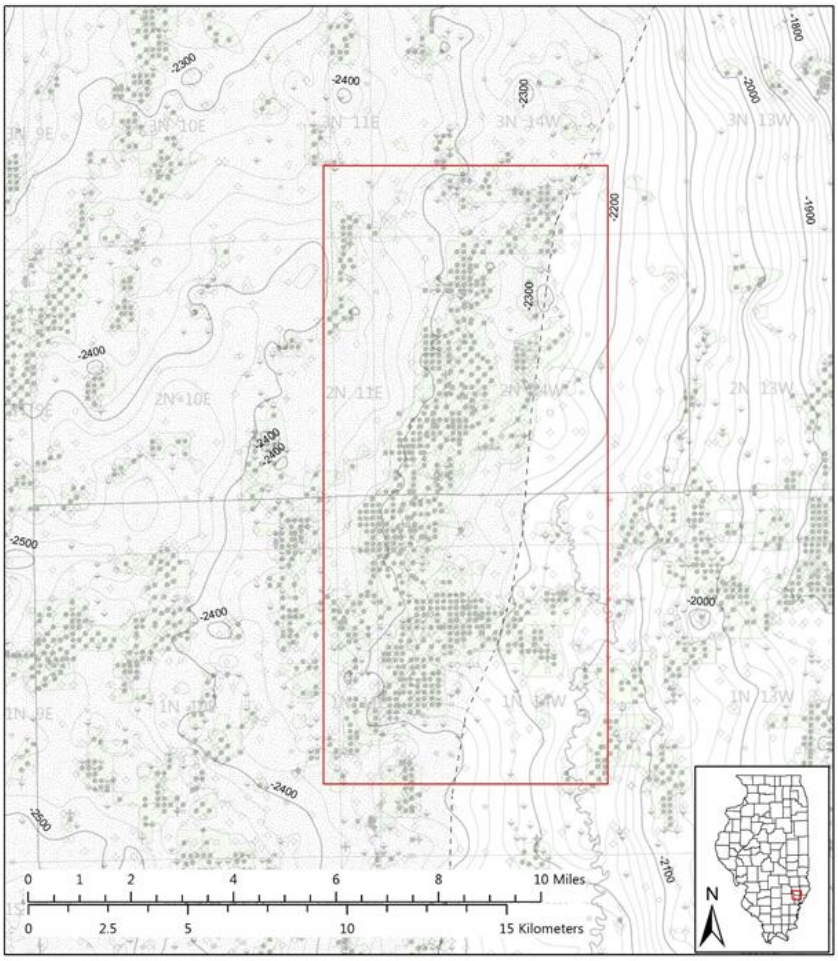

Figure 2.24. Structure map contoured on the base of the Barlow limestone shows the north-south oriented Parkersburg Field situated along the western flank of the La Salle Anticlinorium as it dips westward into the Fairfield Basin. Parkersburg Field is located in the red box. The base of the Barlow limestone is contoured on a 6.1-m (20-ft) interval with index contours and subsea elevations labeled every 30.5 m (100 ft). Oil field areas are highlighted in green.

Most oil production in the field originates from the "McClosky" ooid shoals in the Ste. Genevieve Formation. Most completed wells penetrate through the entire thick Cypress Sandstone interval. Chesterian Sandstones have become an increasingly important secondary oil producing target in the field, with 95,400 m^3 (600,000 BBL) of oil produced from Cypress Sandstone reservoirs in Parkersburg Field since 1943. There were 504 wells drilled in the region before 1990, including 105 whose production emanates from the Cypress Sandstone. While production from the Cypress Sandstone dates back to 1942, much of this production in the field originates from wells that were drilled during the 1970s or

later. Once the McClosky reservoirs were depleted, there was a renewed interest in exploring and developing potential production units in other zones. The success of exploration endeavors in the Cypress Sandstone has been sporadic in Parkersburg Field, as its Cypress Sandstone reservoirs have varying geometries, lithologies, and reservoir qualities and may also be compartmentalized. Recoveries from these Cypress Sandstone reservoirs have, empirically, been lower than those from McClosky oolites, as reservoir volumes and reserves, while substantial, are lesser than in McClosky reservoirs.

The Cypress Sandstone in Parkersburg Field occurs at a depth of approximately 883.9 m (2,900 ft) below the surface. Measured porosity values for Cypress Sandstone reservoirs in the candidate study area range from 12–18%, and measured permeability values range from 0.02–0.197 um^2 (20–200 mD). Yet, none of this data was available for the thick Cypress Sandstone of Parkersburg Field. The thicker Cypress Sandstones which coincide with the more pronounced structural closures are the most productive Chesterian sandstone reservoirs in the candidate study area. After reviewing cross-sections from Parkersburg Field, the Cypress Sandstone was found to be more poorly developed than in other candidate areas.

Although the entire Cypress formation can be greater than 30.5 m (100 ft) thick, some areas are dominated by shale and relatively thin (i.e., less than 6.1 m (20 ft) thick) sandstone bodies occur at various intervals within the formation. In other areas, thick Cypress Sandstone bodies develop with relatively thin (i.e., less than 10 foot) shale intervals which separate sandstones 30 to 50 ft thick. Where these thick sandstones occur, their SP log character is markedly different; instead of exhibiting a distinctly blocky sandstone log character, their SP log exhibits a less blocky log response, which is indicative of stacked sandstone bodies.

Although data availability is sufficient for Parkersburg Field, the lack of a typical thick Cypress Sandstone with a thin oil reservoir in the top makes it an unlikely candidate for further study.

Sailor Springs East Field

Sailor Springs East Field is a small area occupying parts of Sections 27, 28, 33, and 34, T4N, R8E, in Clay County, Illinois. The area was chosen for evaluation based on its proximity to the known production of the thick Cypress Sandstone in Noble Field and the recent attempts to increase oil production from the thin oil zone in the top of the thick Cypress Sandstone by drilling a horizontal well.

The area is in the trough of the Bogota-Rinard Syncline (**Figure 2.25**), and it is one of the few areas reviewed that is not located on a closed structure. This indicates that production may be related to a stratigraphic trap in the thick Cypress Sandstone. Sailor Springs East Field has produced mainly from the thin oil zone in the top of the thick Cypress Sandstone. Most of the wells in the area reach total depth within the top of the thick Cypress Sandstone in order to avoid water coning from the underlying saline aquifer.

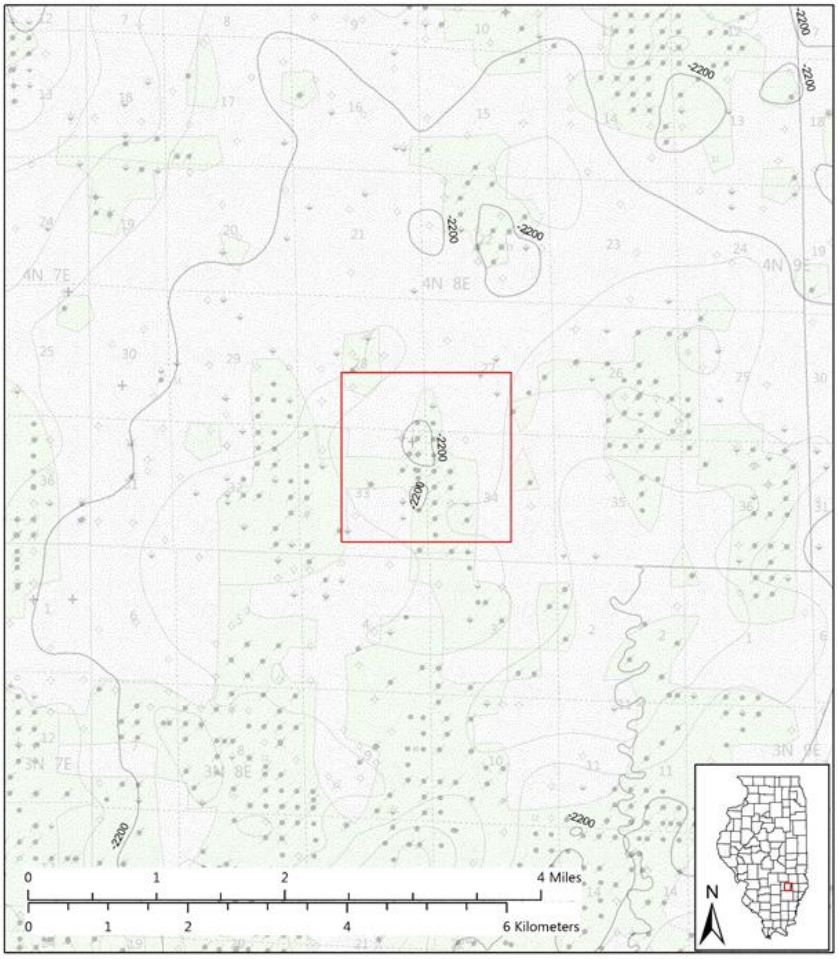

Figure 2.25. Structure map contoured on the base of the Barlow limestone showing the Sailor Springs East Field (inside the red box) located within the relatively broad, flat-bottomed trough at the base of the Bogota-Rinard Syncline. The base of the Barlow limestone is contoured on a 6.1-m (20-ft) interval with index contours and subsea elevations labeled every 30.5 m (100 ft). Oil field areas are highlighted in green.

The top of the thick Cypress sandstone is approximately 15 m (50 ft) below the base of the Barlow limestone. Rare, thin, lenticular sandstone bodies can occur in the intervening space that is otherwise composed of shale. The thick Cypress Sandstone is about 42.7 m (140 ft) thick and occurs at a depth of-approximately 823 m (2,700 ft). The thick Cypress Sandstone is quite blocky on SP logs and, like Noble Field, has few distinct breaks. The oil column within the top of the thick Cypress Sandstone is approximately 4.6 m (15 ft) thick.

Sailor Springs East Field covers only a small area and has relatively few completed wells. Because the Cypress Sandstone was the principal target reservoir and open-hole completions within the top of the sandstone are common, there are very few existing wells or logs which penetrate the entire thickness of the thick Cypress Sandstone. Moreover, there is little available core analysis data, but there may be remnants of a whole core available for detailed study. Two wells for which core analysis data is available have an average porosity value of 16% and an average permeability value of 0.375 um^2 (380 mD). Sailor Springs East Field is being actively drilled and has active production from the thick Cypress Sandstone, its small number of wells and even smaller subset of those which penetrate the thick Cypress

Sandstone both indicate that this area is lacking in the types of available data needed to construct comprehensive geologic maps and 3D models.

Selected Study Areas

Selecting and finalizing an oil field area for study was the first milestone for the project. The selected oil field area was the target for a detailed study of the thick Cypress Sandstone which includes the construction of geologic, geocellular, and reservoir simulation models. The findings from the study area form the framework for the regional and economic assessments of the thick Cypress Sandstone. After reviewing eight candidate oil fields within the thick Cypress Sandstone fairway in the ILB (**Tables 2.1 and 2.2, Figure 2.14**), Noble Field, which is part of the Clay City Consolidated Field in Northwest Richland County, was selected as the oil field study area for this project (**Figure 2.26**).

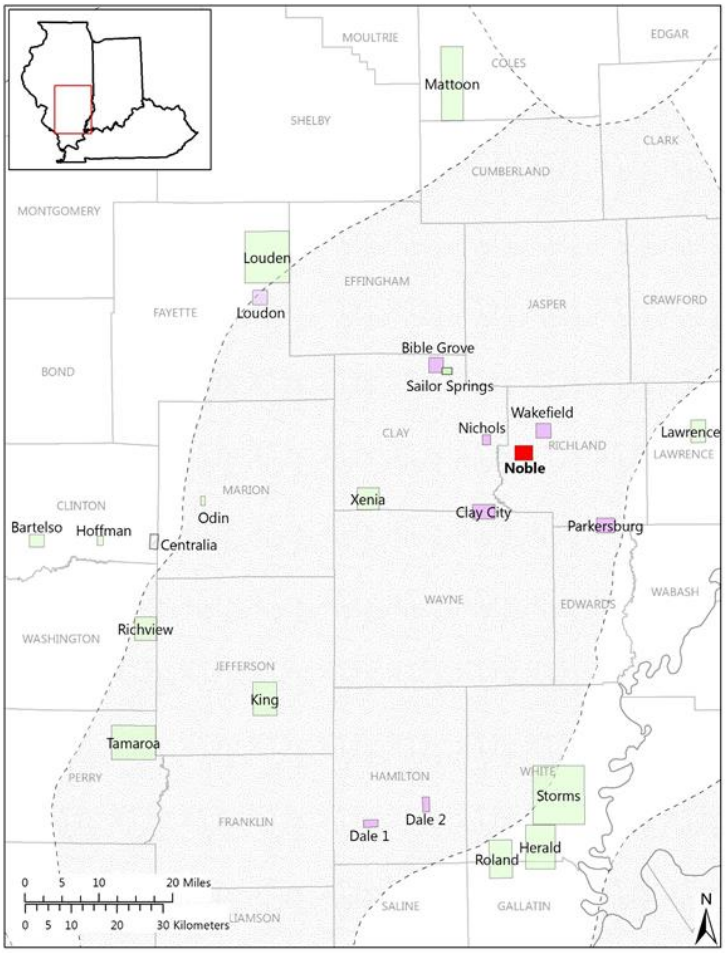

*Figure 2.26. Map showing the eight candidate study areas (in purple; **Table 2.1**) within the fairway of the thick Cypress Sandstone (stippled) in Illinois. The selected study area, Noble Field, is shown in red. Each study area was assessed for available data. Areas where the Cypress Sandstone has been studied in oil fields in the past are shown with green boxes.*

Noble Field has attributes which make it the most favorable area in which to conduct detailed study pursuant to the goals of this project. It lies near the center of the thick Cypress Sandstone fairway

(**Figure 2.14**) and has undergone nearly continuous development since 1937, providing a wealth of geophysical data of various types and vintages. Noble Field has a recorded history of production from the thin oil zone within the top of the thick Cypress Sandstone; some companies established waterflood programs and drilled horizontal wells into this zone since the year 2000. Citation Oil and Gas, currently operating in the field, has two cores within the oil zone in the top of the thick Cypress that were made available for the purposes of this project.

With an oil field selected for detailed study, the project proceeded to create high-resolution geologic maps and develop 3D geocellular models of the thick Cypress Sandstone. The candidate study areas represent a range of geologic characteristics and data availability. Although Noble Field was selected for detailed study in this particular project, the completed evaluation and assessment of the other candidate oil fields, as well as this project's continued effort to compare and contrast their respective thick Cypress Sandstone reservoir characteristics with those of the selected study site, will provide important and informative feedback and guidance for researchers and scientists building geocellular models and reservoir simulations. The variable thickness and character of the thick Cypress Sandstone, the variability of its oil column, and the striking differences in porosity and permeability between the different areas of the ILB raise fundamental questions that must be addressed in order to effectively devise efficient CO_2 EOR and storage development strategies. Attributes from the candidate oil fields may be used to adjust detailed models based on Noble Field to be representative of the thick Cypress Sandstone more generally in other oil fields in the regional study. Further study of these fields, as well as other areas found to exhibit an opportune combination of geology and data availability, helps to provide confidence that the models developed as a result of this project accurately represent the geometry of typical thick Cypress Sandstone reservoirs in the ILB and that the models can be populated with attribute ranges which describe the variations throughout the thick Cypress Sandstone fairway.

3. Geologic Characterization of the Cypress Sandstone

3.1 Data Compilation and Analysis

Prior to beginning the geologic characterization of the thick Cypress Sandstone, ISGS institutional databases were queried to determine the data (e.g., core, geophysical logs, drilling and completion data, and production data) available for development of geologic, geocellular, and reservoir models. Four data types – core, geophysical logs, drilling and completion data, and production data – were compiled for Noble and Kenner West Fields. For Dale and Loudon Fields, core and geophysical logs were compiled. Geologic characterization of the four fields, combined with analysis of more widely available geophysical log, core, and outcrop data, ultimately informed and facilitated regional characterization of the Cypress Sandstone. All correlations and mapping were conducted using IHS Petra and ArcGIS software.

Core

Through a combination of querying the ISGS institutional database, reviewing past publications, and communicating with local oil field operators, over 100 Cypress Sandstone cores from Illinois (over 3,800 linear feet of core) were identified (**Figure 3.1**). Nearly all the cores were given a cursory examination before sub-selecting those that would be used to complete the detailed geologic characterization of the Cypress Sandstone. All whole cores found within the Western Belt were examined and those in strategic locations (such as within the above listed fields) were described in detail. Those cores found outside of the Western Belt of thick Cypress Sandstone were not examined in detail.

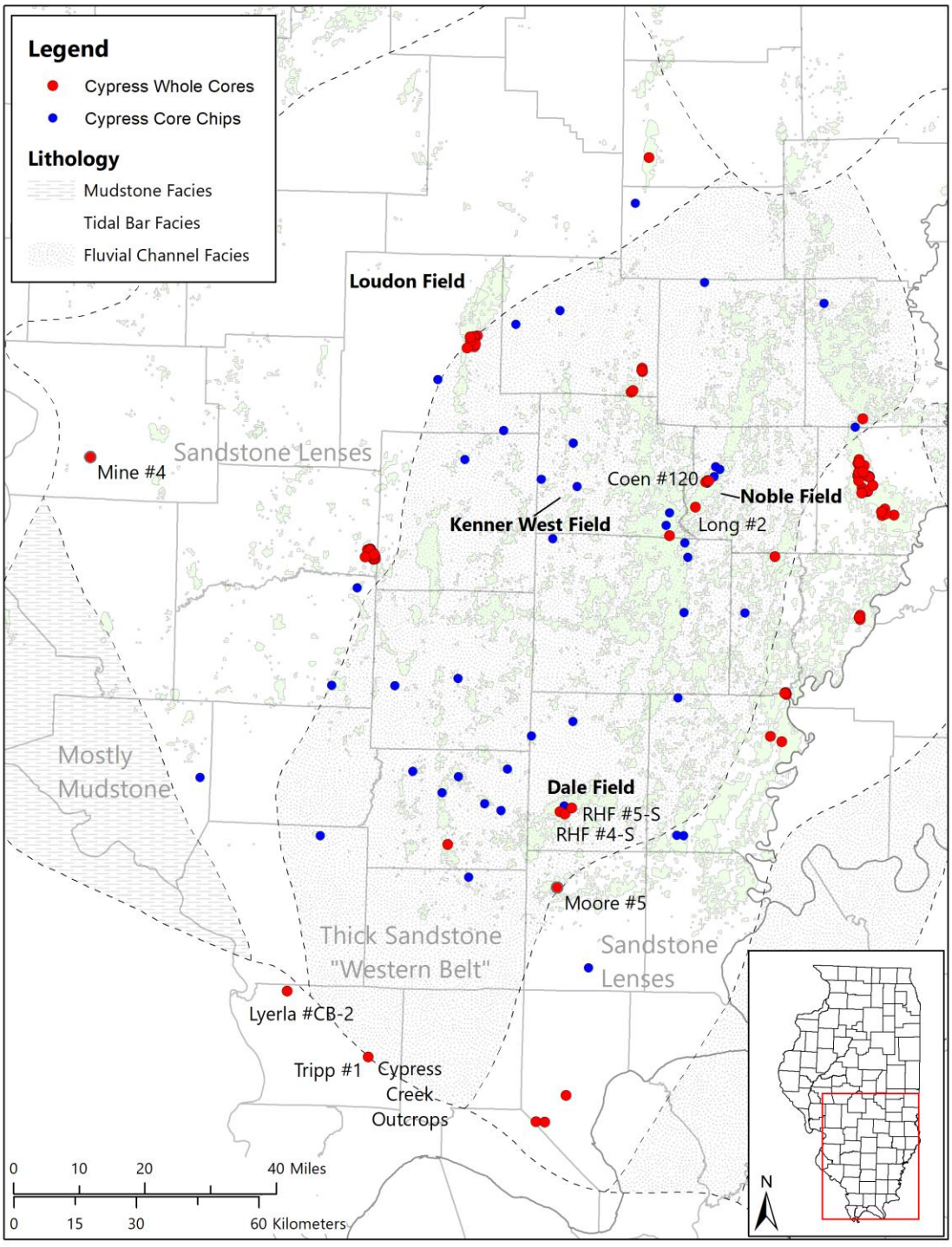

Figure 3.1. Map showing dominant Cypress facies, the location of Cypress Sandstone cores (cores referenced heavily in text are labeled), and the location of the Cypress Creek outcrops in southwestern Illinois. The thick Cypress Sandstone fairway ("Western Belt") is the stippled area. Whole cores are typically 4" diameter cores that were taken through all or a significant portion of the sandstone body present at the well location. Core chips are older, formerly whole core that at one point were subsampled (usually a 1" thick sample per foot) to save space. Core chips were generally less useful for detailed, sedimentological description, but provided samples for routine core analysis and petrographic thin sections, thus improving the spatial distribution of the reservoir dataset.

Collection of New Core

Geologic characterization of the thick Cypress Sandstone is limited by the lack of core data representative of the entire thickness of the sandstone. Existing core coverage within the thick Cypress Sandstone across the ILB is irregularly distributed. Cores were commonly collected from the uppermost part of the formation where conventional oil reservoirs exist. This limits opportunities for a detailed geologic study of the internal architecture of the thick Cypress Sandstone. In addition, the age of most of the oilfields in the Basin means existing geophysical logs are generally e-logs (SP, resistivity). Although plentiful, these logs lack the detail and information that can be gleaned from more modern log suites (such as neutron-density porosity or gamma ray).

To enhance the dataset for studying the thick Cypress Sandstone, two new cores were collected as part of this project to provide a more complete look at sedimentary facies and reservoir properties that can be expected through the entire thickness of the Cypress Sandstone. Data and imagery from the two cores collected for the project were packaged for online core visualization using the accessible PDF portfolio format. The core visualizations portfolios will be available on the Illinois Oil and Gas Online Resources (ILOIL) map and data viewer system (http://maps.isgs.illinois.edu/ILOIL/).

Tripp #1

Drilling the Tripp #1 well (API 121812190900), a shallow well adjacent to thick Cypress outcrops in southern Illinois (**Figure 3.1**), began September 6, 2016 and was completed on September 13, 2016 at a total depth of 79 m (259 ft). The 6.6 cm (2.5 in) diameter whole core is permanently archived in the ISGS samples library (Core Number C-15660). The well location is 2.8 km (1.75 mi) northeast of well-studied roadcuts along I-57 (Cole and Nelson, 1995) and 3.2 to 4.8 km (2 to 3 mi) northwest of extensive outcrops along Cypress Creek (**Figure 3.1**), the type locality of the formation (where the formation was originally named and described) as established by Engelmann (1863). Fieldwork in the fall-winter field season of 2016-2017 focused on these outcrops. The addition of the whole core and geophysical logs to the outcrop study provided needed context for identifying significant features within the formation, including subtle intraformational contacts.

A total of 79 m (259 ft) of whole core was recovered from Tripp #1 well. The upper 7.6 m (25 ft) of the core consisted of surficial deposits that overlaid the bedrock. The first bedrock unit encountered was the Barlow limestone; the base of the Barlow is the upper contact of the Cypress Sandstone and is an important subsurface marker bed that strengthened confidence in the stratigraphic position of the core. One hundred sixty feet of Cypress Formation is present in the core: 18.3 m (60 ft) of upper sandy and shaly deposits and 30 m (100 ft) of thick, continuous sandstone. Twenty-two meters (72 ft) of underlying Ridenhower Shale and Paint Creek Limestone were cored to provide an adequate wellbore depth so that the logging tools could clearly measure the base of the Cypress Sandstone. Logging was conducted by the ISGS (gamma ray, spontaneous potential, resistivity, spectral gamma ray, full waveform sonic, Acoustic Televiewer) and by Weatherford Wireline Services (gamma ray, spontaneous potential, resistivity, neutron density/porosity).

Long #2

Drilling of the Long #2 well (API 121592648800), an oil well in Noble Field, Section 30-T3N-R9E, Richland County, Illinois (**Figure 3.1**), was completed in May 2017. CountryMark Energy Resources was the operator of the well and assisted the project by agreeing to collect core through the Cypress Sandstone as a part of their drilling program. 18.3 m (60 ft) of 10.2 cm (4 in) diameter whole core was collected through the thick Cypress Sandstone and is permanently archived in the ISGS samples library (Core Number C-15661). Logging was conducted by Weatherford Wireline Services (gamma ray, spontaneous potential, resistivity, neutron density/porosity, spectral gamma ray, dipole sonic, and compact micro-imager).

Analogous Pennsylvanian Sandstone Cores

To further enhance the dataset for studying the thick Cypress Sandstone, relatively plentiful core from thick lower Pennsylvanian sandstones was employed as a proxy for the high-porosity end member of the thick Cypress Sandstone and were used in core flood experiments. Lower Pennsylvanian sandstones in the ILB are excellent analogs to the thick Cypress Sandstone from both a depositional environment and reservoir standpoint (Webb et al. 2015; **Table 3.1**). The sandstones are generally thick and may have oil zones developed in their top overlying thick aquifers (**Figure 3.2**). The ISGS possesses a large quantity of core penetrating the Lower Pennsylvanian sandstones in Southeastern Illinois.

Table 3.1. Reservoir properties of the Cypress Sandstone at Noble Field compared with three analogous Pennsylvanian sandstones from Lawrence Field.

Oilfield	*Formation*	*Thickness (m, [ft])*	*Grain size*	*Clay Content (%)*	*Porosity (%)*	*Permeability (um^2, [mD])*
Noble	*Cypress Ss*	*53.3 [175]*	*Very fine to fine*	*<5*	*17*	*0.434 [440]*
Lawrence	*Tradewater ("Robins Sand")*	*45.7 [150]*	*Fine to medium*	*<5*	*19*	*0.311 [315]*
Lawrence	*Caseyville Fm ("Applegate Sand")*	*61 [200]*	*Fine to coarse*	*No data*	*17*	*0.750 [760]*
Lawrence	*Caseyville Fm ("Buchanan Sand")*	*30.5 [100]*	*Fine to coarse*	*No data*	*19*	*0.197 [200]*

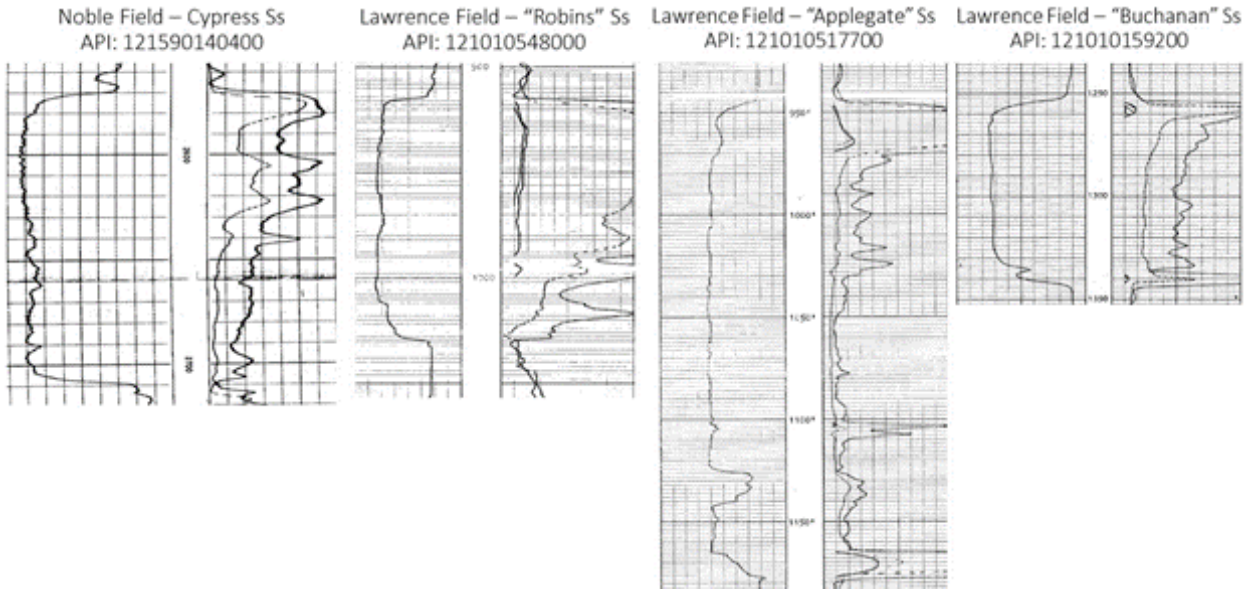

Figure 3.2. Four example logs comparing the thick Cypress Sandstone with analogous Pennsylvanian sandstones. Electric logs with spontaneous potential (SP) and resistivity traces shown (no scales given). Vertical scales are the same. All show thick sandstone bodies with a variable thickness of increased resistivity towards the top, indicating a conventional oil reservoir overlying an aquifer and potential ROZ. Reservoir attributes shown in ***Table 3.1****. Ss, sandstone.*

Geophysical logs

Geophysical logs served two purposes in the project (i.e., correlation for geologic characterization and mapping and well log analysis for fluid saturation determination). All available logs (including old e-logs and modern neutron-density porosity logs) were used for the purposes of correlation and mapping both in the detailed field studies and at the regional scale. In general, modern neutron-density porosity logs were used to conduct well log analysis research to identify and quantify residual oil saturation, though efforts were made in some local areas to use old e-logs for this purpose.

ILB operators are not required to contribute digital well log files (.LAS) to the ISGS database, so logs used in this project had to be digitized so that individual curves could be analyzed. Nearly 1,100 well logs were digitized, and all have been contributed to the ISGS permanent database and are freely available to the public on the ILOIL website.

Drilling and completion data

Drilling and completion data (e.g., drilling permits, completion reports with perforation data, plugging affidavits, drill stem test data, and scout check tickets) provided crucial data for the exploration of ROZs. In the Noble and Kenner West Fields, this data provided key information concerning the complicated production history of individual wells. At the basin-scale, all these data were used to indicate and map the presence of oil saturation within the Cypress Sandstone.

Production data

An accurate oil production history is integral to better understand the historical distribution of production within a field, such as what part of the field was most productive and what formations contributed to that production. An accurate production history is necessary to estimate the current

distribution of oil, water, and pressure within a reservoir, and may also be used to constrain boundary conditions. Reservoir engineers use production data to test simulation results against real-world data. Matching reservoir simulation results with known, past production supports conceptual geologic and geocellular models of interpreted formations, along with the interpretation of the initial oil-water contact. Oilfield data in the form of pipeline reports and operators' records provide a historical perspective on annual production rates on a per lease basis.

3.1.1 Strategy for Undertaking Geologic Characterization

Once data availability had been assessed, detailed geologic and reservoir characterization of the Cypress Sandstone began. This effort required research across multiple scales of investigation:

1. Grain- and facies-scale: The detailed geologic and reservoir characterization began with research on the **Sedimentology of the Cypress Sandstone** (Section 3.2). This entailed studying available core and outcrops to develop a robust facies scheme that could be applied at the field- and basin-scales to interpret the depositional environment and diagenetic history of the rock. Depositional environment and diagenetic history are both factors which control rock fabric and reservoir quality. A better understanding of these controls and how they affect the rock in three dimensions can facilitate better development strategies, including vertical and horizontal well placement and completion strategies, and CO_2 injection with greater sweep efficiencies, and higher CO_2 storage efficiency.
2. Field-scale: Concurrently with the research on the sedimentology of the Cypress Sandstone was targeted **Characterization of Noble, Kenner West, and Loudon Fields** (Section 3.3). This targeted characterization was necessary to determine the geometry of the reservoir bodies, the internal architecture of facies, and the volumetric assessment of the container for the MPZ and the potential ROZ and CO_2 storage resource. The field-scale study resulted in the development of static geologic conceptual models, dynamic flow simulation models, and recommendations for ROZ development strategies within the Cypress Sandstone, primarily for Noble Field.
3. Basin-scale: Lessons learned from the grain-, facies-, and field-scale studies of the Cypress Sandstone were integrated into a broader **Regional Characterization of the Cypress Sandstone** (Section 3.4) which established the overall geologic framework of the Cypress Sandstone and provided a basis for identification and **Characterization of Cypress Sandstone ROZs** (Section 4) and ultimately contributed to the volumetric estimates used in the **CO_2-EOR and Storage Regional Resource Assessment** (Section 6).

3.2 Sedimentology of the Cypress Sandstone

3.2.1 Introduction

Background on the geologic setting, stratigraphy, and oil reservoirs of the Cypress Sandstone is provided in Section 2 and will not be recapitulated here. Motivation for a more detailed sedimentological investigation of the thick sandstones specifically is given in Section 3.1.1. As such, the following efforts were made to analyze the sedimentology and architecture of thick sandstones in the Chesterian (Late Mississippian) Cypress Formation of the ILB, USA, which are herein interpreted to be deposits of a large, fine-grained river with low grain size variance. This research assesses the implications of the sedimentology for reservoir heterogeneity, as relevant to CO_2-EOR and storage. The questions addressed are:

1. What is the depositional environment of the thick sandstone bodies within the Cypress Formation?
2. How is reservoir heterogeneity manifested in sandy, fine-grained fluvial deposits and variations in permeability that control fluid flow?

Much remains unresolved concerning the depositional controls on reservoir architecture and heterogeneity of fine-grained rivers. Identification of grain size shifts, internal stratification, and erosional discontinuities, each occurring at different scales, can be cryptic in fine-grained sandstone bodies with low grain size variance. For example, erosive story bases, which may correspond to subtle grain size or facies shifts, can have a significant impact on reservoir anisotropy by forming discrete flow units (e.g., Ebanks et al. 1992). Identification of stacking patterns and grain size trends in fluvial deposits is important, because grain size and sorting exert strong controls on reservoir porosity and permeability (Selley 2000). Although grain size variance is relatively low in fine-grained fluvial reservoirs, the coarsest grained and highest energy lithofacies typically exhibit greater absolute porosity and permeability than finer-grained, lower energy lithofacies (e.g., Chapin et al. 2014). Therefore, understanding the three-dimensional distribution of porosity and permeability in reservoirs is necessary for constructing and conditioning representative reservoir models that form the basis for well-completion and field-development strategies (Ebanks 1987).

3.2.2 Methods

To assess the sedimentology of the thick Cypress Sandstone, an effort was made to use all available data types (described in Section 3.1). An outcrop study and a new "behind the outcrop" core (Tripp #1) were integrated with findings from subsurface studies in the basin interior of new (Long #2) and existing core to better understand the Cypress Formation throughout Southern Illinois, with specific emphasis on the Western Belt of thick Cypress Sandstone (**Figure 3.1**).

Dataset

Data available for study of the Cypress Formation include outcrop, core, and an abundance of various types of geophysical logs. Thousands of oil wells have been drilled through the Cypress Formation in Southern Illinois, with most having geophysical logs and few having core.

Cores

The cores studied are all held at the ISGS's geological samples library in Champaign, Illinois. Many cores of the Cypress Formation exist from Southern Illinois (**Figure 3.1**) and vary greatly in quality. However, most of the core only capture a small fraction of the Cypress Formation, with only a small percentage (~27%; 29 cores) containing long sections (>15.2 m (50 ft)) of the formation. Seventy cores (**Figure 3.1**) along with outcrops of Cypress Creek were inspected to devise a sedimentary facies scheme, seven of which were logged and described in detail. The cores studied in detail were preferentially selected based on the following criteria:

- inclusion of thick sandstone facies
- percentage of entire formation represented (high percentage preferred)
- length of section through Cypress Formation
- completeness (minimal core loss preferred) and quality (minimal disintegration preferred)
- new cores or previously unstudied old cores
- location (an effort was made to construct an even spatial distribution of cores)

In certain cases, like in Lawrence County where multiple Cypress cores exist in close proximity (**Figure 3.1**), at least one core was logged and chosen as a representative section of the area. When prioritizing cores for description and logging, at least one core from within each of Nelson's (2002) "facies" regions (**Figure 3.1**) was examined. Cores available within the Western Belt were prioritized, logged, and decribed first. New cores previously unstudied include: Mine #4 (API 121190035100), Lyerla #CB-2 (API 121812094100), Tripp #1 (API 121812190900), Moore #5 (API 121652585700), RHF #2-S (API 120650135600), RHF #5-S (API 120650139200), and Coen #120 (121592608300) (**Figure 3.1**).

Outcrops

Although many outcrops of the Cypress Formation exist, they are commonly isolated and do not expose the entire formation, with the thick sandstones being preferentially preserved. Despite weathering, the outcrops provide valuable information about lateral and vertical facies variability and architecture that cannot be obtained from core or geophysical log data in the subsurface of the basin interior. To assess facies, environments of deposition, lateral variability, and the associated reservoir properties of Western Belt thick Cypress Sandstones, outcrops of the understudied Cypress type section at Cypress Creek, Union County, IL, were examined (**Figure 3.3**). The entire Cypress Creek area was examined to determine the quality of exposures. The "outcrops of special note" in Cypress Creek, found on the Mt. Pleasant Quadrangle bedrock geology map (**Figure 3.3**; Nelson & Devera, 2007), were all visited along with other areas not noted by Nelson & Devera.

At Cypress Creek, photos were taken, bed thicknesses were measured using a metric tape measure, and cross-bed orientations and foreset dip angles were measured with a Brunton Geo™ Pocket Transit compass (declination of -2 °). Additionally, samples from selected exposures in Cypress Creek were collected for grain size analysis; samples were collected above and below large-scale erosional boundaries.

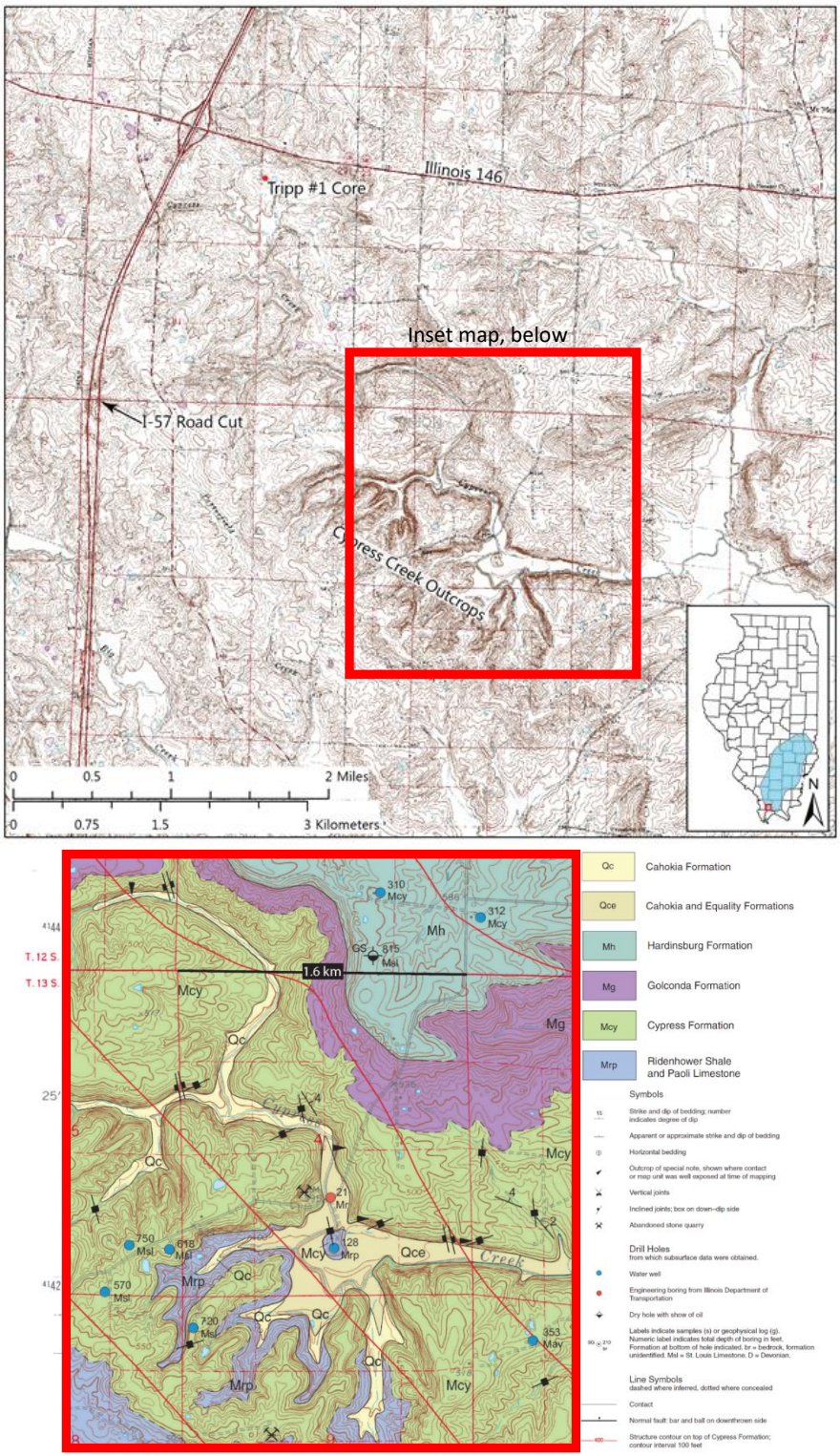

Figure 3.3. ***(A)*** *Topographic map showing the location of the Tripp #1 (API 121812190900) well and its proximity to the Cypress Creek outcrops and the I-57 road cut. Inset map shows location of area of investigation 1 (red box) in relation to Illinois and the Western Belt (highlighted blue).* ***(B)*** *Geologic map of the Cypress Creek area modified from Nelson & Devera (2007).*

Geophysical Logs

Geophysical logs – mostly pre-1970s e-logs – are the most abundant data available for study of the Cypress Formation. Interpretations and correlations herein rely upon these logs, which most commonly include spontaneous potential (SP), gamma ray (GR), and resistivity (RES) tracks. Other newer geophysical logs, such as density (RHO), density porosity (DPHI), neutron porosity (NPHI), spectral gamma ray (THOR, URAN, and POTA), and acoustic televiewer (ATV), were available in certain places and in some instances provided supplementary information.

Given context provided by outcrops, geophysical logs provided a basis for understanding the three-dimensional variability of the Cypress Formation. Where available, cores were used to calibrate and ground-truth the geophysical log data. In Dale Consolidated Oil Field (hereafter referred to as Dale Field), Hamilton County, IL (**Figure 3.1**), an oilfield-scale case study was conducted. Dale Field was used because it is a large oil field (~675 km^2; 255 mi^2) with a high well density, known thick Cypress production, and has three whole core that penetrate almost the entire thickness of the thick Cypress Sandstone (**Figure 3.1**). 874 wells were used in Dale Field for mapping, although many more exist in the field.

Dale Field is located near the south-eastern margin of the Western Belt (**Figure 3.1**) and within the Fairfield Basin, the central, deepest portion of the Illinois Basin. The limited Cypress production that has come from these domes, mainly the Dale Dome in the eastern end of Dale Field, has been from a relatively thin (6.1-18.3m; 20-60 ft), discontinuous sandstone reservoir overlying a thick (18.3-36.6m; 60-120 ft), laterally extensive sandstone. On the crest of Dale Dome where oil saturation occurs in the thin upper sandstone reservoir, low to fair oil saturation is noted on well logs in the top of the underlying thick Cypress Sandstone. Continuous core penetrating through high resistivity zones at the top of the thick Cypress Sandstone at the Rural Hill Dome show no visible oil saturation and corroborate the general lack of production from the thick Cypress Sandstone at Dale Field.

Techniques

Facies Analysis

Seventy cores and several outcrops of Cypress Creek were inspected to establish complementary sedimentary and geophysical facies schemes. Outcrops at Cypress Creek allowed examination of the spatial and vertical process variability associated with thick Cypress reservoir sandstone facies. Sedimentary facies were grouped into facies associations, which were then calibrated to geophysical data (primarily SP and RES logs) at Dale Field to create a geophysical facies scheme.

Subsurface Mapping

PETRA software was used in conjunction with geophysical log data (primarily SP, GR, and RES) to correlate between wells and generate isopach maps within PETRA's correlation module. In some instances, RHO, DPHI, and NPHI logs were available and provided supplementary information which aided in correlations and lithologic interpretations. ArcGIS and PETRA were used to make net and gross isopach maps.

Stratigraphic correlation and mapping within Dale Field was based on a lithostratigraphic approach due to the absence of log-detectable marker horizons within the Cypress Formation. However, in Dale Field, lithostratigraphic surfaces are herein believed to roughly represent chronostratigraphic surfaces (*sensu* sequence boundaries and flooding surfaces) due to their regional lateral extent.

Grain Size, Porosity, and Permeability

Grain size in the Cypress Formation ranges from very fine- to fine-grained and, less commonly, medium-grained sand (Potter 1962; Swann 1964), although the mean grain diameter is unknown. Consequently, subtle grain size variations within the Cypress Formation may be overlooked when using a grain size card and hand lens. To reduce the risk of human error in grain size assessment, the Tripp #1 (API 121812190900) core was assessed quantitatively in thin section. Each thin section was viewed at the same magnification alongside a 200 μm scale bar. Grains were visually compared to the scale bar to estimate mean grain size in μm.

Outcrop samples were also collected for grain size analysis and made into thick sections (>30 μm). Outcrop thick section photomicrographs were then visually compared to estimate grain size and compare grain size differences above and below erosional contacts. These calibrations from grain size shifts identified in thin section and under high magnification microscope served to guide and enhance grain size determination of thick Cypress Sandstone using a grain size card and hand lens in the cores studied herein.

Eighteen additional thin sections were analyzed to quantitatively determine the mean grain diameter (D_{50}) of thick Cypress Sandstones. Individual grains (~300 to 500) within these thin sections were measured to produce mean, maximum, and minimum grain diameter values.

Porosity and permeability were measured using a Vinci™ POROPERM steady state gas porosimeter and permeameter. Core plugs used for measurements were 2.5 cm (1 in) in diameter.

3.2.3 Lithofacies

Overall, the thick Cypress Sandstone is dominated by sandy lithofacies. Six lithofacies descriptions and interpretations were derived from both outcrops and cores (see **Table 3.2**), with a thin, basin-wide pedogenically-altered lithofacies (**Table 3.2**; Lithofacies P) immediately overlying the thick sandstones in the Western Belt and in the upper half of the Cypress Formation outside of the Western Belt. A complete lithofacies scheme, including the non-reservoir muddy and silty lithofacies of the Cypress Formation, can be found in the Supplemental Materials section of Howell (2017).

The mean grain size, D_{50}, of the thick Cypress Sandstone is ~132 μm, which restricts the character of potential bedforms to the far left of the bedform phase stability diagram (**Figure 3.5**). However, as all grain measurements included quartz overgrowths (typically ~10-20 μm thick), which are prevalent throughout the Cypress Sandstone (Pitman et al. 1998), this measured D_{50} represents a slight overestimation, and mean original D_{50} may be *c.* 120 μm.

Table 3.2. Sandy lithofacies and pedogenically altered lithofacies of thick Western Belt sandstones.

Code	Lithology	Description	Depositional Process Interpretation
S_M	Sandstone, Massive	Whitish-tan structureless arenite to sublitharenite, may contain faint contorted bedding, small (<1 cm long) tabular shale intra-clasts, calcite cement	Fluvial upper flow regime traction sedimentation under high suspended load concentration
S_D	Sandstone, Deformed	Whitish-tan arenite to sublitharenite with contorted laminae or bedding, may contain small (<1 cm long) tabular shale intra-clasts, calcite cement	Post or syndepositional soft sediment deformation in fluvial environment
S_R	Sandstone, Ripple-bedded	Whitish-tan asymmetric ripple-bedded arenite to sublitharenite, may contain small (<1 cm long) tabular shale intra-clasts, calcite cement	Fluvial lower flow regime traction sedimentation
S_P	Sandstone, Planar-bedded	Whitish-tan planar-bedded arenite to sublitharenite, may contain small (<1 cm long) tabular shale intra-clasts, shaley-carbonaceous laminae, shale-carbonaceous debris, calcite cement	Fluvial upper-stage plane beds produced from unidirectional traction sedimentation under high suspended load concentration
S_C	Sandstone, Cross-bedded	Simple unidirectional cross-beds (~0.3 m) and short foreset length (<2 m), low angle foresets (<15 º) common, often superimposed on low-angle bar-scale lateral accretion surfaces	High aspect ratio fluvial dunes produced from unidirectional traction sedimentation under high suspended load concentration
S_{LA}	Sandstone, Lateral Accretions	Low-angle (<10 º) and long wavelength (10s of meters) lateral accretion surfaces often with lithofaces S_{C1} superimposed	Master surfaces of longitudinal fluvial bars
C	Conglomerate	Conglomerate displaying a wide range of clast lithologies, commonly matrix supported and may be calcite cemented, commonly fine-grained matric, may contain clay intraclasts, clay laminae, carbonaceous debris, rounded siderite or septarian pebbles, crinoids, brachiopods, gastropods, and bryozoans	Fluvial channel lag produced from high energy unidirectional traction sedimentation
P	Pedogenic Alteration	Commonly variegated (varying red, green, yellow, grey) or gleyed lithologies, may contain carbonate nodules, siderite, pyrite, carbonaceous material, root traces, slickensides, and peds	Pedogenesis post deposition

Massive Sandstone (SM): Description

Lithofacies S_M is a whitish-grey, very fine- to fine-grained (D = 150 μm), well-sorted arenite to sublitharenite that is structureless, contains relatively low volumes (<3%) of detrital clay (**Figure 3.4A**) and often grades to planar-bedding or cross-bedding. Furthermore, this lithofacies may contain calcite cement and small (<10 mm long; <0.39 in) tabular shale intraformational clasts.

Massive Sandstone (S_M): Interpretation

Lithofacies S_M was deposited in a fluvial subaqueous environment by unidirectional traction currents under high suspended load concentrations. Lithofacies S_M is considered to contain bedding, although its extremely low detrital clay volumes and nearly unimodal grain size have rendered the bedding undetectable by visual inspection.

Deformed Bedding (S_D): Description

Lithofacies S_D is a very fine- to fine-grained sandstone ($D = 147\ \mu m$) consisting of deformed bedding (**Figure 3.4B**), that is typically closely associated with a range of sandy facies (most commonly lithofacies S_C, S_P, S_R, and S_M). In outcrops along Cypress Creek, core behind these outcrops (Tripp #1, API 121812190900; see **Figure 3.1** for location), and Dale Field cores, this lithofacies is consistently present in the upper portions of thick sandstones (**Figure 3.4B4, 3.4B5**).

Deformed Bedding (S_D): Interpretation

Lithofacies S_D is interpreted as representing post- or syn-depositional soft sediment deformation from dewatering/fluidization in a fluvial environment (cf. Sambrook Smith et al. 2016). Like dewatering/fluidization structures of the fine-grained Bermejo River (Sambrook Smith et al. 2016), these structures exist in the upper portions of the thick sandstones.

Ripple-bedded Sandstone (S_R): Description

This lithofacies comprises arenite to sublitharenite consisting of whitish-tan, very fine-grained (D = 99 µm) sands that are well-sorted, displaying small-scale asymmetrical cross-stratification (<20 mm thick sets; <0.78 in) with relatively high (3-7%) detrital clay volumes (**Figure 3.4C**), which increase in frequency vertically within thick sandstones. Tabular foresets are most common in lithofacies S_R (**Figure 3.4C2, 3.4C3**), but sporadic trough cross-stratification was observed in some outcrops and cores (**Figure 3.4C1**). Both tabular and trough cross-stratification within lithofacies S_R may be poorly developed. Oil staining, iron-oxide mottles (**Figure 3.4C3**), calcite cement, and very small (<10 mm long; <0.39 in) tabular shale intra-clasts may also be present.

Ripple-bedded Sandstone (S_R): Interpretation

Lithofacies S_R formed in a subaqueous environment within the lower flow-regime where traction transport dominated and is interpreted to represent the depositional product of two-dimensional fluvial current ripples that formed under unidirectional flows. A poorly developed lithofacies S_R that exhibits trough cross-stratification (**Figure 3.4C1**) records the presence of three-dimensional, unidirectional current ripples.

Figure 3.4. A) Lithofacies SM. Left to right: (A1) 930.9 m (3054 ft) RHF #2-S (API 120650139400); (A2) possible distorted bedding, 471.8 m (1548 ft), Heckert #902 (API 120512572400); (A3) 460.9 m (1512 ft), Heckert #902. B) Lithofacies D. Left to right: (B1) 903.1 m (2963 ft), RHF #5-S (API 120650139200); (B2) 902.8 m (2962 ft), RHF #2-S (API 120650139400); (B3) 32.6 m (107 ft), Tripp #1; (B4) 469.4 m (1540 ft), Heckert #902; (B5) Domal structure from north Cypress Creek, (B6) Large-scale fluid escape structure from north Cypress Creek. C) Lithofacies SR. Left to right: (C1) 865.9 m (2841 ft), RHF #4-S (API 120650135600); (C2) poorly developed asymmetric ripples 29.6 m (97 ft), Tripp #1; (C3) oil stained and iron oxide, 881.5 m (2892 ft), Coen #120 (API 121592608300); D) Lithofacies SP. Left to right: (D1) 901.0 m (2956 ft), RHF #5-S; (D2) 901.9 m (2959 ft), RHF #2-S, (D3) low angle, 470.3 m (1543 ft), Heckert #902. E) Lithofacies SC. Left to right: (E1) non-oil stained 881.2 m (2891 ft), RHF #5-S, (E2) shale rip-up clasts on foresets 42.1 m(138 ft), Tripp #1, (E3) oil-stained 790.7 m (2594 ft), Montgomery #B-34 (API 121592606400); F) Lithofacies C. Left to right: (F1) shale rip-up clast and rounded septarian nodule lag from within thick Western Belt Sandstone 922.3 m (3026 ft), RHF #2-S, (F2) calcareous fossiliferous lag from within thick Western Belt Sandstone 891.5 m (2925 ft), RHF #5-S, (F3) shale rip-up clast lag at the base of thick Western Belt sandstone 56.7 m (186 ft), Tripp #1.

Climbing ripples, like those commonly observed in the suspended-load dominated Río Bermejo (Sambrook Smith et al. 2016), were not observed in the thick Cypress Sandstone. Climbing ripples of the Río Bermejo were attributed to flashy discharge produced by rapidly waning flow at the end of frequent flood stages (Sambrook Smith et al. 2016). Allen (1970) has shown that climbing ripples occur only in non-uniform and/or unsteady flows, such as those of the Río Bermejo. Based on this evidence, unidirectional flows depositing lithofacies S_R likely had a less flashy discharge than the Río Bermejo. (Allen 1970; Bristow 1993).

Planar-bedded Sandstone (S_P): Description

Lithofacies S_P is a whitish-tan to brown, very fine to fine-grained (D = 135 μm), well-sorted, planar bedded arenite to sublitharenite with relatively low (<3%) detrital clay volumes (**Figure 3.4D**). Oil staining, shaley-carbonaceous laminations, carbonaceous material, and small (<30 mm long; <1.18 in) tabular shale intra-clasts are also found sporadically. True planar bedding in this facies is rare in outcrop but common in core. Furthermore, in outcrop, planar bedding is transitional, laterally over short distances (<10 m; <32.8 ft), to lithofacies S_C or S_{LA}.

Planar-bedded Sandstone (S_P): Interpretation

Lithofacies S_P is interpreted as being deposited in a subaqueous fluvial environment where unidirectional traction currents persisted. Considering the small characteristic grain diameter of lithofacies S_P (**Table 3.3**), all planar bedding within the thick Cypress Sandstones and rest of the Cypress Formation is interpreted to represent upper-stage plane beds deposited within the upper flow regime (**Figure 3.5**) and produced by the migration of extremely low-amplitude, asymmetrical bed waves upon a near-flat surface (c.f. McBride et al. 1975; Paola et al. 1989; Best & Bridge 1992; Bridge & Best 1997).

Table 3.3. Average grain diameter measurements and associated lithofacies from three relatively complete cores (Tripp #1 [API 121812190900], RHF #2-S [API 120650139400], and Coen #120 [API 121592608300]) through thick Cypress Sandstone in the Western Belt.

Tripp #1			**RHF #2-S**			**Coen #120**		
Depth (m)	*Lithofacies*	*D*	*Depth (m)*	*Lithofacies*	*D*	*Depth (m)*	*Lithofacies*	*D*
27.5	S_R	134	902.3	S_P	71	787.5	S_R	81
34	S_D	138	907.9	S_P	165	789.3	S_R	107
41.5	S_P	160	914.3	S_C	147	790.8	S_R	74
46	S_C	188	921.1	S_C	176	792	S_C	112
49.5	S_D	155	923.5	S_P	142	793.8	S_C	169
54.7	S_C	98	929	S_R	100	795.7	S_C	159

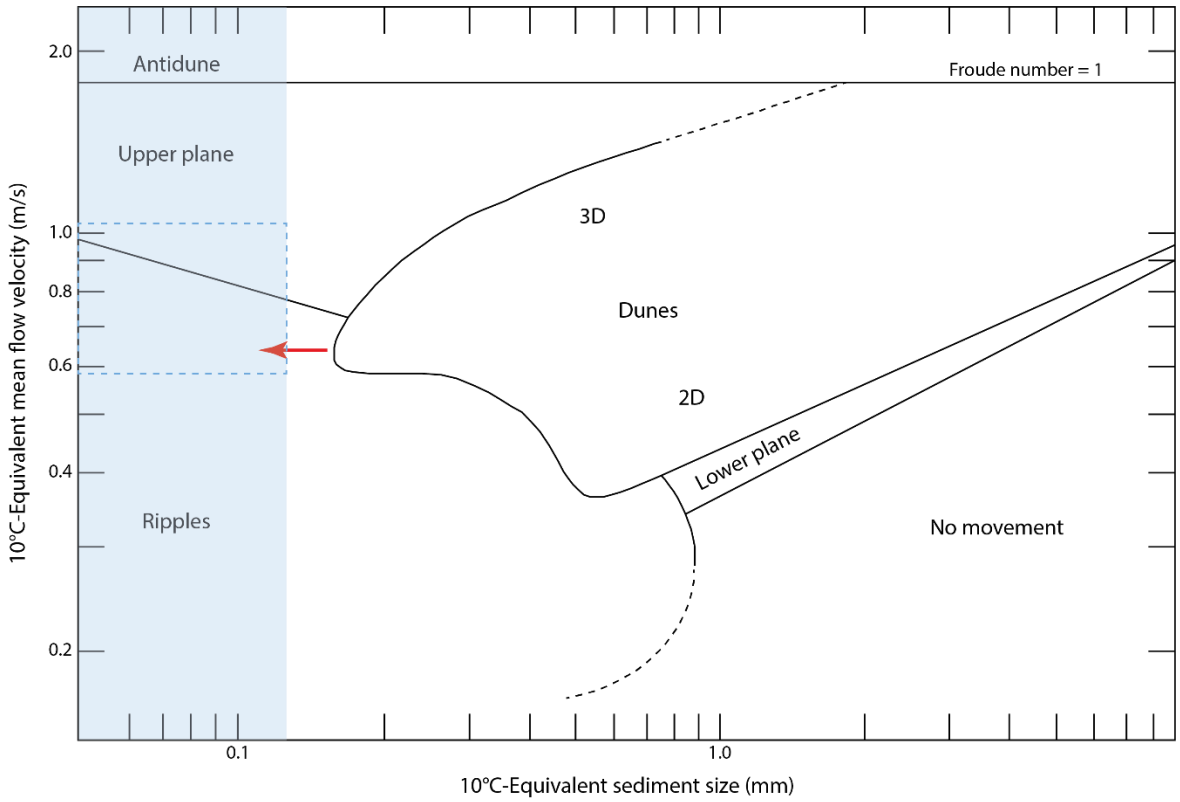

Figure 3.5. Bedform stability diagram highlighting the 'window' (shaded blue) in which unidirectional bedforms of the Cypress Sandstone existed. The upper grain size limit of the blue shaded region is defined by D50 (132 µm) of the coarsest grain sandstones in the Cypress Sandstone, which are manifested as two thick sandstone trends, the Western Belt and the West Baden Trend. Thus, all true planar bedding (lithofacies SP) within the Cypress Sandstone represents upper-stage plane beds since the characteristic grain diameter is less than 200 µm. Simple cross-beds (lithofacies SC1) and low amplitude-long wavelength cross-beds (lithofacies SC2) within the Western Belt fall within the dashed blue box, a 'zone' in which the bedform stability diagram lacks data. The dune stability field likely expands further leftward (red arrow) into this 'zone'. Modified from Figure 5.74 D in Bridge and Demicco (2008).

Cross-Bedded Sandstone (S_C): Description

This lithofacies is a whitish-tan to brown, very fine to fine-grained (D = 150 μm), well-sorted, cross-bedded arenite to sublitharenite sandstone with relatively low (<3%) detrital clay volumes (**Figure 3.4E, Fig. 3.6**). Lithofacies S_C exists on a mesoform scale (i.e., <2 m long; <6.56 ft) and possesses relatively small cross-sets that are approximately 0.27 m (8.85 ft) thick (**Figure 3.5**, scenario 1), with coupled foreset lengths of <1 m (<3.28 ft). The thickest cross-sets are on average 0.8 m (2.62 ft) but are rare (**Figure 3.5**). Low-angle foresets (<15º; see also Cole and Nelson 1995) consistently dip west-southwestward (**Figure 3.6**) and may be overturned. Their morphology is often convex-up or sigmoidal with tangential toesets (**Figure 3.6**), whereas bounding surfaces are most commonly two-dimensional planar to wedge-planar (**Figure 3.6**) but can also be three-dimensional. Lastly, this lithofacies is often superimposed on master surfaces (i.e., large-scale lateral accretion surfaces) of lithofacies S_{LA} (**Figure 3.6B, C, D**), but when superimposed, cross-sets are restricted in size to <0.2 m (0.65 ft) (see **Figure 3.5**, scenario 2).

Cross-Bedded Sandstone (S_C): Interpretation

Lithofacies S_C was deposited by unidirectional traction currents and represents the product of low-angle, two- or three- dimensional fluvial dunes. The average foreset dip-direction is to the southwest (**Figure 3.6**) and supports the interpretation of southwestward-oriented currents through the northeast-southwest-oriented Western Belt of thick Cypress Sandstone (**Figure 3.1**). The absence of marine fossils, herringbone cross-strata, periodic reactivation surfaces, thick clay drapes (>1 mm (>0.03 in) thick), and tidal 'bundles' preclude a tidal origin for lithofacies S_C.

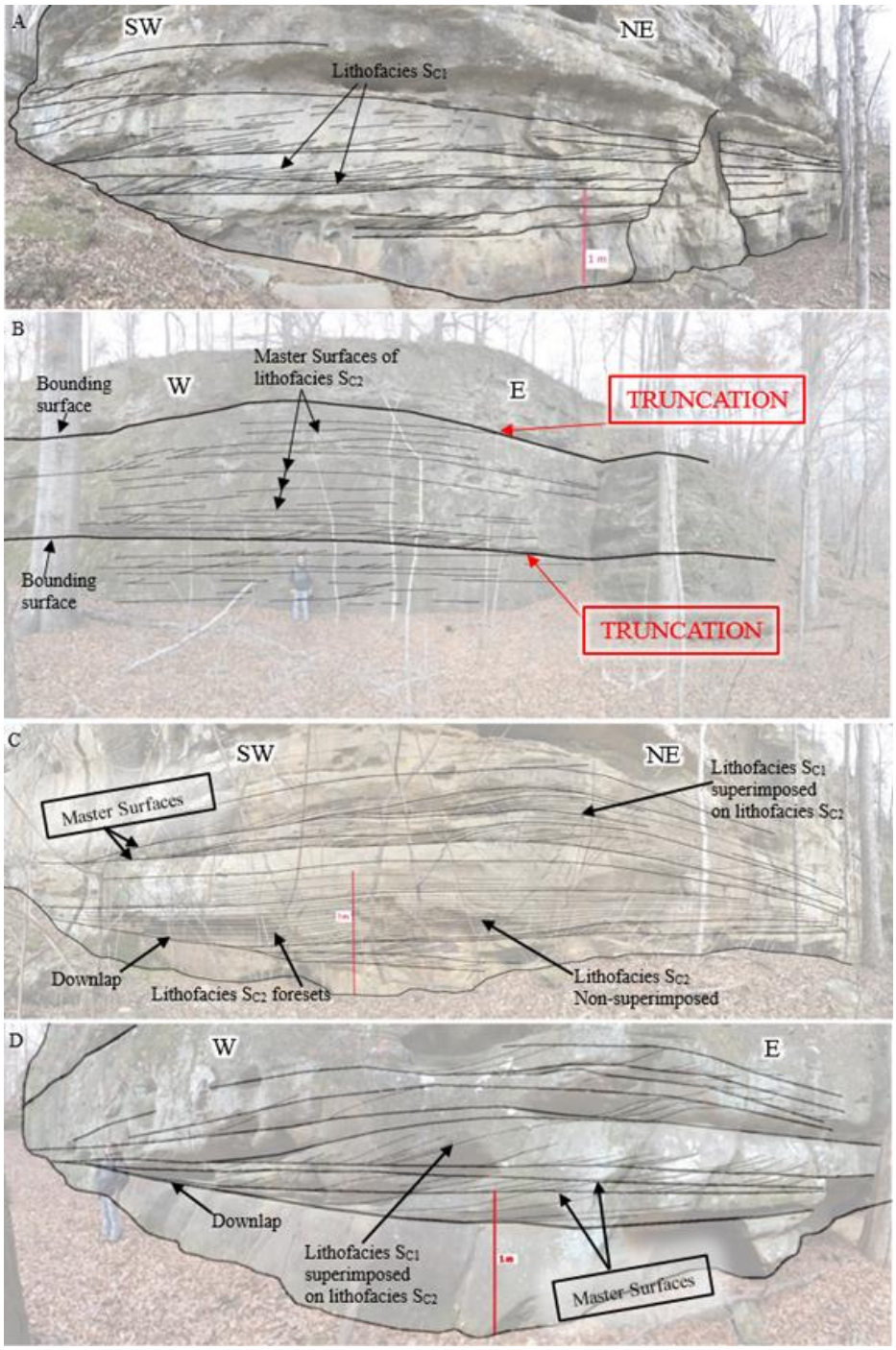

Figure 3.6. Cypress Creek outcrop showing A) stratigraphic context and morphologies of lithofacies SC1. B) relationship between lithofacies SC1 and SC2. Lithofacies SC1 is superimposed on lithofacies SC2, where bounding surfaces of lithofacies SC1 (i.e., master surfaces of lithofacies SC2) dip gently (<10°) west southwestward. Bounding surfaces of lithofacies SC1 (i.e., master surfaces of lithofacies SC2) are here seen to truncate at larger scale bounding surfaces on the macroform scale (i.e., roughly the scale of a bar). C) stratigraphic context of lithofacies SC2. Non-superimposed lithofacies SC2 in the bottom half of the image where bounding surfaces and foresets of lithofacies SC2 downlap to the southwest. In the upper half of the image, lithofacies SC1 becomes compounded on lithofacies SC2. D) lithofacies SC1 compounded on lithofacies SC2, with master surfaces of lithofacies SC2 downlapping to the west.

When examining ancient fine-grained fluvial cross-beds, Turner (1981), Røe (1987), Cotter & Graham (1991), Røe & Hermansen (1993), and Hjellbak (1997) considered the abundance of low-angle foresets, sigmoidal foresets, convex-up foresets, and asymptotic toesets to be the products of high suspended-load to bedload transport ratios. Experimental and ancient studies show that the morphology of these cross-sets is characteristic of flows in the transition from dune to upper-stage plane-bed (Saunderson & Lockett 1983; Røe 1987; Bridge & Best 1988; Røe & Hermansen 1993). In modern alluvial channels, low-angle dunes (leeside <15º) dominate many sand-bed rivers (Best & Kostaschuk 2002), and experimental work further suggests that these low angles are attributable to high suspended- to bedload sand-transport ratios (Yalin 1964, 1972; Kostaschuk and Villard 1996; McLean et al. 1999; Kostaschuk 2000, 2005; Kostaschuk et al. 2008; Naqshband et al. 2014; Hendershot et al. 2016; Bradley and Venditti 2017; Naqshband et al. 2017). Furthermore, as the ratio of suspended load transport to bedload transport increases, the toesets of unidirectional dunes become increasingly asymptotic (Allen 1963; Jopling 1965). Likewise, the small-scale cross-sets of lithofacies S_c, displaying low-angle, sigmoidal and convex-up foresets, in combination with asymptotic toesets, are herein suggested to be the products of fluvial currents with a high suspended-load to bedload transport ratio.

Sandstone with Lateral Accretion Surfaces (S_{LA}): Description

Lithofacies S_{LA} is characterized by low-angle (<10º) bar-scale lateral accretion surfaces (i.e., master surfaces) that extend downflow for 10s of meters (**Figure 3.6B, C, D**). The master surfaces of lithofacies S_{LA} consistently dip west southwestward, in same direction as lithofacies S_C (**Figure 3.6**). This lithofacies is regularly punctuated by outcrop-scale bounding surfaces, where master surfaces downlap onto lower bounding surfaces, and/or toplap onto upper bounding surfaces (**Figure 3.6B, D**). This results in ~5-7 stacked units ~3-4 m (~10-13 ft) thick.

Sandstone with Lateral Accretion Surfaces (S_{LA}): Interpretation

This lithofacies was deposited by unidirectional traction currents and represents the depositional products of large, fluvial sand bars. Master surfaces of lithofacies S_{LA} are typically superimposed with lithofacies S_C (**Figure 3.6B, C, D**), which are interpreted to represent decimeter-scale simple dunes migrating down the lee-side longitudinal bars. The scale of lithofacies S_{LA} units is too large (3-4 m (9.84-13.12 ft) thick) to represent individual compound dunes, such as those recently documented by Galeazzi et al. (2018) and Almeida et al. (2016). In some instances, lithofacies S_{LA} exhibits large-scale reactivation surfaces. These reactivation surfaces are likely the result of flow unsteadiness as flow strength increases (c.f. Best et al. 2003; Reesink & Bridge 2011).

Alternatively, where lithofacies S_C is not superimposed on lithofacies S_{LA} (**Figure 3.6C**), lithofacies S_{LA} may represent the product of large, low-angle, 'washed-out' bedforms (c.f. Simons & Richardson 1966; Saunderson & Lockett 1983; Bridge & Best 1988), transitioning towards upper-stage plane bed (**Figure 3.5**). Since bedforms are washed-out at lower values of stream power than coarser-grained bedforms (Simons & Richardson 1966), many large bedforms within the Cypress fluvial system are potentially washed-out. For example, in the suspended-load dominated, fine-grained Yellow River, China, most surfaces are low-amplitude with long-wavelengths (i.e., washed-out), and thus the bed is nearly flat (Ma et al. 2017).

In summary, both lithofacies S_{C1} and S_{LA} are restricted to a narrow 'window' on the bedform phase stability diagram (**Figure 3.5**) due to their small mean grain size. **Figure 3.5** shows that the dune

stability field pinches out around 150 μm, although dune-forms are known to exist in rivers with mean grain sizes less than this (e.g., Bermejo River, Argentina (Sambrook Smith et al. 2016); Yellow River, China; (Ma et al., 2017)). Thus, the dune stability field likely continues, albeit within a narrower range of bed shear stresses, further to the left on the phase diagram, and into the dashed blue box shown in **Figure 3.5**. Lithofacies S_C and S_{LA} fall within this dashed blue box and are herein considered the depositional products of: i) a fluvial flow regime at lower bed shear stresses than upper-stage plane beds, but higher than asymmetrical current ripples, and ii) high-suspended sediment to bedload transport ratios.

Conglomerate (C): Description

This lithofacies is commonly sharp-based, conglomeratic, and poorly sorted, being dominantly matrix supported with a wide range of clast lithologies and sizes. In many cases, lithofacies C is not truly conglomeratic but contains abundant clay rip-up clasts embedded within a fine-grained sandy matrix (**Figure 3.4F1, F3**). The matrix is typically a fine-grained sublitharenite that may be calcite cemented (**Figure 3.4F2**) that, when present, is associated with fossils (fragmented and abraded crinoids, brachiopods, gastropods, and fenestrate bryozoans) and a spike in the resistivity well log. Lithofacies C commonly contains tabular clay intra-clasts (1-60 mm (0.03-2.36 in)) thick; **Figure 3.4F3**), carbonaceous debris (1-80 mm (0.03-3.14 in) long), rounded carbonate and siderite pebbles that may be septarian (<40 mm (<1.57 in) diameter) (**Figure 3.4F1**). In general, the clasts are not uniformly oriented, but may be imbricated along foresets of lithofacies S_C.

Conglomerate (C): Interpretation

Lithofacies C is interpreted to represent channel lag deposits produced by high energy, unidirectional traction currents. Where marine fossils are present, they are commonly heavily abraded and/or disarticulated and are interpreted to be entrained via erosion of fossiliferous sandstone lenses sometimes found at the base of Cypress Formation (see Smith 1996) or the underlying marine limestone or shale.

Pedogenic Alteration (P): Description

This lithofacies consists of variegated (varying from red to green to yellow to grey) or drab muddy and silty lithofacies (**Figure 3.7**). Lithofacies P exists as a relatively thin (~1-3 m (3.28-9.84 ft)), continuous horizon immediately overlying the thick Cypress Sandstone within the Western Belt and sandstone lenses at the base of the Cypress Formation just outside the Western Belt (**Figure 3.7**). Although less common, lithofacies P may also be developed in sandy lithofacies. When lithofacies P is red or variegated with high-chroma colors, it is commonly developed in muddy and silty lithofacies and in close association with carbonate nodules (**Figure 3.7G**), root traces, and slickensides (**Figure 3.7A**), or peds (**Figure 3.7F**). When lithofacies P is drab, it is commonly developed in muddy and silty lithofacies but in close association with low-chroma colors, abundant carbonaceous material, root traces, siderite, and pyrite. When lithofacies P exists in sandy lithofacies, iron-oxide staining, pyrite, siderite, and/or root traces are most common.

Pedogenic Alteration (P): Interpretation

This lithofacies represents the thin, basin-wide paleosol, or coaly horizon, consistently noted in the upper half of the Cypress Formation in past work (Workman 1940; Swann & Atherton 1948; Chapman 1953; Potter 1962; Swann 1963; Willman et al. 1975; Cole & Nelson 1995; Grube & Frankie 1999; Nelson et al. 2002). Lithofacies P is interpreted as a paleosol horizon, the product of pedogenic

alteration within a floodplain environment during subaerial exposure. When calcite nodules and red coloration are present within muddy and silty lithofacies, lithofacies P represents a calcic vertisol developed in a well-drained, wet-dry environment with seasonal precipitation (c.f. Driese & Ober 2005; Kahmann & Driese 2008). Alternatively, when calcite nodules or red coloration are absent, but a combination of drab, low-chroma colors (Fe reduction), rootlets, abundant carbonaceous material, siderite, or pyrite are present, lithofacies P is interpreted as a gleysol that developed in a poorly drained, water-logged, high water table environment (**Figure 3.7A, C**; c.f. Driese & Ober, 2005; Kahmann & Driese, 2008).

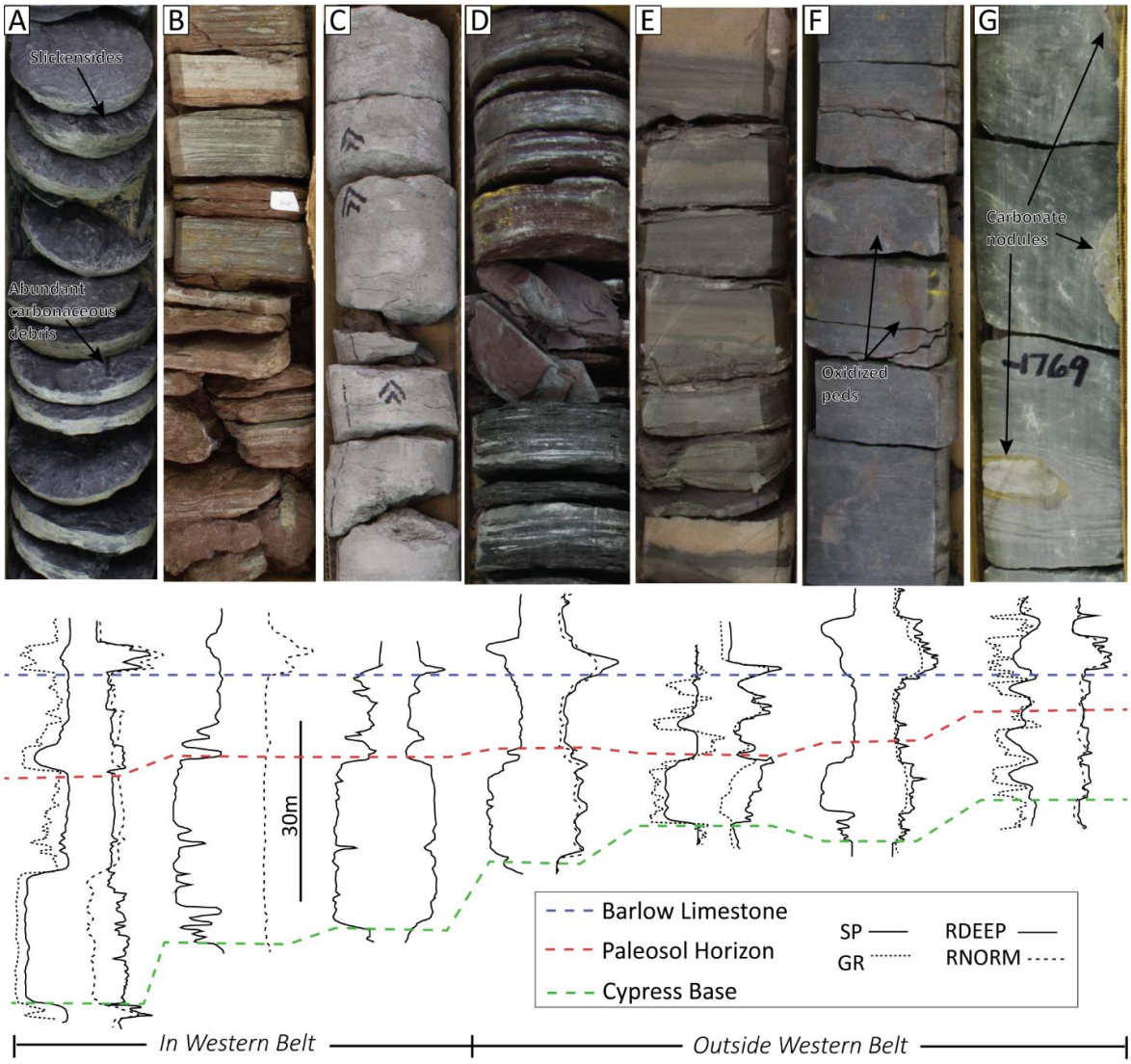

Figure 3.7. Lithofacies P immediately overlying thick Cypress Sandstones within the Western Belt and in the upper half of the formation outside of the Western Belt; A) 805.3m, Long #2 (API 121592648800); B) 373.1 m, CFU #209W (API 120270161200); C) 358.7 m, Tripp #1 (API 121812190900); D) 416 m, Baltzell #MI-2C (API 121012783200); E) 787.6 m, Moore #5 (API 121652585700); F) 460.6 m, King #KM-1 (API 121010717300); G) 539.2 m, Seaman #15 (API 120292361900).

3.2.4 Fluvial Facies Association

Major erosional discontinuities are present within thick sandstones in Cypress Creek outcrops (**Figure 3.8**) and cores (**Figure 3.9**). These discontinuities are marked by abrupt, but consistent, changes above the erosional contact including: (1) a slight (~50-100 µm) increase in mean grain size (**Figure 3.8, 3.9**), (2) a poorly developed lag (lithofacies C) (**Figure 3.9**), (3) a change to lithofacies M, Sc, S_P, S_{LA}, or C (**Figure 3.8, 3.9**), (4) a decrease in detrital clay concentration (**Figure 3.10**), and (5) an increase in permeability (**Figure 3.10**). The association of these characteristics suggests that these erosional surfaces are channel bases. These characteristics further suggest that deposits immediately overlying these erosional surfaces are consistently high energy and most likely represent thalweg deposits.

In cores, the sandstones fine upwards subtly, increase in detrital clay concentration from each erosional discontinuity, and are transitional vertically from lithofacies S_C to lithofacies S_D, and then to lithofacies S_R (**Figure 3.9**). The upper portion of a typical succession is present below the major discontinuity shown in the Long #2 (API 121592648800) core (**Figure 3.9C)**. The Tripp #1 (API 121812190900) core (**Figure 3.9B**), collected 3.5 km from the Cypress Creek outcrop shown in **Figure 3.8**, is topped by a gleyed carbonaceous lithofacies P (see **Figure 3.7C** for close-up) with faint underlying subvertical root traces. Lithofacies P was also observed immediately overlying thick sandstones in the Cypress Creek area by Kehlenbach (1969) and Cole & Nelson (1995).

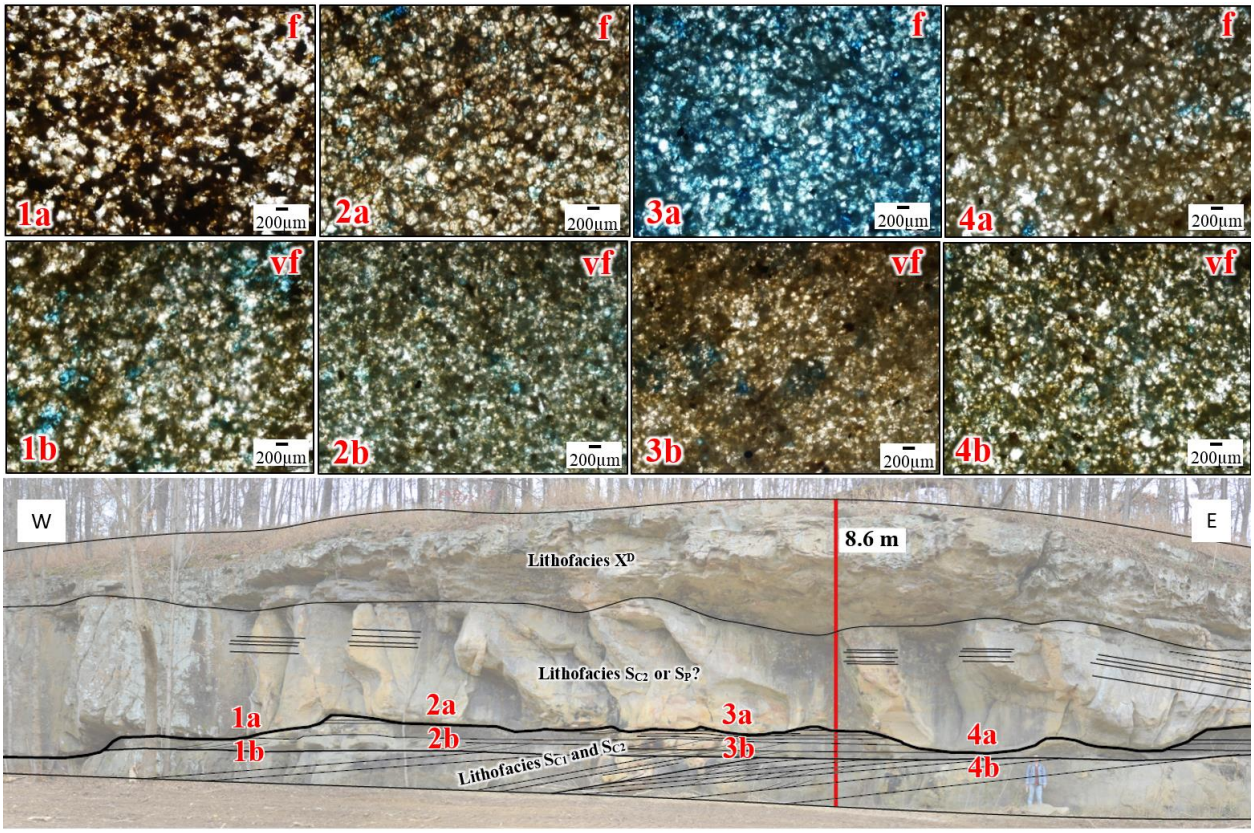

Figure 3.8. Cypress Creek outcrop showing a slight but abrupt grain size increase (~50 µm) across an erosional surface within the thick Western Belt sandstone.

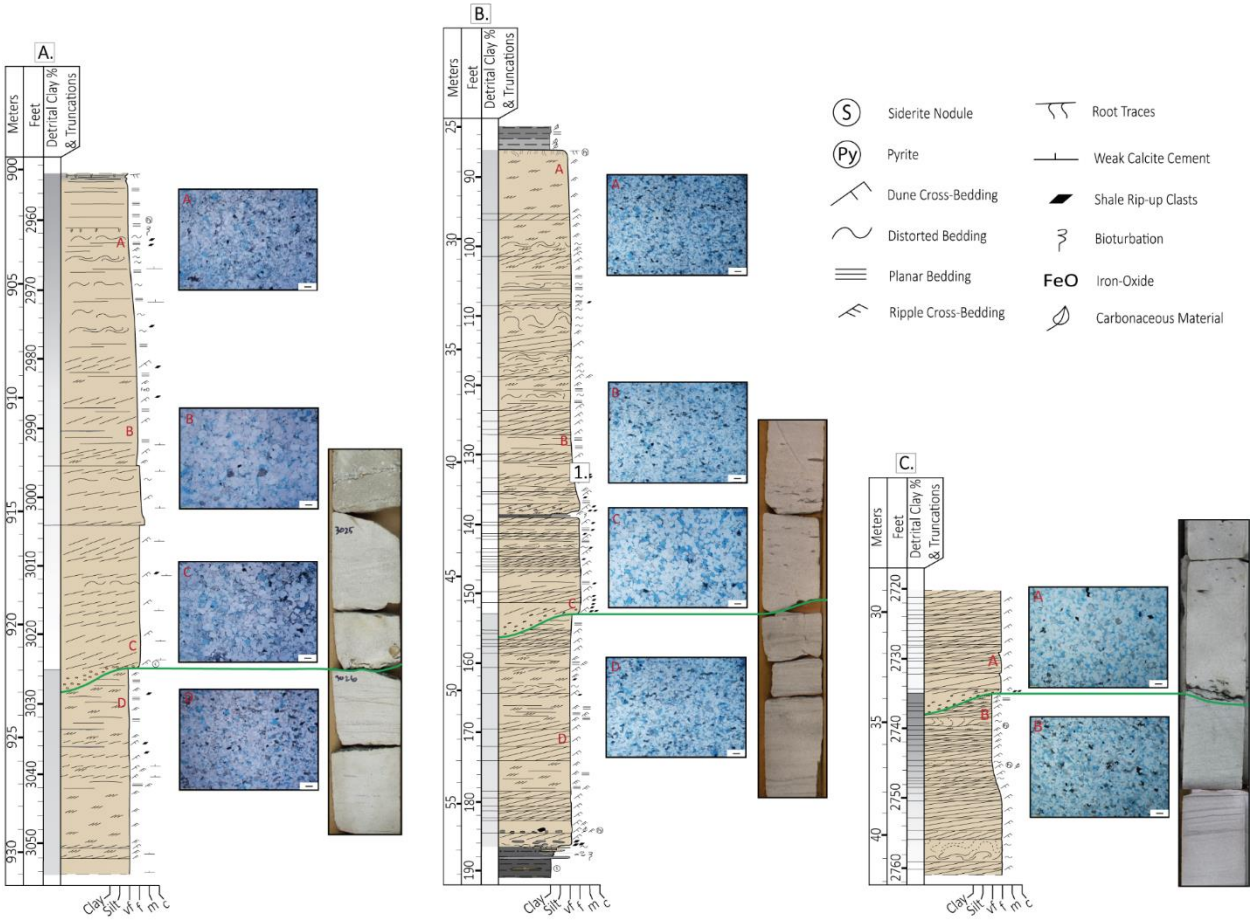

Figure 3.9. Graphic columns with selected thin sections to demonstrate grain size changes on either side of major intraformational discontinuities in the A) RHF #2-S (API 120650139400) B) Tripp #1 (API 121812190900), and C) Long #2 (API 121592648800) cores. Few truncations were documented in RHF #2-S due to core quality. Thin section scale bars are 250 µm.

The thick Cypress Sandstones of the Western Belt occur in outcrop in the Cypress type area and consists dominantly of lithofacies S_{C1}, S_{C2}, S_P, S_R, S_M, X^D, C, and X^P. As with the cores, major erosional surfaces were observed to be embedded within thick sandstones in the Cypress Creek outcrops. The Tripp #1 (API 121812190900) core 3.5 km (2.2 mi) from the outcrop demonstrated that these subtle but major erosional surfaces in the thick sandstones can be obscured within geophysical facies C because they are, by nature, sand on sand contacts (**Figure 3.10B**).

Two to three stacked, genetically continuous storys are present in thick sandstones within the Western Belt (**Figure 3.9**). Each story is approximately 15-22 m (49.2-72.2 ft) thick in the RHF #2-S core (**Figure 3.9A**; green line to core top) and 16-22 m (52.5-72.2 ft) thick in the Tripp #1 core (**Figure 3.9B**; green line to core top). The story bases (i.e., erosional discontinuities) may either be undiscernible (**Figure 3.10B**) or correspond to a subtle inflection in well log signatures (**Figure 3.10A, C**). Data from a new Weatherford Compact Microimager (CMI) log through the Western Belt in the Long #2 well (API 121592648800) in the basin interior (**Figure 3.10C**) shows a change in cross-set dip-direction and

magnitude at the story bases. The beds dip consistently south southwestward in each story (**Figure 3.10A**), which is in accordance with the regional trend and interpreted water transport direction.

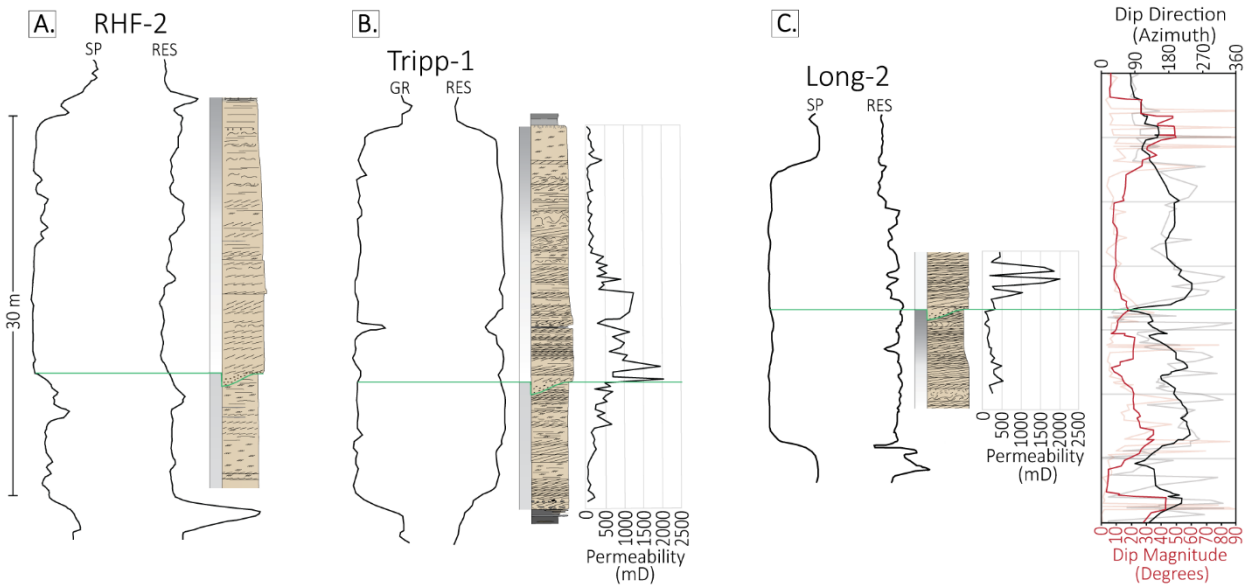

Figure 3.10. A) Well logs and core (detrital clay % to left) of the RHF #2-S (API 120650139400). B) Well logs, core (detrital clay % to left), and permeability of Tripp #1 (API 121812190900). C) Well logs, core (detrital clay % to left), permeability, and CMI log (bedding dip direction and magnitude) of Long #2 (API 121592648800). Major discontinuities (green lines) correspond to abrupt and significant permeability shifts that may be very subtle or completely obscured in traditional well log suites.

From the channel base(s) in the Tripp #1 (API 121812190900) core (~46 m (~151 ft) or ~42 m (~138 ft)) to the top of the thick Western Belt Sandstone at ~16 m (~52.5 ft), the succession is genetically continuous and 16-20 m (52.5-65.6 ft) thick. The ratio of lithofacies S_R to lithofacies S_C and S_P increases upwards and grain size decreases accordingly, suggesting a decrease in flow velocity through time. This fining-upward succession is topped by a gleyed, highly carbonaceous gleysol (lithofacies M_C^P) with evidence of root traces immediately beneath it (**Figure 3.9**). This gleysol indicates that not only were currents decreasing in energy over time, but they were also shallowing.

Roughly 80 km (49.7 mi) northwest of the Tripp #1 (API 121812190900) core, a very similar succession can be observed in the RHF #2-S (API 120650139400) core in Dale Field (**Figure 3.9**). Although the nature of upper and lower contacts of the thick Western Belt sand are unknown in this core, it does capture ~90% of the entire sandstone. Similar to the Tripp #1 (API 121812190900) core, a major erosional channel base embedded within the thick Western Belt sandstone of the RHF #2-S (API 120650139400) core is characterized by a poorly developed basal lithofacies C and a subtle grain size increase associated with thalweg deposits (lithofacies S_C and S_P). Evidence of up to two more erosional channel bases exist above this lower, most obvious channel base.

The top of thick fluvial Western Belt sandstones is commonly transitional into muddy and silty lithofacies modified by X^P before transitioning into marine muddy and silty lithofacies within the upper interval (**Figure 3.7**). On top of thick sandstones, geophysical facies B corresponds to muddy and silty

lithofacies modified by X^P. A funnel transition to the upper interval, was commonly observed in geophysical logs in Dale Oil Field. For wells missing the funnel-shaped log transition, a sharp transition was observed, like the Tripp #1 core (API 121812190900; **Figure 3.9B**), where a gleyed paleosol rests directly upon a bar top. In both cases, the initial marine flooding that eventually inundated the basin and deposited the overlying Barlow Limestone evidently occurred after deposition of the thick, fluvial Western Belt sandstones because the thick Western Belt sandstones are transitional upward to subaerial exposure at their tops before becoming marine. This transition to subaerial exposure at the top of thick Western Belt sandstones is interpreted herein to be evidence of a change to river floodplain deposits.

Given the dominance of fluvial lithofacies and the typical lithofacies succession found in core through thick Western Belt sandstones, a point bar model (e.g., **Figure 3.11**), where the idealized vertical succession is a basal lag, cross-beds, and ripple cross-beds topped by paleosols, is here tentatively suggested for these channel fills. However, nearly identical successions may be found within channel fills of braided river deposits (Bridge 1985, 1993) and cannot be ruled out completely. Nonetheless, channel fills within the Western Belt are commonly stacked upon each other (multistory), with there being evidence of up to three genetically continuous storys in the Tripp #1 (API 121812190900) and RHF #2-S cores (API 120650139400).

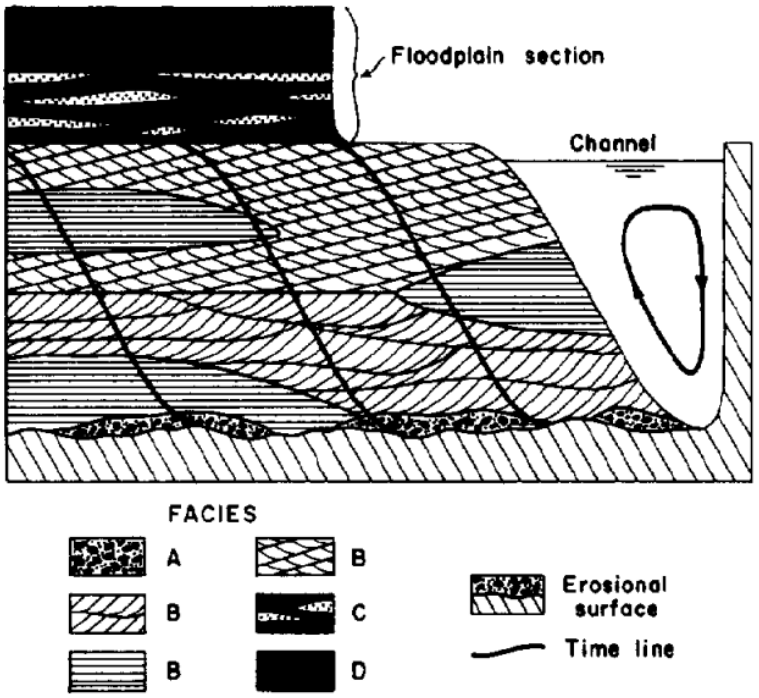

Figure 3.11. Idealized point-bar model from Allen (1970). A = conglomeratic, B = cross-bedded sandstone, flat-bedded sandstone, B = cross-laminated sandstone, and C = alternating beds, siltstone.

Channel bases identified in this study (defined by subtle grain size shifts and poorly developed lags) were not previously recognized within thick sandstones of the Western Belt, which were commonly viewed as being genetically continuous, 'clean' sands with no internal discontinuities. Likewise, Nelson et al. (2002) interpreted these deposits to be dominantly transgressive incised valley fills, being originally braided river deposits that were significantly reworked by tides and waves. Cole and Nelson

(1995) also did not recognize these internal erosion surfaces and suggested a divergent interpretation in which thick Western Belt sandstones represent solely marine products, such as imbricated tidal bars. Although these channel bases were not recognized by previous authors, many have suggested a fluvial to deltaic origin for other thick Chesterian sandstones (e.g., Potter 1962; Swann 1964), although none have specifically differentiated thick Western Belt sandstones of the Cypress Formation. The present study supports and refines the fluvial interpretation, suggesting that thick sandstones of the Western Belt represent dominantly the multistory fluvial lowstand systems tract (LST) deposits.

The sequence stratigraphic model is rooted in the belief that nearly complete sediment bypass occurs through valley systems on low gradient coastal plains during LST, although this 'vacuum cleaner' model has recently been deemed incorrect (Blum et al. 2013). The basal valley-fill surfaces of low gradient, lowstand coastal-plain paleovalleys are strongly diachronous and do not represent an extended period of incision and sediment bypass. Low gradient, LST coastal river systems instead conform to the 'conveyor belt' model, where a significant portion of the total sediment load is stored in the river belt before reaching the ocean (Blum et al. 2013). As such, the sequence boundary of Sequence 8 at or near the base of thick Western Belt sandstones likely does not represent a long period of incision coupled with mostly sediment bypass. Thus, the sequence boundary of Sequence 8 must be roughly the same age as the overlying Western Belt fluvial deposits (c.f. Blum et al. 2013). Since LST fluvial deposits have a high probability of being stored within river belts on low gradient coastal areas, LST fluvial deposits of the ancient, low slope Cypress river have a high probability of comprising the bulk of thick sandstones in the Western Belt. Additionally, whereas little to no evidence of marine reworking exists within thick Western Belt sandstones, evidence of subaerial exposure exists consistently on top of thick Western Belt sandstones, further suggesting that these thick sandstones represent dominantly fluvial LST deposits rather than TST deposits (c.f. Nelson et al. 2002).

3.2.5 Geophysical Facies

Lithofacies of the Cypress Sandstone at Dale Field were calibrated to geophysical logs (**Figure 3.12**; specifically, SP and resistivity due to their prevalence in the ILB) to construct a geophysical facies scheme that could be applied elsewhere in the basin (**Table 3.4**). Most geophysical facies are broken down into subcategories based on the degree of serration in the log signature. Each geophysical facies generally consists of a characteristic assemblage of lithofacies that, when associated together, represent characteristic depositional environments. Thus, geophysical facies are herein proxies for facies associations. See Howell (2017) for the full application of the geophysical facies scheme and resulting depositional model derived for Dale Oil Field.

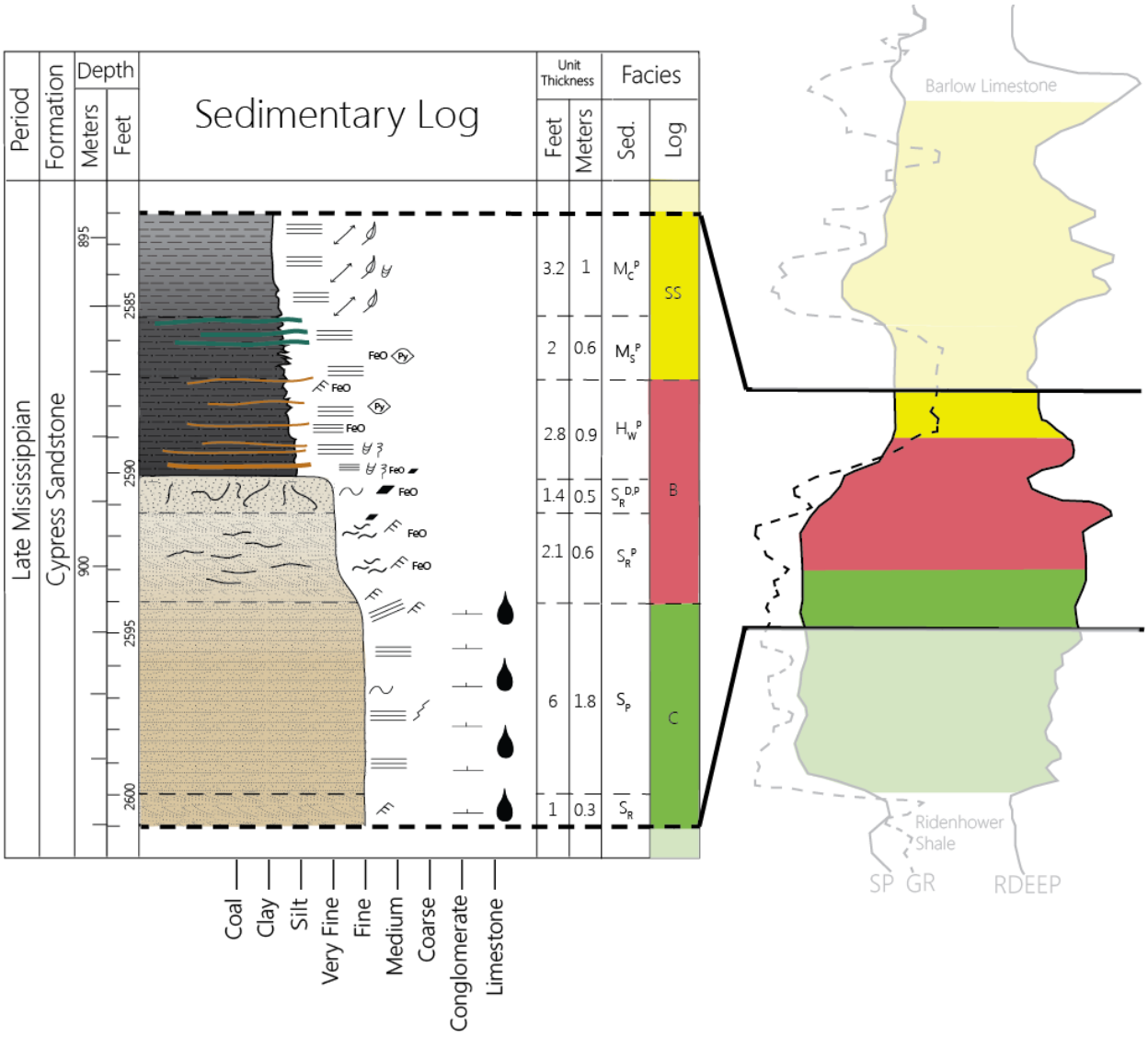

Figure 3.12. Example showing lithofacies of Moore #5 (API 121652585700) calibrated to geophysical logs to form geophysical facies.

Table 3.4. Geophysical facies scheme for the Cypress Formation including thickness, log motif, description, depositional process, lithofacies, and facies associations for each geophysical log facies. All geophysical log motifs are from the Cypress Formation. On motifs, left curve is SP and right curve is resistivity (dashed = short normal).

Log Facies	Net Sand Thickness		SP and Resistivity Log Signature	Description	Depositional Process	Common Lithofacies	Facies Associations
Smooth Shale (SS)	0			Uniformly high SP and low resistivity, may be slightly serrated, upper and lower contacts may be sharp or gradational	Uniform low energy suspension-dominated sedimentation	M, M_S, H_L, H_W OR M^P, $M_S{}^P$, $H_L{}^P$, $H_W{}^P$	Mud flat, delta front, interdistributary bay OR Floodplain, abandoned channel fill
Irregular (I)	~0-3 m	1	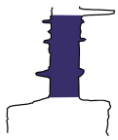 Net sand = 0	Irregular (serrated) SP, overall high gamma-ray and low resistivity	Irregular switching between low energy fall-out sedimentation and moderate energy, bed load-dominated sedimentation	M., M_S, H_L, H_W, H_F, S_{RD}, C OR M^P, M_C, $M_S{}^P$, $H_L{}^P$, $H_W{}^P$, $H_F{}^P$, S_R, C	Tidal bar, intertidal bar, tidal ridges, tidal flat OR Floodplain, overbank, channel levee, crevasse splays
		2	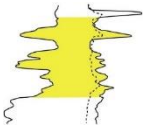 Net sand > 0				
Hourglass (H)	~3-8 m	1	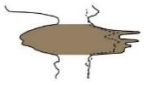 Smooth	Roughly symmetrical increase and decrease in SP that may be serrated, upper and lower contacts gradational	Gradual increase in bedload sedimentation energy followed by a gradual decrease in bedload sedimentation	S_R, S_{RD}, H_W, H_F, H_L, S_P, X^P, C	Tidally-modulated delta front, mouthbars, or shoreface sands
		2	 Serrated				
Bell (B)	~3-15 m	1	 Smooth	Increase in SP upwards with roughly no vertical	Gradual decrease in bedload-dominated sedimentation	S_C, S_R, S_P, S_M, X^D, H_W, M_S, H_F, X^P	Meandering or anastomosing river deposits, floodplain and levee deposits

		2	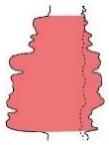 Serrated	change in resistivity, sharp lower contact and gradational upper contact	under the influence of high suspended load		
Funnel (F)	~3-12 m	1	 Smooth	Decrease in SP upwards with roughly no vertical change in resistivity, gradational lower contact and sharp upper contact	Gradual increase in bedload sedimentation followed by abrupt transition to suspension dominated sedimentation	M_S, X^P, X^D, H_W, H_F, S_R, S_{RD}, S_P	Prograding mouthbars or shoreface sands
		2	 Serrated				
Cylindrical (C)	~12-60 m	1	 High serration	High SP and low resistivity that may be serrated, gradational or sharp upper and lower contacts	Abrupt increase in bedload sedimentation under the influence of high suspended load	S_{C1}, S_{C2}, S_P, S_R, S_M, X^D, C	Multistory channel fills of meandering or anastomosing river
		2	 Medium serration				
		3	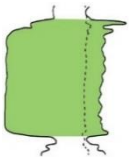 Smooth				

3.2.6 Implications for Reservoir Heterogeneity

The characteristics and preservation of fine-grained river bedforms leads to challenges in discerning their subtle, but significant, genetic features, such as facies discrimination, story bases, and grain size changes. However, this subtle heterogeneity may exert a strong control on subsurface fluid flow, and thus diagenetic evolution, which impacts hydrocarbon production and/or CO_2 injection.

In a petrographic study, Pitman et al. (1998) suggested that although substantial diagenesis has occurred since deposition, "original variations in permeability due to small grain size differences have been preserved" in Cypress reservoirs. An example of this is the preserved covariance of permeability and grain size (**Figure 3.10**). Larger grain sizes (i.e., fine-grained) correlate with lithofacies C and S_C, thalweg deposits overlying erosional channel bases (at 38 m (124.67 ft) and/or 46 m (150.91 ft)), and high permeability zones in the Tripp #1 (API 121812190900) and Long #2 (API 121592648800) cores (**Figure 3.10**). In the Cypress Creek outcrops ~3 km (~2 mi) from the Tripp #1 core, evidence of preferential fluid flow in thalweg deposits above channel bases was observed in liesegang banding, resulting from the preferential transmission of iron-oxide-rich fluids, which is isolated to slightly coarser-grained sandstones above an erosional surface, with a small (<300 mm (<11.8 in)) iron-oxide 'halo' existing below the erosional surface. Iron-rich fluids thus did not flow, or had a lower flow rate, through sandstones below the erosional surface, most likely due to their lower grain size and permeability. Abrupt, but subtle, increases in grain size (very fine-upper to fine sand) and a four-fold increase in permeability correspond with these erosional channel bases (**Figure 3.10**), suggesting that channel bases and overlying thalweg deposits, largely obscured within otherwise visually homogeneous thick sandstones in the Western Belt, may act as higher permeability thief zones during fluid injection, and should thus be considered during the development of reservoir models to ensure accuracy.

At a regional-scale, the thick Cypress Sandstone in the Western Belt hosts significant oil reservoirs that are candidates for future CO_2-EOR and associated storage due to their significant volume. The present research demonstrates that the textural (nearly unimodal) and lithological (nearly mono-mineralogic) homogeneity that is apparent from casual inspection of such sandy, fine-grained deposits belies the complexity of their reservoir heterogeneity. Significant genetic features, such as story bases, which impact the anisotropy of the reservoir porosity and permeability (**Figure 3.10**), may be almost entirely obscured in gamma-ray and resistivity curves (**Figures 3.10**). In core or outcrop, it may even be difficult to discern changes in facies that impact the functional heterogeneity of the unit as a reservoir body composed of discrete flow units.

Reconstructing the vertical dimensions of channel storys and mapping architectural elements at the field-scale provides constraints for geologic models for the dimensions of flow units and contributes to an understanding of reservoir continuity (e.g., George & Stiles 1978). Understanding the vertical sequencing of facies and grain size change, even if subtle (<50 μm grain size changes), provides critical insight into the potential efficacy of different injection strategies depending on whether CO_2-EOR or storage is being prioritized. Thus, the optimum reservoir sweep may be achieved by injecting CO_2 in lower permeability facies near the top of a channel story, with production perforations placed within the higher permeability story base so flow toward the higher permeability may overcome the buoyancy contrast of the CO_2 in water.

3.3 Characterization of Noble, Kenner West, and Loudon Fields

This section describes project activities undertaken to complete geologic characterization of Noble, Kenner West, and Loudon Fields. A range of project activities were completed at each study site including stratigraphic correlation, sedimentary facies analyses, and identifying petrophysical characteristics of the reservoirs present in a specific field. Isopach maps were developed which show variation in the thickness and geometry of the thick Cypress Sandstone. This work facilitated the broader, regional geologic characterization of the Cypress Sandstone (see Section 3.4).

While a range of project activities were conducted in order to complete field-scale geologic characterization, not all project activities pursuant to this goal were undertaken at each individual field. At Noble, project activities included both stratigraphic and facies analyses as well as reservoir characteristics (i.e., reservoir geometry, volumetric analysis, and Isopach maps). At Kenner West, project activities included stratigraphic analysis and reservoir characteristics (i.e., reservoir geometry, volumetric analysis, and Isopach maps). At Loudon, project activities were limited to stratigraphic analysis and reservoir characteristics (i.e., reservoir geometry and Isopach maps).

3.3.1 Noble Field

Introduction

The Noble Oil Field was discovered in 1937 and is in Southwestern Richland County, Illinois. Roughly 50% of Noble Field's cumulative oil production of 7.3 million m^3 (46 MMBO) is derived from a relatively thin oil reservoir that occurs in a thick (up to 50 m (164 ft)) fluvial, valley-fill sandstone within the Mississippian Cypress Sandstone. Attempts at production from such reservoirs suffer from early onset of high water production and low recovery efficiencies (25% in the case of Noble Field). As such, these reservoirs have potential for nonconventional carbon dioxide (CO_2) enhanced oil recovery (EOR), which is CO_2-EOR that includes geologic storage of carbon as a significant component of the process.

Stratigraphy

A stratigraphic column summarizes the middle Mississippian to lower Pennsylvanian strata in Noble Field and indicates hydrocarbon-bearing formations (**Figure 3.13**). The Cypress Sandstone is well developed as a thick, continuous sandstone that generally has a blocky appearance on spontaneous potential (SP) or gamma ray logs. The shape of the top of the Cypress is generally convex upward, with a flat to slightly undulating base. The thickness of the sandstone can vary from 27.0-53.3 m (90-175 ft). A comprehensive reservoir characterization of the valley fill Cypress Sandstone is presented later in this report. There is generally a 6.1-9.1 m (20-30 ft) thick shaly interval between the top of the sandstone and the base of the Barlow limestone. This shaly interval consists of dark gray shale that is generally noncalcareous near the top and bottom. Near the middle of the zone is a variegated dark green and red mudstone that is variably calcareous, contains small calcite nodules, and has a blocky appearance. This section of the shaly interval is interpreted as a paleosol and has been noted in many reports around the Basin (Nelson et al. 2002). The upper portion of the dark gray shale is silty and grades upward into the Barlow limestone.

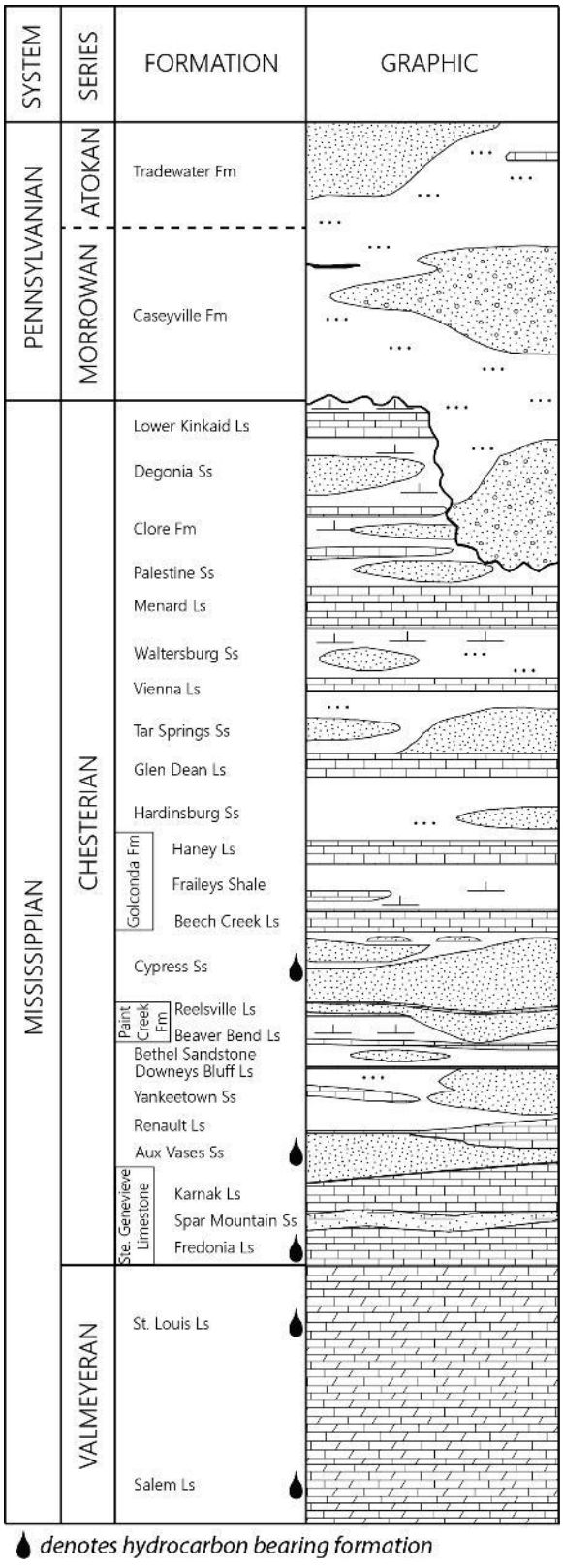

Figure 3.13. Generalized stratigraphic column of Noble Field. Modified from Cole and Nelson (1995).

Facies Analysis

Whole cores from three wells in the north part of Noble Field (Section 4, T3N, R9E) and one well to the south and down structure from the main part of the field (Section 30, T3N, R9E) were available in the ISGS samples library (**Table 3.5**). The Montgomery #B-2 core (API 121590139100) was taken in 1938 and originally represented 21 m (70 ft) of the formation but was later reduced, sampled, or had poor recovery as no more than 15 m (50 ft) remains. The core is heavily oil stained, making identification of sedimentary features other than basic textural descriptions difficult. The Montgomery #B-34 (API 121592606700) and Coen #120 (API 121592608300) wells, the latter of which is included in **Figure 3.14**, were cored in 2004 and 2005, respectively. Although partially oil stained, sedimentary features were discernable in these cores that represent only the upper portion of the valley fill Cypress. The Long #2 well was cored in 2017 as part of this project and penetrated through a sandstone lens and a portion of the underlying shale, as well as through 12 m (40 ft) of the 21 m (70 ft) thick valley fill sandstone at the base of the formation.

In general, the valley fill Cypress Sandstone observed in all cores is fine- to very fine-grained, with rare occurrences of medium-grained sandstone. The Montgomery #B-34 and Coen #120 cores record changes in depositional energy and sedimentary structures near the top of the valley fill succession (**Figure 3.15**). In the Montgomery core, cross-bedded sandstone near the base grades upward into a lower energy ripple-bedded sandstone at 789.0 m (2,588.5 ft) that sharply transitions at 787.8 m (2,584.5 ft) to a heterolithic flaser- to wavy-bedded sandstone, marking another, and more abrupt, drop in energy. The reduced depositional energy produced alternating deposits of bed-load traction of sand with suspension fallout of silts and clays. The heterolithic facies grades upward into very fine-grained ripple-bedded sandstone that extends to the top of the cored interval. The Coen #120 core shows a very similar succession.

The depositional environment, energy, and resulting sedimentary features define the sedimentary facies used in this study. In both cores, sedimentary facies and reservoir quality correlate well with the oil staining of the rock; reservoir facies exhibit oil staining and include cross-bedded and ripple-bedded sandstone; nonreservoir facies lack oil staining and exhibit wavy- and lenticular-bedded sandstones.

Table 3.5. Wells with whole core of the Cypress Sandstone in Noble Field.

Well name and number	API number	ISGS core number	Cored interval, m (ft)
Montgomery B-2	121590139100	835	784.9 to 806.2 (2,575 to 2,645)
Montgomery B-34	121592606400	15658	785.2 to 794.3 (2,576 to 2,606)
Coen 120	121592608300	15659	787.3 to 795.8 (2,583 to 2,611)
Long 2	121592648800	15661	801.3 to 807.4 (2,629 to 2,649)
			829.1 to 841.6 (2,720 to 2,761)

Reservoir Facies

Fine-grained, cross-bedded sandstone was the dominant sedimentary facies observed in the cores (**Figure 3.15**). Cross-sets are visually well-defined by thin laminations of clay that are found along their surfaces. The oil staining of the cores may exacerbate this effect. Very fine-grained, ripple cross-laminated sandstone can be found at the base of some cross-bed sets. Truncation surfaces or thinner sections of ripple bedding mark bed-set boundaries and can occur from a few centimeters (inches) to a little more than 0.3 m (1 ft) apart. Portions of the cross-bedded facies exhibit distorted bedding because

of penecontemporaneous soft sediment deformation. The sandstone is commonly slightly calcareous and exhibits dense calcite-cemented zones in some places. Iron oxide mottling is common in the reservoir facies. Light to medium brown oil staining is present in the cross-bedded and ripple-bedded facies; in the portion of the Montgomery #B-2 core below the oil-water contact, the sandstone is unstained and remains white. Aside from minor amounts of clay found along cross-bed foresets, the cross-bedded facies is largely composed of clean sandstone that constitutes high reservoir quality.

Figure 3.14. The top of the Montgomery #B-34 core is in the upper left corner and proceeds downhole toward the bottom right. Each box segment is 0.6 m (2 ft) long. The core shows a typical upward change in facies from dominantly cross-bedded and ripple-bedded sandstone to heterolithic strata above. The change in color of the core from light brown to light gray reflects the lack of oil staining in the nonreservoir heterolithic facies. Figure 3.15 shows a graphical depiction of facies in the Montgomery core.

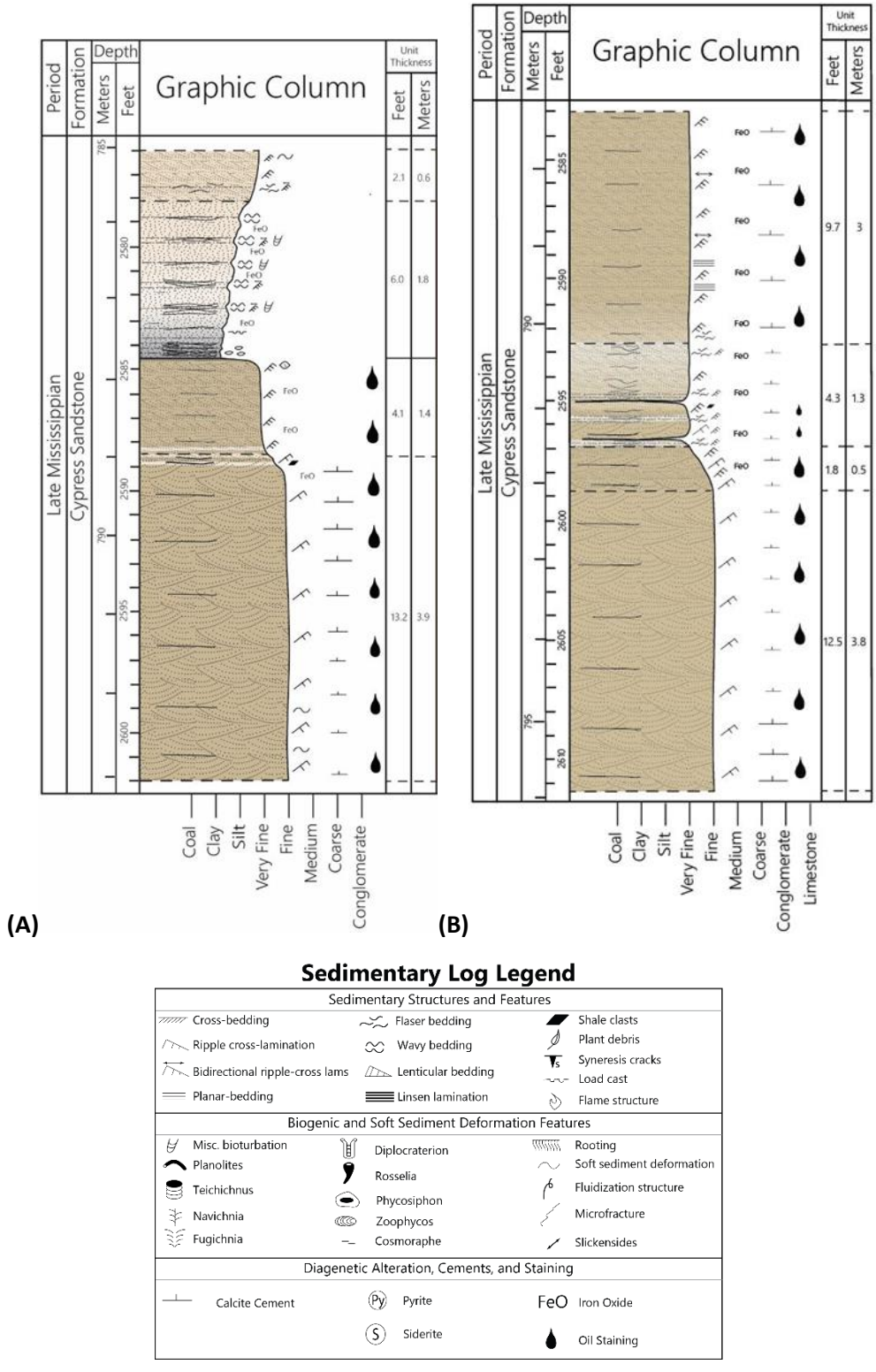

Figure 3.15. A) Lithologic log of the C.T. Montgomery #B-34 well (API 121592606400, Section 4, T3N, R9E) and B) Coen #120 well (API 121592608300, Section 4, T3N, R9E). The sedimentary facies observed in each core, particularly the depositional setting and the associated sorting characteristics, controls the reservoir quality.

Nonreservoir Facies

Non-hydrocarbon bearing sandstones in the upper portion of the Montgomery #B-34 core (**Figure 3.15**) exhibit a sequence of heterolithic strata. Very fine-grained, wavy-bedded to flaser-bedded sandstones are light orange to white, and they appear to have been altered by iron oxide staining. This staining is generally constrained to sections that are relatively free of shaly lenses or drapes. Some ripple cross-laminations occur throughout the heterolithic strata, as do rare horizontal and vertical burrows. Zones of shale-rich, lenticular-bedded sandstones also occur.

Depositional Model

In a regional study of lower Chesterian stratigraphy, Nelson et al. (2002) assigned portions of the Cypress Sandstone and its overlying and underlying formations to three unconformity-bounded depositional sequences. The older part of the Cypress that is transitional with underlying Paint Creek Formation deposits is part of Sequence 7 of the Nelson et al. (2002) scheme. The valley fill Cypress corresponds to Sequence 8, and some of the shaly deposits overlying the flooding surface that transition upward into the Barlow limestone are part of Sequence 9. The mapped geometry of the sandstone bodies, vertical and lateral relationships, geophysical log characteristics, and sedimentary structures observed in cores provided the means to make preliminary interpretations of the depositional environment of the Cypress Sandstone at Noble Field, with some comments on how it fits within the Nelson et al. (2002) scheme. While appearing as a mostly homogeneous sandstone on geophysical logs, detailed mapping has shown internal lithologic breaks, which allow the sandstone to be divided into three successive units (**Figure 3.16**).

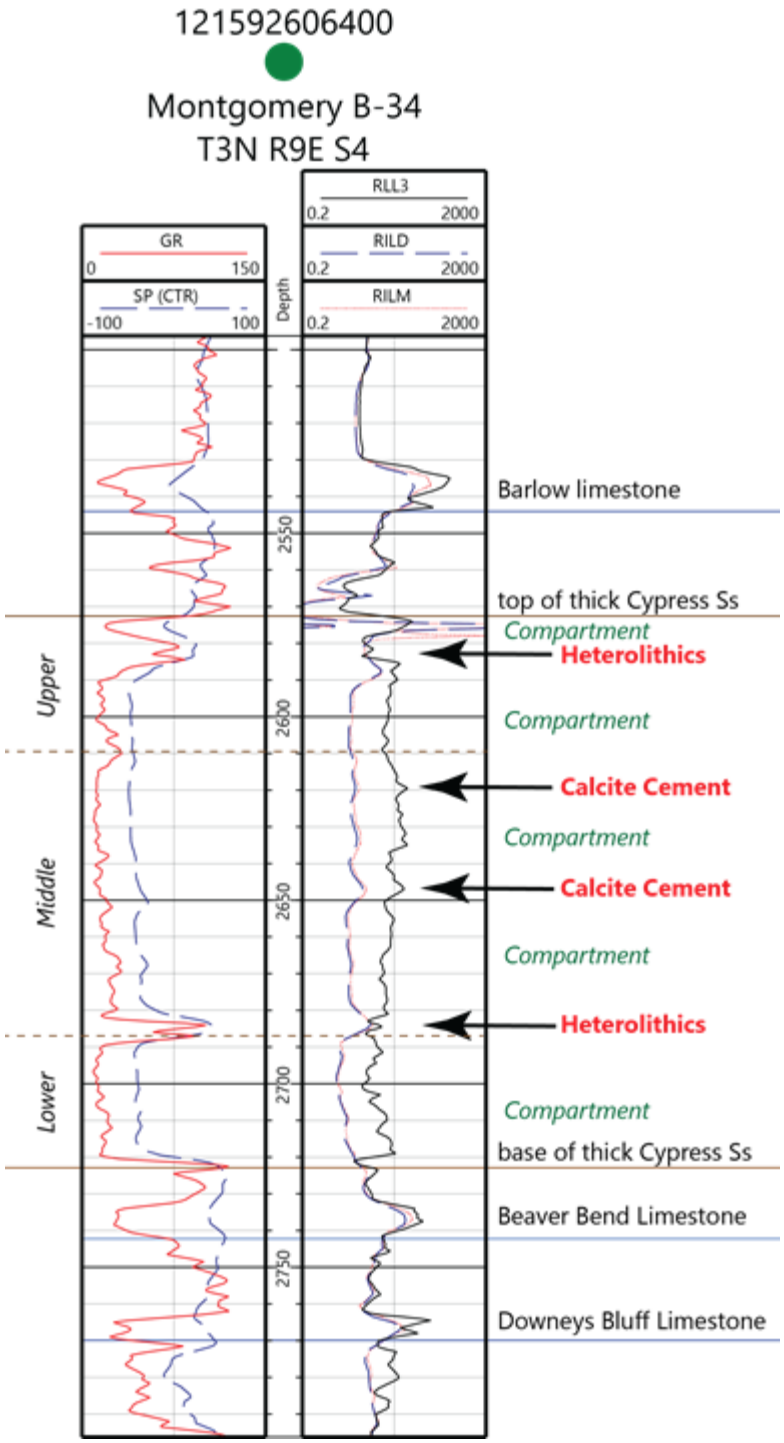

Figure 3.16. Geophysical log of the Montgomery #B-34 well (API 121592606400, Section 4, T3N, R9E) showing possible depositional and diagenetic features within the valley fill Cypress Sandstone (Ss) that create four potential baffles or boundaries to fluid flow, shown in bold red. Possible compartments within the thick sandstone are shown in green italics. The three main portions of the sandstone include a lower portion below a consistent shale break, as shown in Figure 3.17, 3.18, and 3.19, a middle portion composed of a clean and blocky section, and an upper, more heterolithic and variable portion.

Lower Sandstone

The lower boundary of the sandstone is assumed to be erosional, as geophysical log correlations indicate that, in some places, it incises through the Reelsville Limestone, a member of the underlying Paint Creek Formation. Roughly 7.9 m (26 ft) of erosional relief into the Paint Creek Formation was observed in this study of Noble Field. Nelson et al. (2002) previously documented the erosional nature of the base of the sandstone and noted that, based on geophysical log correlations in Richland County, the Cypress Sandstone incised valleys do not cut as deeply into underlying strata as is the case near the outcrop belt, where the Cypress can cut through several underlying formations.

A sandstone 6.1-21.3 m (20-70 ft) thick rests along the erosional lower contact and is continuous across Noble Field (**Figure 3.17, 3.18 and 3.19**). The Long #2 core penetrates about 7.6 m (25 ft) of the lower sandstone in Noble Field. Cross bedding dominates the core with some sections of convolute bedding. The base of the sandstone was not cored, however, and the interpretation of the base of the sandstone on an accompanying Weatherford Compact Micro-Imager log is equivocal, meaning the erosional basal contact of the formation remains speculative.

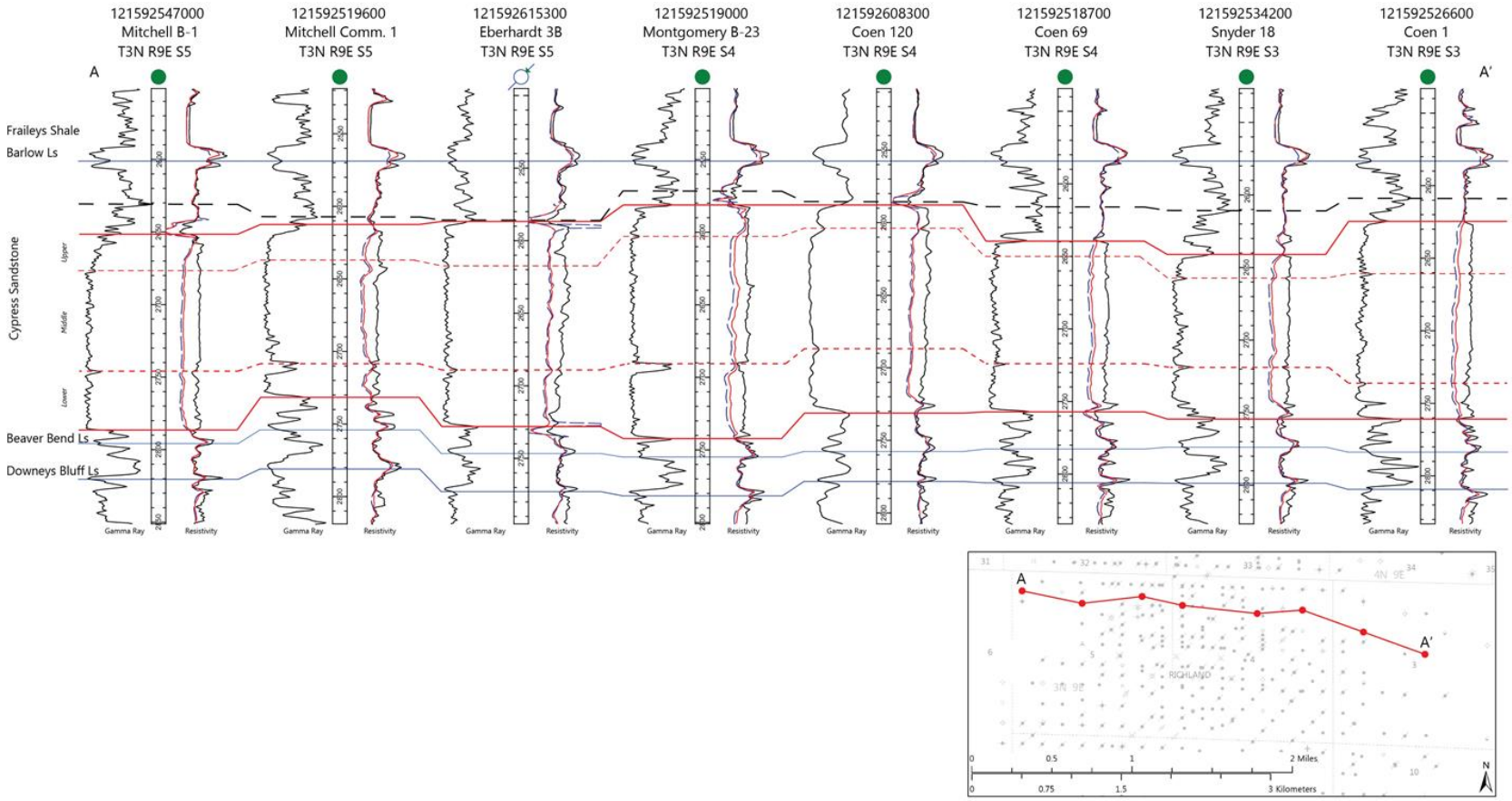

Figure 3.17. West to east cross section showing the log signatures of the valley fill Cypress Sandstone across Noble Field. The cross section is flattened at the base of the "Barlow" limestone. The erosional base of the Cypress is indicated by the pinch and swell of the interval between the base of the sandstone and the base of the Beaver Bend Limestone. The well log profile through the sandstone is aggradational, showing stacked sandstone storys that can most obviously be differentiated where shale breaks are present (red dashed line), but may be indistinguishable where sandstone-on-sandstone contacts occur. The retrogradational deposits immediately above the sandstone may be overbank/floodplain or estuarine sediments that fill abandoned channels. Zones of low resistivity above the thick sandstone may indicate areas of patchy coal or carbonaceous shale (Figure 3.18). A gamma ray maximum likely marks a significant marine flooding surface (black dashed line), above which transgressive deposits compose the remainder of the formation up to the Barlow limestone.

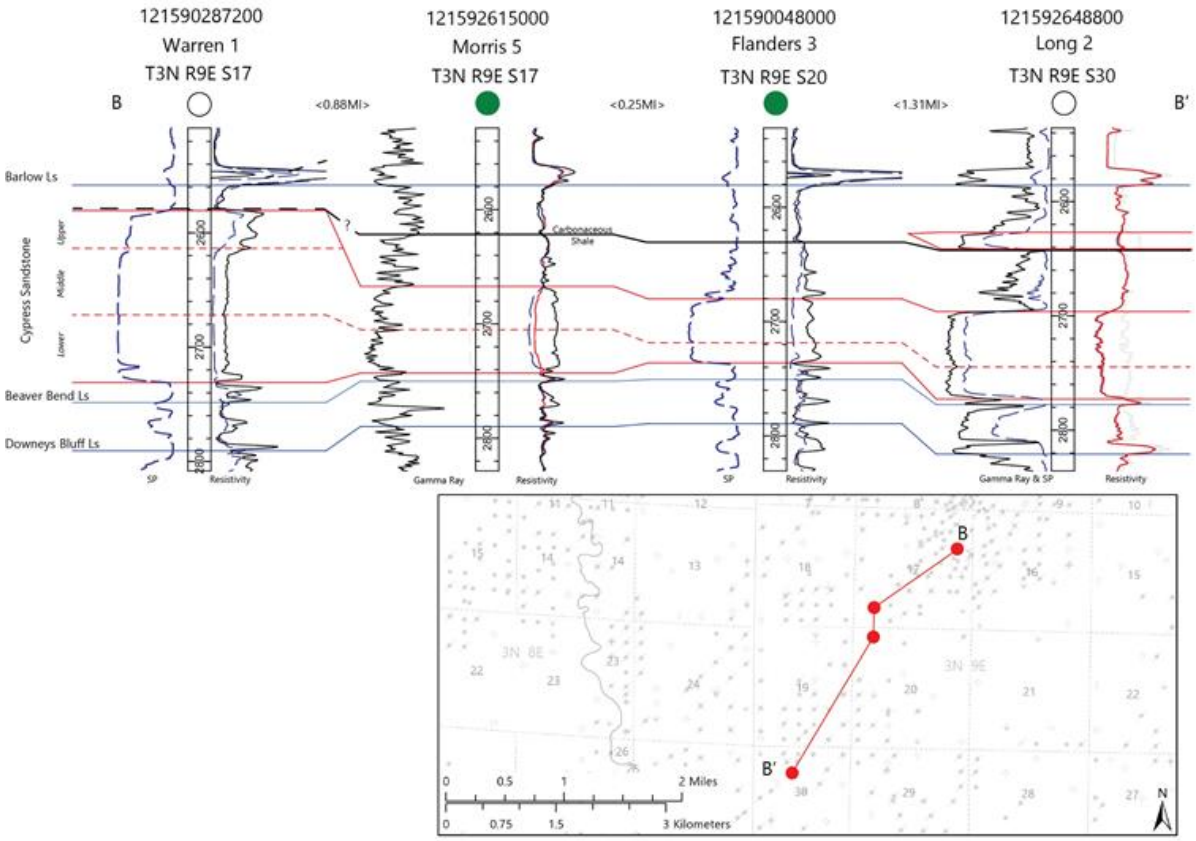

Figure 3.18. NE to SW cross section showing how the Cypress Sandstone thins southwestward going out of Noble Field. The cross section is flattened at the base of the Barlow limestone. A thin zone of low-density rock correlates to a zone of low resistivity and occurs roughly at the stratigraphic position where a thin coal has been previously described from drill cuttings. Core through this interval in the Long #2 (Section 30, T3N, R9E) revealed a thin carbonaceous shale with ubiquitous plant fossils.

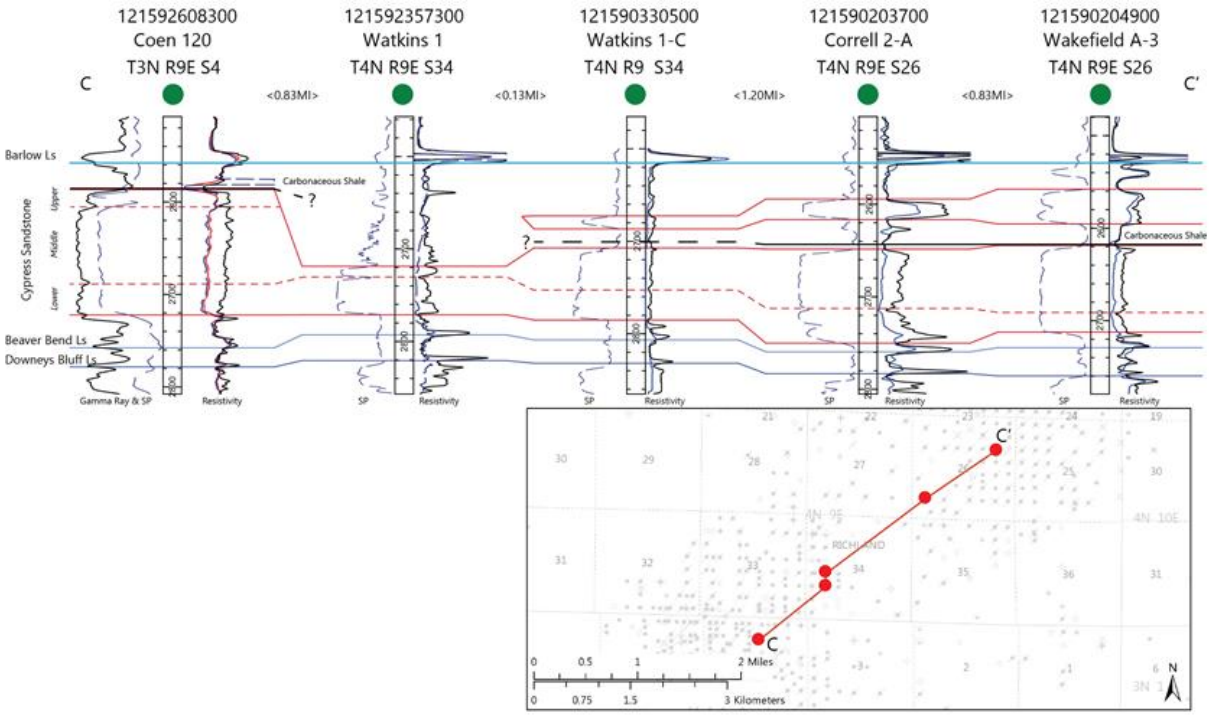

Figure 3.19. SW-NE cross section showing how the Cypress Transitions from Noble Field to Noble North Field. The cross section is flattened at the base of the Barlow limestone. The thick sand body on the left is hydraulically connected with the lower sandstone on the right side of the cross section. A middle sandstone overlies the lower sandstone and thickens to about 12.2 m (40 ft). A thin, lenticular sandstone body directly underlies the Barlow limestone in Noble North Field.

The lateral persistence of the lower sandstone was previously noted by Phillips (1954) and Chapman (1953), who described the basal part of the Cypress Sandstone as a discontinuous sheet deposit of fine-grained, white quartz sandstone that covers most of Richland and Clay Counties, respectively. Cross-section correlations from this study confirmed the persistence of this sandstone across Richland County. The sandstone generally thins and pinches out against the Charleston Monocline, the steep western flank of the La Salle Anticlinorium.

In a previous regional study of the Cypress Sandstone, Cole and Nelson (1995) interpreted the lower sandstone to have been deposited in a shallow, subtidal environment, citing bidirectional current indicators, clay drapes on ripples, oscillatory ripples, and a normal marine fossil fauna as evidence of its marine origin. Cole and Nelson (1995) asserted that the lower Cypress Sandstone intertongues with shallow marine shales and limestones of the Paint Creek Formation. Later correlations by Nelson et al. (2002) refined this interpretation: in some areas of the basin, a basal, coarsening-upward marine sandstone grades upward from the underlying Paint Creek Formation deposits as part of Sequence 7. In other areas, apparent lateral intertonguing is the result of the deposition of Cypress Sandstone in incised valleys along an unconformable contact where Cypress Sandstone may be laterally juxtaposed to and lap onto the truncated surface of the underlying marine shales and limestones of the Paint Creek Formation as part of Sequence 8. In areas where sandstone of Sequence 7 is unconformably overlain by sandstone of Sequence 8, it may be difficult to differentiate the two. Nelson et al. (2002) favor an estuarine interpretation for the valley fill portion of the Cypress (Sequence 8), stating that extensive tidal reworking of lowstand fluvial deposits within a tidal embayment during transgression seems

probable, implying that the incised valley systems were first filled with fluvial sediments before being reworked.

Mud drapes and bidirectional sedimentary structures, typical of tidally influenced deposits, were not observed, nor was a normal marine fossil fauna pervasive within the Long 2 core. The common cross bedding and presumed erosional lower contact are indicative of fluvial deposition. A fluvial sheet sandstone is thus the favored interpretation for the lower sandstone at Noble Field; in this case, the expected marine portion of the Cypress Sandstone (part of Sequence 7) is assumed to be eroded. Fluvial sheet sandstones are formed through the amalgamation of fluvial channel belts during periods of low aggradation (Wright and Marriott, 1993; Shanley and McCabe, 1994; Blum et al., 2013). The overextension of rivers over long, low-gradient coastal plains can also form sheet sandstones, as a result of the reduction in stream power and the resultant storage of sand in channels on the coastal plain (Holbrook, 1996). Sediment-choked channels cause frequent avulsion, which, over time, leads to the development of a regionally continuous sandstone sheet (Holbrook, 1996). Multivalley sandstone sheets thus form where the need for sediment storage exceeds accommodation within a single valley, resulting in lateral reworking (Holbrook et al., 2006). Thus, the lower part of the valley fill Cypress Sandstone is probably regressive, lowstand deposits composed predominantly of thalweg sandstones. Floodplain deposits were eroded or reworked during lateral channel migration and are not typically preserved. Such sheet sandstones are capable of being deposited by multiple fluvial styles, including sinuous meandering systems, low-sinuosity braided systems, and anastomosing systems.

Middle Sandstone

The most consistent discontinuity within the whole of the valley fill Cypress succession occurs at the top of the lower sandstone. This discontinuity occurs nearly everywhere in the field and manifests as a minor positive deflection to a shale break a few feet thick on gamma ray logs in different areas of the field (**Figure 3.17, 3.18 and 3.19**). Well cuttings from six wells show the shale break is generally composed of dark gray to reddish gray shale that contains bryozoan fossil fragments (**Figure 3.20**). The middle sandstone overlies this shale break and is the cleanest portion of the valley fill Cypress Sandstone, based on the highest deflection of the log from the shale baseline, and the blocky, aggradational log profile (**Figure 3.16**). The middle sandstone is generally 27.0-33.5 m (90-110 ft) thick and contains thin shale breaks. While these breaks may provide some basis to subdivide this unit, the breaks are not laterally persistent and traceable; in many places, the middle sandstone appears continuous on logs.

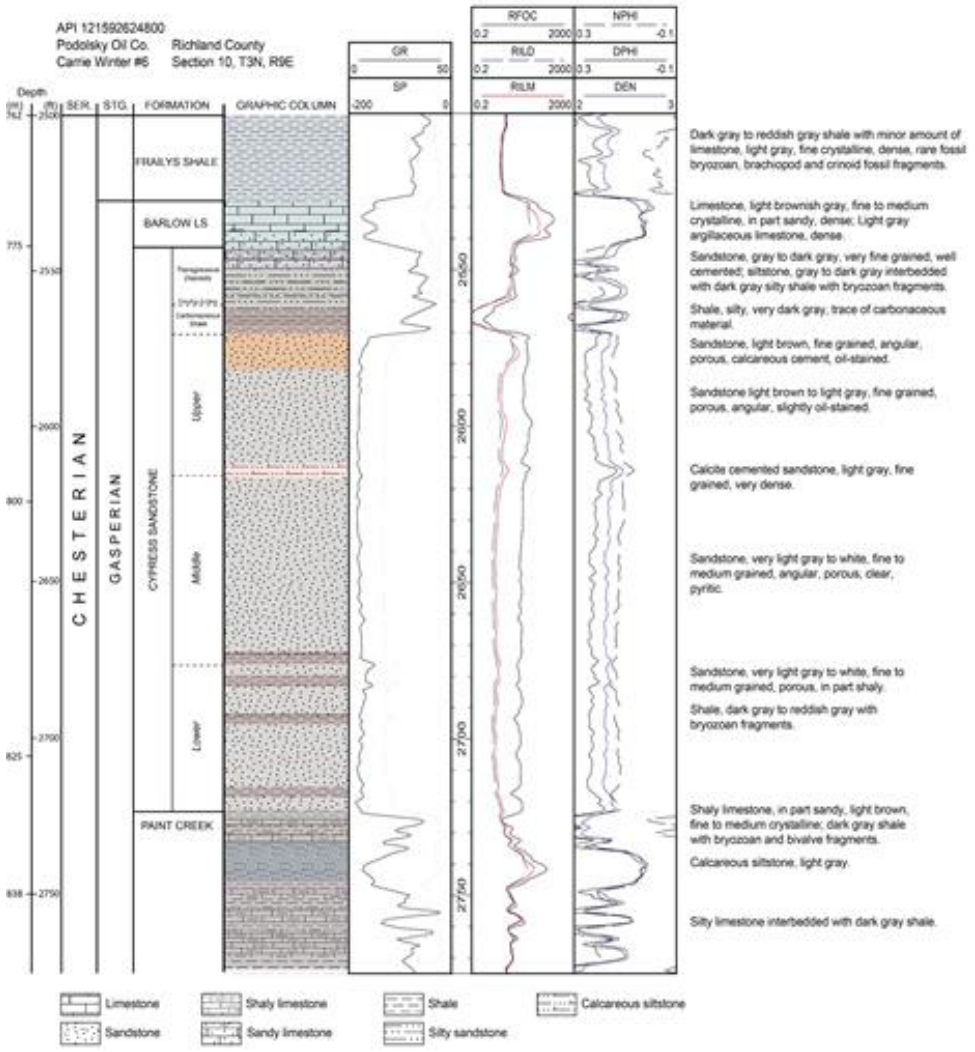

Figure 3.20. Graphical log and geologic description from a sample study of Podolsky Oil Company, Winter 6 well (API 121592624800, northwest of the northwest Section 10, T3N, R9E), in Noble Field. Samples were studied in the 762-845.8 m (2,500-2,775 ft) interval. Samples indicate lithologic changes coincident with inflections in the SP curve (reddish gray to dark gray shaly zones that can be fossiliferous), spikes in the resistivity curve within the sandstone (calcite-cemented zones), and low resistivity values above the sandstone (carbonaceous shales). Sample studies indicate oil-stained sandstone below the producing oil-water contact.

The middle sandstone is present everywhere in Noble Field but pinches out or grades laterally into green shale with thin, nonporous sandy shale partings northeast and southwest of Noble Field (Lee, 1939; **Figure 3.18; Figure 3.19**). Chapman (1953) described this sandstone as being composed of northwest-trending bodies composed of fine-grained, well-sorted, and angular to subangular quartz sandstone that is light gray or greenish gray, but is usually white, and can contain calcite cement. Available core description records on file at the ISGS corroborate this lithologic description, though some medium-grained sandstone was observed in sample sets (**Figure 3.20**). About 4.6 m (15 ft) of the middle sandstone is preserved in the Long 2 core, showing uniformly fine-grained cross-bedded sandstone. The contact between middle and lower sandstones in this core appears erosional, with some small clay chips occurring within the basal portion of the middle sandstone.

Based on the limited core data and the cross-section correlations of the middle sandstone, it is also interpreted to have a fluvial origin. Compared with the lower sandstone, the middle sandstone is thicker, but less laterally persistent, with a greater degree of floodplain preservation, as indicated by the lateral transition to variegated, likely paleosol bearing shale. The reduction in lateral reworking may reflect a rise in base level and a commensurate increase in accommodation. Therefore, the sandstones above the lower sandstone are likely fluvial deposits dominated by aggradation, rather than lateral migration and reworking.

Upper Sandstone

The upper portion of the valley fill Cypress Sandstone is the thinnest of the three subunits but has the most core data because it contains the oil reservoir. As described above, the general facies trend within the upper sandstone is somewhat transitional, from predominantly cross-bedded with associated ripple-bedded sandstone upward into more heterolithic strata before entering the shaly interval above the sandstone, as observed on geophysical logs. Clay laminations are found along some cross-bed foreset surfaces. Contorted cross-bedding and convolute bedding are observed within this interval. These features formed because of soft sediment deformation of previously deposited cross-beds, with deformation likely caused by compaction of the water-saturated sand, indicating rapid deposition.

As with the underlying sandstone units, the dominance of cross-bedded sandstone and lack of features indicating tidal influence (e.g., bidirectional bedding structures, tidal rhythmites) suggest that a fluvial interpretation is reasonable. The higher proportion of detrital clay, within the cross-bedded facies as well as within wavy- to flaser-bedded facies may indicate waning energy of the fluvial system or a lateral shift of the thalweg away from the cored area. This upper sandstone marks the uppermost fluvial sandstone body in Noble Field.

Together, the lower, middle, and upper sandstones in Noble Field comprise an amalgamated, multistory sandstone. These valley fill sandstones of Sequence 8 are immediately overlain in places by a zone of low resistivity (e.g., **Figure 3.18**). A core description through this zone of the 1930s Arbuthnot #1 well (API 121590012100, northwest of the northwest Section 8, T3N, R9E) by L.E. Workman of the ISGS shows about 1 m (4 ft) of green to red mudstone that contains <2 mm (<0.08 in) diameter calcite nodules, features indicative of a calcic vertisol (Mack et al., 1993). Samples described for the present study indicated a zone of carbonaceous material that also corresponds to a low-resistivity log signature and low-density signature on geophysical logs (**Figure 3.20; Figure 3.18**), which likely represents this paleosol horizon. Core from the Long #2 well through this interval confirmed the presence of <0.3 m (<1 ft) of carbonaceous shale overlying a dark grey shale with pervasive root marks. About 10 km (6 mi) to the southwest in Section 33, T3N, R8E, Chapman (1953) noted a 0.3 m (1 ft) thick seam of coal overlying the thick sand, providing further evidence of a paleosol horizon—in this case, a histosol (Mack et al., 1993). The paleosol horizon likely caps the valley fill sequence, except in places where active channels were flooded or where it may have been scoured by later marine transgression.

As continued base-level rise began to overtake the sediment supply, the low gradient of the coastal plain and concomitant rivers would have been subject to marine inundation over great distances. Estuarine reworking of the upper portion of the fluvial sandstone succession may have occurred in some areas, while other areas may have experienced some minor transgressive scour.

Geophysical log cross sections show an inflection point, mainly on the gamma ray log, but on the SP log also where the general profile of the log switches from retrogradational to progradational (**Figure**

3.17). This inflection may represent a significant marine flooding surface, above which some sandstone lenses may exist, but sample descriptions indicate they are very-fine grained and well cemented (**Figure 3.20**). They may also be bioturbated, as has been observed in cores and outcrops (Cole and Nelson, 1995).

Reservoir Characteristics

Geometry and Isopach Maps

Geophysical logs available for correlation and mapping included 1940s- to 1970s-era electric logs with SP and resistivity curves (generally long normal, short normal, and lateral resistivity) from roughly 380 wells within the study area. There were also around 130 wells with more recent logs, including neutron density porosity, gamma ray, SP, and induction resistivity traces.

The geophysical log expression of the valley fill Cypress Sandstone is characterized by a blocky, aggradational profile on the SP and gamma ray logs, with a slight fining upward trend at the top of the sandstone that transitions into a shalier, retrogradational log profile (**Figure 3.21**). The basal contact of the sandstone is generally sharp and well-defined (**Figure 3.21**). Resistivity curves typically show a relatively high resistivity at the top of the sandstone body that either gradually becomes less resistive with depth or, in some cases, is somewhat jagged with sharp spikes that disrupt an otherwise gradual downward decrease in resistivity. The high resistivity zone is thickest in the older logs, indicating the original thickness of the oil reservoir. Newer logs show a thinner zone of high resistivity that reflects decades of oil production.

Some wells exhibit a spike of high resistivity at the base of the Cypress Sandstone near its contact with the underlying Paint Creek Formation. In such cases, either the Cypress rests conformably on top of the intact Reelsville Limestone and the resistivity spike is the Reelsville Limestone, or the basal portion of the sandstone contains an erosional lag of clay clasts or limey fossil fragments and may be calcite cemented as a result (e.g., Morad et al., 2010). Both scenarios have been noted in studies of analogous Cypress outcrops in Southern Illinois (Cole and Nelson, 1995).

Geophysical log cross sections indicate that the basal contact of the Cypress Sandstone with the underlying strata is erosional (Nelson et al., 2002; **Figure 3.17, Figure 3.18**). The Reelsville Limestone is absent and likely eroded over most of the field. A shaly interval is usually present between the base of the Cypress and the underlying Beaver Bend Limestone, but the Cypress eroded through the shale and rests directly on top of the Beaver Bend Limestone in many areas. Locally, the Cypress erodes through the Beaver Bend Limestone entirely.

The top and base boundaries of the valley fill Cypress Sandstone were determined, and the resulting gross thickness of the sandstone was mapped (**Figure 3.22**). The gross sandstone thickness refers to the thickness between the top and base of the entire valley fill Cypress Sandstone body and may include thin intercalated shales or shaly sandstone intervals (**Figure 3.22**).

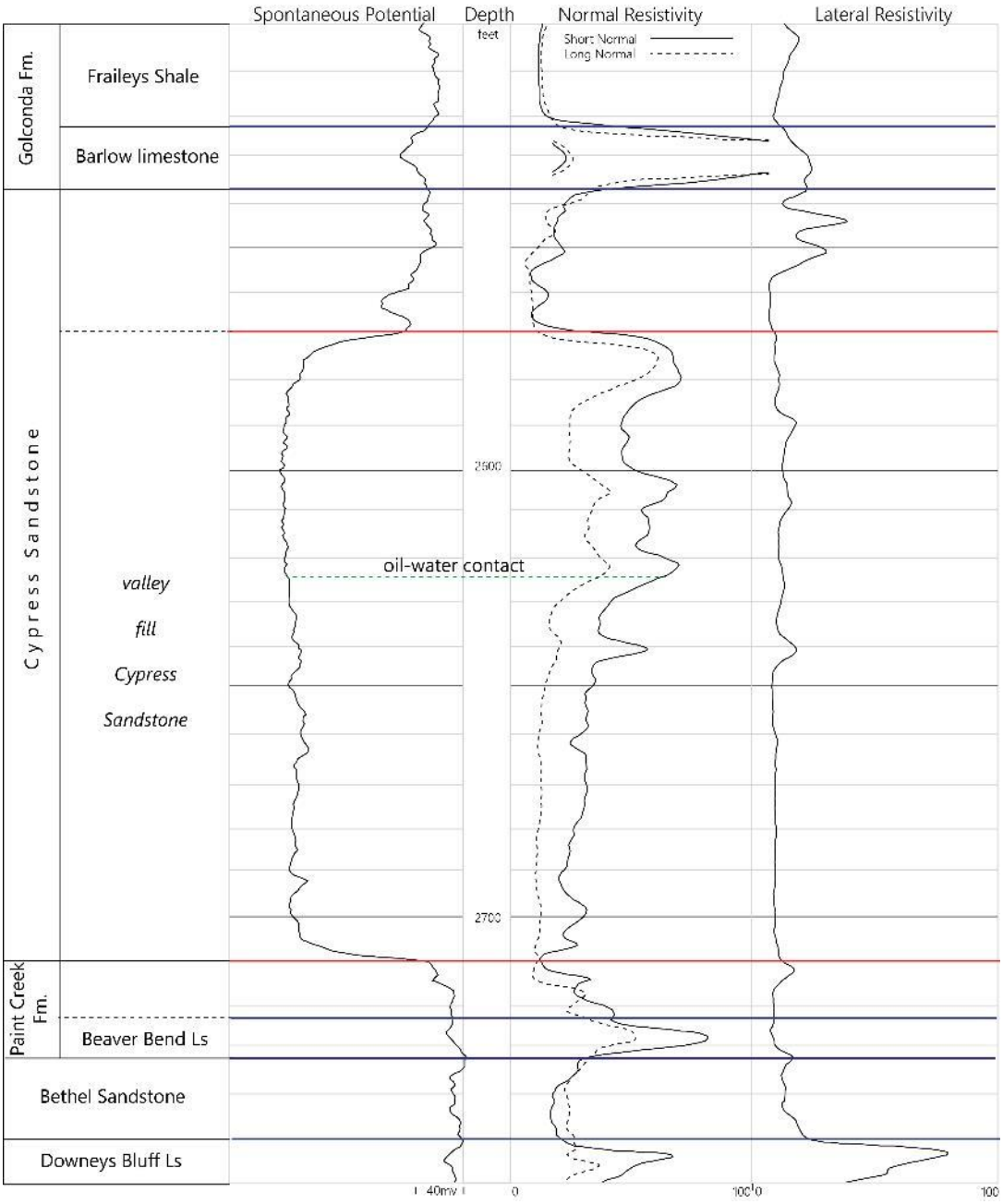

Figure 3.21. Type electric log of the valley fill Cypress Sandstone in Noble Field from the C.T. Montgomery #B-15 well (API 121590140400, southwest of the northwest Section 4, T3N, R9E). The Cypress Sandstone consists of approximately 42.7 m (140 ft) of sandstone overlain by approximately 11 m (35 ft) of shale and shaly sandstone. Roughly 16 m (53 ft) of oil reservoir is developed in the top of the sandstone, as indicated by the resistivity profile and confirmed by sample descriptions on file at the ISGS.

Normalized SP logs were used to derive net thickness data for the Cypress Sandstone. The Fraileys Shale was set as the shale baseline, or 0% clean sandstone (**Figure 3.21**). The 100% clean sandstone SP response was calibrated using the lower, water-saturated portion of the valley fill Cypress Sandstone that had the greatest amount of negative deflection of the SP from the shale baseline. Net sandstone thickness refers to the cumulative thickness of sandstone above a certain normalized SP

value cutoff; 50% has commonly been used in previous Cypress Sandstone studies (Grube, 1992; Grube and Frankie, 1999). Because of the blocky nature of the valley fill Cypress on SP logs, the net/gross ratio of the sandstone in Noble Field is high, with data from 385 normalized SP logs indicating an average of 87% clean sandstone. Thus, the gross isopach map shown in **Figure 3.22** for all practical purposes represents the net (50% clean) sandstone thickness.

The Cypress Sandstone forms an inverted V-shape of two intersecting sandstone trends in the mapped area: one that trends northwest-southeast and one that trends northeast-southwest. The former dominates and is roughly 11 km (7 mi) long and 4.4 km (2.75 mi) wide, narrowing toward the southeast (**Figure 3.22**). The latter, a subordinate northeast-southwest-trending sandstone body, intersects the larger body and is about 2.4 km (1.5 mi) wide. The sandstone reaches a maximum thickness of more than 53.3 m (175 ft) just east of the crest of the Clay City Anticline, in Sections 10, 11, 14, and 15 (T3N, R9E). The sandstone reaches a minimum thickness of approximately 9.1 m (30 ft) along the southern border of the mapped area (**Figure 3.22; Figure 3.18**).

The net sandstone isopach map is a composite of three amalgamated sandstone stories that are stacked in Noble Field. Areas of the map (**Figure 3.22**) where the sandstone thickness drops below roughly 21.3 m (70 ft) indicate one of two things:

1. The upper part of the formation has changed facies to shale, as can be seen in **Figure 3.18**. These shales may represent floodplain/overbank facies, or may represent abandoned, clay-filled channel. A possible, arcuate shaped clay filled channel is shown in **Figure 3.22** in the southern half of the map where the Cypress sandstone is near its thinnest.

2. The valley fill Cypress has broken up into multiple sandstone bodies separated by shales as much as 6.1-9.1 m (20-30 ft) thick. In areas where there are multiple sandstone bodies separated by shales that are tens of feet thick, the isopach only reflects lower, blocky SP sandstone that is hydraulically connected with the valley fill Cypress Sandstone. To the northeast, in Noble North Field, the lower continuous sandstone is overlain by an additional sandstone that can be 9.1-12 m (30-40 ft) thick and, above that, thin lenticular sandstone bodies lie below the base of the Barlow limestone (**Figure 3.19**). Lee (1939) and MGSC (2005) have described the Cypress in this area previously.

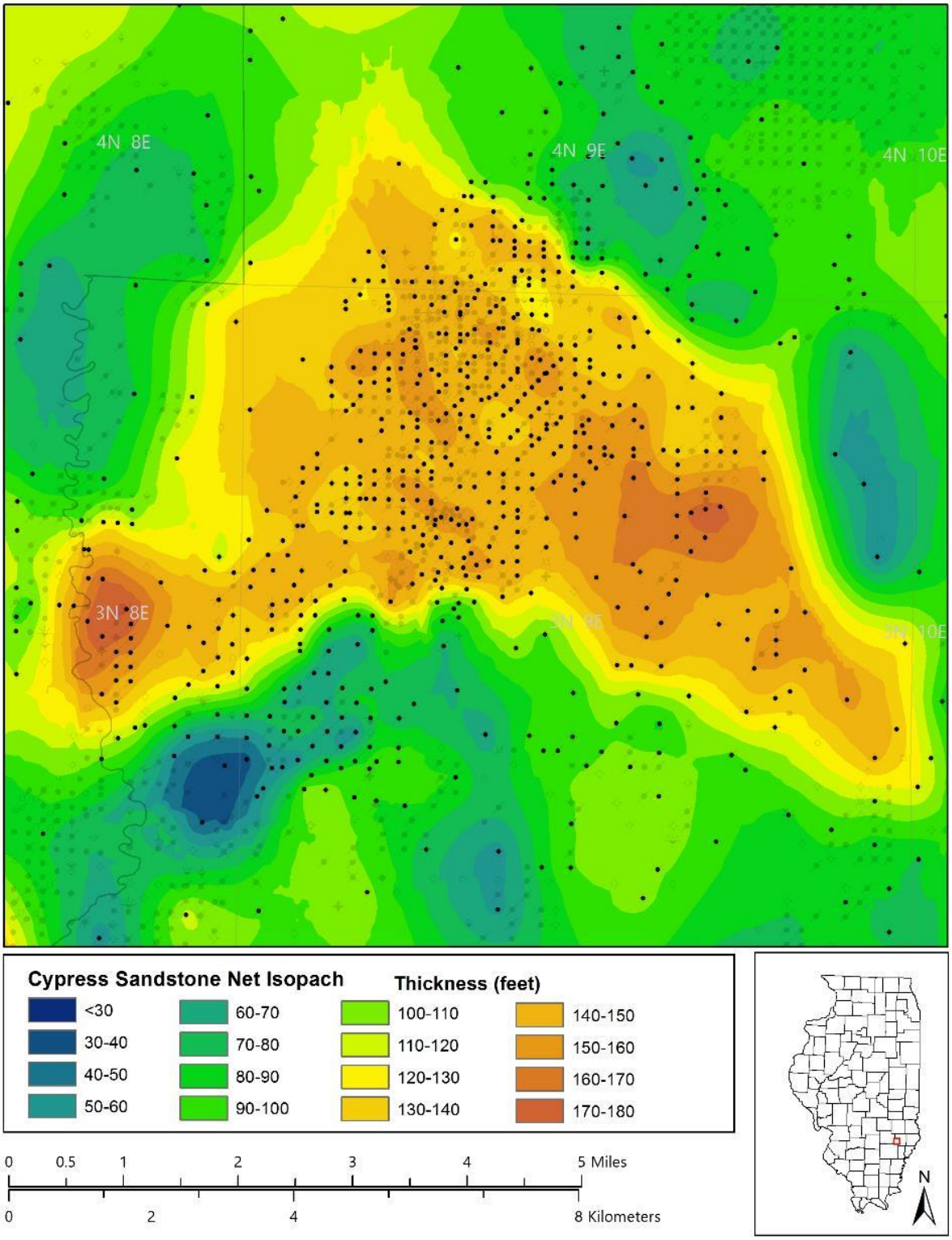

Figure 3.22. Isopach map of Noble Field showing the valley fill Cypress Sandstone. Contour interval is 3 m (10 ft). Map shows an intersecting northwest–southeast and northeast–southwest trending of maximum thickness, which is oblique to the northeast–southwest trend of the overall Western Belt of thick Cypress Sandstone. Data points are shown on the map as black dots.

Volumetric Analysis

Original oil in place (OOIP) was determined for the Cypress Sandstone reservoir at Noble Field. The OOIP value was calculated by using a modified volumetric formula:

$$OOIP = \left(\frac{7{,}758 \times \phi \times (1 - S_w) \times A \times h}{B_{oi}}\right) \times net, \qquad (3.1)$$

Where:

- 7,758 = barrels of oil per acre foot
- Φ = porosity
- S_w = water saturation
- A = area
- h = height
- B_{oi} = formation volume factor
- *net* = the average net/gross ratio within the reservoir as derived from normalized SP logs

Three different approaches were taken to calculate the OOIP to compare traditional methods of calculating OOIP with a model-based approach. The first two used methods based on the traditional volumetric formula. The third used values taken from a three-dimensional geocellular model of the valley fill Cypress Sandstone in Noble Field to be documented in a future report.

For the traditional approaches, the reservoir area (A) was the area within the line that represents the oil-water contact (**Figure 3.23**), and height (h) was the average thickness of the reservoir from the oil-water contact to the top of the Cypress Sandstone. An average porosity of 17.3% was previously determined. Because of the blocky nature of the Cypress Sandstone on geophysical logs, the entire thickness was considered of equal reservoir quality; data from 385 normalized SP logs across the field indicate that the average net/gross ratio within the valley fill Cypress Sandstone was 87%. Thus, the calculated OOIP was multiplied by 87% to get the final OOIP (**Table 3.6**). Two typical values for water saturation (S_w), 30% and 40%, were used to give a range of possible OOIP values.

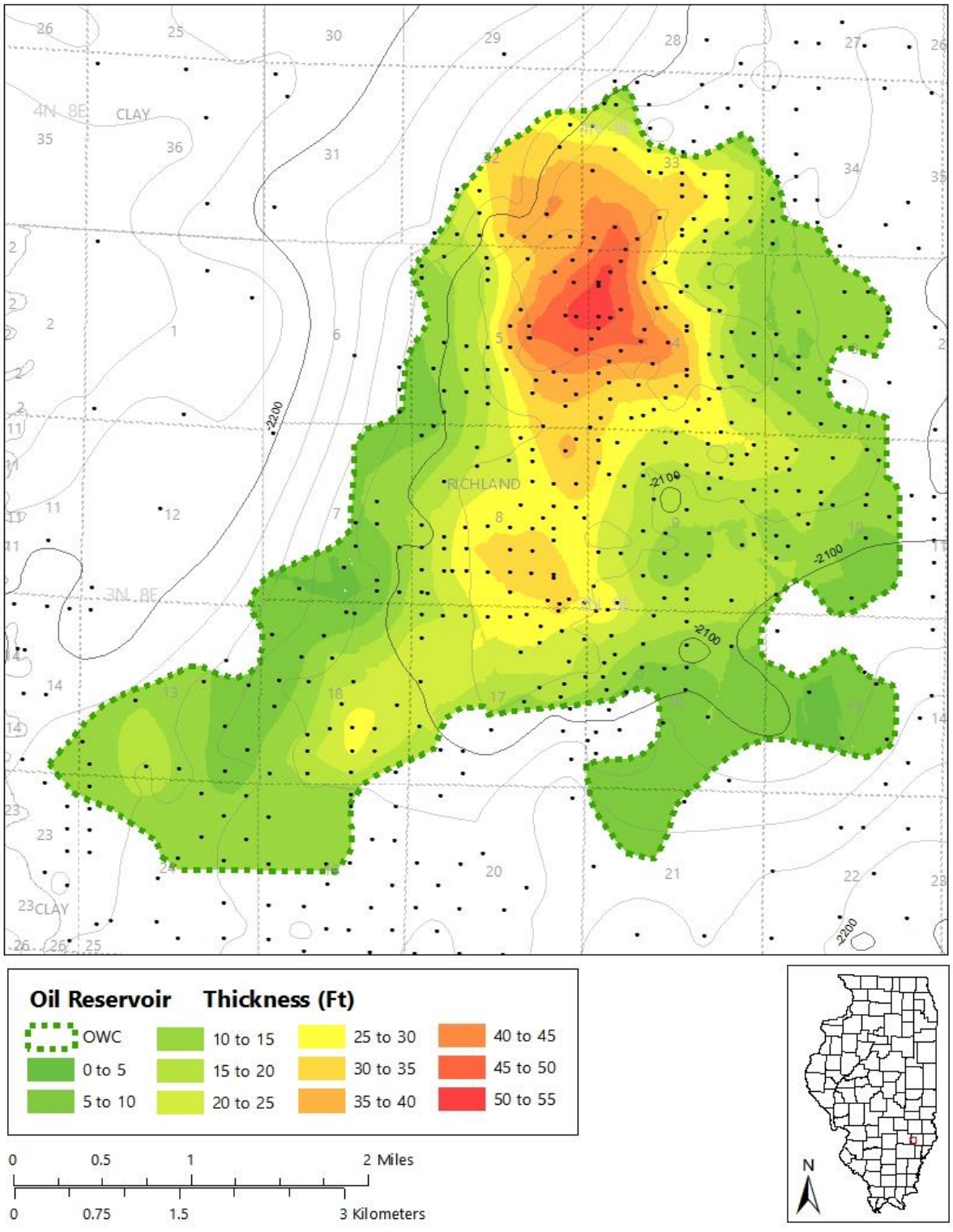

Figure 3.23. Isopach map of the oil reservoir developed in the top of the valley fill Cypress Sandstone. The green dashed line represents the oil-water contact in Noble Field. The thickest oil column coincides with the peak of the structure, as can be seen in the overlaid structure contours of the Barlow limestone. Structural contour interval is 6.1 m (20 ft).

The Cypress Sandstone reservoir is impacted by variable shale content and calcite cement, so a second approach was used to apply a porosity gradient to obtain a refined value for OOIP that perhaps better represents the heterogeneity of the reservoir. The reservoir was divided into 1.5 m (5 ft) thick slices with the volume and average porosity (from porosity logs) calculated for each slice (**Table 3.6**). OOIP was calculated for each slice and summed to determine the final OOIP reported in **Table 3.7**.

Table 3.6. Table of volumetric characteristics of the Cypress Sandstone at Noble Field. Calculations are described in the text.

Noble Field Cypress reservoir volumetric characteristic[1]	Production
OOIP (traditional volumetrics, average porosity, 87% net/gross) =	15.0 to 17.52 million m^3 (94.5 to 110.2 million BBL)
OOIP (traditional volumetrics, porosity gradient) =	14.8 to 17.30 million m^3 (93.3 to 108.8 million BBL)
OOIP (geocellular model-based volumetrics, average porosity) =	14.1 to 16.46 million m^3 (88.7 to 103.5 million BBL)
Mobile OOIP (to water, assuming 25% S_{or}) =	8.68 to 11.1 million m^3 (54.6 to 70.1 million BBL)
Cumulative production =	3.80 million m^3 (23.9 million BBL)
Recovery efficiency =	26.3 to 22.5%
Remaining mobile oil =	4.88 to 7.35 million m^3 (30.7 to 46.2 million BBL)

[1]OOIP, original oil in place; S_{or}, residual oil saturation.

Table 3.7. Area, volume, and average porosity for each 1.7 m (5 ft) slice of the valley fill Cypress Sandstone oil reservoir used to calculate OOIP[1].

Iso contour	Area, ha (acres)	Volume, ha m (acre ft)	Average porosity, %
5	2,798.8 (6,915.8)	4,265.3 (34,579.0)	11.4
10	2,768.9 (6,841.9)	4,219.7 (34,209.3)	14.0
15	2,083.9 (5,149.3)	3,175.8 (25,746.6)	15.5
20	1,415.8 (3,498.5)	2,157.7 (17,492.7)	17.8
25	994.8 (2,458.0)	1,516.0 (12,290.1)	18.3
30	673.3 (1,663.6)	1,026.0 (8,318.2)	17.3
35	415.1 (1,025.6)	632.5 (5,127.8)	17.8
40	229.2 (566.4)	349.4 (2,832.2)	16.5
45	119.5 (295.2)	182.0 (1,475.8)	16.8
50	56.6 (139.8)	86.2 (699.1)	17.8
55	13.7 (33.9)	20.9 (169.3)	17.1

[1]*The iso contour column indicates the base of the slice, measured in feet below the top of the reservoir.*

A third alternative calculation of OOIP was conducted using values of the reservoir volume (reservoir area [A] × reservoir height [h]) and average porosity (Φ) determined from a three-dimensional geocellular model created in Isatis software by Geovariances. The surface elevations for the top of the valley fill Cypress Sandstone and the oil-water contact used in the geocellular model were the same as

those used in the traditional volumetric calculations. This permits comparison of the modeling and traditional approaches to determine OOIP.

The formation volume factor (B_{oi}) of 1.06 for an oil sample from the Coen #23 well (API 121590138200, Section 4, T3N, R9E) was used to convert the volume of oil in the reservoir to the volume of produced oil at the surface. Volume loss was attributable to degassing of the oil at atmospheric pressure. As with the traditional volumetric calculations, two typical values for S_w, 30% and 40%, were used in the model calculations to give a range of OOIP values.

The resulting OOIP values derived from traditional- and model-based volumetrics are listed in **Table 3.7**. The OOIP calculated by the modeling approach yielded a lower value, likely due to the model's ability to better incorporate localized, log indicated zones of low-quality reservoir (e.g., shaly or cemented sandstone zones that are not represented in core plug data). In other words, the model better honors all the data where the traditional approaches tend to generalize the data, and in this case, are probably overly optimistic. The average reservoir porosity calculated from the geocellular model was 12.6%, which is nearly 5% lower than core plug data used in the traditional calculations.

Mobile OOIP is a calculation of the portion of oil that can be removed above residual oil saturation (S_{or}). The mobile OOIP value was calculated using the standard volumetric formula:

$$Mobile\ OOIP = \{7758 * \phi * [1 - (S_o - S_{or})] \times A \times h\}/B_{oi} \quad (3.2)$$

Where:

- A, h, and B_{oi} are defined the same as in the OOIP equation
- S_o = oil saturation
- S_{or} = residual oil saturation

Recovery efficiency was calculated using the average of the two OOIP values derived from the porosity gradient method and the geocellular model method. Residual oil saturation (S_{or}) into water was assumed to be 25% (MGSC, 2005). The remaining mobile oil is the difference of cumulative production from mobile OOIP.

The results of the volumetric calculations show that the three methodologies for calculating OOIP produced comparable results, with an average estimated OOIP of 15.9 million m^3 (100 million bbl) of Cypress oil. With cumulative production of 3.8 million m^3 (23.9 million bbl), more than 11.9 million m^3 (75 million bbl) of oil remains in the reservoir, of that an estimated 4.9 to 7.4 million m^3 (30.7 to 46.2 million bbl) is movable oil.

3.3.2 Kenner West Field

Introduction

Although Kenner West was not an initial candidate study site for this project, the discovery of ample core and production data made the field an attractive study site for geologic characterization. Kenner West Field, located in southwestern Clay County, Illinois, is approximately (8 km (3.5 mi) north of Xenia, Illinois. The field mainly occupies Section 23, T3N, R5E (**Figure 3.24**). Kenner West was discovered in February 1947 by the Phillips Petroleum Company (Bell and Kline, 1948). The discovery well, the Spiker #1 well (API 120250250200, southeast ¼ of the southwest ¼ Section 23, T3N, R5E), had an initial production of 15.1 m^3 (95 bbl) of oil and 11.1 m^3 (70 bbl) of water from the Cypress Sandstone. Other oil

producing formations in Kenner West Field include the Yankeetown (Benoist) Sandstone, and Ste. Genevieve (McClosky) Limestone.

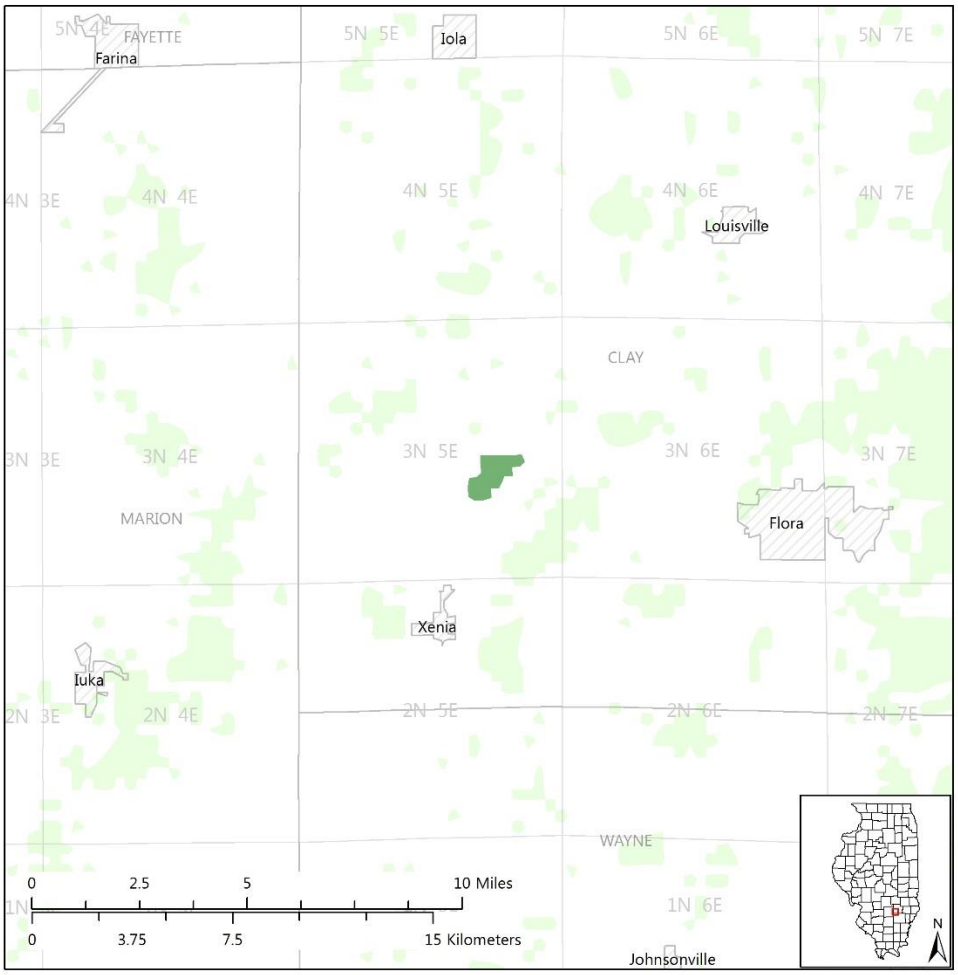

Figure 3.24. Index map showing the location of Kenner West Field, shaded in dark green, in southwestern Clay County. Township lines are shown in gray and are labeled, and municipalities are shown in gray crosshatch.

Stratigraphy

Kenner West Field lies north of the Fairfield Basin, the central deep portion of the ILB, and is situated within the central part of the northeast-southwest trending axis of the thick Cypress Sandstone fairway (**Figure 3.1**). Kenner West Field is located on a satellite dome west of the Kenner Anticline, both of which are situated on a terrace of a southeast facing homocline that dips down into the Bogota-Rinard Syncline (Nelson 1995). A regional structure map contoured on the top of the Barlow limestone (**Figure 3.25**) shows the location of Kenner West Field with respect to these structural features.

The structure of the Kenner West dome was mapped on two horizons; the map constructed on the base of the Barlow limestone is shown in **Figure 3.26**. The dome was found to be slightly elongated NE-SW and has a diameter of about 2.4 km (1.5 mi) with a closure of around 12.2 m (40 ft). A NE-SW trending saddle separates the Kenner West dome from the Kenner Anticline to the southeast.

As with Noble Field, Kenner West Field exhibits a typical Chesterian succession (**Figure 3.13**). The Yankeetown (Benoist) Sandstone is an oil reservoir in the field, occurring at a depth of around 832.1 m (2,730 ft). 6.1-9.1 m (20-30 ft) of shaly, coarsening upward Benoist sandstone is indicated on geophysical logs. A regional study of the Benoist sandstone indicates that its thickness in Kenner West Field should average around 6.1-9.1 m (20-30 ft) of net clean sandstone (Leetaru et al. 2005). About 3 m (10 ft) or less of shale commonly separates the top of the Benoist sandstone from the overlying Downeys Bluff Limestone marker bed. The Downeys Bluff Limestone forms a widely traceable marker bed that reaches a maximum thickness of 2 m (6 ft) but is commonly only a few feet thick. In the northern part of the field, the succession between the base of the Cypress Sandstone and the top of the Benoist sandstone becomes shaly and the Downeys Bluff Limestone becomes difficult to identify on logs by its typical high resistivity peak. Above the Downeys Bluff Limestone, the Bethel Sandstone interval is commonly represented by 6.1-9.1 m (20-30 ft) of shale.

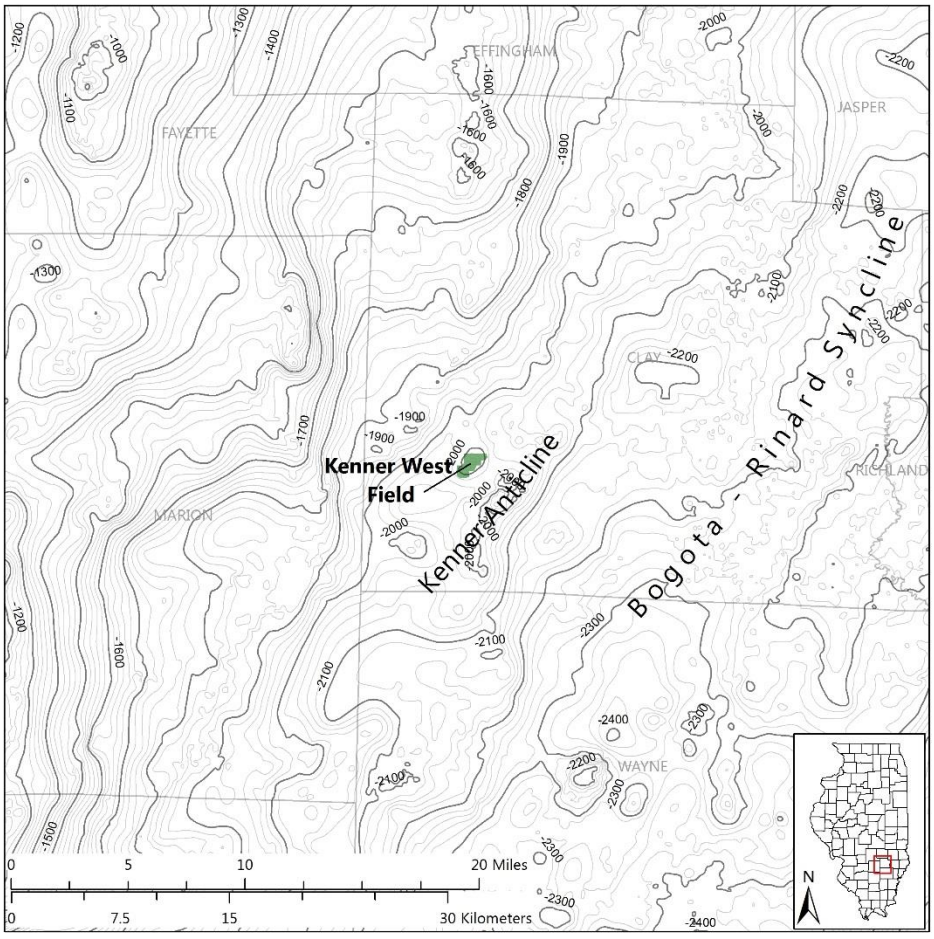

Figure 3.25. Structure map contoured on the subsea elevation of the base of the Barlow limestone. Contour interval is 6.1 m (20 ft) with 30.5 m (100 ft) index contours darkened and labeled. Kenner West Field (shaded in green) is located just west of the Kenner Anticline. Nearby structural features are labeled.

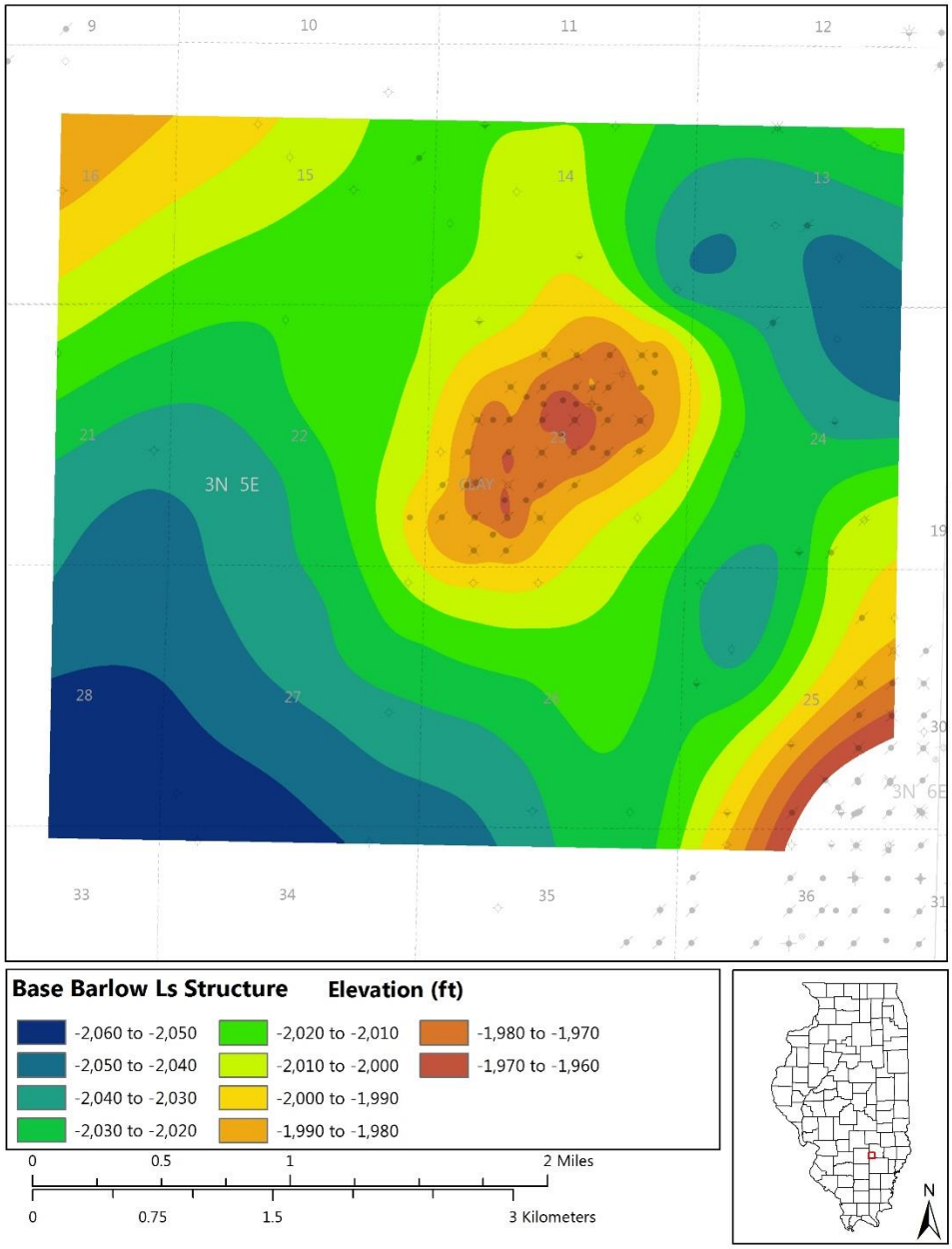

Figure 3.26. Map of Kenner West Field showing structure on the base of the Barlow limestone. Contour interval is 3 m (10 ft) with contours color coded.

The Ridenhower Formation overlies the Bethel Sandstone interval and consists generally of shale and sandstones. Over much of the field, the formation consists of approximately 6.1 m (20 ft) of shale. However, in some areas, the formation contains up to about 12.2 m (40 ft) of sandstone. The lithologic variability of the formation can make the contact between the Ridenhower and the Cypress Sandstone difficult to identify, but the base of the Cypress Sandstone generally exhibits a thin spike of higher resistivity (**Figure 3.27**), making it distinguishable from the underlying sandstones.

The Cypress Sandstone in Kenner West Field consists of a thick, lower sandstone overlain by shales and shaly sandstone (**Figure 3.27**). The lower sandstone is well developed and laterally persistent, with a generally blocky appearance on spontaneous potential (SP) or gamma ray logs. The lower sandstone forms a generally N-S trending, somewhat sinuous sandstone body that passes through Kenner West Field and is about 1.6 km (1 mi) wide. The thickness of this sandstone is consistently about 24.4-30.5 m (80-100 ft) within Kenner West Field but thins considerably to the northwest and southeast outside of the field to about 15.2 m (50 ft) or less. Above the thick, lower sandstone and below the base of the Barlow limestone is a 12.2-15.2 m (40-50 ft) thick interval that contains a lower shale, middle shaly sandstone, and upper shale that divide the interval into thirds (**Figure 3.27**).

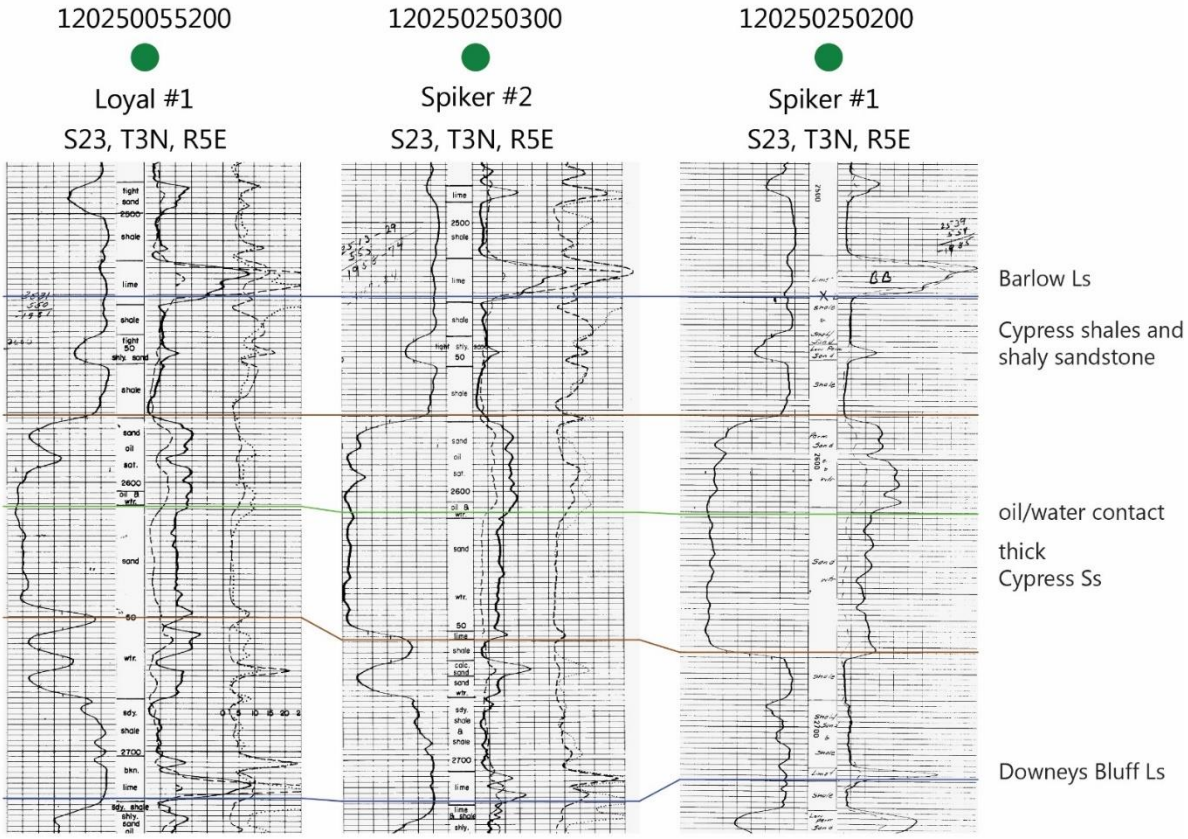

Figure 3.27. Representative west-east cross section showing the typical characteristics of the thick Cypress Sandstone in Kenner West Field.

Reservoir Characteristics

Geometry and Isopach Maps

Maps of the thick Cypress Sandstone at Kenner West Field were developed based on geophysical well log correlations. The primary geophysical logs available for correlation and evaluation were 1940s to 1970s era electric logs with SP and resistivity curves (generally long normal, short normal, and lateral resistivity) and some additional wells with recent induction logs, which included gamma ray, SP, and induction resistivity traces. Neutron-density porosity logs were also generally available for these

wells. Roughly 80 wells were used to map the thick Cypress Sandstone within the study area. The top and base boundaries of the thick Cypress Sandstone were determined from geophysical logs and the resulting thickness of the sandstone was mapped (**Figure 3.28**).

Thickness data for the Cypress Sandstone were derived from normalized SP logs. The shale baseline, or 0% clean sandstone, for normalizing the SP logs was established by using the consistently flat-line response of the Fraileys Shale. The 100% clean sandstone SP response was calibrated using the water-saturated portion of the Cypress Sandstone that had the greatest amount of SP deflection from the shale baseline. The gross sandstone thickness refers to the thickness between the top and base of the entire thick Cypress Sandstone body and may include thin intercalated shales or shaly sandstone intervals. Net sandstone thickness refers to the cumulative thickness of sandstone above a certain normalized SP value cutoff; 50% has been a commonly used value for previous Cypress Sandstone studies (Grube, 1992; Grube and Frankie, 1999). Because of the blocky nature of the thick Cypress Sandstone on SP logs, the net-gross ratio of the sandstone in Noble Field is nearly 100%; data from 24 digitized and normalized SP logs indicate an average of 86% clean sandstone. Thus, the isopach map shown in **Figure 3.28** is a gross isopach of the thick Cypress Sandstone that, for all practical purposes, serves as a net sandstone, where the net is greater than 50% clean sandstone above the shale baseline.

The Kenner West Field is 5.6 km (7.5 mi) north of the Xenia East Field that was previously studied by Xu and Huff (1995). The geology of the two fields is somewhat similar, as the ~1.6 km (~1 mi) wide north-south trending belt of thick Cypress that passes through Kenner West proceeds south to and is hydraulically connected to Xenia East Field. The thickness and continuity of this trend was previously shown on an isopach map of the lower thick sandstone by Chapman (1953). In Kenner West Field, the upper part of this sandstone is oil saturated, with up to 10.7 m (35 ft) of reservoir and an oil-water contact at roughly -626.1 m (-2,054 ft) (**Figure 3.29**). At Xenia East, the top of the thick sandstone has an elevation of -622.7 m (-2,043 ft). If the two fields shared an oil-water contact, the thick Cypress Sandstone at Xenia East should have around 3 m (10 ft) of oil saturation in the top, but logs indicate that it is water saturated. The main difference between the geology of the two fields is that Xenia East has a thin (4.6 m (15 ft)) clean sand above the lower thick Cypress Sandstone that is oil saturated. An equivalent sandstone at Kenner West is of similar thickness, but logs indicate it is much shalier and not of reservoir quality and is not oil bearing.

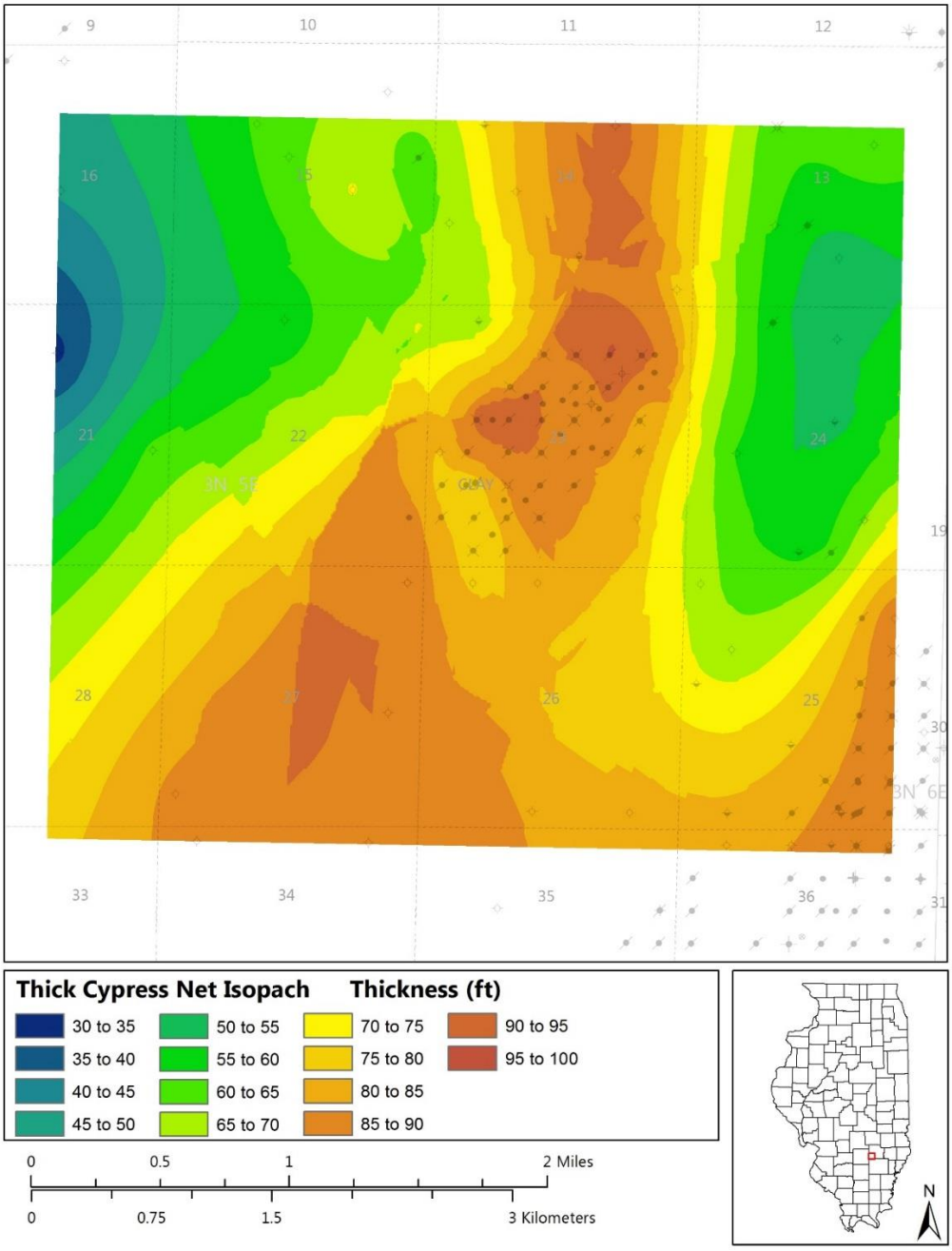

Figure 3.28. Isopach map of Kenner West Field showing thickness of the lower, thick Cypress Sandstone body. Contour interval is 1.5 m (5 ft). Map shows a slightly sinuous north-south trending sandstone body, which is aligned with the trend of the overall thick Cypress Sandstone fairway.

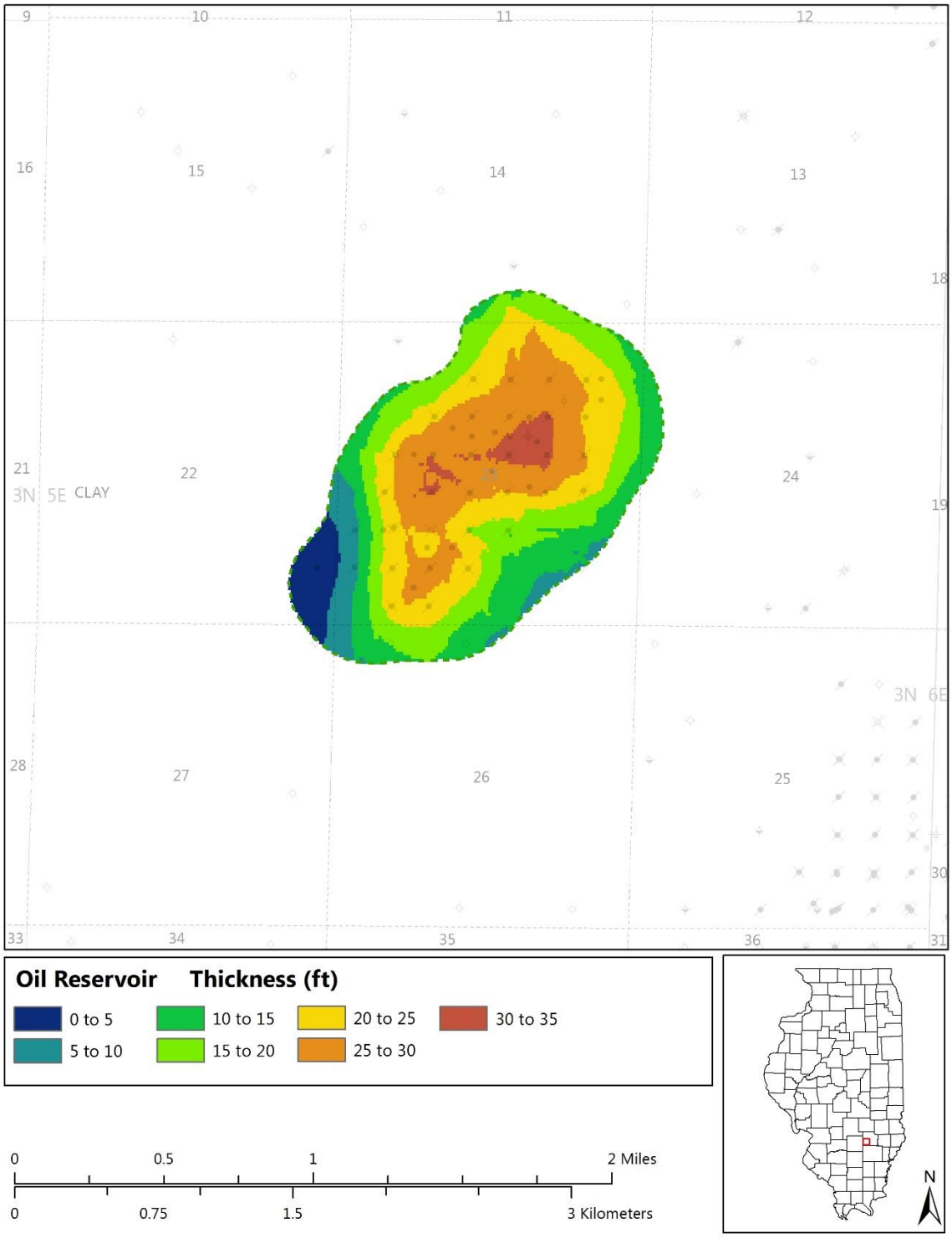

Figure 3.29. Isopach map of the oil reservoir developed in the top of the thick Cypress Sandstone. The green dashed line represents the oil-water contact in Kenner West Field. The thickest oil column coincides with the peak of the structure.

Volumetric Analysis

OOIP was determined for the oil reservoir in the thick Cypress Sandstone at Kenner West Field using the equation described in Section 3.3.1. The reservoir area (*A*) was determined using GIS by calculating the area within the contour line that represents the oil-water contact (**Figure 3.29**), which was found to be 261 ha (644 acres). The height (*h*) of the reservoir was calculated by taking the average thickness of the reservoir from the oil-water contact to the top of the thick Cypress Sandstone and was found to be 5.9 m (19.4 ft). A 17.75% porosity value, derived from the mean of core plug-measured porosities within the reservoir portion of the thick Cypress Sandstone in several wells within Kenner West Field, was used. Because of the blocky nature of the thick Cypress Sandstone on geophysical logs, this entire thickness was of equal reservoir quality; data from 24 normalized SP logs across the field indicates that the average net to gross ratio within thick Cypress Sandstone is 86%. The calculated OOIP was thus multiplied by 86% to get the final OOIP (**Table 3.8**). Two typical values for water saturation (S_w), 30% and 40%, were used to give a range of possible OOIP values.

There are no records from oil sampling and analysis within Kenner west Field; but samples from the southwest Clay County area indicate a typical formation volume factor (B_{oi}) of 1.05. This value was used to convert the volume of oil in the reservoir to the volume of produced oil at the surface with volume loss attributable to degassing of the oil at atmospheric pressure. Two typical values for S_w, 30% and 40%, were used to give a range of possible OOIP values. The resulting OOIP values are listed in **Table 3.8**.

Recovery efficiency was calculated using the average of the two OOIP values derived from the porosity gradient method and the geocellular model method. Residual oil saturation (S_{or}) to water was assumed to be 25% (MGSC, 2005). Remaining mobile oil is the difference of cumulative production from mobile OOIP.

Table 3.8. Table of volumetric characteristics of the Cypress Sandstone at Kenner West Field. Calculations are described in the text.

Kenner West Field Cypress Reservoir	
OOIP (traditional volumetrics, average porosity, 86% net:gross)=	1.4 to 1.6 million ($m^3$8.5 to 9.9 million bbl)
Cumulative production=	0.2 million m^3 (1.3 million bbl)
Recovery efficiency=	13.2 to 15.4%

3.3.3 Loudon Field

Introduction

Loudon Field, located in Fayette County, is one of the largest oil fields in Illinois, having produced approximately 63 million m^3 (398 MMbbl) of oil through 2009. ISGS data indicate that 2,939 wells have been drilled up to 2009, commonly on 4-ha (10-acre) spacing. Loudon Field has eleven separate geologic horizons that have recorded production (See **Figure 3.13** for reference). Nine of these are Mississippian age, including the siliciclastic Cypress, Bethel, Benoist, Paint Creek, Renault, Aux Vases, Spar Mountain, and Carper, and the McClosky Limestone. The Cypress Sandstone is commonly the thickest, most widespread and prolific reservoir in the field. Devonian Grand Tower and Ordovician Kimmswick (Trenton) formations are also productive. A focus on the stratigraphic aspects of the Cypress Sandstone are reviewed and included in this field report.

The field is located on the western structural flank of the ILB and coincides with the western edge of the central basin thick Cypress Sandstone (**Figure 3.1**). Cypress Sandstone reservoirs are

generally at a drilling depth of less than 487.7 m (1,600 ft) and therefore are not miscible candidates for CO_2-EOR. The ROZ potential of the field was not evaluated. Only the southern 31 km^2 (12 mi^2) of the 119.1 km^2 (46 mi^2) field were studied. Geophysical well log data from 178 wells, 135 of which included the entire Cypress sections, were employed. There are 836 wells recorded in the study area. Research of this area shows that variations of the depositional setting create a heterogeneous character of the sandstone depositional units that limit reservoir continuity. The field was studied because the Cypress Formation at Loudon is at the western margin of the basin depocenter where the Cypress shows stratigraphic variations that are useful for depositional analysis of the central basin stratigraphy and help refine Cypress conceptual geologic modeling.

Reservoir Characteristics

Geometry and Isopach Maps

The depositional setting in which the Cypress Sandstone reservoir sediments were deposited in the study area appears to be uncomplicated, while the characterization of the reservoir depositional environments and their relationship is more complex. An isopach map (**Figure 3.30**) of the entire Cypress interval shows the thickness of the sedimentary section from the base of the overlying Barlow limestone to the base of the basal scour contact with the underlying Paint Creek Formation or older underlying units depending on the extent of the Cypress incision. This contact is considered regionally unconformable. Thickness of the Cypress sediments which include sandstone, mudstone, shale, and minor carbonates range from 17.4-32.0 m (57-105 ft) within the oil field portion of the study area. Immediately east of the present anticlinal structure and trending southwest, the Cypress interval thickens to at least 54.9 m (180 ft) where the incised contact shows scouring deeper into the units underlying the Paint Creek. This thick trend continues to the southwest of the anticline.

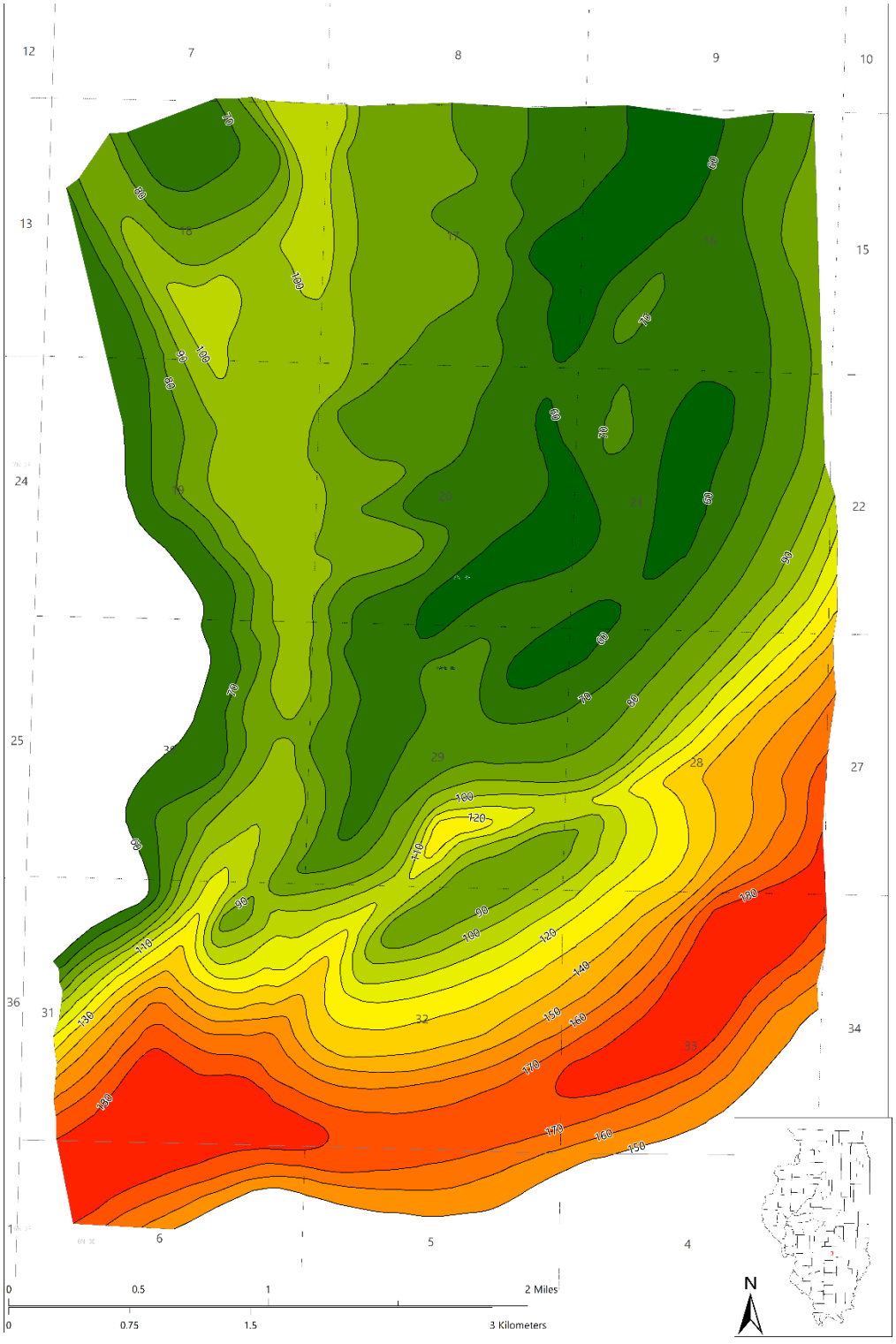

Figure 3.30. Isopach map of the Cypress interval showing the thickness of the sedimentary section from the base of the Barlow limestone to the base of the basal scour contact with the underlying Paint Creek Formation or older underlying units depending on extent of the Cypress incision.

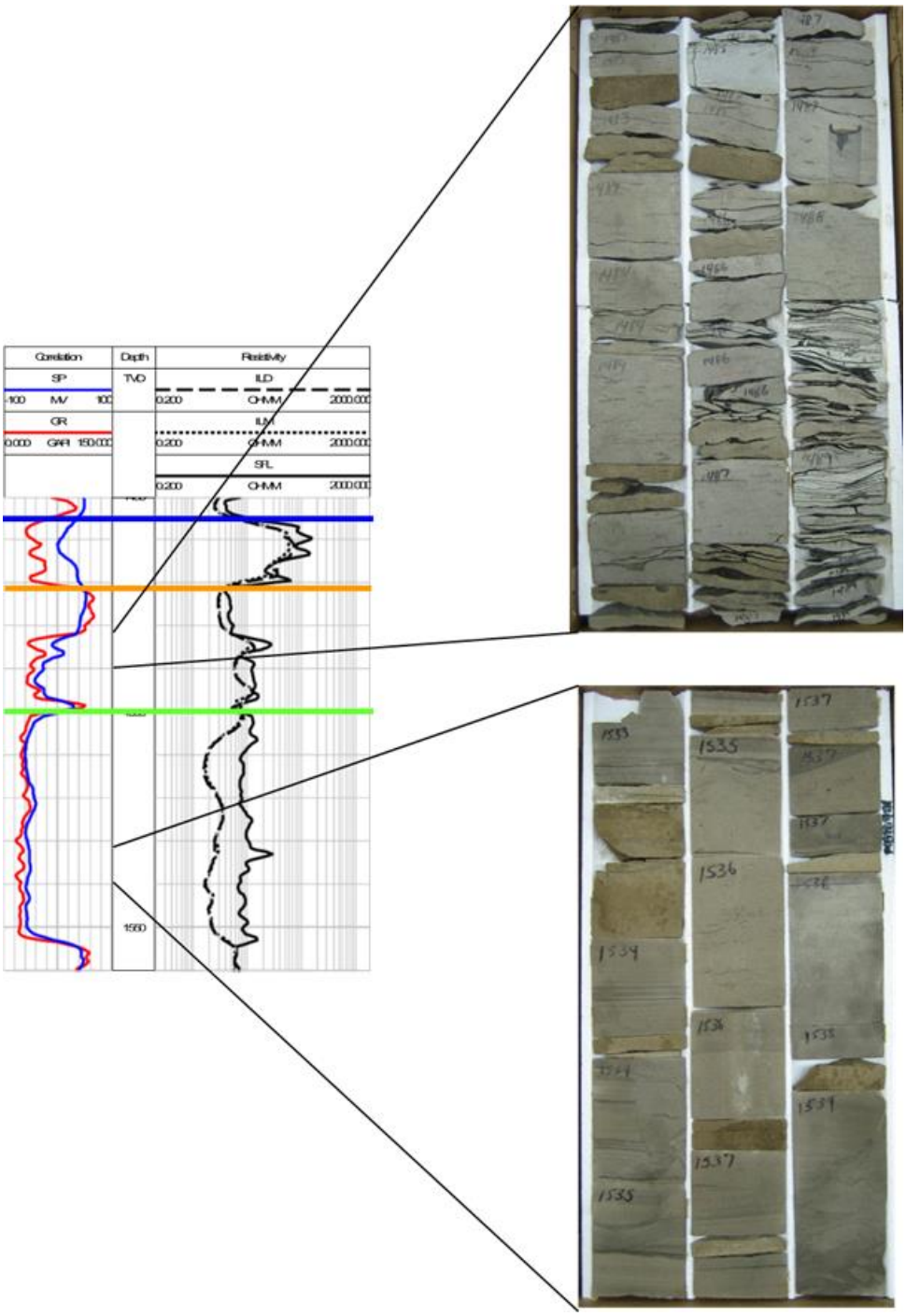

Figure 3.31. Geophysical well log from the Heckert #902 well (API 120512572400), SE SW NW Section 20-T7N-R3E, with core from the Cypress Sandstone. The lower core is the channel facies with subtle rhythmite bedding that indicates possible tidal influence in this channel facies. The upper core is the tidal bar facies with tidal couplets (rhythmites), mostly in the right two columns. Note that the spontaneous potential (SP) trace (blue) of the blocky channel facies shows a more consistent and "cleaner," less muddy, sandstone response than the tidal bar facies. The uniform response and separation of the resistivity traces (right-black) of the channel facies indicate a uniform, permeable, and porous reservoir character while the tidal bar facies indicates a lower capacity and more heterogeneous reservoir. The Barlow limestone is the high resistivity, upper 4.6 m (15 ft) of the log.

An incised valley pattern is evident on the Cypress isopach map (**Figure 3.30**) as shown by a north-south, thick trend through Sections 17, 18, 19, 20, 29, and 30 (all in T7N-R3E). Thickness of the Cypress sediments within the trend are 24 to 32 meters (80 to 105 feet). This valley merges in Section 31-T7N-R3E with the more deeply incised valley that borders the field to the east and extends southwest around the south end of Loudon Field. Thickness of the Cypress within the valley that borders the field ranges up to 200 feet. Well logs show that blocky, channel-like sandstone is the dominant facies that is deposited in this valley and particularly the valley bordering the field.

A north-south to southwest trending Cypress thin separates the area between the two valley trends on the Cypress isopach map. This isopach thin is between 15.8 and 21.3 m (52 and 70 ft) thick and forms a ridge roughly a 0.8 km (0.5 mi) wide bordering the line between Sections 16 and 17, and Sections 20 and 21. It is truncated by the incised valley at the south end of the field.

The stratigraphy of the Cypress Formation within the study area can be complex and change over short distances. Two prominent sandstone reservoir facies associated with the incised valley are recognized. The first facies within the central valley is a blocky sandstone, 6.1-15.2 m (20-50 ft) thick that is prevalent in Sections 19, 20, 29, and 30. A blocky character on geophysical logs and the occurrence within the central valley position, indicate that these are channel fill sandstones. Wells with a Cypress interval thickness greater than 24.4 m (80 ft) commonly display a channel facies in the central valley, particularly in the southern area of the valley. Flow direction of this channel is to the south where it merges with the more prominent channel system.

A section of core with the well log from the Heckert #902 well (**Figure 3.31**) shows the character of the blocky channel facies from the incised valley in Section 20. There are subtle tidal rhythmites in the Heckert channel facies core suggesting that this blocky channel facies was deposited within the tidal influenced portion of a tidal delta system.

A second major reservoir sandstone facies that is both within and flanks the central valley shows elongated, lenticular bar geometries when mapped (Finley, 2009). Other oil fields within the Illinois Basin have similar log characteristics that display elongate bar geometries (Grube, 1992, Grube and Frankie, 1999). Cores from stacked Cypress tidal bar reservoirs that have this geometry at Lawrence Field, Lawrence County, Illinois on the eastern flank of the Basin show tidal couplets and reversed bedding that are tidal indicators (Seyler and Grube, 2012). An electric log (**Figure 3.32**) from the Lawrence Field Baltzell #N-23 well shows the log character of stacked tidal bars like those observed on the cross section at Loudon Field (**Figure 3.33**). The log character from this facies has an irregular spiked or sawtooth appearance that is attributed to muddy sandstone deposition interlayered between the tidal bars. **Figure 3.34** is an example of the elongate tidal bar geometry from interval D at Lawrence Field. These elongate bars coalesce laterally and appear as a complex bar configuration in plan view. Individual tidal bars are typically 0.6-3 m (2-10 ft) thick. Multiple bars commonly stack, making correlation of individual bars difficult. Therefore, defining the geometry of an individual bar is challenging. Bars can vertically coalesce and become thicker than 3 m (10 ft), appearing blocky or channel-like on well logs. This causes the well log character of the bars and channels to appear similar and therefore difficult to distinguish. on logs. he individual bars themselves, by the nature of their tidal dominated, turbid water deposition, are not homogeneous clean sandstones as shown by the Heckert core. The tidal bar facies at Loudon Field is shown in the upper 6.1 m (20 ft) of a core from the Heckert

#902 well in Section 20 (**Figure 3.31**). Tidal couplets are observed in the center and right columns of this core.

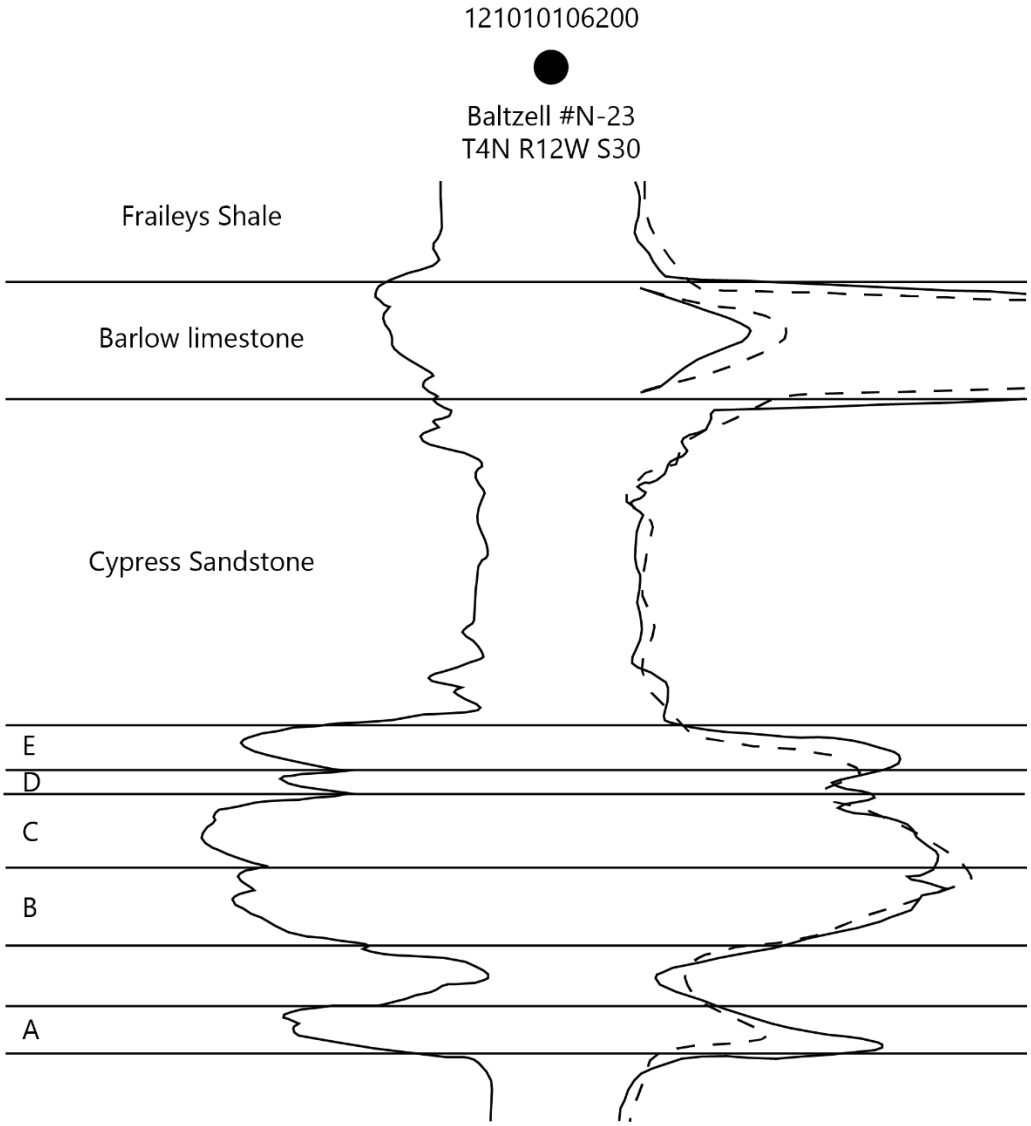

Figure 3.32. Baltzell #N-23 well log, SE NW of Section 30, T4N R12W from Lawrence Field showing Cypress Sandstone stacked tidal bars intervals "A" through "E". Note the log similarity of the tidal bar character at Lawrence Field to those in the Figure 3.33 cross section of the Owens #1 well and the Morrison wells at Loudon Field. The individual Cypress sandstone intervals have lenticular, tidal bar geometry where each bar may act as a discreet reservoir flow unit. Characteristic of the Cypress section is a 10-foot genetic thickness tendency of units that is probably a function of accommodation space, and the rates of deposition vs. subsidence in cratonic basins. These intervals commonly coalesce which may show up as thicker units. The "10-foot rule" can be very useful tool for correlating these thinly bedded units in cratonic settings. Modified from Seyler et al., 2012.

Research at Loudon Field for an experimental huff' n' puff CO_2 injection test in the Cypress Sandstone using the Owens #1 well (API 120510266800) included correlating and generating isopach

maps of individual tidal bars in the vicinity of the well (Finley, 2009). Individual bars form as elongate sandstone bodies that coalesce into larger bodies up to 80.9 ha (200 acres) in extent and trend northeast-southwest. Thin shale or shaly sandstones layers between these stacked bars compartmentalize the reservoirs into multiple, poorly connected flow units. A well log of the Owens well is included within a cross section showing the Cypress Sandstone interval (**Figure 3.33**). The well is in the northwest quarter of Section 20, 0.8 km (0.5 mi) north of the Heckert #902 well.

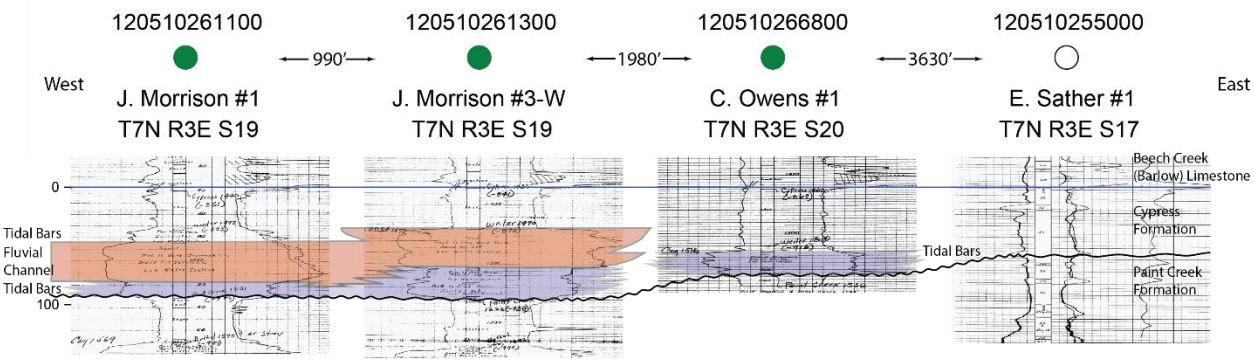

Figure 3.33. A 1.25-mile-long, east-west, four well, electric log cross section showing examples of the stratigraphic characteristics typical in Loudon Field.

Starting from east to west, the Sather #1 (120510255000) well on the cross section shows the thin Cypress ridge interval that separates the two channel fairways located on either side of the central ridge displayed on the isopach map. The section traverses west from the ridge area into the incised valley. The Sather #1 well consists of minor sandstones and muddy sandstone. Cypress sediments in the ridge well are 16 feet thinner than the Owens #1 well to the west. The Owens log shows the character of the Cypress stacked, sawtooth tidal bars but has no channel sandstone. West of the Owens is the Morrison #3-W well (API 120510261300) with 7.9 m (26 ft) of tidal bars at the base, 10.1 m (34 ft) of channel, and no tidal bars at the top. The Morrison #1 well (API 120510261100), a ten-acre (4-ha) offset well west of the Morrison #3-W, has 3.7 m (12 ft) of tidal bar at the base, 10.1 m (34 ft) of channel, and 3m (10 ft) of tidal bar overlying the channel. Not included in the cross section is an offset well about 518.1 m (1,700 ft) north of the Morrison wells, the Burtschi #15 well (API 120510150800). It is mentioned because it shows mostly tidal bars, 11.3 m (37 ft) at the base, 2.1 m (7 ft) of muddy sandstone, capped by a 2.4 m (8-ft) channel or possible tidal bar, all within the same stratigraphic interval as the Morrison wells. Other nearby wells show only tidal bars throughout this correlative interval. The location of reservoir facies varies appreciably over short distances within this valley, particularly the tidal bar facies. Channels overlying tidal bars would not be expected during sea level rise and transgression. Sea level variation, channel avulsion or migration, and floods are possible events that may account for this complex stratigraphy. The basic assumption of the depositional model in a transgressive setting is that ultimately, tidal bars, if present, should onlap and override the channels. This is the more prevalent relationship apparent at Loudon.

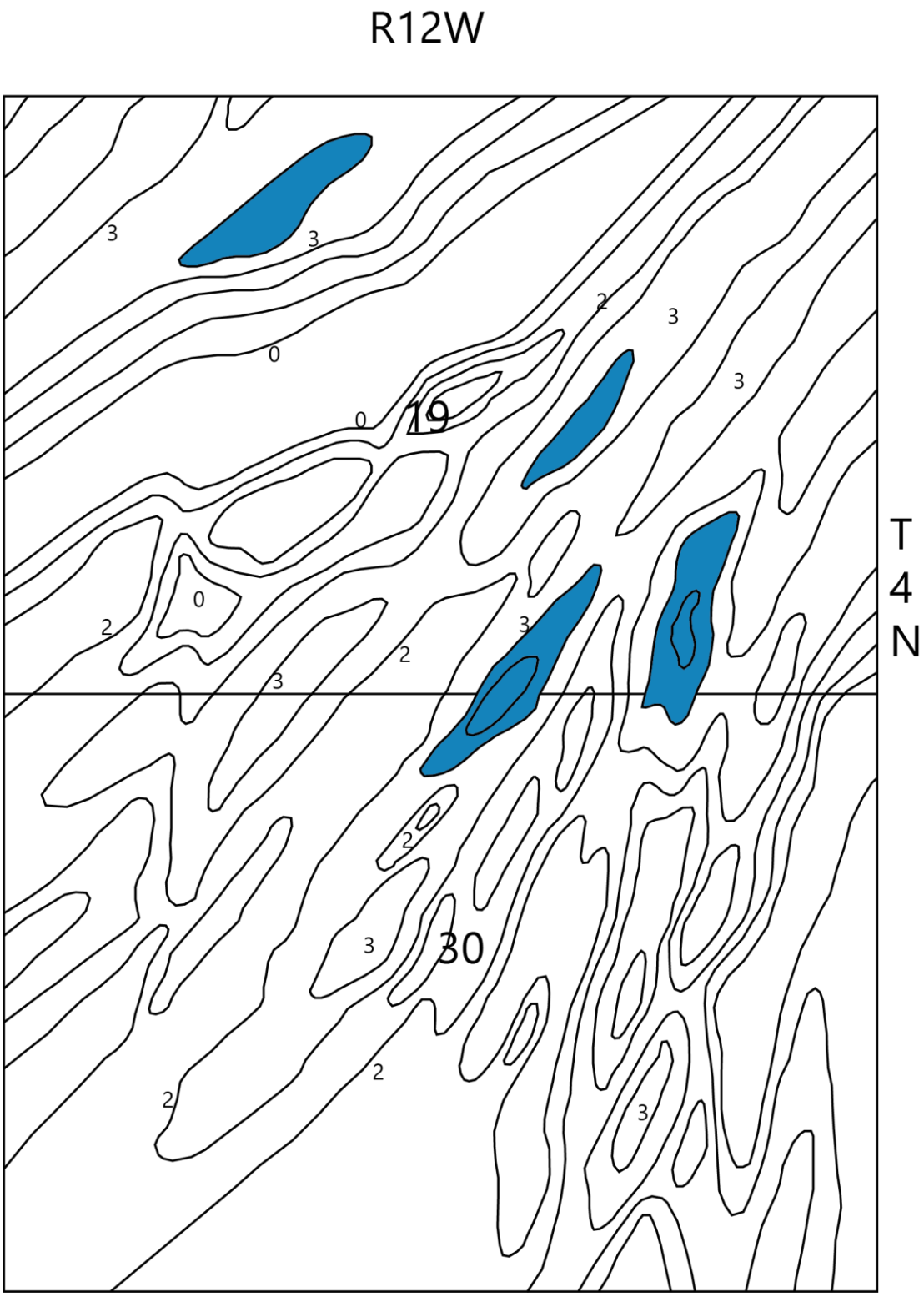

Figure 3.34. Cypress interval D isopach map from Sections 19 and 30, T4N-R12W Lawrence Field showing the geometry, trend and coalescing characteristic of tidal bars that are like those at Loudon Field. (C.I. 1 m (3 ft)). Modified from Seyler et al., 2012.

3.4 Regional Characterization of the Cypress Sandstone

Although the Western Belt of thick Cypress Sandstone appears as a discrete fairway of thick sandstone on the regional map (**Figure 3.1**), it is important to understand that the thick sandstones exist in a complex, three-dimensional architecture with other facies within the Cypress Formation. The following section describes the complexity of the geology and compartmentalization of the Cypress Sandstone across the region that plays a role in the modern configuration of oil reservoirs, potential ROZs, and CO_2 storage targets of the Cypress Sandstone.

3.4.1 Stratigraphic Variability and Lithofacies

Across the Illinois Basin region, the Cypress Formation underlies the Barlow limestone; it overlies the Ridenhower Shale that commonly consists of shale or interbedded shale, limestone, and sandstone (**Figure 3.35**). The boundaries of Cypress with the overlying Barlow and the underlying Ridenhower are generally conformable. However, in places thick Cypress sandstone cut into Ridenhower and a persistent paleosol horizon is present near the top of Cypress recording subaerial unconformities (Nelson et al., 2002; and described in Section 3.2).

The lateral and vertical lithofacies variations of the Cypress Formation across the Clay City Anticline are shown in the geophysical log cross-sections AA' and BB' (**Figure 3.36**). The Cypress varies from interbedded shale and lenticular sandstone bodies (**Figure 3.36** cross section AA' well 1 and cross section BB' well 6) - to dominantly sandstone facies within the Western Belt thick Cypress capped by shale or interbedded shale and sandstone interval (**Figures 3.35 and 3.36**, cross sections AA' wells 2 through 7 and cross section BB' well 1 through 5). In the eastern part of the study area, southeast of the Clay City Anticline, the Cypress consists dominantly of shale with thin sandstone or siltstone beds (**Figure 3.37**).

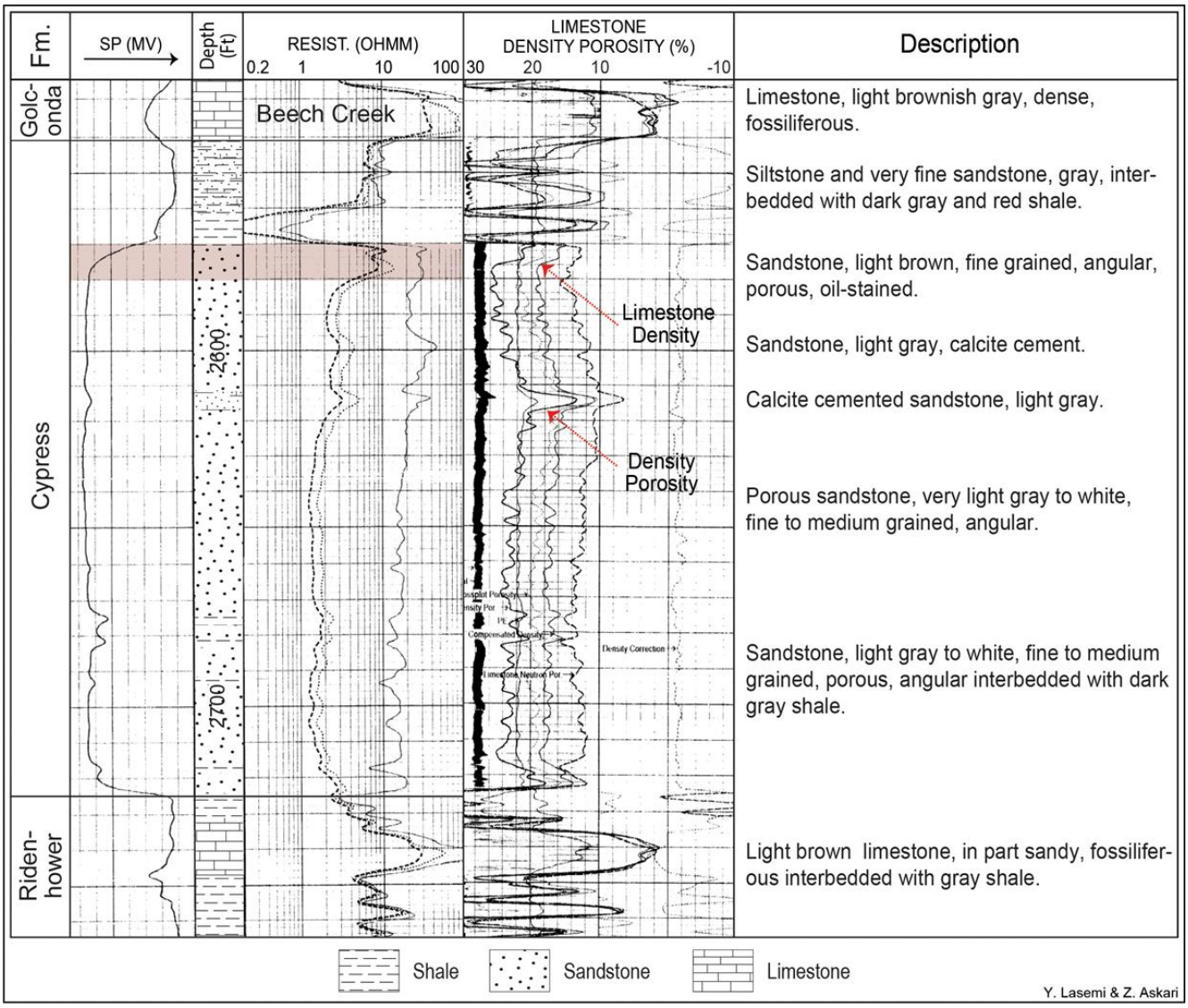

Figure 3.35. Type log of the Cypress Formation in Richland County (API 121592624800) showing stratigraphic column and sample desacription of the Cypress and the bounding formations. Note that the Cypress consists mainly of amalgamated sandstone bodies showing bell and barrel shaped log signatures capped with shale partings/thin shale beds. Note the oil saturated productive interval (in brown) in the upper part of the thick Cypress.

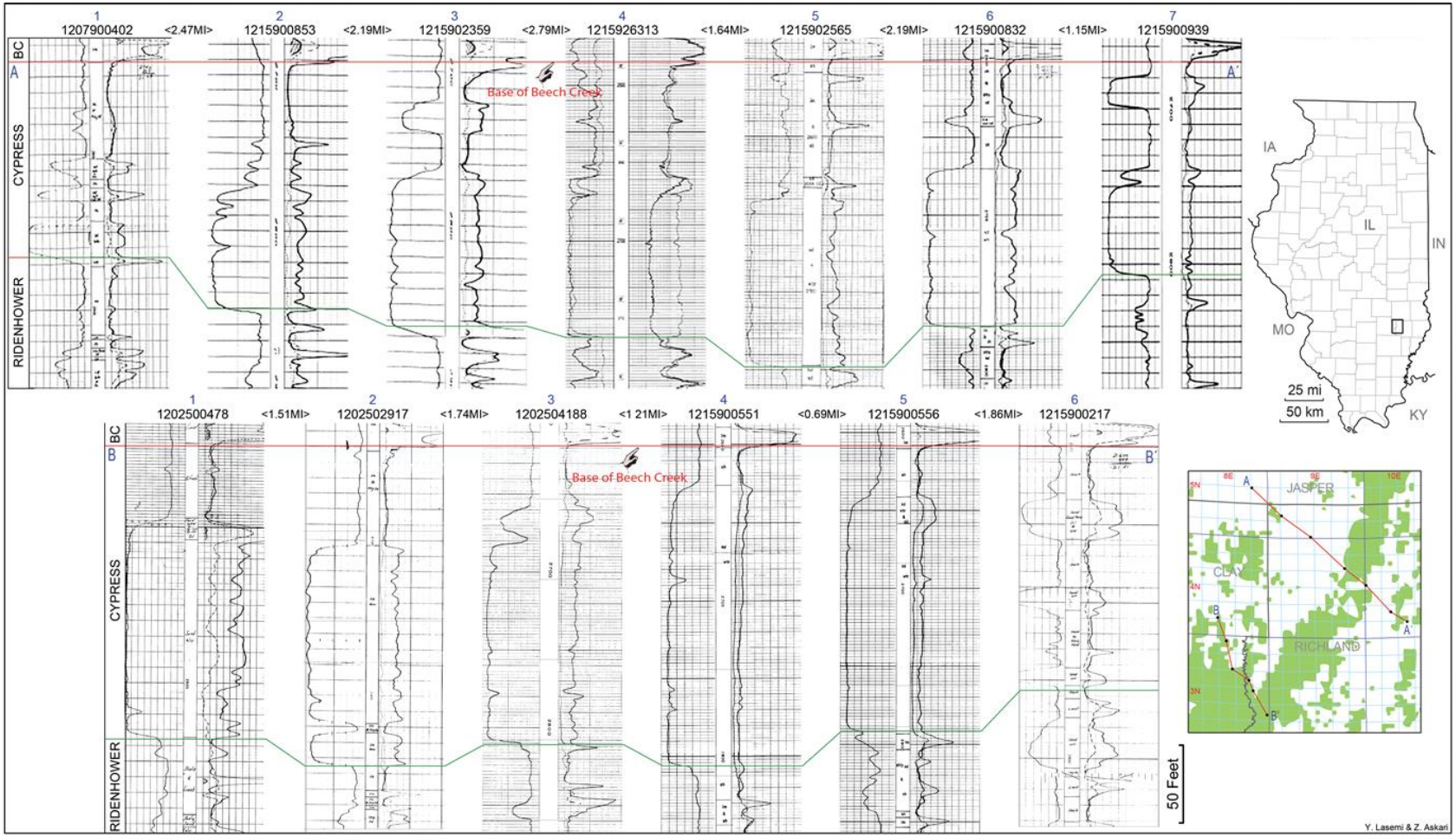

Figure 3.36. Geophysical log cross sections AA' and BB' across the Clay City Consolidated Field showing lateral and vertical variation of the Cypress deposits. Note the uneven erosional topography of the lower boundary of the formation. The Cypress varies from interbedded shale and lkenticular sandstone bodies (cross ection AA' well 1 and cross section BB' well 6 to dominantly sandstone facies, the thick Cypress, capped by shale or interbedded shale and sandstone interval (cross sections AA' wells 2 through 7 and cross section BB' well 1 through 5).

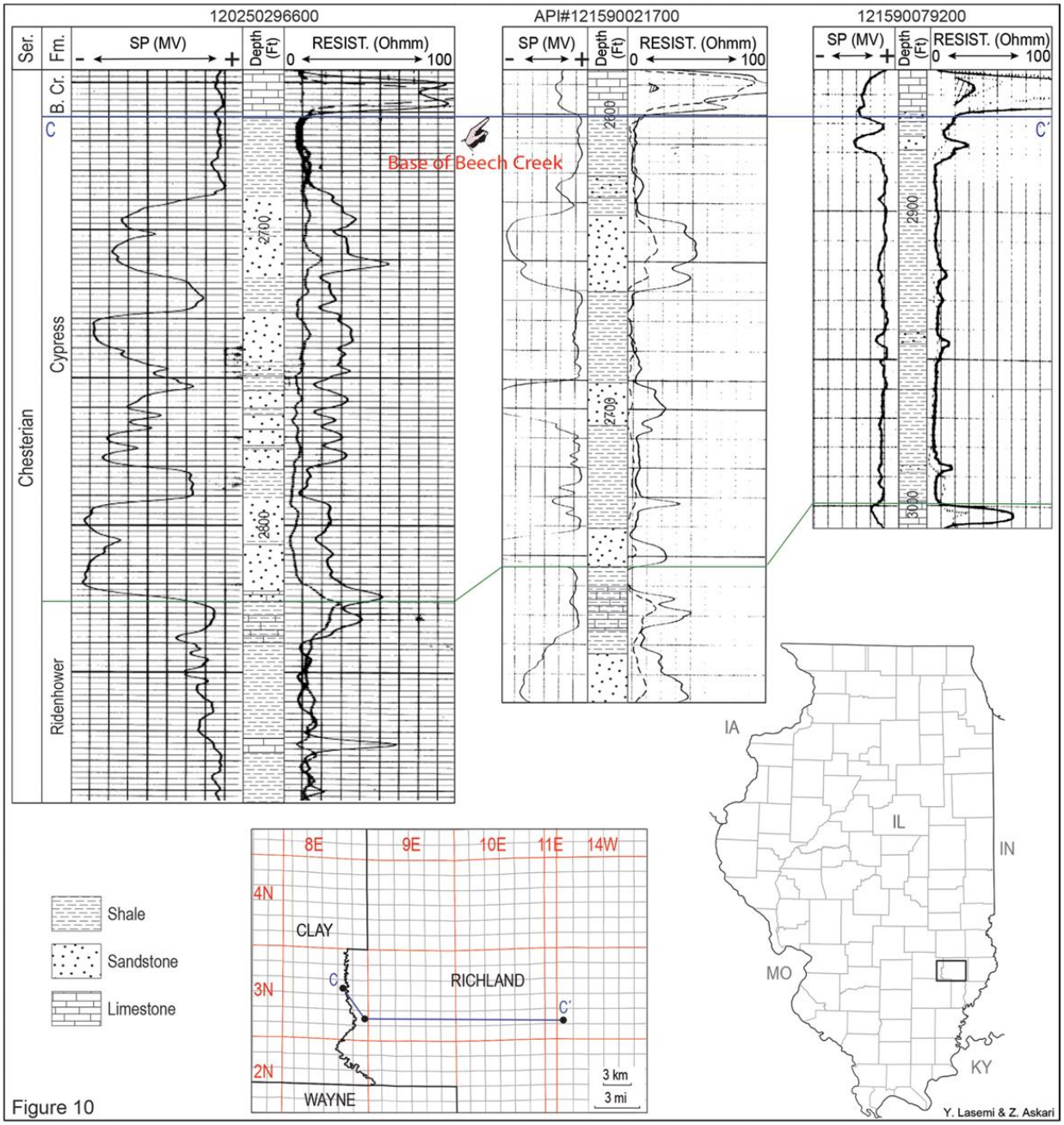

Figure 3.37. Geophysical log cross section CC' showing stratigraphic variability of the Cypress strata. Note interbedded shale and sandstone in the west and dominantly shale with thin sandstone or siltstone beds in the east of the study area, southeast of the Clay City Anticline.

In places, the middle sandstone intervals coalesce with the lower Cypress thick sandstone forming a much thicker amalgamated sand body over 45.7 m (150 ft) thick due to the absence of shale beds or presence of very thin intervening shale partings (for examples see wells 4 and 5 in cross section BB, **Figure 3.36**). The thick Cypress Sandstone of the Western Belt is characterized by stacked sand bodies commonly displaying cylindrical shape geophysical log signature (e.g., **Table 3.4**) in which sand bodies are separated by thin shale beds or shale partings (**Figure 3.35**). In these sandstones, cylindrical shape geophysical log signature may change to bell shape near the top of the succession due to presence of shale partings or interbedded shale and sandstone (see basal part of Cypress in well 6, cross section AA', **Figure 3.36** for an example).

Cypress sandstone intervals are characterized by a rather high compositional maturity consisting of quartzarenite, sublitharenite, and subarkose (Pitman et al., 1998). The lower Cypress sand bodies commonly are

cross bedded (e.g., Nelson et al., 2002; Howell, 2017) and consist of sorted, subangular- to rounded fine grained quartzose sandstone with grains showing evidence of a recycled origin. They consist of less than 10% minor components, including opaque minerals and feldspars with signs of dissolution and alteration to clay minerals (**Figure 3.38B, C**). Locally calcite cement may partially occlude pore spaces (**Figure 3.38C**). A thin layer (about 1 m (2 ft) thick of dense, calcite cemented sandstone is present in the upper part of the stacked sandstone body in some locations (**Figure 3.35**) in which quartz grains are partially replaced by calcite (**Figure 3.38D**). Quartz cement overgrowth showing signs of erosion is present on a few sand grains (**Figure 3.38C**).

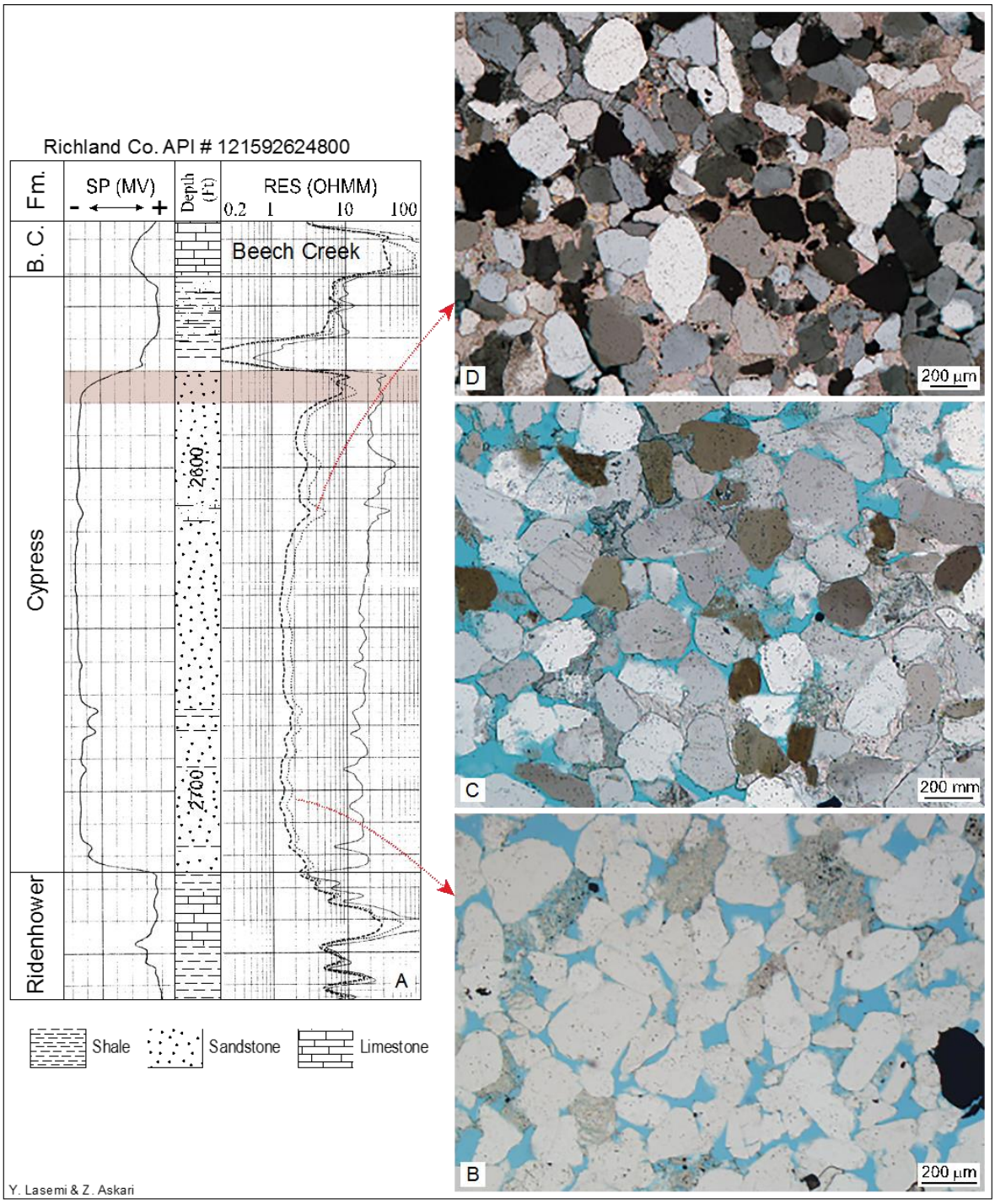

Figure 3.38. Type log of Figure 3.61 A) and photomicrographs of the Cypress stacked sandstone bodies showing subangular- to rounded quartzose sandstone (pore space in blue). B) Photomicrograph under plain light; opaque minerals (black) and altered feldspars (gray) with signs of dissolution. C) Same as B under polarized light. Note partial calcite cementation in the lower right. Note also evidence of erosion on quartz cement overgrowth in a few grains. D) Dense calcite cemented quartzose sandstone under polarized light showing loss of porosity due to calcite cementation and partial replacement of quartz by calcite.

The lenticular sand bodies in the interbedded shale and sandstone intervals in the middle and upper part of Cypress may display bell shape (fining upward) or funnel shape (coarsening upward) gamma ray and SP

log signatures (**Figures 3.36 and 3.39A**). Sandstone beds with finning upward profiles may consist of fine grained, angular to subrounded, submature sandstone (**Figure 3.39B**), although the presence of mature quartzose sandstone with fining upward motif cannot be rolled out. Mature sandstone intervals with coarsening upward motif are recognized (**Figure 3.39C**). They may be quartz cemented (**Figure 3.40B**) showing hetrolithic stratification with herringbone and hummocky cross lamination/cross bedding (**Figure 3.40C**). Sandstone intervals with coarsening upward log signature may also consist of submature quartzose sandstone.

The Cypress Sandstone intervals are generally porous (**Figures 3.35, 3.38B, C, and 3.39**) with both primary intergranular and secondary dissolution porosities present (**Figures 3.38B, C, and 3.39B**). Reservoir permeability of up to 0.77 μm^2 (780 mD) has been reported. Average reservoir porosity using core data and porosity logs were determined to be about 16%. However, reservoir porosity may reach to over 20% in some areas. Original porosity was reduced because of post depositional compaction and cementation by calcite (**Figure 3.38C**), silica (**Figure 3.39C**), and clay minerals. The clay minerals in the Cypress sandstone reservoirs includes kaolinite, chlorite, illite, and illite/smectite mixed layered clays (Rehak, 2014; Webb et al., 2016). Net sandstone thickness map of massive and lenticular sandstones in the study area reveals sandstone thickness in the range between 3-49 m (10-160 ft) (**Figure 3.41**) and displays southwest trending paleovalleys for the Cypress Formation.

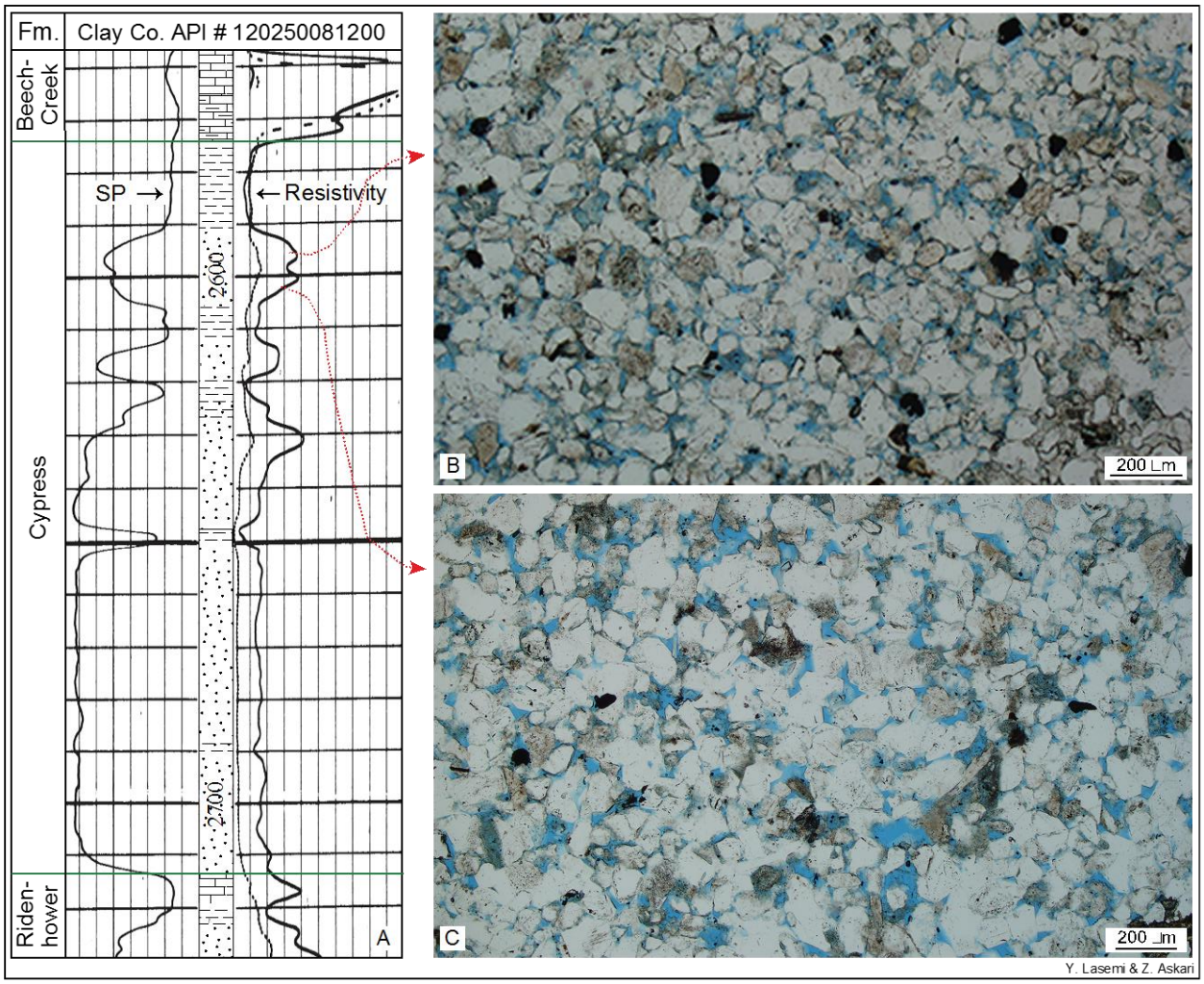

Figure 3.39. A type log in Clay County showing stratigraphic column and photomicrographs of core samples of a lenticular sandstone in the upper part of the Cypress Formation (for lithologic symbols, see Figure 3.64).

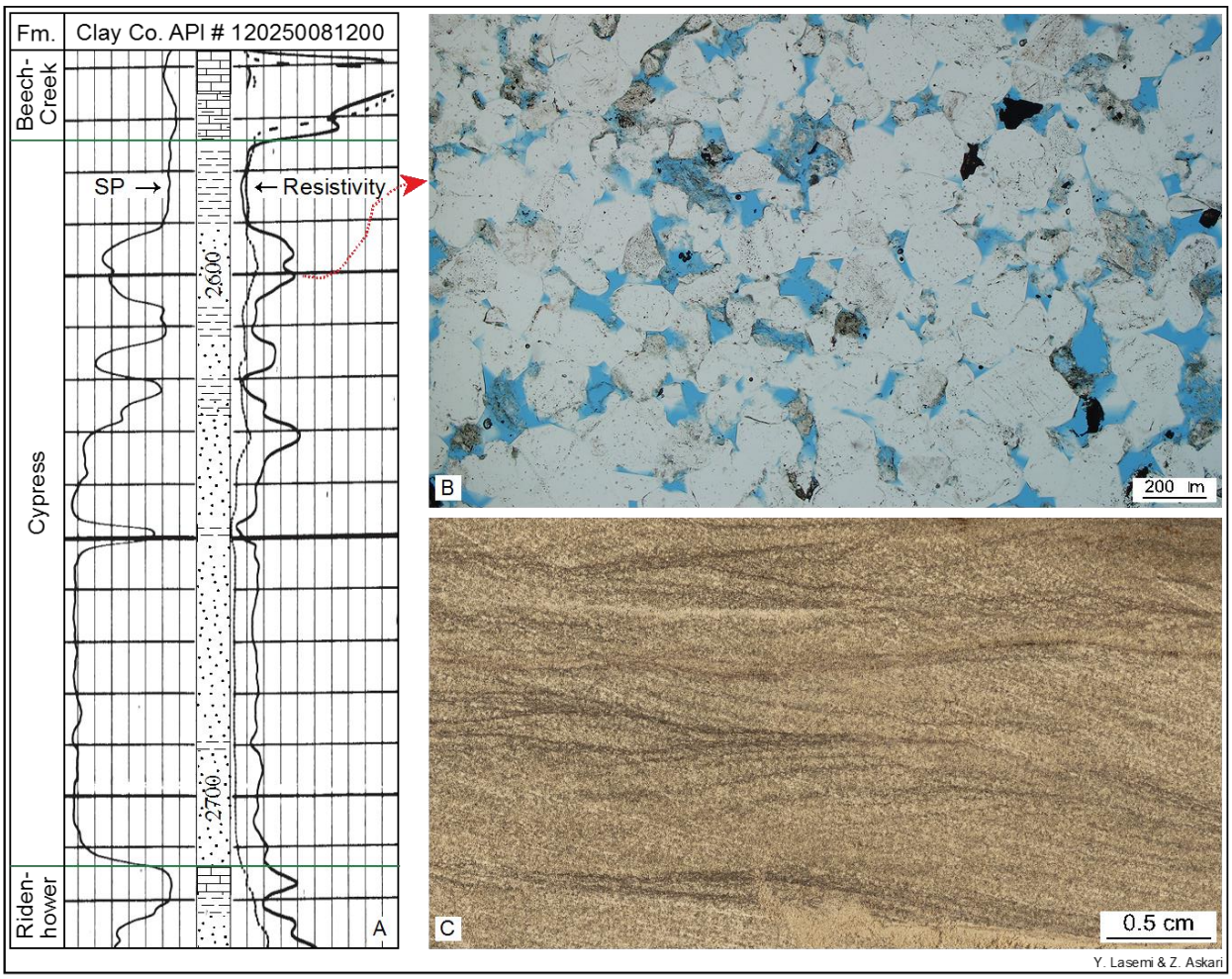

Figure 3.40. Same as Figure 3.65 showing enlarged portion of photomicrograph in Figure 3.65C and core sample of the same interval. Note quartz overgrowth cement on quartz grains in B. Photograph C is the core sample (core diameter is 6.35 cm (2.5 in) showing heterolithic stratification and bidirectional cross lamination.

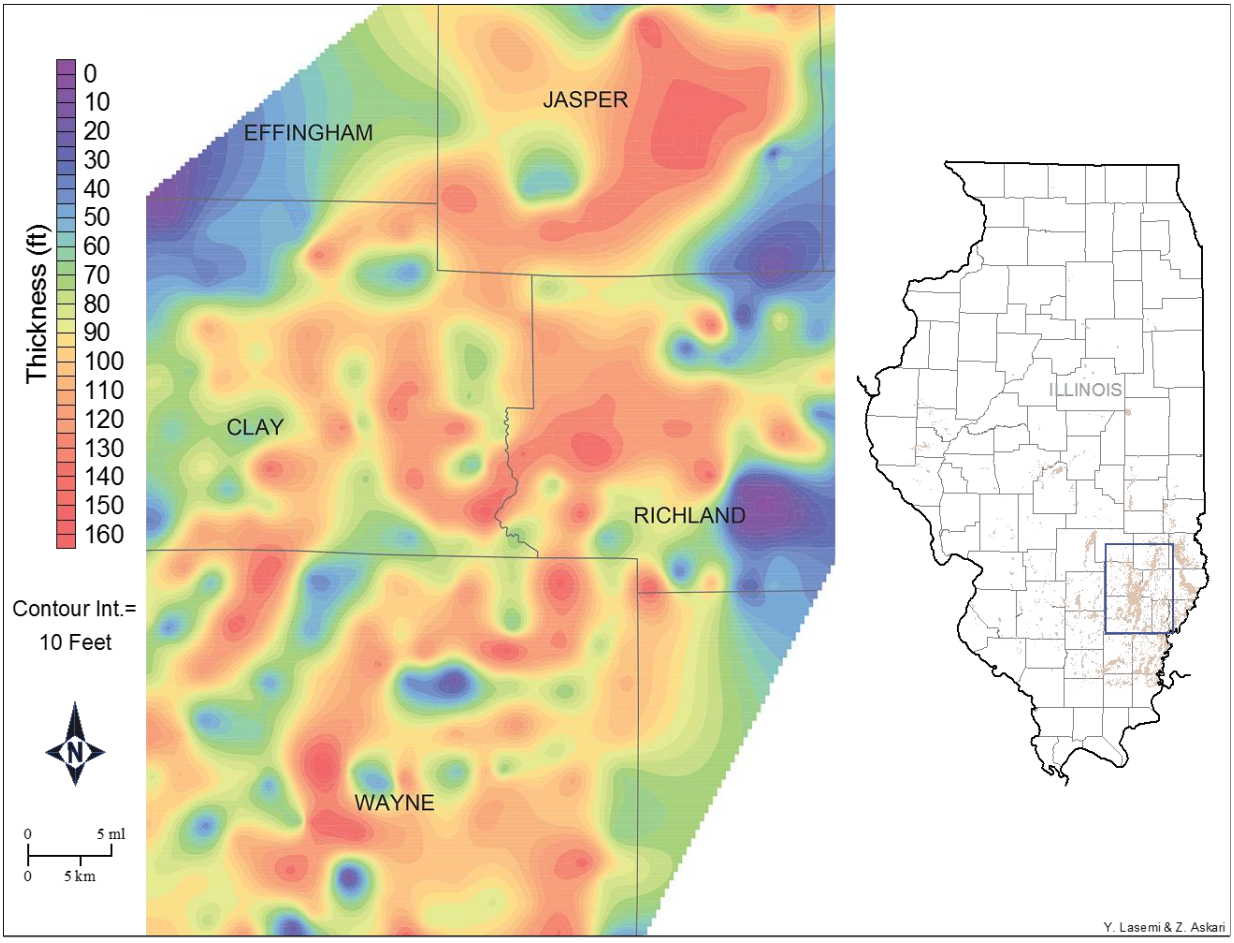

Figure 3.41. Net sandstone isopach map of the Cypress Formation interval showing and overall northeast-southwest trend for sandstone bodies.

3.4.2 Petroleum Traps and Controls

Sandstone reservoirs within the Cypress Formation commonly produce from lenticular reservoirs that trend in a northeast-southwest direction (e.g., Grube and Frankie, 1999; Webb and Grube, 2014). In the study area, oil production is from tacked porous sandstone lenses developed in the middle and uppermost part of the formation (**Figure 3.42**, wells 1 and 2). In addition, the upper part of the thick Cypress multi-story sand bodies are commonly productive (**Figure 3.42**, well 3). Petroleum entrapment in the Cypress is mainly stratigraphic and controlled by updip facies change in laterally discontinues sandstone reservoirs (**Figure 3.43**). The upper thick Cypress multi-story sand body is commonly productive on anticlinal closures along the crest of the Clay City Anticline (**Figure 3.44**) forming a structural-stratigraphic combination trap. As shown in **Figure 3.44**, the well away from anticlinal closure (API 121590155100) is water saturated. The upper part of thick Cypress is also productive in stratigraphic updip pinch outs away from structural closures (for an example, see well 1 in cross section BB'). An ROZ underlies the oil saturated interval (Webb et al., 2016).

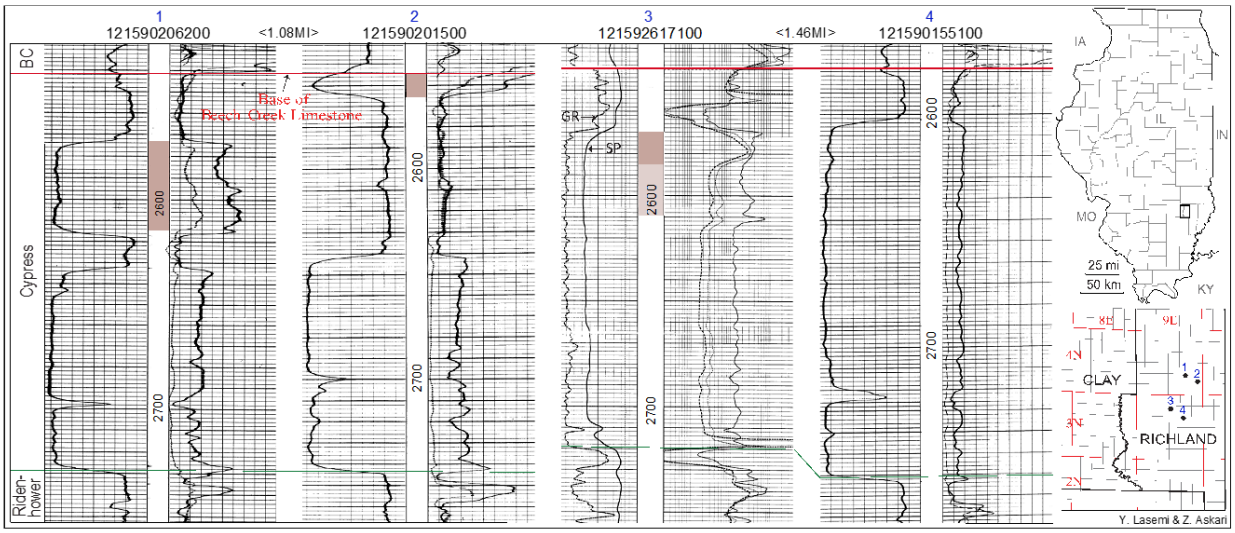

Figure 3.42. Type logs showing the productive Cypress Sandstone bodies in brown lolor. Note laterally discontinuous oil saturated sandstones. Note also oil saturated upper thick Cypress in well 3. The same interval in well 4 shows a very low true resistivity because it is water saturated.

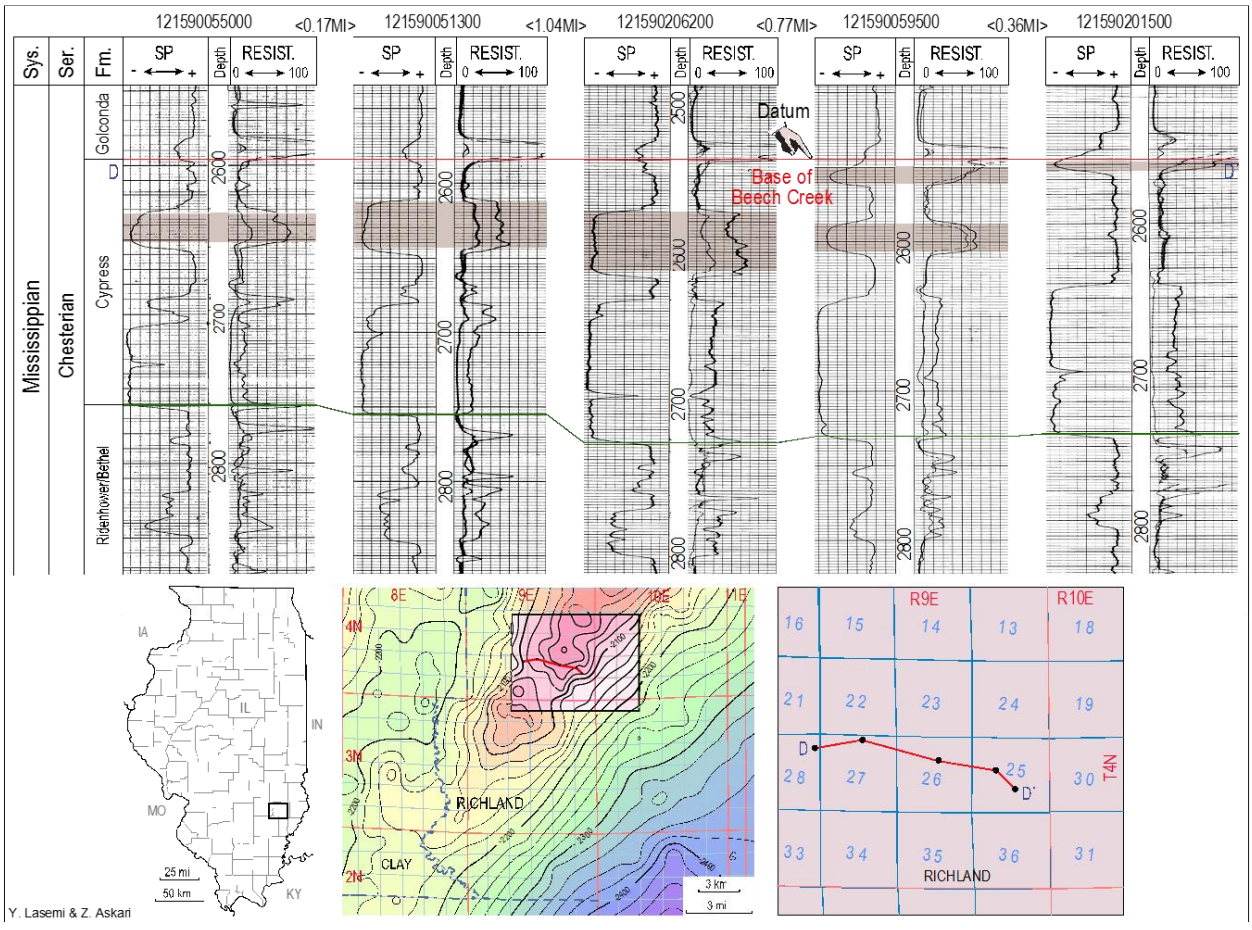

Figure 3.43. Stratigraphic cross section DD' across the Clay City Anticline showing the lateral variation of the Cypress Sandstone. Note oil saturated compartmentalized sandstone lenses (in light brown).

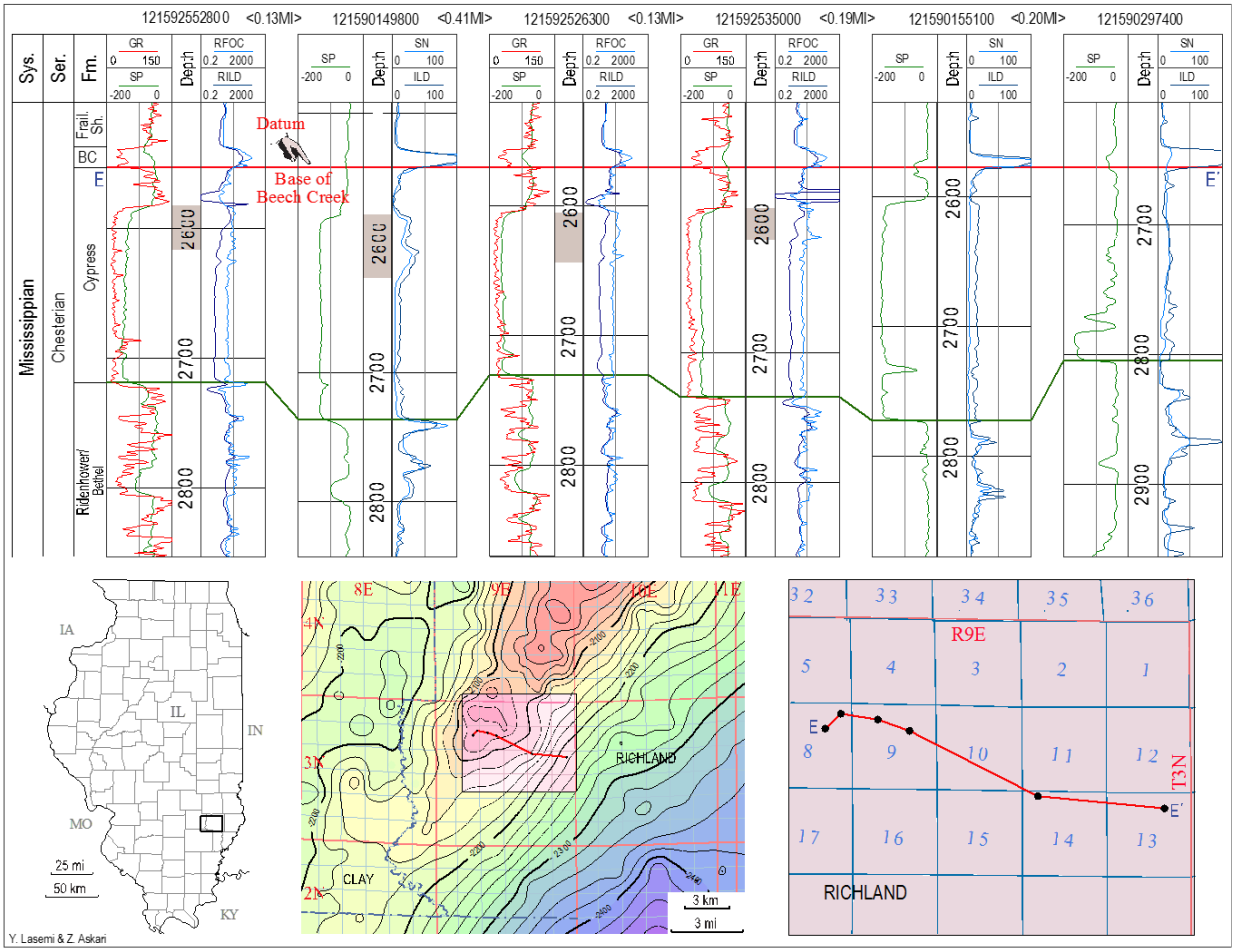

Figure 3.44. Stratigraphic cross section EE' across the Clay City Anticline showing lateral variation of the Cypress Sandstone. Note oil saturated horizons (in light brown) in the upper part of the thick Cypress. The porous upper part of the thick Cypress in well 5 (API 121590155100) is water saturated because it is too low on the flank of the anticline.

3.4.3 Reservoir Characterization

Detailed geological characterization of the Cypress Sandstone in the deep part of the ILB (Fairfield Basin) indicated compartmentalized sandstone reservoir bodies related to shallow marine, deltaic, and fluvial depositional systems. The Cypress succession comprises:

- A mainly deltaic unit in which prodelta mudstone passing upward into distal to proximal coarsening-upward distributary channel mouth-bar sandstones or blocky to fining-upward sandstone lenses interpreted as distributary channel fill deposit. Angular to subrounded grains and funnel, cylindrical, and bell-shaped log signatures in the sandstones are interpreted to indicate delta distributary and mouth bars, and inner delta plain fluvial channels.

- A shallow marine succession of mudstone to mature sandstone interpreted as offshore bar or shoreface deposit. Hetrolithic stratification and rounded to subrounded grains in sandstones showing funnel shape log signature in the upper part of Cypress indicate deposition in high energy setting under wave and/or tide influence. Bell shaped fining upward cycles in places may record deposition in the lower intertidal or a meandering tidal channel setting. Similar facies have been reported in the upper part of the Cypress in other parts of the ILB, which are interpreted to have been deposited in tidally influenced delta plain setting (Grube and Frankie, 1999; Webb and Grube, 2014).

- Major lenticular, multistory sandstone bodies at several horizons with shale partings or interbeds displaying cylindrical or bell-shaped profile. These sandstone bodies cut down several meters into the succession and the lowermost horizon may reach the limestone or shale of the underlying Ridenhower Shale. The rather thin calcite cemented sandstone in the upper part of the thick Cypress may correspond with a short-term sea level fall. Partial erosion of quartz cement overgrowth on sand grains indicate inherence from various Lower Paleozoic and Proterozoic sources. The southwest trending paleovalleys for the Cypress Formation (**Figure 3.41**) corresponds with the southwest trending paleovalleys and a northeast source for the Cypress Formation as suggested by previous authors (e.g., Potter et al., 1958; Swann, 1964; Nelson et al., 2002; Seyler et al., 2012).

During the time of Cypress deposition, two western and eastern clastic belts existed, running south-southwest in Southeastern Illinois and Southwestern Indiana, respectively separated by shale and interbedded shale and sandstone (Nelson et al., 2002, **Figure 3.1**). Nelson et al. (2002) indicated the deposition of Cypress "thick sandstones" as lowstand fluvial incised valley fills along unconformable boundaries on which the Cypress Formation is incised deeply into underlying formations and extensively reworked by tidal current during transgression in an estuarine setting. We are in accord with Nelson et al. (2002) and interpret these texturally submature sandstones as lowstand fluvial incised-valley fill deposits that eroded underlying deposits (**Figure 3.36**) during the falling stage of fourth-order sea level cycles. These low sea level events may correlate with the time of paleosol development that Nelson et al. (2002) reported within the Cypress Formation away from thick Cypress sandstone belt. Tidal sedimentary structures have been reported in the upper part of the thick Cypress sandstone bodies (Nelson et al., 2002), which could have been the consequence of subsidence due to sediment load, paleoslope change, or sea level fluctuation that resulted in periodic tidal influx into the fluvial system. Webb et al. (2016) interpreted the thick Cypress sandstones occur as multistory fluvial sandstone bodies that become estuarine upward in an accommodation limited setting.

Howell (2017) proposed the western belt thick Cypress sandstones as three sheet-like packages deposited in meandering or anastomosing fluvial system within a ~50 km (~30 mi) wide and ~200 km (~125 mi) long composite, sinuous belt with a high affinity toward suspended load transport because of its exceptionally fine grain size. However, absence of capping flood plain deposits or presence of thin shale beds/shale partings and sheet like character of the sand bodies suggest a major sandy-braided fluvial system as a trunk river, similar to South Saskatchewan River (Miall, 1978, 1996). Braided channels normally have flat bases with the main sand bodies indicated only by blocky-shaped log signatures (Miall, 2014), as is the case in the amalgamated thick Cypress sand bodies. As was mentioned above, incised valley fills are commonly multi-story sand bodies displaying a regional basal erosion surface that records sea level lowstand and the progressive rise in base-level (Fielding, 2007; Miall, 2014).

Diagenetic processes, including compaction and cementation by quartz, calcite, and clay minerals in the Cypress sandstones resulted in the reduction of porosity and permeability. However, dissolution of feldspar grains and formation of clay mineral coatings or partial calcite cementation on grains resulted in the increase and preservation of porosity, respectively. Clay minerals in the sandstone interstices of the thick Cypress sandstone intervals may have been formed as the consequence of late diagenetic processes (e.g., Rehak, 2014; Webb et al., 2016). However, a new study by Virolle et al. (2019) suggest that, in estuaries and the adjacent fluvial/tidal streams, clays could be deposited as detrital with clays binding to sand grains forming 1 µm to more than 200 µm clay coats on sand grains despite strong hydrodynamic conditions. Up to 30% of grains are coated along the entire length of the estuary; tidal bars and heterolithic point bars in the estuary funnel and estuarine channels are the main areas and potentially form good reservoir quality in deeply buried sandstones (Virolle et al., 2019). Quarts cement overgrowth in the thick Cypress is rare or inherited from recycled older deposits

(**Figure 3.37C**). Chloritization or illitization of clay coats during burial diagenesis prevent quartz overgrowth cement development, allowing preservation of high porosity and permeability in deeply buried sandstones (Tang et al., 2018; Virolle et al., 2019).

In the study area, in addition to the lenticular sand bodies in the middle and upper part of Cypress (**Figure 3.43**), the upper part of the thick Cypress is also productive (**Figure 3.42**, well 3 and **Figure 3.44**). Webb et al., (2016) suggested enhanced stratigraphic trapping due to differential compaction over the thick sandstones forming the areas with the highest potential for CO_2-EOR and storage. Although differential compaction may locally be important, the results of this study suggest that stratigraphic updip pinch outs and combination structural-stratigraphic traps on anticlinal closures appear to control petroleum entrapment in the thick Cypress. Even in Noble Field (northwest quarter, T3N, R9E, Richland County), which is a part of the Clay City Anticline, thick Cypress producing interval is located on anticlinal closure (**Figure 3.44**). The stacked sandstone intervals in the thick Cypress succession are laterally discontinuous and are encased in impermeable marine and marginal marine shale, which make them potential targets for storage of anthropogenic CO_2.

3.5 Petrography of Cypress Sandstone

3.5.1 Data and Methods

The ISGS geologic samples library houses Cypress Sandstone cores from approximately 110 wells. Howell (2017) selectively described and analyzed the facies of those core representative of the fluvial portion of the Cypress Sandstone. Samples from these cores were selected for further petrographic analyses.

Core logs helped to identify various facies at different depths that need to be further studied by drilling core plugs perpendicularly at the cores. The drilled plugs were put into Steady state gas permeameter and porosimeter (PoroPerm), manufactured by Vinci technologies, to collect permeability and porosity data. Samples, cut at same depth as the plugs or trimmed from plug ends, were shipped to Wagner Petrographic Inc. to be made into thin sections. Thin sections were stained with iron stain, k-spar stain, and dual carbonate stain on the left half of each slide.

Thin sections were analyzed using a Zeiss Axiophot Upright Microscope, combined with Olympus D72 camera to capture images. Point-counting the thin sections was conducted by taking photos with appropriate magnification lenses (higher magnification lenses for finer grained samples, and lower magnification lenses for coarser grained samples (objectives vary from 2.5X to 10X)) on two representative zones of each slides. Grids were then laid on these photos using photo editing software. Minerals and pores located at the intersections of the grid were identified and counted for at least 400 points for each thin section. In total, 112 point-counts (56 thin sections) were conducted.

Twenty-nine thin sections were from cores that had been analyzed by Howell (2017); these thin sections were each assigned a sedimentary facies. These thin sections were mainly from producing oil fields, such as Noble, Dale, and Loudon Field (**Figure 3.45**). Wells that were both stratigraphically interpreted and had thin section point counted are: RHF #2-S (Dale Field, API 120650139400), RHF #4-S (Dale Field, API 120650135600), Ripley #26 (Loudon Field, API 120512569900), Montgomery #B-34 (Noble Field, API 121592606400), and Coen #120 (Noble Field, 121592608300). The remainder of the samples were chosen from minor oil fields or plugged dry wells to increase the spatial distribution of samples across the fluvial facies of the Cypress Sandstone in the basin (**Figure 3.45**). Of the 56 thin sections that were studied, some of the wells had multiple plugs/thin sections taken from different depths and facies, and others may have only had one plug/thin section taken. SEM was used was needed to examine the details of authigenic clay minerals in the intergranular pore space.

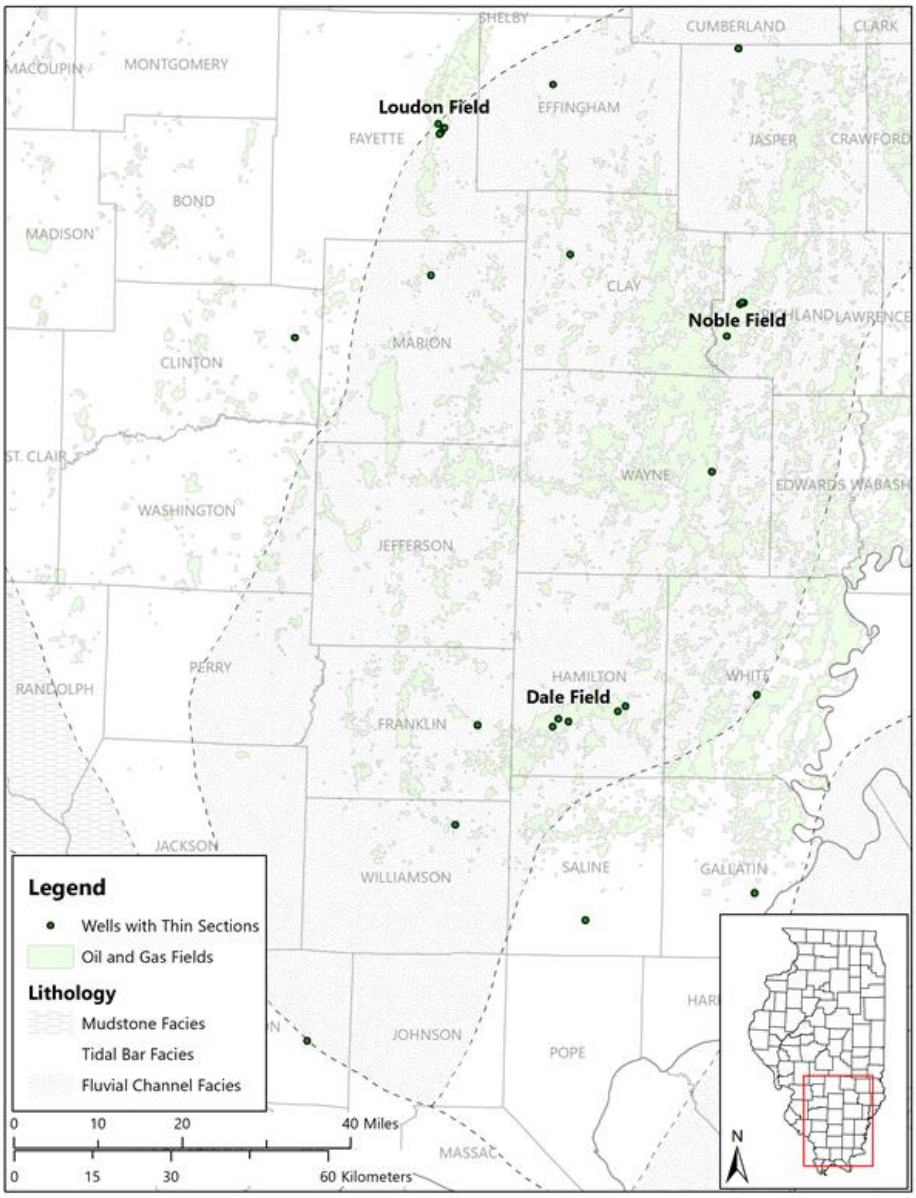

Figure 3.45. Localities of wells with thin sections point counted for this study with major oil fields labeled on the map.

3.5.2 Mineralogy

Following the sandstone classification scheme of Folk (1980), the Cypress Sandstone is predominantly quartz arenite (**Figure 3.46**), with 84% of samples being classified as such. Subarkose (8% of samples) and sublitharenite (8% of samples) compose a minor proportion of the Cypress (**Figure 3.46**).

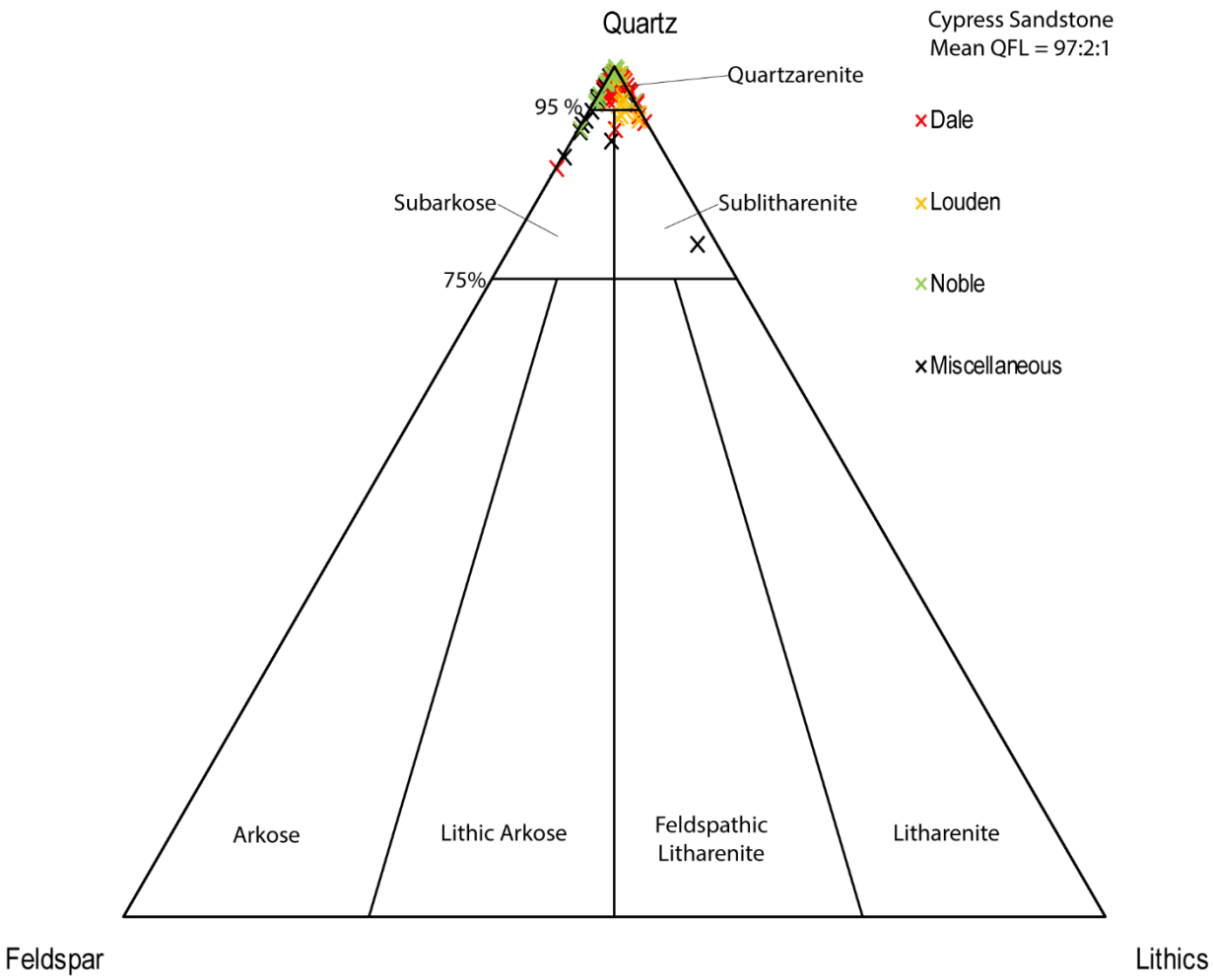

Figure 3.46. Ternary QFL (quartz, feldspar, lithic fragments) plot for showing the results of point counting from 56 Cypress Sandstone thin sections. Samples from different major oil fields color coded as shown in legend.

Monocrystalline quartz is the most common mineral in the Cypress Sandstone. Subhedral and euhedral grains are more common than anhedral ones. Feldspar grains such as plagioclase, microcline, sanidine, orthoclase, and perthite occur in pristine or partially dissolved condition, and comprise 1.7% of the total framework grain mineral content for Cypress Sandstone on average. Lithic fragments, as defined by Folk (1980), are predominantly chert, and they comprise a small percentage (1.2% on average) of the framework grain mineral composition.

Kaolinite, illite, chlorite, and smectite are the major kinds of authigenic clay minerals found in Cypress. Clay minerals like illite occur as a layer on the framework grains, normally seen as a dark rim on the perimeter of quartz (**Figure 3.47**). On the other hand, kaolinite formed from altered feldspar grows on the dissolved feldspar grains or fill pore spaces between grains.

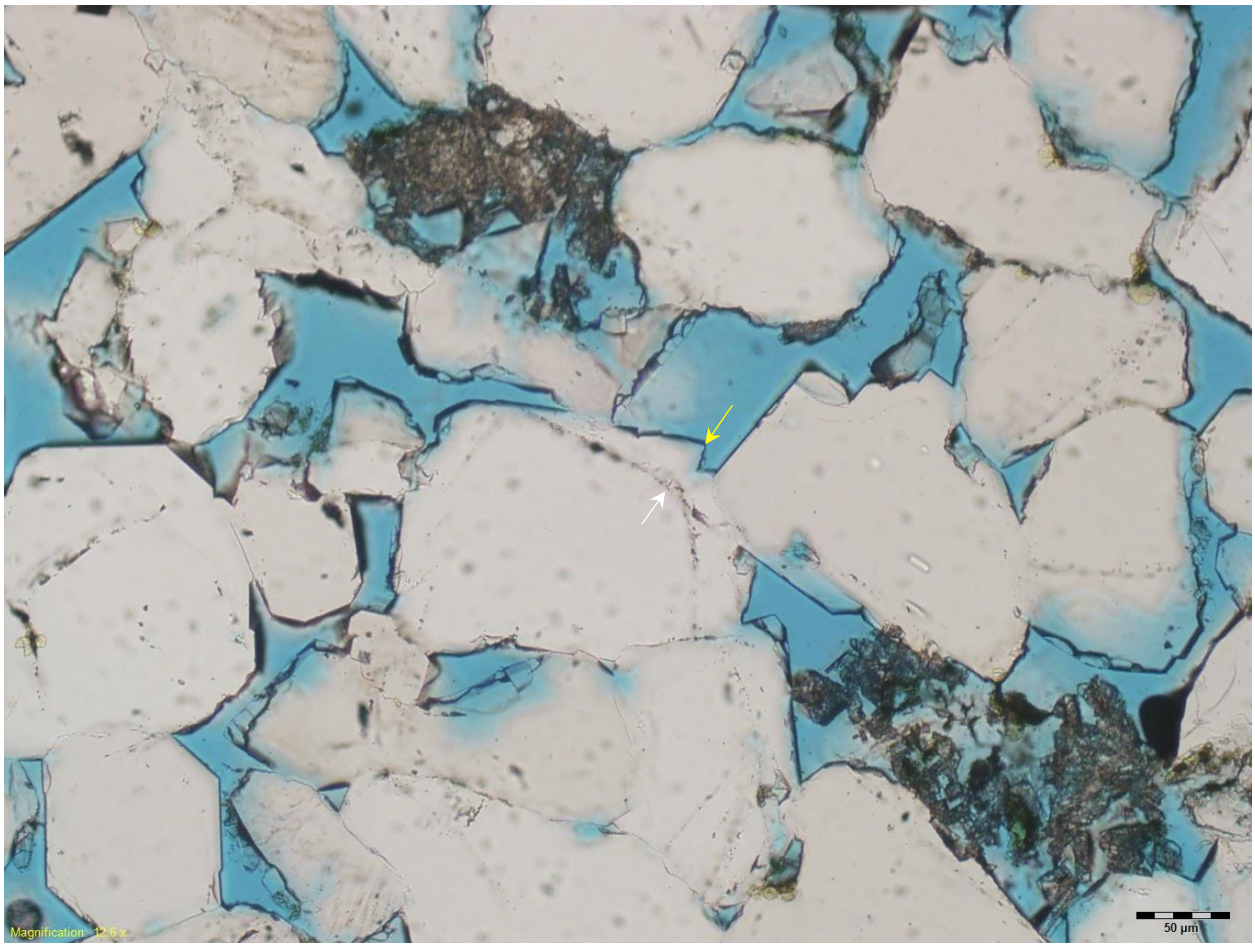

Figure 3.47. Syntaxial quartz overgrowth outlined by inclusions (white arrow). The dark clay line (illite stained by hematite) marks the boundary of overgrowth (yellow arrow). Long #2 (API 121592648800) 2737.8' 20x plane polarized light, the scale bar at the bottom right is 50 µm.

Horizontal beds of fine silt layers are composed of detrital clay flocculates (**Figure 3.48**). They are most common in facies with upper fine grains and medium-well sorting (**Figure 3.49**).

Figure 3.48. Scanned thin section showing fine bedded silt layers (indicated by white arrow) at RHF #2-S (APR 120650139400) 2954.8'.

Figure 3.49. Fine bedded silt layers (indicated by white arrow) from the previous thin section under the microscope with 5x objective under plane polarized light, scale bar down right is 200 µm.

Carbonate cement including calcite and dolomite occur across the Cypress Sandstone (**Figure 3.50**). Poikilotopic cement is the most common form for carbonate cement. Euhedral dolomite can also be found at many locations. In regions rich in carbonate cement, fossil fragments are relatively common. However, due to the poor preservation condition of these fossil fragments, it is difficult to identify the species.

Figure 3.50. Scanned thin section with left side stained with dual-carbonate staining, calcite cement stained with a red color (indicated by white arrow) RHF #2-S (API 120650139400) 3050.4'.

Accessory minerals including muscovite, biotite, and zircon are rare in Cypress Sandstone. Opaque minerals like hematite and pyrite occur but are indistinguishable under optical microscope and compose less than 1% of all samples on average. Therefore, they will not be included in further discussion in this study.

3.5.3 Diagenesis

Quartz Cement

Syntaxial quartz overgrowths are the most common type of cementation observed in Cypress. The source for such overgrowth can come from both pressure dissolution at grain contacts and dissolutions of silica in pore fluids (**Figure 3.51**). Quartz overgrowths are distinguished from the framework grains by the textural change; for example, the original grain is free of fluid inclusions, but the overgrowth is filled with fluid inclusions, or vice versa. In other examples, impurities like clays and silt would partially cover the quartz grains and outline the boundary between the grain and its overgrowth (**Figure 3.47**).

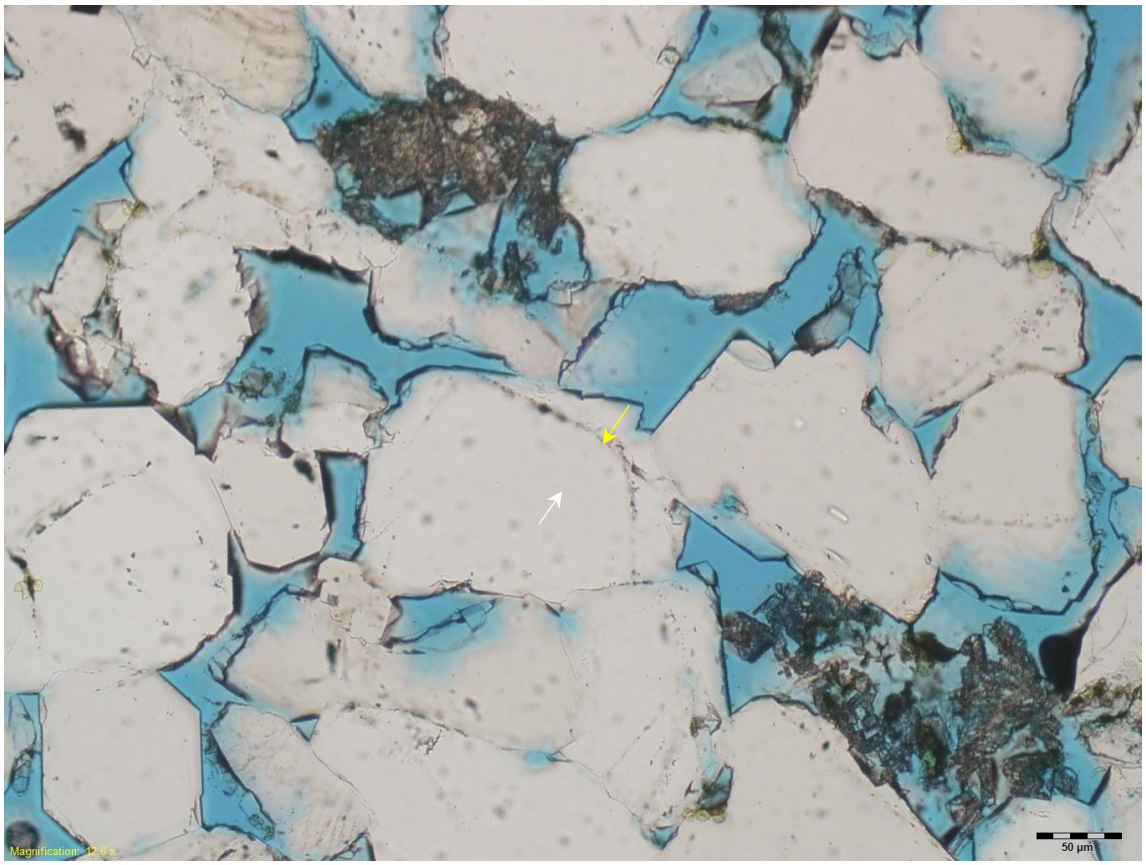

Figure 3.51. Syntaxial quartz overgrowth outlined by inclusions (white arrow). The dark clay line (illite stained by hematite) marks the boundary of overgrowth (yellow arrow). Long #2 (API 121592648800) 2737.8' 20x plane polarized light, the scale bar at the bottom right is 50 µm.

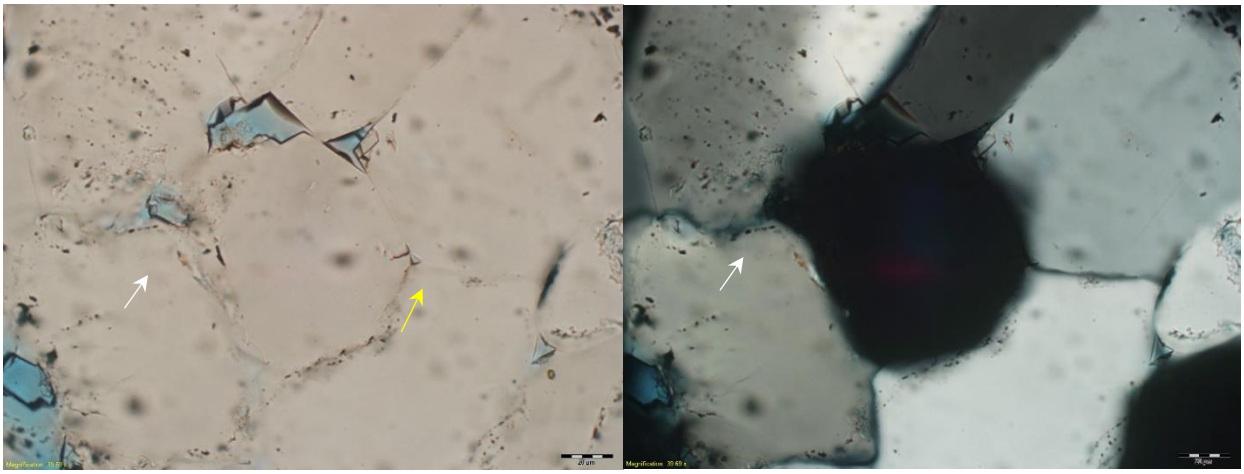

Figure 3.52. Quartz cement caused by pressure dissolution (indicated by yellow arrow). The original grains can be distinguished by the inclusion rich boundary (indicated by white arrow) and different extinction under cross polarized light, Tripp #1 (API 121812190900) 108' 63X plane and cross polarized light, the scale bar at bottom right is 20 µm.

Feldspar Alteration

Detrital feldspars commonly undergo dissolution or alteration and replacement in subsurface settings (Ulmer-Scholle et al. 2014), and such alteration and dissolution are observed in Cypress Sandstone to such an extent that few unaltered feldspar grains are seen to occur in thin sections (**Figure 3.53**).

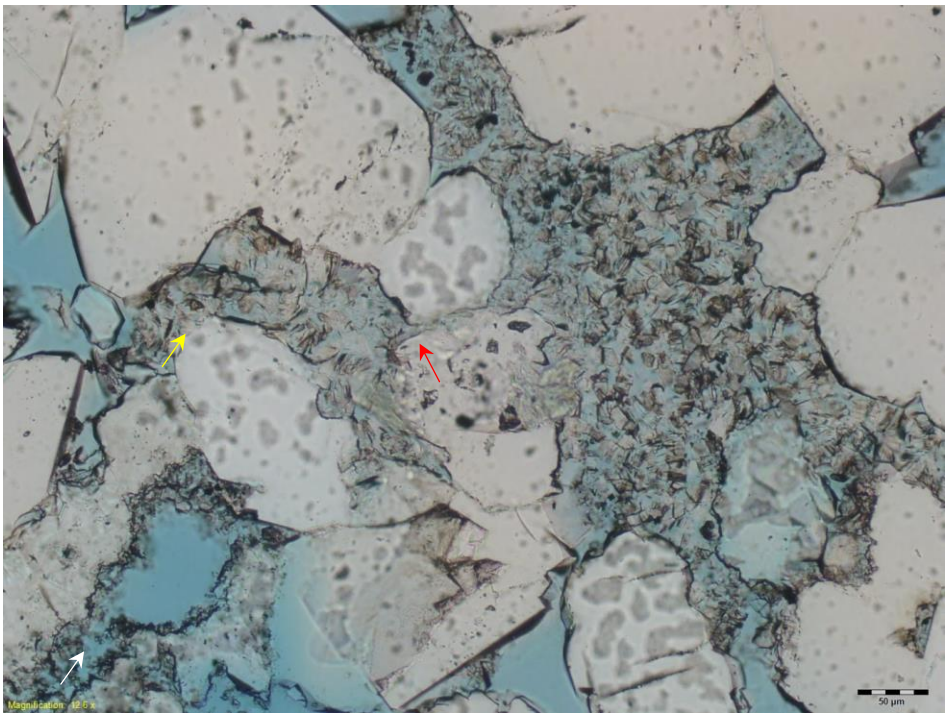

Figure 3.53. The pore space at the bottom left resembles a feldspar grain (white arrow), the kaolinite bundle at the center to the left of the photo has a boundary close to a feldspar grain (yellow arrow), which is likely to be the product of replacement, kaolinite grows into pore spaces and blocks the pore throat (red arrow). 121930121800 (Puckett. F. E. 1) 3183', 20X plain polarized light, the scale bar at the bottom right is 50 µm.

Authigenic Clay Minerals

Kaolinite

Kaolinite is commonly the replacement product of feldspar, as seen in **Figure 3.53**. They form at the site of feldspar grains and expand to block the intergranular pore spaces and pore throats. Previous studies according to Ulmer-Scholle et al. (2014), indicate that kaolinite replaces feldspar at temperatures ranging from 20 to 90°C (68 to 194 °F), which can represent a wide range of depths (180-4,000 m (600 ft-13,200 ft)) in the ILB when only considering geothermal gradient (equation 1 and 2, from Webb and Grigsby 2017, personal communication). That kaolinite can be further altered into illite, dickite, and chlorite in higher temperature by geothermal, hydrothermal fluid events or oil migration. However, the abundance of kaolinite preserved in the sandstones has indicated these further alterations are not common, and thus provide insight into the maximum burial temperature of Cypress sandstone.

$$62\ °\mathrm{F} + \frac{1°\mathrm{F}}{100ft} * (Depth - 100ft) = Temperature\ at\ given\ depth \qquad (3.3)$$

or

$$16.7℃ + \frac{1.82℃}{100m} * (Depth - 30.5m) = Temperature\ at\ given\ dept \quad (3.4)$$

Dicktite

Dickite is the product of kaolinite altered under high temperature (90-140°C). This SEM photo (**Figure 3.54**) shows the 'booklet' shaped kaolinite being altered into blockier shaped dickite.

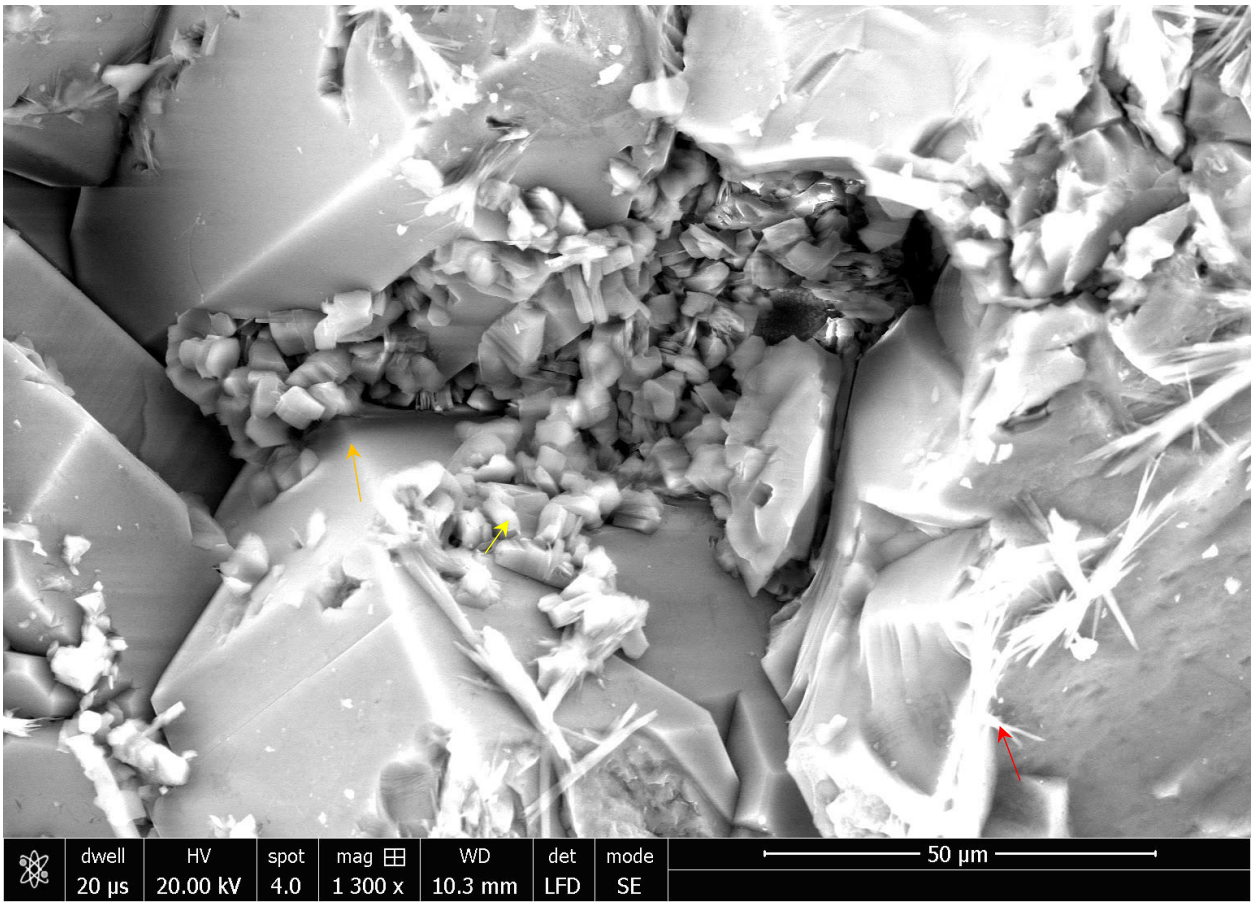

Figure 3.54. Pore filling clay minerals: kaolinite (orange arrow), dickite (yellow arrow) and illite (red arrow) on top of quartz grains, SEM, Tripp #1 (API 121812190900).

Illite

Illite is normally associated with other clay minerals like smectite and sericite. Although illite in most cases is colorless, it is easily stained by hematite or hydrocarbon, giving it a distinctive black or brown color under plane polarized light (**Figure 3.55**). Illite normally occurs on the faces of quartz overgrowths (**Figure 3.56**).

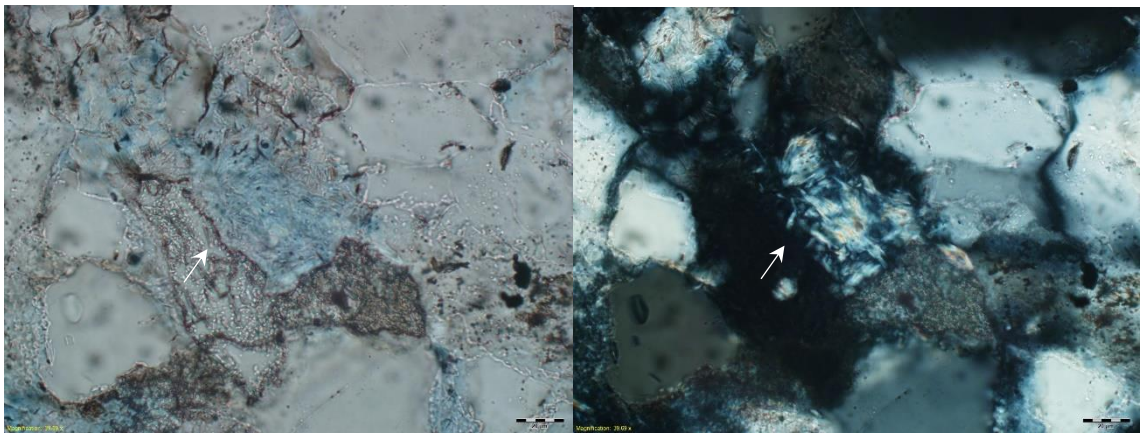

Figure 3.55. Illite and sericite (white arrow), RHF #2-S (API 120650139400) 2960.4' 63X plane and cross-polarized light, the scale bar at bottom right is 20 µm.

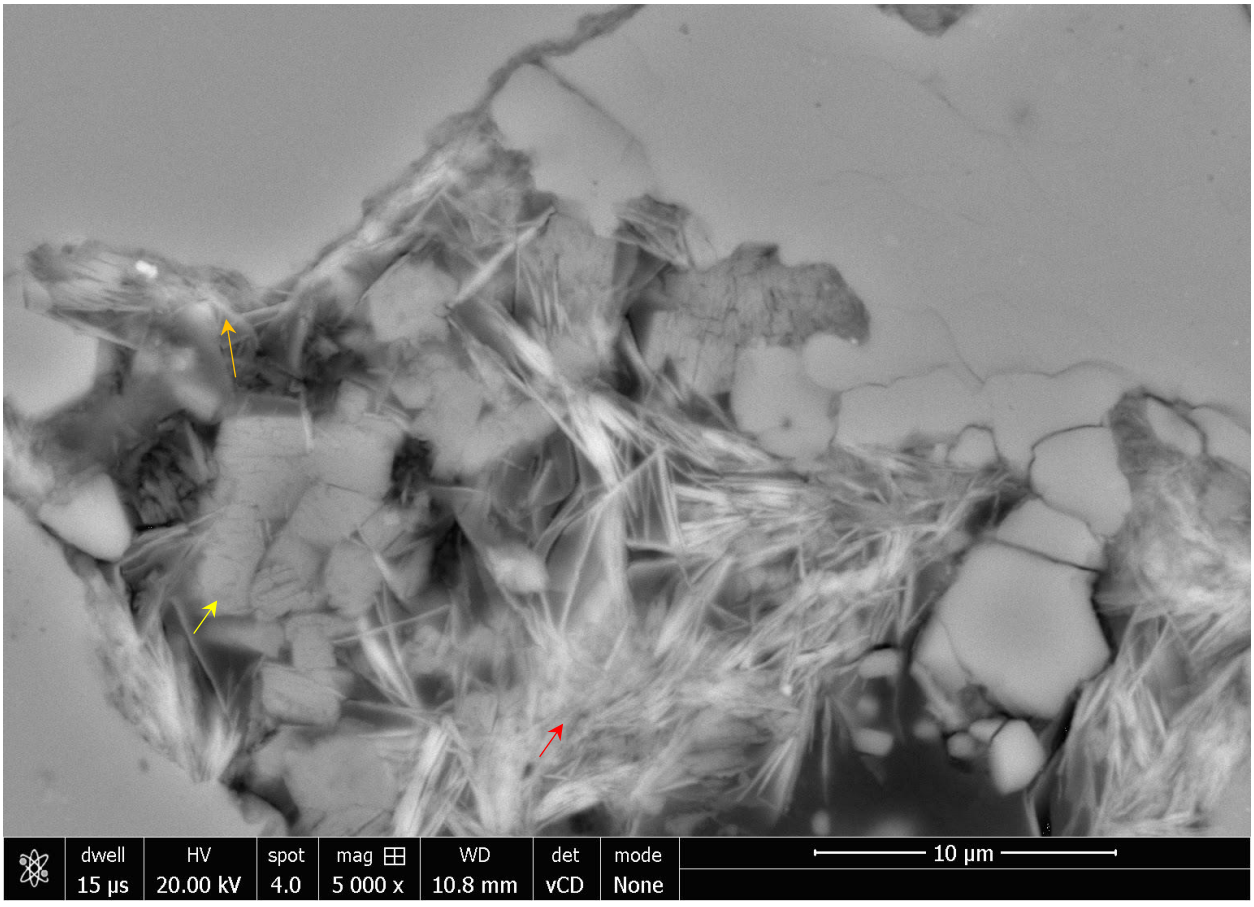

Figure 3.56. Pore filling illite (red arrow) and kaolinite (yellow arrow), also Illite blocking quartz surface from syntaxial overgrowth (orange arrow), SEM on thin sections, 121592606400 (CT Montgomery B-34) 2580.5'.

Chlorite

In Cypress, chlorite tends to form on quartz surface as well. Its formation is closely associated to ferromagnesian grains or Fe/Mg ions in general. Chlorite forms at above 80°C (176°F), thus occurring in later stage where temperature is much higher. (Ulmer-Scholle et al. 2014). It has a distinctive green color under plain polarized light (**Figure 3.57**). Chlorite is not commonly observed in thin section, but can be easily analyzed by XRD.

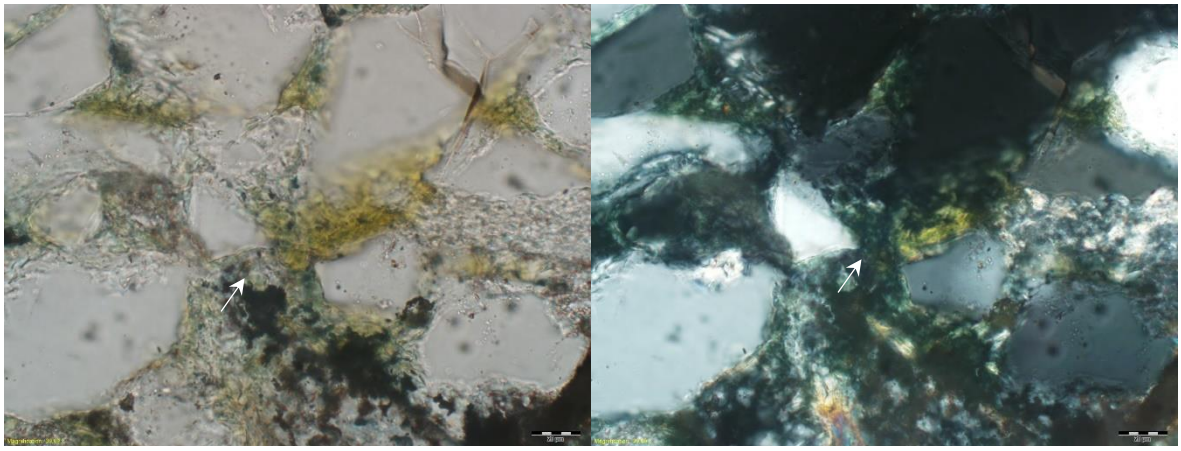

Figure 3.57. Chlorite (white arrow), 121592606400 (CT Montgomery B-34) 2580.5' 63X plane and polarized light, the scale bar at bottom right is 20 µm.

<u>Carbonate Element</u>

Calcite was stained red by dual carbonate stain in thin sections. Such staining helped to distinguish calcite from dolomite, which both are colorless under plane polarized light, and highly birefringent under cross-polarized light. Calcite cement commonly engulfs multiple framework grains, creating a poikilotopic cement (**Figure 3.58 and Figure 3.59**). Analysis of the carbonate cements using cathodoluminescence shows that there are multiple generations of carbonate cement (**Figure 3.60**).

Dolomite not only forms poikilotopic cement, but also euhedral crystals that can be seen in **Figure 3.61**. It is worth noting that some of the euhedral dolomite crystals have a yellow-brownish stain either inside or on the parameters of the crystals (**Figure 3.62**). These are likely to be iron staining, but could also possibly be impurities from cutans.

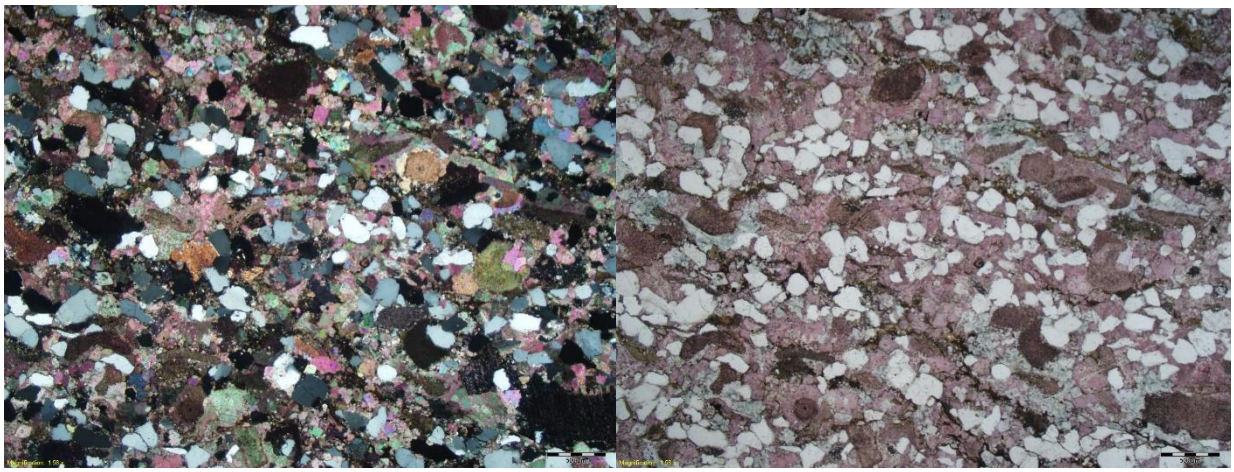

Figure 3.58. Stained calcite poikilotopic cement (red), 120650139400 (Rural Hill Flood 2-S) 3050.4' 2.5X plain and cross polarized light, the scale bar at bottom right is 500 µm.

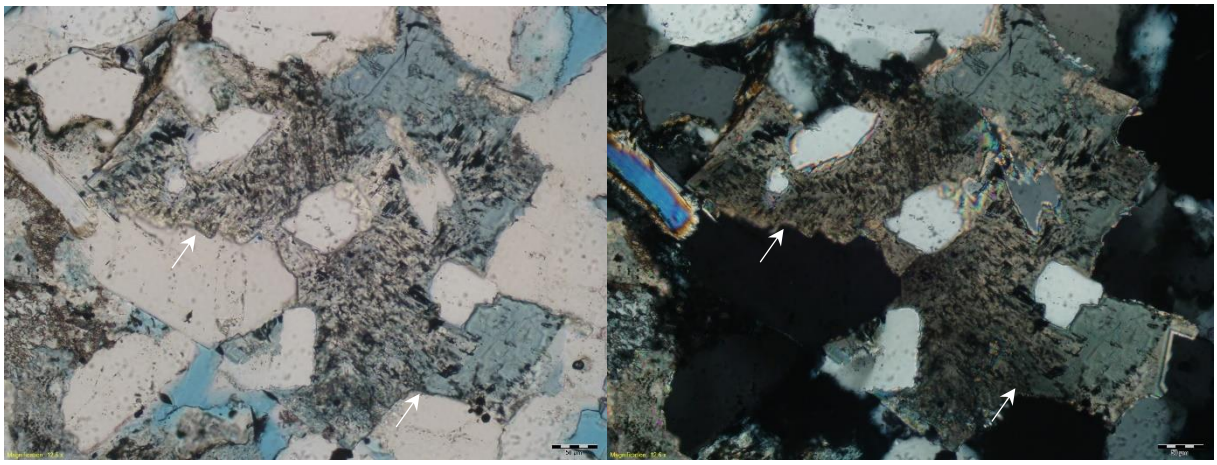

Figure 3.59. Poikilotopic/saddle dolomite cement (white arrow), 121592648800 (Long 2) 2745' 20X plain and cross polarized light, the scale bar at the bottom right is 50 µm.

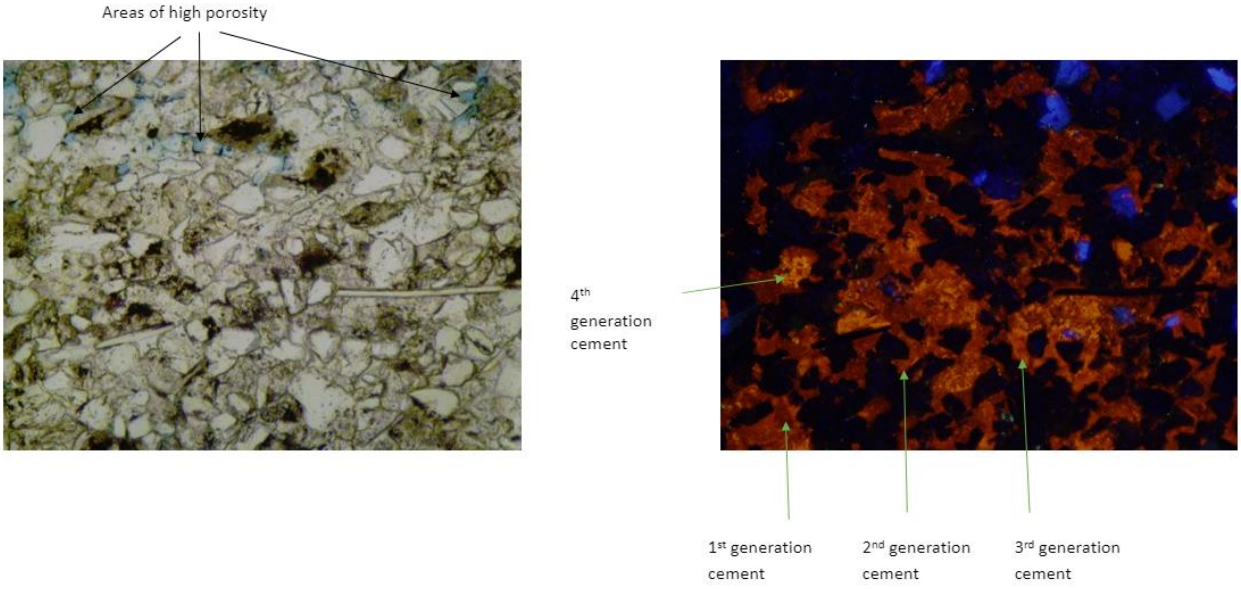

Figure 3.60. Plain polarized light and cathodoluminescence photograph on heavily calcite cemented thin section, 120270084000 (Hanseman 3) at 1202'.

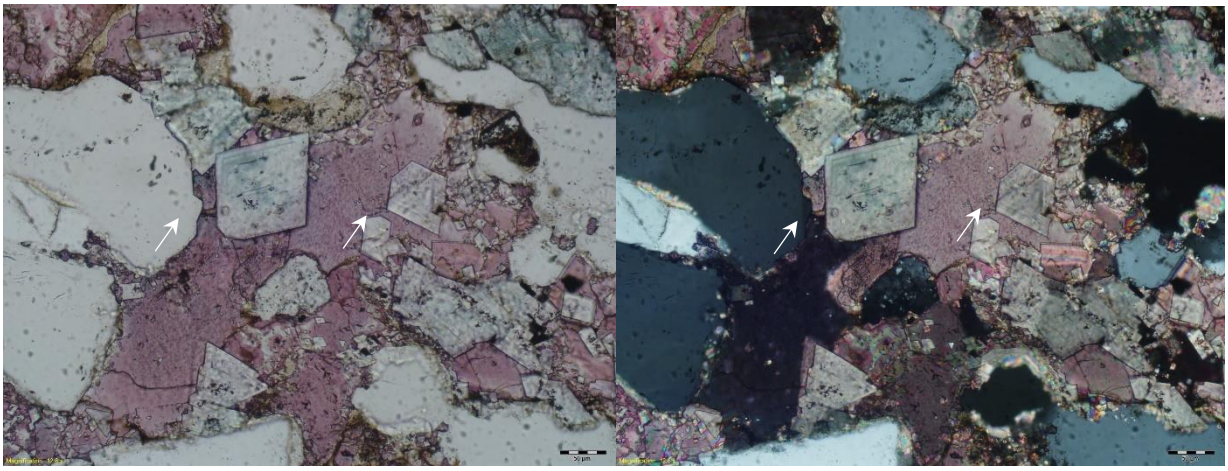

Figure 3.61. Euhedral authigenic dolomite inside the poikilotopic calcite cement (stained red), 120650139400 (Rural Hill Flood 2-S) at 3050.4' 20X plain and polarized light, the scale bar at the bottom right is 50 µm.

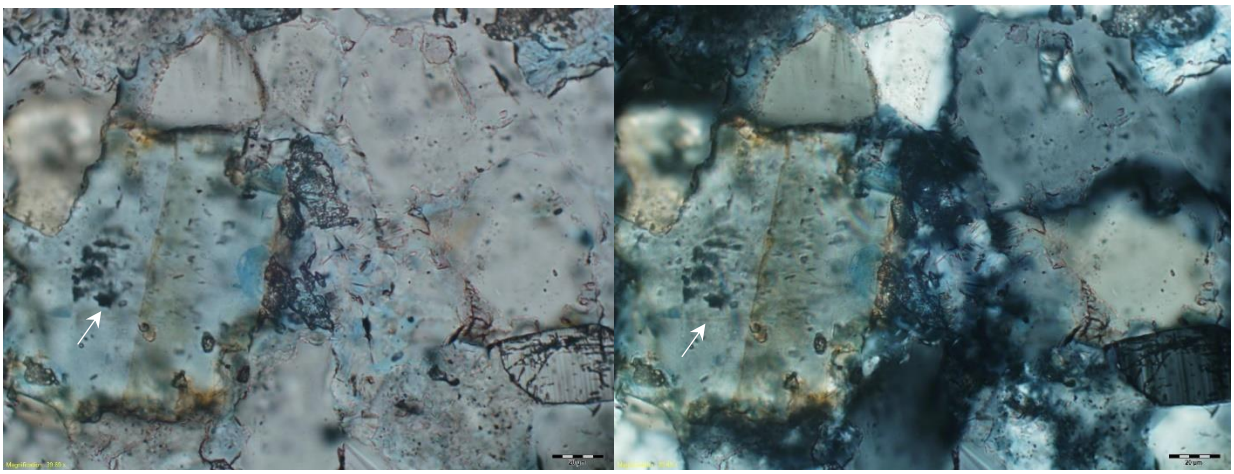

Figure 3.62. Dolomite stained by hematite (white arrow), 120650139400 (Rural Hill Flood 2-S) at 2960.8'63X, plain and crossed polarized light, the scale bar at bottom right is 20 µm.

Hydrocarbon emplacement

Bituminous residue was observed trapped in pore spaces for some samples. In **Figure 3.63**, the brownish stains are dead oil, or oil that lacks volatile components. Hydrocarbon residues can have similar optical behavior to that of iron stained clay minerals. To distinguish them, fluorescence microscopy is a general approach. However, this method is only applied to samples with live oils, because dead oil normally does not yield much fluorescent under UV light. Hydrocarbon residue here are identified by its affinity with kaolinite cement and, where available, well records that indicate oil at the sampled depth. In **Figure 3.63**, hydrocarbon is within the microporosity between vermicular kaolinite. The wettability of hydrocarbon to kaolinite is known (Fassi-Fihiri et al. 1995).

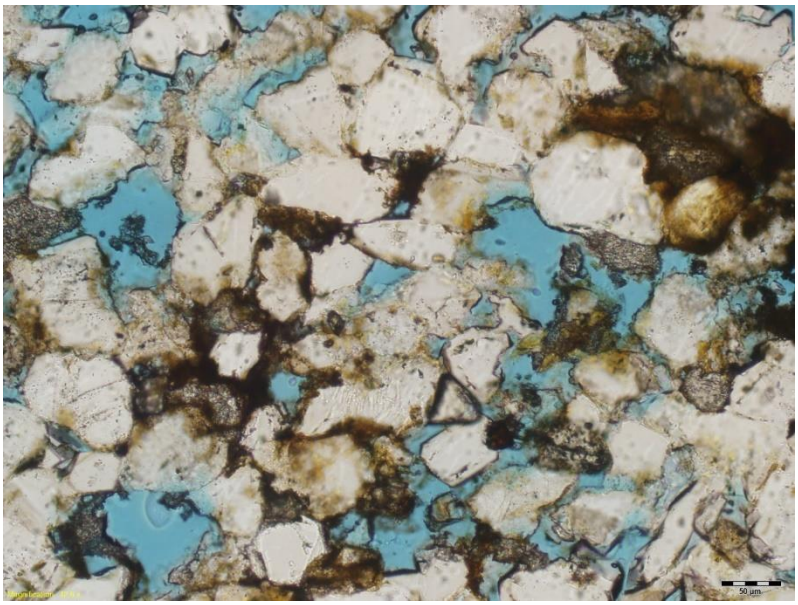

Figure 3.63. Hydrocarbon trapped in sandstone, Coen #120 (API 121592608300) at 2595.5' 20X plane polarized light, the scale bar at the bottom right is 50 µm.

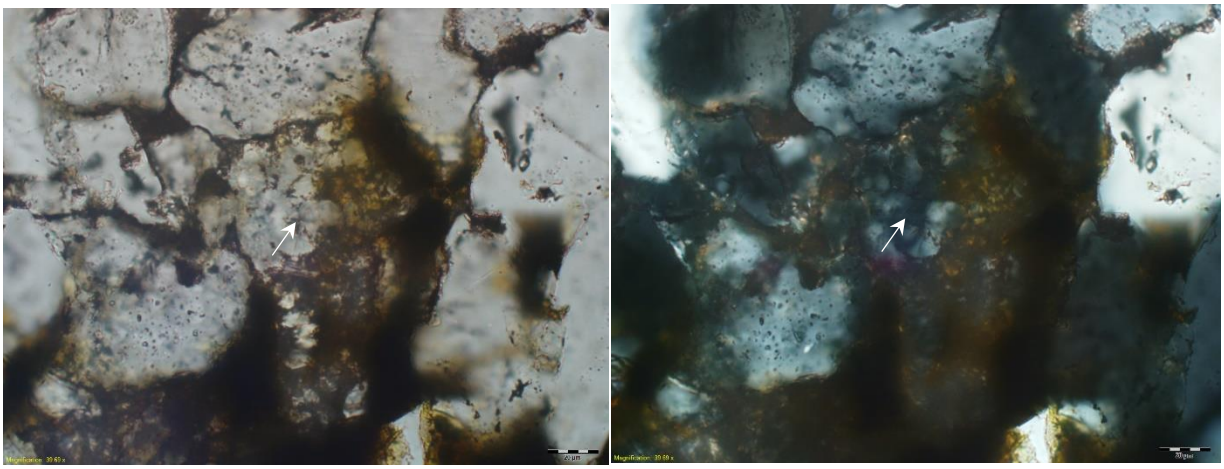

Figure 3.64. Hydrocarbon within vermicular kaolinite, Coen #120 (API 121592608300) at 2596.5' 63X plane and cross polarized light, the scale bar at the bottom right is 20 µm.

3.5.4 Paragenetic Sequence

Carbonate cementation is one of the earliest stages of diagenesis (**Figure 3.65**) observed in Cypress Sandstone thin sections. Pore spaces in the Cypress Sandstone show that an early cementation had helped to preserve the porosity, which was otherwise destroyed by compaction (**Figure 3.66**). As seen in **Figure 3.58**, its intergranular volume (IGV) is much larger than that of similar depth, indicating that calcite cement supported mineral grains from compaction and preserved much of the initial IGV.

Authigenic dolomite predate calcite cement, as shown in **Figure 3.61**. Euhedral dolomite crystal formed first and was then engulfed by the poikilotopic calcite cement. Both calcite and dolomite cement predate syntaxial quartz overgrowth. In **Figure 3.58** and **Figure 3.59**, the quartz grains seem to be much rounded than the common euhedral shape caused by syntaxial quartz overgrowth. (**Figure 3.47**).

With the aid of cathodoluminescence, multiple generations of carbonate cements have been revealed (**Figure 3.60**). However, without further detailed analysis of hydrothermal fluid events, it is hard to pinpoint these diagenetic events on the paragenetic sequence.

Feldspar replacement is also interpreted to have occurred early in eogenesis, as it does not require high temperature. In **Figure 3.54**, both kaolinite and quartz overgrowth occur in a small area, suggesting similar timing for these two diagenetic events.

Syntaxial quartz overgrowth is caused by mechanical compaction caused by pressure dissolution and chemical dissolution resulting silica dissolved in pore fluid. Noticeable quartz overgrowth stopped when illite starts to form at the overgrowth surface (**Figure 3.47**).

In mesogenesis, higher temperature and pressure allowed reactions of altering kaolinite into chlorite and dickite to occur. Feldspar dissolution comes in later, which dissolved those feldspars that has survived previous diagenesis. Those feldspars formed in a later stage during which compaction could no longer destroy them; they then formed secondary porosity (**Figure 3.54**).

Hydrocarbon emplacement occurred in late stage diagenesis. Most of the samples that have been stained by hydrocarbon have relativelymatured diagenetic features (**Figure 3.63**), as mentioned above. It is common to see bituminous hydrocarbon residues blocking pore spaces trapped in clay matrix, especially authigenic kaolinite (**Figure 3.64**).

Previously, Pitman et al. (1998) and Seyler (2000) interpreted the paragenetic sequence of the Cypress Formation. Compared to their work, this study focused more on petrographic analysis. Instrumentational analyses like XRD, CL, SEM, etc. were used to help identify diagenetic features and authigenic clay mineral compositions; therefore, this study lacks analysis on thermal evolution history. However, new petrographic evidence has moved the timing of certain diagenetic events to an earlier stage. For example, the lack of quartz overgrowths inside a poikilotopic carbonate cement shows that carbonate cementation predates syntaxial quartz overgrowth, whereas in previous study, carbonate cementation was thought to appear in late stage diagenesis. Illite overgrowth is also shifted to a later stage, as most commonly observed in thin sections on the rims of hematite stained illite covering surface of quartz overgrowth.

Due to the absence of thermal history analysis, this study cannot draw any conclusions on hydrothermal fluid related diagenesis. More isotopic study is necessary to date and correlate these events and adjust the interpreted paragenetic sequence proposed by this study.

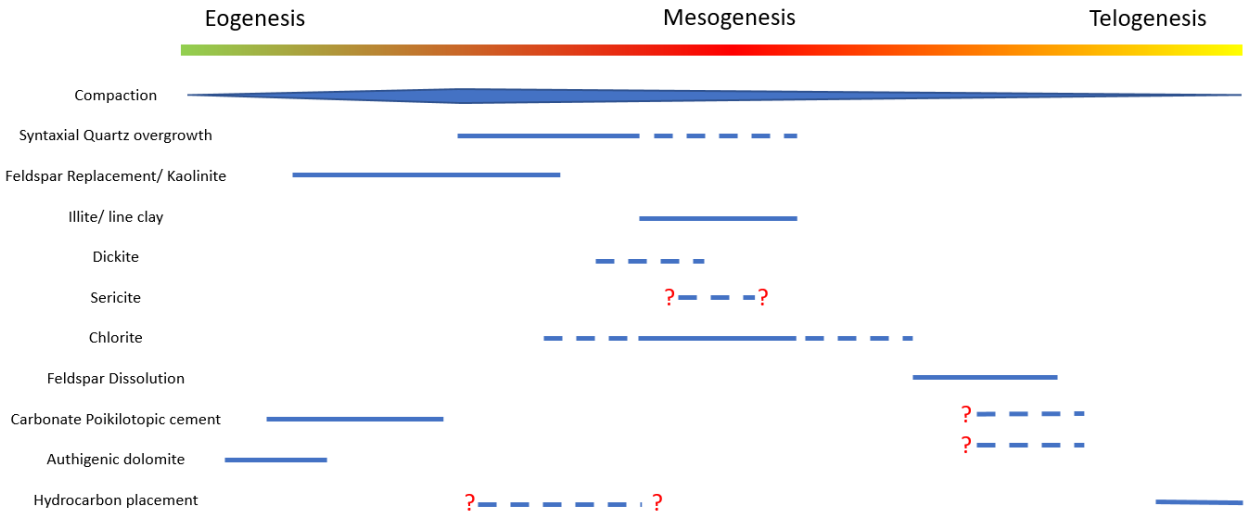

Figure 3.65. Paragenetic sequence of the Cypress Sandstone. The solid line shows diagenesis with petrographic evidence. The dotted line shows inferred diagenetic events. The question marks show possible diagenetic events.

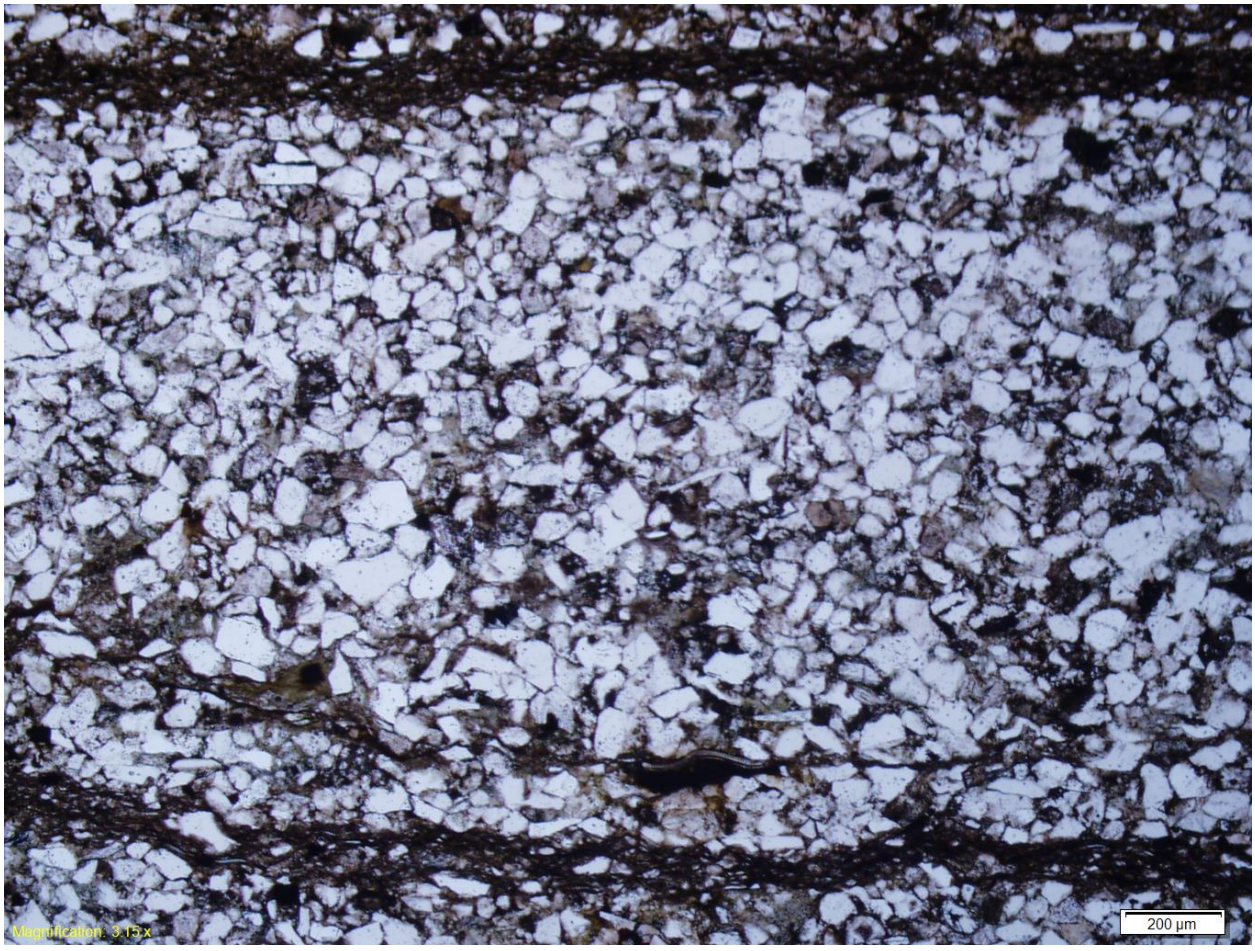

Figure 3.66. 121592606400 (CT Montgomery B-34) at 2578.5', 5X plane polarized light. The scale bar at bottom right is 200 µm.

3.5.5 Reservoir Quality

Quantitative porosity control analysis

Following Ehrenberg (1995), a quantitative approach was adapted for converting point-count data to intuitive values showing the causes of porosity loss. Equations for compactional porosity loss (COPL), porosity loss due to cementation (CEPL), and index of compaction (ICOMP) are shown below:

$$COPL = P_i - \frac{(100-P_i)\times IGV}{100-IGV} \quad (3.5)$$

$$CEPL = (P_i - COPL) \times \frac{C}{IGV} \quad (3.6)$$

$$I_{COMP} = \frac{COPL}{COPL+CEPL} \quad (3.7)$$

I_{COMP} is a value between 0 to 1, when I_{COMP} <0.5, the porosity loss would be majorly contributed by cementation, and when I_{COMP} >0.5, the porosity loss would be majorly due to cementation. Initial porosity, Pi, is calculated by averaging the initial porosity of all thin sections based on their sorting and grain size.

Table 3.9. Sample data and interpretations from thin sections and plugs.

	S_P	S_C	S_M	S_R	S_{RD}
Samples (n)	6	11	2	9	1
COPL	20.63	25.84	18.33	23.83	31.53
CEPL	5.65	5.15	7.68	4.38	0.22
I_{COMP}	0.79	0.86	0.70	0.79	0.99
P_i	40.37	38.42	39.80	40.56	41.80
IGV	24.82	21.90	26.15	20.85	15.00
Thin Section Porosity	5.14	8.32	6.14	8.44	0.00
Lab He porosity (%)	13.92	16.18	15.04	15.10	7.70
Total quartz (%)	78.26	77.17	79.02	78.04	67.43
Authigenic quartz (%)	5.46	3.15	4.12	7.30	1.25
Total Feldspar (%)	1.47	0.77	0.00	1.10	4.12
Lithic (%)	0.91	0.55	1.89	0.72	0.00
Clay (%)	12.54	9.43	10.46	10.93	29.20
Sorting Class	Very well to well	Very well to moderately well	Very well to well	Very well to well	Very well
Grain Size Class	Lower medium to upper very fine	Upper fine to lower medium	Lower fine to lower medium	Upper very fine to upper fine	Lower very fine
Depositional Environment	Fluvial	Fluvial	Subaqueous	Lower fluvial	Marine/brackish

As shown in **Table 3.9**, all facies (determined by Howell (2017); **Figure 3.67**)), exhibit porosity loss that can be attributed primarily to compaction rather than cementation. Although there's no statistical correlation, authigenic quartz percentage is suspected to play a minor role in controlling the porosity of sandstone; clay percentage has a stronger negative relationship with porosity. (**Figure 3.68, 3.69**) It should be noted that both

authigenic and detrital clay are accounted for in the clay percentage; therefore, it is hard to tell which part played a more major role in reducing porosity.

Code	Lithology	Description	Grain Size	Cross-Set Thickness	% Bioturbation	Depositional Process Interpretation
S_R	Sandstone, Ripple-bedded	Whitish-tan very fine to fine-grained asymetric ripple-bedded arenite to sublitharenite, commonly asymmetric ripples, may or may not contain: oil staining, calcite cement, bidirectional ripples, shale rip-up clasts, calcite cement	D = ~100µm	1-2 cm	0- 2%	Fluvial lower flow regime traction sedimentation
S_{RD}	Sandstone, Ripple-bedded with clay Drapes	Whitish-tan very fine to fine-grained ripple bedded arenite to sublitharenite with clay drapes on foresets (<1mm thick), commonly bidirectional (short period reversals) with laterally migrating or slightly climbing foresets, may or may not contain: oil staining, calcite cement, sigmoidal ripples, asymmetric ripples shale rip up clasts, calcite cement	D = ~100µm	<2 cm	0- 15%	Traction sedimentation in a brackish or marine setting with elevated concentrations of clay in suspended load
S_P	Sandstone, Planar-bedded	Whitish-tan to brown very fine to fine-grained planar bedded arenite to sublitharenite; may or may not contain: oil staining shaley-carbonaceous laminae, shaley-carbonaceous debris, shale rip up clasts, calcite cement	D = ~135µm	----	0- 4%	Upper stage plane beds produced from unidirectional traction sedimentation in a fluvial setting
S_C	Sandstone, Cross-bedded	1 Simple unidirectional cross-beds with low thickness (~0.3 m) & short foreset length (<2 m), low angle foresets (<15°) common, commonly superimposed on bar-scale lateral accretions or low amplitude & long wavelength cross-sets (S_{C2})	D = ~150µm	~0.27 m	0%	High aspect ratio fluvial dunes produced from unidirectional traction sedimentation under the influence of high suspended load
		2 Low-amplitude (<3 meters) & long wavelength (10s of meters) unidirectional cross-sets, commonly very low angle (<10°) foresets, commonly aggradational		<3 meters		Low aspect ratio fluvial dunes produced from unidirectional traction sedimentation under the influence of high suspended load
		Whitish-tan to brown very fine to fine-grained arenite to sublitharenite, frequent oil staining; may or may not contain: shaley-carbonaceous laminations, carbonaceous debris, shale rip-up clasts, calcite cement				
C	Conglomerate	Conglomerate displaying a wide range of clast lithologies, commonly matrix supported and calcite cemented, commonly fine-grained sand matrix; may or may not contain: clay clasts, clay laminations, carbonaceous fragments, rounded carbonate or siderite pebbles or septarian nodules, crinoids, brachiopods, gastropods, and bryozoans	Clay to coarse gravel	----	0%	Fluvial lag produced from high energy unidirectional traction currents
X^D	Deformed Bedding	Distorted laminae or bedding within a wide range of lithofacies, commonly contains disturbed bedding and/or convolute bedding	Clay to fine-grained	----	0-100%	Post or syndepositional soft sediment deformation
X^P	Pedogenic Alteration	Commonly variegated (varying from red to green to yellow to grey) or gleyed lithologies, may or may not contain: carbonate nodules, siderite, pyrite, carbonaceous material, root traces, slickensides, peds	Clay to fine-grained	----	0-20%	Pedogenesis post deposition

Figure 3.67. Part of facies interpretation table from Howell (2017).

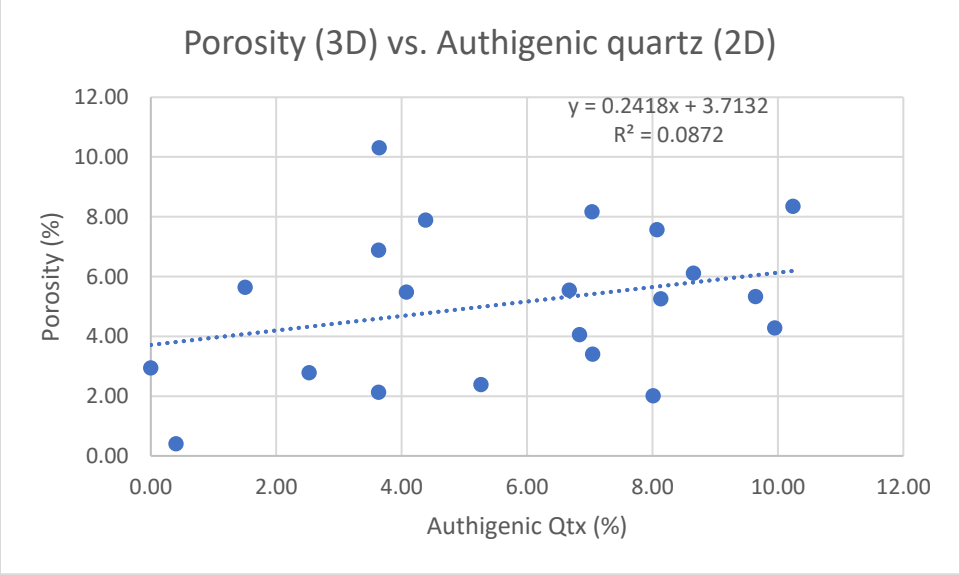

Figure 3.68. Porosity from plug testing vs. authigenic quartz from point-counting.

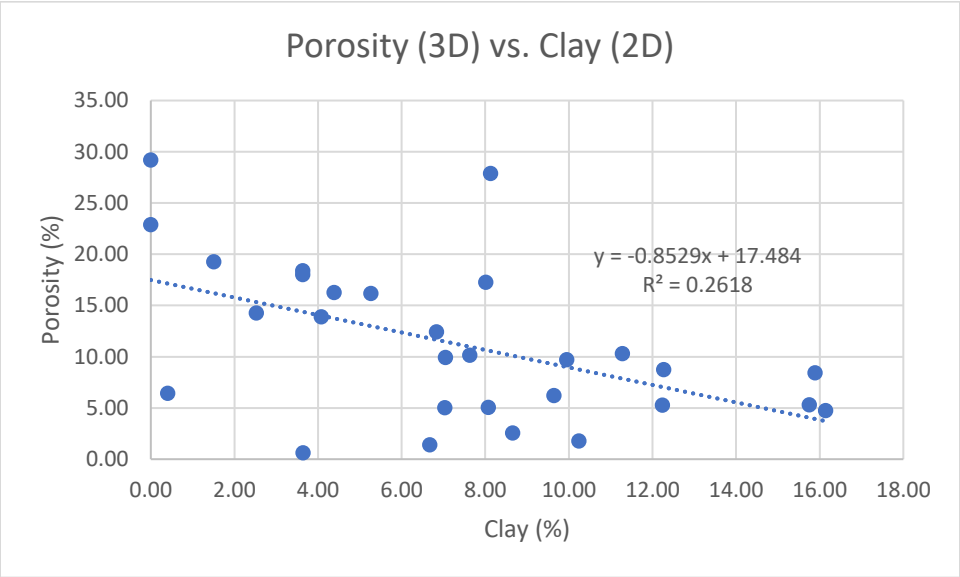

Figure 3.69. Porosity from plug testing vs. Clay content from point-counting.

Ripple-bedded with clay drape sandstone facies (S_{RD}; **Figure 3.70**) represent the lowest porosity of all samples. It has highest clay content (29.2%, compared to the second highest clay content of 12.54%), the majority of which is detritus, and the finest grain size (lower very fine, the finest class in Beard and Weyl, 1973). Although logically sound, more samples of S_{RD} should be examined to draw more universal conclusions.

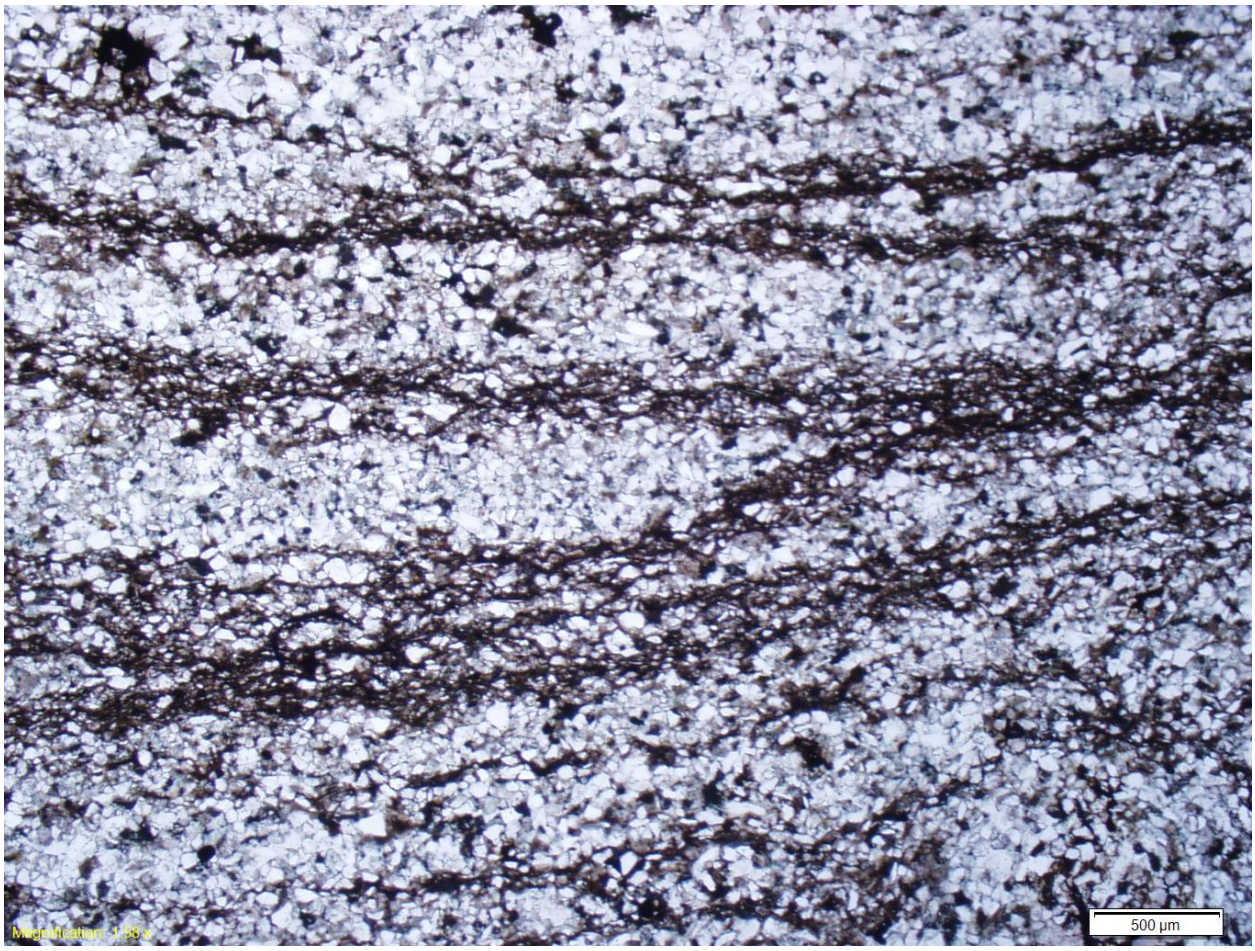

Figure 3.70. SRD facies sandstone thin section, Montgomery B-34, API# 121592606400, at 2583.5'. 2.5X plane polarized light. The scale bar at bottom right is 500 µm.

Both the ripple-bedded with clay drape sandstone facies (S_{RD}) and the ripple bedded sandstone (S_R) facies have high initial porosity and low IGV, indicating that they have lost more porosity than any other facies. Additionally, they have more clay content than other facies, and as a result, the plastic detrital clay can easily fit into intergranular pore spaces, facilitating compaction.

Although all facies have I_{COMP} greater than 0.5, massively bedded sandstone (Facies S_M) has the lowest I_{COMP} of all other facies, indicating that more cementation took place in zones with less sedimentary features and detritus clay content.

Porosity destruction

Mechanical compaction is the primary cause of porosity loss. Without support from pore fluid, clay matrix, or cement introduced in the early diagenetic stage, porosity can be eliminated during burial. Especially with poorly or moderately sorted samples, during compaction, detritus clay and silt can easily fill gaps and pore spaces between larger grains.

Although cementation helps to preserve IGV during burial, if such cement is not dissolved in a later stage, the sandstone could also lose a significant amount (if not all) of its initial porosity. Syntaxial quartz cement is likely the cause of most of the cementation related porosity loss. Unlike the carbonate cement which, due to its geochemistry can precipitate and dissolute easily, quartz cementation, especially quartz overgrowth, is

unlikely to be dissolved away once formed. Luckily, quartz cementation is only related to several facies as well as grain size and sorting, and early stage carbonate cementation or detritus clay can limit syntaxial overgrowth.

Authigenic clay lowers porosity, but in many cases, authigenic clay minerals like illite block quartz overgrowth, thus preserving porosity. In such cases, porosity loss caused by authigenic illite also help preserve more porosity than there would be in the absence of illite. Kaolinite, the predecessor of illite, acts in an opposite way, as it tends to grow into pore spaces. Kaolinite may have helped stop syntaxial overgrowth, but it also contributed to significant porosity loss. In many cases, bituminous hydrocarbon got trapped in clay matrix and cements, thus reducing porosity (**Figure 3.64**).

Porosity creation

Carbonate cement not only preserves IGV, but also creates secondary porosity when it dissolves. It is worth noting that kaolinite creates microporosity, which can implicate efforts to determine fluid saturation in the reservoir via well log analysis (Giannetta et al. in revision), but the extent to which microporosity would impact the effective porosity and permeability or reservoir quality for carbon sequestration generally is debatable. In later stage diagenesis, post-compaction feldspar dissolution has previously been studied and discussed in other formations in the ILB (Freiburg 2016). In the Cypress Formation, similar structures have been observed (**Figure 3.54**), and due to the Cypress Formation's relatively low feldspar content (**Figure 3.46**), this diagenetic event is very likely to have taken place.

Permeability control

Porosity is crucial to reservoir quality, as it shows available accommodation. However, to adequately assess the potential for CO_2-EOR and carbon sequestration, permeability data is essential. Regions with adequate porosity may not be suitable EOR candidates if pathways between pore spaces are sealed by various cements. Although measured porosity may be good, much of the pore volume will not be accessible for CO_2.

Permeability data collected from plug testing combined with petrographic analysis can help to correlate mineralogical factors that control permeability. Four wells of different permeability distributions have been selected for studying such correlations: 1) Noble Field – Montgomery #B-34 (API 121592606400), 2) Noble Field – Coen #120 (API 121592608300), 3) Dale Field – RHF #2-S (API 120650139400), and 4) Loudon Field – Homan #B2-19 (API 120510119000) (**Figure 3.71, 3.72, 3.73**).

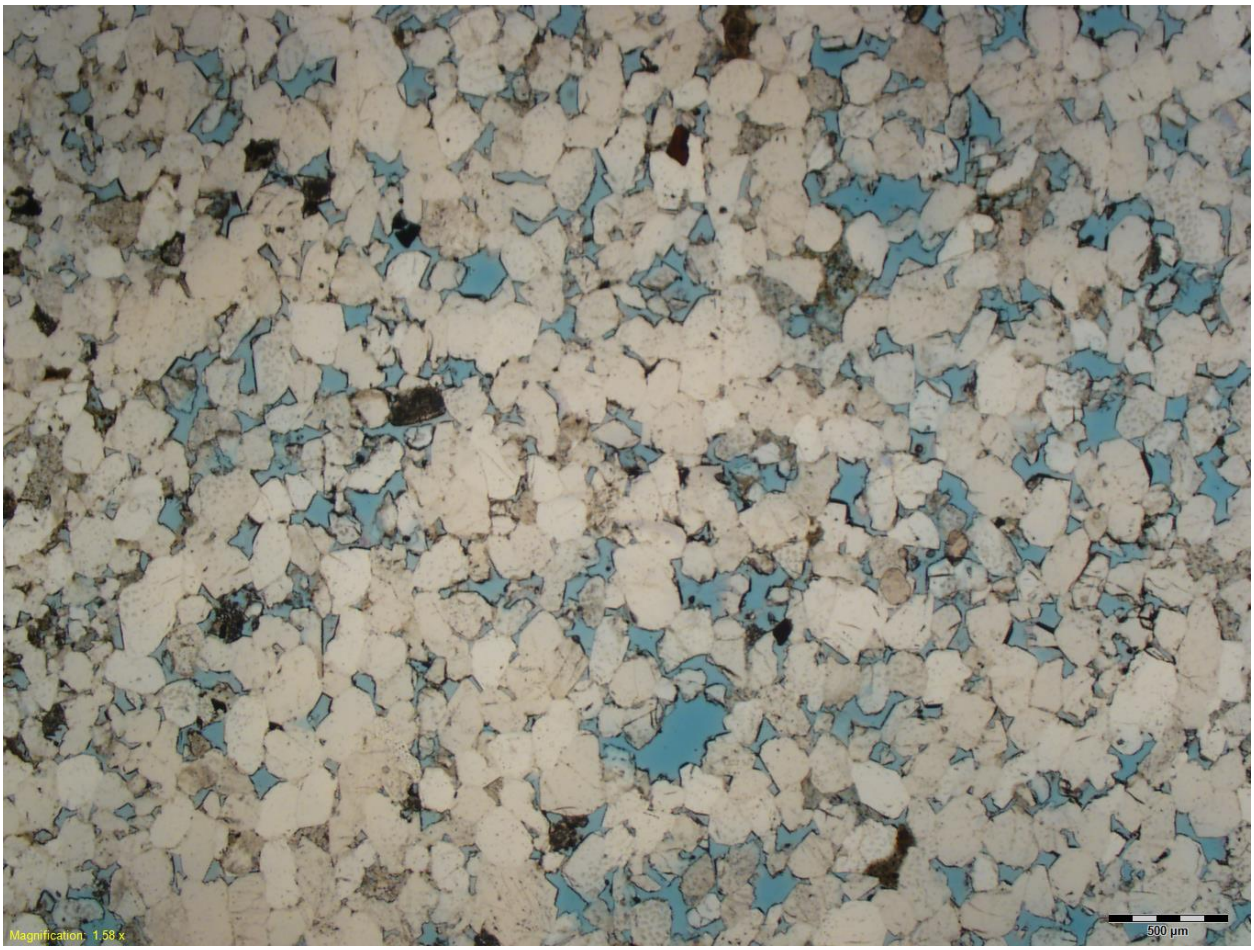

Figure 3.71. RHF # 2-S at 914.3 m (2999.8 ft), Sc, Φ = 18.29%, k = 0.28 µm^2 (284.1mD) Sc, 2.5X plane polarized light. The scale bar at bottom right is 500 µm.

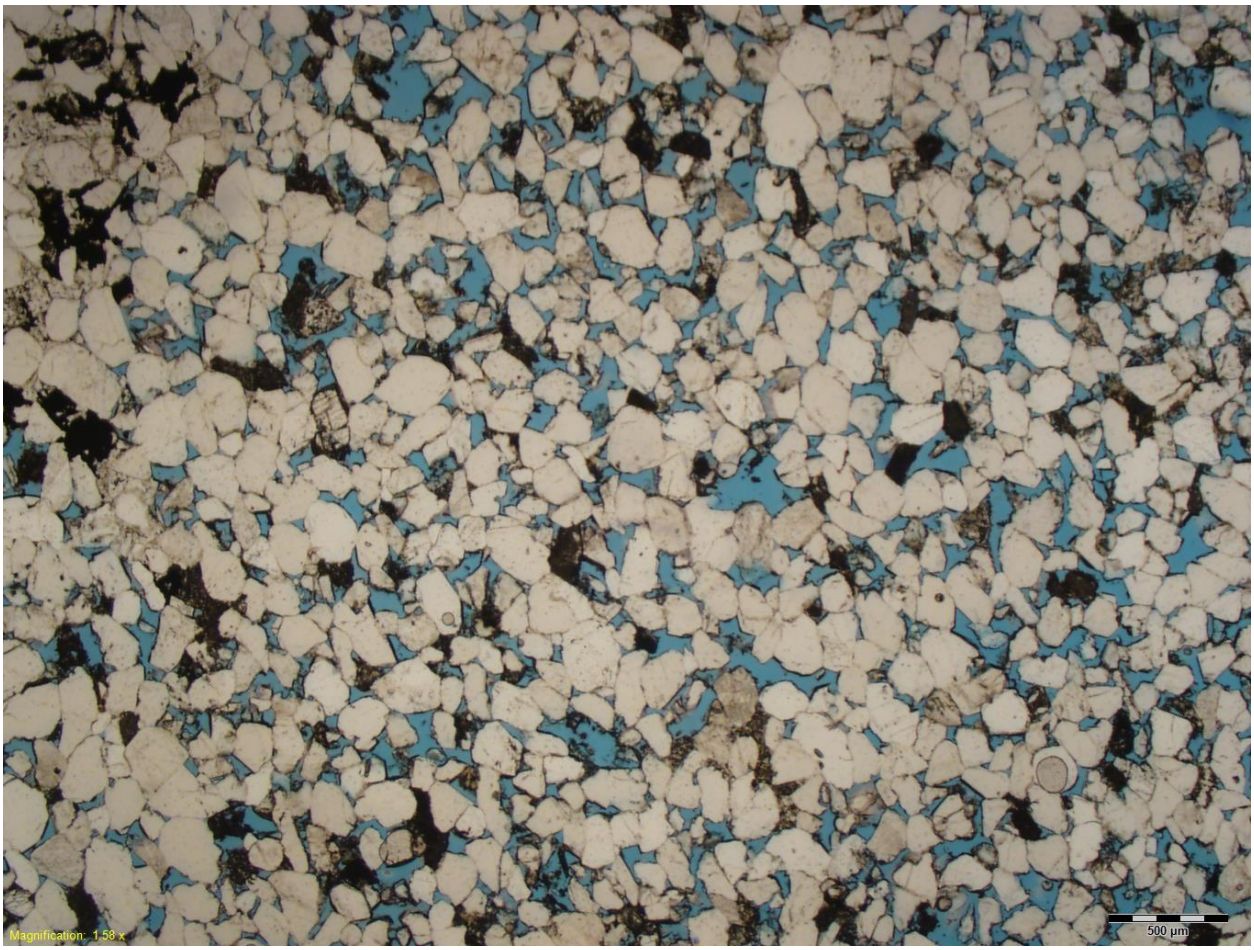

Figure 3.72. Coen #120, at 793.5 m (2603.5 ft), Sc, Φ = 16.2%, k = 0.50 µm^2 (502mD), 2.5X plane polarized light, the scale bar at bottom right is 500 µm.

Figure 3.73. Montgomery #B-34 at 790.2 m (2592.5 ft), Sc, Φ = 20.1%, k = 2.56 µm^2 (2592.5mD), 2.5X plane polarized light. The scale bar at bottom right is 500 µm.

3.6 Cypress Sandstone Reservoir Characterization: Conclusions

- Depositional Environments
  - Major lenticular, multistory sandstone bodies occur at several horizons with shale partings or interbeds displaying cylindrical or bell-shaped geophysical log profile. These sandstone bodies cut down several meters into the succession and the lowermost horizon may reach the limestone or shale of the underlying Ridenhower Shale.
  - The thick Cypress Sandstones are dominantly multistory lowstand deposits of a suspension-dominated river. Characteristic features of the sandstone include but are not limited to: large washed-out cross-sets, low angle cross-sets, asymmetrical current ripples, planar bedding, massive bedding, distorted bedding, and subtle basal lags that are often defined by small magnitude grain size changes and very few lithic intra-clasts.
  - Deposits of sandy fine-grained rivers are a story of subtlety: subtle inflections on traditional well logs highlight storys, slight grain size shifts denote channel story bases and fills, subtle facies change and subtle textures (i.e., low grain size variance) make it difficult for bedforms to be distinguished in outcrop and core – especially in outcrop because the magnitude of preferential weathering is low; thus, outcrops do not necessarily produce weathering profiles that are indicative of bedding changes and boundaries.

- The valley fill Cypress Sandstone is interpreted to be composed of multistory fluvial sandstone deposited during lowstand and transgression with evidence of a change to estuarine conditions near the top. Despite some internal heterogeneity, where multiple sandstone storys amalgamate (as in Noble Field), they create thick, relatively widespread sandstone bodies that have characteristics (such as high lateral and vertical permeability, limited compartmentalization, and large pore volumes) favorable for CO_2 storage.

- Reservoir Characteristics
  - Subtle variations in sandy fine-grained rivers are significant and telling, whether it be in the grain size, clay content, well log response, or facies and facies transitions. Sedimentary architecture in sandy fine-grained systems with low grain size variance may be difficult, or impossible, to recognize in traditional log suites, but are much easier to identify with CMI logs and permeability. Small variations in sandy fluvial deposits of low grain size variance are herein shown to be significant, and thus may be significant in studying sandstones from other depositional environments.
  - Channel bases in fine-grained deposits show subtle, but abrupt, increases in permeability that may act as thief zones or preferential flow paths.
  - The thick Cypress Sandstone exhibits some of the highest permeability values known from sandstone reservoirs anywhere in the Illinois Basin. Petrographic analysis of the cross-bedded sandstone revealed a hybrid pore system of primary intergranular and secondary porosity. Long, well-connected pores resulted from carbonate cement dissolution, which likely controls the high permeabilities.
  - Petrographic date from various sandstone facies shows a majority (84.2%) of all samples as quartz arenite, with a small percentage of subarkose (12.4%) and sublitharenite (4.4%).
  - Quantitative analysis on point-counting data has shown compaction than cementation caused more porosity loss in all sandstone facies in Cypress Sandstone.
  - Permeability is controlled by both sorting/grain size and diagenesis; high porosity, low permeability observed at Loudon Field could be a result of its finer grains and high authigenic clay mineral content relative to the lower porosity but higher permeability Cypress at Noble Field.

3.7 Other Reading

The preceding material dealing with the geologic characterization of the Cypress Sandstone represents a compilation of material from manuscripts from several authors who contributed to this project. The material has been edited. For the complete works, readers should refer to the original manuscripts (listed below), which are in various stages of publication.

Giannetta, L.G., N.D. Webb, S.K. Butler, and N.P. Grigsby, in review, Using clay microporosity to improve formation evaluation in potential residual oil zones: Cypress Sandstone, Illinois Basin. *AAPG Bulletin*.

Grube, J.P., Geology of the Cypress Sandstone in Loudon Oil Field.

Howell, K.J., 2017, Sedimentology of multistory fluvial sandstones of the Mississippian Cypress Formation, Illinois, USA: MS Thesis.

Howell, K.J., N.D. Webb, J.L. Best, and E.W. Prokocki, *in prep*, The Sedimentology of a Large Carboniferous Fine-Grained River: Facies, Paleohydraulics, and Implications for Reservoir Heterogeneity. *Sedimentology.*

Lasemi, Y., and Z. Askari, Stratigraphic variability and reservoir characterization of the Cypress Formation, Clay City Consolidated Field, southeast Illinois

Webb, N.D., and N.P. Grigsby, *in press*, Assessing the Cypress Sandstone for CO_2-Enhanced Oil Recovery and Carbon Storage: Part I - Reservoir Characterization of Noble Oil Field, Western Richland County, Illinois.

Yu, M. and N.D. Webb, Diagenetic Pattern and Petrographic Analysis of the Cypress Sandstone, Illinois Basin.

4. Characterization of Cypress Sandstone ROZ

4.1 Data Compilation and Analysis

The previous section of this report described the detailed geologic characterization of the Cypress Sandstone. That characterization effort focused on the "container" within which the prospective residual oil zones (ROZs) exist. Understanding the container is important because it controls the storage capacity of the Cypress and the spatial distribution of prospective ROZs. Additional research was required to understand the distribution of oil saturation within the container in order to assess the CO_2-EOR resource. Thus, in this section of the report, the focus is on:

- Development of a methodology using well logs to identify critical fluid contacts that bound the top and base of a ROZ (i.e., the producing oil-water contact and the oil-water contact, respectively).
- Characterizing the fluid saturation within the Cypress Sandstone at Noble and Kenner West Fields using the well log methodology.
- Determining residual oil saturation to water using laboratory experiments with analog fluids to better calibrate well log analysis.

4.2 Well Log Analysis

4.2.1 ROZ characteristics

Residual oil is commonly considered in the context of oil remaining in a main pay zone (MPZ) after primary and secondary recovery and is specific to a displacing fluid use (e.g., residual oil to water or residual oil to CO_2). Naturally occurring residual oil is possible as groundwater movement over geologic timescales can sweep oil reservoirs resulting in thick intervals of residual oil (i.e., ROZs) that can exist beneath an MPZ or, if the entire oil column is swept, without an associated MPZ.

ROZ studies have focused on carbonate formations in the Permian (Koperna and Kuuskraa, 2006), Big Horn, and Willison Basins (Burton-Kelly et al., 2014; Yang and Qing, 2016) and have advanced the understanding of the processes, occurrence, characteristics, and identification of ROZs. To characterize the lateral distribution of ROZs, basin-scale studies have used indirect indicators, such as sulfur in formation fluids, extensive dolomitization, and tilted oil water contacts, as preliminary screening tools to identify areas that have high ROZ potential (West, 2014; Trentham and Melzer, 2015). Recently, basin evolution models have been developed for the Williston Basin to simulate the generation, transport, and fate of hydrocarbons (Burton-Kelly et al., 2014, 2017). When calibrated to core and log data, these models have been able to predict oil accumulations in areas with known oil saturation and could potentially locate greenfield ROZs in areas that lack other indicators.

Residual oil saturation to water is highly variable (typically 15 to 35% in sandstones) and controlled by rock (e.g. lithology, pore/grain size and shape, wettability) and fluid (e.g. viscosity, interfacial tension, flow velocity) characteristics (Valenti et al., 2002; Teklu et al., 2013). Methods have been developed to estimate residual oil saturation remaining in depleted MPZs to maximize oil recovery. These methods can be applied to natural ROZs, but often involve core or modern well logs; therefore, they can be expensive and time consuming to acquire in mature oilfields (Chang et al., 1988; Pathak et al., 2012).

Because there is little log contrast between the low oil saturation characteristic of ROZs, the overlying depleted MPZ, and the underlying aquifer, it is difficult to identify ROZs' oil-water contacts, making traditional well log analyses unreliable. We have developed a methodology to identify fluid contacts between MPZ, ROZ, and aquifers using a combination of established well log analyses techniques derived from neutron-density

porosity and resistivity well logs. In addition, water saturation calculated from well logs was used to estimate oil saturation within the MPZ and ROZ.

4.2.2 Methods to Identify ROZs

The methodology is a combination of log derived water saturation (S_W), moveable hydrocarbon index (MHI), apparent water resistivity (R_{WA}), and bulk volume water (BVW) (Archie, 1942; Asquith, 1985; Asquith and Krygowski, 2004) to pick fluid contacts (producing oil water contact (POWC) and oil water contact (OWC)) and determine if the analyzed well has an ROZ.

The moveable hydrocarbon index (MHI) can be used to identify the boundary between mobile and immobile oil (i.e., the POWC or top of the ROZ). Apparent water resistivity (R_{WA}) is directly affected by water saturation and, consequently, has distinct characteristics within the MPZ, ROZ, and underlying aquifer that can be used to help guide the selection of both the POWC and OWC. Bulk volume water (BVW) is used to identify intervals that are at irreducible water saturation (i.e. the MPZ), and apparent changes in saturation that maybe attributable to grain size changes. A S_W profile can be used to validate the OWC and to characterize the oil saturation of the well by determining the oil saturation in the MPZ, ROZ, and at the POWC.

This methodology is meant to use existing data as a preliminary screening tool for identifying the presence of a ROZ. However, analysis of well logs involves some degree of uncertainty, so additional data was used to support findings whenever possible. For example, historical data (such as oil shows, oil production/perforations, core analysis data, drill stem tests) for nearby wells was used to validate occurrence of mobile oil.

Water Saturation Profile

Water saturation profiles (S_W vs depth) can be created by using established methods of calculating S_W from resistivity and neutron-density porosity logs, e.g., Archie (Archie, 1942) or Dual Water (Waxman and Smits, 1968; Clavier et al., 1984). A ROZ below a MPZ will have S_W that varies with depth according to a predictable behavior shown in **Figure 4.1** (Koperna and Kuuskraa, 2006; Harouaka, A. et al., 2013; Yang and Qing, 2016). Within the MPZ, water saturation is low and at irreducible saturation. Below the base of the MPZ at the top of the ROZ, water saturation increases to a constant water saturation (i.e. the residual oil saturation); referred to here as the ROZ transition zone. Below the constant water saturation within the main ROZ, the water saturation increases to 100%, in the underlying aquifer; referred to here as the capillary transition zone. The lower boundary of irreducible water saturation is defined here as the producing oil water contact (POWC) and the depth where water saturation increases to 100% is the oil water contact (OWC). The ROZ is defined here as the interval between the POWC and the OWC. These definitions make a distinction between MPZ, main residual oil zone (MROZ), and two capillary transition zones.

Some input parameters (such as Archie's cementation exponent or the shale properties used in Dual Water equations) can be difficult to estimate or do not remain constant throughout the thickness of the formation, and even a small error in one of these parameters can cause a ROZ to appear as 100% S_w. Furthermore, even if S_w is calculated accurately, additional information is needed to determine the oil saturation that is necessary to be mobile, making the POWC pick difficult. Nevertheless, water saturation profiles can be used to estimate the amount of oil in the MPZ and ROZ and as the basis of regional ROZ resources assessments, and individual ROZ field studies.

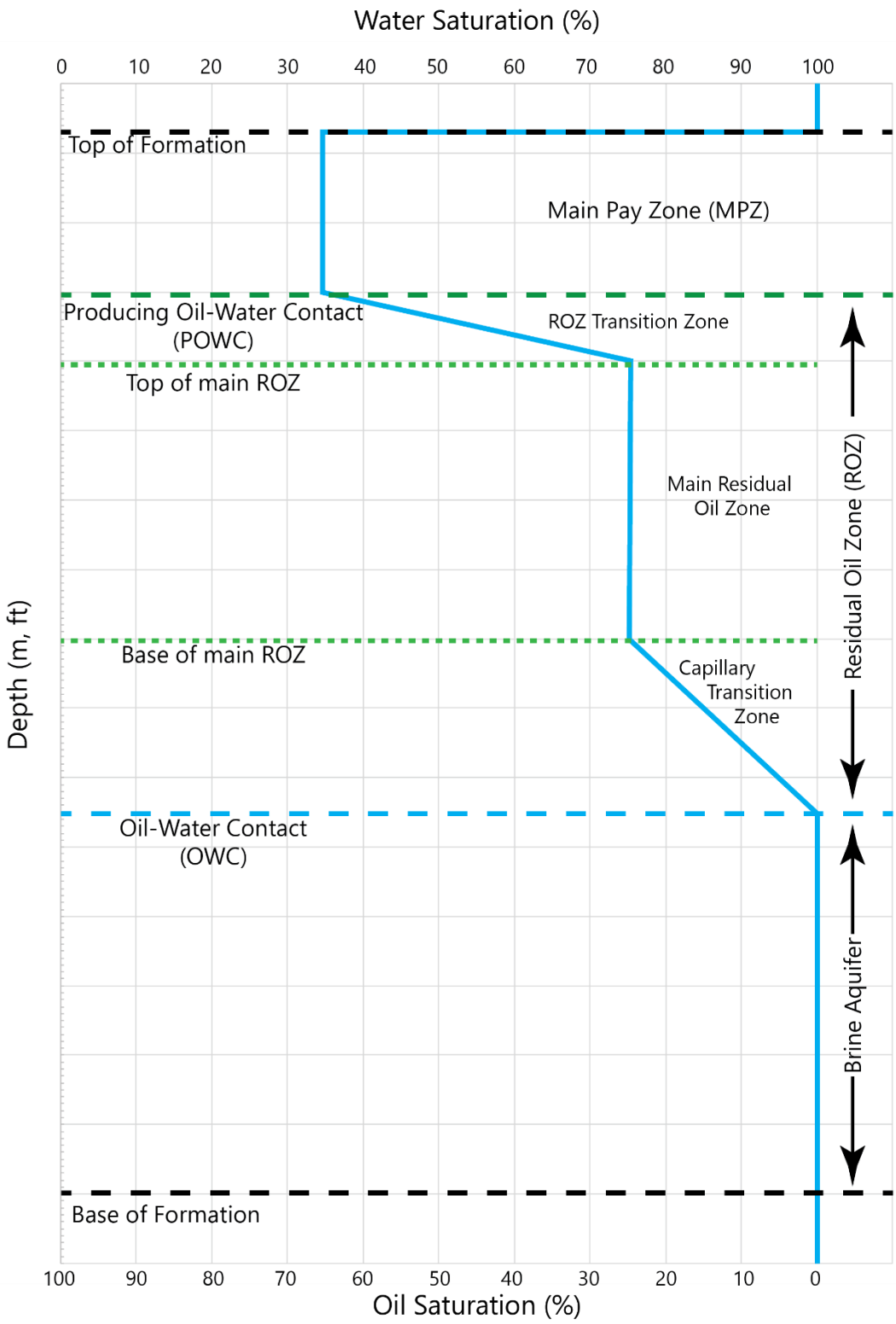

Figure 4.1. Idealized water saturation (S_W) profile. Top and base of the porous formation indicated with black dashed lines, water saturation profile shown with solid blue line. The ROZ exists between the producing oil-water contact (POWC – green dashed line) and the oil-water contact (OWC), below which water saturation becomes 100%. Irreducible water saturation is 35%, and residual oil saturation in this figure is 25% (75% S_W). The ROZ is comprised of the ROZ transition zone, main ROZ, and capillary transition zone.

Moveable Hydrocarbon Index

The moveable hydrocarbon index (MHI) was developed as a quick look method to identify reservoirs that contain movable hydrocarbons by comparing the water saturations of the uninvaded formation and the flushed zone (Asquith, 1985; Asquith and Krygowski, 2004). Mud filtrate invades permeable hydrocarbon-bearing zones and displaces the hydrocarbons from the flushed zone immediately adjacent to the drilled wellbore, resulting in the flushed zone having a higher water saturation than the uninvaded formation. For hydrocarbon-bearing zone in which the hydrocarbon has been flushed or moved by the mud filtrate, MHI is calculated as follows:

$$MHI = \frac{S_w}{S_{xo}} = \sqrt{\frac{R_{xo}/R_t}{R_{mf}/R_w}} \quad (8)$$

Where:

- S_{xo} = water saturation of the flushed zone
- R_t= resistivity of the uninvaded zone (ohm-m)
- R_{xo} = resistivity of the flushed zone (ohm-m)
- R_{mf} = resistivity of the mud filtrate (ohm-m at formation temperature)

It is generally accepted that, for sandstones, an MHI <0.7 (<0.6 for carbonates) indicates that hydrocarbons are present, and that the formation has adequate hydrocarbon mobility (Asquith, 1985; Asquith and Krygowski, 2004). If this holds true, the MHI will be <0.7 in the productive portion of a sandstone reservoir (i.e. the MPZ and ROZ transition zone) and > 0.7 in the unproductive portion (i.e., the ROZ and 100% S_W intervals).

Apparent Water Resistivity

Apparent Water Resistivity (R_{WA} in ohm-m) is mathematically defined by assuming 100% S_W and using Archie's equation as follows:

$$R_{wa} = \frac{\phi^m * R_t}{a} \quad (9)$$

Where:

- ϕ = porosity
- m = cementation exponent
- a = tortuosity factor

Each interval (MPZ, ROZ, 100% S_W) will have a characteristic R_{WA} signature. Resistive hydrocarbon-filled pore space will result in a very high R_{WA} in the MPZ. Conversely, conductive brine filling the pore space within a 100% S_W interval will result in the lowest R_{WA} (equal to the R_W) of the formation. A ROZ is a mixture of oil and water and will have an R_{WA} values between that of the MPZ and 100% S_W interval.

The minimum R_{WA} can be compared to the known value for R_w for the formation; this can be used to validate a 100% S_W interval below the ROZ. The depth at which R_{WA} meets the true R_W (the known resistivity of the formation water) can be used to pick the OWC.

Bulk Volume Water

Bulk volume water (BVW) is the product of water saturation and porosity and is commonly used to identify MPZs that will produce water-free oil; i.e., S_W is at irreducible saturation (S_{WIRR}). BVW is calculated as follows:

$$BVW = S_w * \emptyset \quad (10)$$

The assumption is that BVW is constant at S_{WIRR} for similar grain sizes and increases with decreasing grain sizes (**Table 4.1**) (Asquith, 1985; Asquith and Krygowski, 2004). Therefore, an interval of the upper reservoir that has a constant BVW indicates an MPZ at S_{WIRR} within a homogenous formation. If the MPZ is at S_{WIRR}, BVW will maintain a stable value related to the grain size in the MPZ and begin to increase immediately below the POWC. A thick MPZ that exhibits two different but constant BVW values indicates that the zone is at S_{WIRR} but has two unique grain sizes. In the aquifer, BVW is expected to be equal to porosity.

Table 4.1. Relationship between grain size and bulk volume water at S_{WIRR} in sandstone reservoirs; from Asquith, 1982.

Grain Size		Bulk Volume Water at S_{WIRR}
Coarse	0.5-1.0 mm	0.020-0.025
Medium	0.25-0.5 mm	0.025-0.035
Fine	0.125-0.25 mm	0.035-0.050
Very Fine	0.062-0.125 mm	0.050-0.070
Silt	<0.0625 mm	0.070-0.090

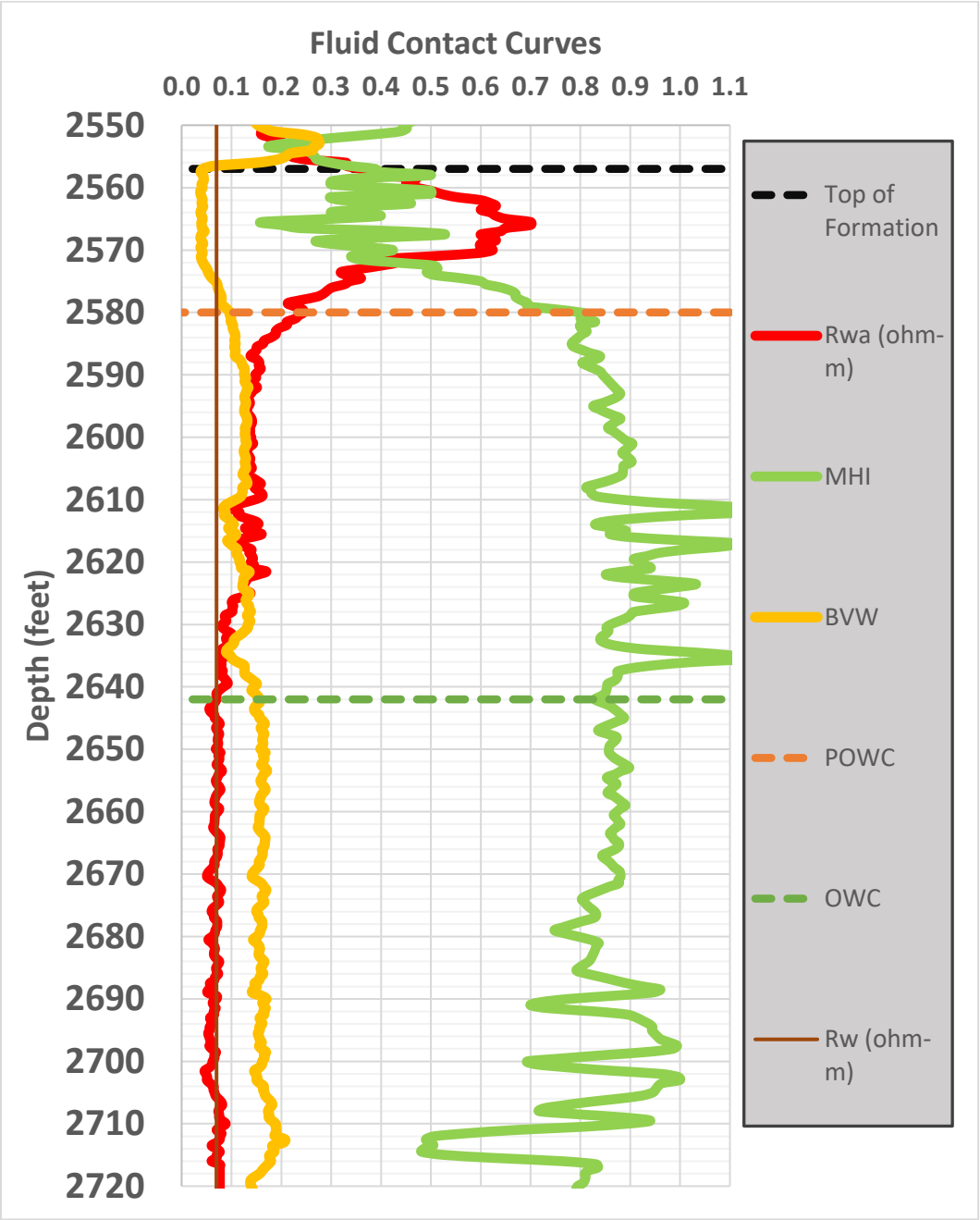

Figure 4.2. Idealized Fluid Contact Curves. Moveable hydrocarbon index (solid green line), R_{WA} (solid red line), and BVW (solid orange line) curves plotted against depth. The POWC (dashed orange line), top and base of the ROZ (dashed red and blue lines), and OWC (dashed green line) are the same depths from Figure 4.1. BVW is low and constant within the MPZ, increases to the value of porosity as water saturation increases. MHI is less than 0.7 in the MPZ and increases to greater than 0.7 where there is no moveable hydrocarbon (in the ROZ and 100% S_W zone). R_{WA} is very high in the MPZ, decreases and stabilizes in the ROZ, and decreases again before stabilizing at the true R_W in the 100% S_W zone. This behavior can be used to aid in selection of POWC and OWC.

4.2.3 Application to Noble Oil Field

Field Background

Noble Field produced oil from a MPZ approximately 18 m (60 ft) thick at the top of the 27 to 53 m (90 to 175 ft) thick Cypress Sandstone. Wells with neutron density porosity and resistivity logs necessary for this study

were completed after the 1980 and reflect decades of primary production and waterflooding; consequently, these logs reflect MPZ oil saturation below S_{WIRR}. Waterflooding complicates the estimation of water resistivity for the water saturation calculations from resistivity logs.

The reservoir temperature for the Cypress Sandstone at Noble Field was determined to be 31.7°C (89°F), in agreement with the temperature expected based on the standard geothermal gradient for the Illinois Basin. Reservoir pressure was determined to be of 7,424.5 kPa (1,076.80 psi) at 778.2 m (2,553 ft) based on a 2006 drill stem test of the Foss #8 well (API 121592619300, southwest of the northeast Section 8, T3N, R9E). The standard hydrostatic pressure gradient of 9.8 kPa/m (0.433 psi/ft) for the normally pressured Illinois Basin gives an expected pressure of 7,621.5 kPa (1,105.4 psi) at this depth. The standard hydrostatic gradient is close to the calculated gradient of 9.6 kPa/m (0.422 psi/ft) for this well. The primary drive mechanism for the Cypress Sandstone is likely a combination of solution gas and bottom water drive.

Records of oil analyses from the Coen #23 well (API 121590138200, southwest quarter of the southeast quarter Section 4, T3N, R9E) from 1942 indicate that oil from the formation has an API gravity of 37.5°. A waterflood summary for the Grubb-Evans waterflood unit lists an API gravity of 31.8°. A new oil sample from a Cypress Sandstone-only tank battery yielded an API gravity of 33.3° and a viscosity of 7.1 cP. Density of the oil was 0.851 to 0.850 g/mL (0.492 and 0.491 oz/in^3) at temperature of 24.7°C and 31.5°C (76.5°F and 88.7°F), respectively. The wells contributing Cypress oil to the battery included Coen 90, 91, 92, 94, 98, 100, Palmer-Taylor 26, and CL Wilson 4 (southwest quarter of Section 4 (Coen), southeast quarter of Section 5 (Palmer-Taylor), and northeast quarter of Section 8 (Wilson), T3N, R9E).

The disparity in oil gravity from the various samples likely relates to the original setting of the oil within the reservoir. The Coen #23 well was drilled in the early development of the field, perforated in the upper 1.2 m (4 ft) of the reservoir, and sampled shortly after completion, resulting in a higher API gravity. Oil gravity commonly increases from the base to the top of the reservoir because higher volatiles naturally migrate upward over geologic time. The later waterflood unit and tank battery oil samples, which were collected farther down the production curve and likely have lower gas content, may reflect oil that was originally lower in the reservoir that has migrated up over time with development and production in the field, particularly as water coning moves oil from lower in the reservoir upward.

An operator in Noble Field has reported to the author that biodegradation has increased the viscosity of the oil produced from the Cypress, as evidenced by chunks of paraffin and “slime balls” recovered from produced oil. The operator must circulate biocide through their equipment every few months to prevent corrosion and biomass plugging of reservoir permeability. The brine–oil interactions responsible for the biodegradation of the oil may not be limited to the oil–water contact and may reflect the incursion of brine into the reservoir because of water coning, which is associated with the production or disposal of formation waters into the Cypress over several decades.

Meents et al. (1952) recorded the brine composition of 98,182 parts per million (ppm) of total dissolved solids (TDS) from an unspecified well in Section 8, T3N, R9E. An analysis by Demir (1995) of a brine sample from a well northeast of Noble Field had slightly more than 101,000 ppm of TDS. A new brine sample was collected from the Coen #92 well (API 121592607500, northwest quarter of the southwest quarter Section 4, T3N, R9E) and yielded 98,121 ppm of TDS, consistent with the previous findings.

Water resistivity values for Cypress Sandstone can be calculated by using Equation 3 from Demir (1995):

$$R_{w(T)} = 957/[(TDS)^{0.778} \times (1.017)^{T}], \quad (11)$$

Where:

- $R_{W(T)}$ = water resistivity (in ohm-m) at temperature °C (°T)
- TDS = total dissolved solids concentration (in mg/L or ppm)

With a reservoir temperature of 31.7°C (89°F) and a TDS value of 98,121, the R_W for the brine is 0.073 ohm-m.

The Cypress Sandstone at Noble Field is a thick, homogenous, fine- to very-fine grained sand that transitions into an overlying heterolithic, shale-rich interval. The formation has few shale breaks throughout, and two thin (< 1 m (< 3 ft) thick) laterally extensive calcite cement layers. Ninety-five wells that fully penetrate the thick Cypress Sandstone in Noble Field and the surrounding area were logged with resistivity and neutron density porosity logs. Four of these wells were also logged with cased-hole pulsed neutron logs (PNLs) in 2017. Based on analysis of core and neutron-density porosity logs, porosity is typically between 16 and 20% and permeability is high (up to a Darcy). Petrographic analysis performed on core suggests that the thick Cypress has low clay content (on average around 4% by volume) (Giannetta et al., in press).

Noble Field-Wide Results – ROZ Characterization

For validation using nearly 100 wells only the POWC and OWC were picked, and the POWC was picked where MHI = 0.7. This method groups both transition zones into the ROZ. From the well log analyses, oil was detected in 86 of the 95 wells analyzed; a MPZ overlying a ROZ was detected in 71 and a ROZ with no overlying MPZ was detected in 15 wells. The OWC was consistently around 652.3 m (2,140 ft) below sea level with a small standard deviation (**Figure 4.3** and **Table 4.2**). The top of the Cypress was around 640.1 m (2,100 ft) and the POWC was around 637.0 m (2,090 ft) (**Figure 4.3** and **Table 4.2**). Both had much more variability shown by the larger standard deviation and maximum and minimum. This is attributed to the lateral variability in structure and oil production.

The median oil saturation in the MPZ was ~55%, the median oil saturation in the ROZs was ~24%, and median oil saturation at the POWC was ~42% (**Figure 4.4** and **Table 4.2**). The standard deviations show residual oil saturation (to water in the ROZ) is between 20 and 29% and the oil saturation necessary to be mobile is between 38 and 49% (at the POWC).

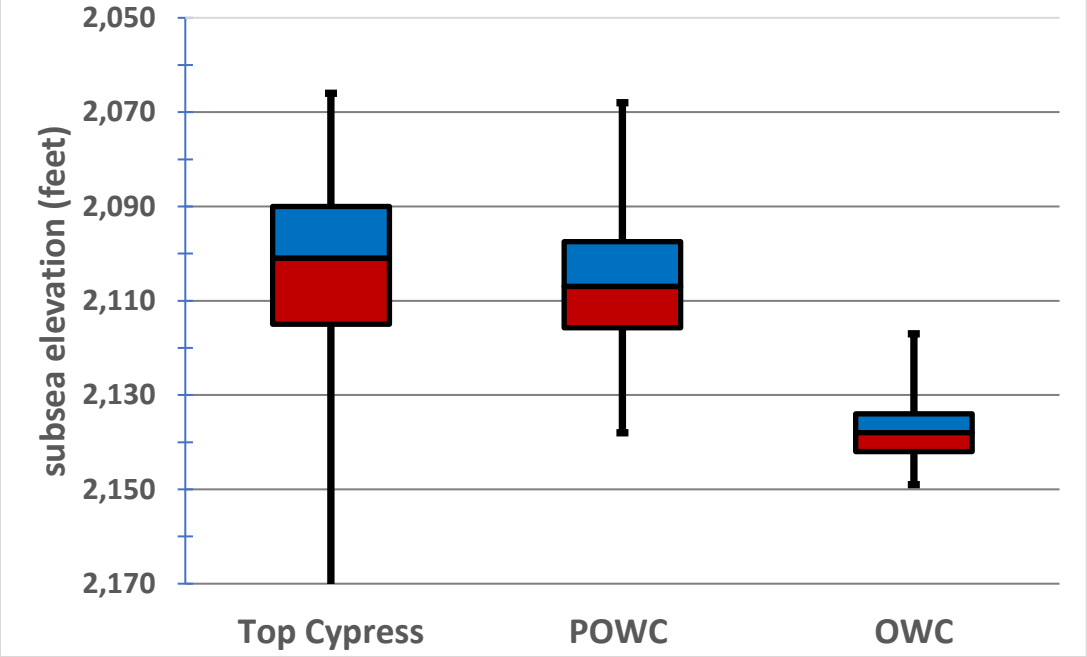

Figure 4.3. Box and whisker plot of the depths of the top of the Cypress, POWC, and OWC derived from fluid contact curves for 96 wells at Noble Field. Boxes represent the median (where blue meets red) and standard deviations (bottom of red is

median -1 standard deviation, top of blue is median + 1 standard deviation). Whiskers represent the maximum and minimum extent. There is less variability in the OWC than in the POWC and top of the Cypress and the overlap between top of the Cypress and POWC is indicative of the thin and/or depleted MPZ.

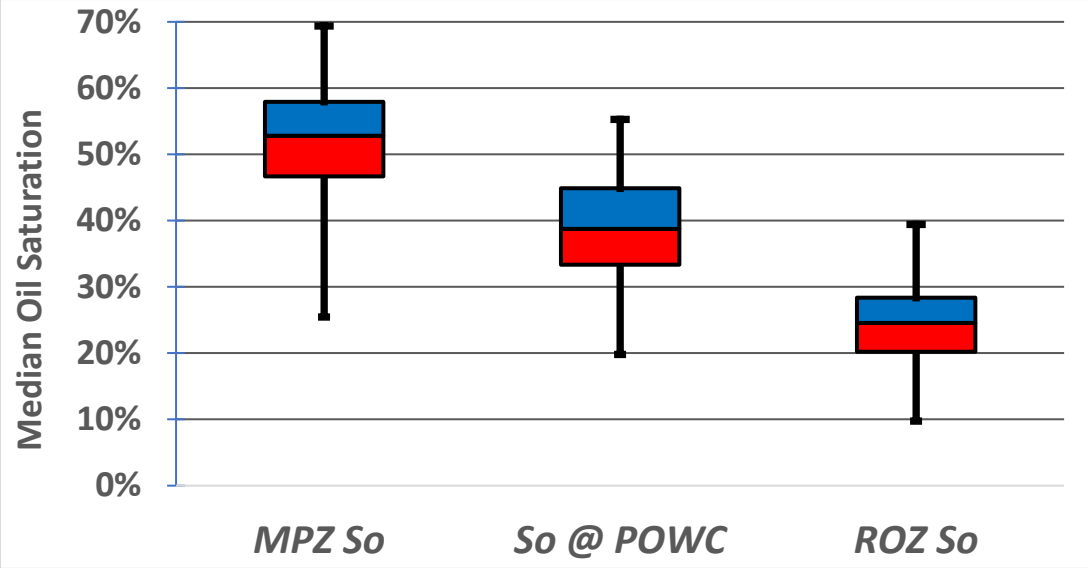

Figure 4.4. Box and whisker plot of the median oil saturation within the MPZ and ROZ and the saturation at the POWC for 86 wells at Noble Field that had oil saturation. Boxes represent median (where red box meets blue box, and standard deviations). Whiskers represent the maximum and minimum observed oil saturations. The data shows a clear trend of decreasing oil saturation with depth. These results indicate that the oil saturation necessary to be mobile is around 38 to 48% and the residual oil saturation is between 20 and 28%.

Table 4.2. Field wide statistics for MPZ and ROZ dimensions and oil saturations.

	MPZ median S_O (%)	S_O @ POWC (%)	ROZ median S_O (%)	Top Cypress Subsea elevation (m, [ft])	POWC Subsea elevation (ft)	OWC Subsea elevation (ft)
Median	54	42	25	639.5 [2,098]	641.9 [2,106]	652.0 [2,139]
Standard Deviation	9	7	5	5.2 [17]	4.0 [13]	1.8 [6]
Minimum	29	20	14	653.8 [2,145]	652.6 [2,141]	655.6 [2,151]
Maximum	69	57	34	629.7 [2,066]	630.3 [2,068]	647.7 [2,125]

Validation

Two approaches were used to validate the reliability of using the fluid contact curves: historical records (i.e., oil shows recorded while drilling) and recent cased-hole PNLs.

Historical records

Historical data (such as oil shows listed on drilling and core analysis reports and perforated intervals of oil producing wells) was compiled for each well and compared to the interpreted MPZs and ROZs. The analysis requires modern wells (with neutron-density porosity logs) that fully penetrate the Cypress, so most wells

analyzed were targeting deeper formations. This results in Cypress producing perforations in only 7 of the 95 wells analyzed. Forty-four of the wells recorded oil shows in the Cypress. All producing perforations occurred within the fluid contact curve derived MPZ. The top of oil shows occurred between the top of the Cypress and the POWC. The base of the oil shows usually occurred within a few feet of the POWC, but sometimes occurred slightly below it; within the fluid contact curve derived ROZ.

Pulsed-Neutron logs

Schlumberger's Reservoir Saturation Tools (RST), a cased-hole PNL, was acquired on four wells from two leases within Noble Field: Winter #4, Winter #6, Foss #6, and Foss #7. The Foss #6 and Foss #7 were Cypress oil producing wells. The Winter #4 and Winter #7 were never perforated in the Cypress, but oil saturation for the Cypress was noted on their completion reports. All four wells fully penetrate the thick Cypress and were logged with open-hole neutron-density porosity and resistivity logs when originally drilled. Analysis of the resistivity and neutron density porosity logs indicate that all four wells had a 3-4.6 m (10-15 ft) MPZ overlying a ~6-meter (20-foot) ROZ (**Table 4.3**). Nearby wells had similar interpreted OWCs, supporting the local occurrence of a ROZ. These four wells were selected for PNLs for a few reasons; interpretation of the resistivity and neutron-density porosity logs suggest that each has a strong likelihood of MPZ overlying a ROZ, each has production and/or oil shows that support the interpretation, and operator willingness.

For the wells in which the PNLs were run, the contacts and oil saturations within each interval were analyzed (**Table 4.3**). The OWC derived from the fluid contact curves was within five feet of the OWC from the PNL logs in the Foss #6 well and within two feet in the other three wells, and the POWC was close in the Winter wells and shifted upward in the Foss wells (that had undergone production before the PNLs were taken). However, there is some disagreement between the oil saturations within each interval; PNL oil saturation was higher in the MPZ and lower in the ROZ.

Water saturation curves derived from the PNLs were used to validate the OWC. The PNLs can be used to better understand the oil saturation within the MPZ and at the POWC for the Winter wells, but the Cypress production in the Foss wells between the time they were originally drilled and logged and when they were logged with PNLs was expected to reduce the oil saturation of the MPZs and shift the POWCs upward.

Table 4.3. Drill date and interpreted thickness of the MPZ and ROZ for the four wells that received PNLs.

Well Name	Year drilled	MPZ thickness (feet)	ROZ thickness (feet)
Foss 6	1994	14	25
Foss 7	2006	10	25
Winter 4	2008	11	21
Winter 7	2011	12	21

Saturations derived from PNLs were plotted with fluid contact and Archie saturation curves as a function of depth (**Figures 4.5, 4.6, 4.7, 4.8**). The contacts and oil saturations within each interval were recorded for each well (**Table 4.4**). The OWC derived from the fluid contact curves was within five feet of the OWC from the PNL logs in the Foss #6 well and within two feet in the other three wells, and the POWC was close in the Winter wells and shifted upward in the Foss wells (that had undergone production before the PNLs were taken). However, there is some disagreement between the oil saturations within each interval; PNL oil saturation was higher in the MPZ and lower in the ROZ.

Water saturation curves derived from the PNLs were used to validate the OWC. The PNLs can be used to better understand the oil saturation within the MPZ and at the POWC for the Winter wells, but the Cypress production in the Foss wells between the time they were originally drilled and logged and when they were logged with PNLs was expected to reduce the oil saturation of the MPZs and shift the POWCs upward.

Table 4.4. POWC, OWC, and interval oil saturation for four wells that received pulsed neutron logs.

		Foss 6	Foss 7	Winter 4	Winter 7
Identification	POWC depth	2600	2600	2589	2592
	OWC depth (ft)	2625	2625	2610	2613
	PNL OWC depth (ft)	2620	2627	2610	2612
Characterization	Archie So in MPZ (%)	65	44	69	68
	Archie So @ POWC (%)	52	37	47	44
	Archie So in ROZ (%)	21	25	25	29
	PNL So in MPZ (%)	24	20	83	78
	PNL So in ROZ (%)	13	27	18	16

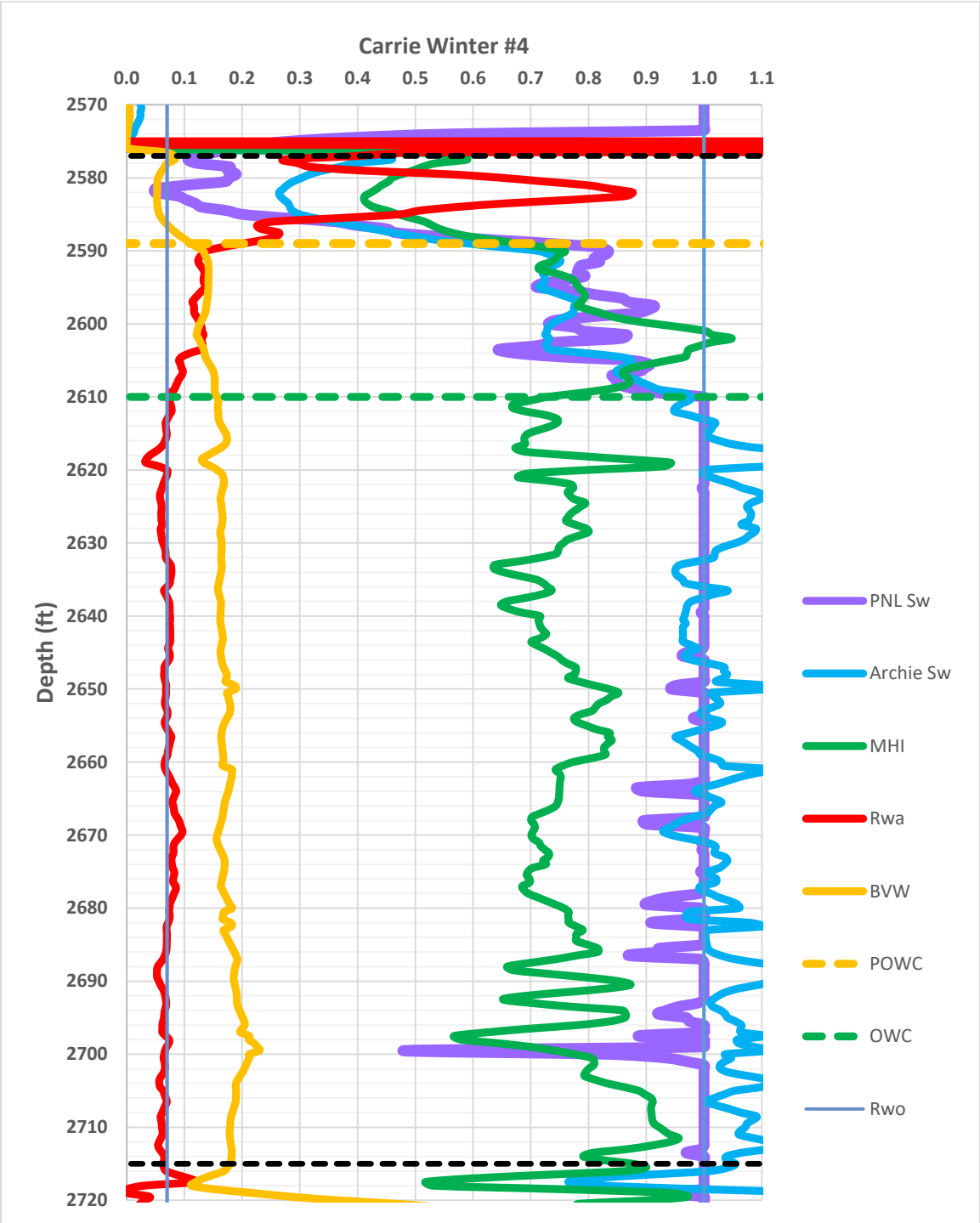

Figure 4.5. Fluid contact curves, picked OWC and POWCs, and Archie and PNL water saturation profiles for the Carrie Winter #4 well (API # 121592624600, NW NW Section 10, T3N, R9E).

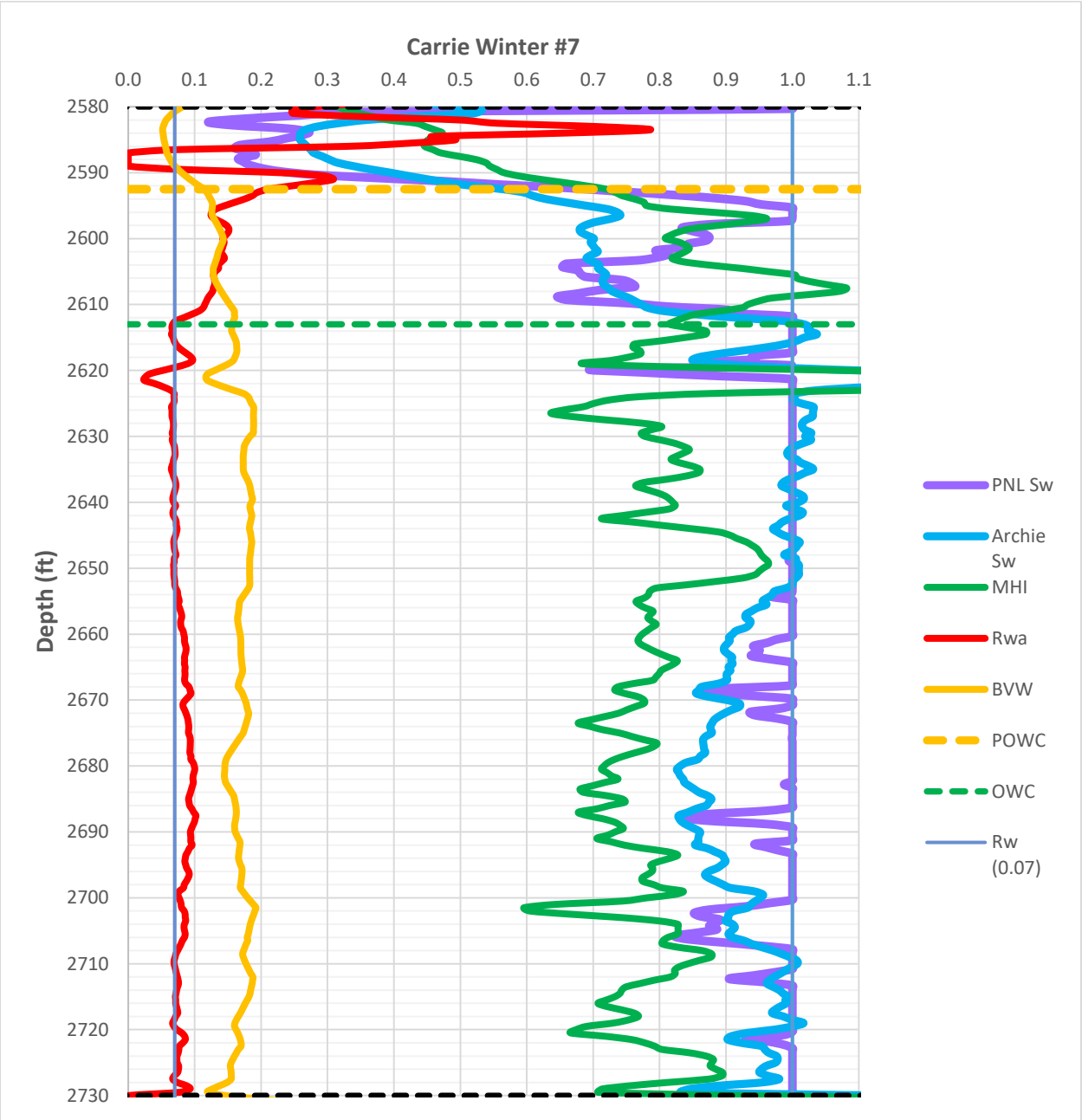

Figure 4.6. Fluid contact curves, picked OWC and POWCs, and Archie and PNL water saturation profiles for the Carrie Winter #7 well (API # 121592631000, SW NW Section 10, T3N, R9E).

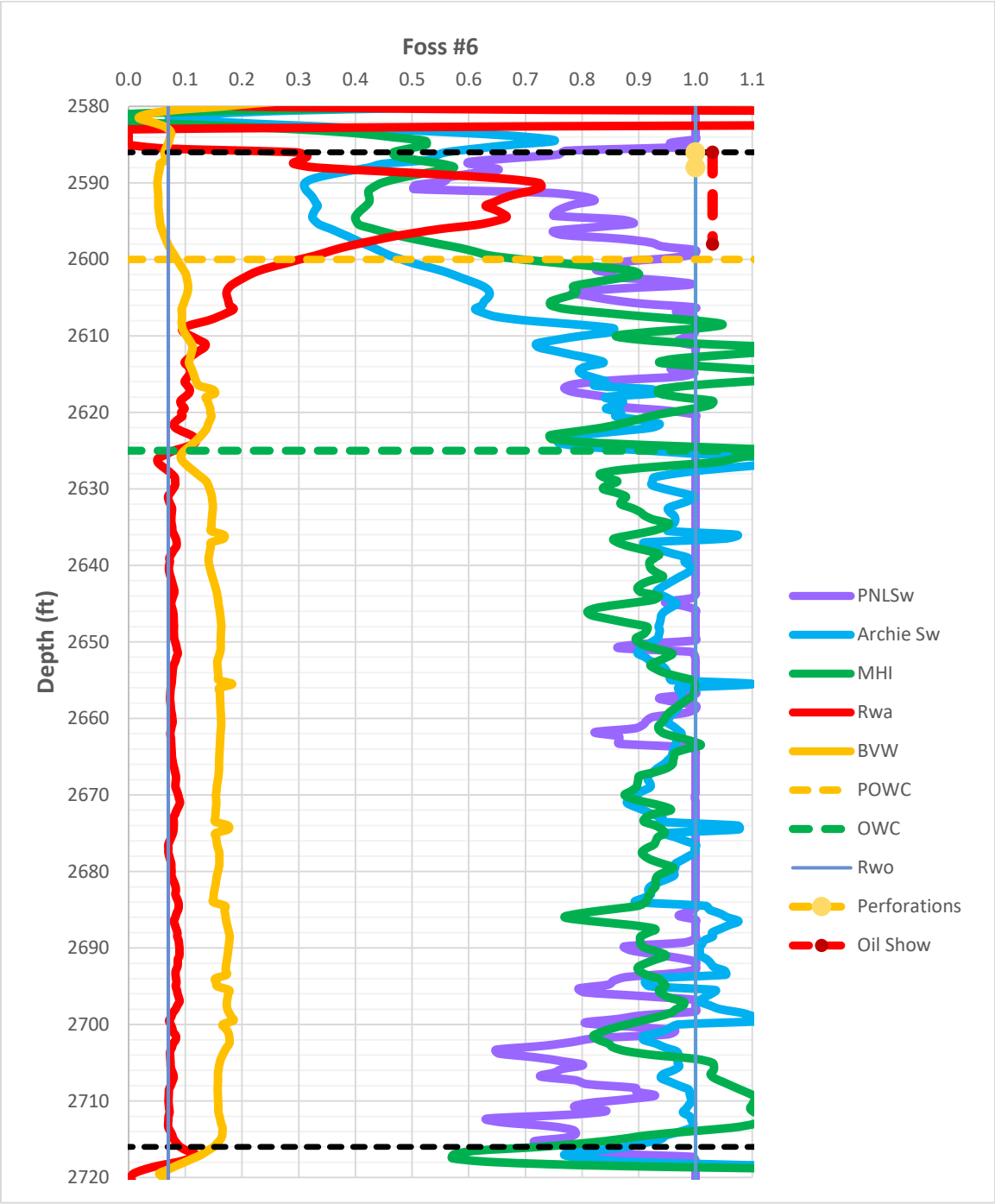

Figure 4.7. Fluid contact curves, picked OWC and POWCs, and Archie and PNL water saturation profiles for the Foss #6 well (API # 121592552800, SW NE Section 8, T3N, R9E). This well had a show of oil from 2586 to 2598 and was perforated from 2586 to 2588 with an initial production of 12 bbls oil, 28 bbls water. It is still producing oil as of 2019.

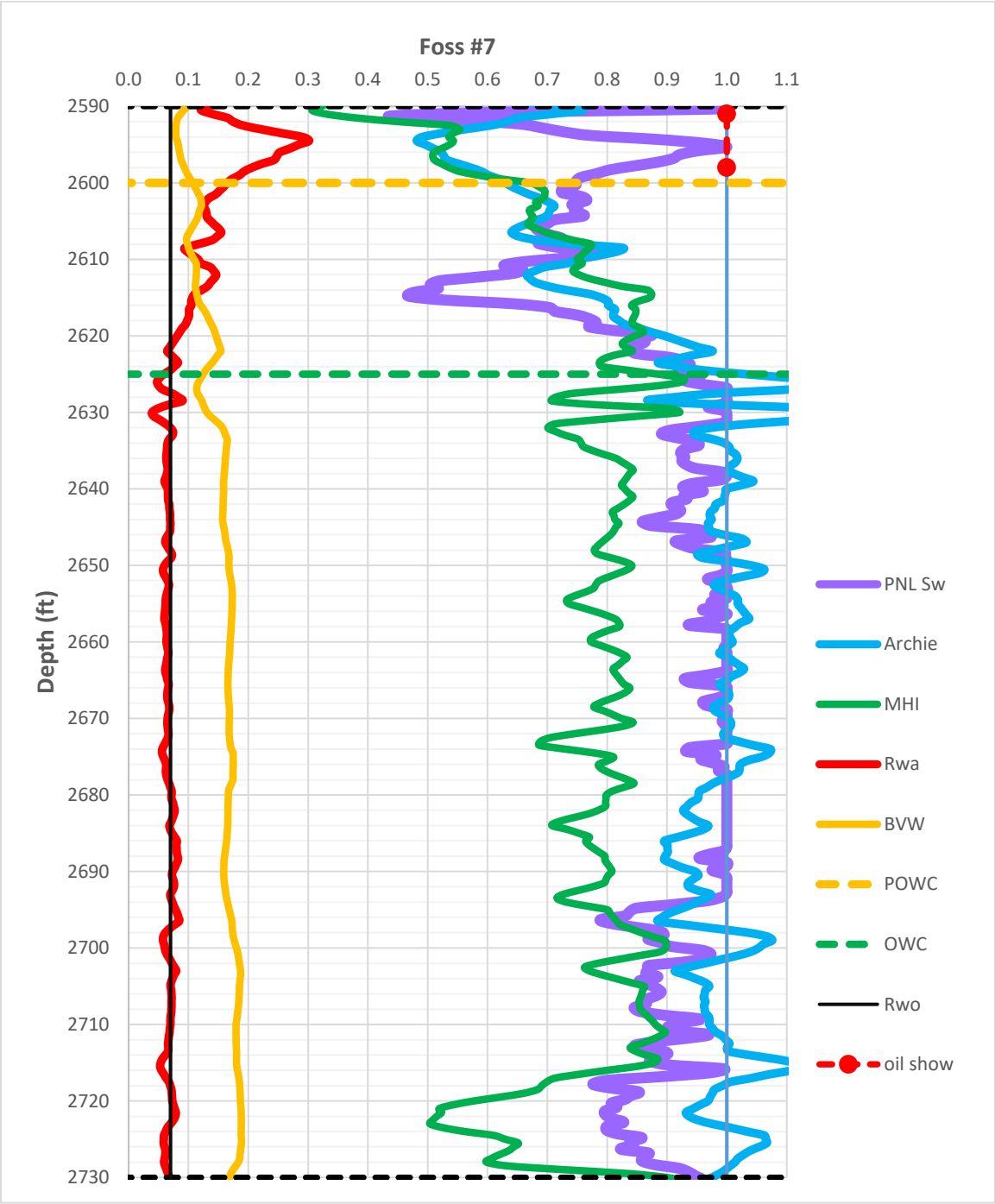

Figure 4.8. Fluid contact curves, picked OWC and POWCs, and Archie and PNL water saturation profiles for the Foss #7 well (API # 121592619200, NW NW NE Section 8, T3N, R9E). The well had a show of oil from 2591 to 2598. The well was a Cypress oil producer, but perforation depths and IPs were not available.

4.2.4 Application to Kenner West Oil Field

Methods developed to identify and characterize the ROZ at Noble Field were also applied at Kenner West Field. Recorded depths of the POWC, OWC, and top of Cypress, and the oil saturation within the MPZ, ROZ, and at the POWC were recorded for all wells and used to create maps of the MPZ, ROZ, and oil column thicknesses and the elevations of the POWC and OWC. The R_w used in the analyses is 0.059 ohm-m and is based on values published by Meents et al. (1952) and Demir (1995).

Wells at Kenner West were generally drilled and logged in two distinct eras; one in the 1940s with SP and resistivity logs (e-logs) that represents the virgin reservoir properties, and another in the 1990s with modern gamma ray and neutron density porosity logs in addition to the e-logs that represents a post-production reservoir. Nine wells had usable resistivity and neutron density porosity logs (post-production) and 26 additional wells had usable e logs (virgin reservoir properties) (**Figure 4.9**).

The method developed at Noble Field relies on porosity from neutron density porosity logs. It was therefore applied directly to the wells with neutron density porosity logs. These wells were drilled and logged after the 1980s, so the results represent reservoir conditions post primary and secondary recovery. An effort was made to use old wells that did not have neutron density porosity logs to characterize the virgin (pre-production) distribution of oil and water. An SP to porosity transform created during geocellular model development was used to calculate a porosity curve that was used in Archies equation to construct water saturation profiles. These wells did not have gamma ray logs, so volume of shale and dual water saturations could not be calculated.

Calculating porosity from SP logs and the lack of shale estimates introduces an added source of uncertainty, so several steps were taken to help improve confidence in the analysis of the e logs. SP derived water saturation was calculated for wells with neutron density porosity logs. This was compared to the saturation derived from neutron density porosity logs (assumed to be more accurate) to determine how closely the SP derived water saturation approximated results. Also, the results for the wells with no neutron density porosity logs were compared to historical records and mapped to identify outliers. Finally, statistics for key results (oil saturation at the POWC and residual oil saturation) for all wells were compared to ensure that values were reasonable.

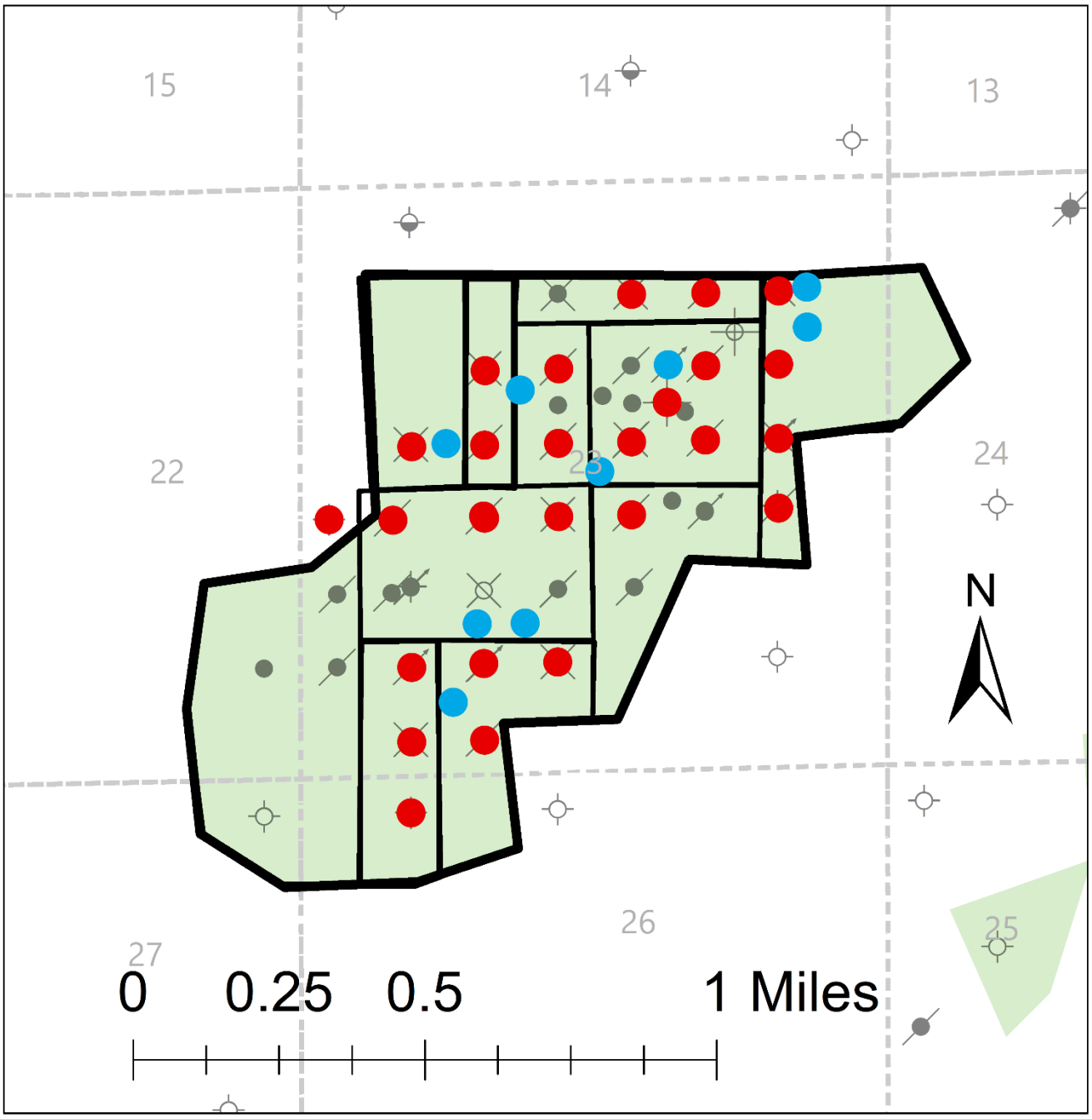

Figure 4.9. Locations of wells used for well log analysis. Wells with neutron density porosity logs shown in blue dots and wells with only old e logs are shown in red dots. Lines indicate leases and black dots indicate wells that did not have logs that fully penetrate the Cypress.

1990s wells

The nine wells with neutron density porosity logs are evenly distributed (**Figure 4.9**). Two of the wells (120252895200 and 120252895300) were perforated in, and produced oil from, the thick Cypress. The other seven wells had shown of oil listed on the scout tickets. The water saturation and fluid contact curves were calculated and plotted against depth and POWC and OWC were selected (**Figure 4.10, 4.11**). Depths of shows of oil listed on drilling reports, perforated intervals, drill stem tests, and core were also recorded and added to the profiles.

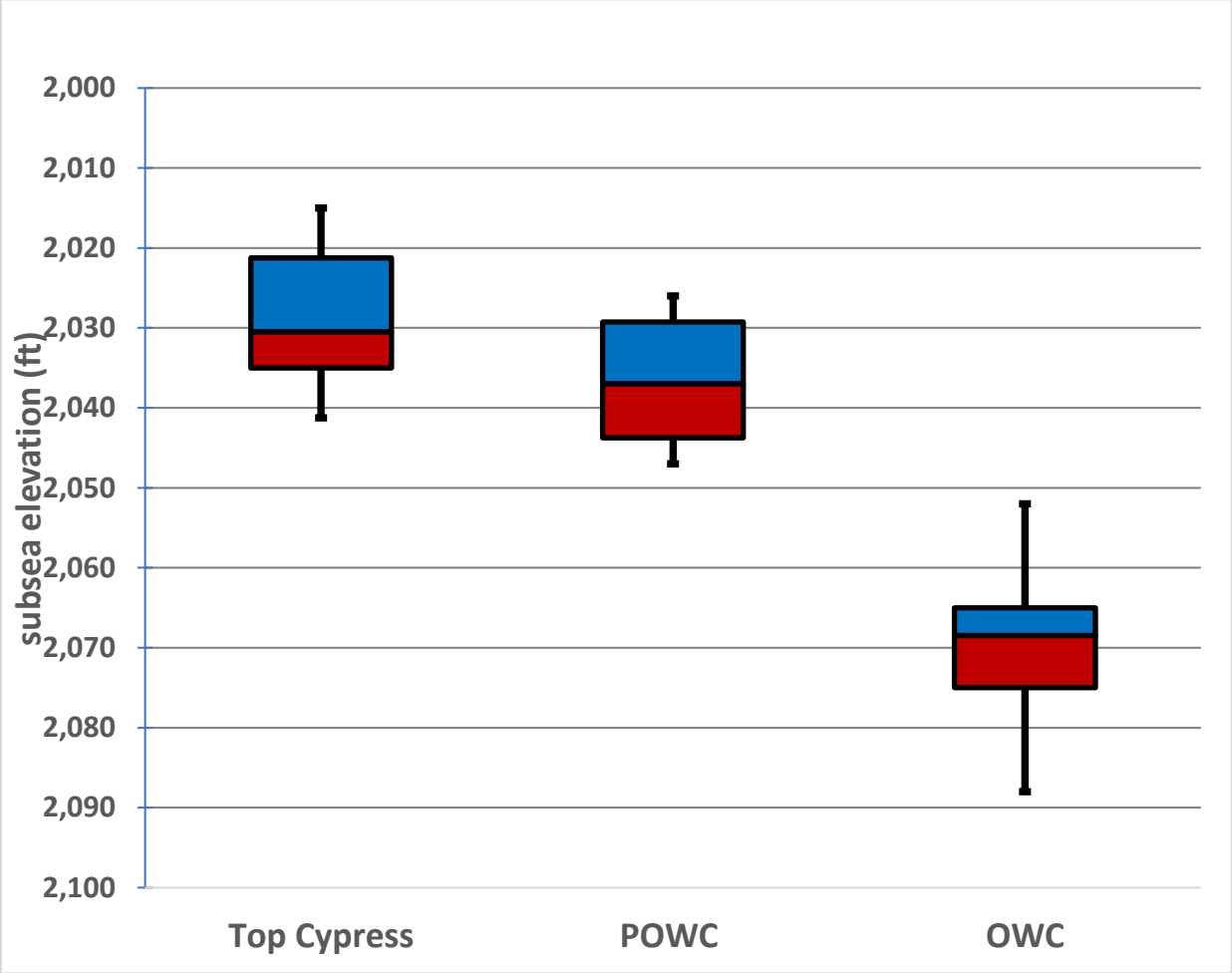

Figure 4.10. Box and whisker plots of the median oil saturations of the MPZ, and the POWC and in the ROZ for the 1990s vintage logs.

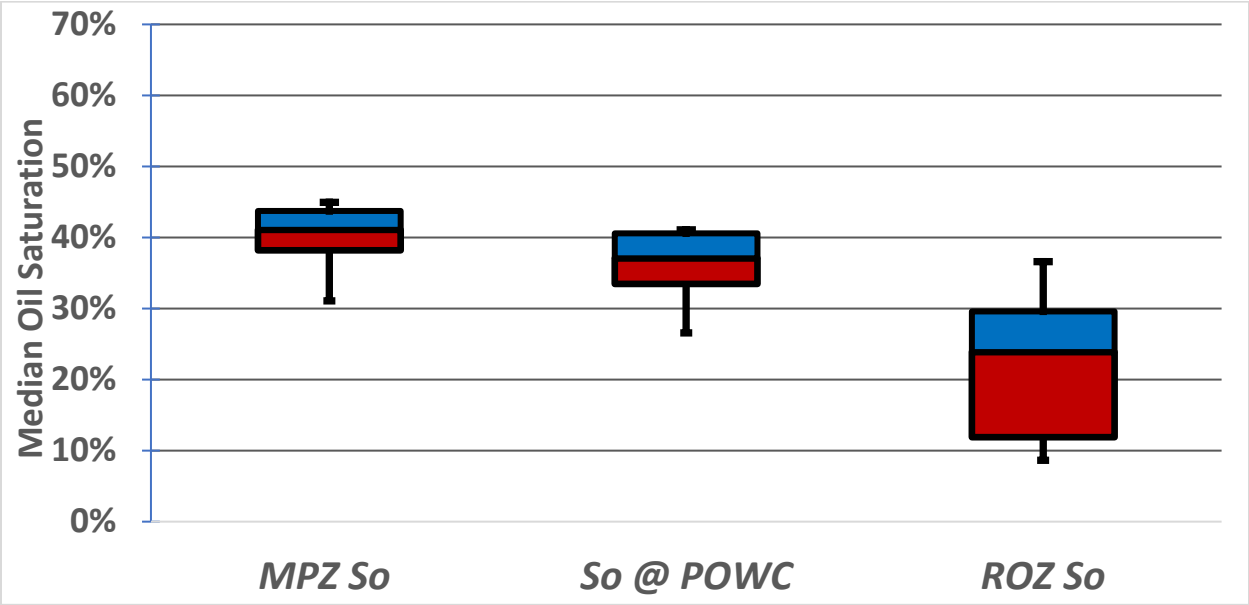

Figure 4.11. Box and whisker plots of the median oil saturations of the MPZ, and the POWC and in the ROZ for the 1990s vintage logs.

3D models

3D models of the interpreted MPZ, ROZ, and 100% S_w base were constructed to better understand the distribution of oil. The grid used for geocellular models was used to delineate cell spacing (30.48 m x 30.48 m x 0.91 m (100 ft x 100 ft x 3 ft)) and model bounds. Subsea elevations of the POWC and OWC for each well were extrapolated over the model domain and used to define the upper and lower bound of the ROZ and the lower bound of the MPZ. The top of the MPZ was the upper most active cell. The model was populated by assigning each interval (MPZ, ROZ, and 100% S_w base) an indicator value. The resulting model (**Figure 4.12**) shows a thin MPZ in the middle of the field surrounded by a thick ROZ that extends beyond the field boundary.

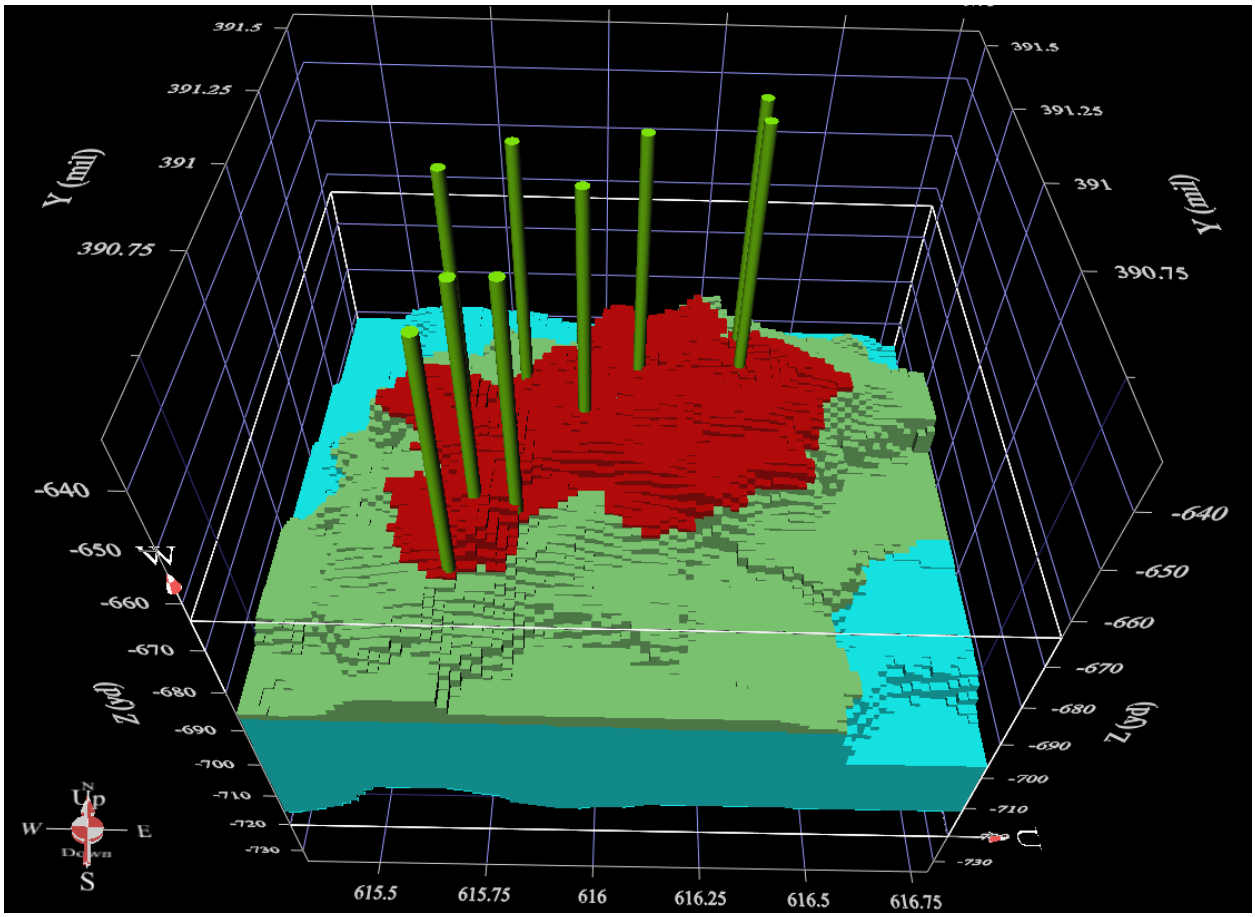

Figure 4.12. MPZ shown in red, ROZ shown in green, and 100% Sw shown in light blue. Conditioning wells shown as green tubes.

1940s wells

An attempt was made to use old wells without neutron density porosity logs to characterize the ROZ. SP derived porosity was calculated for each well and used in Archies equation to calculate water saturation profiles. POWC and OWC were picked from these curves. These wells also lacked gamma ray curves, so volume of shale and Dual water saturations could not be calculated. However, 19 of the 26 wells produced from the Cypress and 22 had Cypress core. Perforated intervals within these wells were assumed to contain moveable oil. This can validate POWC selection.

SP logs

Because of the lack of wells with neutron density porosity logs, it was necessary to make use of SP logs. SP logs were first normalized to a sand/shale ratio by picking clean sand and pure shale baselines and rescaling the curves to represent a percent clean sand (Leetaru, 1990; Webb and Grigsby, 2018). The shale baseline was picked in the shale interval above the thick Cypress Sandstone and below the overlying Barlow Limestone and the clean sand baseline was picked within the thick Cypress Sandstone. Normalized SP logs were used to construct omnidirectional variograms that were used in sequential Gaussian simulations to create a grid of normalized SP values.

Transforms

An attempt was made to relate SP logs to porosity. Normalized SP logs were cross plotted against porosity from core analysis reports. The equation defining the line regressed through them was used to transform simulated normalized SP values into porosity (**Figure 4.13**). The resulting SP derived porosity was plotted against core data for each well (**Figure 4.14**). SP logs follows the general trends observed in the core data but lacks the variability. This can be attributed to the poor vertical resolution of the SP log. It was therefore considered representative on the scale of a grid cell (30.48 m by 30.48 m by 0.91 m thick (100 ft by 100 ft by 3ft thick)).

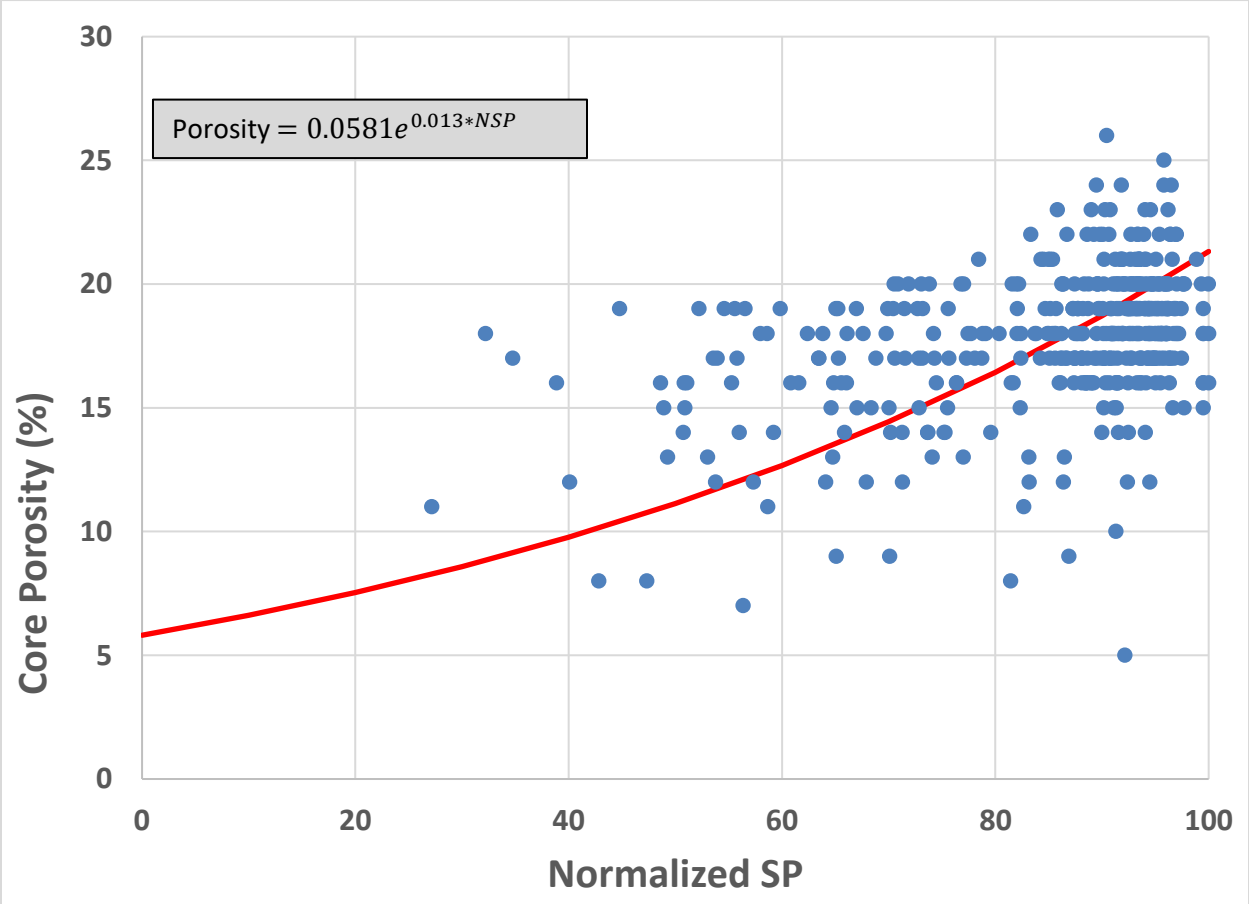

Figure 4.13. Cross plot of normalized SP and porosity data from core analysis reports.

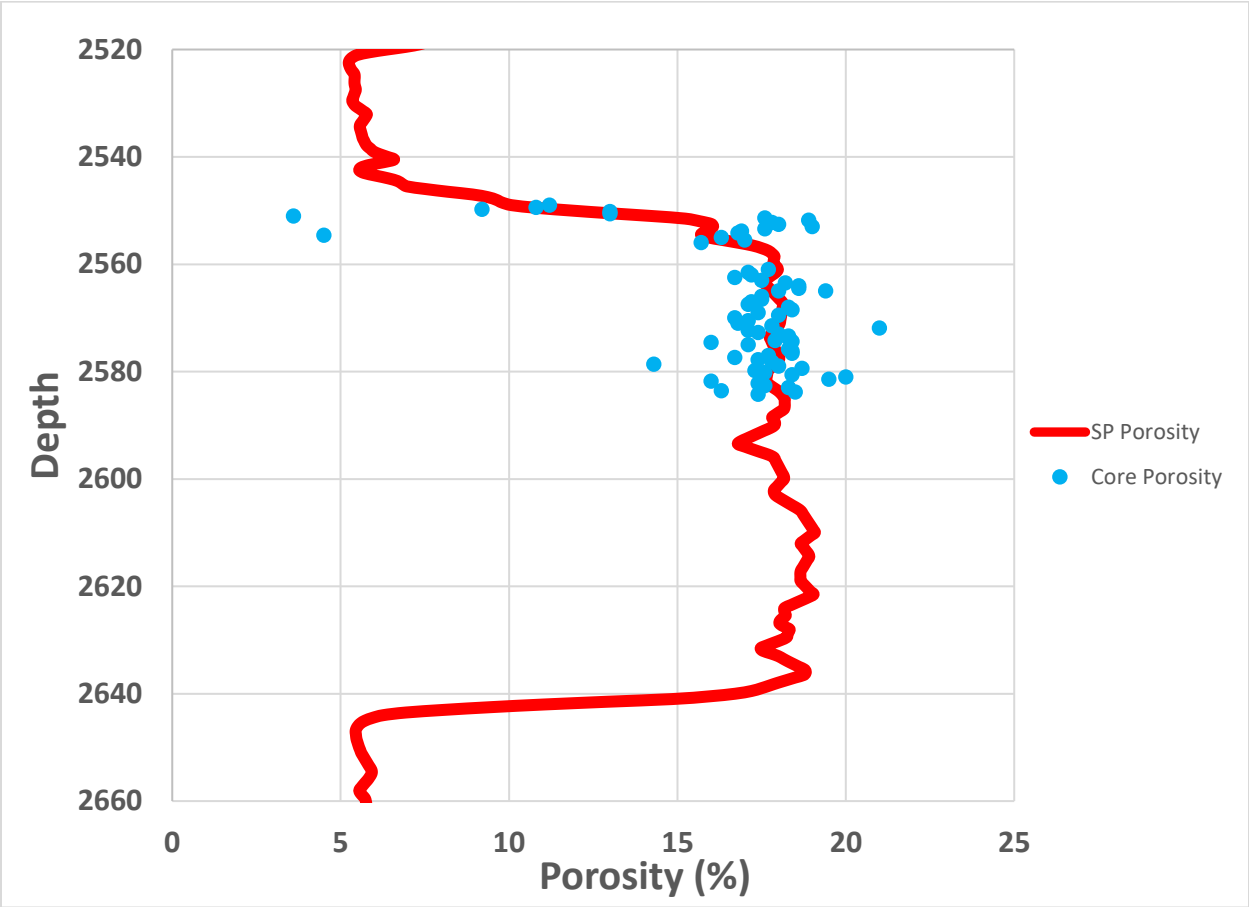

Figure 4.14. Porosity from core analysis reports and derived from normalized SP log plotted against depth. SP derived porosity lacks the variability of the core data but matches the general trend.

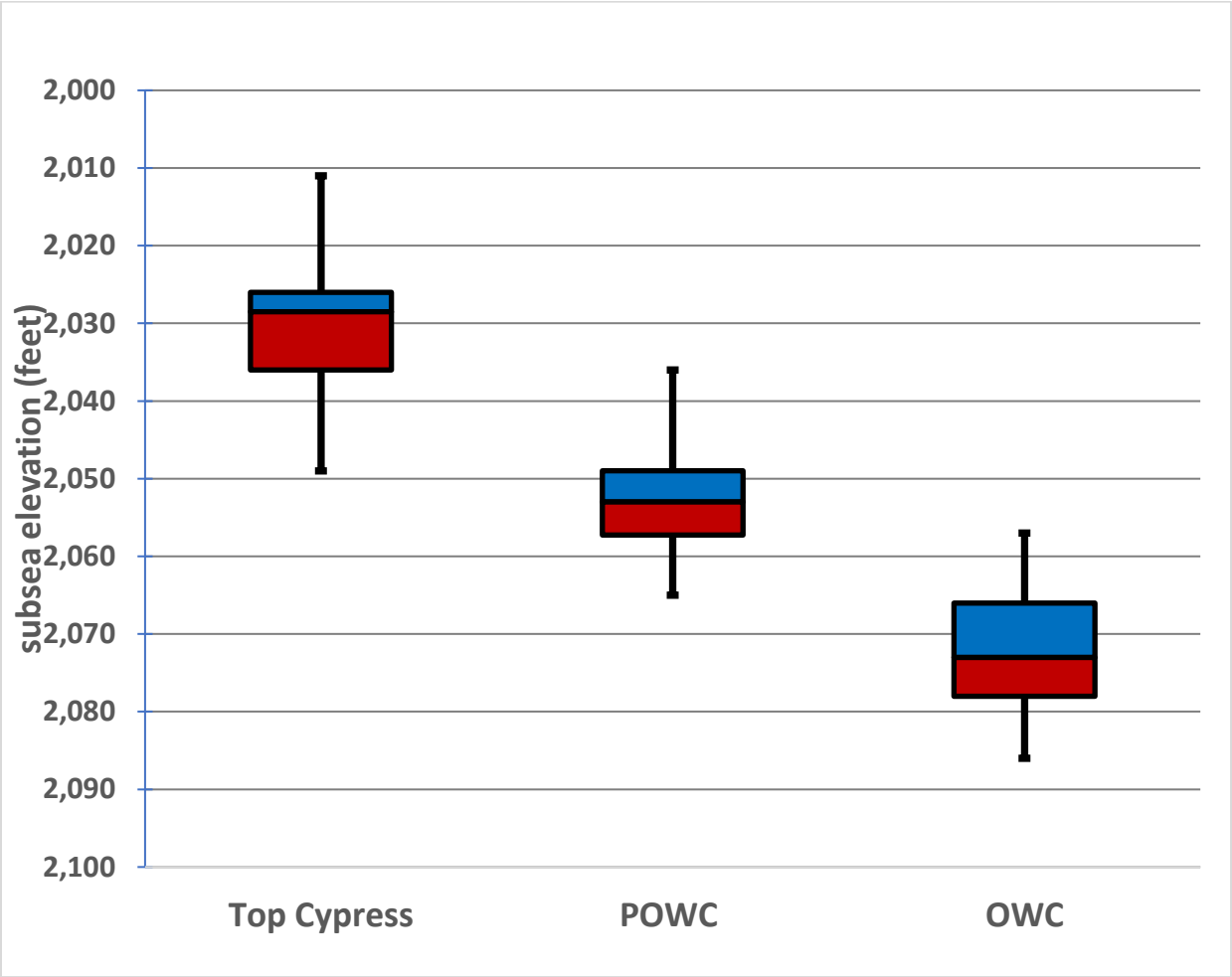

Figure 4.15. Box and whisker plots for the elevation of the top of the Cypress, POWC and OWC from the 1940s vintage logs.

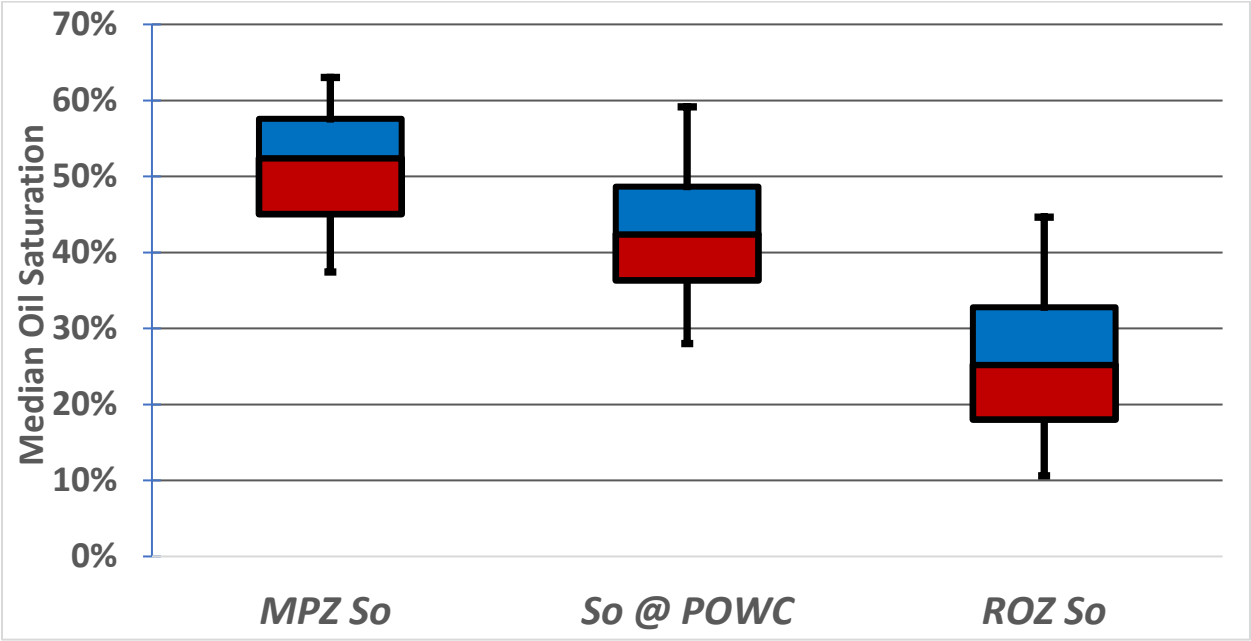

Figure 4.16. Box and whisker plots of the median oil saturations of the MPZ, and the POWC and in the ROZ for the 1940s vintage logs.

3D model

The same method used to construct the oil model of Kenner West from the 1990s wells was used to construct a 3D model of the 1940s intervals. This model has a much thicker MPZ that thins but extends to the boundary to the southwest. The ROZ beneath the MPZ has similar lateral extent and depth as the 1990s model but is thinner due to the thicker MPZ.

Comparison: 1990s vs 1940s results

The results from the 1990s vintage wells (post-production) were compared to the 1940s vintage wells (pre-production) to determine if the SP derived porosity used for the 1940s vintage was able to adequately estimate oil saturation and to evaluate how the distribution of oil and water changed over time. Comparison of the oil water contacts (**Figure 4.17**) shows no significant difference in OWC (about -2,070) and an upward shift in the POWC over time. This reduction in MPZ thickness is indicative of decades of primary and secondary recovery.

Comparison of the saturation within each interval shows that the oil saturation within the ROZ did not change over time (~25% in both cases) and that the saturation within the MPZ decreased over time (about 55% in the 1940s and 40% in the 1990s) (**Figure 4.18**).

Residual oil saturation is a function of rock and fluid properties and is not expected to change as a result of production, so the agreement in ROZ saturation increases confidence that the SP derived porosity was able to adequately calculate oil saturation. The change in MPZ So is indicative of the MPZ being depleted over time (though not all the way to residual oil saturation).

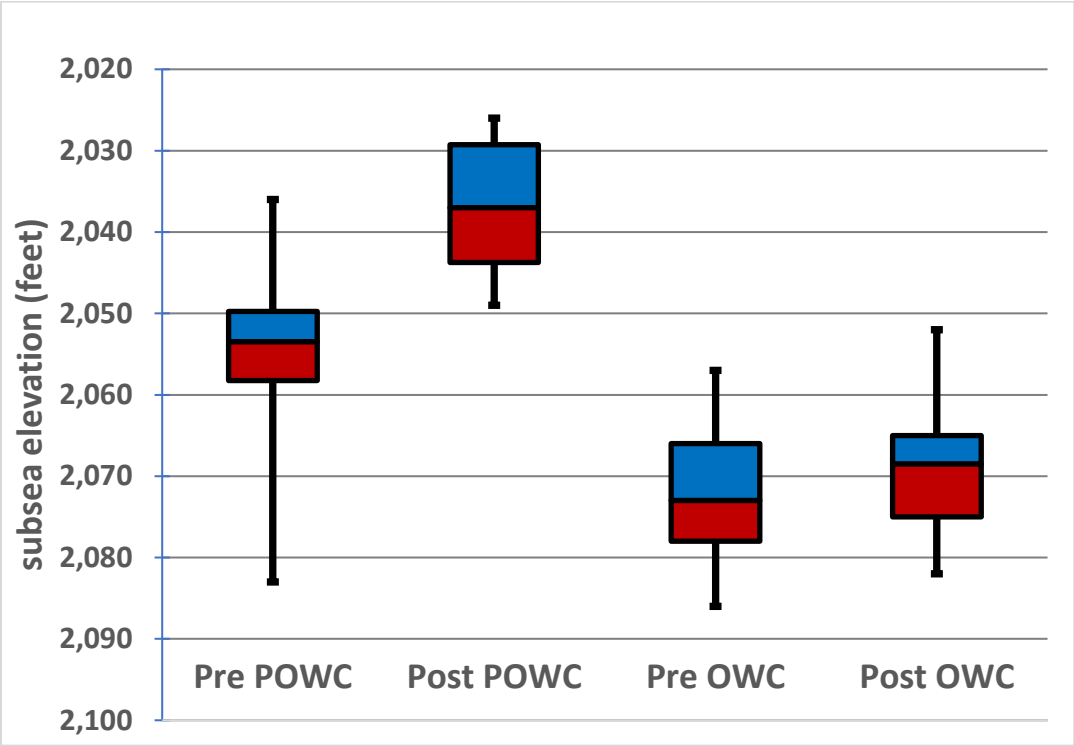

Figure 4.17. Box and whisker plots for the POWCs and OWCs of the post- and pre-waterflood vintage logs. The significant upward shift in POWC over time is indicative of a thinning of the MPZ resulting from decades of primary and secondary recovery.

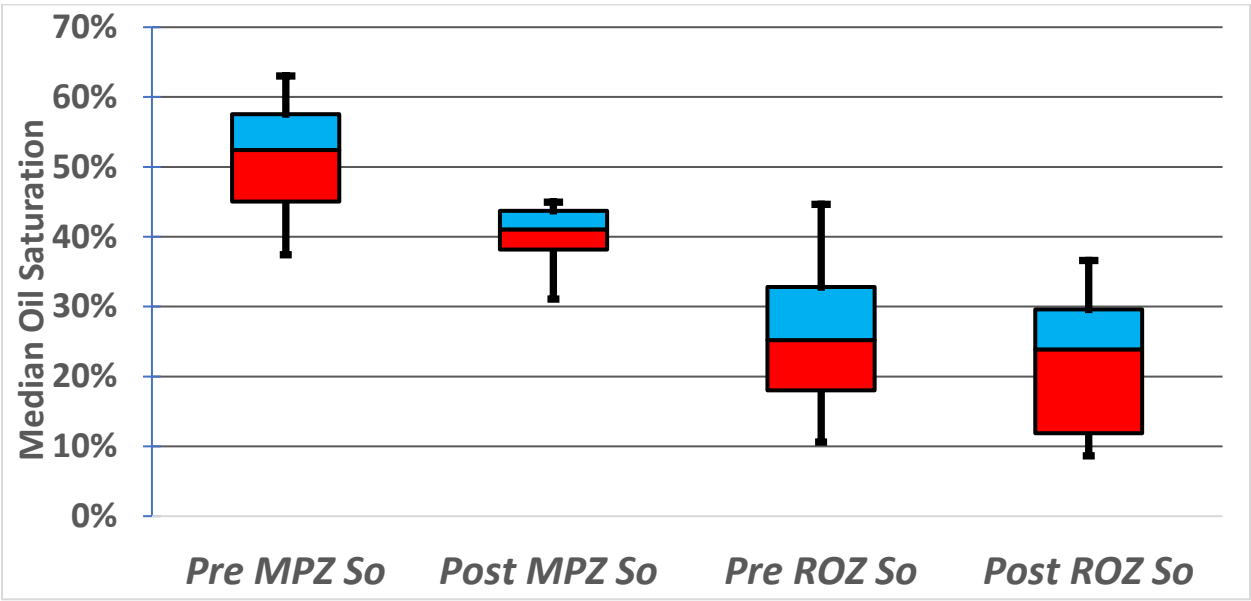

Figure 4.18. Box and whisker plots of the median oil saturations of the MPZ and ROZ for the 1990s and 1940s vintage logs. The oil saturation within the ROZ remains constant over time while the saturation decreases in the MPZ. This is indicative of the depletion of the MPZ.

4.2.5 Conclusions

Analysis of well logs was able to consistently identify oil, differentiate between mobile and residual oil, and characterize oil saturation within the MPZ and ROZ. Application of the method at Noble and Kenner West identified a ROZ below the MPZ at both fields. The ROZs at both fields had similar characteristics (**Table 4.5**). These findings were supported by historical evidence at both fields and modern PNLs at Noble Field.

The characteristics of the ROZs at both fields matched expectations. Oil columns were thickest in the middle of the fields and thinned to the periphery. The median oil saturation within the interpreted ROZs converged at ~25% at both fields (within the range expected for sandstones). Oil saturation in the MPZ was interpreted to be between 40-50%, but interpretation of the bulk volume water curves suggests that the MPZ was rarely at irreducible water saturation. An upward shift in POWC resulting in a thinning MPZ over time at Kenner West, indicative of the decades of oil production, was observed.

Table 4.5. Summary of MPZ and ROZ characteristics at Noble and Kenner West Fields

	Noble	**Kenner 1940s**	**Kenner 1990s**
MPZ S_O (%)	53	51	41
S_O at POWC (%)	39	44	37
ROZ S_O (%)	23	25	24
MPZ thickness (m [ft])	2.4 ([8]	7.6 [25]	2.1 [7]
ROZ thickness (m [ft])	9.4 [31]	5.5 [18]	9.1 [30]
Well count	94	26	9

It is believed that this method can be applied on the basin scale to identify and characterize ROZs. However, the analyses at Noble and Kenner West were aided by the geology (the thick Cypress is a thick, clean, homogenous sandstone), thick underlying aquifer, and amount of data (core analysis reports, water samples to estimate Rw, wells with oil shows and producing perforations). The method may not be as successful in areas that don't have these ideal circumstances.

The analysis of the 1940s vintage wells at Kenner West suggest that SP derived porosity was adequate to detect and characterize the ROZ within the thick Cypress. This may indicate that SP derived porosity can be used across the basin, but the interpretation at Kenner West was aided by the large amount of wells with SP logs and core derived porosity (which allowed for a normalized SP to porosity transform) and the fairly consistent porosity within the clean homogenous Cypress Sandstone (which may compensate for the poor resolution of the SP log). SP derived porosity may not be as successful in areas that don't have these ideal circumstances.

4.3 Residual Oil Saturation Experiments

4.3.1 Introduction

Oil saturation (S_O) in ROZs typically ranges between 20% and 40%, making them functionally like conventional reservoirs that have been depleted by decades of waterflooding and are therefore well suited to tertiary oil recovery processes like CO_2 flooding (Harouaka et al.; 2013). Well log analyses used to estimate S_o rely on accurate measurements (or estimates) of site-specific properties such as the formation water resistivity and volume of shale. What is lacking are *in situ* observations of the residual oil saturation (S_{OR}) within the prospective Cypress Sandstone ROZ against which the log analyses could be calibrated. As such, coreflood experiments were developed to provide independent information on the S_{OR} values that should be expected within the Cypress Sandstone ROZ.

4.3.2 Methods

Fifteen 2.5-cm (1-in) diameter core plugs were selected from Cypress Sandstone cores as well as an analogous, fluvial Pennsylvanian sandstone core to be subject to coreflood. The samples were chosen to represent the typical range of porosity and permeability values observed within the Cypress Sandstone across the ILB.

The plugs were prepared for experimentation by Dean-Stark extraction, whereby any water in the sample is vaporized and any oil is extracted by boiling solvent (in this case, toluene); extraction continues for a minimum of 24 hours (and up to 48 hours) until the extracted solvent is clean.

The clean, dry core plug was weighed and, using a caliper, three length measurements were taken, rotating the plug between each measurement, and averaged to get the final length measurement. Using the final length with the known 1-in (2.5-cm) diameter, the volume was calculated. Bulk density of the plug was calculated. The plugs were subjected to porosity and permeability measurements using a Vinci PoroPerm machine.

The plugs were then prepared for the core flooding experiment by vacuum saturating the plug with a 10% KCl brine. The plug was inserted into a stainless-steel Hassler-type core holder and the end plugs were installed. 1723.6 kPa (250 psi) of confining pressure was applied to the core plug to prevent core flood fluids from leaking past the core plug.

Fluid was pumped through the core plug via a motor-driven plastic syringe pump controlled by an Arduino microcontroller at a rate of 0.28 mL/min. Measurements of resistance across the saturated plug were taken using a Genrad Digibridge (ohmmeter) at the end of each pore volume of fluid that was flowed through the plug. Effluent was measured with a graduated cylinder.

With the brine-saturated plug inserted in the core holder, brine was initially flowed through the core plug to ensure 100% brine saturation. The plug was removed from the core holder and quickly weighed to determine the water saturated mass. The plug was reinserted and the water injection continued to purge any air bubbles from the flow lines. The syringe was then replaced with a syringe containing oil. An oil was selected based on its weight and viscosity to be analogous to Cypress crude oil at ambient temperature and pressure conditions. The oil was injected through the plug until the effluent from the core plug was entirely composed of oil and the resistance values increased and leveled out. At this point, the plug is assumed to have reached irreducible water saturation (S_{WIRR}). The plug was removed from the core holder and weighed. The volume of the effluent oil was measured and subtracted from the volume of the injected oil to determine the volume of oil occupying pore space within the plug.

The core plug was then replaced in the core holder once more, the syringe was switched back to 10% KCl brine, and the waterflood resumed. The brine was injected through the plug until the effluent from the core plug was entirely composed of brine and the resistance values decreased and leveled out. At this point, the plug is assumed to have reached residual oil saturation (S_{or}). The plug was removed from the core holder and weighed. The volume of the effluent brine was measured and subtracted from the volume of the injected brine to determine the volume of water occupying pore space within the plug.

4.3.3 Results

The 15 selected core plugs (**Table 4.6**) represent the range of porosity and permeability values typical of the thick, fluvial facies of the Cypress Sandstone. The porosities range from 11.7 to 24.9% and permeabilities range from 0.02 to 0.85 μm^2 (15.2 mD to 856.8 mD). One core plug was tested three times to determine the veracity of the saturation results produced by the experiment.

Table 4.6. Listing of well ID and depths of 15 plugs chosen for core flood experiments. Rock properties for each sample, including porosity, permeability, and matrix density, are included.

Well API Number	Formation	Plug Depth (ft)	Porosity (%)	Permeability (μm² [mD])	ρ_{MATRIX} (g/cm³)
120650139400	Cypress	3029.8	11.7	0.02 (15.2)	2.65
120650139400	Cypress	2989.4	13.7	0.08 (77.2)	2.64
121592648800	Cypress	2757.7	15.0	0.17 (174.0)	2.65
121592648800	Cypress	2726.4	16.0	0.17 (176.1)	2.65
120650139400	Cypress	3052.9	16.3	0.10 (102.8)	2.63
121592648800	Cypress	2758.9	16.7	0.34 (342.2)	2.66
121592648800	Cypress	2736.4	17.0	0.11 (110.2)	2.64
121592648800	Cypress	2729.9	17.0	0.29 (297.6)	2.64
121592648800	Cypress	2737.8	18.2	0.15 (150.9)	2.66
121592648800	Cypress	2728.9	19.2	0.80 (807.7)	2.64
121012872700	Pennsylvanian	905.5	22.2	0.34 (344.4)	2.62
121012872700	Pennsylvanian	940.5	22.6	0.41 (410.5)	2.64
121012872700	Pennsylvanian	914.5	23.0	0.46 (470.0)	2.69
121012872700	Pennsylvanian	902.5	23.6	0.85 (856.8)	2.43
121012872700	Pennsylvanian	927.8	24.9	0.40 (406.9)	2.68

Irreducible water saturation (S_{WIRR}) and S_{OR} values were determined for each sample (**Table 4.7**) based on three different calculations:

$$S_{w\ Mass} = \frac{water\ pore\ volume}{He\ pore\ volume} \quad (12)$$

Where:

- He pore volume = Total pore volume of the plug (mL)
- Water pore volume = Volume of the water (mL) defined by:

$$Water\ pore\ volume = \frac{plug\ weight - dry\ plug\ weight - mass\ pore\ volume * oil\ density}{brine\ density - oil\ density} \quad (13)$$

Where:

- Plug weight = measured weight of the plug at S_{OR} and S_{WIRR} (g)
- Dry plug weight = mass of the dry plug (g)
- Oil density= density of the oil used (0.0866 g/cm³)
- Water density = density of the water used (1.06 g/cm³)
- Mass pore volume = mass of the pore volume at 100% S_W (cm³) defined by:

$$mass\ pore\ volume = \frac{plug\ weight - dry\ plug\ weight}{brine\ density} \quad (14)$$

Where:

- Plug weight = measured weight of the plug at 100% S_W (g)

$$S_{W\ Archie} = \sqrt{\frac{R_O}{R_T}} \quad (15)$$

Where:

- R_O is the resistivity of the plug at 100% S_W (ohm-m)
- R_T is the resistivity of the plug at Sor and S_{WIRR} (ohm-m)

$$S_{W\ Volume} = \frac{Brine\ Volume\ Injected - Brine\ Volume\ Produced}{He\ Pore\ Volume} \quad (16)$$

Table 4.7. Values of initial water saturation, irreducible water saturation, and residual oil saturation for each plug.

API	Plug Depth	Swirr			Sor		
		Mass	Archie	Volume	Mass	Archie	Volume
121012872700	902.5	17%	18%	17%	39%	37%	37%
121012872700	905.5	25%	26%	27%	16%	14%	15%
121012872700	914.5	26%	26%	27%	21%	22%	19%
121012872700	927.8	21%	26%	27%	42%	37%	45%
121012872700	940.5	16%	22%	14%	36%	36%	46%
121592648800	2726.4	22%	19%	21%	30%	32%	32%
121592648800	2728.9	21%	24%	23%	33%	29%	32%
121592648800	2729.9	22%	24%	23%	25%	27%	25%
121592648800	2736.4	18%	17%	19%	19%	20%	20%
121592648800	2737.8	23%	22%	24%	22%	19%	23%
121592648800	2757.7	23%	21%	20%	31%	35%	32%
121592648800	2758.9	25%	21%	22%	26%	25%	27%
120650139400	2989.4	24%	25%	20%	35%	33%	35%
120650139400	3029.8	23%	26%	23%	19%	18%	18%
120650139400	3052.9	22%	23%	20%	31%	33%	35%
Average		***22%***	***23%***	***22%***	***28%***	***28%***	***29%***
Median		***22%***	***23%***	***22%***	***30%***	***29%***	***32%***

Table 4.7 shows the mean values of S_{WIRR} and S_{OR} that resulted from the core flood experiments. Overall, there was some agreement in the S_{WIRR} determined for all samples, with a mean S_{WIRR} for all samples of 21.4%, median of 21.1%, and a range of 15.0 to 28.9%. The S_{OR} values had more variability, with a mean S_{OR} for all samples of 32.0%, median of 33.3%, and a range of 15.3 to 52.3%.

4.4 Conclusions

A well log analysis methodology was developed and applied to Noble and Kenner West Oil Fields, where it observed a ROZ of variable thickness beneath the MPZs at both fields. These results were validated by historical records and modern pulsed neutron logs. Application of the methodology to Kenner West Field suggests that "old" well logs can be used to identify ROZs. However, both fields have high data density and clean, homogenous sandstone, which makes them ideal candidates. Well log analyses may not be as effective in less ideal conditions.

The well log analysis methodology was also used to characterize the oil saturation within the MPZ and ROZ. Findings suggest that the MPZ was not at irreducible water saturation (indicative of reservoirs that have undergone decades of primary and secondary recovery) and that the residual oil saturation is between 20-30%. There was some disagreement between the oil saturation observed in the log analysis methodology and PNL logs (which predicted higher oil saturation in the MPZ) and core (which suggests a higher S_{or}). This may indicate that the log analysis methodology is underestimating oil saturation and highlights the importance of fluid contact curves. The core flood tests also included samples from Pennsylvanian sand, which had the highest porosity and residual oil saturation. Removing these points brings the average S_{OR} down to ~27%.

It is known that many geologic parameters (such as porosity, permeability, grain size distribution, pore geometry, wettability) influence residual oil saturation. More work is required to better understand these controls to determine if (or under what conditions) a single residual oil saturation can be assumed.

5. Field Development Strategies

5.1 Modeling and Reservoir Simulation Overview

With a ROZ resource identified within the thick Cypress Sandstone in the ILB, research turned to focus on the practical aspects of recovering the resource via CO_2-EOR. The detailed geologic reservoir characterization of the Cypress Sandstone and the research to identify fluid saturation distribution within the reservoir provided the basis for developing representative geocellular and static reservoir models to be used for reservoir simulation. The simulations were then used to develop injection scenarios meant to maximize oil production and the storage of CO_2.

Reservoir structure and isopach maps produced as part of the characterization were used to define the volumetric parameters of the sandstone container, both as an oil productive reservoir and a CO_2 sink. Three-dimensional digital geocellular models based on the results of reservoir characterization were developed to reflect detailed reservoir features, including lithologic heterogeneity, depositional trends, facies changes, and rock fabric.

The modeled container was populated with fluid saturation distribution representative of the initial conditions of the oil field. Historical well completion data was used to simulate historical oil production. Matching reservoir simulation results with actual historical production validated the conceptual geologic and geocellular models of interpreted formations and estimates of initial conditions such as the OWC and OOIP. An accurate production history is also necessary for decline curve analysis to forecast future performance, estimate the current distribution of oil, water, and pressure within a reservoir, and constrain boundary conditions.

With a calibrated (history-matched) dynamic model, reservoir simulations proceeded with testing various development strategies to determine the optimal approaches for CO_2-EOR and CO_2 storage with respect to the MPZ, the ROZ, or targeting both simultaneously. Because the a of CO_2-EOR in ROZs is the potential to offset oil production with carbon storage, for all simulated CO_2-EOR and storage injection scenarios, carbon balance was calculated to determine the effectiveness of the CO_2-EOR program regarding producing net carbon negative oil (NCNO).

5.2 Geocellular Modeling

The regional geologic characterization described in Section 3 informed the development of a geocellular model that represents the static reservoir properties (i.e., porosity and permeability) in the Cypress Sandstone at Noble Field. The geologic characterization was also necessary to infer interwell characteristics and properly incorporate important small-scale features into the model.

Understanding the geology of the Cypress Sandstone at Noble Field played a role in three key areas: (1) delineating bed boundaries for separating the model into discrete, genetically related elements based on lithofacies to detect anisotropy and properly represent transitional behavior, (2) incorporating diagenetic calcite cement within an otherwise lithologically homogeneous sandstone, and (3) assigning data to the proper facies so that relationships between parameters could be understood. The model is used for hypothetical CO_2-EOR injection simulations to determine if, and under what conditions, the ROZ could add to incremental oil production at the field.

5.2.1 Methods

Data

Three hundred eighty-six wells in the study area had geophysical logs; 385 of the wells had spontaneous potential (SP) curves, and 126 of those wells also had neutron-density porosity logs (**Figure 5.1**). Fourteen wells in the study area also had core measured porosity and permeability data. To make the porosity to permeability correlation more robust, core porosity and permeability values from 13 other wells outside of the immediate

study area but within Richland County were also incorporated into the dataset. Both log and core data are available on ILOIL.

There were enough wells with SP logs in Noble Field to clearly delineate lithofacies boundaries and detect large-scale anisotropy within the sandstone. However, SP logs have poor vertical resolution and fail to detect mineralogical changes in the sandstone that may create heterogeneity in an otherwise thick, homogeneous sandstone. Conversely, there were not enough wells with neutron-density porosity logs to quantify large-scale trends in sandstone and shale, but the logs did detect two parallel layers of calcite cement observed in core and sample sets that were not detected by the SP logs (**Figure 5.2**). Thus, the strengths of both data types were leveraged to capture different aspects of the geologic heterogeneity within the Cypress Sandstone: SP logs were used to develop a model of the depositional distribution of lithofacies (i.e., sandstone and shale) (herein referred to as the depositional model), and porosity logs were used to develop a model of the diagenetic calcite cement within the sandstone (herein referred to as the diagenetic model). The two models were combined to create a geocellular model representative of the internal architecture of the Cypress Sandstone at Noble Field that included depositional and diagenetic geologic features believed to control fluid flow.

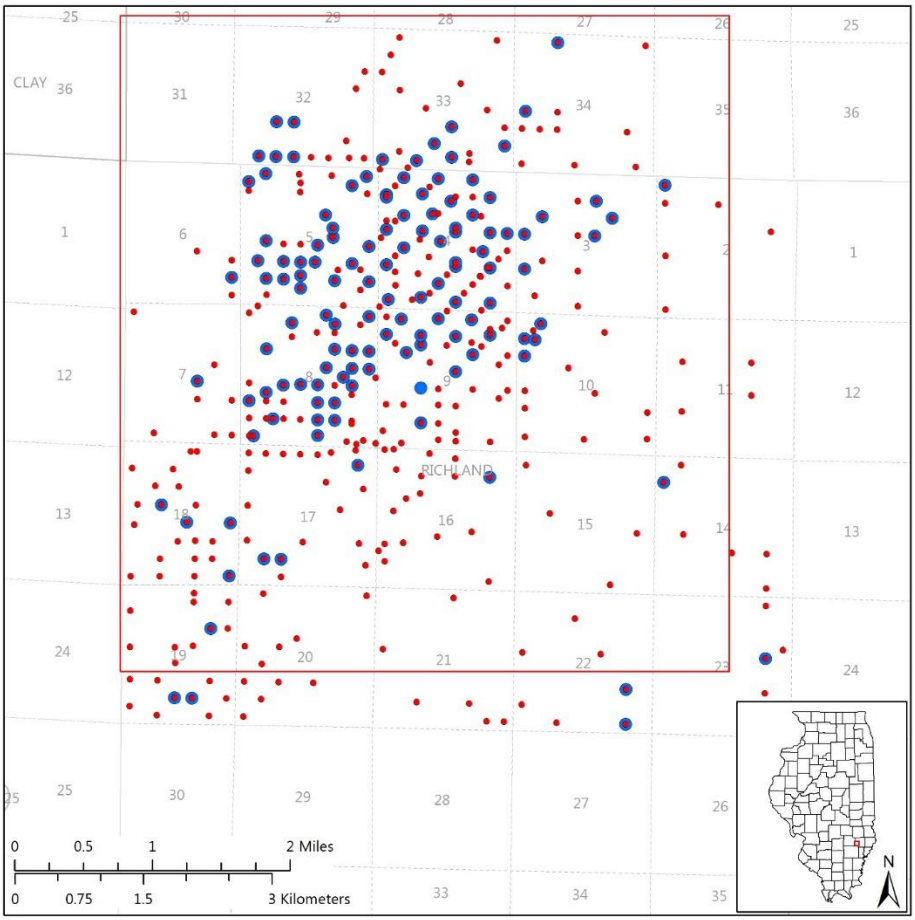

Figure 5.1. Map of Noble Field showing the model extent (black box) and data distribution. Small red dots are wells with SP logs, and big blue dots are wells with neutron-density porosity logs.

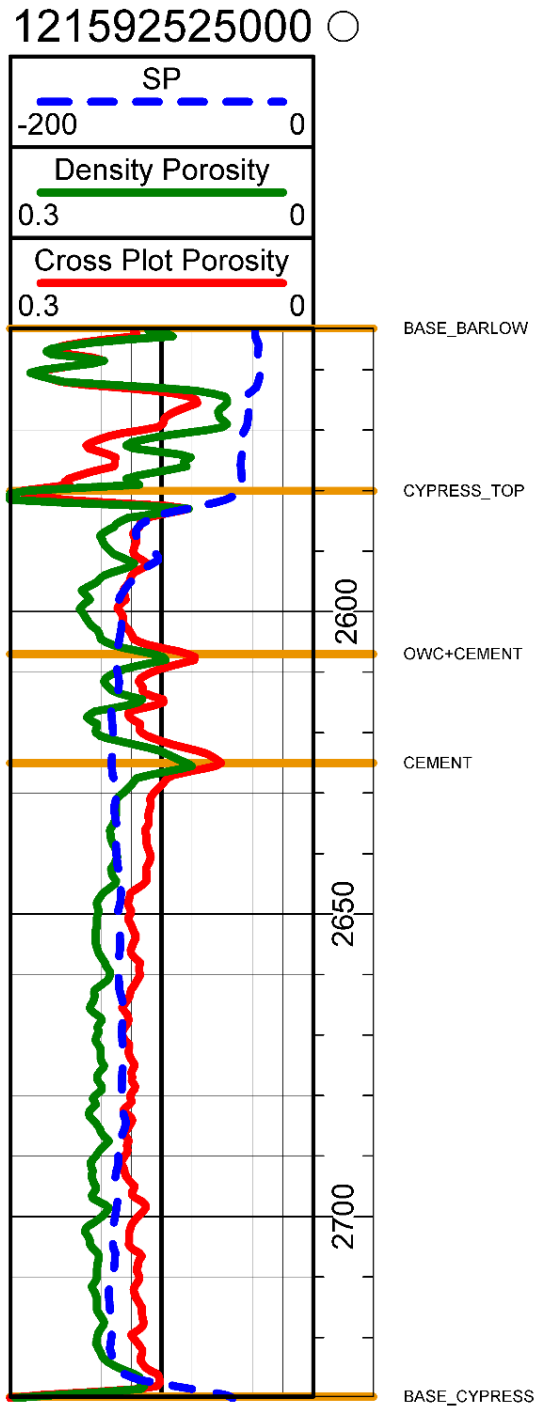

Figure 5.2. Digitized log data from the thick Cypress from Noble Field. The logs are flattened along the stratigraphic datum; the base of the Barlow Limestone. Cross plotted porosity log is red line, density porosity is green line, and SP values is dashed blue line. Orange lines are picked tops (base of the Barlow, top of the thick Cypress, oil water contact/upper cement layer, lower cement layer and base of the Cypress). The SP log is not as sensitive to thin beds because it is a much lower resolution tool, but is able to approximate the porosity log, except for two calcite cement layers that occur at the oil-water contact (at a depth of 795 m (2,608 ft) and about 9.1 m (30 ft) below it at a depth of 800 m (2,625 ft).

Grid Development

Both models are based on a 3-dimensional grid constructed to encompass the lateral extent of the study area, covering approximately 62 km^2 (24 mi^2) with an approximate volume of 7 million m^3 (250 billion ft^3 ; **Figure 5.1**). The grid was divided into ~25 million cells (260 × 256 × 375) with cell spacing of Δx = Δy = 30.5 m (100 ft) and Δz = 0.3 m (1 ft).

Structural maps of the base of the Barlow limestone and the base of the thick Cypress Sandstone developed during geologic characterization provided boundaries for the vertical extent of the grid. An additional structural map of the top of the thick Cypress Sandstone was used to demarcate a gross lithofacies change of the lower, reservoir quality sandstone portion of the Cypress Sandstone (referred to here as the thick Cypress) to the upper, non-reservoir quality shale-rich zone (referred to here as the upper Cypress).

Depositional Model Development

Spontaneous potential logs had the highest data density and were used to quantify the lithofacies distribution. The SP logs for each well were normalized to compensate for well-to-well variation that occurs because of differences in fluid chemistry or other borehole conditions (Leetaru, 1991). Log normalizing was described in detail in Section 3.3.1. For the purposes of modeling, the normalized curve is considered analogous to the proportion of sandstone vs shale.

The base of the Barlow limestone was used as a stratigraphic datum to convert the grid and log data from structural to stratigraphic space. This aligns features, such as shale beds and equivalent sandstone facies, which were assumed to have been deposited on a horizontal plane before being deformed by structure. This alignment is necessary for variograms to detect anisotropy and spatial correlation.

Normalized SP logs were used to develop variogram maps to detect the direction of anisotropy. A map was initially created for the entire Cypress Formation, but no clear anisotropy could be detected, so separate maps were created for the lower thick sandstone interval and the upper shaly interval (**Figure 5.3**). Each map was created using 18 directions and 30 lags of 700 feet. The resulting variogram map of the thick Cypress shows anisotropy with maximum connectivity in the N110° direction. This matches the dominant northwest-southeast-oriented thick sandstone body (**Figure 3.22**). The amount of shale in the upper Cypress resulted in strong connectivity in every direction. Although the upper shaly unit is much thinner than the thick Cypress, its strong omnidirectional connectivity masked the anisotropic trend of the thick Cypress when the two were combined.

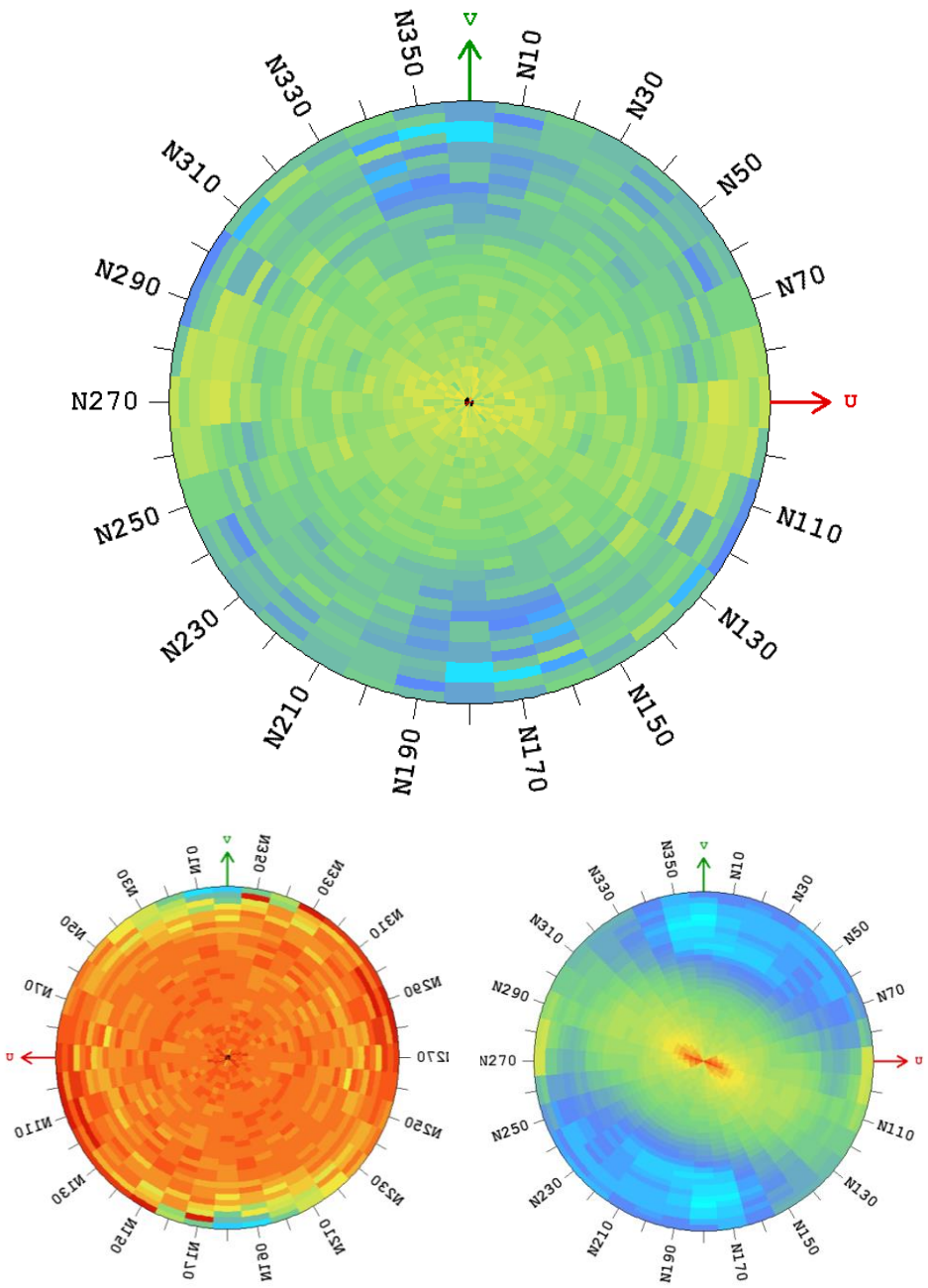

Figure 5.3. A visual representation of spatial correlation in every compass direction. Warm colors indicate normalized SP values that are like the point of origin. No clear trends can be seen in the entire Cypress Formation (top) or shaly upper Cypress (lower left). Warm colors aligning along N110° within the lower thick sandstone (lower right) indicate a long range of spatial correlation along that direction, which aligns with the trend of the dominantly NW-SE trend of the Cypress Sandstone. Conversely, cool colors perpendicular to N110° indicate that values become different near the point of origin and a short range of spatial correlation in that direction.

The spatial correlation of the thick Cypress Sandstone was quantified using two empirical horizontal variograms: one aligned with the direction of maximum connectivity (110°) and one perpendicular to it (200°). One empirical vertical variogram was also used.

Models fit to each variogram had two nested structures: one with short ranges that control the data assigned to cells close to conditioning data, and one with much longer ranges that control the data assigned to

cells far from conditioning data (**Figure 5.4**). Each structure had the same sill and a small nugget to honor the conditioning data. The model aligned with the direction of maximum connectivity had much longer ranges (**Table 5.1**), which results in features within the model elongating in that direction. Because no anisotropy could be detected in the upper Cypress, an omnidirectional variogram was used.

The variogram models were used in Sequential Gaussian Simulations to create 50 unique, equiprobable realizations of the distribution of normalized SP for both the thick Cypress and the upper shale-rich zone. The realizations were compared to the geologic characterization (Section 3.3.1), and ISGS geologists assisted with choosing the realization that best represented the internal architecture and heterogeneity.

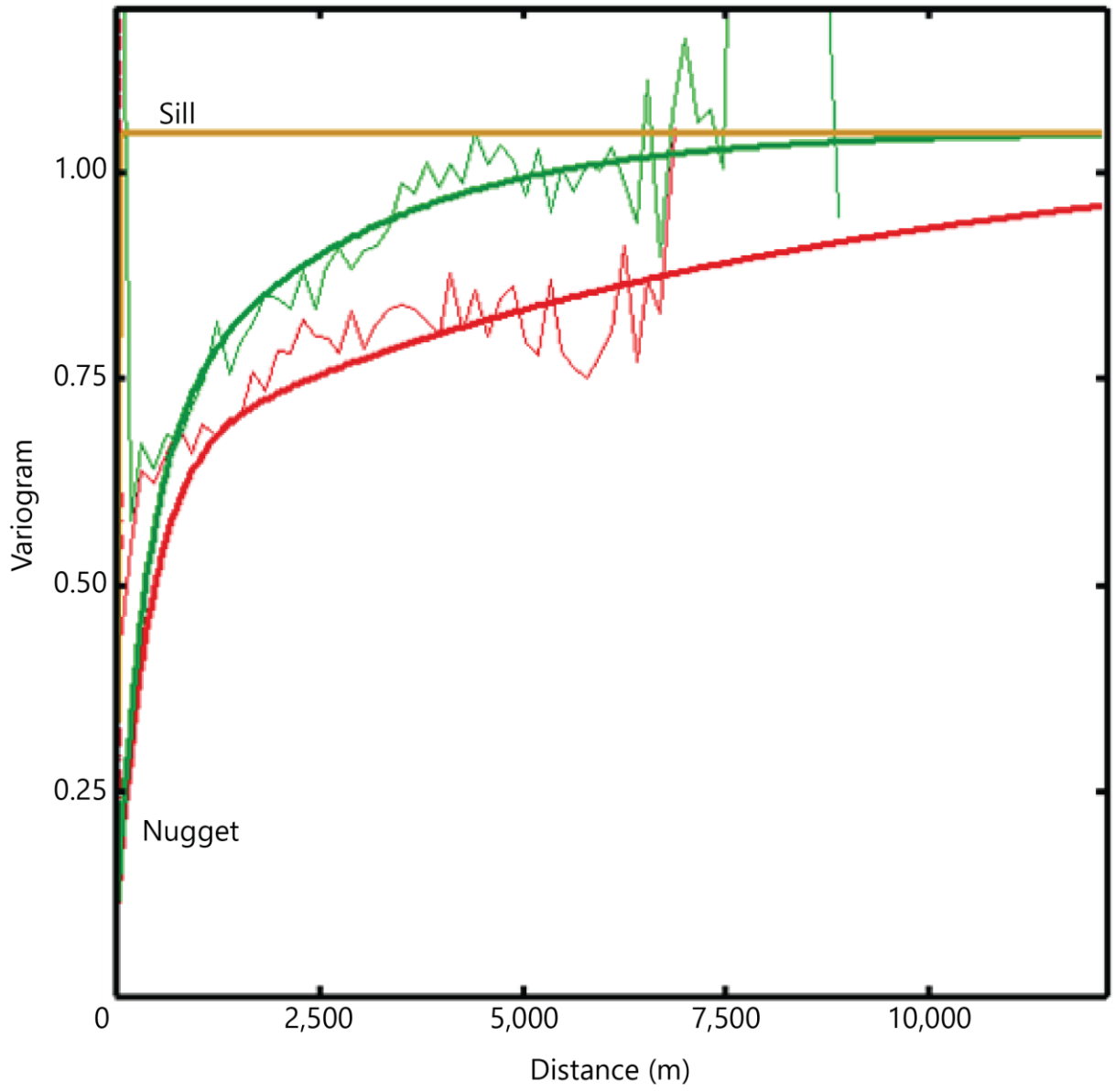

Figure 5.4. Models fit to the horizontal variograms for the thick Cypress, including the one in the direction of maximum connectivity (N110°, red lines) and the one perpendicular to it (N200°, green lines). The model variograms (thick lines) fit the empirical variograms (thin lines), indicating transitional behavior was captured.

Table 5.1. Statistics for the horizontal variograms aligned with the anisotropy (N110°) and perpendicular to it (N200°) and the vertical variogram (z). Nugget represents measurement errors (extent to which model deviates from conditioning data).

Direction	Nugget	Close Sill	Close Range, m (ft)	Far Sill	Far Range, m (ft)
N110°	0.1	0.5	1,676 (5,500)	0.4	18,288 (60,000)
N200°	0.1	0.5	1,067 (3,500)	0.4	7,620 (25,000)
z	0.1	0.5	12 (40)	0.4	36.6 (120)

Diagenetic Model Development

Neutron-density porosity logs from 126 wells were used to create a diagenetic model of the calcite cement and unaltered sandstone intervals. Because the calcite cement is a diagenetic feature believed to have been formed at the oil water contact (See Section 3.3.1), the grid and log data were flattened along the oil-water contact instead of the base of the Barlow limestone. Using the base of the Barlow as the stratigraphic datum would have misaligned the cement layers and made the continuity of the feature difficult to detect. Using the oil water contact instead shifts the data to the orientation in which the geologic feature was believed to be created.

A porosity cutoff of 15% was used to classify the logged data into “cement” (<15%) and “unaltered sandstone” facies (>15%; **Figure 5.5**). It was known from core data that the calcite cement has very low porosity (<5%), but the cement layers were not thick enough for neutron density porosity logs to record their true porosity. Multiple cutoffs were selected, and it was iteratively determined that 15% was adequate to separate the calcite cement from the unaltered sandstone.

There were too few neutron-density porosity logs to detect laterally variable trends in sandstone and shale, but geostatistical analysis of the logs did detect two parallel layers of calcite cement, one at the OWC and one about 9.1 m (30 ft) below it. Of the 126 wells with neutron-density porosity logs, both layers of calcite cement were present in 97 wells, and an additional 12 wells only had the deeper layer of calcite cement (**Figure 5.5**). The cement was absent in the remaining 17 wells. The calcite cement was most prevalent in the middle of the model and absent in the northeast. Low porosity “cement” facies also occurs sporadically near the base of the model.

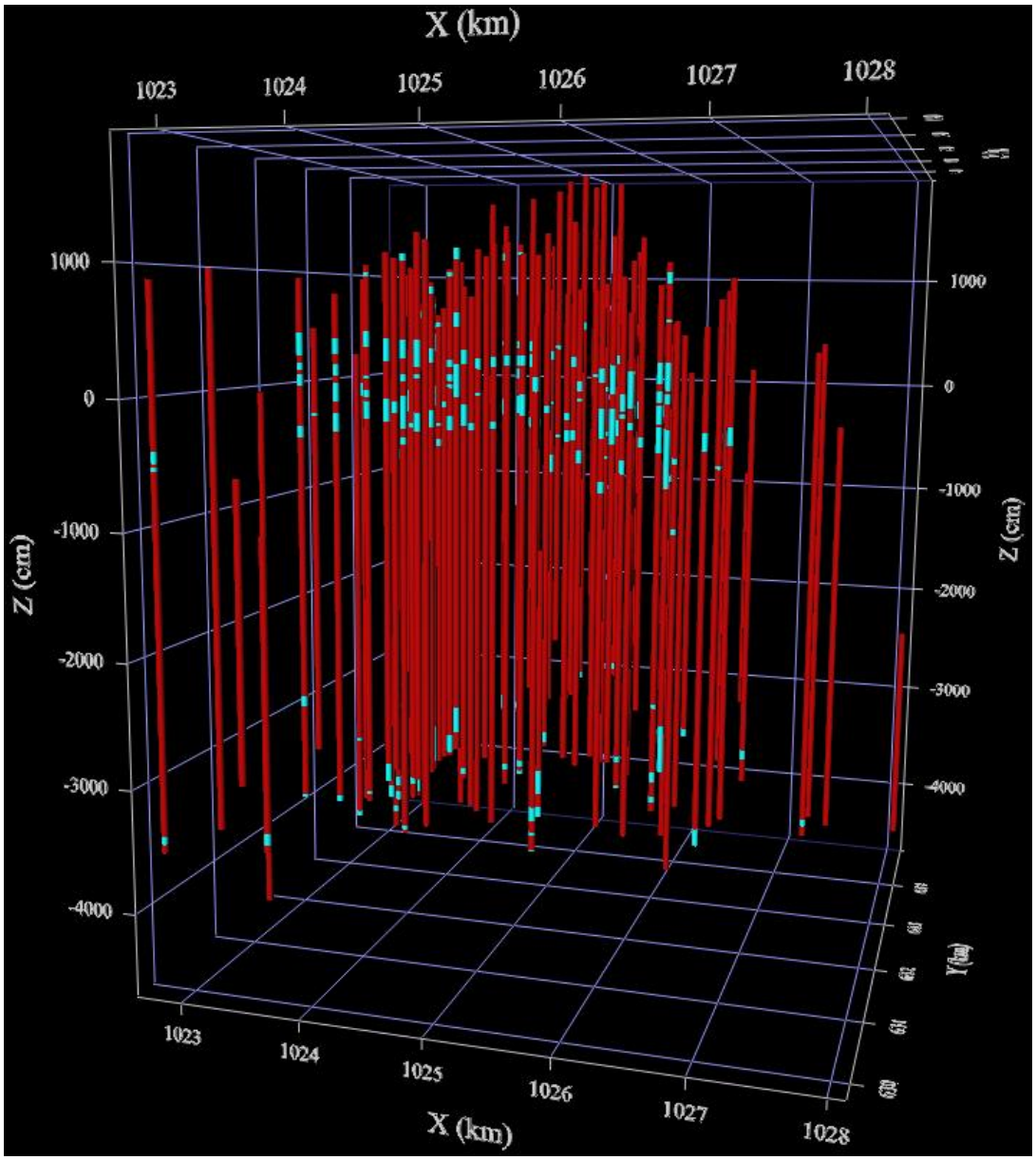

Figure 5.5. Blue represents the low porosity facies (meant to capture the cement) and red represents the high porosity facies (meant to capture the unaltered clean sandstone). The data is flattened along the OWC. Most of the low porosity facies occurs in two bands near the top and sporadically near the base.

The grid was divided into three zones: one with wells with two cement layers, one with wells with one cement layer, and one with wells without a cement layer. The odds of encountering the cement facies was calculated for each layer within each zone. Trends were interpolated between zones and each cell was assigned the odds of encountering the cement facies. This method extrapolates trends over entire grid and is not good at detecting lateral variability, but was appropriate to recreate the calcite cement, which was interpreted to be laterally continuous.

Assignment of Petrophysical Properties

The depositional and diagenetic models were returned to structural space and combined to create a model that includes the geologic heterogeneity including lithofacies distribution and diagenetic calcite cement.

Porosity values were assigned to each cell by developing a transform based on wells that had both SP and neutron-density porosity logs. The data were plotted against each other and linear and reduced major axis lines were regressed through them (**Figure 5.6**). Ideally, the equation defining the best fit regression line would be used to transform the normalized SP values in each cell into porosity. However, it was known that the neutron-density porosity logs include the low-porosity calcite cement facies that appeared as clean sand on SP logs. So, to create a transform for the uncemented sandstone, log-derived porosity data from the calcite-cemented intervals was identified (**Figure 5.7**). The SP and porosity curves for each well were analyzed and data points that fell within cement zones were identified. The points that fell within the cement zones generally had high SP and low porosity values. These points were removed, and new lines were regressed through the remaining data (**Figure 5.8**). The new lines based on clean sand data points only had a better fit and resulted in modeled porosity that was closer to core values (**Table 5.2**), so the equation defining the reduced major axis curve was used to transform the simulated normalized SP in each cell into porosity.

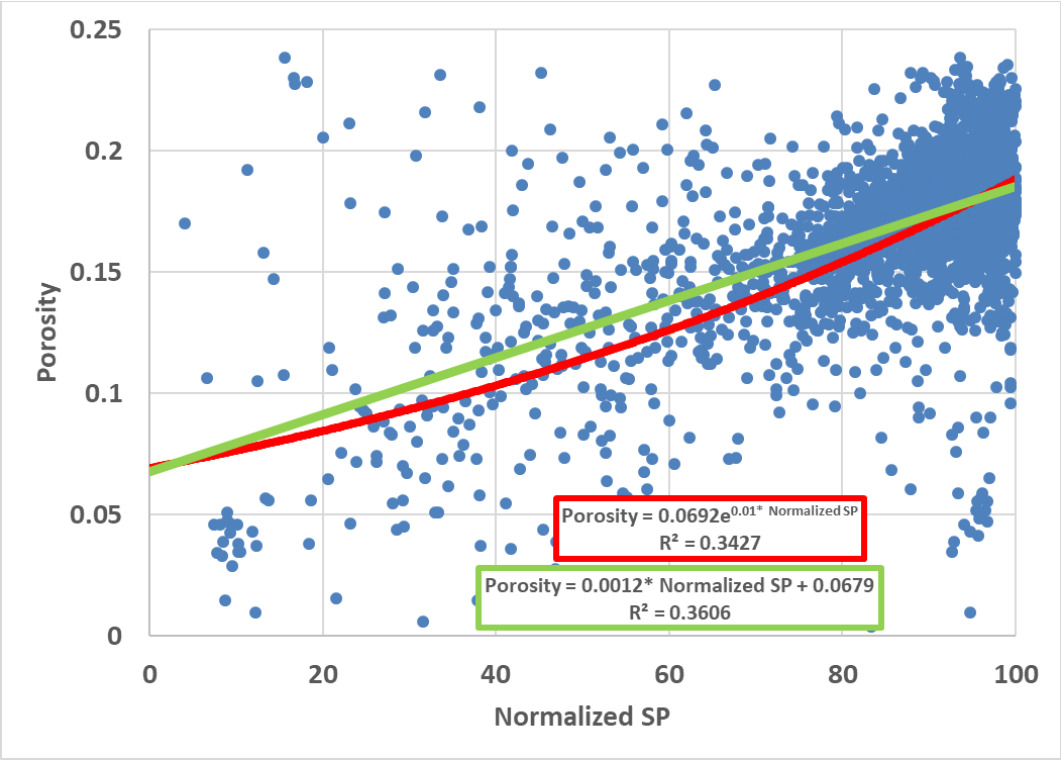

Figure 5.6. Cross plots of normalized SP and neutron-density porosity log data. Linear (green line) and reduced major axis (red line) regressions are plotted.

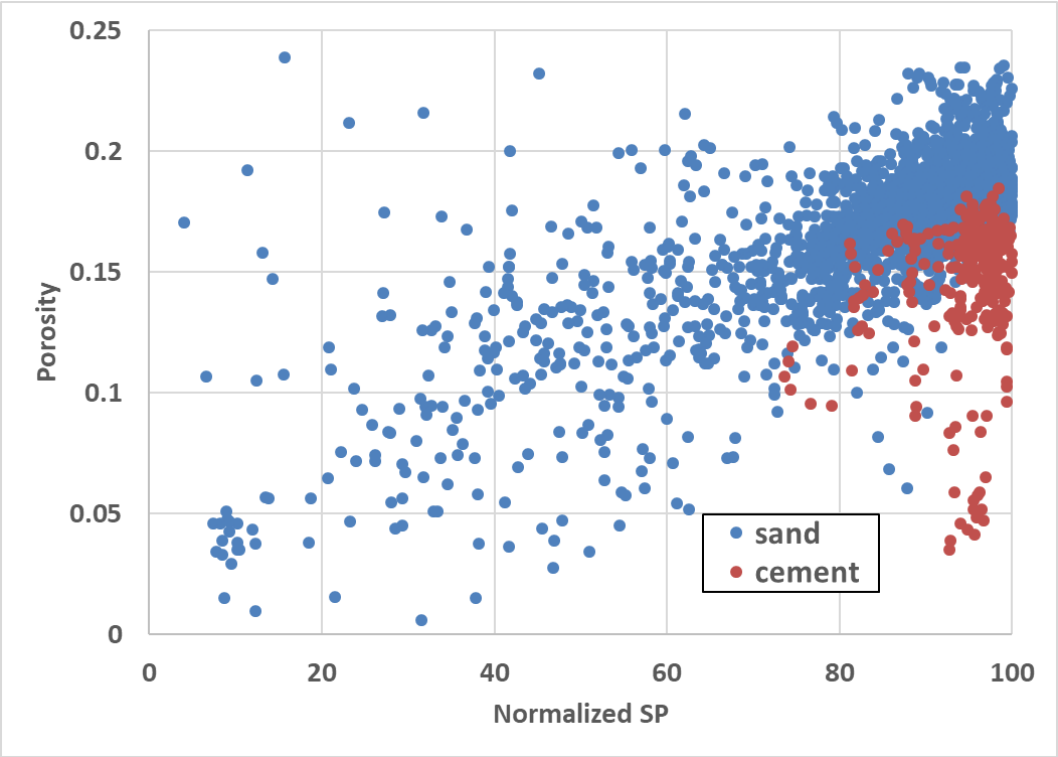

Figure 5.7. Cross plots of normalized SP and neutron-density porosity log data. Same porosity dataset as Figure 5.6, but porosity values corresponding to calcite cemented sandstone have been highlighted.

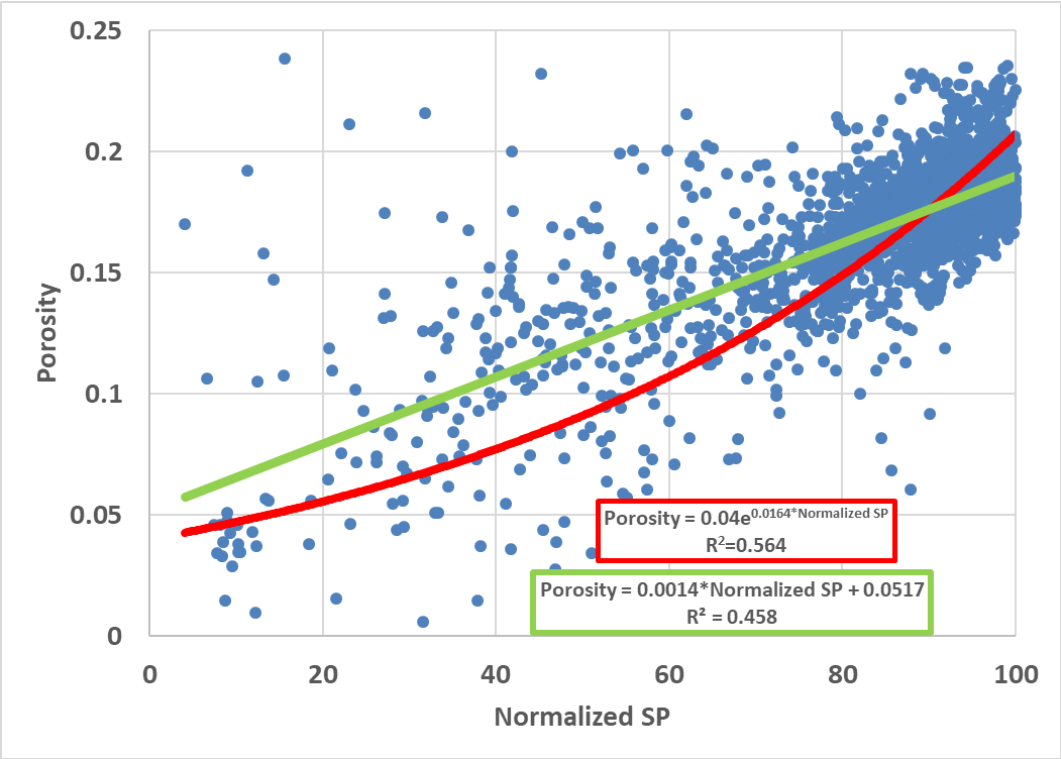

Figure 5.8. Cross plots of normalized SP and neutron-density porosity with calcite cemented sandstone points removed. Linear (green) and reduced major axis (red) lines are fit to the data. The equation defining the red line was used to transform simulated normalized SP into porosity.

Table 5.2. Porosity from core analysis reports and derived from SP using transforms based on all data and clean sand only.

	Core Porosity (%)	Model Porosity (%)	
		All Data Transform	Clean Sand Only Transform
Minimum	6	8	5
Maximum	25	18	21
Mean	17	17	17
Median	18	17	18

The diagenetic model was returned to structural space and cells that had a high probability of containing the low porosity facies (>90%) were embedded in the depositional model. These cells were then assigned a porosity of 10%.

A porosity-to-permeability transform was developed using data from conventional core plug analysis reports for the Cypress Sandstone at Noble Field available within the ISGS data repository. A cross plot of the raw data appeared to contain two trends, one with high permeability and one with lower permeability (**Figure 5.9**). The existence of two separate trends suggested two porosity-to-permeability relationships exist within the Cypress Sandstone, most likely related to changes in facies within the sandstone.

The upper shaly estuarine portion of the sandstone was expected to have lower porosity and permeability values than samples in the cleaner fluvial sandstone because of the abundance of lower energy bedforms and higher clay content. The depth of each data point was subtracted from the depth to the top of the thick Cypress for each well. The results were sorted into three groups: one containing data from the upper

Cypress, one with data from less than below the top of the thick Cypress (near the contact of the thick and upper Cypress), and one with data from the middle of the thick Cypress.

Data from the middle of the thick Cypress, where higher energy cross bedded sandstones with very little clay content are dominant, generally fell within the higher permeability trend, whereas the data from the upper Cypress fell within the lower permeability trend. Two reduced major axis lines were created for each trend: one fit to the data from the heterolithic estuarine upper Cypress and one fit to the data from the more homogeneous, fluvial middle of the thick Cypress. Data that fell within 3 m (10 ft) below the top of the thick Cypress fell into both trends and were not included in either regression (**Figure 5.10**). Averaging the data for each core reduces scatter and makes both trends more distinct (**Figure 5.11**).

The equation defining the line fit to the data from the thick Cypress (green line in **Figure 5.11**) was used to transform the porosity into permeability in the model of the thick Cypress, and the equation defining the line fit to the data from the upper Cypress (blue line in **Figure 5.11**) was used to transform porosity to permeability in the model of the upper Cypress.

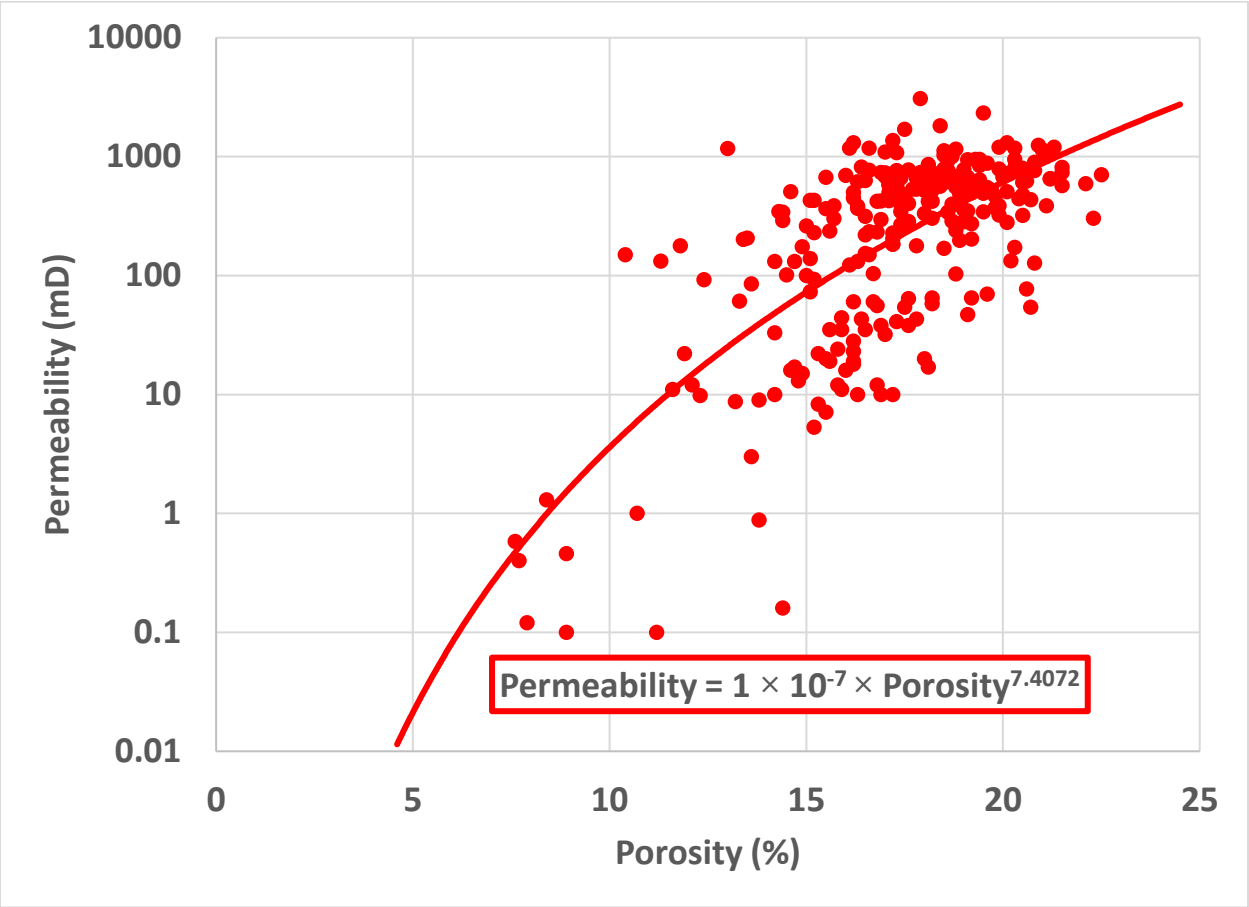

Figure 5.9. Cross plot of all porosity and permeability from core analysis reports of the Cypress Sandstone at Noble Field.

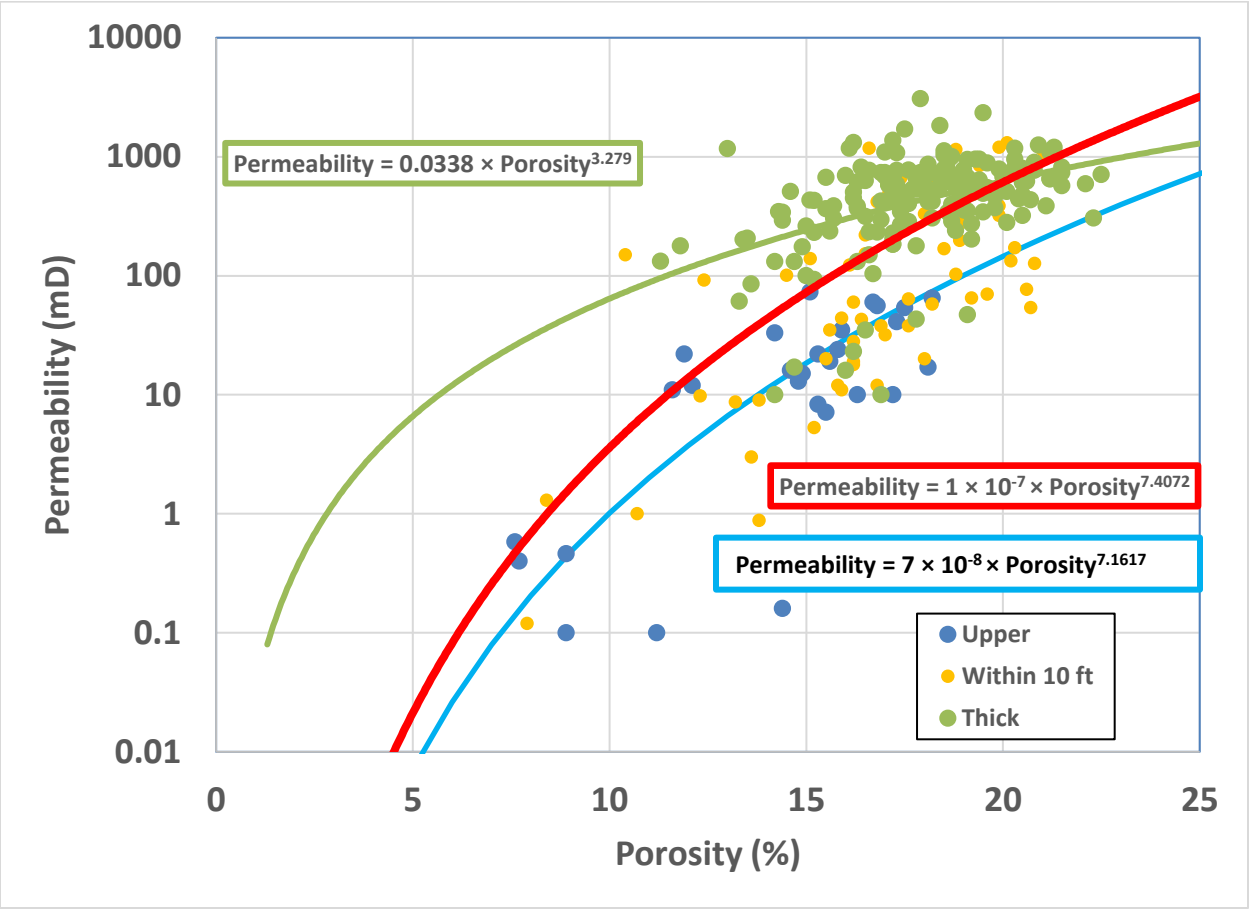

Figure 5.10. Cross plot of porosity and permeability from core analysis reports of the Cypress Sandstone at Noble Field. The raw data (Figure 5.9) appeared to contain two trends, so data were grouped by depth above or below the top of the thick Cypress. This revealed that the data from the upper Cypress occurred in a lower permeability cluster, whereas data from the thick Cypress occurred in a higher permeability cluster. Data near the interface occurred in both trends.

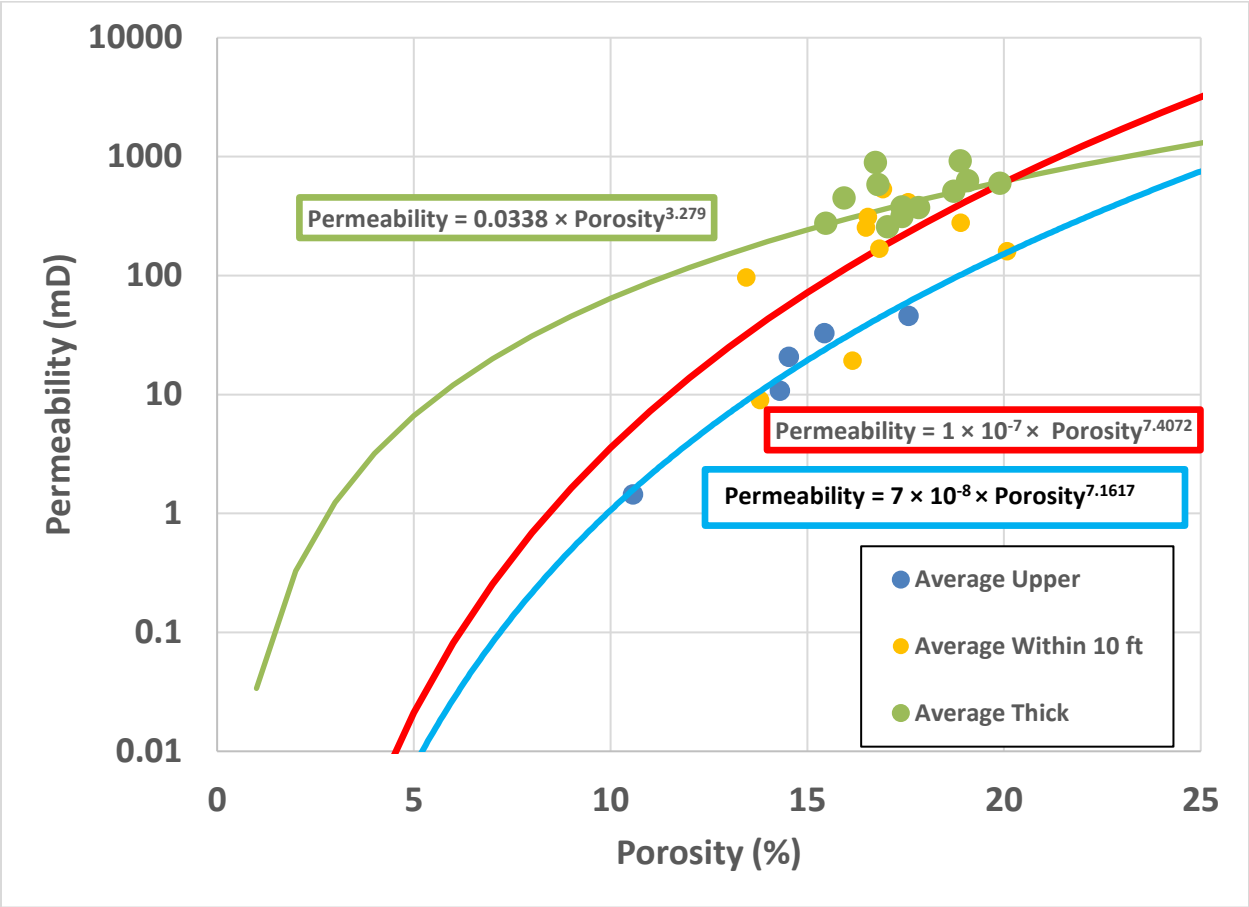

Figure 5.11. Cross plot of porosity and permeability averaged for each core Cypress Sandstone at Noble Field. The shale rich facies of the upper Cypress has a different porosity to permeability relationship than the clean sand facies within the thick Cypress.

Table 5.3. Permeability statistics from core analysis reports and derived from porosity for the model using two transforms.

	Core (µm² [mD])	Combined Transform (µm² [mD])	Thick Only Transform (µm² [mD])
Minimum	0.00 (0.10)	0.00 (0.00)	0.00 (3.07)
Maximum	0.61 (617.0)	0.54 (543.6)	0.68 (689.5)
Mean	0.56 (562.9)	0.21 (215.1)	0.40 (409.1)
Median	0.34 (342.0)	0.22 (222.3)	0.46 (461.2)

5.2.2 Static Models

Depositional Model

The modeled distribution of sandstone and shale matched expectations from the geologic characterization. The thick Cypress is primarily composed of sandstone with a low clay content (**Table 5.4**), and isolated shale breaks transition into shale at the top (**Figures 5.12 and 5.13**). The character of the model begins to change to the northeast as the thick Cypress thins and becomes slightly more shaly, corresponding with the transition into Noble North Field. Also, the large-scale anisotropy observed along N110° in the variogram map coincides with the elongation of the thickness of the sandstone body observed in the isopach map.

The model of the upper Cypress is much more shale rich than the lower thick sandstone with northeast-southwest trending sandstone lenses only occurring in the northeast corner (**Figure 5.14**). This coincides with an overall thinning of the thick Cypress and the development of discrete sandstone lenses in the shale-rich upper Cypress in Noble North Field. The upper Cypress will not be used for reservoir simulations because it is not hydraulically connected to the main thick Cypress sandstone body. However, the fact that the model matched expectations from the geologic conceptual model described in Section 3.3.1 demonstrates that (1) the SP logs can detect changes in lithofacies and (2) the data coverage is adequate to detect anisotropy and to condition simulations to create a representative distribution. Both (1) and (2) improve confidence in the depositional model of the thick Cypress.

Table 5.4. Normalized SP values are analogous to the percentage of clean sandstone. The thick reservoir portion contains much cleaner sandstone, whereas the upper shale-rich zone has low sandstone content.

	Upper Cypress (% clean sand)	**Thick Cypress (% clean sand)**	**All Cypress (% clean sand)**
Minimum	0	0	0
Maximum	100	100	100
Mean	13.75	88.2	67.24
Median	8.87	93.57	89.2
Standard Deviation	14.67	15.03	36.22

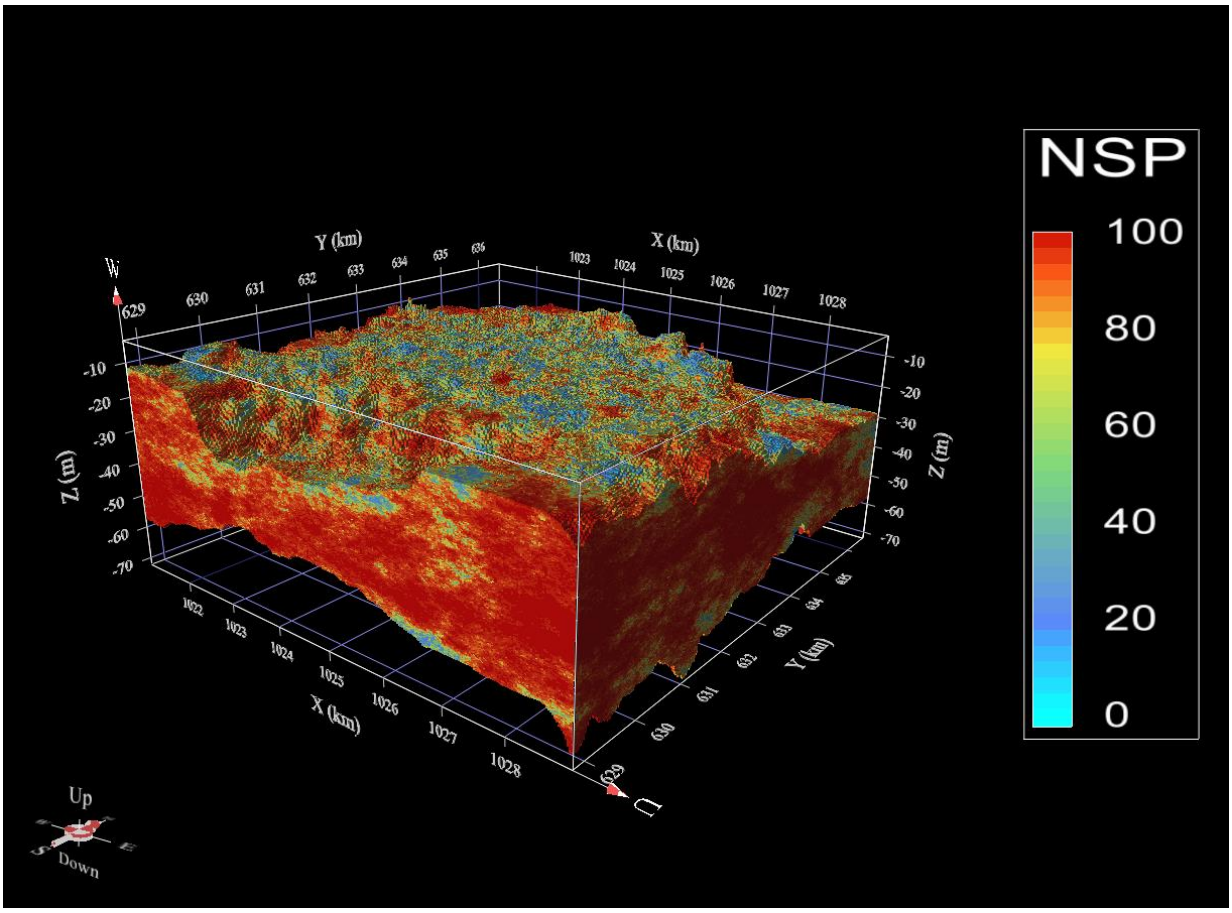

Figure 5.12. Distribution of the normalized SP (NSP) in the depositional model. Warm colors indicate cells with a high percentage of sand and cool colors indicate cells with a high percentage of shale. The middle of the model is very sand rich, and the upper and lower bounds are much more shale rich than the middle of the model. The model is shown in stratigraphic space with 50× vertical exaggeration.

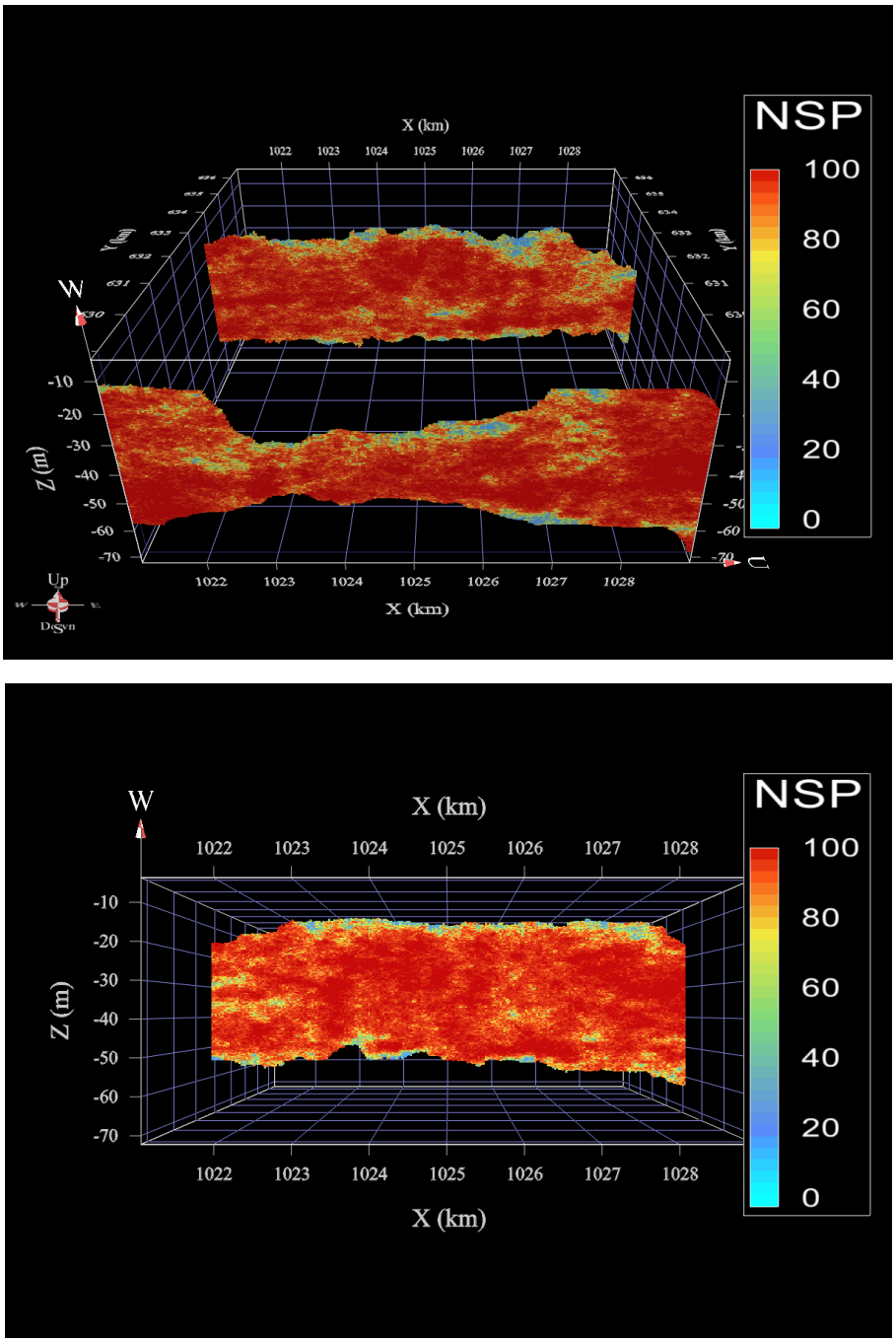

Figure 5.13. East-west slices of the depositional model showing the internal distribution of sandstone and shale. The slices in the upper image represent the distribution at the southern and northern borders (the northern border is ~16,000 ft (4,877 m) from the southern border). The slice in the lower image represents the middle of the model and is ~10,000 ft (3,048 m) from the southern border. All slices reveal that the middle of the model is mostly clean sand with a few discontinuous shale units and that the most pronounced shale appears at the upper and lower boundaries. The northernmost slice has more shale in the eastern corner, coinciding with the transition to Noble North Field. All slices are shown in stratigraphic space with 50× vertical exaggeration.

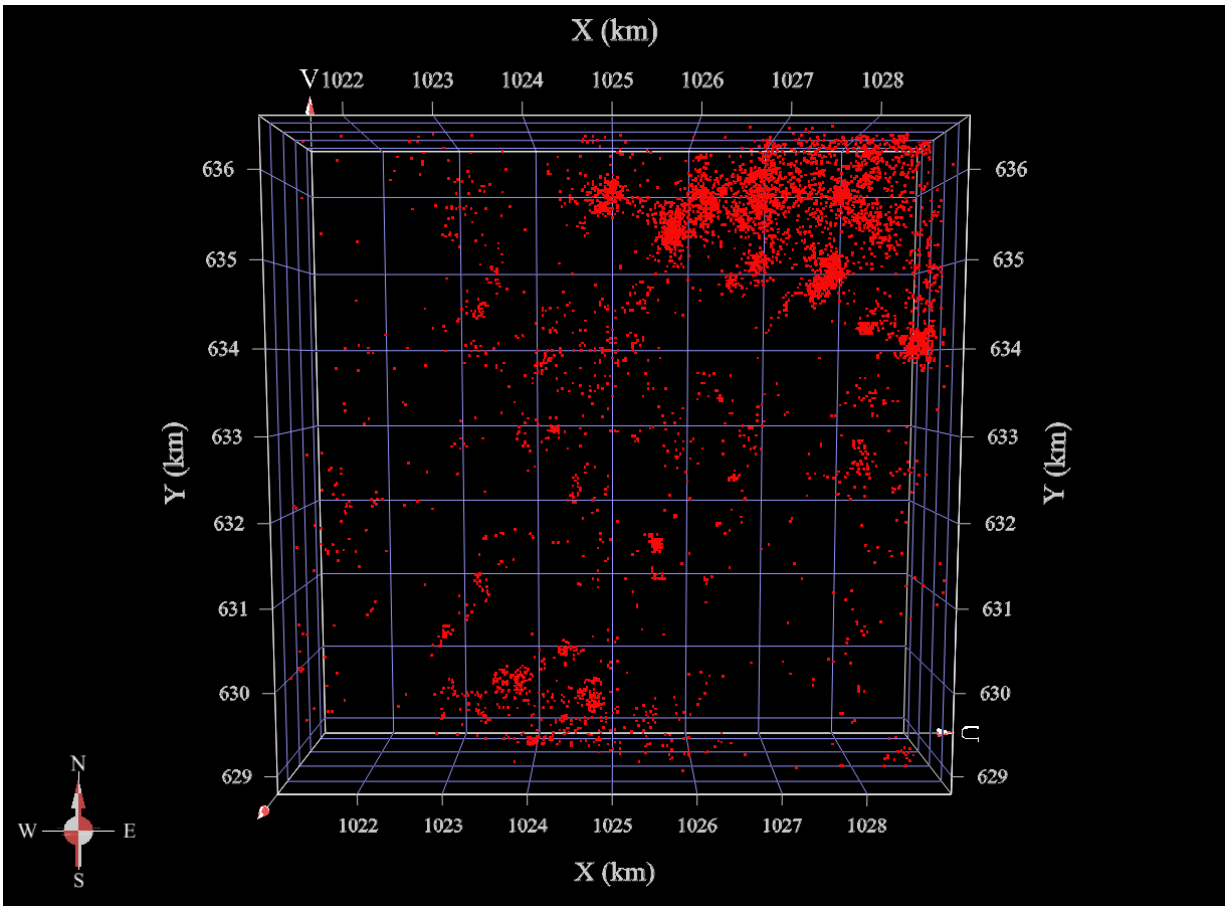

Figure 5.14. Depositional model of the upper Cypress after a 90% cutoff has been applied to make only the clean sand cells visible. The model is mostly shale with a scattering of clean cells. Northeast-southwest trending lenses are visible in the northeastern corner, which corresponds with the transition to Noble North Field.

Diagenetic Model

The diagenetic model has two parallel layers of cement: one concurrent with the existing oil-water contact and one about 9.1 m (30 ft) below it (**Figures 5.15 and 5.16**). The lower layer is often more pronounced, but both layers were present throughout the model, except in the northeast corner where the cement thins and disappears. This corresponds with the transition to Noble North Field, where the upper thick Cypress becomes more shale rich and the top of the sandstone dips below the plane of the cement.

The diagenetic model had low porosity near the base of the thick Cypress. These data points were interpreted to be discontinuous shale units that appear as the clean sandstone transitions to shale at the base of the reservoir. The depositional model properly represented these discontinuous shale bodies, and the odds of encountering these layers in the diagenetic model were below the threshold used to embed cement in the final model. Thus, the layers were not included in the final model.

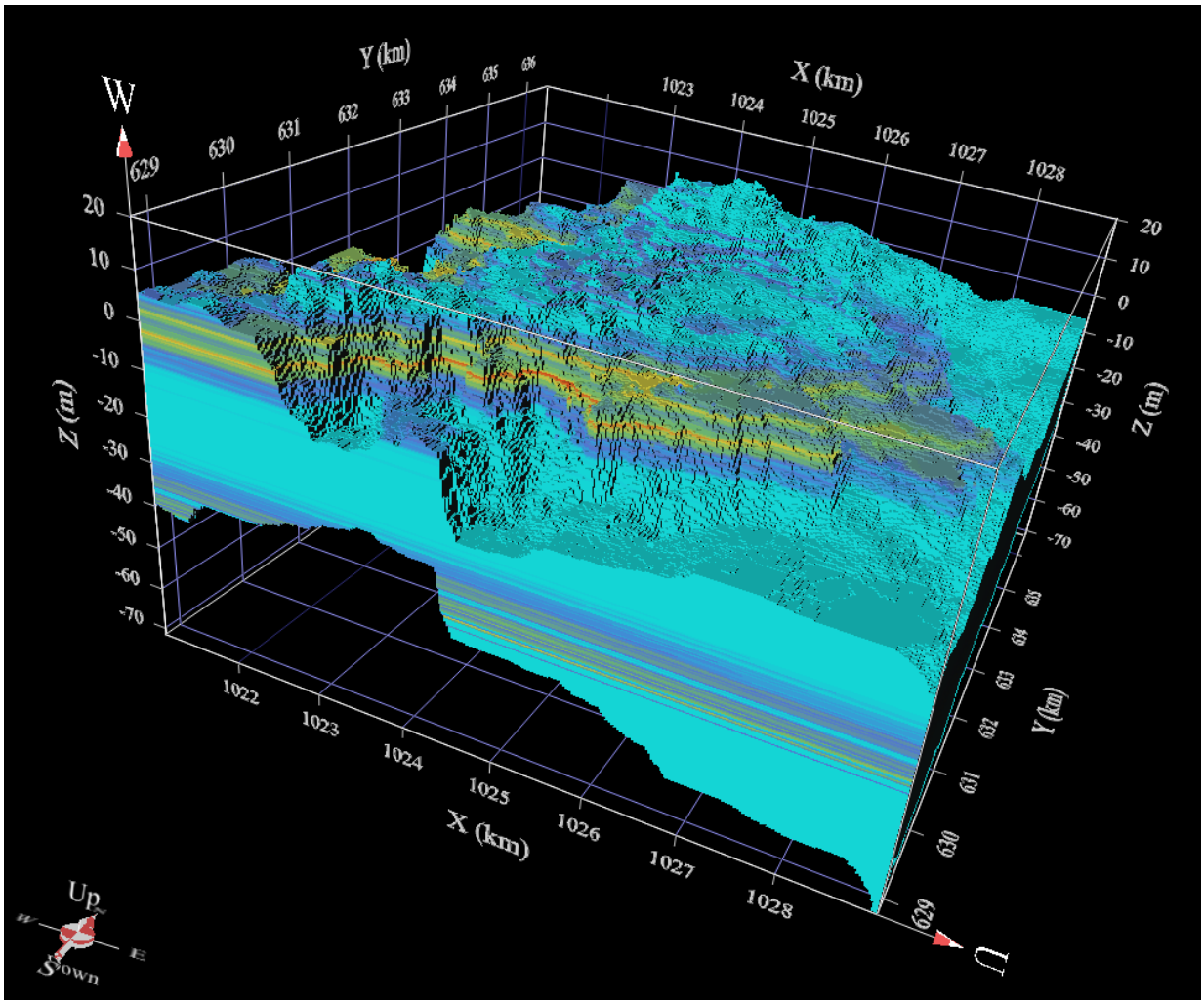

Figure 5.15. The diagenetic model: warm colors indicate high odds of encountering the low-porosity facies, whereas cool colors indicate low odds. The low-porosity facies is mostly found in two distinct bands interpreted as calcite cement at the oil-water contact and 9.1 m (30 ft) below the oil-water contact. The low-porosity facies also occurs near the base of the model, which is caused by shale appearing in some logs when the sandstone transitions to shale at the base of the thick Cypress. 50× vertical exaggeration.

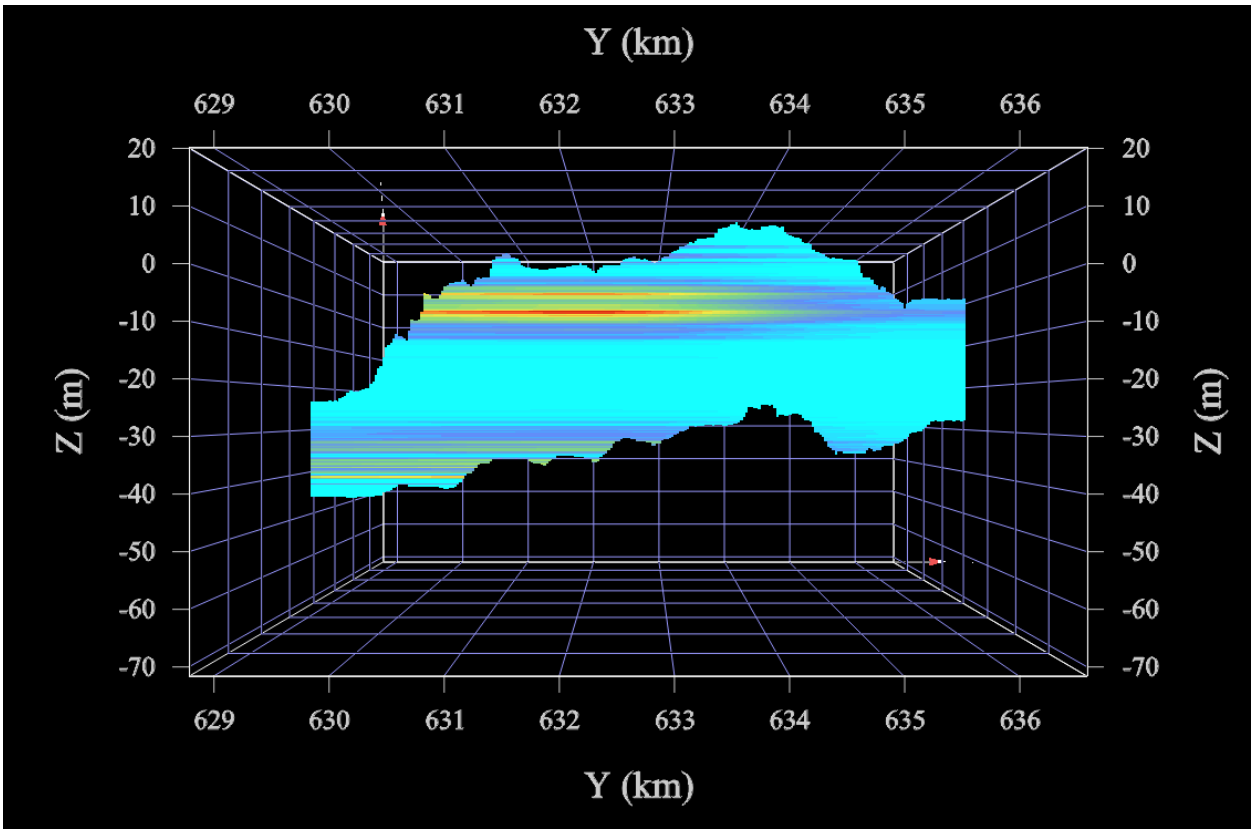

Figure 5.16. A north-south-oriented slice of the diagenetic model. Warm colors indicate better odds of encountering low-porosity facies. The calcite cement appears as two parallel layers of low-porosity facies in the upper reservoir. The model has been flattened on the oil-water contact, so the upper layer occurs at contact). The lower band is more pronounced and occurs about 10 m (33 ft) below the oil-water contact. Both layers disappear near the northern edge. There is also a chance of encountering low-porosity facies, which are interpreted as discontinuous shale bodies, in the lower portion of the reservoir (>30 m (>98 ft) below the oil-water contact). 50× vertical exaggeration.

Combined Model

The final combined model integrates the porosity and permeability based on the normalized SP simulated in the depositional model with two bands of calcite cement from the diagenetic model. **Figures 5.17 and 5.18** show the distribution of the petrophysical properties, and **Table 5.5** lists the statistics of the final model. This model reflects the heterogeneity and internal architecture of the sandstone presented in the geologic conceptual model described in Section 3.3.1.

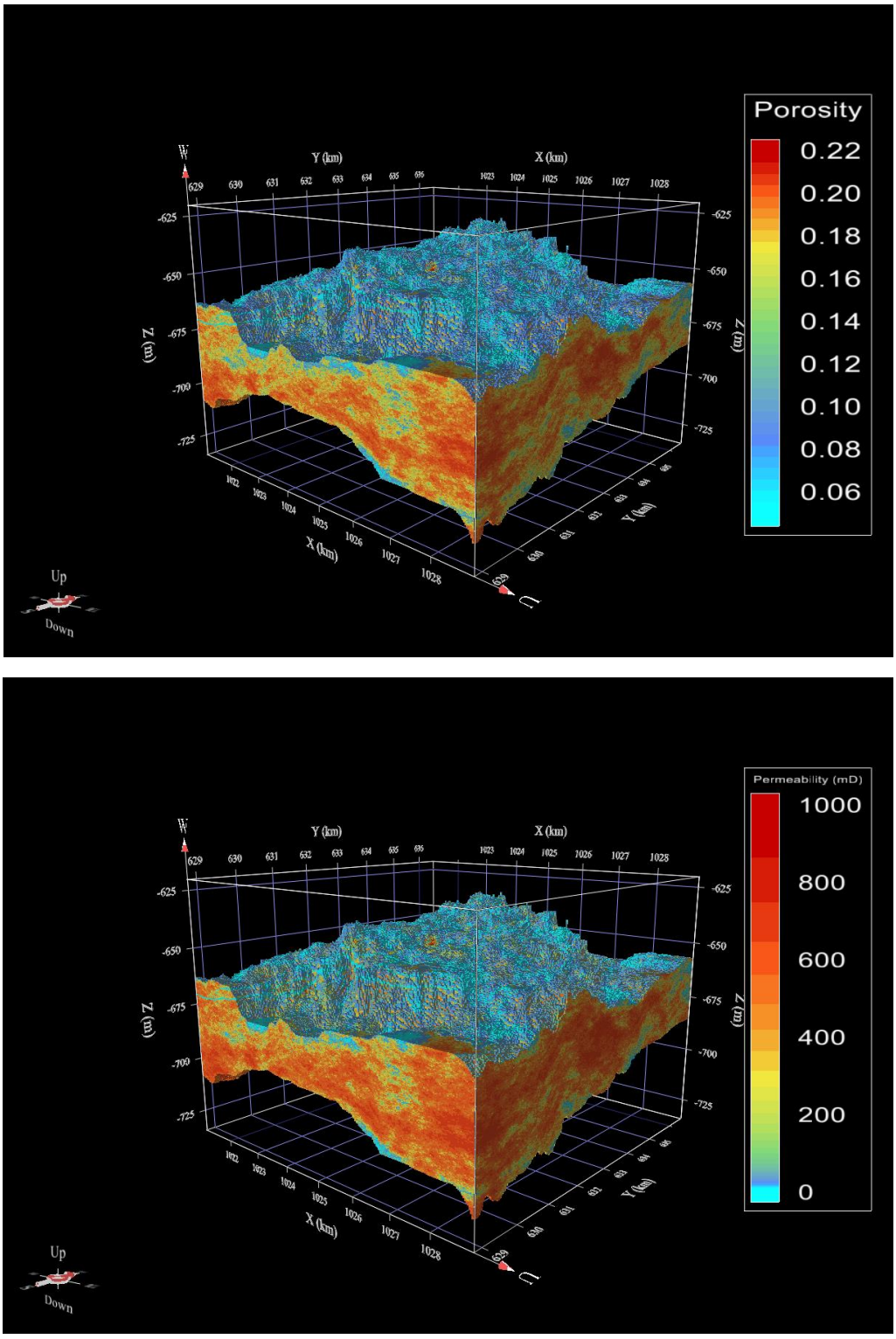

*Figure 5.17. Final model of porosity (upper image) and perm*eability (lower image). The upper boundary has high shale content, which results in low porosity and permeability. The middle of the model is fairly clean sand with typical porosity of 17% and permeabiltiy of 0.39 μm^2 (400 mD).

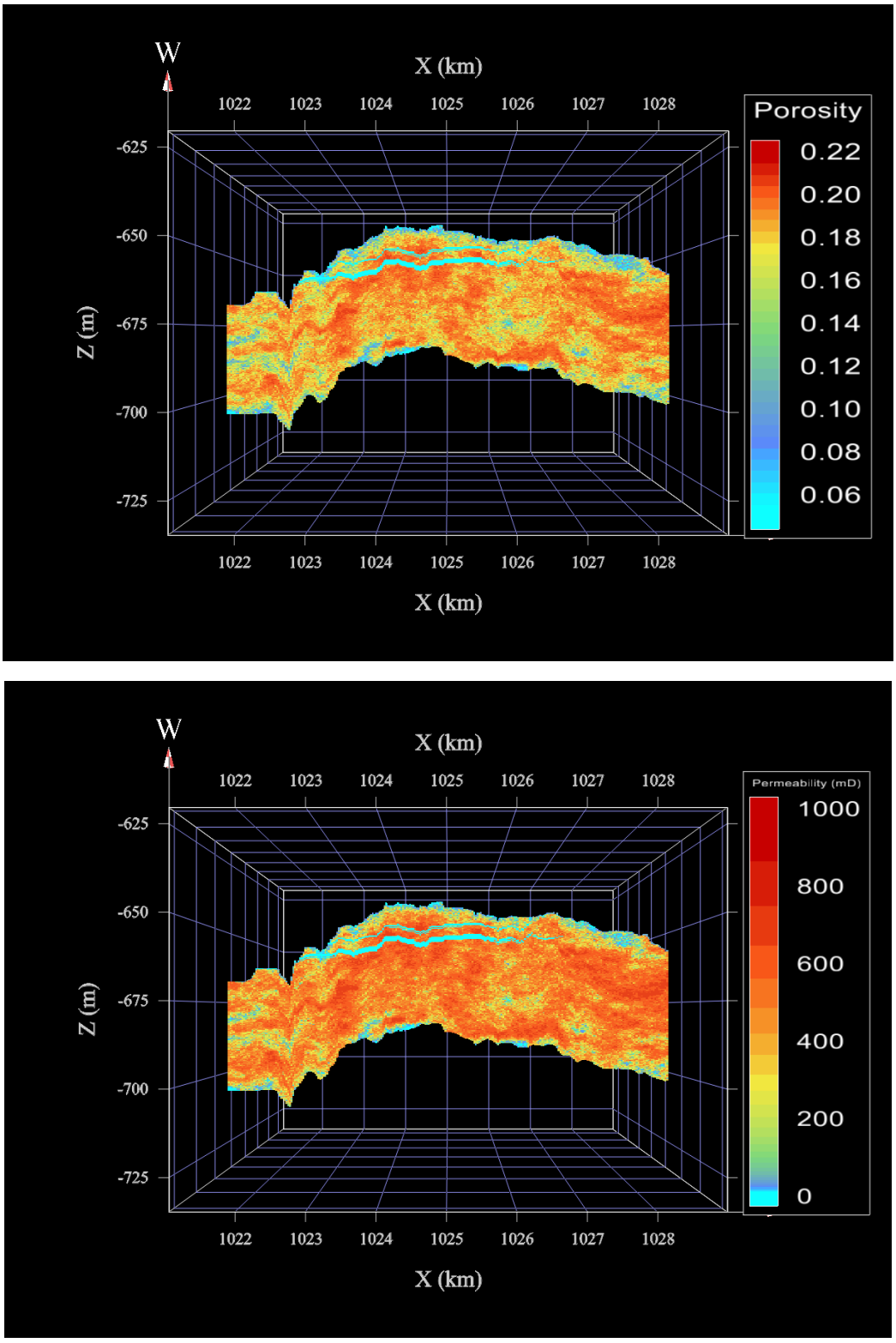

Figure 5.18. Slice from the middle of the final model showing the internal distribution of porosity (upper image) and permeability (lower image). The internal distribution reveals the stark contrast between clean sand and two parallel layers of cement in the upper reservoir. This slice is from the approximate middle of the model (3,048 m (10,000 ft)) from the southern boundary) and is shown with 50× vertical exaggeration.

Table 5.5. Statistics from the embedded model.

Attribute		Model Value
Number of cells	Total	1,980,160
	Defined	734,180
	x	130
	y	128
	z	119
Spacing, ft (m)	*x*/*y*	200 (61)
	z	3 (0.9)
Elevation (subsea, ft [m])	Min.	–2,053.5 (625.91)
	Max.	–2,410.5 (734.72)
Thickness, ft (m)	Min.	45 (14)
	Max.	189 (57.6)
	Mean	129.77 (39.554)
Porosity	Min.	0.04
	Max.	0.21
	Mean	0.17
	Median	0.18
	St. dev	0.04
kH (mD)	Min.	2.85
	Max.	689.47
	Mean	401.56
	Median	456.35
	St. dev	186.9
kZ (mD)	Min.	0.41
	Max.	371.55
	Mean	159.22
	Median	173.44
	St. dev	104.07

5.3 Oil Field Crude Oil and Brine Characterization

5.3.1 Minimum Miscibility Pressure Analysis

The minimum miscibility pressure (MMP) of crude oil is an important design parameter when evaluating potential sites for carbon dioxide enhanced oil recovery (CO_2-EOR). The MMP of crude oil is the pressure at a given temperature that oil and CO_2 mix to form a homogeneous solution. Reservoir pressure above the MMP is generally considered miscible and those below are considered immiscible. Miscible floods are expected to have higher oil recovery and immiscible floods are expected to have lower oil recovery. This section summarizes the results of an MMP slim tube test on a crude oil sample collected at the surface in Noble Field. Additionally, the density and viscosity of the crude oil were measured under atmospheric pressure.

A crude oil sample was collected by the Citation Oil and Gas Corp from a battery of wells that only produced from the Cypress and the water sample came from the well Coen #92 (API 121592607500) in the Clay City Consolidated oil field. The estimated reservoir temperature at the completion depth of the well was 33°C (91.4°F).

The ISGS measured the physical properties of the oil near reservoir temperature and atmospheric pressure (**Table 5.6**). The density was measured with a Mettler Toledo Densito 30PX digital hydrometer and the viscosity with a Precision Scientific Viscosity apparatus. The composition of the oil was analyzed by the Illinois Sustainable Technology Center by simulated distillation following ASTM method 7169-05 with results shown in **Figure 5.19**.

Table 5.6. Summary of the physical properties of the Cypress oil at several temperatures.

Temperature °C	density (g/cm^3)	viscosity (cP)
31	0.8556	7.114

The concentration of major ions in the brine was determined by the ISGS using ion chromatography for anions and by the Illinois State Water Survey using inductively coupled plasma mass spectrometry for cations (**Table 5.7**). Anion analysis show a Cl^- concentration of 58,744.6 mg/L, a Br^- concentration of 460.2 mg/L and a SO_4^- concentration of 1,115.31 mg/L.

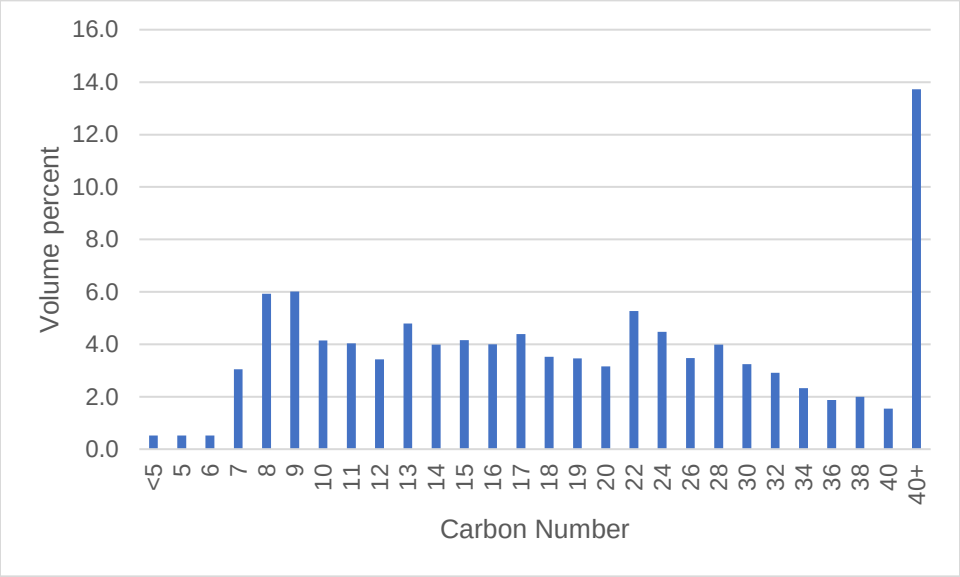

Figure 5.19. Composition of Cypress oil sample measured by simulated distillation with results as volume percent.

Table 5.7. Anion and Cation concentrations measured from Cypress brine. Units are mg/L.

ICP analyses by the Illinois State Water Survey
Samples received: 10/20/2015
Samples analyzed: 10/23/2015
Report date: 11/06/2015
All concentrations are in mg/L

Sample name/#	**Al**	**As**	**B**	**Ba**	**Be**	**Ca**	**Cd**	**Co**	**Cr**	**Cu**
MDL:	**0.93‡**	**1.1‡**	**0.58‡**	**0.021‡**	**0.0055‡**	**0.29‡**	**0.12‡**	**0.13‡**	**0.058‡**	**0.040‡**
Cypress brine	<0.93‡	<1.1‡	6.91	0.208	<0.0055‡	2730	<0.12‡	<0.13‡	<0.058‡	<0.040‡

Sample name/#	**Fe**	**K**	**Li**	**Mg**	**Mn**	**Mo**	**Na**	**Ni**	**P**	**Pb**
MDL:	**0.24‡**	**0.40‡**	**2.8‡**	**0.27‡**	**0.015‡**	**0.22‡**	**0.26‡**	**0.43‡**	**0.73‡**	**0.41‡**
Cypress brine	<0.24‡	214	11.1	1307	0.198	<0.22‡	32516	<0.43‡	<0.73‡	<0.41‡

Sample name/#	**S**	**Sb**	**Se**	**Si**	**Sn**	**Sr**	**Ti**	**Tl**	**V**	**Zn**	**Zn**
MDL:	**2.2‡**	**1.5‡**	**1.3‡**	**1.7‡**	**0.86‡**	**0.0037‡**	**0.0056‡**	**0.43‡**	**0.47‡**	**0.097‡**	**0.097‡**
Cypress brine	919	<1.5‡	<1.3‡	5.3	<0.86‡	81.8	<0.0056‡	0.67	<0.47‡	<0.097‡	<0.097‡

[1]Dagger (‡) indicates method detection limit (MDL) is elevated and was estimated because of a difficult matrix.

The MMP point of the oil was determined using a 15.8 m (52 ft) long slim tube with a pore volume of 120 mL. For each test, 1.5 pore volumes of toluene were first flushed through the slim tube to remove oil residue and then nitrogen was pumped through to displace the toluene and evacuate the slum tube. After the evacuating the slim tube, oil was injected, and a back-pressure regulator was set to control the outlet pressure. An ISCO model 500D syringe pump was used to inject mineral oil to displace CO_2 into the slim tube. A total of 1.2 pore volumes was injected over 12 hours for each of the tests. This test was performed several times at a temperature of 33°C. A fraction collector collected the effluent over ten-minute intervals to determine produced oil volume over time.

The data points collected for a range of pressures are reported in **Table 5.8**. We then ran an additional test to verify that the points above the MMP would not change as a result of the repacked slim tube. The experimental results are presented in **Table 5.8** and **Figures 5.20 and 5.21**. The results show that the break in the slope between the low pressure and high-pressure measurements is between 7,584.5 and 8,274.0 kPa (1,100 and 1,200 psig) (**Figure 5.19**), which is the estimate of the MMP of the thick Cypress Sandstone crude oil at the reservoir temperature of 33°C.

Table 5.8. Oil recoveries at the tested outlet pressures.

Pressure (kPa, psig)	% Recovery
5929.7 (860)	54.5
6619.2 (960)	82.8
7929.3 (1150)	87.3
8411.9 (1220)	88.5

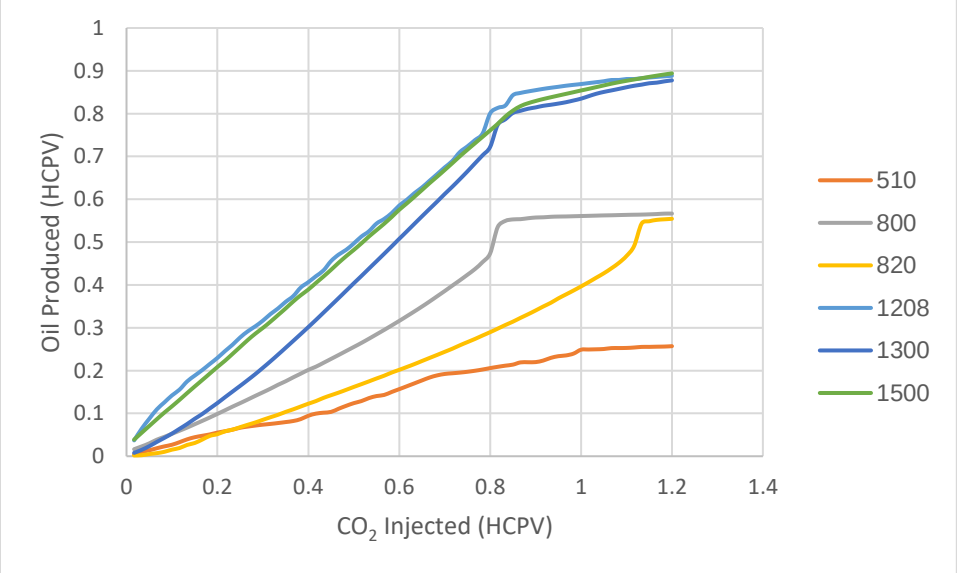

Figure 5.20. Amount of oil produced per amount of carbon dioxide injected measured in units of hydrocarbon pore volume (HCPV) at outlet pressures from 3,516.5 to 10,342.5 kPa (510 to 1,500 psig).

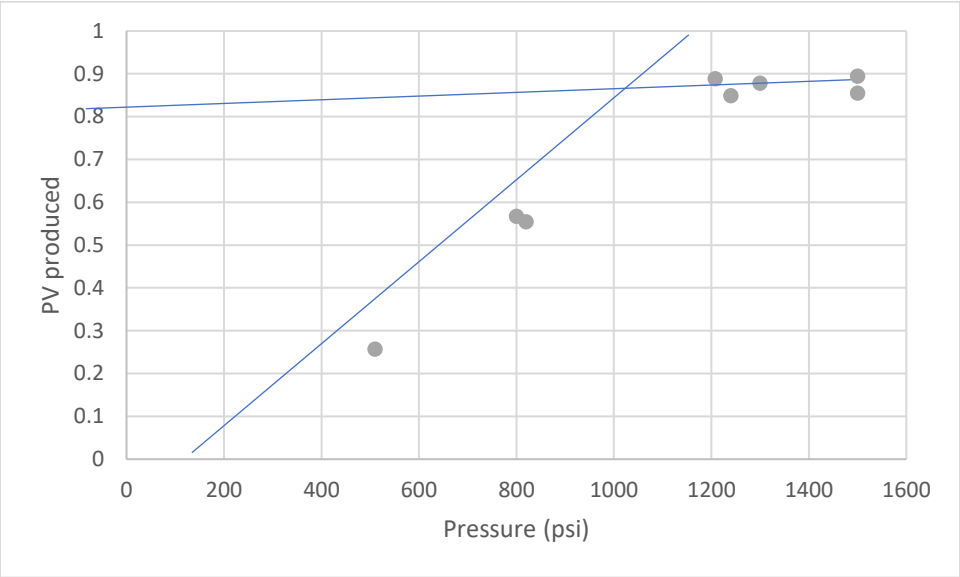

Figure 5.21. Pressure vs pore volume injected plot showing data from the slim tube tests. The trend lines for the low pressure and high-pressure tests intersect indicating a MMP of 7,584.5 to 8,274.0 kPa (1,100 to 1,200 psia) at reservoir temperature of 33°C (91.4°F).

5.3.2 Brine-CO_2 interaction Analysis

The act of injecting CO_2 into a reservoir fundamentally changes the chemistry of the system. The pH can drop to around 3 and mineral dissolution/precipitation can occur at accelerated rates. These changes can have a significant impact on the injection process. Accelerated mineral precipitation or dissolution can lead to formation damage. Decreased pH can drive trace metals into solution, causing problems with reservoir brine disposal, and changes in mineral distribution can alter the capillary pressure properties of the formation. To evaluate these potential changes, we performed a core flood experiment and monitored the effluent chemistry. This data was then input into a set of models to evaluate which processes might be occurring and what the major controls of the chemical system might be.

Experimental Setup

A core sample from the Montgomery #B-35 well (API 121592606400) at a depth of 791.4 m (2,596.5 ft). was placed into Hassler type core holder with at least 17,237.5 kPa (2,500 psi) of confining pressure in an oven at 32.2°C. Two cylinders were connected to the inlet, one with Cypress reservoir brine and the other with CO_2. The entire system could equilibrate overnight. After equilibration, an ISCO 500D syringe pump displaced brine into the vacuum-evacuated core to saturate it. Brine was injected until it overcame the threshold pressure of 8,343 kPa (1210 psi) set by the back-pressure regulator (BPR).

The pump then continuously injected brine at a rate of 1.76 ml/min for 30 minutes (10 pore volumes) while a fraction collector sampled the effluent. A sample (FT-1) of the effluent was then taken over the last 15 minutes of initial brine injection. The inlet fluid was then changed to CO_2 pumping at a rate of 1.76 ml/min for 50 minutes. After this, the inlet fluid switched back to brine with samples FT-2, FT-3, and FT-4 collected over 15-minute intervals for the last 45 minutes of brine injection.

Analysis

Before the experiment began, the end was trimmed off the core plug for XRD analysis. The results show a quartz arenite composition (**Table 5.9**). The small clay fraction is dominated by Kaolinite.

Table 5.9. Mineral composition (volume %) measured by XRD of the sandstone plug.

Clay	Quartz	K-feldspar	P-feldspar	Calcite	Pyrite/Marcasite	sum%
2%	92%	1%	2%	1%	1%	100%

Because the effluent had already gone through the BPR, samples no longer at reservoir pressure or temperature and degassed significant CO_2, the aqueous CO_2 concentrations and pH values were not measured. The Illinois State Water Survey analyzed the cation concentrations of the brine effluent (**Table 5.10**).

Table 5.10. Concentrations of cations in effluent samples (mg/L).

Sample	Al	Ca	Fe	K	Mg	Na	S	Si
FT-1	<0.37 ‡	2726	0.66	499	1293	31356	503	5.50
FT-2	1.40	2700	6.47	365	1263	30239	495	8.12
FT-3	1.32	2592	2.98	299	1304	31972	502	6.14
FT-4	0.88	2561	1.56	295	1307	31954	503	5.71
‡ below detection limit								

Throughout the experiment, a set of pressure transducers and a data logger recorded the inlet and outlet pressure of the core. A constant pressure was maintained at the outlet via the BPR, except when the fluid was being changed, but the inlet varied according the saturation state of the sample and what fluid was being injected (**Figure 5.22**).

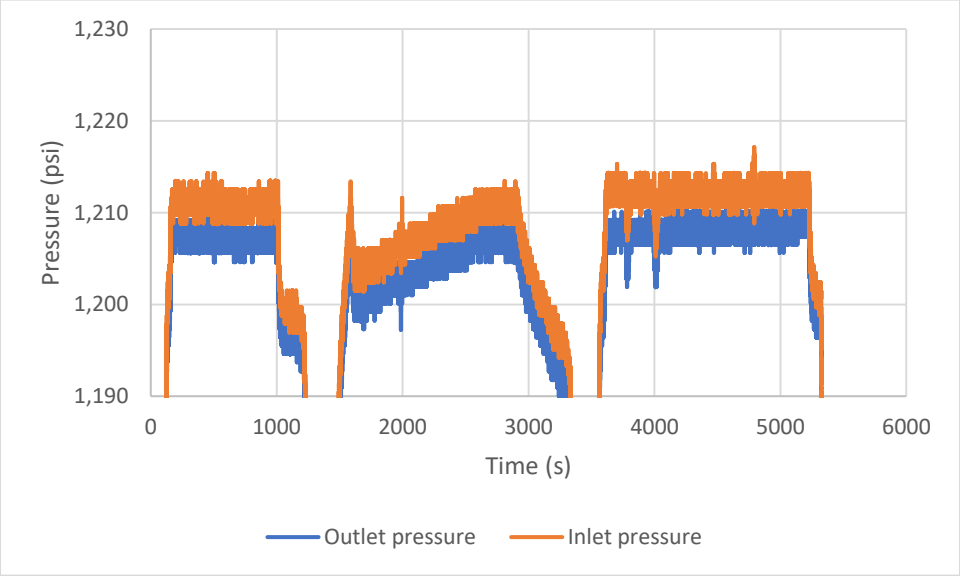

Figure 5.22. Inlet and outlet pressure over the course of the experiment. Drops below 1,190 psi represent periods of changing between fluids.

Model Setup

To simulate the chemistry of the system, a 1D model consisting of 10 nodes was created using the software X1t (Bethke, 2008). Each node had the same cross-sectional area (5.07 cm) and porosity (18%) as the core plug. We did not model the initial saturation period of brine or CO_2 flow. Instead, the initial chemistry was set to the measured composition of the brine effluent from the initial saturation period with a CO_2 fugacity set to the average pressure of the system (1205 psi). This allowed for the modeling of CO_2-saturated brine being displaced by normal reservoir brine.

A second model was created with the same geometry using the software TOUGHREACT (Xu, et al., 2004). This model did not release the CO_2 into solution properly, but it did allow for an investigation into the effects of physical multi-phase flow parameters on the geochemistry of the system. The optimization software Ucode (Poeter and Hill, 1998) was used to perform sensitivity analyses on the both the chemical and physical parameters of the experiment. The analyses consisted of perturbing the values and then determining how much the sum of the squared weighted residuals (SSWR) changed.

$$SSWR = \sum \left(\frac{measured\ value - simulated\ value}{0.01 * measured\ value} \right) \quad (17)$$

The sum of the squared weighted residuals (SSWR) gives a measure of the deviation of the measured values from that of the simulated values.

Results and Discussion

For the geochemical model built in X1t, the results are dominated by the displacement of CO_2-saturated brine. This process removes H^+ which decreases acidity (**Figure 5.23**) and significantly alters the rates and amounts of mineral dissolution and precipitation. This is also shown in the changes in mineralogy: the increase in pH corresponds to the precipitation of kaolinite and the end of calcite dissolution. A similar trend is observed in the geochemical data collected during the test, as there is a decrease in Al and Si over time, which likely reflects dilution resulting from the incoming fresh brine and a slowing rate of mineral dissolution. The Ca concentration also stabilizes at a point that is consistent with it being at equilibrium with calcite in a slightly acidified solution.

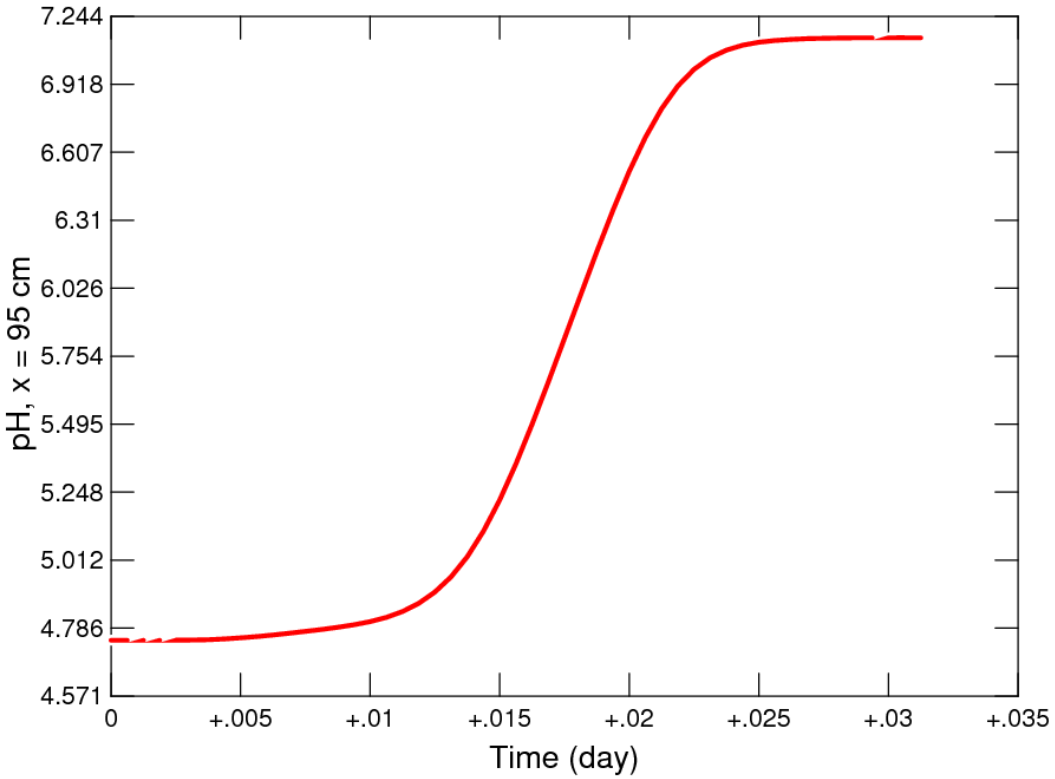

Figure 5.23. Image showing the pH at the last node of the simulated end plug.

The overall amount of minerals being dissolved is minor because the sample is 92% quartz. Quartz is inert to changes in pH and the kinetics of feldspar dissolution are slow relative the length of this experiment (Palindri and Kharaka, 2004). Therefore, carbonates and clay minerals, while a minor component of the rock, dominate the geochemical changes. These changes can still have a significant effect on CO_2 injection, because these minor mineral components coat the quartz and feldspar grains and their alteration can change the wettability of the system. Removing clay minerals from a pore throat, for example, could make it either easier or harder for CO_2 to pass through and, therefore, alter the residual gas and brine saturations.

While the model created in TOUGHREACT does not reproduce geochemical changes as accurately, it does allow an investigation into the sensitivity of the system to changes in the parameters controlling gas and brine saturation (**Table 5.11**).

Table 5.11. Sensitivity of effluent concentration SSWR normalized to the largest sensitivity.

Parameter	Sensitivity
lambda (parameter for capillary pressure and relative permeability	0.109
Residual brine saturation	0.831
Residual gas saturation	1.000
Inverse capillary entry pressure (1/Pa)	0.018
K-feldspar kinetic rate parameter	0.773
Grouped clay kinetic reaction rate	0.004

Residual gas and brine saturation are the two most sensitive parameters for the outlet chemistry. These two parameters determine how much the brine interacts with CO_2. When the brine is displaced by CO_2, the residual brine remaining is acidified and subsequently mixes with the incoming fresh brine introduced into the system after CO_2 injection concludes. Thus, the residual brine saturation (to CO_2) determines the amount of maximum acidified brine present in the system and its ratio relative to the incoming fresh brine. The residual gas saturation determines how much gas remains in the system once it is flushed through with fresh brine. This residual CO_2 then buffers the brine CO_2 concentration, thereby decreasing pH of the system.

5.4 Historical Production and Injection Data Analysis

Oil production for the Illinois Basin is reported in monthly-issued pipeline production reports that have been issued since the 1930s. These reports represent a snapshot in time, and using them to create a long-term production history for a given oil field can be problematic because they contain a large amount of variability, namely from inconsistent record-keeping practices that change over time. In addition, lease names change over time and subtle errors could exist due to transcription or transposition errors. Therefore, in order to use the reports to gather lease-based production data, identified where pre-existing errors commonly occur, organized the data in a format suitable for time tracking, and analyzed available well documents to apportion a fraction of the total comingled production to a target formation.

5.4.1 Production History

Developing production histories involved three main parts: 1) analyzing well information to determine from which formation(s) each well was producing and when; 2) compiling, organizing, and tracking lease-based oil production data through time; and 3) analyzing waterflood reports to characterize water injection. The well information is available on the ISGS's Oracle database and on ILOIL, an interactive map that can be found online at: http://maps.isgs.illinois.edu/iloil/. The production data comes from pipeline production reports available to ISGS employees at the geological records unit (GRU) in the Forbes building.

5.4.2 Well Data

Establishing an accurate history for each well in Noble Field was necessary to properly determine what portion of the total comingled production was from the thick Cypress Sandstone. The well information was also used to create preliminary lease maps of the field.

ILOIL and Well Records

Documents for every well drilled in Illinois can be found on ILOIL using the well's API number, a unique, permanent numeric identifier assigned for identification purposes to a well drilled for the purpose of finding or producing oil and/or gas (API, 1979).

Scout Tickets

A scout ticket consists of notes made by the driller during drilling or reworking of a well. It contains basic information such as the well name, location, ground level elevation, drilling company name, and total depth. It may also contain depths to each formation, potential shows of oil, and information about the treatments, casing, perforated intervals, initial production of oil and water, and drilling, workover, and plug dates. There is typically one scout ticket per well, so a scout ticket may contain information on several APIs.

A basic knowledge of well completion practices is necessary to use scout tickets to understand a well's history. The well is typically drilled to the depth of the primary target formation. Tests can then be run on specific depths within the open hole to determine properties of the subsurface formations. Depths of cores that were extracted and drill stem tests that were conducted are recorded on the scout ticket. A metal sleeve known as a casing is inserted into the well and cemented in place to keep the borehole separate from the subsurface. Holes, known as perforations (often abbreviated on a scout ticket as pf, shots, or s) are punched in the casing to allow communication with the reservoir. Inserting a sleeve and then punching holes in it allows operators to control which parts of the subsurface are in communication with the borehole. The depths of these perforations show what formations the well was producing from. Once the well is completed, the initial production of oil and water (IP) is recorded. A completed well can be re-entered or reworked. This is typically done to change the well from a producer to an injector, to perforate another interval, or to apply a treatment. The purpose and dates of each workover are listed on the scout ticket. A well should be assigned a new API each time it is worked over, and the dates of each workover listed on the scout ticket should correspond to the start and end dates for each API.

Early scout tickets were handwritten and many of these were transcribed to a typed copy. Typed copies are much easier to read, but the handwritten versions sometimes contain information that was not transcribed. However, handwritten scout tickets are often written for the drillers benefit, so abbreviations, handwriting, and even names of formations can be inconstant or difficult to decipher.

Scanned Documents

In addition to the scout tickets, ILOIL scanned documents such as drilling permits, plugging or coring reports, injection information, and driller's logs. Documents found here can vary widely, as each well has a unique history and not everything that was recorded was submitted to the ISGS. However, information can appear here that is not recorded on the scout ticket. For example, a plugging report may reveal that a well was producing from a formation not recorded on the scout ticket. This information may only be stored in the file cabinets at the GRU if it has not been digitized and added to ILOIL.

Developing a Preliminary Lease Map

Pipeline production reports list production by lease. Farm names assigned to each well when they were drilled were used to create preliminary lease boundaries. The resulting lease maps were used to anticipate the size and expected production for each lease and identify leases that may have changed names or get misplaced in the records. Knowing which Cypress producing leases were within the fields before gathering production data minimized the number of leases and name changes that needed to be tracked and identified. A preliminary lease map was developed initially as a rough hand-sketched estimating lease boundary and was updated as more information became available.

5.4.3 Production and Injection Data

The ISGS Geologic Records Unit houses pipeline production reports dating back to 1937. A field-wide production history was created by compiling monthly data for Noble Field, digitizing the data into spreadsheets, creating and assigning a unique and consistent code to each individual production history, tracking each individual production code through time, creating both field-wide and individual cumulative and yearly production curves, and identifying and resolving errors. Once the production curves were completed, wells were assigned to each production history and the Cypress Sandstone was assigned a portion of the total comingled production for each year.

Production curves that show the cumulative and annual production over time were developed for each lease to identify errors that commonly occur when the production data was initially recorded, transcribed onto spreadsheets, or processed. Pipeline production reports do not contain production on a well by well basis for Illinois. Instead, the reports contain production data grouped by operating company first, and then listed by lease. Thus, production data is generally considered to be listed by lease. However, it is important to recognize that this is not entirely accurate. A lease can contain multiple production histories. This most commonly occurs when multiple operating companies own wells within the same lease or when a lease stops producing and then restarts later. It is important to keep each of these production histories separate (even if they are in the same lease) to help identify and minimize errors in both the production and well data.

Noble Field contained large scale waterflood projects. These were characterized by using yearly waterflood reports that contain information on the formation targeted, number of injecting and producing wells, volume of water injected, average well head pressure, and oil and water production.

5.4.4 History Matching

Oil field production history is necessary to accurately estimate current reservoir conditions and to validate the static geocellular model. History matching is the process by which the model attempts to match the known production. A good match indicates that the geocellular model properly represents the geology and validates the initial conditions (such as the oil-water contact, OOIP, and initial reservoir pressure). Once validated, the model can be used to predict future performance under multiple production and injection scenarios.

There are inherent limitations in the production history data that can lead to issues with the history matching process. History matching assumes that the production history is correct, however, it is important to understand that the production histories are an educated estimate. Disagreement between production history and simulated results may be caused by the geocellular model not properly representing the petrophysical properties of the reservoir, but it may also be caused by issues with the production history data.

Missing data is a source of error that may be impossible to identify. For example, a well that was perforated in the target formation without a written record will not be included. The increase in production that such a well creates may be erroneously assigned to another formation or masked if the well was completed around the same time as other wells or if the lease contains multiple wells. Leases may also be misplaced in the pipeline production reports. This can result in entire leases missing from the production history.

It is difficult to confidently distribute a portion of the total comingled production to a target formation. Production within each formation can vary from well to well for a variety of reasons that are difficult to account for (e.g., local variations in petrophysical properties, different treatments, completion problems, perforating the well at incorrect depths). It is also possible that formations were perforated or plugged without a written record. Well perforations and ratios in leases that are not matching simulated results should be inspected closely. It

may be necessary to adjust ratios based solely on reservoir simulation results. This is acceptable given the uncertainties listed above, but care should be taken to ensure that the ratios are edited by a reasonable amount, and that there is a reasonable explanation.

Production data for Noble begins upon discovery in 1937. In 1948, it was lumped into Clay City Consolidated and continued to produce. Historical well data indicates that 219 of the 658 wells in the field were perforated in the Cypress. However, close examination of handwritten scout tickets and other scanned documents (such as well plugging reports) identified an additional 29 wells that were reworked to perforate the Cypress without being assigned a new API. It was determined that 67 leases had wells that were perforated in the thick Cypress. The distribution of these wells were used to construct a preliminary lease map for the field (**Figure 5.24**). Production histories were compiled for each of these leases and checked for errors.

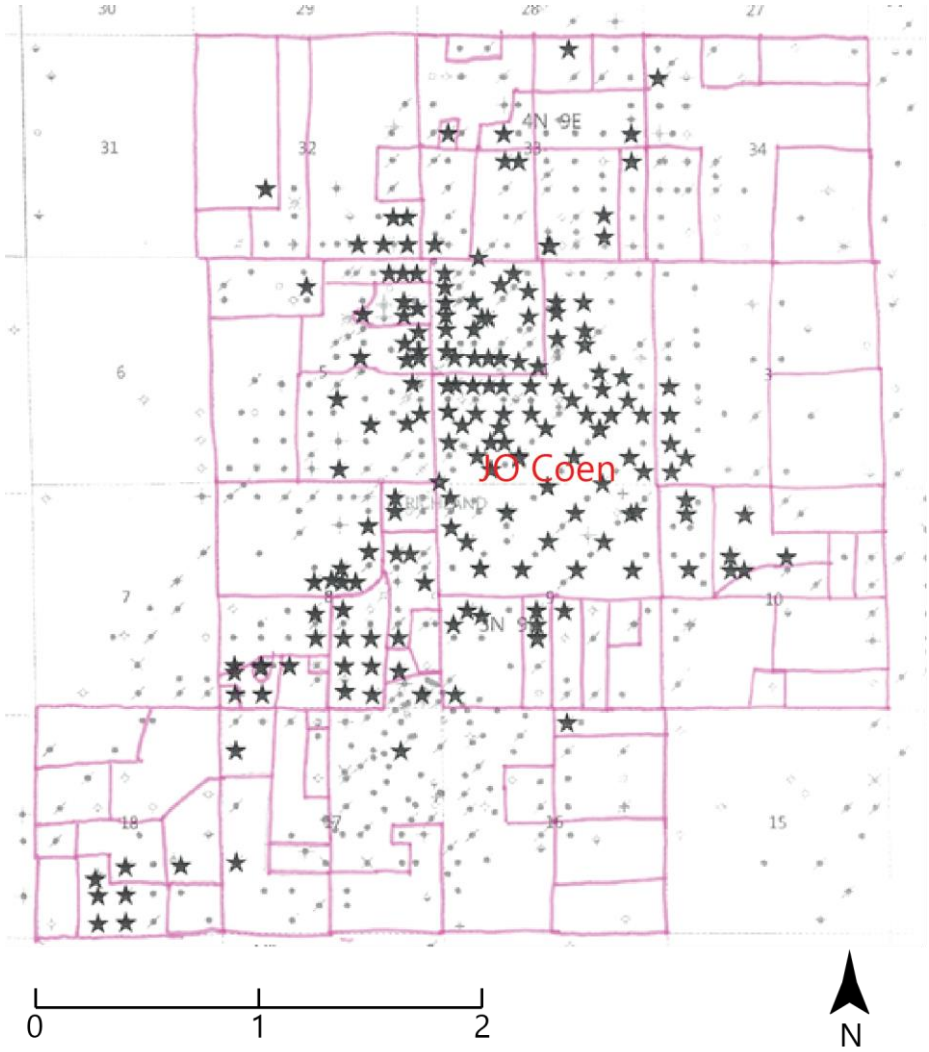

Figure 5.24. Preliminary lease map for Noble Field. Wells perforated in the thick Cypress Sandstone shown in stars.

The JO Coen lease is shown here as an example. It occurs in the middle of the field and takes up 50% of Section 9 and 75% of Section 4. Its production history also highlights the difficulty of managing production data and the necessary assumptions required when doing so. The production history for the Coen lease begins in 1937 and ends in 1967, when production histories for Coen A, Coen B, and Coen D begin. This change corresponds to a change in operator from Pure Energy to Union Oil of California. Production for these subleases

is reported for 1968-1970, but not for 1971-1979. No producing wells are plugged during this time, so it was necessary to interpolate data between 1970 and 1980 to create a smooth decline. A similar interpolation was used to fill a gap in missing data in the mid-1990s (**Figure 5.25**).

A similar method was applied to each of the 67 leases that contain Cypress production to assign a proportion of the comingled production to the Cypress for each year. The sum of the comingled and Cypress-only annual productions were used to create full field production (**Figure 5.26**).

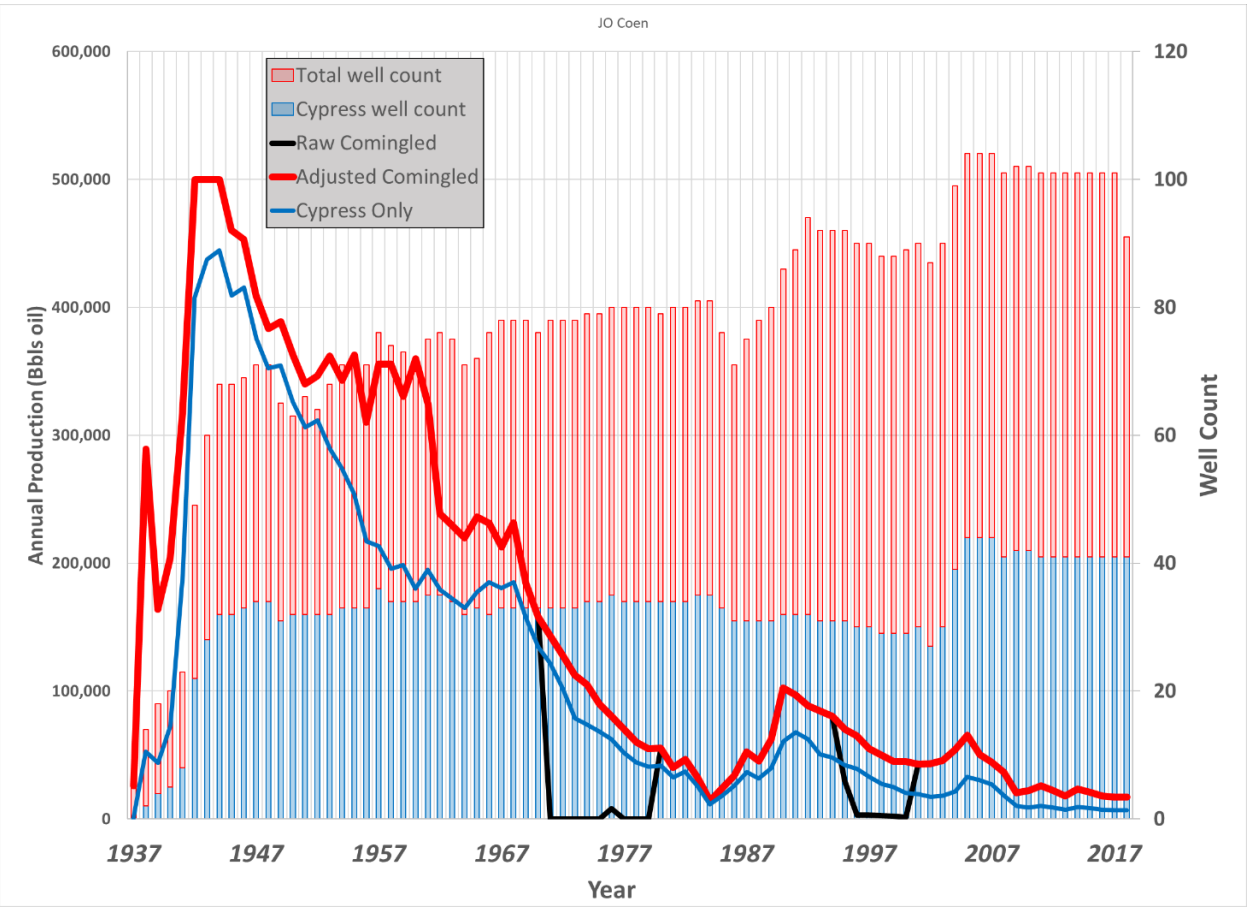

Figure 5.25. Example production plot for the JO Coen lease. Raw comingled production shown in black line, adjusted comingled production shown in red line, and Cypress production in blue line. The number of wells for each year are shown in red (all wells) and blue (wells with Cypress perforations) bars.

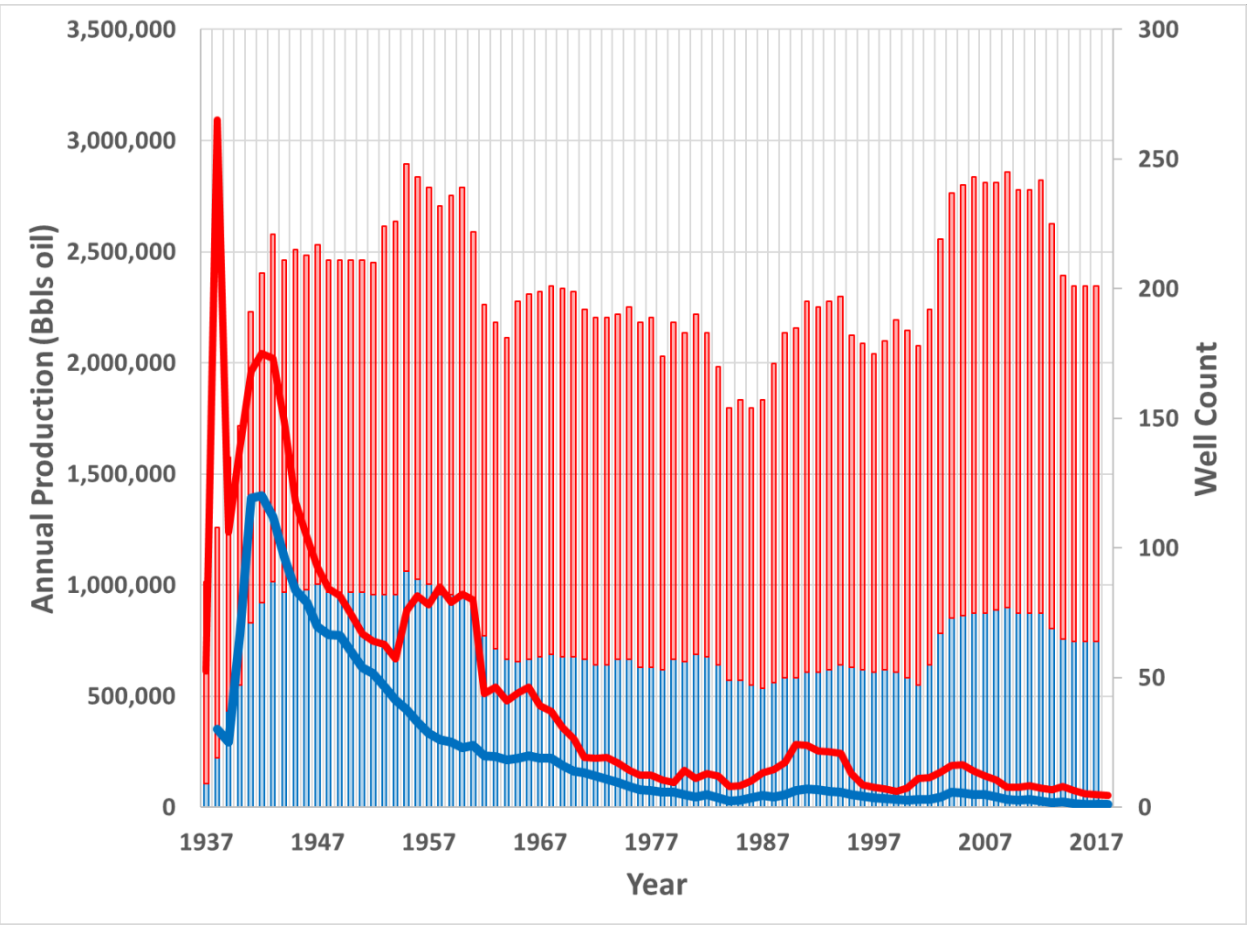

Figure 5.26. Production plot for the Noble Oil Field. Adjusted comingled production shown in red line and Cypress production in blue line. The number of wells for each year are shown in red (all wells) and blue (wells with Cypress perforations) bars.

5.5 CO_2-EOR and Storage Development Strategies for Cypress Sandstone ROZs

5.5.1 Introduction

This study aims to employ a reservoir simulation approach to provide economic development strategies for CO_2-EOR and CO_2 storage in brownfield ROZs of the thick, fluvial facies of the Cypress Sandstone. The procedure included using a geologic model (described in Section 3.3.1) representing the multistory fluvial architecture of the Cypress Sandstone at Noble Field, developing a reservoir model based on measured fluid properties, calibrating the reservoir model to site-specific historical production and injection, and using the calibrated model to predict CO_2-EOR and storage performance. Multiple CO_2-EOR development scenarios were studied that varied well spacing, injection pattern, and perforation interval, and considered the applicability of vertical versus horizontal wells. The findings of this study add to the knowledge base for developing mature fields that contain geologically complex reservoirs with thin MPZs, underlying brownfield ROZs, and strong bottom water drive aquifers.

5.5.2 Motivation

The Illinois Basin is a mature petroleum province with thousands of oil and gas reservoirs in over 60 pay zones (Howard, 1991), with approximately 2,250 oilfields identified as suitable targets for miscible CO_2 flooding (MGSC, 2005). Medium- to high-gravity, low-sulfur oil is commonly produced from pay zones between 305 to 1,524, (1,000 to 5,000 ft) deep with an average depth of 732 m (2,400 ft). Although CO_2 miscible flooding is the

most common EOR method in the US, it has yet to be deployed commercially in the Midwest, where no economically priced CO_2 is available. Primary challenges to the adoption of CO_2-EOR methods in the US Midwest identified by Frailey et al. (2013) are oilfield operator resources, perception, technical, operational, and regulatory. Although the ISGS has conducted prior CO_2-EOR pilots that demonstrated oil response (MGSC, 2012; Frailey et al. 2013), they were of short duration and did not reach peak oil production. While recognizing the efficacy of CO_2-EOR, smaller operators have not made further attempts of CO_2-EOR in the ILB because of uncertain capital expenses, low oil prices, and lack of available CO_2 at reasonable price.

ROZs in the Permian basin have had successful oil recovery via CO_2-EOR (Melzer, 2006). In the ILB, ROZs are suspected within a fairway of thick (up to 50 m) multistory fluvial sandstones of the Cypress Formation. These sandstones form laterally continuous and vertically amalgamated containers with high porosity and permeability. The coincidence of anticlinal structures and the multistory fluvial sandstones form structural-stratigraphic traps in which oil could accumulate, and later be swept away under changing hydrodynamic conditions. The ROZs are of interest because of the CO_2-EOR potential to offset carbon capture and storage costs. Additionally, the amount of CO_2 stored during CO_2-EOR operations is increased in areas with ROZs where CO_2-EOR has not previously been applied. The ROZs may enable CO_2 storage beyond the level of conventional utilization practices, ultimately allowing net carbon negative oil (NCNO) production. As such, nonconventional CO_2-EOR in brownfield ROZs may provide an economic incentive to mitigate CO_2 emissions by storing more CO_2 rather than recycling CO_2 as is typical of conventional CO_2-EOR floods. The added resource that ROZ oil production and tax credits from associated CO_2 storage may provide the incentive needed to jumpstart CO_2-EOR in the Midwest.

5.5.3 Advanced EOR Screening

The Oil & Gas Journal compiled a list of variables (i.e., location, operator, depth, rock and fluid properties, start year, area, and number of wells) for successful CO_2-EOR projects worldwide (Koottungal, 2014). This data has been used to develop preliminary screening criteria that can be broadly applied to candidate reservoirs for miscible CO_2 floods (Al Adsani and Bai, 2011; Sandrea and Dharod, 2016; Kamari et al., 2014; Bachu, 2015; Lake et al., 2014). The rock (porosity and permeability), fluid (oil density and viscosity), and reservoir (depth and temperature) properties of the thick Cypress Sandstone at Noble Field was compared to those from eight immiscible and 47 miscible projects from Koottungal (2014) to see if they fall within the range of other successful projects in sand or sandstone reservoirs. The depth to the Cypress at Noble Field varies from approximately 792 to 823 m (2,600 to 2,700 ft). The porosity and permeability of the sandstone from core reports is generally about 18% and 0.10 to 0.50 μm^2 (100 to 500 mD), respectively. Based on historical records and the typical geothermal gradient for the midcontinent, the reservoir temperature is approximately 32.2°C (90°F). Records of oil analyses from the Cypress in the area indicate that oil has an API gravity in the mid-30° range.

The rock (**Figure 5.27**) and fluid (**Figure 5.28**) properties of the Cypress Sandstone fall within the range of other successful CO_2-EOR projects, but the depth and temperature are below normal (**Figure 5.29**). Only Salt Creek (which has a depth of 350.1 m (1,150 ft) for immiscible and between 488 to 671 m (1,600 to 2,200 ft) for miscible floods), Velma Hoxbar (with a depth of 679 m (2,228 ft)), East Ford (with a depth of 817 m (2,680 ft)), and North Ward Estates (with a depth of 792 m (2,600 ft)) are shallower. Only the Velma Hoxba (with an oil temperature of 28.9°C (84°F)), East Ford (with an oil temperature of 27.8°C (82°F)), and North Ward Estates (with an oil temperature of 28.3°C (83°F)) have lower oil temperatures.

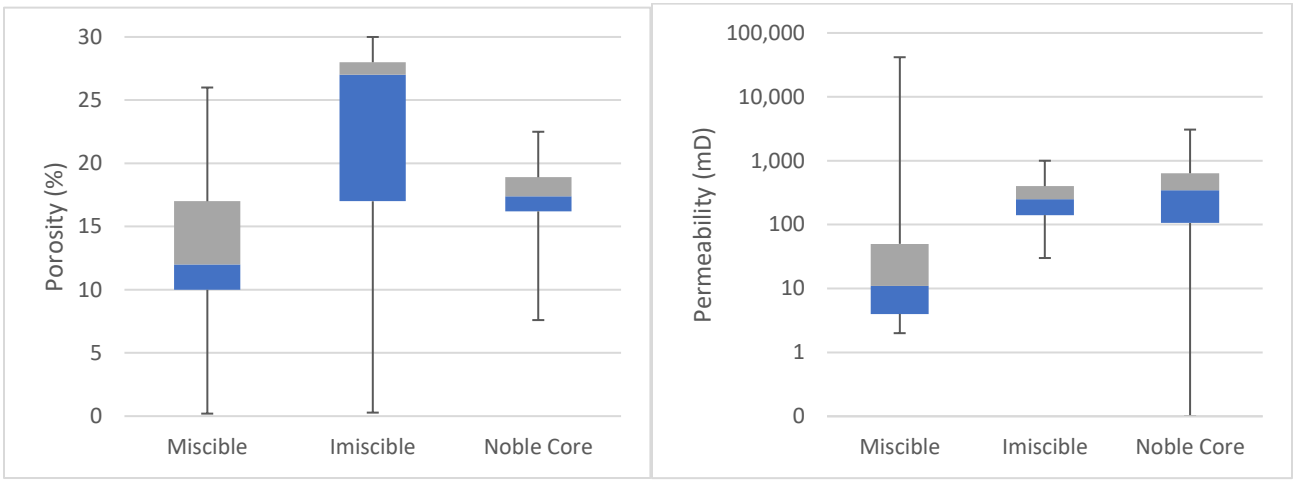

Figure 5.27. Box and whisker plots of the static rock properties (porosity and permeability) from successful miscible and immiscible CO2-EOR projects (from Koottungal 2014) and the Cypress Sandstone at Kenner West Field. The properties at Noble and Kenner West fall within the range of successful CO2-EOR projects.

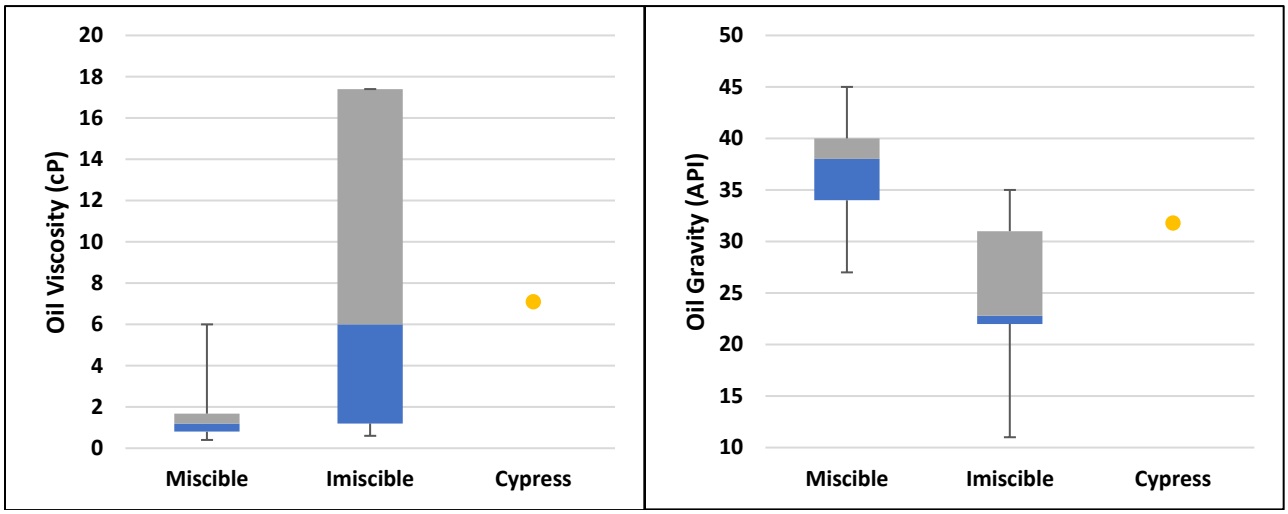

Figure 5.28. Box and whisker plots of the fluid properties (oil viscosity and density) from successful miscible and immiscible CO2-EOR projects (from Koottungal 2014) and the Cypress Sandstone. The properties from the Cypress fall within the range of successful CO2-EOR projects.

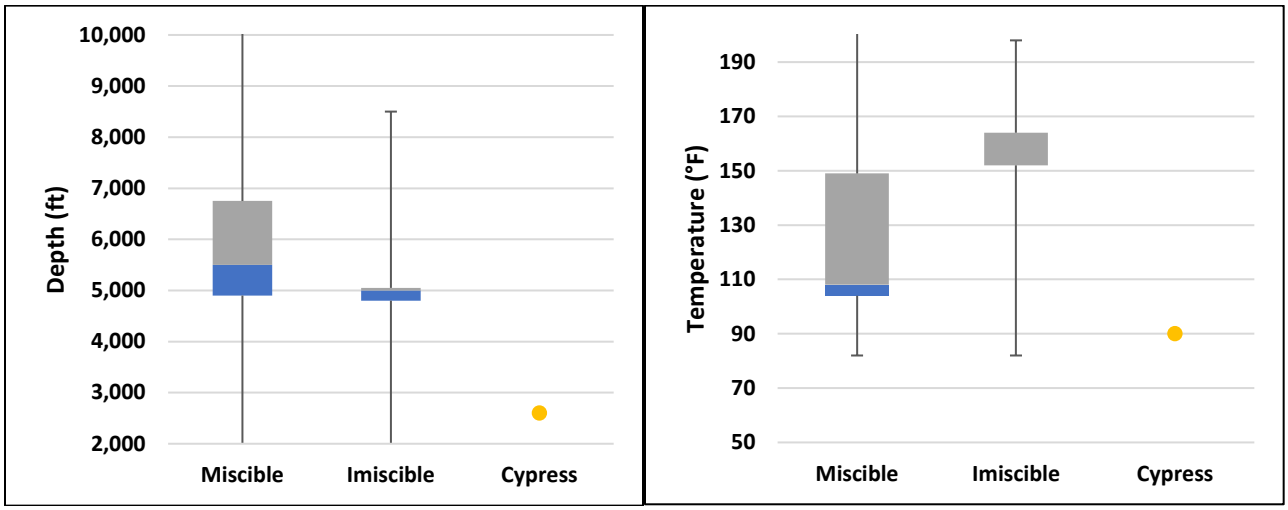

Figure 5.29. Box and whisker plots of the reservoir properties (depth and temperature) from successful miscible and immiscible CO2-EOR projects (from Koottungal 2014) and the Cypress Sandstone. The properties from the Cypress are on the extreme low end of successful CO2-EOR projects.

5.5.4 Numerical Simulation

Methodology

The purpose of numerical simulation is to provide estimates of oil recovery and CO_2 storage from nonconventional CO_2 floods in potential ROZs. Landmark's Nexus (version 5000.4.12), a commercial software package, was used to conduct numerical simulations. Nexus allows simulations of multiphase flow with multiple compositions for one or multiple assets and models the reservoir, wells, and surface and subsurface facilities as a single system for a comprehensive representation of asset behavior (Nexus Reservoir Simulation, 2017).

The static reservoir or geocellular model was developed from geologic, fluid properties, and well data from the Cypress Sandstone in Noble Oil Field (as described in Section 5.2) and was used as input to reservoir simulations. The static models were developed to properly represent geologic features that control fluid flow. Porosity and permeability data were populated with reservoir depth, thickness and well locations into the static reservoir model. Figure 5.30 shows porosity distribution of the Cypress at Noble Field. The crude oil pressure-volume-temperature (PVT) data used in simulations was generated using a five-component Peng-Robinson equation of state (EOS). The EOS was developed from laboratory measurements of oil composition, density, and viscosity of samples collected from Noble Field (see Section 4.2.3). Halliburton's Desktop-PVT software was used to simulate the behavior of crude oil (hydrocarbon fluid) mixtures and to fine-tune the EOS to match measured crude oil properties. The well data were compiled by collecting all the well location, configuration, perforation, and operating data and considering only the production and injection data in Cypress Sandstone.

The reservoir models were first calibrated to the oil production history by adjusting the most important influencing parameters. The calibrated reservoir models were then used to simulate various water flooding and CO_2 flooding scenarios (as described in previous section) to predict CO_2-EOR and Storage performance.

Simulation Inputs

The simulation inputs include primarily static model, crude oil PVT data, and rock-fluid properties. The static reservoir model of Noble Field consisted of 130 × 128 × 72 gridblocks in the x-, y-, and z-directions, respectively, i.e., 1,198,080 gridblocks (**Figure 5.30**). Each gridblock had dimensions of 61 m × 61 m × 0.9 m (200 ft × 200 ft × 5 ft). A porosity cutoff of 8% was applied to the upper shale-rich Cypress to eliminate portions of the model considered non-reservoir. Application of porosity cut-off reduced the total number of active gridblocks from 1,198,080 to 441,265. The maximum and average porosity of the reservoir are 21% and 15% and the

horizontal permeability ranges between 0.3 md to 689 md with a mean of 319 md. The vertical permeability of the reservoir was approximately 85% of the horizontal permeability (i.e. kv/kh = 0.85) throughout the model except for the top two active layers, where it is reduced to 30% (i.e. kv/kh = 0.30) due to finer grain size and increased clay content, and in cells containing the two cement layers, where it was set to 10% (i.e. kv/kh = 0.10). The initial water-oil contact was 659 m (2,163 ft) below ground level. Completion intervals of the wells were taken from well records.

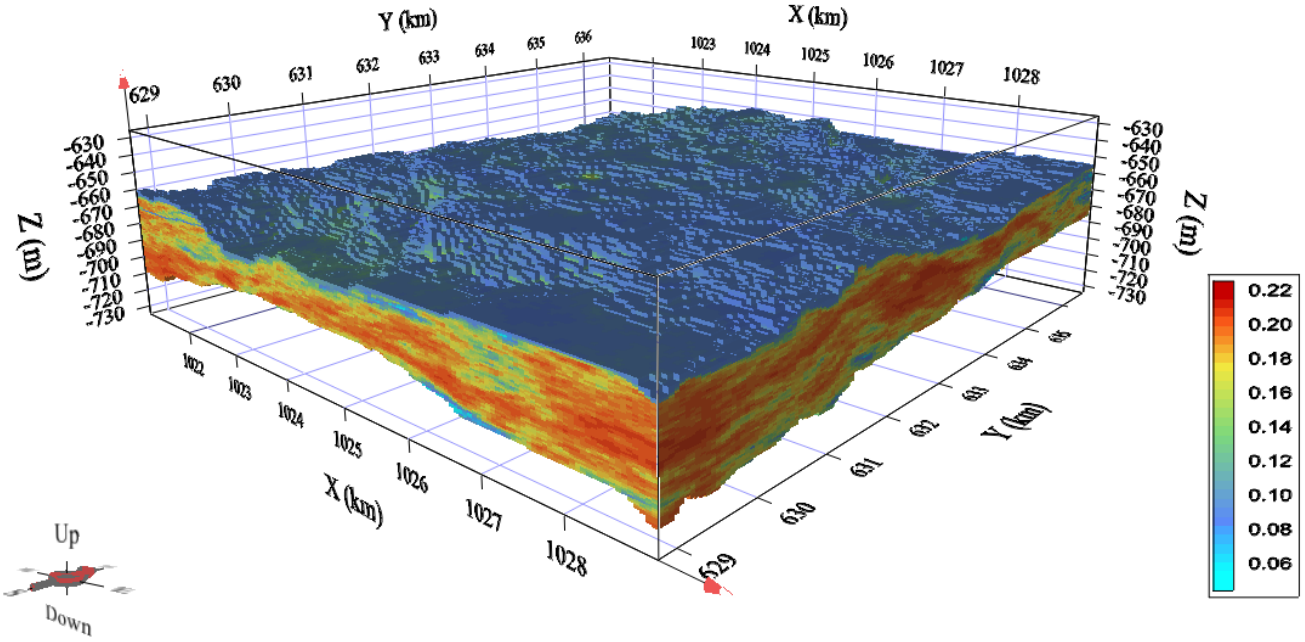

Figure 5.30. Geocellular model of Noble Field showing porosity distribution.

Five pseudo-components were used to characterize crude oil at Noble Field. The mole fractions of the pseudo-components (**Table 5.12**) were adjusted in Desktop-PVT until the EOS-derived fluid properties matched the observed density and viscosity of crude oil, at initial reservoir pressure (approximately 1158 psia) and temperature (~31.7°C (~89°F)). The minimum miscibility pressure (MMP) of CO_2 and oil at reservoir temperature of 31.7°C (89°F) ranged from 1,000 to 1,100 psi using correlations from Yellig and Metcalfe (1980), Chen et al., (2013), and Zhang et al. (2015); this estimation compared favorably with the laboratory-determined of 1,100 to 1,200 psia at reservoir temperature (33°C (91.4°F)) for a crude oil sample from Noble Field (see Section 5.3.1). The Lohrenz–Bray–Clark correlation was used to calculate the viscosity of the crude oil. Generalized water-oil and gas-oil relative permeability correlations were used in the simulations. **Table 5.13** shows the brine properties and rock compressibility.

Table 5.12. Mole fractions of the pseudo-components used in the five-component equation of state to match the crude oil properties of Cypress Sandstone.

Component	Pseudo-component	Mole Fraction
CO_2	CO_2	0.0001
C_1–C_5	C_2	0.0489
C_6–C_{11}	C_8	0.3765
C_{12}–C_{25}	C_{15}	0.4248
C_{25}^+	C_{32}	0.1498

Table 5.13. Reservoir brine and rock parameters.

Parameter	Value
Water density, ρ_{wb}	1.08 g/cm^3 (67 lb/ft^3)
Water formation volume factor, B_{wi}	1.03 rb/stb
Water viscosity, μ_w	0.92 cP
Water compressibility, c_w	2.57× 10^{-6} psi^{-1}
Rock compressibility, c_r	5.0 × 10^{-6} psi^{-1}

The following assumptions were made in the simulations, based on generalities of ILB geology and oilfield operations: (1) Capillary pressures between oil and water and between gas and water are negligible, as a result, relative permeability hysteresis effect was assumed negligible; (2) initial pressure within the reservoir is hydrostatic (i.e., the reservoir is assumed to be normally pressured at discovery); and (3) the crude oil in the reservoir was assumed to contain small amounts or proportions of dissolved hydrocarbon gas.

Due to limited availability, the relative permeability data were synthetically generated using Corey's function to mimic water-wet conditions. **Table 5.14** lists the end-point saturations and relative permeabilities, which were chosen based on previous simulation work in the ILB (Knepp et al., 2009). These data were kept constant while the Corey exponents were adjusted until reasonable history-match was achieved.

Table 5.14. Saturation and relative permeability end points.

Parameter	Value
Irreducible water saturation, S_{wr}	0.35
Residual oil saturation to water, S_{orw}	0.25
Residual oil saturation to gas, S_{org}	0.15
Critical gas saturation, S_{gc}	0.10
Water relative permeability at residual oil saturation, $k_{rw,max}$	0.20
Gas relative permeability at irreducible water saturation, $k_{rg,max}$	0.90
Oil relative permeability at irreducible water saturation, $k_{row,max}$	0.80
Oil relative permeability at residua gas saturation, $k_{rog,max}$	0.80

5.5.5 Development Scenarios

Pattern simulations

Before starting full-field simulation, simple pattern simulation was performed to understand and identify dominant displacement mechanisms during CO_2 injection and to determine strategies for maximizing ROZ oil recovery in brownfields or depleted MPZs in the full-field simulation. Well patterns, such as 5-spot, 9-spot, line drive, and a combination of 5-spot and line drive were considered in the pattern simulations.

Based on the pattern simulation, CO_2 distribution is controlled by the process of oil displacing water, and water production. Favorable mobility of ROZ water counters CO_2 buoyancy, but gravity override prevails (**Figure 5.31**). An oil bank was developed due to CO_2 injection, and it moved laterally and downwards (**Figure 5.32**). Two water banks were formed during CO_2 injection, which can be attributed to an initial displacement of water by oil, followed by water banking due to CO_2 displacing water left behind by the oil (**Figure 5.33**). This displacement mechanism was shown in all other simulations performed. As such, the ROZ developing strategies are to minimize downwards movement of the oil bank into the ROZ and to inject/store CO_2 throughout ROZ.

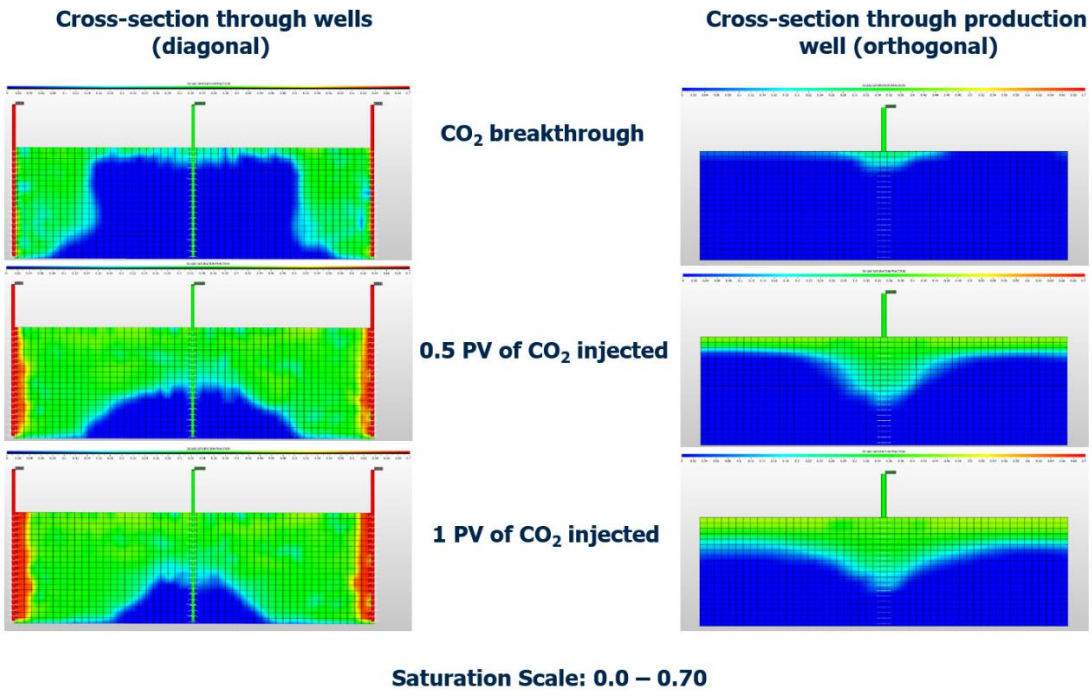

Figure 5.31. Cross-sectional and diagonal views of gas saturation distribution of an 80-acre 5-spot pattern CO2 flood. The blue colored areas represent the unswept portions of the model.

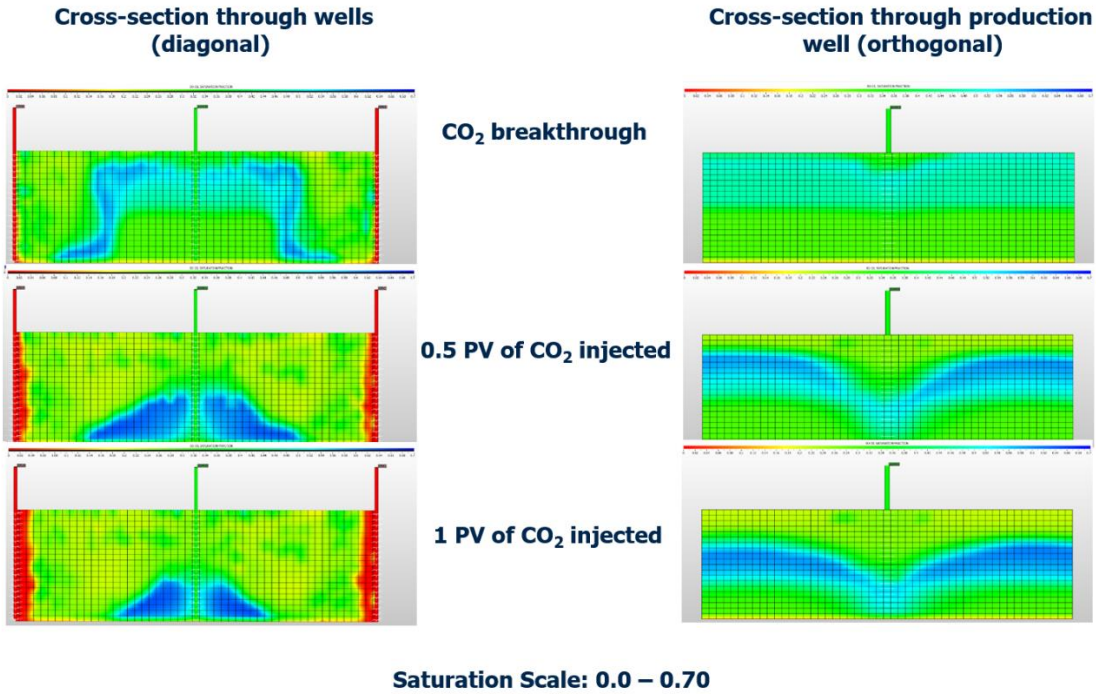

Figure 5.32. Cross-sectional and diagonal views of oil saturation distribution of an 80-acre 5-spot pattern CO_2 flood. Two oil banks (blue) were developed, an oil bank sinking into the ROZ (Diagonal view) and another developing in the bottom section of the MPZ (orthogonal view).

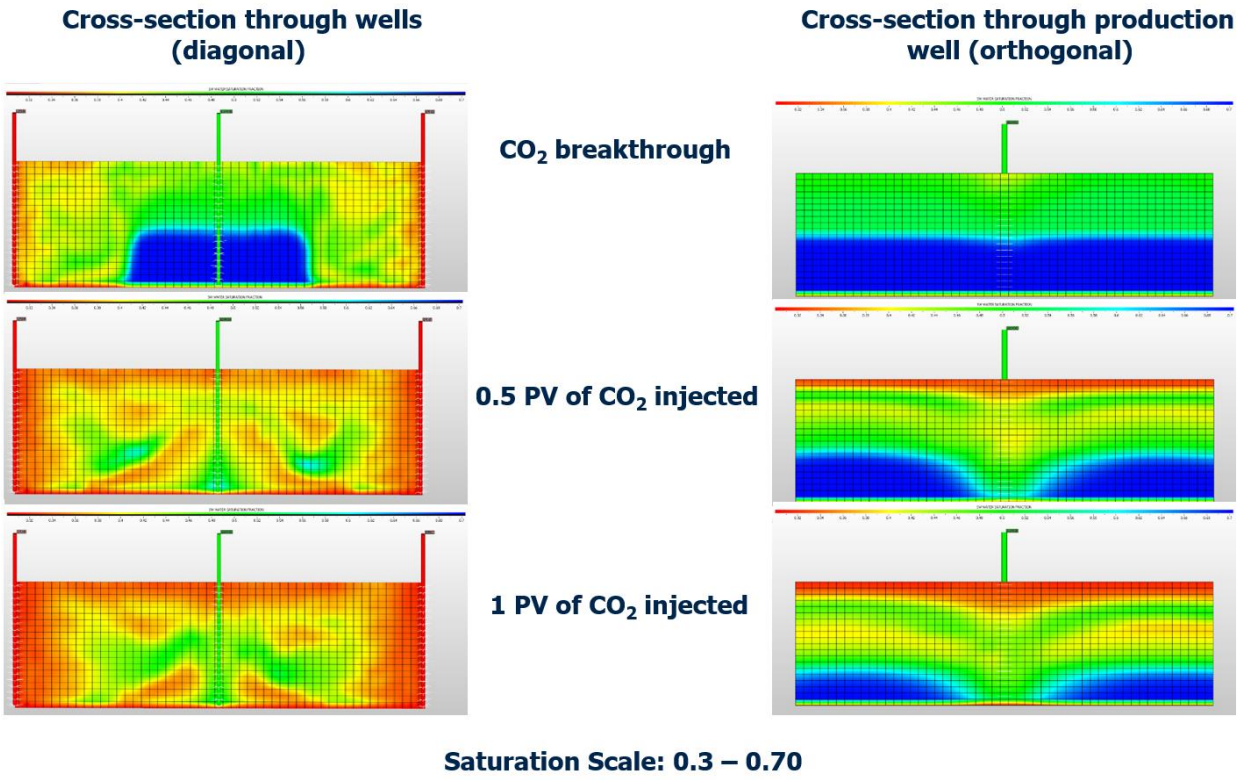

Figure 5.33. Cross-sectional and diagonal views of water saturation distribution of an 80-acre 5-spot pattern CO_2 flood. The blue colored areas represent the unswept portions of the model. Two water banks developed (in situ WAG) during CO_2 flood

Full-field simulations

To provide development strategies for CO_2-EOR and CO_2 storage in brownfield ROZs, multiple development scenarios were simulated to evaluate the CO_2-EOR and storage performance using the Noble Field reservoir model (**Table 5.15**). Presently, no attempt was made to co-optimize traditional CO_2-EOR with CO_2 storage. The simulations presented in this report are therefore biased towards excessive CO_2 storage (or inefficient utilization during CO_2-EOR).

The scenarios were designed to vary in injection pattern and well spacing, perforation interval, injection scheme, MPZ flood, ROZ flood, and high injection rate. The injection patterns included 5-spot, 9-spot, and peripheral injection. Pattern wells were selected based on the existing well layout, and the spacing was varied from 40-acres to 80-acres, except for one 160-acre case involving pattern realignment and expansion. The perforation interval of producers were either within the MPZ only or both MPZ and ROZ. Parameter sensitivity simulations were run to evaluate the effect of gas processing capacity and the producing BHP on CO_2-EOR performance. In the gas processing case, the maximum field gas production rate (gas processing capacity) was constrained at 10.5 MMscf/d. The BHP of producers was increased from 1,100 psia to 1,150 psia (at datum of 643 m (2,108 ft)) for the producing BHP case.

Multiple injection schemes were considered, including continuous, water-alternating-gas (WAG) injection (Jarrell et al., 2002), soak-alternating-gas (SAG) (Murray et al., 2001), and pattern realignment and expansion (PRE). SAG and PRE are described below.

The soak alternating gas (SAG) injection method combines continuous, WAG, and huff-and-puff injection schemes, excluding water injection to eliminate associated injectivity and production expenses, and increases

near wellbore CO_2-crude oil miscibility. The SAG method involves cycles of injection and well shut in to allow for near wellbore CO_2-oil mass transfer (soak) by injectors. Each SAG cycle is like the huff and puff method except that instead of producing the well CO_2 is injected after shut-in (Murray et al., 2001).

Pattern realignment and expansion (PRE) method involves changing the injector-producer configuration to direct injected CO_2 to poorly flooded areas and increasing injector-producer well spacing to delay CO_2 breakthrough. The PRE method involves converting (1) 'initial' CO_2 injectors to water injectors and (2) a proportion of oil producers to CO_2 injectors. The conversion of 'initial' CO_2 injectors to water injectors is intended to prevent flow of CO_2 into previously flooded areas and to increase average reservoir pressure. Lastly, conversion of a proportion of existing producers to CO_2 injectors increases the size of the realigned patterns by a factor of 4. For example, the initial and final pattern sizes of the PRE case in **Table 5.15** are 40-acre and 160-acre, respectively.

Two scenarios were simulated to evaluate the effect of separately flooding the MPZ and ROZ i.e. ROZ flood and MPZ flood (**Table 5.15**). Lastly, a scenario involving simulation cases with high CO_2 injection rates, allowing for out of pattern CO_2 injection, were simulated to asses effects of excessive injection on CO_2-EOR and storage.

Reservoir Model Calibration

For Noble Field, historical production and injection data were available from pipeline production reports (IOCC, 1952) on lease-by-lease basis during primary recovery and on field-wide basis during secondary recovery (waterflood). The reservoir model was therefore calibrated using production and injection data on field-wide basis. Completion dates of wells were obtained from scout tickets. In cases where precise dates were unavailable, the last day of the month was used. Some wells were completed in multiple pay zones so, production or injection from such wells were allocated based on the proportion of perforations within each well that were in the Cypress.

Bottom water drive was the predominant recovery mechanism during primary recovery due to presence of an active aquifer below the MPZ. As a result, high water-cut was achieved during primary production due to water conning. Producing wells were generally perforated at the top (1.5 to 3 m (5 to 10 ft)) interval of the reservoir to minimize excessive water production (personal communication with field operator). The Corey exponents for both oil and water relative permeability curves were iteratively adjusted to match oil production during primary recovery and waterflooding. Water injection was constrained to the equivalent volume of produced water during waterflooding. Simulation results closely match historical production (**Figure 5.34**). The calibrated model was used as input in subsequent CO_2 flood simulations to project EOR and storage.

Table 5.15. Development scenarios simulated for Noble Field to evaluate CO2 flood performance. All cases had injection into both MPZ and ROZ except the MPZ case. Each case has a corresponding water injection baseline. Bottom hole pressure for all cases constrained to 7,584.5 kPa (1,100 psi).

Scenario	Case	Description							
					Completion		Constraints		
		Spacing	Pattern	Injection Scheme	MPZ	ROZ	Injectors (MMscf / day)	Producers (MMscf / day)	Notes
Injection pattern and well spacing	As-is				As-is	As-is			Continue water injection with existing well locations
	40-acre	40-acre	5-spot	Continuous	All	All	12.55		
	80-acre	80-acre	5-spot	Continuous	All	All	12.55		
	80-acre*	80-acre	9-spot	Continuous	All	All	12.55		
	Peripheral	N/A	Peripheral	Continuous	All	All	12.55		
Perforation interval	MPZ	80-acre	5-spot	Continuous	All	Base	12.55		
	MPZ-bottom ROZ	80-acre	5-spot	Continuous	All	Base	12.55		
	Bottom MPZ-ROZ	80-acre	5-spot	Continuous	All	Base	12.55		
Parameter sensitivities	Producing BHP	80-acre	5-spot	Continuous	All	Base	12.55		
	Gas processing limit	80-acre	5-spot	Continuous	All	Base	12.55	10.5	
Injection design	WAG	80-acre	5-spot	WAG	All	Base	0 – 12.42		40% initial CO_2 slug and 0.5:1 WAG ratio
	SAG	80-acre	5-spot	SAG	All	Base	0 – 12.55		40% initial CO_2 slug and maximum 30-day soak period
	PRE	40 → 160-acre	5-spot	Continuous	All	Base	12.55		40-acre → 160-acre spacing after 3 years of injection. Initial CO_2 Injectors converted to water injectors and 33% of producers converted to CO_2 injectors.
	Gravity drainage	N/A	Line drive	Continuous	Base	None	12.55		Crestal injectors perforated at the top (3 m [10 ft]). Producers placed around the perimeter of the structure
MPZ flood	40-acre Blanket MPZ	40-acre	5-spot	WAG	All	None	12.55		Injectors also perforated in the upper 6.1 m (20 ft) of the aquifer
	40-acre Blanket MPZ-aquifer injection	40-acre	5-spot	WAG	All	None	12.55		
	80-acre Blanket MPZ	80-acre	5-spot	WAG	All	None	12.55		
ROZ flood	40-acre CO_2 injection	40-acre	5-spot	Continuous	None	Base	12.55		Injectors perforated across entire ROZ
	40-acre WAG	40-acre	5-spot	WAG	None	Base	0 – 12.55		
	80-acre WAG	40-acre	5-spot	WAG	None	Base	0 – 12.55		
High CO_2 injection rate	40-acre ROZ	40-acre	5-spot	Continuous	None	All	143 – 500	21	
	80-acre MPZ	80-acre	5-spot	Continuous	All	None	69.3 – 247		
	40-acre MPZROZ	40-acre	5-spot	Continuous	All	All	142 – 500		
	80-acre MPZROZ	80-acre	5-spot	Continuous	All	All	125 – 250		

*Perforate entire MPZ and ROZ for both producers. Corner injectors are perforated in the ROZ. Edge injectors are perforated in the MPZ.

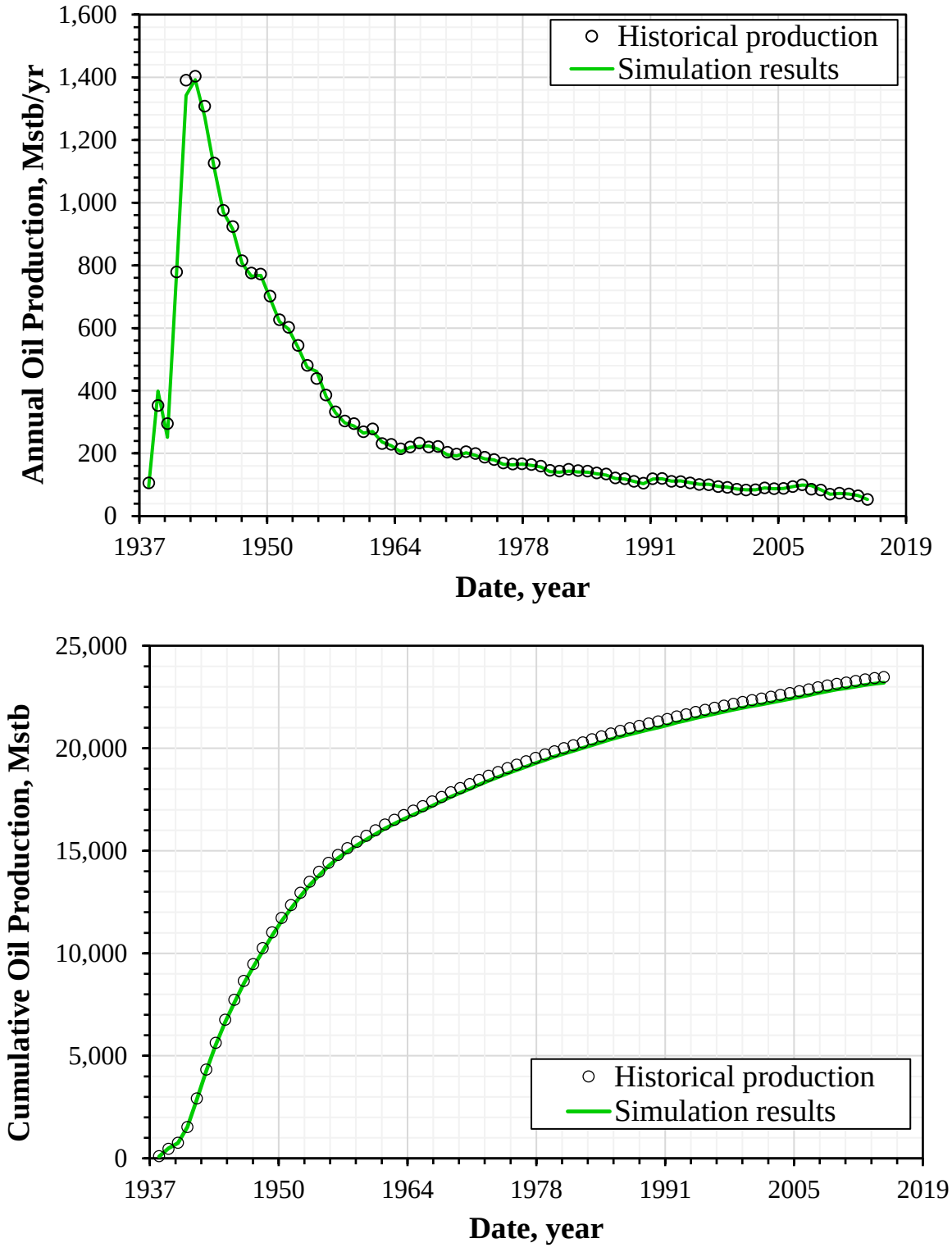

Figure 5.34. History-match of annual oil production (above) and cumulative oil production (below) during primary recovery and waterflooding at Noble Oil Field.

CO_2-EOR and storage performance

The metrics used to evaluate the CO_2-EOR and storage performance include CO_2-EOR, CO_2 storage, oil recovery factor, net utilization factor, CO_2 storage factor, storage efficiency, and carbon balance of oil produced (CB). They were calculated using the equations below:

$$CO_2EOR = N_{p,CO_2} - N_{p,WF} \quad (18)$$

$$G_{store} = G_{inj,CO_2} - G_{p,CO_2} \quad (19)$$

$$RF = \frac{CO_2EOR}{OOIP} \quad (20)$$

$$NUF = \frac{G_{store}}{CO_2EOR} \quad (21)$$

$$SF = NUF \times RF \quad (22)$$

$$E_{CO_2} = \frac{G_{store}}{HCPV} \quad (23)$$

$$CB = \frac{G_{store}}{CO_2EOR} \quad (24)$$

Where:

- CO_2-EOR = incremental oil produced
- $N_{p,CO2}$ = cumulative oil production of CO_2 flood (Mstb)
- $N_{p,WF}$ = cumulative oil production of waterflood (Mstb)
- G_{store} = CO_2 storage (MMscf or Mrb)
- $G_{inj,CO2}$ = CO_2 injected (MMscf)
- $G_{p,CO2}$= CO_2 produced (MMscf)
- RF = oil recovery factor (-)
- OOIP = original oil in place (Mstb)
- NUF = net utilization factor,
- SF = CO_2 storage factor (MMscf/Mstb)
- E_{CO2} = CO_2 storage efficiency (Mrb/Mrb)
- HCPV = hydrocarbon pore volume (Mrb).

The OOIP in the equations is the OOIP of the pattern area rather than the whole field OOIP. Injected CO_2 that moves out of pattern area was not accounted for in storage efficiency calculations. **Table 5.16** summarizes the performance parameters at Noble Field after 20 years of simulated CO_2 injection.

The ROZ development strategies were identified by comparing the EOR performance of the cases in each simulated scenario as a function of time. Simulation results suggest that the 5-spot pattern flood had better EOR performance than other pattern floods (**Table 5.16 and Figure 5.35**). The fluid saturation distribution indicates that movement of injected CO_2 within the reservoir is controlled primarily by gravity (as with the simple pattern simulations) and secondarily by geological factors such as permeability heterogeneity. Because vertical permeability (k_z) of the reservoir is high (**Figure 5.36**), the relatively buoyant CO_2 rises to the top of the reservoir in the MPZ and below a low-permeability calcite layer in the ROZ and eventually breakthrough at top perforations of producing wells (**Figure 5.37**). As a result, strategies to mitigate gravity effects and excessive gas production were tested, including selective perforation, injection design, and high injection rate.

As shown in **Figure 5.38,** perforating intervals in both MPZ and ROZ may not substantially increase oil production compared to perforating the MPZ alone. However, a significant increase in production could be

achieved by perforating the entire MPZ and the bottom 3 m (10 ft) of the ROZ, compared to blanket perforation of both intervals; a WAG simulation using the same well completions predict incremental oil production significantly greater than the continuous CO_2 injection case (**Figure 5.38**). Limiting field gas production to a maximum processing capacity of about 10.5 MMscf per day by shutting in high gas producers led to a slight increase in oil recovery (broken red line in **Figure 5.38**) due to increase in average reservoir pressure. Increasing producing BHP (broken blue line in **Figure 5.38**) reduced oil production due to decrease in the pressure gradient (Δp) between the wellbore and reservoir.

There is established success in producing economic quantities of oil from ROZs and the need to shift the carbon balance from net positive to net negative. This leads the discussion towards storing a significant portion of CO_2 while producing as much oil per injected unit of CO_2 as possible; a goal that would be met through the optimization of sweep and storage efficiency. In all simulated CO_2-EOR and storage injection scenarios, carbon balance was calculated (see Eq. 7) to determine the effectiveness of the CO_2-EOR program regarding producing NCNO. For this study, a ratio of 1 tonne of CO_2 injected and stored for every 2.5 barrels of oil recovered is considered to have a neutral carbon balance (e.g., Kuskraa et al. 2013). Using this ratio, the Carbon Balance value reported in **Table 5.16** represents carbon neutral if the value is equal to 0.4 and represents NCNO if the value is greater than 0.4. 18 cases produce NCNO, 3 are carbon neutral, and only one is net carbon positive. The net carbon positive example coincides with the case that has the highest EOR performance. The cases that have the most negative carbon balance are those that have a high CO_2 injection rate in which CO_2 moves outside of the pattern boundaries.

Table 5.16. CO_2-EOR and storage metrics at Noble Field after 20 years of simulated CO_2 injection. The five highest EOR, Storage, Oil Recovery, and Net Utilization examples are shaded.

Scenarios	Cases	EOR (Mstb)	CO_2 Storage (million tonnes)	Oil Recovery	Net Utilization (Mscf/stb)	CO_2 Storage Factor (Mscf/stb)	CO_2 Storage Efficiency*	HCPV injected	Carbon Balance (tonne/stb)
Injection pattern and well spacing	40-acre (5-spot patterns)	1,539	1.5	3.5%	18	0.6	19%	1.2	1.0
	80-acre (5-spot patterns)	1,627	1.6	4.2%	19	0.8	21%	1.3	1.0
	80-acre (9-spot patterns)	1,154	1.8	3.0%	29	0.8	24%	1.6	1.5
	Peripheral	1,221	1.1	2.8%	18	0.5	14%	0.7	0.9
Perforation interval	MPZ	2,284	1.7	7.7%	14	0.8	31%	1.7	0.8
	MPZ-bottom ROZ	2,411	1.7	6.3%	14	0.8	22%	1.3	0.7
	Bottom MPZ-ROZ	1,200	2.3	3.1%	36	1.1	38%	1.3	1.9
Parameter sensitivities	Producing BHP	903	3.1	2.4%	64	1.5	41%	1.2	3.4
	Gas processing limit	2,507	1.9	6.5%	15	0.9	25%	1.3	0.8
Injection design	WAG	3,599	1.4	9.4%	7	0.7	19%	0.9	0.4
	SAG	1,743	1.4	4.0%	15	0.6	18%	1.2	0.8
	PRE	3,041	1.1	7.0%	7	0.4	14%	0.8	0.4
	Gravity drainage	3,090	2.9	4.7%	18	0.8	19%	0.7	0.9
MPZ WAG flood	40-acre Blanket MPZ	2,226	1.0	6.6%	8	0.5	20%	1.0	0.4
	80-acre Blanket MPZ	3,501	1.1	11.4%	6	0.6	22%	1.1	0.3
ROZ WAG flood	40-acre CO_2 injection	186	1.0	1.9%	107	2.0	26%	4.7	5.7
	40-acre WAG	208	1.1	2.1%	104	2.1	23%	3.2	5.5
	80-acre WAG	136	1.5	1.6%	211	3.3	42%	3.7	11.2
++High injection rate	40-acre ROZ	810	63.6	8.2%	1479	121.3	919%	54.1	78.5
	80-acre MPZ	3,043	9.5	9.1%	59	22.4	79%	2.6	3.1
	40-acre MPZROZ	2,260	29.2	5.2%	243.9	27.2	240%	5.7	12.9
	80-acre MPZROZ	3,395	36.0	10.1%	200	34.7	373%	7.8	10.6

**Calculated using OOIP of the pattern, MPZ case used OOIP of MPZ only without OOIP from ROZ.*

+Calculated using Pore volumes (PV) of pattern, MPZ case used PV of MPZ only without PV from ROZ.

++Excessive net utilization, storage factor, and storage efficiency due to significant out of pattern injection.

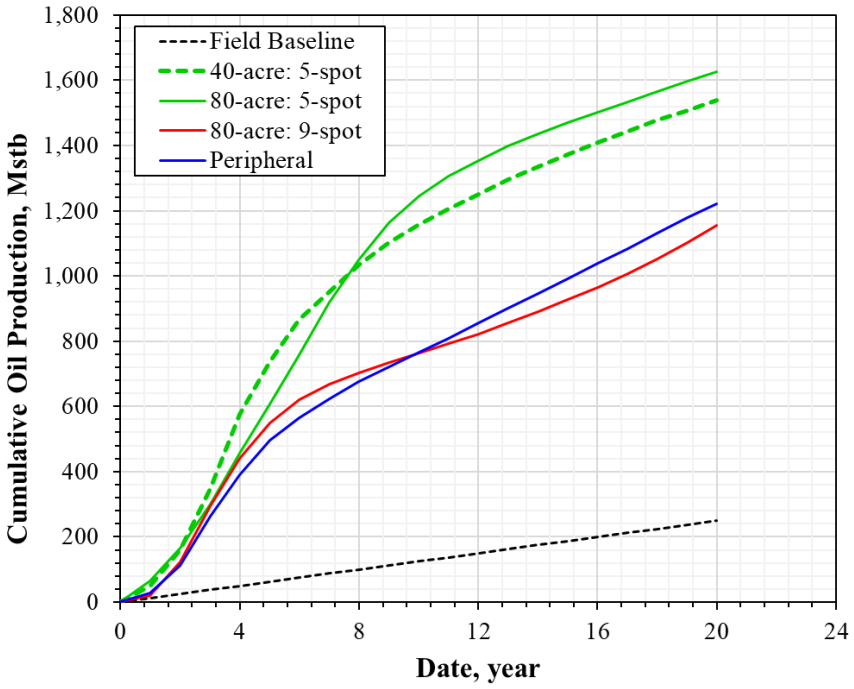

Figure 5.35. Effect of pattern size and type. The cumulative EOR of the 80-acre 5-spot is not significantly greater that of the 40-acre case. Nine spot pattern and peripheral cases have lower EOR performances compared to the 5-spot pattern cases.

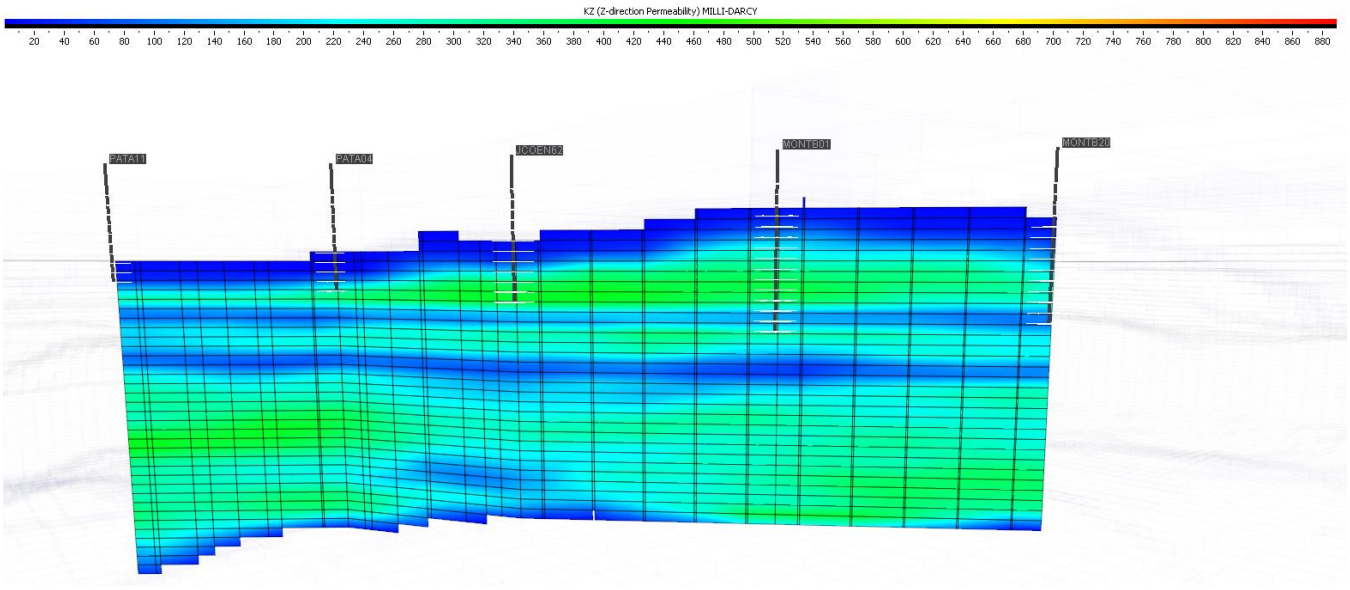

Figure 5.36. Cross-section through injection and producing wells showing vertical permeability (kz) distribution. Warmer colors represent high kz (> 100 md) gridblocks and cooler colors represent low kz (< 100 md) gridblocks. The top of the MPZ is less permeable than its lower section. Two low-permeability calcite layers separate the MPZ and ROZ (upper blue layer) and the ROZ and a thick aquifer (lower blue layer).

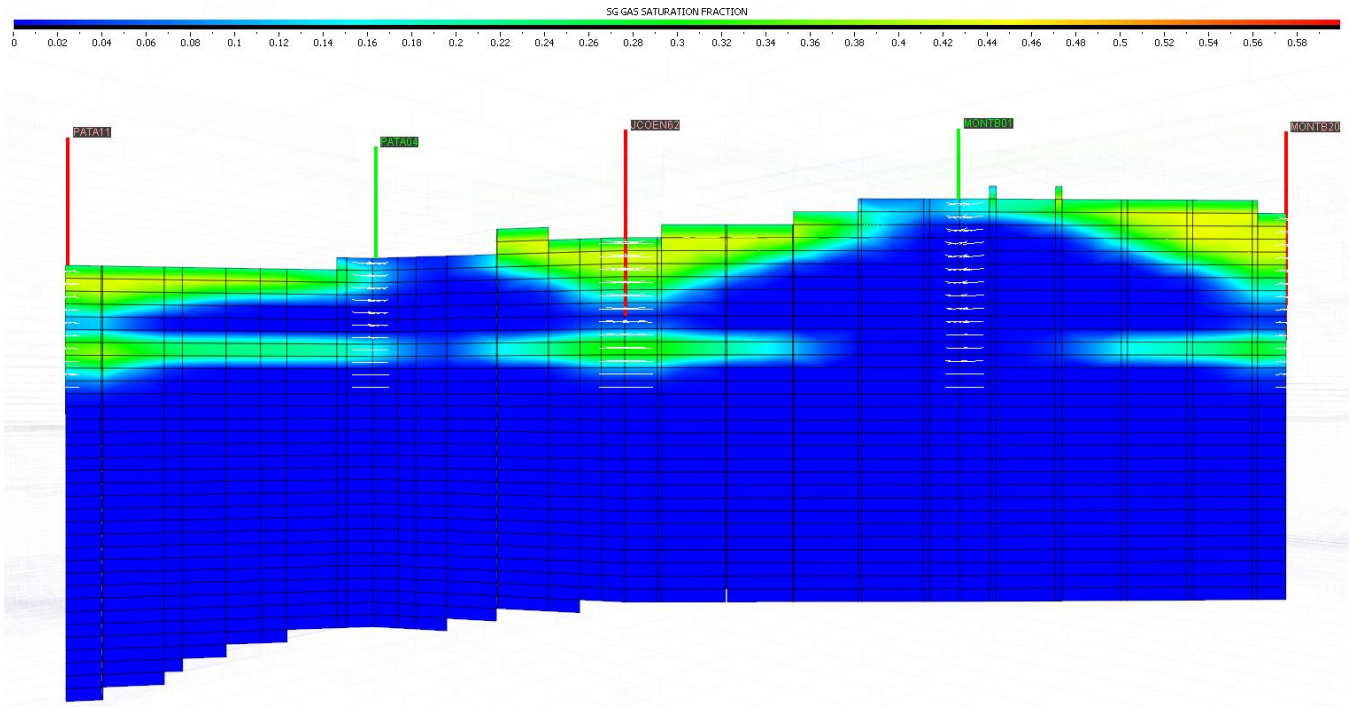

Figure 5.37. Cross-section through injection (red lines) and producing (green lines) wells showing CO2 saturation distribution (warmer colors) at breakthrough.

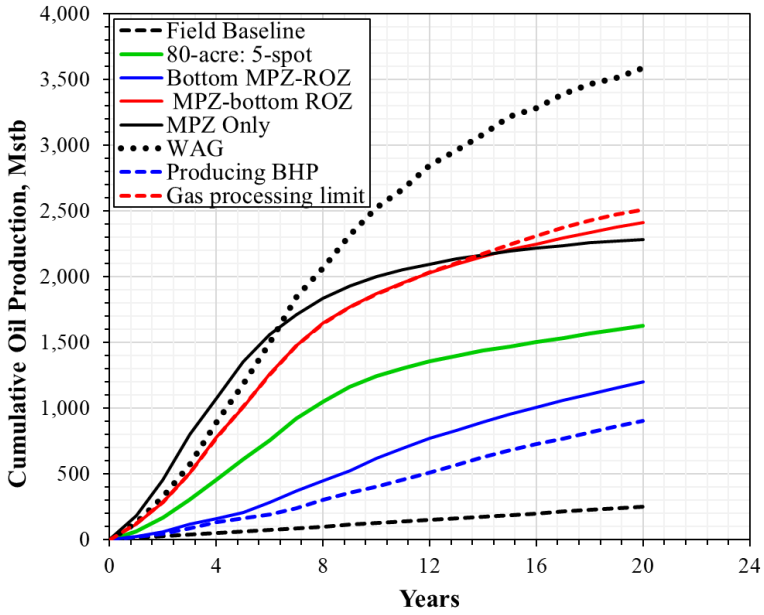

Figure 5.38. Effect of selective perforation of the ROZ and/or MPZ. Selective perforation of the MPZ and ROZ is not significantly effective than flooding only the MPZ.

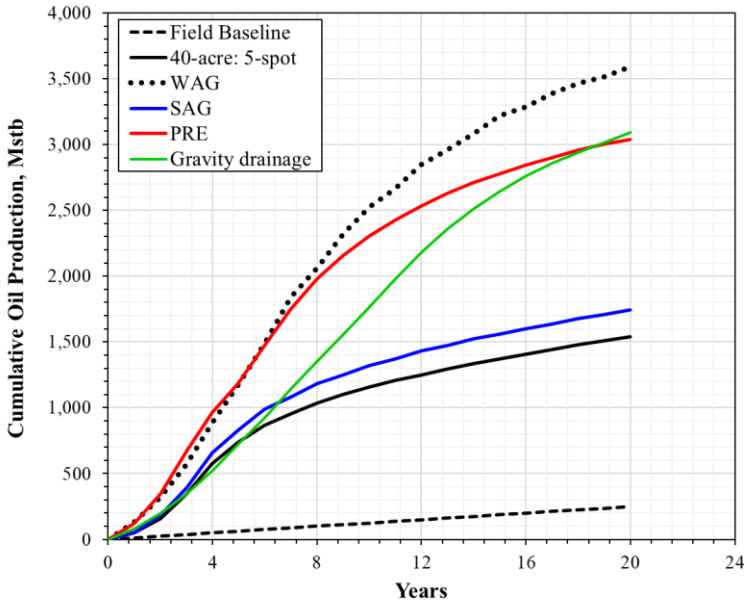

Figure 5.39. Effect of injection design. The PRE EOR performance is significantly greater than that of SAG and conventional 40-acre 5-spot pattern case.

A moderate increase in oil production was shown using the SAG injection method. However, oil recovery of the PRE case is significantly higher than those of SAG and conventional 40-acre 5-spot pattern CO_2 flood cases. The cumulative oil production after 20 years of the gravity drainage case is slightly higher than that of PRE case (**Figure 5.39**), however, it has lower EOR performance because it has a higher OOIP than the latter (i.e., lower recovery factor, **Table 5.16**). Overall, the 80-acre WAG case

has the best EOR performance compared to PRE and SAG cases (**Figure 5.39**) and the preceding cases (**Figures 5.35**).

The WAG EOR potential of MPZ and ROZ (**Table 5.15**) were assessed by comparing performances of the 40-acre and 80-acre 5-spot pattern floods. The WAG EOR performance of the 80-acre pattern case is better than that of the 40-acre pattern for MPZ flood scenario (**Figure 5.40**). However, the 40-acre pattern performed better than 80-acre pattern for the ROZ flood scenario (**Figure 5.40**).

The CO_2 injection rate was constrained at 12,550 Mscf/d in the preceding cases to mitigate out-of-pattern injection so that the average reservoir pressure in these simulations ranged from 1,200 to 1,250 psia, which is about 100 – 200 psia above the MMP of Cypress crude oil. Additional simulations were performed to assess the effect of injection rate on CO_2-EOR and storage performances. **Figure 5.41** indicates that increasing CO_2 injection rate increases EOR and storage (**Table 5.15**). However, the estimated storage factors and efficiencies of these cases are significantly high because of out-of-pattern displacement of CO_2. Oil recovery increased with increasing injection rate because CO_2 becomes more miscible with oil as a result of the increase in average reservoir pressure to about 1,600 psia, which is significantly greater than MMP. Results in **Figure 5.41** also corroborate those in **Figure 5.35**, **Figure 5.40**, and **Table 5.15**, which indicated that the 40-acre and 80-acre 5-spot pattern injection schemes are best suited for flooding the ROZ and MPZ, respectively, due to high EOR performance.

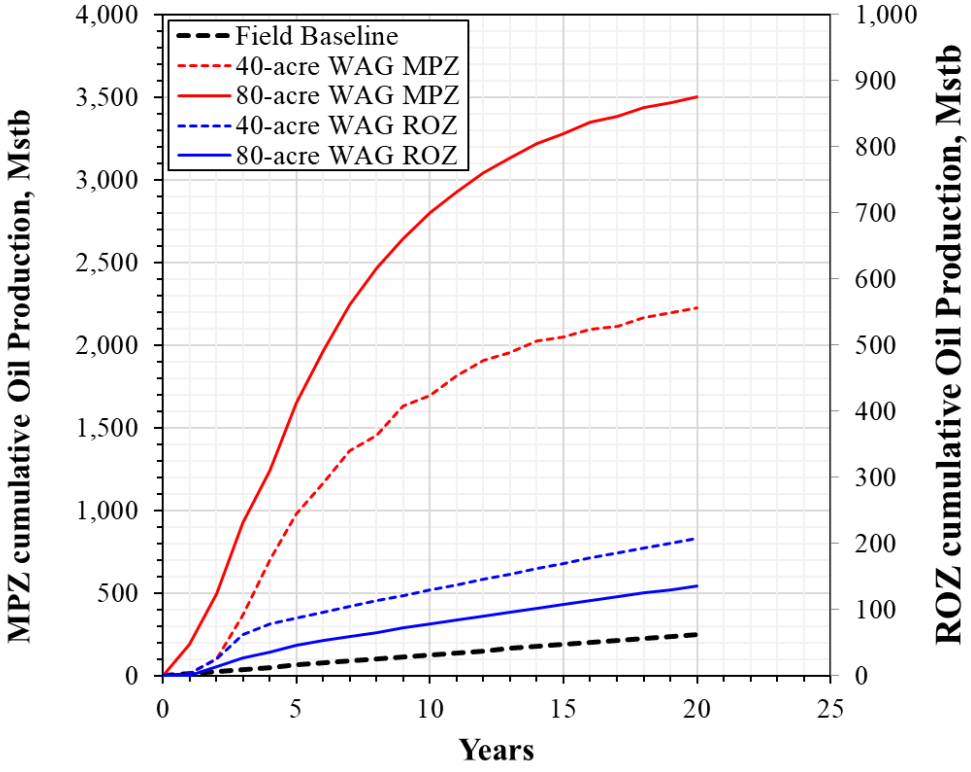

Figure 5.40. MPZ (primary axis) and ROZ (secondary axis) WAG flood scenarios.

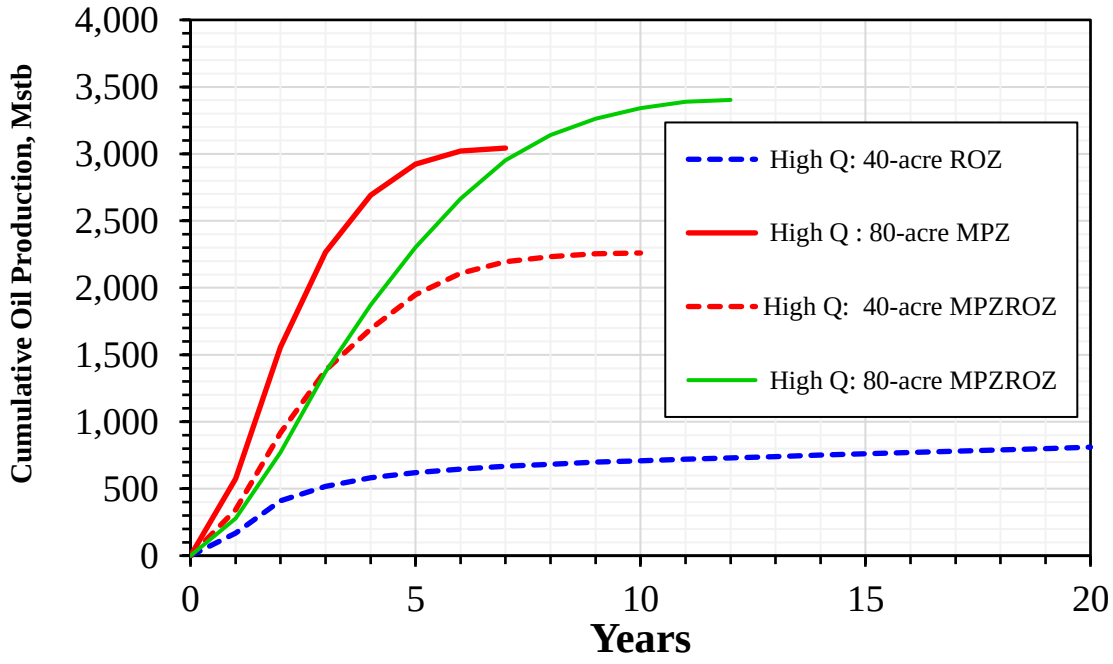

Figure 5.41. High injection rate (pressure constrained) continuous CO2 injection cases. The oil production rates of the 80-acre MPZ, 40-acre MPZROZ, and 80-acre MPZROZ cases become equivalent to the oil rates of the their respective waterflood baselines after 7, 10, and 12 years, respectively.

Direct comparison of the performance of the simulated scenarios were also made through normalization of simulation results to original oil in place (OOIP) or hydrocarbon pore volume (HCPV). Parameters calculated from simulation results include dimensionless cumulative oil and water production and CO_2 injection and storage. The dimensionless cumulative oil production (N_{pd}) was estimated as the ratio of produced oil volume (N_p) to the OOIP.

$$N_{pd} = \frac{N_p(Mstb)}{OOIP\ (Mstb)} \quad (25)$$

The dimensionless cumulative water production (W_{pd}) was calculated as the ratio of cumulative water production (W_p) to hydrocarbon pore volume (HCPV) at reservoir conditions.

$$W_{pd} = \frac{W_p\ (Mrb)}{HCPV\ (Mrb)} \quad (26)$$

The dimensionless cumulative CO_2 injection (G_{injd}) was estimated as ratio of cumulative CO_2 injection (G_{inj}) and to *HCPV*.

$$G_{injd} = \frac{G_{inj}\ (Mrb)}{HCPV\ (Mrb)} \quad (27)$$

The dimensionless cumulative CO_2 storage (G_{sd}) was estimated as ratio of the difference between the injected (G_{inj}) and produced volumes of CO_2 (G_p) to *HCPV*.

$$G_{sd} = \frac{G_{inj}\ (Mrb) - G_p(Mrb)}{HCPV\ (Mrb)} \quad (28)$$

The performance of the simulation scenarios was compared based on N_{pd}, and G_{sd} because the primary objectives of this study are to optimize oil production and CO_2 storage. The dimensionless water production curves were used to identify scenarios with low water production per unit volume of CO_2 injection because produced water disposal or handling could be a major challenge.

Figures 5.42 to 5.44 show the dimensionless curves of simulation cases that reveal effects of: (1) Pattern type (5-spot vs 9-spot vs peripheral flood), (2) Pattern size (40-acre vs 80-acre), (3) Injection scheme (continuous, WAG, SAG, PRE, and gravity drainage), and (4) High CO_2 injection Rates (MPZ, ROZ, MPZ-ROZ) on CO_2 EOR performance for Noble Field. **Figure 5.42** shows that the EOR performance 5-spot pattern simulations are better than those of 9-spot and peripheral flood cases, which corroborates results in **Figure 5.35**. The EOR of the high injection rate simulation cases are low (**Figure 5.42**) because the HCPV of CO_2 injected per barrel of oil produced is high. On the other hand, the high injection rate cases produce less gas (**Figure 5.43**) and water (excluding the gravity drainage case), on a HCPV basis, than other simulation cases. As shown in **Figures 5.38, 5.39, and 5.42,** WAG is the best injection scheme for Noble Field because it has the highest EOR compared to other injection schemes. The difference in normalized volume of gas produced per unit volume of injected CO_2 between the simulated case in **Figure 5.43** is relatively small (about 0.2 HCPV) except for the 40-acre WAG ROZ and high CO_2 injection rate cases. Simulation results project the gravity drainage and PRE cases to produce the lowest and highest amount of water per unit HCPV, respectively (**Figure 5.44**).

The following conclusions can be drawn from the Noble Field simulation results presented herein:

- Of the injection design cases, WAG has the highest oil recovery.
- For low injection rates, flooding the MPZ and ROZ separately has higher oil recovery.
- For WAG cases, the 80-acre 5-spot pattern has higher oil recovery than the 40-acre 5-spot pattern in the MPZ; the inverse is true for the ROZ.
- ROZ floods have higher oil recovery when producers are perforated in the bottom 10 ft of the ROZ.
- High continuous CO_2 injection rate increases oil recovery from the ROZ.
- In terms of carbon balance, 21 of the cases are NCNO or carbon neutral.

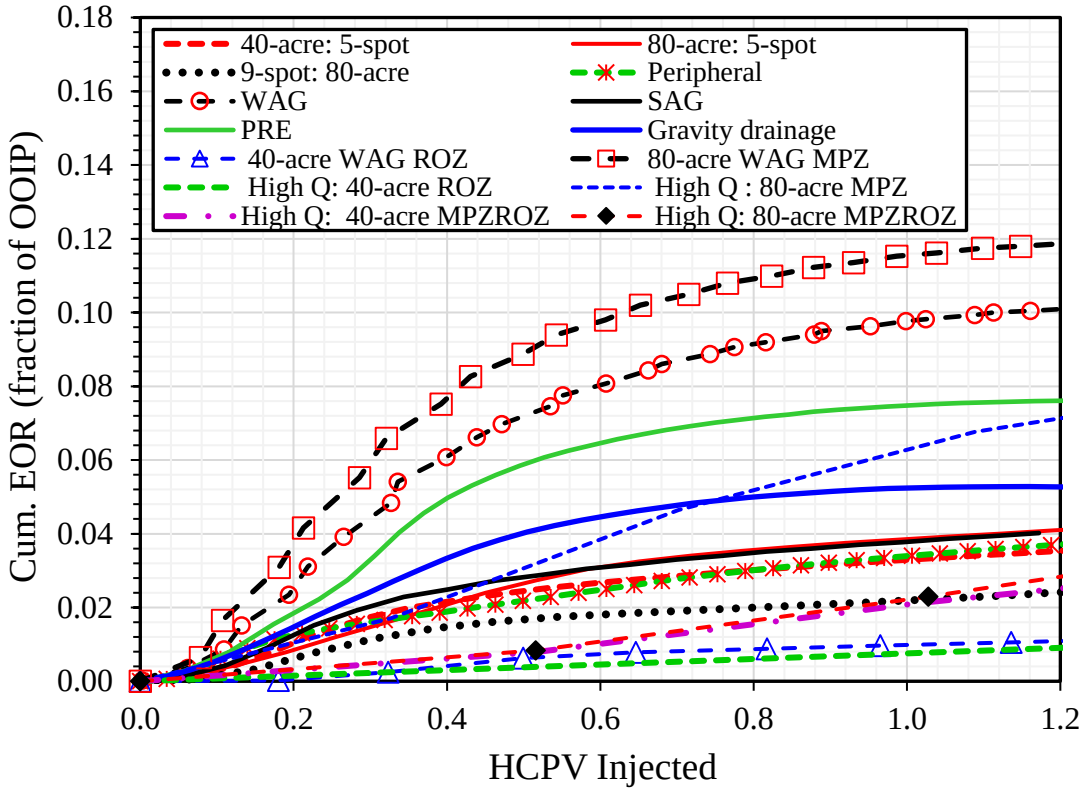

Figure 5.42. Dimensionless incremental oil recovery (Npd) for injection pattern and well spacing, injection scheme, MPZ flood, ROZ flood and high injection rate CO2 flood scenarios. This allows for direct comparison of the EOR performances of simulated cases based on HCPV of CO2 injected. For example, the '80-acre WAG MPZ' and 'High Q: 40-acre ROZ' cases have the highest and lowest incremental oil recovery per unit HCPV of CO2 injected.

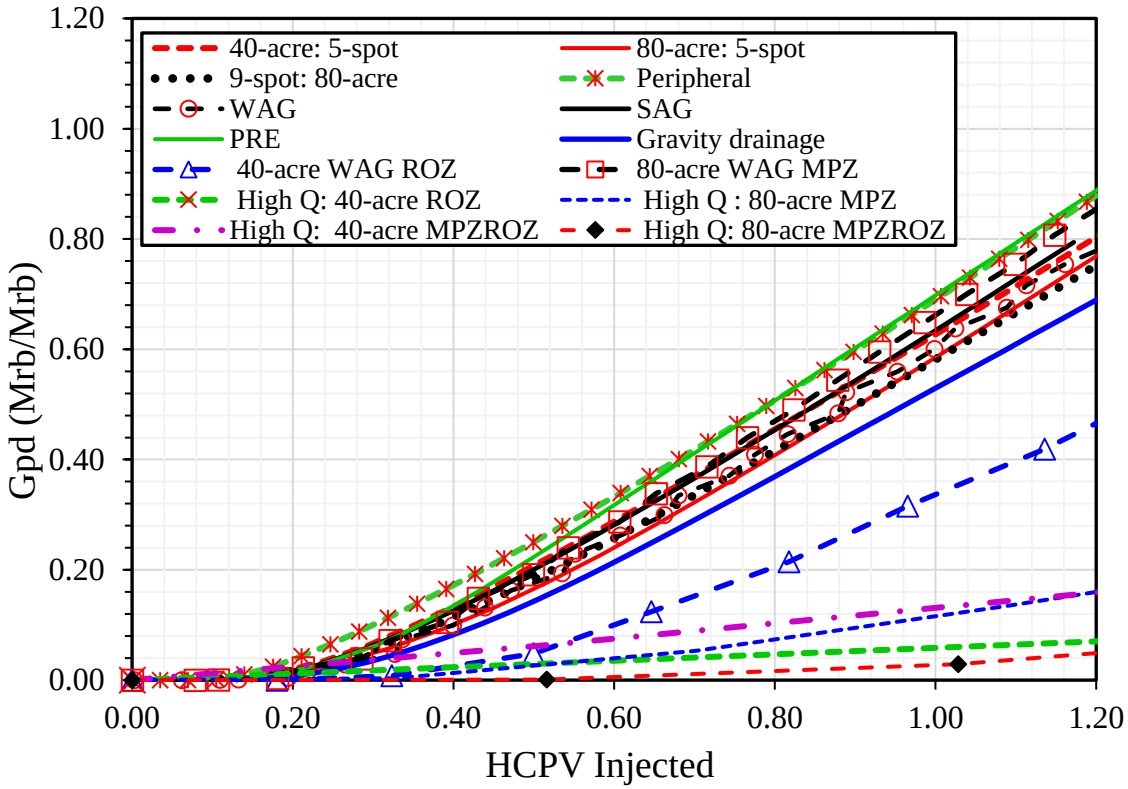

Figure 5.43. Dimensionless incremental gas production for injection pattern and well spacing, injection scheme, MPZ flood, ROZ flood and high injection rate CO2 flood scenarios. Direct comparison of normalized gas production indicates that 'PRE' and 'High Q: 80-acre MPZROZ' cases produced the highest and lowest volumes of gas per unit HCPV of CO2 injected.

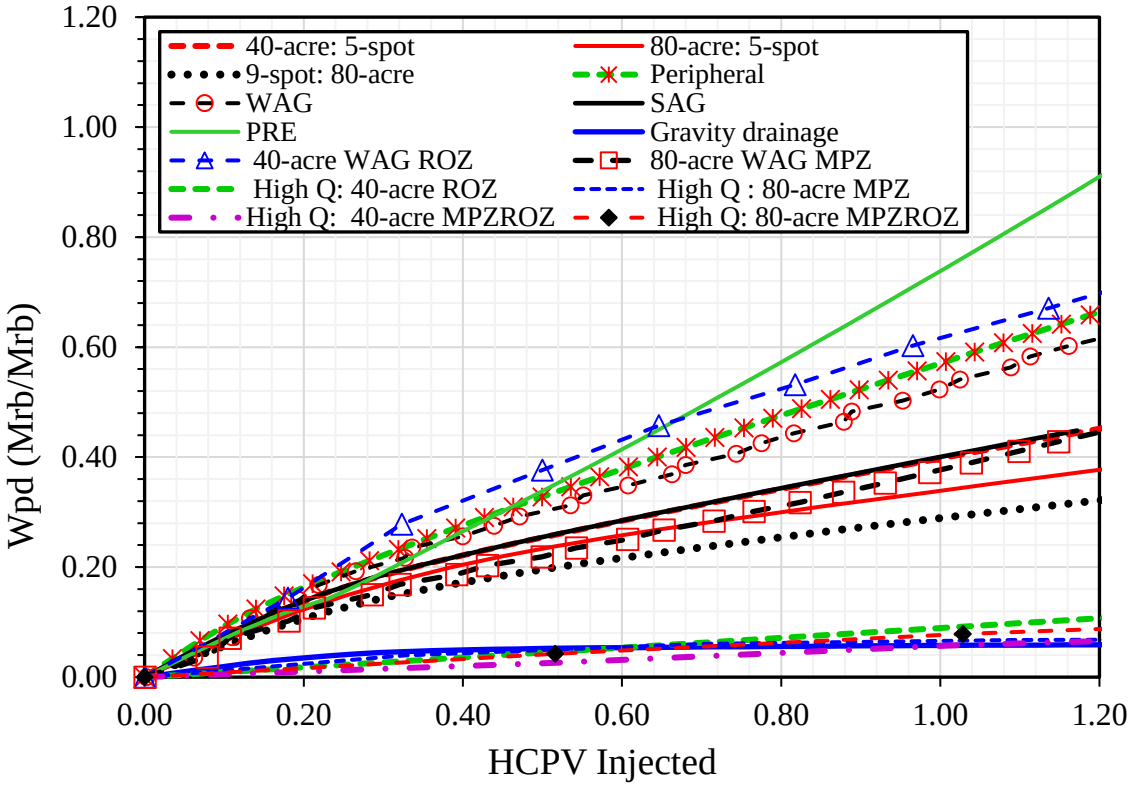

Figure 5.44. Dimensionless incremental water production for injection pattern and well spacing, injection scheme, MPZ flood, ROZ flood and high injection rate CO2 flood scenarios. The 'PRE' and 'High Q: 40-acre MPZROZ' cases production the highest and lowest amount of water per unit HCPV of CO2 injected.

5.5.6 Economic Evaluation

Methodology

Economic metrics were estimated for CO_2-EOR cases of the Noble Field to identify plausible commercial development strategies for the ROZ in the ILB. The comparative economic metrics were the internal rate of return (IRR) and net present value at 20% discount rate (NPV_{20}), payout time for capital expense (CapEx), project life, profit/investment ratio, and cumulative cash flow for each case. The economic life was defined as the year in which net revenue was zero. All other metrics were calculated for each case's economic life.

While numerous CO_2-EOR cases were simulated, a general economic scenario was required to define expenses and revenue. The major elements of this scenario are as follows:

- A major CO_2 pipeline exists, and a trunk line is required to connect the CO_2-EOR project to the pipeline.
- The size (and cost) of the CO_2 recycling facility is based on the projection of the annual CO_2 production. (The sizes are 1, 2.1, 10.45 and 21 MMscf/d at a cost of $1.5, $2.1, $5.8, and $7.9MM, respectively) (McKaskle et al., 2017).
- Existing wells not in CO_2 injection patterns are plugged. All wells in patterns require workover for CO_2 service, and annual well work. Wells are pumped and have an associated "lift" cost.
- The CO_2-EOR project is deployed as a single phase for the entire field.

Economic Inputs

Many assumptions of future prices and expenses are required for CO_2-EOR economics. Unless otherwise specified, well and surface equipment estimates are based on responses from ILB oilfield operators. All economic analyses were compiled before federal income taxes (FIT).

Prices

Oil price: The Society of Professional Engineers recommends that reasonable historical averaged oil prices should be projected as constant or flat. Price of oil was set at a flat $50/bbl.

CO_2 Price: Although the economics presented here were pre-FIT, IRS tax credits for CO_2 storage with CO_2-EOR (i.e. 45Q) were included. Because the tax credit would be available to a company's finances and not necessarily a specific CO_2-EOR project's finances, cost of CO_2 was set at $0 for the project. In cases where oil production was low (<1 MMstb) and economic metrics were poor, $20 was assigned to each ton of CO_2 stored as revenue to the project. ROZ only cases required $40/ton revenue for better economic metrics.

Capital and Operating Expenses

Unit costs were used in this study (**Table 5.17**). The costs were grouped as follows:

- CapEx included:
  - plugging wells
  - drilling and completing new wells
  - well workover/cleanup
- Operating Expenses (OpEx) included
  - annual well cost
  - total fluid production cost (i.e. lift costs)
- Ad valorem (on surface equipment only) and royalty payments

Table 5.17. *CapEx and OpEx unit costs for well and surface equipment.*

cost per new well	**$250,000**
cost per surface equipment	$100,000
cost per workover/conversion	$20,000
cost of plugging	$5,000
cost of CO_2 recycling (10.5 Bscf/d)	$5,800,000
cost of CO_2 recycling (21 Bscf/d)	$7,900,000
cost of trunk line construction	$1,000,000
cost of CO_2 gathering system	$250,000
cost per well per year	$10,000
cost per well per year	$5,000
Royalty	12.5%
Ad valorem Tax	0.5%
Lift costs, $/bbl-fluid	$0.48
Recycled CO_2, $/ton	$10
Oil price, $/bbl	$50

Specific well counts for each scenario determined the capital and operating expenses. **Table 5.18** lists the well status for CO_2-EOR field development cases at Noble Field. The well arrangement made use of existing wells and minimized the number of new wells. The wells used in each case included currently active wells, re-entered previously plugged wells, and new wells. The unused existing active wells were shut-in and plugged and abandoned. The plugged and abandoned wells may require monitoring or re-plugging; costs to monitor or re-plug previously abandoned wells were not included in these analyses.

Table 5.18. Well status for CO_2-EOR field development cases at Noble Field.

Case	Producers				Injectors				Active well count	Pattern count
	Active	Re-entered	New	Shut-in	Active	Re-entered	New	Shut-in		
40-acre (5-spot)	32	16	2	26	50	38	2	7	82	32
80-acre (5-spot)	14	8	—	34	25	17	2	16	39	14
80-acre (9-spot)	14	8	—	34	60	17	3	7	74	14
Peripheral	35	16	2	24	30	18	1	6	65	—
Gravity drainage	24	20	0	36	24	7	7	0	7	7

Goods and administrative (G&A) costs were assumed 20% of CapEx and OpEx. Illinois has no severance tax on oil production. All CapEx was expensed at t=0; depreciation was not used.

Results

The economic metrics are shown in **Table 5.19**. In comparison to **Table 5.16** of the simulation results, which has CO_2-EOR performance metrics after 20 years of injection, the economic metrics are calculated over the economic life of each project. Payout varied from 1-4 years while the economic life varied from back 6 to 20 years. (20 years was the maximum value based on the period of CO_2-EOR simulations.). Net revenue from oil production only (no inclusion of CO_2 storage related revenue) varied from $50 to over $150 M. (Excludes cases requiring >0$/ton for stored CO_2, the cases with asterisks below.) The ROZ only cases could only yield positive IRR if $40/ton revenue was generated.

Table 5.19. Economic metrics for Noble Field CO_2-EOR cases (the top five scenarios for each economic metric is shaded; payout is shaded 1 and 2 years).

Case Name	Payout (yr)	Economic Life (yr)	Net Revenue-Oil ($M)	Capital Investment ($M)	CO_2 Costs ($M)+	Operating Costs ($M)	Cum Cash Flow ($M)	IRR %	NPV @ 20%	P/I
40-acre (5-spot patterns)	4	9	47.9	-12.9	-9.8	-13.6	24.5	18.3	-0.7	1.9
80-acre (5-spot patterns)	4	11	56.8	-10.7	-12.4	-10.7	33.7	28.5	3.5	3.2
80-acre (9-spot patterns)*	3	8	30.5	-14.5	15.5	-9.7	36.3	39.4	6.9	2.5
Peripheral*	3	20	52.8	-12.0	5.2	-24.0	34.1	32.7	4.6	2.8
MPZ	2	11	89.5	-10.7	-11.5	-8.3	69.6	85.2	24.7	6.5
MPZ-bottom ROZ	3	14	93.7	-10.7	-17.7	-12.6	63.4	57.0	16.8	6.0
Bottom MPZ-ROZ*	3	20	51.9	-10.7	19.8	-13.3	58.4	45.6	10.5	5.5
Producing BHP*	3	20	38.9	-10.7	43.0	-11.7	70.3	45.9	11.2	6.6
Gas processing limit	3	18	105.7	-10.7	-25.3	-14.9	65.6	57.0	17.0	6.2
WAG	2	20	156.5	-10.7	-16.5	-19.0	120.9	68.5	28.9	11.4
SAG	3	11	59.7	-10.7	-13.1	-11.9	34.6	36.3	6.2	3.3
PRE	2	18	128.8	-10.7	-17.6	-19.8	91.3	68.4	24.8	8.6
Gravity drainage	3	20	134.6	-10.2	-19.3	-10.5	104.8	49.5	18.1	10.3
40-acre Blanket MPZ	3	15	89.0	-10.7	-11.8	-13.4	63.7	44.5	13.8	6.0
80-acre Blanket MPZ	2	17	147.5	-10.7	-17.1	-13.6	116.7	98.1	38.1	11.0
40-acre CO_2 injection**	2	7	3.6	-10.7	24.0	-5.1	22.5	48.7	5.0	2.1
40-acre WAG**	2	8	4.7	-10.7	23.7	-6.9	21.5	36.1	3.3	2.0
80-acre WAG**	2	6	2.1	-10.7	27.5	-4.2	25.5	47.9	5.7	2.4
40-acre ROZ*	1	20	34.7	-13.2	1190	-8.7	1216	449	268.6	92.4
80-acre MPZ	1	6	131.9	-13.2	-19.4	-5.0	107.5	200	57.0	8.2
40-acre MPZROZ	2	7	95.8	-13.2	-27.6	-6.5	61.7	94.9	25.0	4.7
80-acre MPZROZ	2	10	145.8	-13.2	-33.0	-8.9	103.9	108.	41.4	7.9

Discussion

No single case tops all economic metrics. The High CO_2 Injection, 80-acre Blanket MPZ, and MPZ cases have the highest IRR, and three of the highest NPV@20%. For all cases, 80-acre patterns have higher economic metrics than 40-acre cases due to delay in CO_2 breakthrough leading to cost to capture and re-inject the produced CO_2. CO_2 injection in to MPZ is necessary for strongest economic metrics. The PRE and Gravity Drainage cases did not have the highest metrics but were above the median for most cases' metrics. ROZ only cases have the lowest metrics and require the highest unit revenue for CO_2 stored.

Selection of a development strategy based on economic criteria will be specific to an individual company's business strategies. For example, payout or time to return capital investment maybe more important to one company compared to the IRR for another. Nevertheless, the 80-acre and High CO_2 Injection cases have more favorable economic metrics. A combination of higher CO_2-EOR, higher CO_2 purchased, and lower CO_2 produced gave the best results.

(This economic analysis is intended to provide a comparison economic metrics of different CO_2-EOR development strategies. Although, representative of specific development scenarios, it is not intended to be used for making a specific commercial decision because economic generalizations were made.)

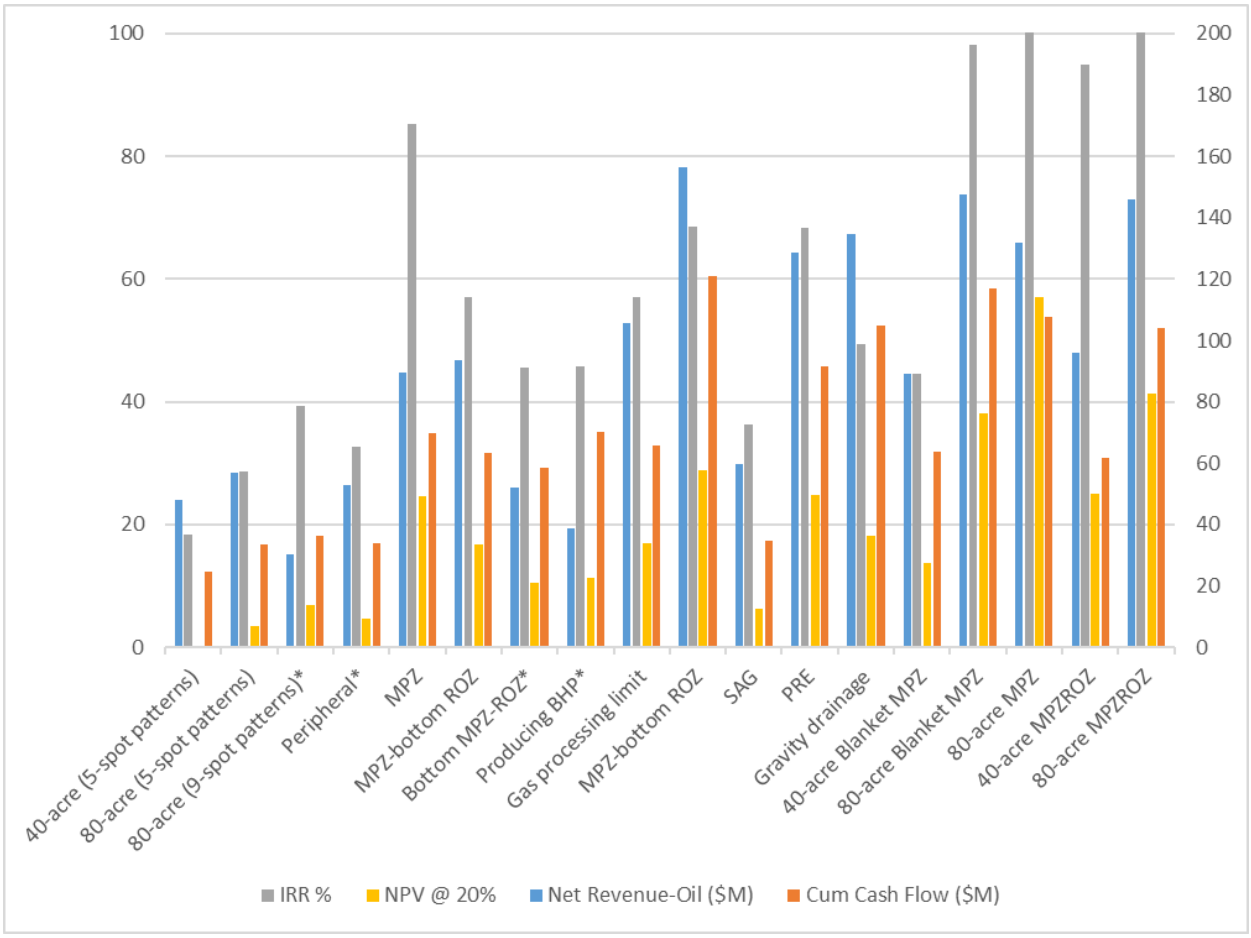

Figure 5.45. Economic metrics for Noble Field CO2-EOR Cases (left axis for IRR and Cumulative Cash Flow; right axis for Net Revenue and NPV@20%).

5.5.7 Development Strategies

Based on the economic results of the cases simulated, traditional flooding approaches (scenario: injection pattern and spacing) that minimize CO_2 leaving the outer patterns (i.e. moving down dip away from the oil reservoir) did not have high economic metrics, while cases with relatively higher injection rates that had more significant CO_2 move out of pattern had higher metrics. ROZ only CO_2-EOR without substantial CO_2 storage revenue (e.g. tax credits) had the lowest metrics and were uneconomic. Like traditional CO_2-EOR, WAG process had higher metrics for MPZ and ROZ CO_2-EOR.

Because of the Noble Field geologic setting (i.e. a large anticline) any case could be augmented with a single CO_2 storage well into the aquifer that could generate revenue that could improve the economic metrics dramatically.

The elements of a development strategy for CO_2-EOR in the Noble Field (and presumably other similar brownfield ROZs) are as follows:

- 80-acre injection pattern
- MPZ and ROZ injection or MPZ only
- High injection rates (leading to out-of-pattern CO_2)
- WAG if using low injection rates
- Continuous injection if using high injection rates

Three example development strategies for Noble Field are:

- EOR, CO_2 storage, and economic metrics with NCNO: 80-acre, MPZ and ROZ injection, continuous high injection rate strategy
- EOR and economic metrics from the MPZ only but has net carbon positive oil production: 80-acre, MPZ only, WAG strategy
- CO_2 storage and economic metrics with NCNO: 40-acre, ROZ only, continuous high injection rate strategy

Specific development strategies depend on the goals of the project (prioritizing EOR performance vs. storage performance and NCNO) and geologic setting (brownfield vs greenfield), and company's business strategies (economic metrics). Changes in oil and/or CO_2 price would impact the choice to prioritize (or balance) EOR or storage in the development strategy.

6. CO_2-EOR and Storage Regional Resource Assessment

6.1 Data Compilation and Analysis

An important part of the regional resource assessment is the expansion of the work at Noble Field to conceptually define the Cypress Sandstone ROZ play within the Illinois Basin. The geographic limits of the play are defined by the lateral extent of the thick Cypress Sandstone fairway (**Figure 6.1**). Lewan et al. (2002) indicated that this entire area falls within the window of the extent of Cypress Sandstone oil emplacement. The stratigraphic limits are likewise bounded within the Cypress Sandstone. Analogous plays may exist in several analogous Chesterian reservoirs within the Illinois Basin, but no other formations were assessed as part of this research.

Oil can migrate by buoyancy through porous, water-wet rock and/or by hydrodynamic flow. To form a ROZ, oil must be emplaced within the formation and then be displaced over geologic time, either by natural brine migration or by tectonic tilting or faulting after emplacement causing oil to buoyantly migrate out of the reservoir. Studies have focused on the mechanisms of ROZ formation and localized ROZ indicators, but by understanding the regional consequences of ROZ formation, additional criteria emerge for ROZ identification. For example, if the Cypress Sandstone contains a ROZ, the thickness and areal extent of the sandstone across the Basin implies huge fluid flux. Thus, a regional ROZ has broad implications for the Basin, raising questions as to where the displaced oil went and from where the invading water was sourced.

The Cypress Sandstone is truncated in the subsurface along its northern and western termini by younger Pennsylvanian strata along an angular unconformity, whereas the southern and eastern boundaries are exposed in outcrop. Depending on the timing of oil emplacement and subsequent migration out of Cypress Sandstone reservoirs, three possible scenarios for oil migration are postulated: (1) oil was trapped below the unconformity to the north or west or passed into overlying or laterally juxtaposed Pennsylvanian sandstones, (2) oil migrated to the south or east where oil seeps and tar mats might be expected in the outcrop belt, or (3) oil migrated into updip Cypress strata that were subsequently eroded in the geologic past.

To systematically expand on the promising findings of the Noble Field study, the Trentham and Melzer (2016) “cookbook” approach to exploring for and evaluating ROZs in the Permian Basin that is predicated on documenting and reinterpreting existing data was used in the Illinois Basin. Identification of prospective areas with siliciclastic Cypress Sandstone ROZs within the Illinois Basin and an overall assessment of the resource was based on a compilation of empirical evidence directly documented or interpreted from the hundreds of thousands of existing well records in the ISGS database.

6.1.1 Mapping Geological Data

Regional Cypress Sandstone isopach and facies maps were necessary for volumetric calculations as part of the resource assessment of CO_2-EOR and storage potential in the thick Cypress Sandstone. Regional isopach maps of the Cypress Sandstone were developed previously by Willman et al. (1975) and by Seyler et al. (2000). The data control used to make the Willman et al. map is not specified and is a map of gross thickness of the formation. The Seyler et al. map is a net isopach map for the Cypress Sandstone that was based on a grid of 1,700 wells selected at a minimum density of four wells per township.

For the new regional Cypress isopach and facies maps, formation tops were identified using geophysical-wireline logs from approximately 4,500 wells distributed across the basin (**Figure 6.2**). The wells used for the study were selected at a minimum data density of six wells per township (36 mi^2) across the Illinois Basin, except in areas near the boundary where the Cypress either pinches out or is eroded. Additional wells were added for this assessment following initial iterations of the map to fill in well-coverage gaps to complete thickness trends. Three areas have significantly increased data density relating to detailed characterization at Noble Field in Richland County (e.g., Webb and Grigsby, *in press*), Kenner West Field in Clay County, and Dale Field in Hamilton County (e.g., Howell. 2017). The well control is shown in in Figure 4. The boundary extent of the Cypress Sandstone is outlined (**Figure 6.2**) based on mapped extents of the Cypress from previous publications (Bristol and Howard, 1971; Willman et al., 1975; Cole and Nelson, 1995; Nelson et al., 2002) and from thickness data interpreted for this study. All maps generated for the region were clipped to the boundary extent.

In each log, the base of the Barlow Limestone and base of the Cypress Formation were picked to calculate the gross thickness of the Cypress Formation. The net sandstone thickness was determined by summing the thickness of sandstone that has a 50% or greater deflection of the SP curve above the SP shale baseline, normalized to the nearest thick, clean sandstone, which in some cases was within the Cypress. Greater than 50% clean sandstone commonly distinguishes reservoir quality from non-reservoir based on porosity and permeability and has been used in previous Cypress Sandstone studies (Grube, 1992; Grube and Frankie, 1999). The SPE response to the Fraileys Shale was set as the 100% shale baseline, or 0% clean sandstone. Net sandstone thickness refers to the cumulative thickness of sandstone above a certain normalized SP value cutoff. The thickness data were plotted at each well location and mapping was completed using the kriging algorithm in ArcGIS (ArcToolbox > Spatial Analyst Tools > Interpolation > Kriging). The resulting net thickness map is shown in **Figure 6.3**. The thickest net sandstone is in a northeast-southwest trending belt that is up to approximately 56 km (35 mi) wide and best developed in Richland, Wayne, and Hamilton Counties.

The regional mapping, combined with detailed sedimentological studies of core from across the Basin (Howell, 2017; Howell et al, in prep) and field scale studies (Webb and Grigsby, *in press*), allowed for development of a generalized regional facies map (**Figure 6.4**). The northeast-southwest oriented thick sandstone trend is dominantly multistory channel sandstones (Howell et al. in prep; Howell, 2017; **Figure 6.5**). Sandstone lenses outside of these belts are dominantly tidal bars and tidal ridges that can be stacked or shingled (Leetaru, 1996; Damico et al., 2014; Grube and Frankie, 1999; Grube, 1992; Whitaker and Finley, 1992). Mudstones on the eastern and western shelves of the Basin are dominantly paleosols that are coincident with the paleosol horizon within the upper half of the formation, which exists throughout the Basin. During this lowstand, thick sandstones of the Cypress were deposited within the thick sandstone fairway, which were eroded down through tidal bars and tidal ridges coeval with tidal bars and tidal ridges outside thick sandstone trend (**Figure 6.5**).

Core analysis data, including existing records and new data generated from laboratory tests of available core samples from the ISGS, were used to develop a regional database of Cypress Sandstone porosity (**Figure 6.6**). Some areas in the central part of the Basin have very limited Cypress core data, so neutron-density porosity logs were used to characterize porosity (**Figure 6.6**). This data was used in conjunction with the Cypress net thickness map to generate a map of pore volume (**Figure 6.7**).

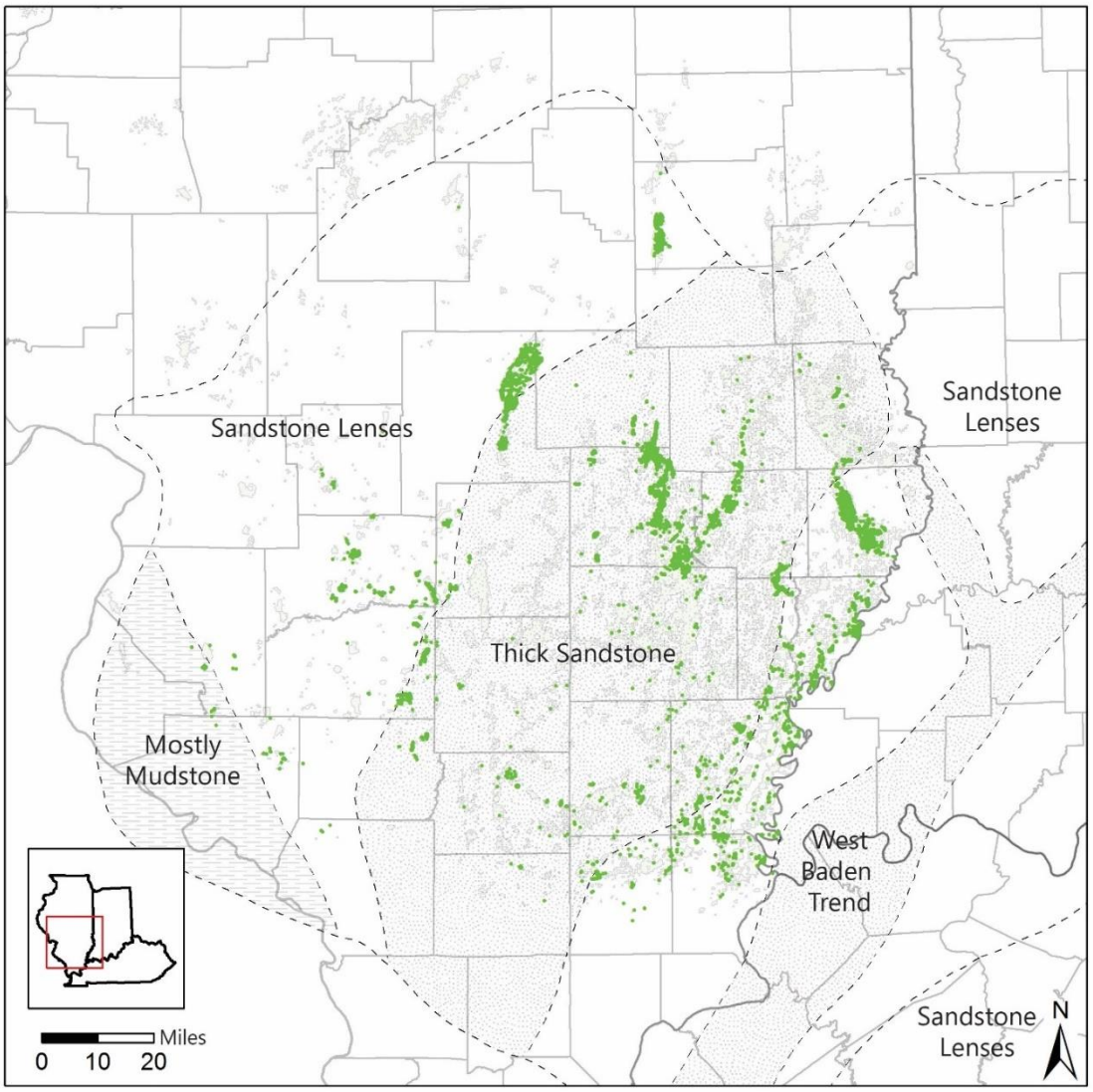

Figure 6.1. Regional province map of the Cypress Sandstone showing the dominant reservoir types. Oil fields are shown in light green and Cypress producing wells are shown as green dots. Modified from Nelson et al. (2002).

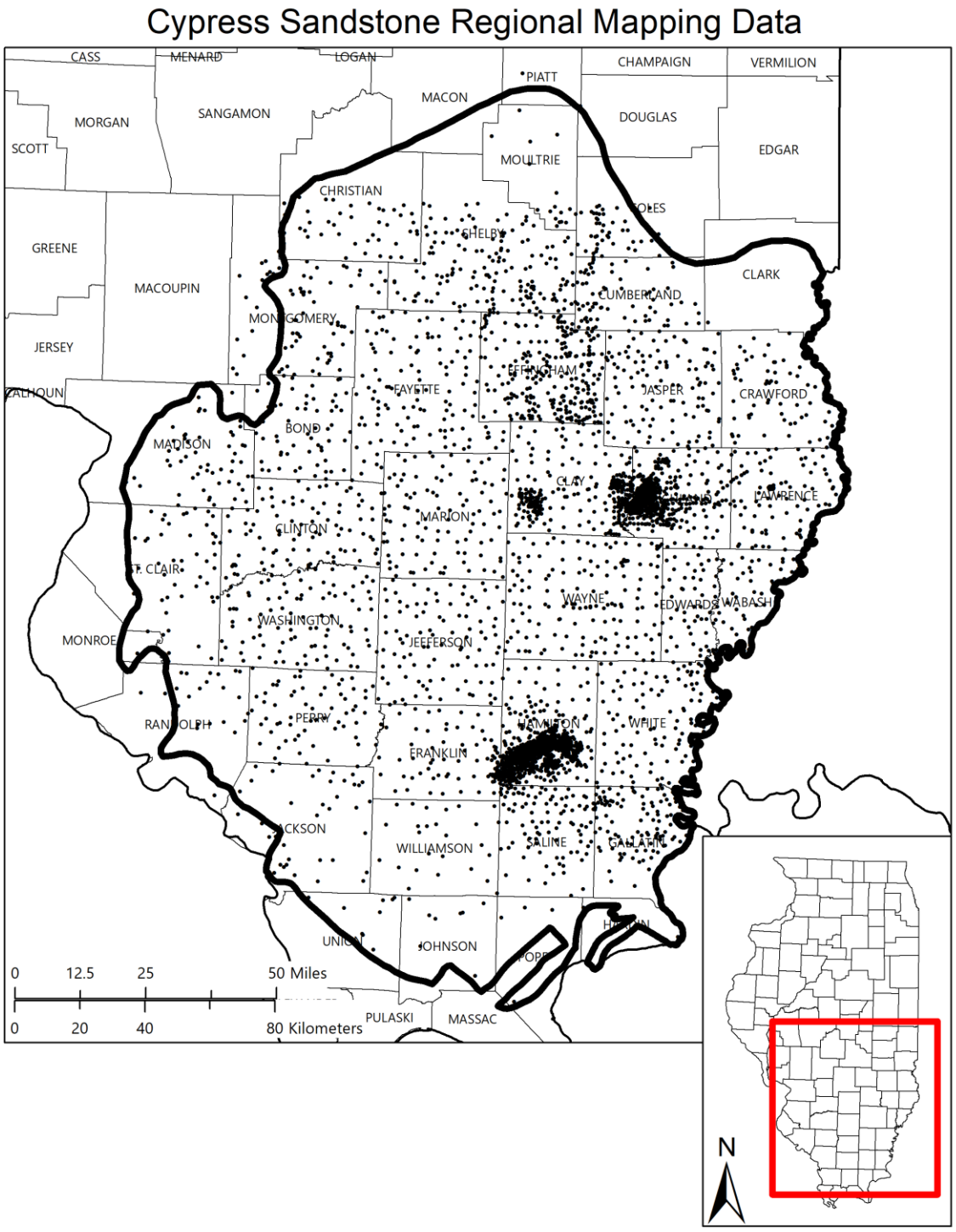

Figure 6.2. Distribution of wells used to map the thickness of the Cypress Sandstone. The thick black line represents the boundary of the Cypress Sandstone within Illinois.

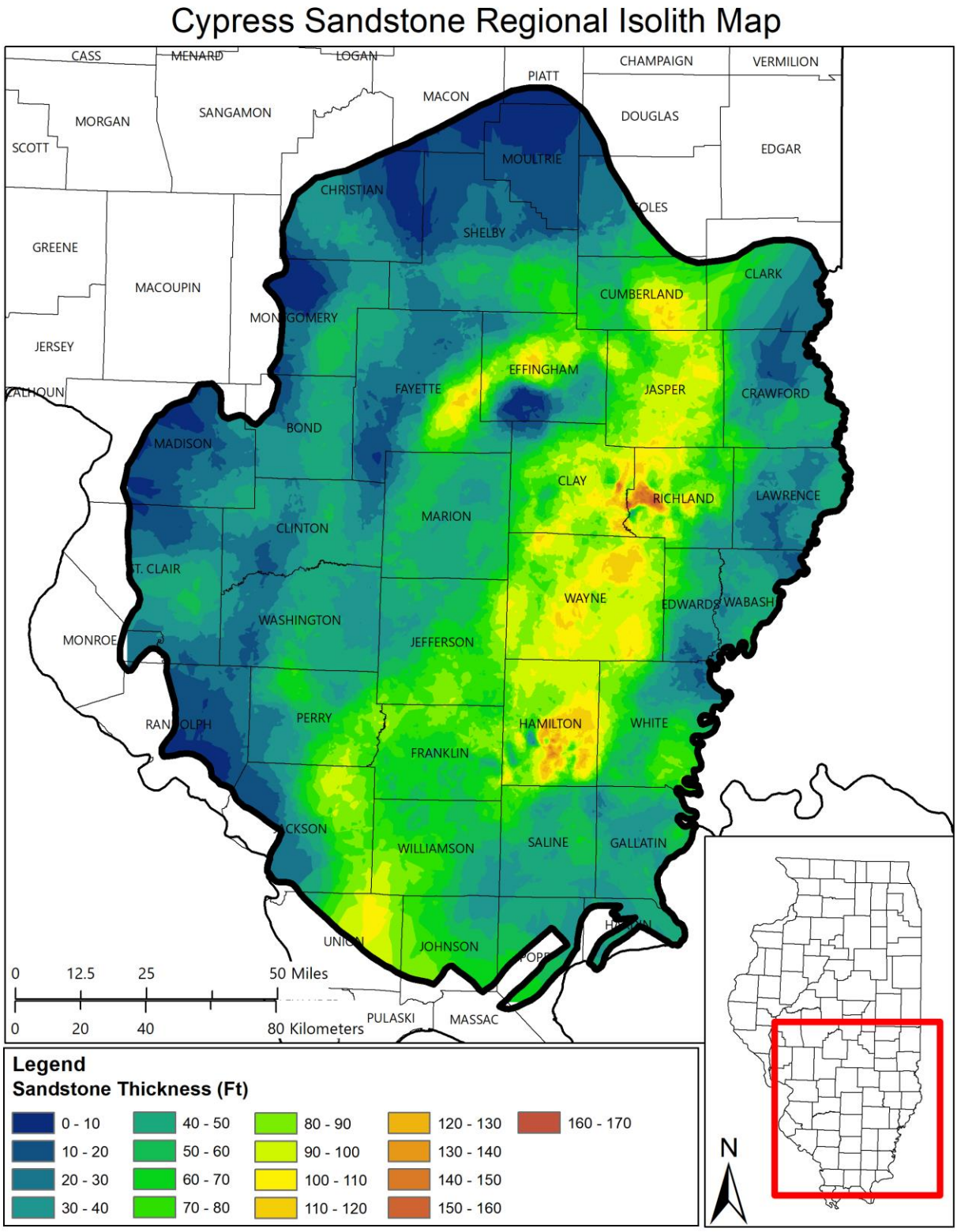

Figure 6.3. Net sandstone thickness map of the Cypress Sandstone.

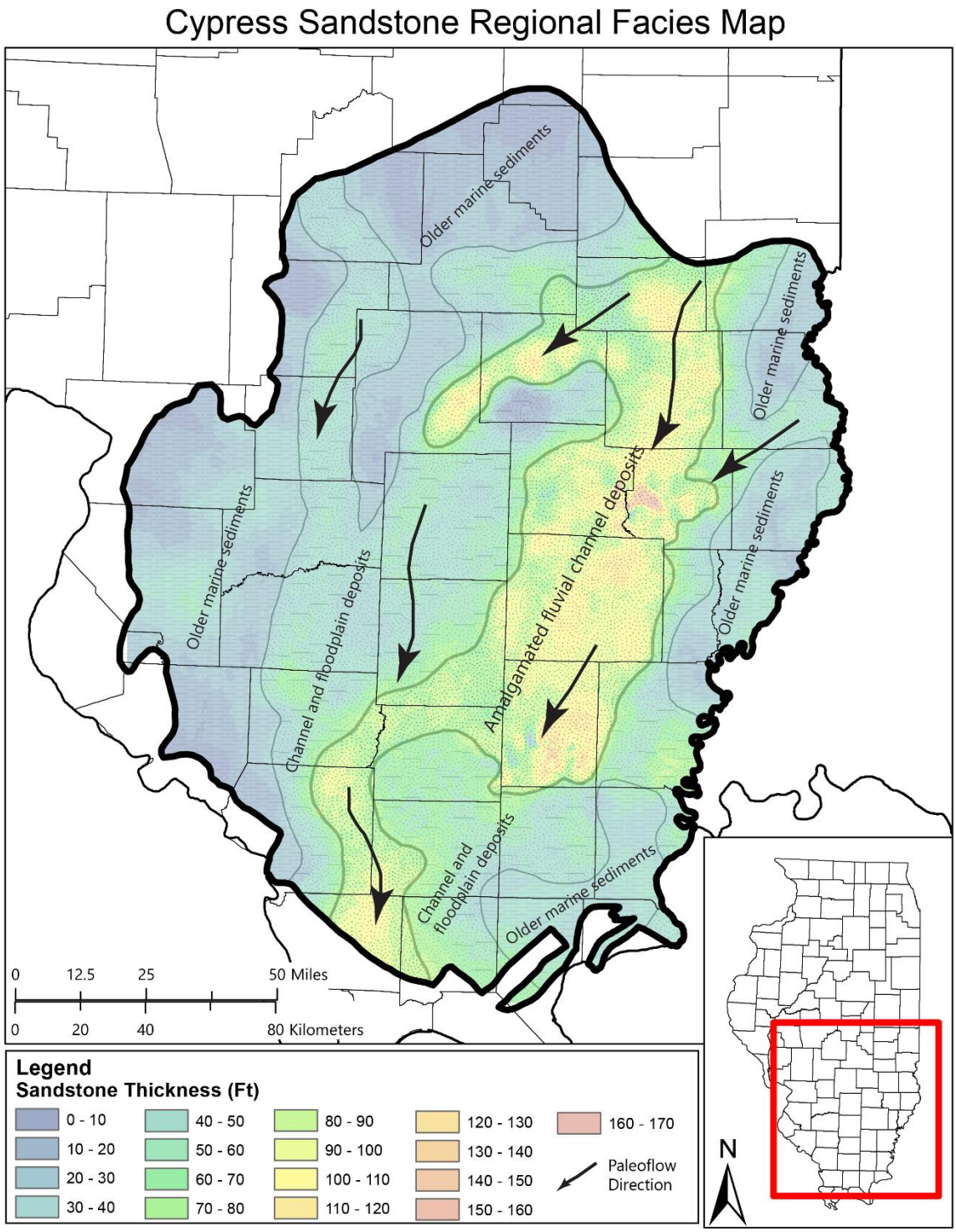

Figure 6.4. Generalized facies map of the Cypress Sandstone.

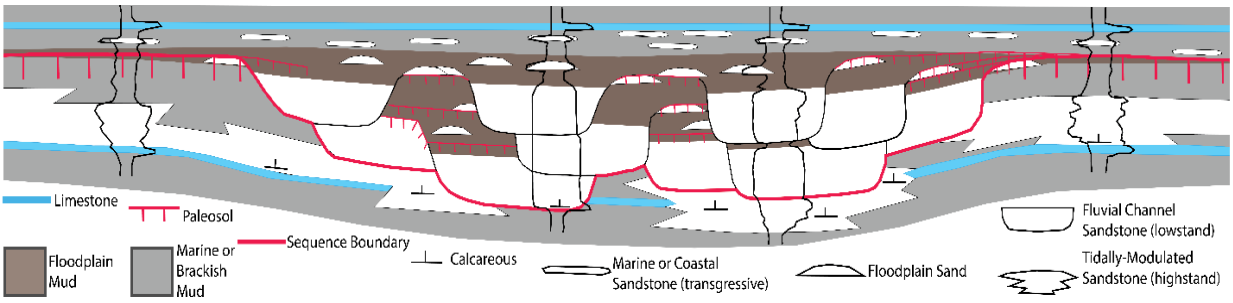

Figure 6.5. Regional diagrammatic West-East cross section across the central part of the Illinois Basin showing the relationship of the fluvial facies of the Cypress Sandstone with older marine facies. Note the upward vertical thickening and amalgamation, of the fluvial, channel-fill sandstones that can create stratigraphic traps. Fluvial channel sandstones eroded down through tidal bars and tidal ridges coeval with tidal bars and tidal ridges outside thick sandstone trend.

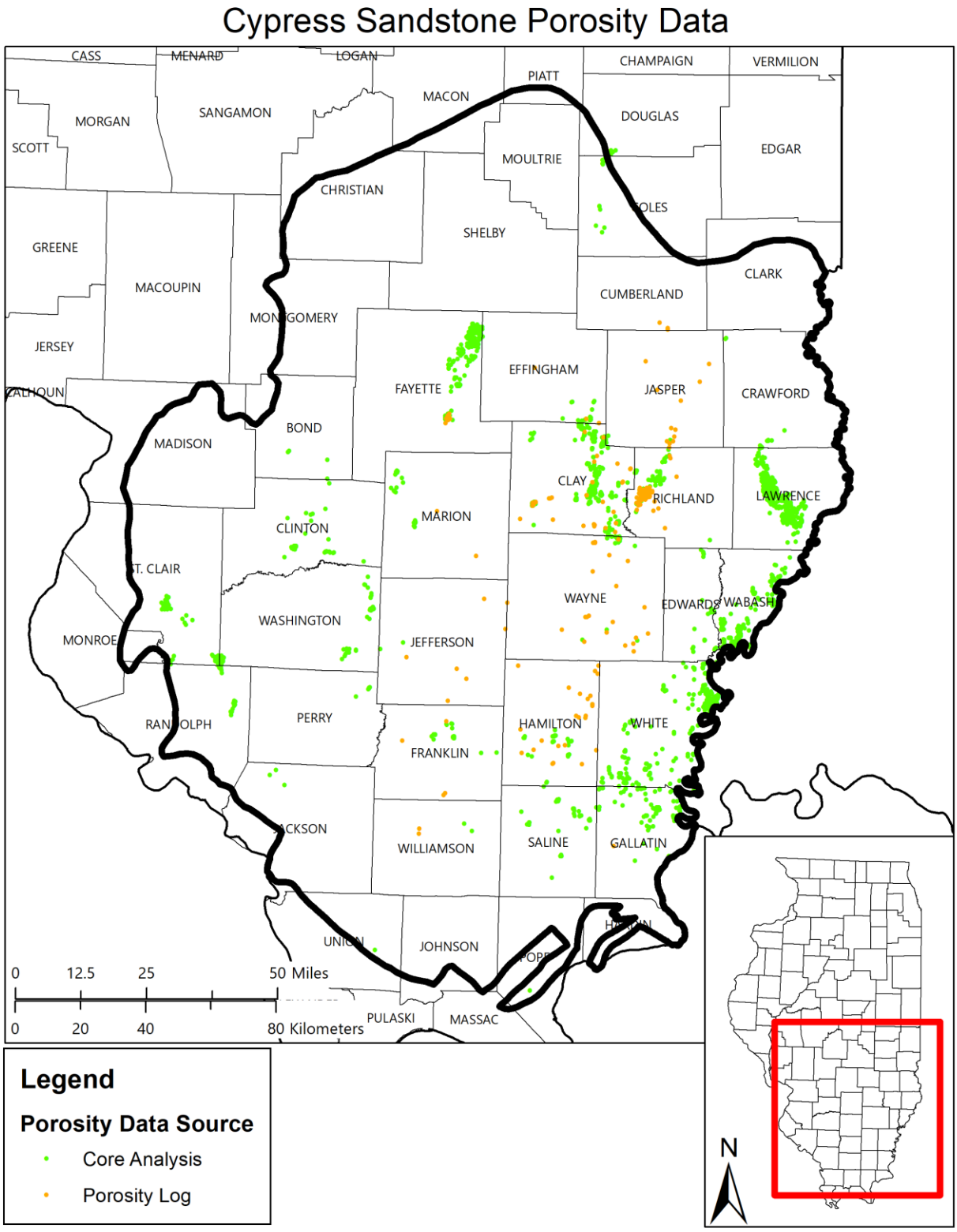

Figure 6.6. Regional distribution of Cypress Sandstone porosity data, from core and from porosity logs, used to generate porosity-thickness map.

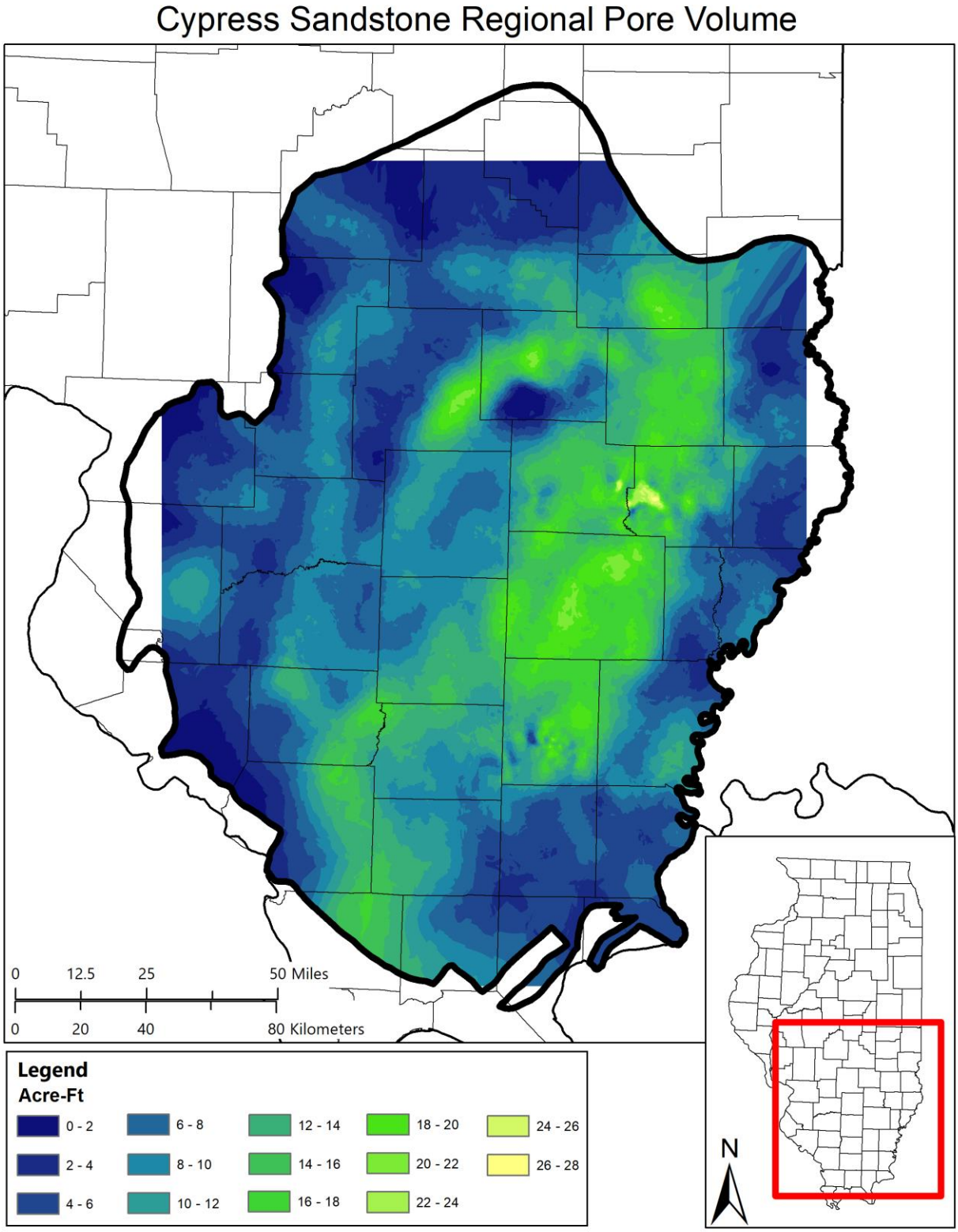

Figure 6.7. Porosity-thickness map showing the regional variation in pore volume within the Cypress Sandstone in acre-feet.

6.1.2 Mapping Oil Saturation Data

Several data types were used to estimate the spatial distribution of oil saturation within the thick Cypress ROZ play. The ISGS institutional databases contain more than a century's worth of oil well data with information relating to the presence of oil saturation in a given formation within the well. Data types used in this study include oil shows from drilling records, oil saturation measurements from conventional core analysis, production and perforation records, and drill stem tests. Of these data types, successful production perforations and drill stem tests are inferred to indicate mobile oil. The other data types do not distinguish between mobile and residual oil and are not considered quantitative measures of oil saturation, but are considered direct evidence that oil is present within the Cypress at that well location. The oil shows data were compiled and mapped to understand the distribution of oil encountered within the Cypress (**Figure 6.8**).

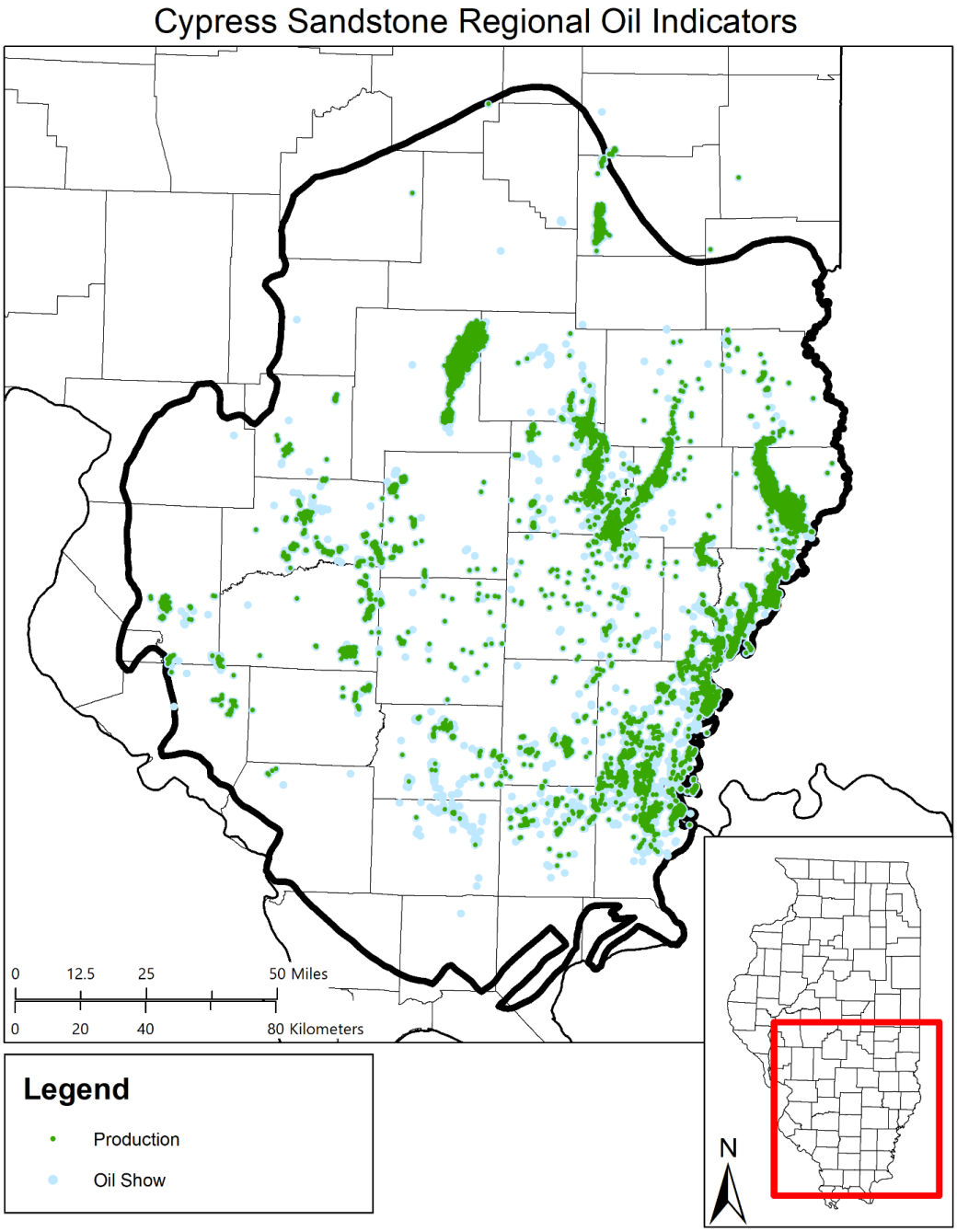

Figure 6.8. Map of Cypress oil production (green dots) and oil shows (blue dots) from the ISGS institutional databases. Both are clustered in established oil fields and were used to guide the search for residual oil.

In addition to the historical data, a method of analyzing well logs developed at Noble and Kenner West fields (Grigsby and Frailey, in prep) was applied to ~300 wells within the thick Cypress ROZ play. The method involves calculating water saturation using Archie's equation and using fluid contact curves (moveable hydrocarbon index, apparent water resistivity, and bulk volume water) to validate whether the well has mobile or residual oil. This analysis allows for an estimation of the thickness of mobile and residual oil (if present), the boundary between mobile and residual oil, the ultimate oil-water contact (the base of the ROZ), and residual oil saturation. Examples of this analysis are shown in **Figure 6.9**. Each well was assigned an indicator value based on whether this well log analysis indicated a main pay zone and ROZ (114 wells), ROZ only (89 wells), or had no indication of oil (104 wells) (**Figure 6.10**).

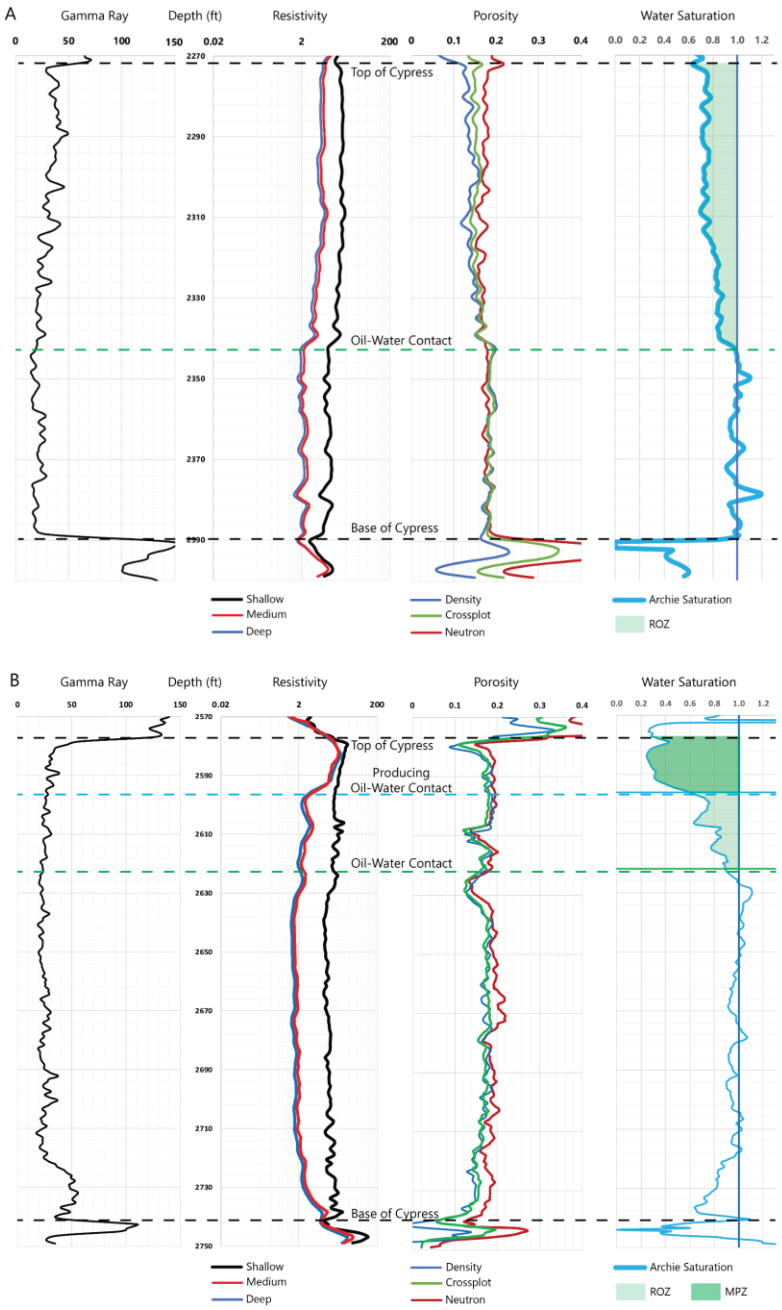

Figure 6.9. (A) Example well log analysis from the Swim #1 well (API 120352328200) showing the Cumberland greenfield ROZ. Gamma-ray log shown in left track, resistivity log shown in left-center track, neutron-density porosity log shown in right-center track, and calculated water saturation shown in right track. Water saturation stabilizes at around 75% (25% oil saturation) for the upper 21 meters (70 feet) of the reservoir, indicating a thick greenfield ROZ. (B) Example well log analysis from the Bourne #1 well (API 121592409403) showing the Noble Brownfield ROZ. Gamma-ray log shown in left track, resistivity log shown in left-center track, neutron-density porosity log shown in right-center track, and calculated water saturation shown in right track. Water saturation is very low (~25%) in the top ~ 6m (20 ft) of the reservoir (the main pay zone), stabilizes at around 75% (25% oil saturation) for ~6 m (20 ft) below the main pay zone, indicating a brownfield ROZ.

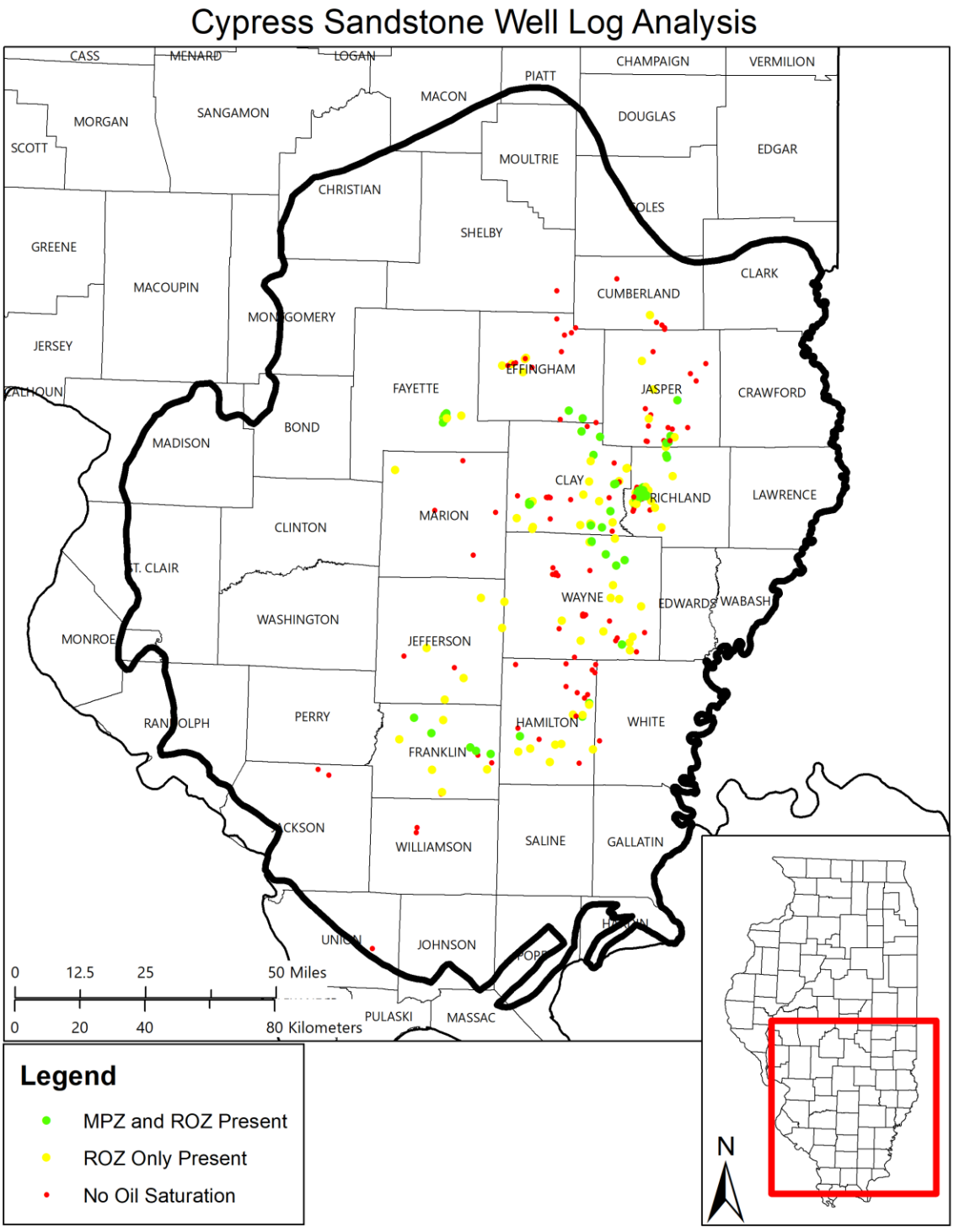

Figure 6.10. Map of oil indicators from well log analysis. Wells with both main pay zone (MPZ) and ROZs are shown in green dots, wells with only ROZ are shown with yellow dots, and wells with no indications of oil are shown with red dots.

6.2 Well Log Validation

To validate that the well log analyses methodology, to ensure that the method was properly applied (to account for transcription or calculation errors), and to evaluate the impact of uncertain input parameters (namely Archie's cementation exponent, R_w, and R_{mf}), an independent study was performed by Dr. Steve Henderson and Dr. George Asquith of Texas Tech University.

6.2.1 Formation Water Resistivity (R_w) Determination

Determining estimates of formation water resistivity is an important first step in the evaluation process. Apparent water resistivity (R_{wa}) is a log-derived estimate of water resistivity in the uninvaded zone. In a water-saturated interval, and assuming S_w = 1.0, R_{wa} is estimated from the Archie equation by:

$$R_{wa} = \frac{{\emptyset_t}^m \times R_t}{a} \qquad (29)$$

Where:

- $\emptyset_t$ = total porosity, estimated from neutron-density
- m = cementation exponent (2.0)
- R_t = resistivity of the uninvaded zone
- a = tortuosity factor (1.0)

In that same water-saturated interval, the magnitude of SP deflection is proportional to the ratio R_{mf}/R_w. Accordingly, with a temperature-corrected value of R_{mf} taken from the log header, R_{wsp} is estimated from the SP deflection by:

$$R_{wsp} = 10^{\left\lfloor \frac{K\left(logR_{mf}\right)+(SP)}{K} \right\rfloor} \qquad (30)$$

Where:

- $K = 61 + 0.133\left(T_f\right)$
- T_f = formation temperature
- R_{mf} = resistivity of mud filtrate at formation temperature
- SP = SP deflection (including sign - or +)

Given that the Cypress is, by every indication, an Archie-type rock (i.e., clean, water-wet, and with high effective porosity), it is reasonable to expect Archie R_{wa} to provide accurate estimates. It is also reasonable to expect that, in an Archie-type rock, R_{wSP} determined from the SP deflection should approximately equal Archie R_{wa}, provided R_{mf} is accurately known. However, on the regional scale, Archie R_{wa} values show a much narrower distribution than R_{wSP} values. For 144 wells in which Archie R_{wa} was evaluated (**Figure 6.11**), values range from 0.025 Ωm to 0.125 Ωm, with a median value of 0.042 Ωm. R_{wSP} in 115 wells where the SP response is usable (**Figure 6.12**) ranges from 0.023 Ωm to 0.169 Ωm (same range as Noble Field individually), with a median value of 0.056 Ωm.

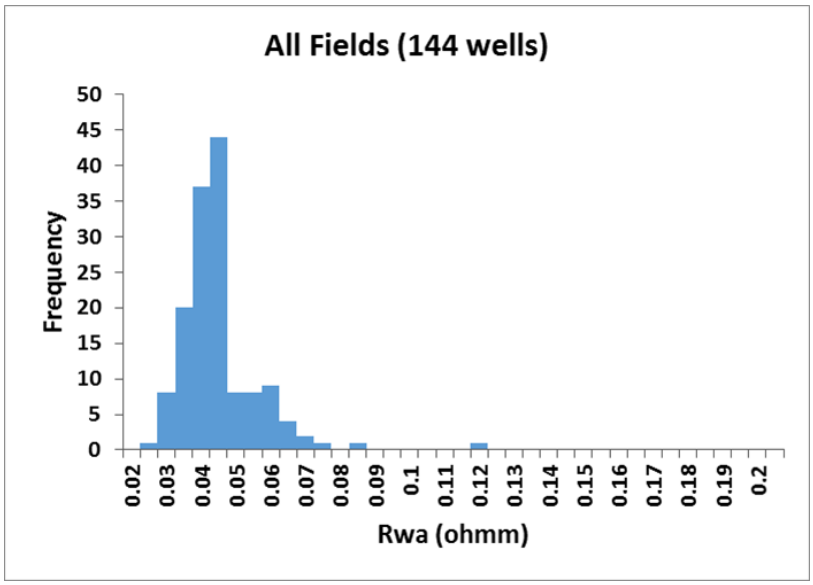

Figure 6.11. Frequency distribution of R_{wa} results in 144 wells from all fields (median value of 0.042 Ωm).

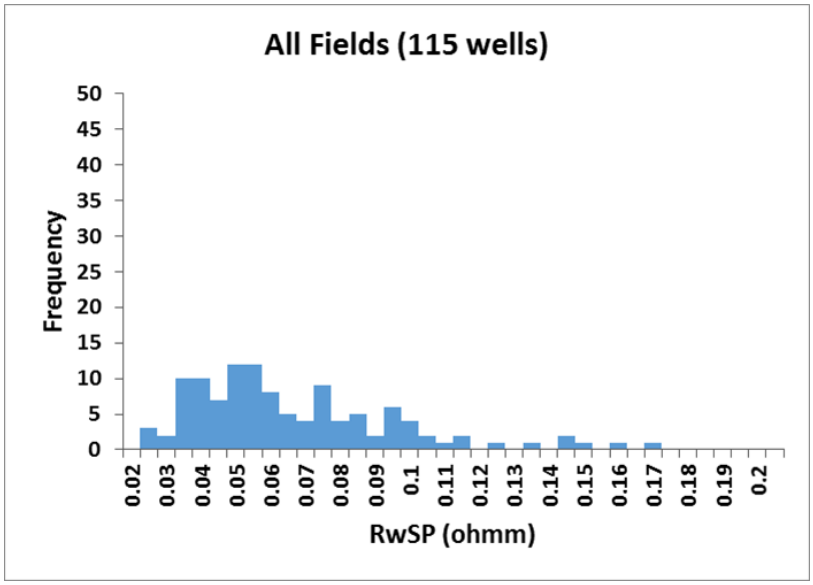

Figure 6.12. Frequency distribution of R_{wSP} results in 115 wells with usable SP response from all fields (median value of 0.056 Ωm).

On a regional scale, (**Figure 6.13**), R_{wa} and R_{wSP} differ by more than 0.005 Ωm in a total of 73 wells. These discrepancies are reason for concern. The poor correlation between wells in which R_{wa} and R_{wSP} are significantly different suggests the possibility that R_{mf} values recorded in many log headers are not accurate.

If the thick Cypress is, as it appears to be, an Archie-type rock, then better agreement between Archie R_{wa} and R_{wSP} values is expected. The narrow distributions of R_{wa} values suggest the Archie method is the most effective for producing repeatable and accurate estimates of water resistivity. Independent data seem to also support this claim. In the East Xenia Field, a water resistivity of 0.046 Ωm is reported for the thick Cypress (Xu and Huff, 1995).

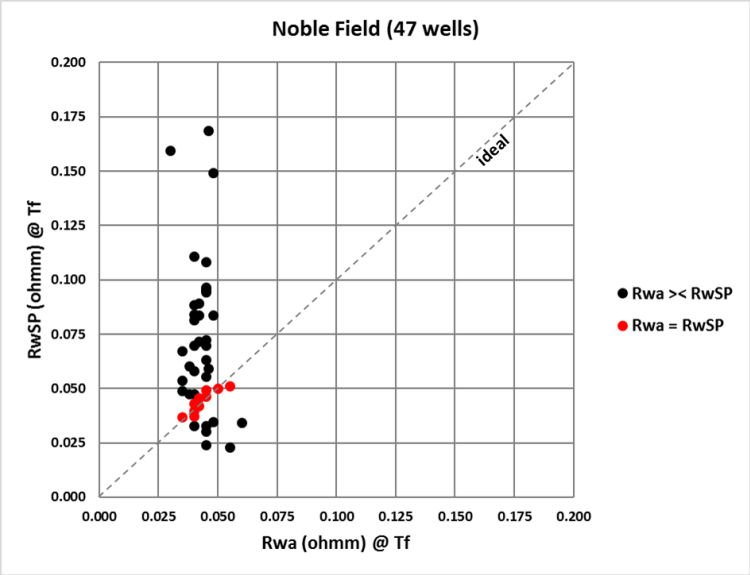

Figure 6.13. R_{wSP} versus Archie R_{wa} in 47 wells of Noble Field where adequate data exist for a comparison. Red points represent 10 wells in Noble Field where R_{wa} and R_{wSP} are approximately equal (< 0.005 Ωm difference).

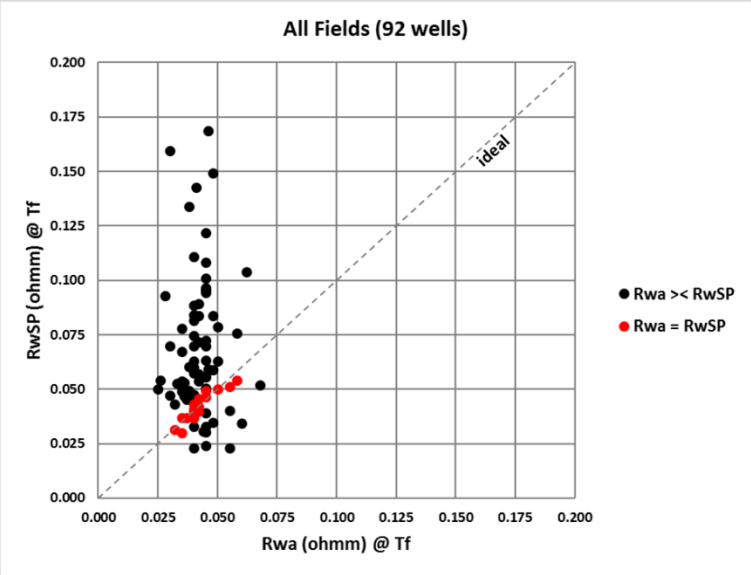

Figure 6.14. R_{wSP} versus Archie R_{wa} in 92 wells where adequate data exist for a comparison. Red points represent 19 wells where R_{wa} and R_{wSP} are approximately equal (< 0.005 Ωm difference).

6.2.2 Identifying the Original Oil-Water Contact (OWC)

The TTU study used two additional methods to pick the OWC; a R_o-R_t overlay and analysis of micrologs. The R_o-R_t overlay often provided perfectly correlatable indications of the OWC with the R_{wa} and water saturation profiles used previously. This should come as no surprise, given that the three methods are different applications of the same equation. However, cases are observed where one method does not provide as conclusive an indication of the OWC as other methods. Accordingly, a comparison of indications provided by all three methods may enable a more accurate determination of the OWC.

In demonstrating the application of the techniques evaluated, responses in the Bourne #7 well (API 1215925687), Noble Field, are used as examples. Responses from additional wells are shown when necessary and noted in figure captions.

R_o-R_t Overlay

A quick and convenient visual method for estimating apparent water resistivity (R_{wa}) is also useful for identifying the OWC. Wet resistivity of the uninvaded zone (R_o), when saturated with formation water of a given resistivity, is calculated by:

$$R_o = \left(\frac{a}{\emptyset_t^{\,m}}\right) \times R_w \qquad (31)$$

Where:

- a = tortuosity factor (1.0)
- $\emptyset_t$ = total porosity, estimated from neutron-density
- m = cementation exponent (2.0)
- R_w = resistivity of formation water at formation temperature

When R_o is plotted as a continuous curve on a logarithmic track with uninvaded zone resistivity (R_t), a comparison of curves provides a means of identifying the presence of hydrocarbon (**Figure 6.15**). If the R_w estimate is accurate, then in a water-saturated interval $R_o = R_t$ and the two curves overlay. This is the basis for using the plot to quickly and visually estimate R_{wa}. By manipulating the R_w variable until the condition $R_o = R_t$ is observed, an estimate of R_{wa} at formation temperature is determined.

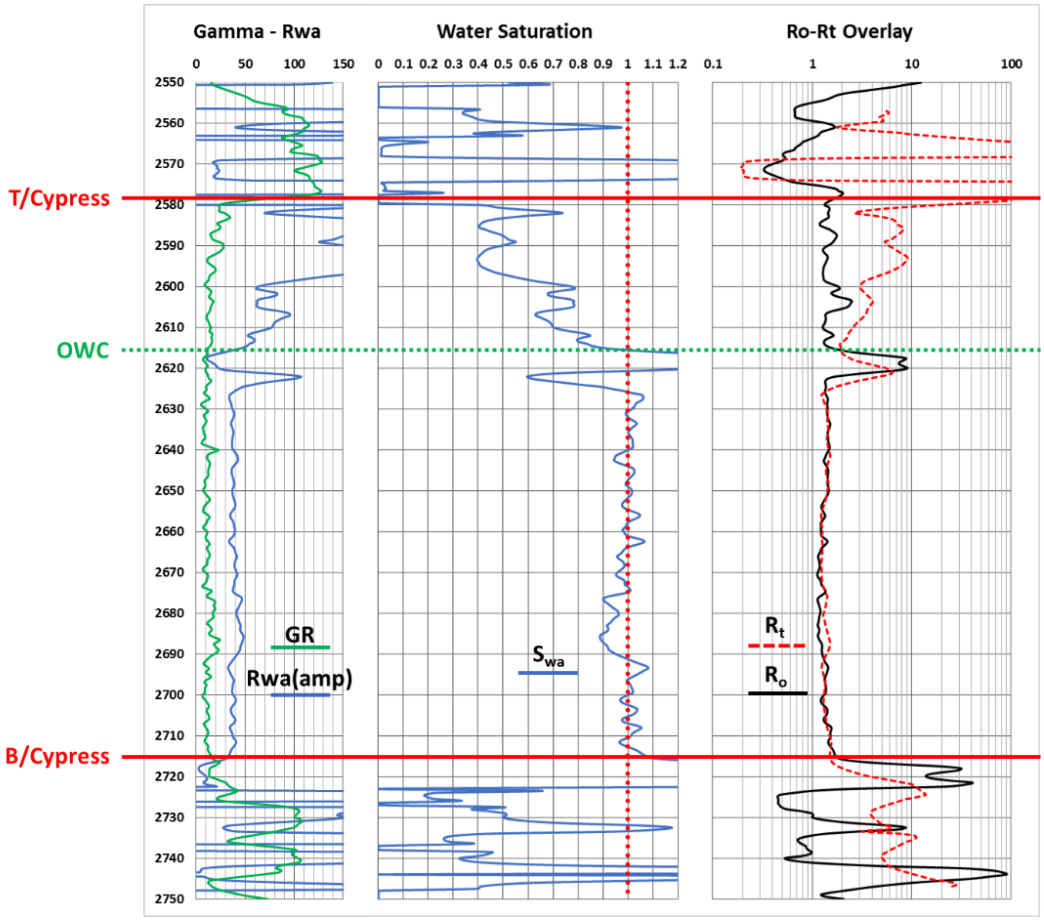

Figure 6.15. R_o-R_t overlay (right track) indicating OWC at 797 meters (2,616 feet) where R_t first increases greater than R_o. R_o calculated using R_w = 0.038 Ωm @ T_f, determined for the interval 800-828 m (2,625-2,715 ft). Data from Bourne #7 well (API 121592568700), Noble Field.

In a hydrocarbon-bearing interval (**Figure 6.15**), $R_o < R_t$. Accordingly, the OWC is identified as the depth at which R_t first increases greater than R_o. This method is demonstrated to be helpful in the Thick Cypress for defining the OWC in wells where the amplified R_{wa} curve shows only a very subtle increase over its baseline response in the water-saturated interval, or where R_{wa} may indicate multiple possibilities for the OWC. The amount of separation observed between R_o and R_t curves is a function of water saturation, with lower S_w producing larger separation.

MicroLog

In less than half of those wells where a microlog is available, changes in micro-resistivity values are observed to coincide with the OWC defined by other methods. Given the very shallow depth of investigation of microlog measurements, changes in fluid saturations within the flushed zone at the OWC might influence one or both measurements. Evidence of the OWC (**Figure 6.16**) may be manifested by increases in micro-inverse and/or micro-normal resistivity curves, or by an increase in the amount of separation between the two curves.

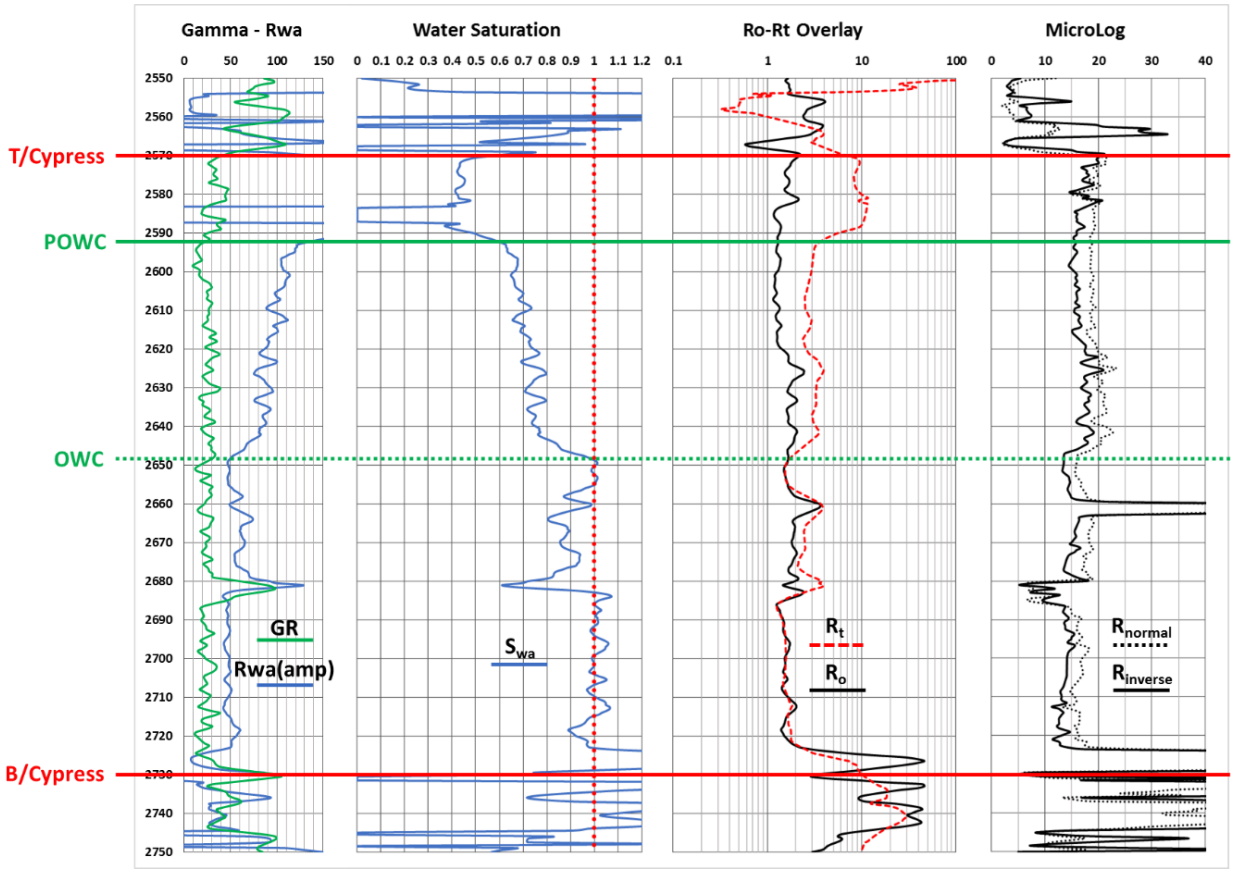

Figure 6.16. Microlog response (right track) in a well where micro-normal and micro-inverse resistivity curves show a distinct increase at the OWC (807 m (2,648 ft)). Data from Montgomery #B-38 (API 121592610700), Noble Field.

The microlog does not provide as conclusive an indicator of the OWC as other techniques. Changes in micro-inverse and micro-normal responses can result from several factors beyond a change of fluid saturations in the flushed zone. These include variations in mudcake thickness and the quality of contact between the tool's pad-mounted electrodes and the borehole wall (i.e., stand-off). In many wells, microlog response provides absolutely no indication of the OWC (**Figure 6.17**).

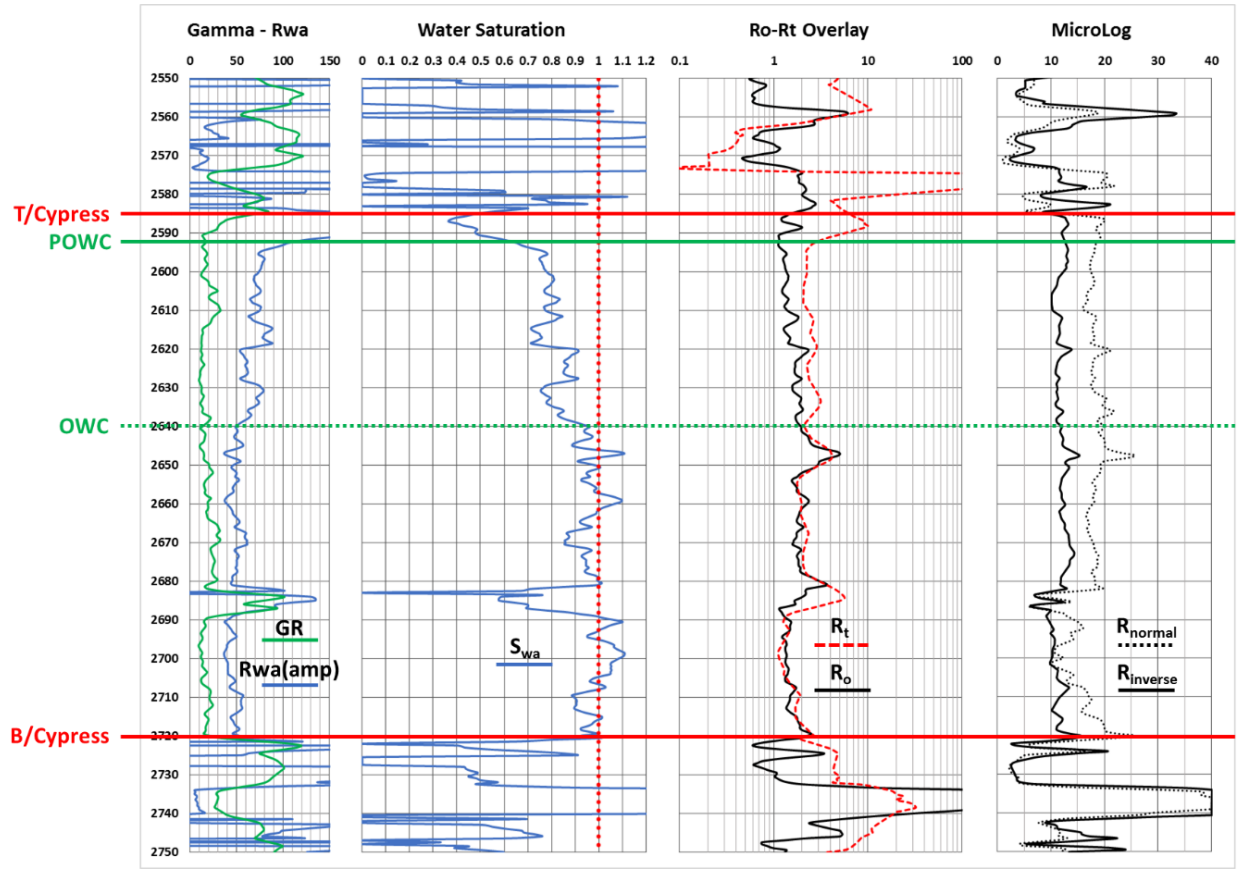

Figure 6.17. Microlog response (right track) in a well where micro-normal and micro-inverse resistivity curves provide no indication of the OWC (805 m (2,640 feet)). Data from Montgomery #B-34 (API 121592606400), Noble Field.

6.2.3 Identifying the Producing Oil-Water Contact (POWC)

The elevation of a reservoir's producing oil-water contact (POWC) is dependent upon parameters such as pore diameter and fluid density, making it difficult to identify with conventional well log responses. The most accurate methods for identifying the POWC are those that rely upon pressure gradient and fluid density data provided by wireline formation testers, drill stem tests and production tests (Bradley, 1987). Accuracy of the POWC pick, therefore, comes with the price of additional cost. Producing oil-water contacts are characterized by changes in saturation and mobility, thus making movable hydrocarbon index (MHI) a logical choice for defining the POWC using resistivity and porosity logs. However, the dependency of MHI upon mud filtrate resistivity (R_{mf}) present problems to a standard MHI evaluation under conditions of resistive invasion.

To eliminate sensitivity to R_{mf}, a method is developed whereby MHI is calculated using a log-derived estimate of mixed water resistivity. Apparent mixed water resistivity (R_{za}) is used to generate an MHI response that is calibrated to the water-saturated interval, providing the basis for applying a fixed cut-off to identify the POWC in multiple wells. As a bonus, R_{za} is also used to calculate resistivity-derived porosity ($\emptyset_{rxo}$) which is useful as another method of identifying the original OWC.

In demonstrating the application of the MHI and $\emptyset_{rxo}$ techniques, responses in the same well shown previously (Bourne # 7, (API 121592568700), Noble Field) are used as examples. Responses from additional wells are shown when necessary and noted in figure captions.

Standard Method for Estimating MHI

Movable hydrocarbon index (MHI) is a unitless parameter representing the ratio of water saturation in the uninvaded zone (S_w) to water saturation in the flushed zone (S_{xo}), where:

$$MHI = \frac{S_w}{S_{xo}} \quad (32)$$

If hydrocarbon is residual and cannot be displaced during invasion, then $S_w = S_{xo}$ and MHI = 1.0. On the other hand, when hydrocarbon is moved during invasion, $S_w < S_{xo}$ and MHI < 1.0. Ideally, a value of MHI decreases in proportion to a volume of hydrocarbon moved. MHI values less than 0.6 to 0.7 are traditionally used to indicate movability (Asquith, 1985).

When S_w is divided by S_{xo}, the $a\emptyset^{-m}$ term of the Archie equation cancels, leaving MHI to be expressed in terms of resistivity ratios by:

$$MHI_{std} = \left[\frac{R_{xo}/R_t}{R_{mf}/R_w}\right]^{0.5} \quad (33)$$

Where:
- R_{xo} = resistivity of the flushed zone
- R_t = resistivity of the uninvaded zone
- R_{mf} = resistivity of mud filtrate at formation temperature
- R_w = resistivity of formation water at formation temperature

In this ratio form (Eq. 6), the standard MHI equation can be used to demonstrate its primary limitation in formations containing saline water that are drilled with fresh water-base mud. Under conditions of resistive invasion where $R_{mf}/R_w > 2$, MHI values calculated using a temperature corrected R_{mf} from the log header give optimistically low results. Movable hydrocarbon might be indicated (i.e., MHI < 1.0) in a water-saturated interval (**Figure 6.18**).

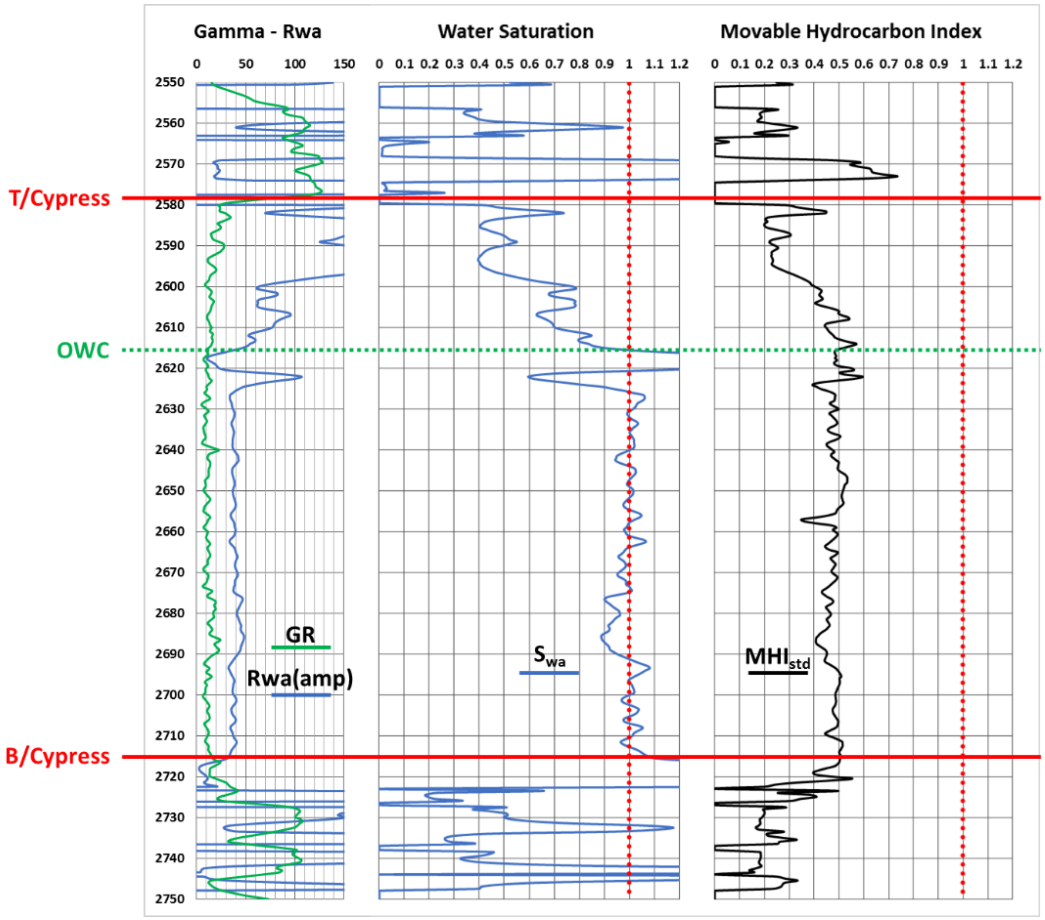

Figure 6.18. MHI_{std} response (right track) calculated by Equation 6, using temperature corrected R_{mf} from log header (1.967 Ωm @ T_f). MHI_{std} indicates the presence of movable hydrocarbon throughout the entire Cypress interval. Data from Bourne #7 (API 12159256870), Noble Field.

The false indication of movability in the water-saturated and ROZ intervals results from the fact that, under conditions of resistive invasion, R_{mf} at formation temperature is not representative of the unknown mixture of mud filtrate and formation water present in the flushed zone. When R_{mf} is greater than the resistivity of this mixed water (R_z), MHI values indicate hydrocarbon is movable even when it is residual.

R_z Method for Estimating MHI

Under conditions of resistive invasion ($R_{mf}/R_w > 2$), an improvement over the standard MHI calculation is to employ an R_z approach, in which MHI is calculated by:

$$MHI_{Rz} = \left[\frac{R_{xo}/R_t}{R_z/R_w}\right]^{0.5} \qquad \text{(Eq. 7)}$$

Where:
R_{xo} = resistivity of the flushed zone
R_t = resistivity of the uninvaded zone
R_z = resistivity of mixed water at formation temperature
R_w = resistivity of formation water at formation temperature

Resistivity (R_z) of the unknown mixture of mud filtrate and formation water in the flushed zone is estimated by:

$$R_z = \frac{1}{\left(\frac{z}{R_w}\right)+\left(\frac{1-z}{R_{mf}}\right)} \quad \text{(Eq. 8)}$$

Where: z = mixing constant
R_w = resistivity of formation water at formation temperature
R_{mf} = resistivity of mud filtrate at formation temperature

Mixing constant (z) represents the relative contributions of formation water and mud filtrate to the resistivity of mixed water and is a function of the radial distance to which a formation is invaded. For example, in the uninvaded formation, z = 1 and $R_z = R_w$; mud filtrate is absent from the mixture. As invasion progresses deeper, the relative contribution of mud filtrate increases while that of formation water decreases. If a formation is very deeply invaded and the flushed zone completely saturated with mud filtrate, then z = 0 and $R_z = R_{mf}$; formation water is absent from the mixture. Accordingly, mixing constant (z) is a value ranging from 0 to 1.0, depending upon depth of invasion.

Values of mixing constant (z) are usually assumed based upon some qualitative assessment of invasion depth. Commonly assumed values are listed in **Table 6.1**.

Table 6.1. Commonly assumed values of mixing constant (z), assigned based upon depth of invasion.

Mixing Constant (z)	Depth of Invasion
0.10	Very shallow
0.075	Shallow
0.05	Average (default)
0.035	Deep
0.025	Very deep

If a resistivity invasion profile shows $R_{ILD} \approx R_{ILM}$, indicating a condition of "very shallow" to "shallow" invasion, then an assumption of z = 0.10 or z = 0.075 may be appropriate. A greater difference between R_{ILD} and R_{ILM}, indicating deeper invasion, may justify the assumption of a lower value. Mixing constant (z) might also be assumed based upon an estimate of invasion depth provided by a resistivity invasion correction ("tornado") chart. Regardless of the method employed, selecting a value of mixing constant is highly subjective, as there are no defined physical boundaries separating the relative depths of invasion used as selection criteria.

The advantage of the R_z approach is that it reduces – but does not eliminate – the sensitivity of MHI_{Rz} to R_{mf}. As the R_{mf}/R_w ratio decreases, MHI_{Rz} approaches 1.0 in a water-saturated interval. In a case of "average" resistive invasion where $R_{mf}/R_w \approx 20$, MHI_{Rz} remains slightly optimistic (i.e., too low). Under higher R_{mf}/R_w conditions (e.g., $R_{mf}/R_w \approx 100$), MHI_{Rz} is grossly optimistic.

Figure 6.19 illustrates movable hydrocarbon index calculated by the R_z method (MHI_{Rz}; Eq. 7). In this example, R_z at formation temperature was calculated using a default assumption for mixing factor (z) of 0.05 ("average" invasion depth). As expected, MHI_{Rz} values are greater than MHI_{std} values (see **Figure 6.18** for comparison); however, MHI_{Rz} remains less than 1.0 in the water-saturated interval. In some wells, MHI_{Rz} is found to be greater than 1.0 in the water-saturated interval. Ideally, MHI should equal 1.0 when $S_w = 1.0$.

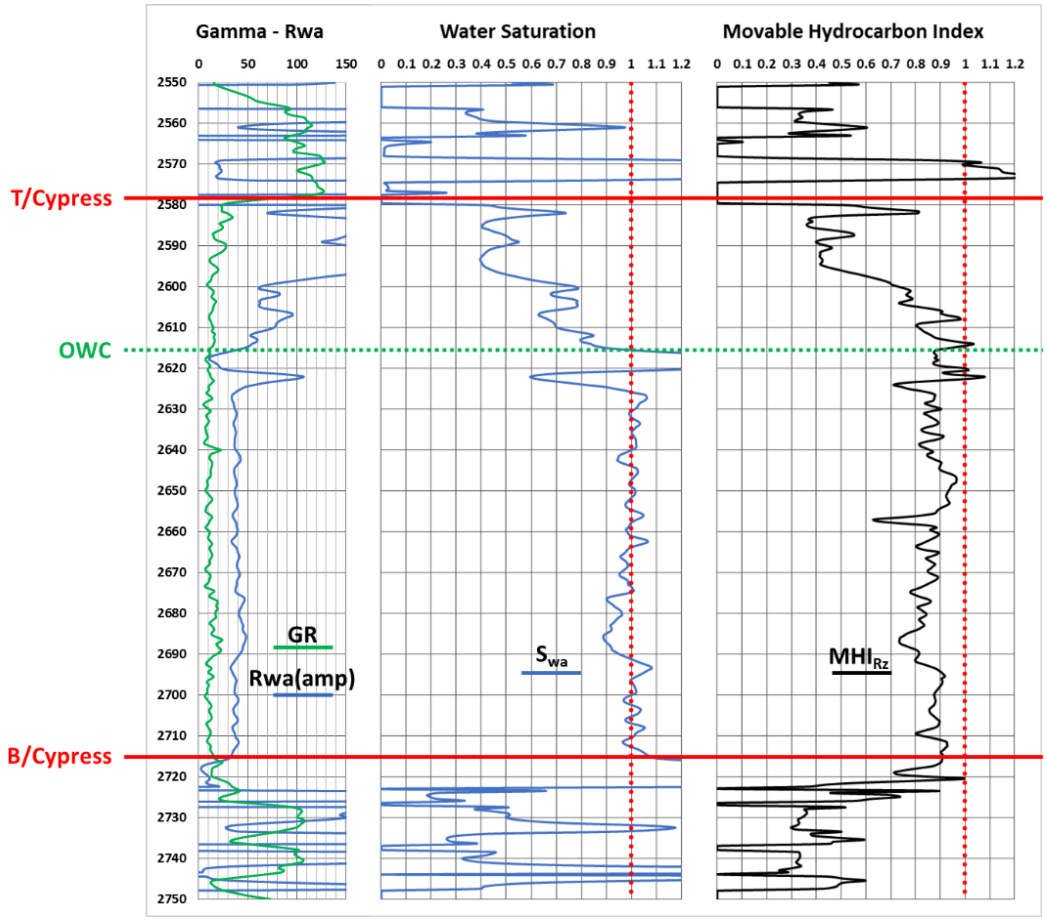

Figure 6.19. MHI_{Rz} response (right track) calculated by Equation 7, using header R_{mf}. = 1.967 Ωm @ T_f, R_w = 0.038 Ωm @ T_f, and default assumption of z = 0.05 ("average" invasion). Note that MHI_{Rz} remains less than 1.0 in the water-saturated interval. Data from Bourne #7 (API 12159256870), Noble Field.

R_{za} Method for Estimating MHI

When header-derived R_{mf}/R_w ratios vary considerably between wells (as is certainly the case in wells of this study), the result is similar variability of MHI responses between wells. Using MHI_{std} or MHI_{Rz} to define the POWC on an equal basis in multiple wells is not practical because the pick is dependent upon an individual well's R_{mf}/R_w ratio. In order to apply a common MHI cut-off for defining the POWC in multiple wells, the dependency of MHI upon R_{mf} must be eliminated. This is accomplished by determining a log-derived estimate of mixed water resistivity.

Apparent mixed water resistivity (R_{za}) is a log-derived estimate of mixed water resistivity and is determined by methods analogous to determining R_{wa}. In a water-saturated interval, Sw = 1.0 and MHI = 1.0. Therefore, assuming S_w = 1.0, R_{za} is estimated from the Archie equation by:

$$R_{za} = \frac{(\emptyset_t{}^m)\times R_{xo}}{a} \qquad \text{(Eq. 9)}$$

Where:
- $\emptyset_t$ = total porosity, estimated from neutron-density
- m = cementation exponent (2.0)
- R_{xo} = resistivity of the flushed zone
- a = tortuosity factor (1.0)

In that same water-saturated interval, and assuming MHI = 1.0, R_{za} can also be estimated from the ratio form of the MHI equation by:

$$R_{za} = \left(\frac{R_{xo}}{R_t}\right) \times R_w \qquad \text{(Eq. 10)}$$

Where: R_{xo} = resistivity of the flushed zone
R_t = resistivity of the uninvaded zone
R_w = resistivity of formation water at formation temperature

When plotted as continuous curves, both Archie R_{za} and Ratio R_{za} provide essentially equal responses in a water-saturated interval (**Figure 6.20**). A comparison of statistical values (e.g., median or mean) produced by both equations in the water-saturated interval permits a judicious determination of R_{za} at formation temperature.

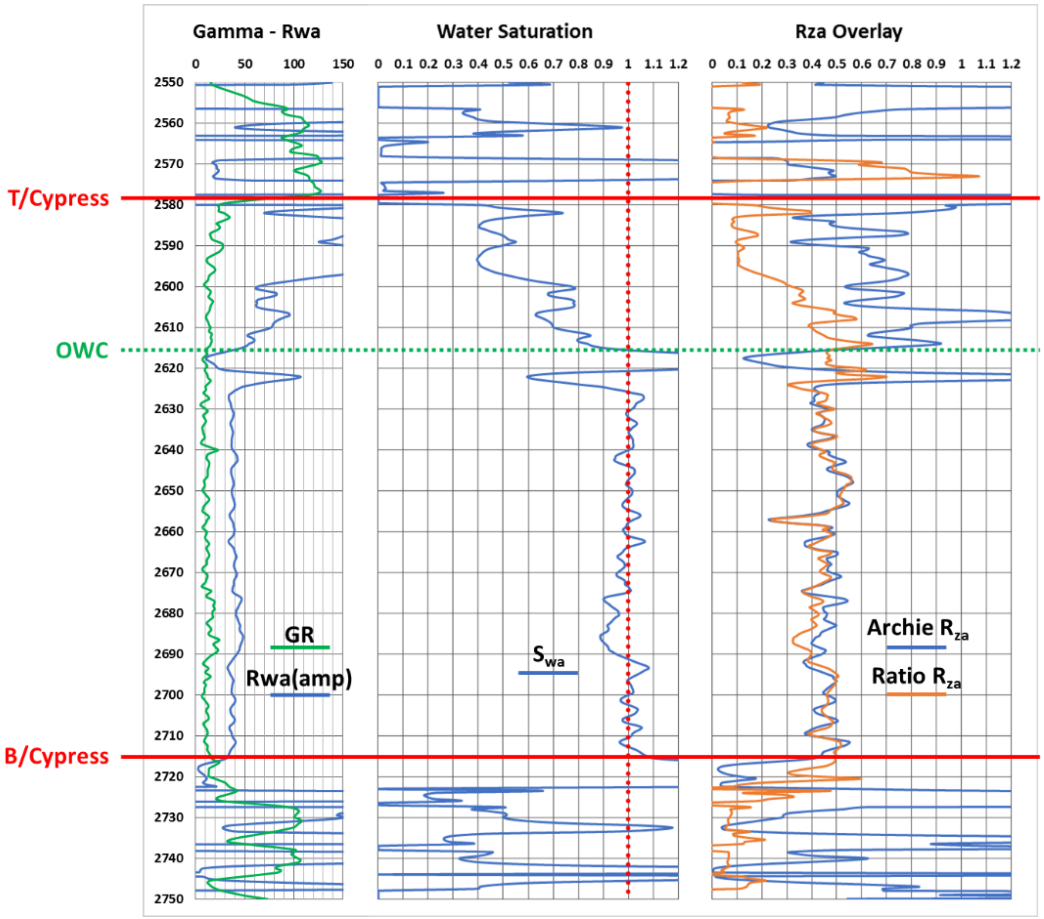

Figure 6.20. R_{za} overlay (right track) showing comparison of Archie R_{za} (Eq. 9) and Ratio R_{za} (Eq. 10). In the water-saturated interval (797-828 meters [2,616-2,715 feet]), median Archie R_{za} = 0.456 Ωm @ T_f and median Ratio R_{za} = 0.451 Ωm @ T_f. Data from Bourne #7 (API 121592568700), Noble Field.

A visual method analogous to the R_o-R_t overlay used for estimating R_{wa} can also be applied to determine R_{za}. Wet resistivity of the flushed zone (R_{oxo}) when saturated with a mixed water of given resistivity is calculated by:

$$R_{oxo} = \left(\frac{a}{\emptyset_t{}^m}\right) \times R_{brine} \qquad \text{(Eq. 11)}$$

Where: a = tortuosity factor (1.0)
$\emptyset_{nd}$ = total porosity, estimated from neutron-density
m = cementation exponent (2.0)
R_{brine} = resistivity of saturating brine at formation temperature

Using the condition $R_{brine} = R_{mf}$ at formation temperature as a starting point, R_{oxo} is calculated and plotted as a continuous curve with R_{xo} on a logarithmic track (**Figure 6.21**). R_{brine} is then varied until the R_{oxo} and R_{xo} curves overlay in the water-saturated interval. At that point, a static value of R_{za} at formation temperature is known. R_{za} determined by this visual method is very similar in value – though not necessarily equal – to statistical values of R_{za} resulting from the Archie (Eq. 9) and ratio (Eq. 10) solutions.

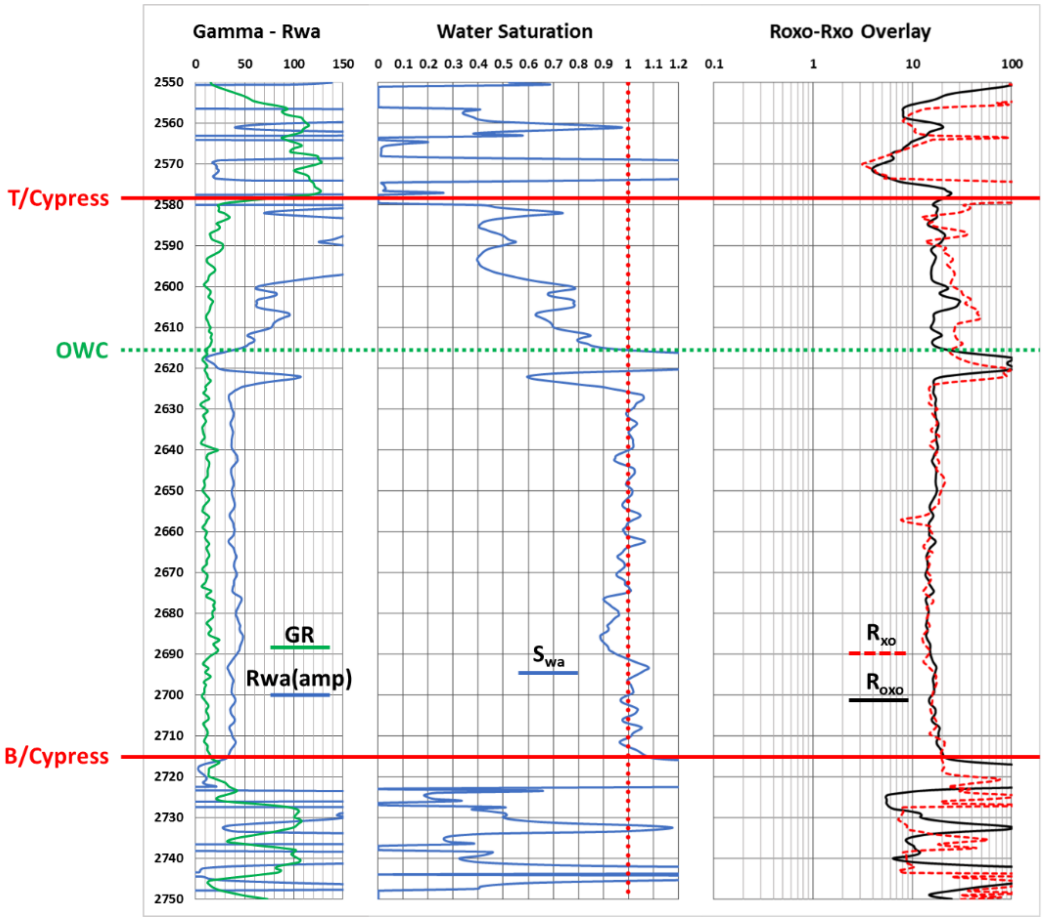

Figure 6.21. R_{oxo}-R_{xo} overlay for determining R_{za} at formation temperature. In the water-saturated interval (2,616-2,715 feet), R_{za} = 0.46 Ωm @ T_f is required for R_{oxo}-R_{xo} curve overlay, corresponding with median Archie R_{za} = 0.456 Ωm @ T_f and median Ratio R_{za} = 0.451 Ωm @ T_f. Data from Bourne #7 (API 121592568700), Noble Field.

Once an estimate of R_{za} at formation temperature is obtained by the preferred method, it is used to calculate an MHI response that is calibrated to equal 1.0 in the water-saturated interval. This final – or calibrated – MHI is calculated by:

$$MHI_{cal} = \left[\frac{R_{xo}/R_t}{R_{za}/R_w}\right]^{0.5} \quad \text{(Eq. 12)}$$

Where: R_{xo} = resistivity of the flushed zone
R_t = resistivity of the uninvaded zone
R_{za} = apparent resistivity of mixed water (log-derived) at formation temperature
R_w = resistivity of formation water at formation temperature

When MHI_{cal} is plotted as a continuous curve, it is approximately equal to 1.0 in a water-saturated interval (**Figure 6.22**). At the OWC where S_{wa} begins to decrease, MHI_{cal} often remains close to and may exceed 1.0 within the ROZ interval (if present). High values of MHI_{cal} in the ROZ interval are indications that oil is, indeed, residual.

For wells in this study, a common cut-off of MHI_{cal} = 0.8 was selected to define the POWC. Theoretically, any cut-off value (e.g., 0.7, 0.6) can be applied, thus resulting in similarly defined POWC elevations in multiple wells. Selecting a higher cut-off value yields slightly more conservative estimates of ROZ thickness.

A pronounced decrease in MHI_{cal} at the top of the ROZ interval, if present, correlates with the change in mobility that characterizes the POWC. When MHI is calibrated to the water-saturated interval in each well, a common fixed cut-off value can be applied to define the POWC in multiple wells. The POWC picked using the MHI_{cal} response may be slightly deep or shallow to a POWC pick based upon an uncalibrated response. In reservoirs where fluid contacts are known or thought to be tilted, such small differences can be critical, making a common criterion effective for mapping purposes.

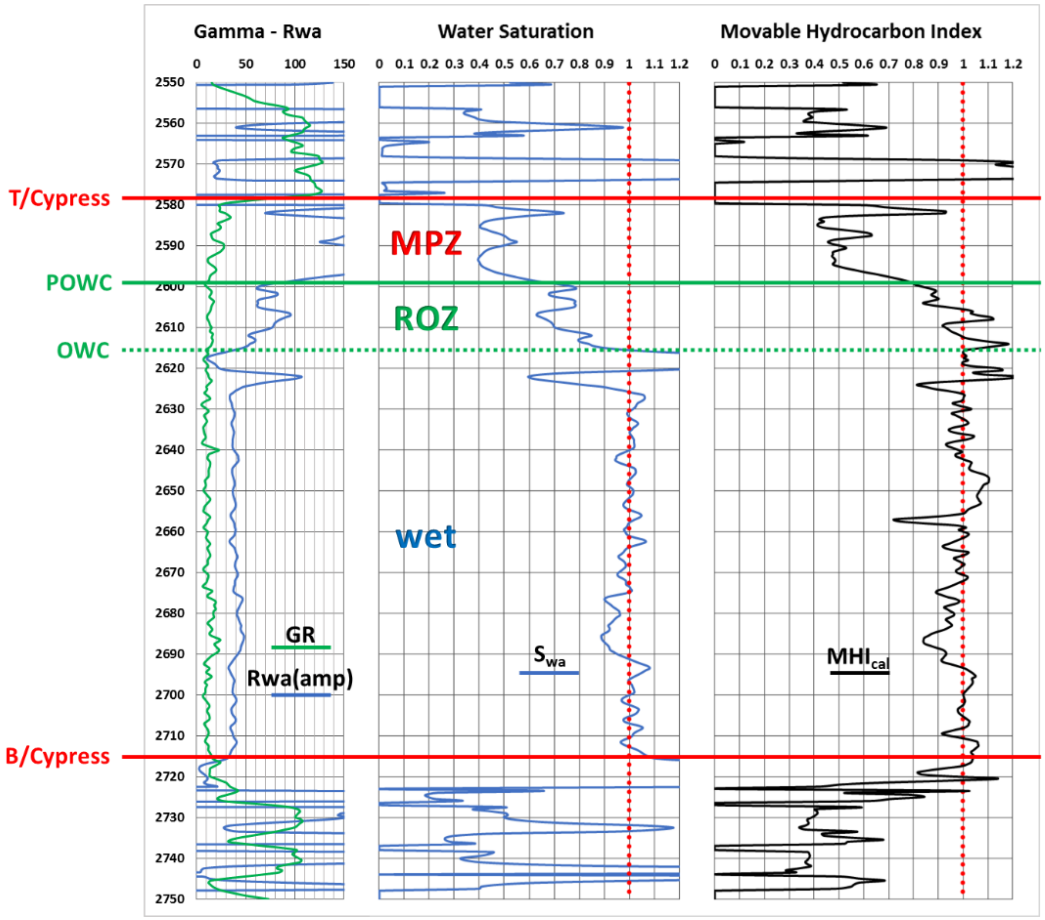

Figure 6.22. MHI_{cal} response (right track) calculated by Equation 12, using R_{za} = 0.46 Ωm @ T_f. Applying a fixed cut-off of MHI_{cal} = 0.8, the POWC is indicated at 792 m (2,599 feet). Note that MHI_{cal} values within the ROZ indicate hydrocarbon is mostly residual. Data from Bourne #7 (API 121592568700), Noble Field.

The most obvious advantage to the R_{za} method for estimating MHI_{cal} is its complete independence of a header R_{mf} value. The POWC can, therefore, be picked based upon a common MHI cut-off in each well without regard to an individual well's R_{mf}/R_w ratio. An additional advantage is that uncertainty resulting from the subjective assumption of mixing constant (z) is also eliminated. There are, of course, limitations to the R_{za} approach. The technique applied here is only valid for an Archie-type rock (i.e., clean, water-wet, and with effective porosity), of which the Thick Cypress sandstone is an example. Perhaps the greatest limitation involves the basis of the MHI calibration routine itself; there must be a water-saturated interval, preferably one contiguous with the overlying ROZ, and there must be a reasonable degree of confidence in a water resistivity (R_w) value.

6.2.4 Conclusions and Recommendations

The primary objective of this investigation was to evaluate methods and establish a process for identifying fluid contacts (producing oil-water contact, POWC, and original oil-water contact, OWC) in the Thick Cypress sandstone using conventional resistivity and porosity logs. Identifying those contacts, where present, permit a determination of whether a residual oil zone (ROZ) exists, its thickness, and its fluid saturations.

Conclusions of the study include the following:

- The Thick Cypress interval is, by all indications, an example of an Archie-type rock (i.e., clean, water-wet, and with effective porosity). Accordingly, results obtained from a standard Archie analysis (e.g., R_{wa}, S_{wa}, R_o) are expected to provide accurate results. Furthermore, the presence of a water-saturated interval in all wells makes such an analysis tenable.
- Apparent water resistivity (R_{wa}) calculated by the Archie method provides repeatable estimates of formation water resistivity in the Thick Cypress interval. Results are confirmed by historical data and pulsed neutron R_w analysis.
- The original oil-water contact (OWC) in the Thick Cypress interval can be defined based on products of a standard Archie evaluation, including apparent water resistivity (R_{wa}), Archie water saturation (S_{wa}), and wet resistivity (R_o). Wet resistivity is applied in a visual overlay technique (the R_o-R_t overlay) for identifying the OWC.
- For some wells, the microlog response provides an indication of the original oil-water contact (OWC).
- The producing oil-water contact (POWC) in the Thick Cypress interval can be identified using movable hydrocarbon index (MHI). However, because preliminary indications suggest R_{mf} (and, by proxy, R_m) values in most log headers are not accurate, a method of calculating MHI that is independent of R_{mf} is required.
- A log-derived value of apparent mixed water resistivity (R_{za}) can be determined for a water-saturated interval by three separate methods, all three of which produce very similar results. The methods of determining R_{za} are independent of a header R_{mf} value.
- Apparent mixed water resistivity (R_{za}) can be used to calculate a calibrated MHI response (MHI_{cal}) that meets the requirement MHI = 1.0 in a water-saturated interval. The method of determining MHI_{cal} is independent of a header R_{mf} value, and independent of a subjective assumption of mixing constant (z).
- Using MHI_{cal}, a common cut-off (here, MHI = 0.8) can be used to define the POWC on an equal basis in multiple wells.
- Apparent mixed water resistivity (R_{za}) can be used to calculate a value of resistivity-derived porosity ($\emptyset_{rxo}$) that is independent of R_{mf}, and which provides an additional method for identifying the original oil-water contact (OWC) in the Thick Cypress.
- Results of an evaluation performed using the described methodology indicate that a residual oil zone (ROZ) of variable thickness and variable quality (i.e., median oil saturation to water, S_o) is present in the Thick Cypress in many fields.

6.3 Regional Resource Assessment

6.3.1 Enhanced Oil Recovery and Associated Storage

Cypress ROZ Fairway

The Cypress Sandstone ROZ fairway is defined as the area of the Basin that, based on regional mapping and data analysis, has potential to contain ROZ prospects. The Cypress ROZ fairway is defined here as the preliminary boundaries of the Cypress ROZ play in the Illinois Basin. (A play is an oil and gas term describing a prospective trend of potential prospects, but which requires more data acquisition and/or evaluation in order to define specific leads or prospects.) Criteria for defining the Cypress Sandstone ROZ fairway included the presence of oil saturation indicators and sandstone of suitable reservoir quality (thickness, porosity) to host ROZs; for areas outside of the ROZ fairway, one or both of those criteria were not met. Though there is evidence, from historical records and well log analysis, that

ROZs are present within the fairway, ROZs are not expected to occur everywhere within the mapped area. Local variations in reservoir properties and structure exert a strong control on the occurrence of ROZs and petroleum traps in general. Several potential ROZ prospects were mapped within the ROZ fairway.

To define the boundaries of the ROZ fairway, Cypress oil indications were mapped and overlaid on regional structure maps of the top of the Karnak Limestone (below the Cypress) and the base of the Barlow Limestone (above the Cypress). Potential oil migration pathways were drawn on the map from the area of intense oil generation from the New Albany Shale in southeastern Illinois (c.f. Barrows and Cluff, 1984). The migration pathways were drawn to flow up structural dip and emanate from known faults. Because the thick, porous and permeable Cypress Sandstone is believed to have been a significant carrier bed for secondary petroleum migration in the Illinois Basin (Lewan et al., 2002), the sandstone thickness as well as distribution of oil saturation indicators and oil production was also used to guide the selection of the petroleum migration pathways. The fairway contained the various migration pathways, resulting in the area shown in **Figure 6.23**. The Cypress ROZ fairway is the area that is most likely to have had oil migrate through it and thus the most likely to contain residual oil.

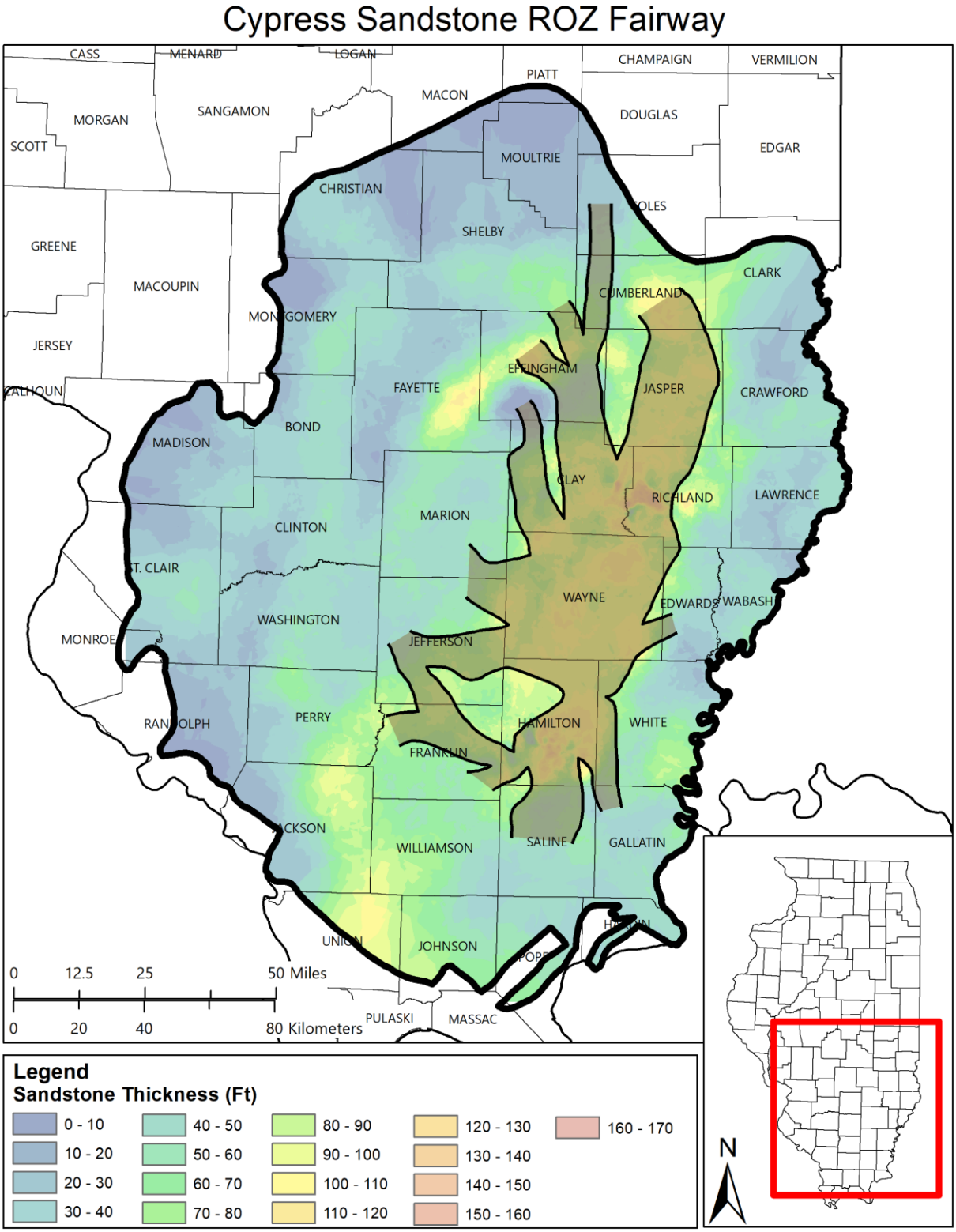

Figure 6.23. Cypress Sandstone ROZ fairway map.

Cypress ROZ Prospects

Cypress ROZ prospects are defined as areas within the ROZ fairway that meet the criteria of having a combination of well log analysis and historical records indicative of the presence of a ROZ. (Prospect is an oil and gas term used to for a potential oil and/or gas accumulation that is sufficiently well defined to represent a viable drilling target.) The ROZ prospects are considered discrete brown- or greenfields within the larger thick Cypress ROZ fairway. Prospects, by definition, are potential oil accumulations that must be evaluated by drilling to determine whether they contain commercial quantities of petroleum (AAPG Wiki). The ROZ prospects defined here are based on careful examination of a limited dataset. The prospects were delineated by grouping wells with historical indications of Cypress oil saturation (**Figure 6.8**) with wells in which well log analysis indicated ROZs (green and yellow dots in **Figure 6.10**). Structure and thickness maps are used to delineate the boundaries of the potential prospect, where appropriate; some prospects lack clearly defined structural closure. Site-specific research is required within a given prospect to evaluate whether the prospect has adequate potential to be developed.

Because many of the ROZ prospects were defined based on data from established oil fields, fewer data were available at the periphery or outside of oil fields to define the outer boundaries of the ROZ prospects. A total of 27 prospects were defined as part of this study (**Figure 6.24**). Most of the prospects are considered brownfield ROZs and underlie a main pay zone in the Cypress Sandstone. A few prospects, including Cumberland, Effingham, and Newton, are potential greenfield ROZ prospects with no associated Cypress main pay zone.

To quantify the regional ROZ resource, porosity, thickness, and residual oil saturation data derived from well log analysis were compiled for each prospect (**Table 6.2**). The thick Cypress Sandstone porosity ranges from 15% to 21%. Residual oil saturation (S_{or}) values range from 14 to 35% with an average of just over 23%, which is comparable to the lower end of the range of saturations observed in the Permian Basin ROZs. Overall ROZ thickness varies widely from 2.7 to 21.6 m (9 to 71 ft) with an average of 9.1 m (30 ft) thick.

The thickness and saturation parameters derived from well log analysis were used to estimate original oil in place (OOIP), from which the EOR and associated storage potential for each ROZ prospect could be determined. Many of the smaller prospects had only a single well from which logs were analyzed (**Table 6.3**), so the parameters from that well were used directly in the volumetric calculation for the prospect. Larger prospects had multiple wells whose logs were analyzed with the wells being unevenly distributed across the prospect. A method was therefore required to apply the parameter of a given analyzed well to only the area nearest to that we. A Voronoi map was generated in ArcGIS (Analysis Tools > Proximity > Create Thiessen Polygons) that partitioned the area covered by the analyzed wells into regions based on the distance to each well. The generated region for each analyzed well contains all points closer to that well than to any other well. The regions were clipped to the boundaries of the ROZ prospects (**Figure 6.25**) and the thickness, porosity, and saturation values for each well was then applied to the corresponding region. The OOIP values for the regions within each ROZ prospect were summed to get the resulting OOIP values for each prospect. An alternative method was applied for comparison by simply multiplying each prospects area, oil column thickness, average porosity, by median residual oil saturation plus and minus one standard deviation (23%, 30%, and 16%, respectively) as derived from the complete well log analysis dataset for the Basin. The residual oil saturations from the log analysis of all wells represents the range of likely residual oil saturation for the

entire thick Cypress Sandstone ROZ play and for each prospect (**Figure 6.26**). Estimations for OOIP within the ROZs in each prospect are reported in **Table 6.3**. Using the approach of relying on the nearest well log data, a total OOIP in the ROZ prospects is 290.8 million m^3 (1.8 billion barrels) of oil. Applying the regional statistics of S_{or} to the area, porosity, and thickness of each prospect gives a range of total OOIP in the ROZs from 207 to 382 million m^3 (1.3 to 2.4 billion barrels) of oil.

Determining the proportion of OOIP recoverable via CO_2-EOR and the amount of pore space available for the associated CO_2 storage was done by applying EOR factors to the estimated oil in place values and net CO_2 utilization factors to the cumulative volume of oil produced via EOR. Reservoir simulation studies of thick Cypress Sandstone at Noble Field (See Section 5.5) provided factors for CO_2-EOR and net CO_2 utilization for a range of injection scenarios. For this research, two of the example development strategies for Noble Field were used for the estimation; one that favors EOR and economic metrics from the MPZ only but has net carbon positive oil production (80-acre blanket WAG flood) and another that prioritizes CO_2 storage and economic metrics with NCNO (40-acre high CO_2 injection rate flood) (**Table 6.4**). The simulated cases assume miscible CO_2 injection. Reviewing the depth parameter of all the prospects (**Table 6.2**) shows that only three of the prospects fall within the depth range for immiscible CO_2 injection (<640 m (<2,100 ft); e.g., MGSC, 2005): Effingham, Patoka, and St. James. For those three prospects immiscible EOR (5.9%) and net CO_2 utilization (2.9 Mscf/stb) factors from MGSC (2005) were applied. For all other prospects the miscible factors derived from reservoir simulation of Noble Field were applied in calculating CO_2-EOR and CO_2 Storage. Results of the calculations are given in **Table 6.5**. In all, a total of 31.1 million m^3 (196 million barrels) of oil was calculated to be recoverable using the 80-acre blanket WAG flood whereas 21.3 million m^3 (144 million barrels) of oil is estimated to be recoverable using the 40-acre high CO_2 injection rate flood. Storage of CO_2 associated with EOR in these ROZ prospects alone, not accounting for associated main pay zones or underlying brine formation, is estimated to be 60.4 million tonnes and 10.4 billion tonnes for 80-acre blanket WAG flood and 40-acre high CO_2 injection rate flood, respectively.

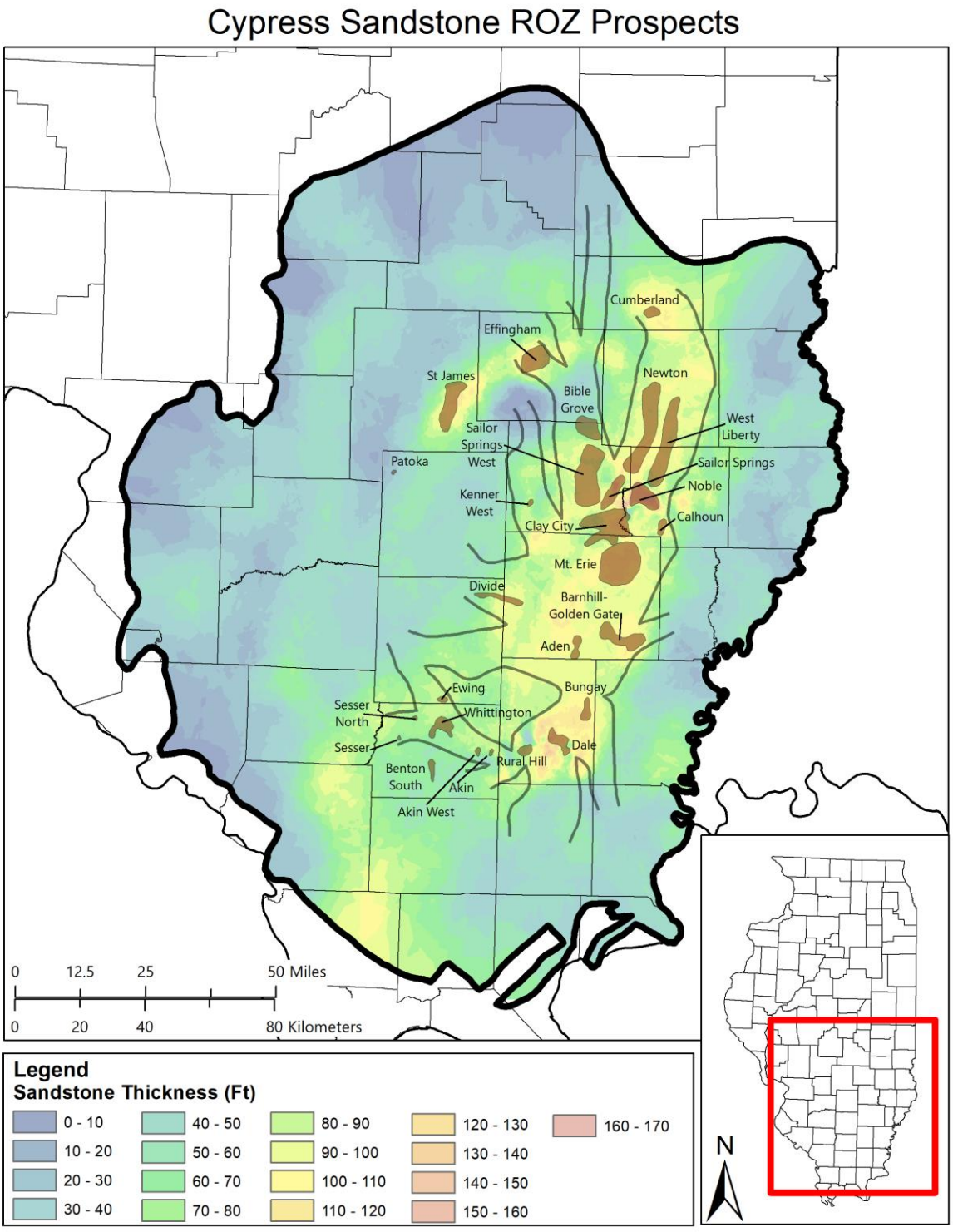

Figure 6.24. Map of potential ROZ prospects within the Cypress ROZ Fairway. The fairway boundaries are outlined in black and the prospects are shaded in brown. The prospect polygons are overlaid on the regional net isopach map.

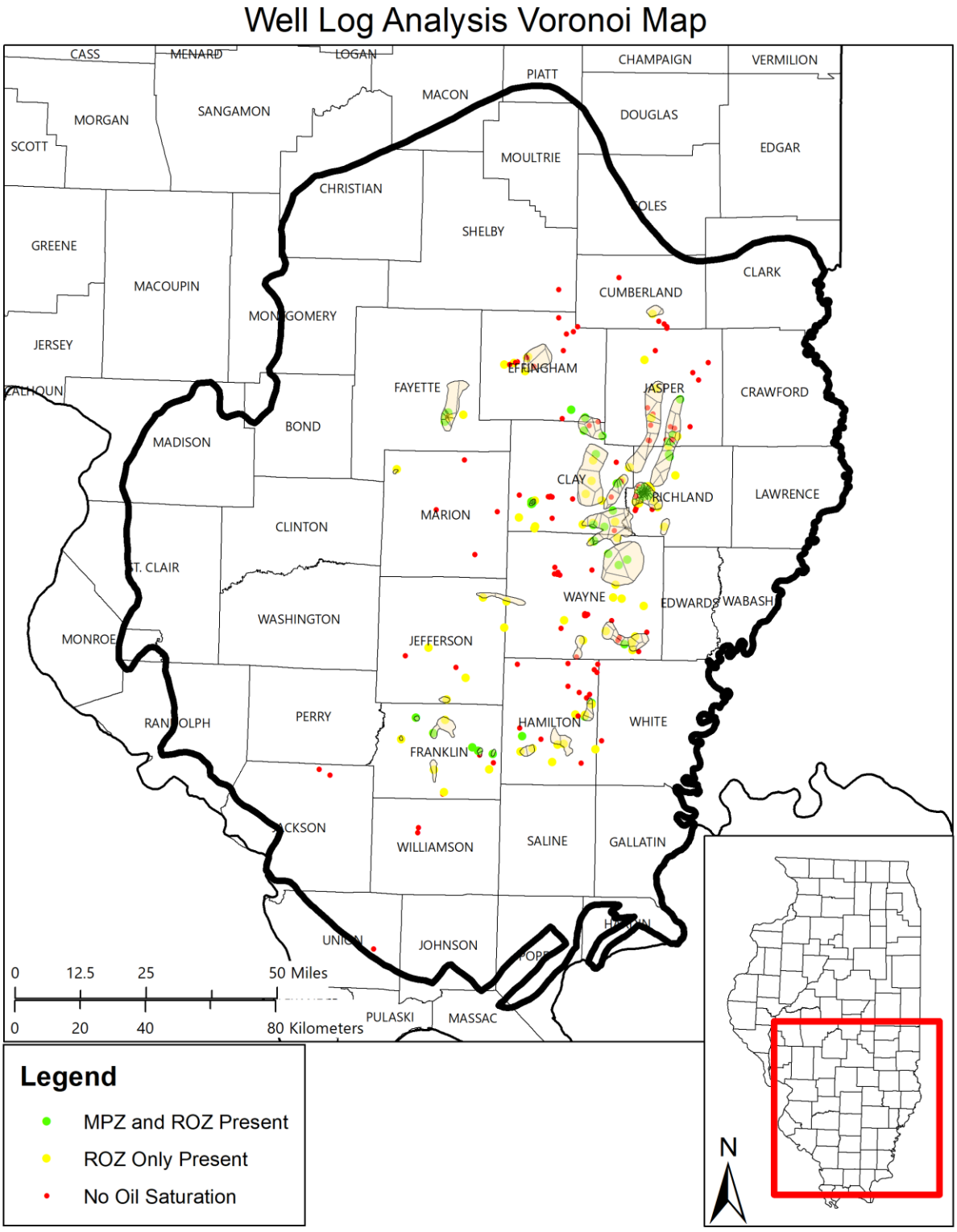

Figure 6.25. Voronoi map of regions generated based on well log analysis wells. Voronoi regions are colored in beige and are clipped within the Cypress ROZ prospects outlined in light black lines.

Table 6.2. Summary of statistics for each of the mapped ROZ prospects. Well count is the number of wells from which logs were analyzed within the boundary of a given potential prospect. The median and mean residual oil saturations (S_{or}) reported are within the ROZ. Map of labeled potential prospects is shown in ***Figure 6.24****.*

Prospect Name	Well Count	OWC Elevation (subsea m [ft])		OWC depth (m, ft)		Mean Porosity (%)	Median S_{or} (%)	Mean ROZ thickness (m, ft)	
Aden	1	-793.4	-2,603	909.5	2,984	19	26	16.5	54
Akin	1	-727.6	-2,387	874.8	2,870	16	30	4.6	15
Akin West	2	-680.3	-2,232	830.9	2,726	17	27	4.9	16
Barnhill-Golden Gate	5	-797.1	-2,615	928.1	3,045	17	26	12.5	41
Benton South	1	-629.7	-2,066	757.4	2,485	18	15	2.7	9
Bible Grove	4	-631.5	-2,072	794.9	2,608	17	24	6.7	22
Bungay	3	-789.4	-2,590	934.2	3,065	17	29	4.3	14
Calhoun	1	-733.7	-2,407	859.5	2,820	20	21	18.3	60
Clay City	13	-697.7	-2,289	836.1	2,743	17	22	6.1	20
Cumberland	1	-633.7	-2,079	794.6	2,607	17	20	21.6	71
Dale	1	-729.7	-2,394	846.1	2,776	14	18	4.9	16
Divide	2	-626.1	-2,054	781.8	2,565	19	28	6.4	21
Effingham	5	-447.8	-1,469	614.5	2,016	17	20	6.4	21
Ewing	1	-665.7	-2,184	797.1	2,615	16	35	8.5	28
Kenner West	9	-630.0	-2,067	794.6	2,607	17	28	10.7	35
Mt. Erie	4	-717.5	-2,354	849.2	2,786	19	21	10.7	35
Newton	6	-682.4	-2,239	841.2	2,760	17	18	8.2	27
Noble	95	-645.9	-2,119	796.1	2,612	17	24	8.5	28
Patoka	1	-258.2	-847	405.4	1,330	20	23	5.5	18
Rural Hill	2	-755.6	-2,479	905.0	2,969	15	19	11.6	38
Sailor Springs	4	-698.9	-2,293	833.6	2,735	17	16	3.7	12
Sailor Springs West	5	-672.1	-2,205	811.7	2,663	18	14	6.4	21
Sesser	1	-586.7	-1,925	729.1	2,392	17	19	13.1	43
Sesser North	1	-634.9	-2,083	793.7	2,604	21	35	15.5	51
St. James	16	-324.0	-1,063	503.2	1,651	19	27	14.3	47
West Liberty	12	-624.5	-2,049	775.1	2,543	17	24	6.7	22
Whittington	2	-633.7	-2,079	769.0	2,523	16	19	5.8	19

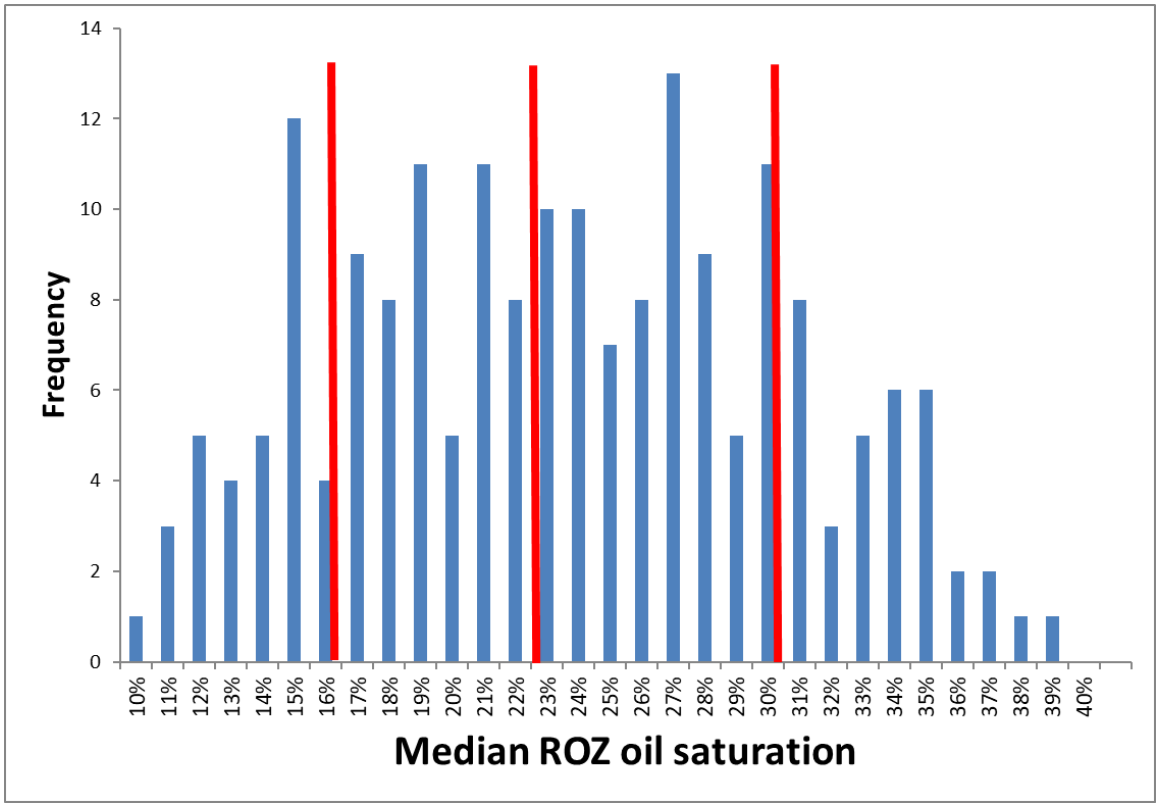

Figure 6.26. Probability distribution function of median residual oil saturation for 194 wells across the Basin that contained a ROZ. Median (23%) and standard deviations (16% and 30%) are shown with red lines.

Table 6.3. Estimated OOIP values for ROZs within each of the mapped prospects.

Prospect	OOIP median S_{or} (million m^3, MMstb)		OOIP 16% S_{or} (million m^3, MMstb)		OOIP 23% S_{or} (million m^3, MMstb)		OOIP 30% S_{or} (million m^3, MMstb)	
Aden	6.3	39.6	3.8	24.2	5.5	34.8	7.2	45.3
Akin	0.5	2.9	0.2	1.4	0.3	2.0	0.4	2.6
Akin West	0.7	4.4	0.4	2.7	0.6	3.8	0.8	5.0
Barnhill-Golden Gate	19.2	120.9	11.5	72.4	16.6	104.1	21.6	135.8
Benton South	0.7	4.1	0.7	4.4	1.0	6.4	1.3	8.3
Bible Grove	6.9	43.7	5.2	32.4	7.4	46.6	9.7	60.7
Bungay	5.9	37.1	2.9	18.3	4.2	26.4	5.5	34.4
Calhoun	7.5	47.1	5.8	36.2	8.3	52.0	10.8	67.8
Clay City	20.5	129.1	13.4	84.0	19.2	120.8	25.1	157.6
Cumberland	9.4	59.2	6.2	39.2	9.0	56.4	11.7	73.5
Dale	2.9	18.5	2.7	17.0	3.9	24.4	5.1	31.8
Divide	5.9	37.4	3.5	22.0	5.0	31.6	6.6	41.2
Effingham	6.6	41.8	5.5	34.7	7.9	49.9	10.4	65.1
Ewing	2.1	13.1	1.0	6.0	1.4	8.7	1.8	11.3
Kenner West	1.2	7.7	0.7	4.5	1.0	6.4	1.3	8.4
Mt. Erie	48.8	306.8	33.2	208.5	47.6	299.6	62.1	390.8
Newton	28.7	180.2	26.6	167.4	38.3	240.6	49.9	313.9
Noble	8.6	53.8	6.3	39.4	9.0	56.6	11.8	73.9
Patoka	0.3	2.0	0.2	1.4	0.3	2.0	0.4	2.7
Rural Hill	3.9	24.8	3.2	20.3	4.6	29.2	6.1	38.1
Sailor Springs	2.4	15.3	2.2	14.1	3.2	20.2	4.2	26.3
Sailor Springs West	21.0	131.9	24.2	152.5	34.9	219.2	45.5	285.9
Sesser	0.4	2.8	0.4	2.3	0.5	3.3	0.7	4.3
Sesser North	1.2	7.5	0.9	5.9	1.4	8.5	1.8	11.1
St James	23.3	146.3	17.6	110.7	25.3	159.1	33.0	207.5
West Liberty	28.2	177.1	18.7	117.7	26.9	169.2	35.1	220.7
Whittington	6.4	40.4	5.2	32.7	7.5	46.9	9.7	61.2
Totals	269.6	1,695.4	202.3	1,272.2	290.8	1,828.7	379.3	2,385.3

Table 6.4. CO_2-EOR and net utilization factors from two simulation cases that maximize EOR and storage (see Section 5.5) as well as for immiscible continuous CO_2 injection (e.g. MGSC, 2005).

Case	CO_2-EOR (%)	Net Utilization (Mscf/stb)
80-acre blanket WAG flood	11.4	6
40-acre high CO_2 injection rate flood	8.2	1479
Immiscible continuous CO_2 injection	5.4	2.9

*Table 6.5. CO_2-EOR and CO_2 Storage for the Cypress Sandstone ROZ prospects. An asterisk (*) next to the prospect name denotes prospects with ROZs that were shallower than the 640 m (2,100 ft) depth cutoff where the miscible EOR and storage factors were not applied. See **Table 6.4** to review the factors used in the calculations.*

		80-acre Blanket WAG Flood		40-acre High CO2 injection Rate Flood	
Prospect	**Oil in place (million m^3; Median S_{or}=23%)**	**CO_2-EOR (m^3)**	**CO_2 Storage (million tonnes)**	**CO_2-EOR (m^3)**	**CO_2 Storage (million tonnes)**
Aden	5.5	630,053	1.3	453,196	224
Akin	0.3	36,290	0.1	26,103	13
Akin West	0.6	69,250	0.1	49,811	25
Barnhill-Golden Gate	16.6	1,886,559	3.8	1,356,999	670
Benton South	1.0	115,161	0.2	82,835	41
Bible Grove	7.4	844,088	1.7	607,151	300
Bungay	4.2	477,995	1.0	343,821	170
Calhoun	8.3	942,028	1.9	677,599	334
Clay City	19.2	2,189,467	4.4	1,574,880	777
Cumberland	9.0	1,021,397	2.0	734,689	363
Dale	3.9	442,016	0.9	317,941	157
Divide	5.0	572,302	1.1	411,656	203
Effingham*	7.9	428,159	0.4	428,159	0
Ewing	1.4	157,584	0.3	113,350	56
Kenner West	1.0	116,659	0.2	83,912	41
Mt. Erie	47.6	5,430,822	10.9	3,906,381	1,927
Newton	38.3	4,361,106	8.7	3,136,936	1,548
Noble	9.0	1,026,535	2.1	738,384	364
Patoka*	0.3	17,530	0.0	17,530	0
Rural Hill	4.6	529,304	1.1	380,727	188
Sailor Springs	3.2	366,083	0.7	263,323	130
Sailor Springs West	34.9	3,972,551	8.0	2,857,449	1,410
Sesser	0.5	60,029	0.1	43,179	21
Sesser North	1.4	154,525	0.3	111,149	55
St. James*	25.3	1,365,853	1.3	1,365,853	0
West Liberty	26.9	3,066,861	6.1	2,205,988	1,088
Whittington	7.5	850,908	1.7	612,057	302
Totals	290.8	31,131,113	60.4	22,901,058	10,406

6.3.2 Results and Discussion

Basin-wide processes control the emplacement and later natural waterflooding of oil reservoirs required to form ROZs, but the occurrence and distribution of ROZs in a given geological formation is incumbent on local scale geologic heterogeneity. In the Cypress Sandstone, this heterogeneity includes changes in facies, vertical or lateral amalgamation of channel sandstone bodies, and sandstone thickness, and is therefore highly variable. In comparison with Permian Basin ROZs, which are hundreds of feet thick and occupy a thick succession of diagenetically altered carbonate rocks, the ROZs of the Cypress Sandstone are thinner (9.4 m [31 ft] on average) and occur within quartz sandstones that are up to about 53.3 m (175 ft) thick. The thickest observed oil column within the fluvial facies of the Cypress Sandstone occurs within Noble Field where 16.8 m (55 ft) of main pay zone is underlain by a ROZ that is 8.5 m (28 ft) thick, totaling 25.3 m (83 ft) of oil saturation. In some areas, well log analysis has indicated ROZs well over 15.2 m (50 ft) thick (**Table 6.2**). In these areas, the oil column can be 50% or more of the thickness of the porous and permeable formation. Notably, nowhere in the basin was the oil column found to occupy the entire thickness of the fluvial sandstone. For this to occur would mean that the entire formation, basin-wide without regard to local structure, was charged with oil, which seems impossible. This observation has implications for mapping the distribution and occurrence of ROZs within the Cypress ROZ play or analogous siliciclastic ROZ plays.

Compared to the diagenetic carbonate ROZs of the Permian Basin, channel sandstone bodies are easily defined in the subsurface and follow established predictable patterns of scale and orientation (Bridge and Tye, 2000). In the Cypress Sandstone, these channel sandstone bodies range in thickness from 4.6 to 19.8 m (15 to 65 ft) and are on the scale of a few to several kilometers in width (Webb and Grigsby, *in press*; Howell et al., *in prep*). The channel sandstone bodies amalgamate vertically and laterally within the fairway and are most prone to being oil bearing in areas where two or more channel elements are vertically amalgamated, forming a stratigraphic trap. The thickness of channel sandstone bodies and the nature of their amalgamation means that lateral changes in facies (e.g. from fluvial channel to muddy floodplain deposits) representing the loss of the upper amalgamated sandstone body can be the difference between having a main pay zone with an underlying ROZ to having only a thin ROZ. The thickness of ROZs observed in the Cypress is at the same order or magnitude as the thickness of channel sandstone bodies within the Cypress. Thus, the presence or absence of the uppermost channel sandstone body can be the difference between a ROZ being present or absent within a given potential prospect.

An understanding of these geologic controls on ROZ distribution, in combination with the increased data density in existing oil fields, makes the certainty of brownfield ROZs assessments greater. Residual oil is likely to extend beyond the boundaries of these oil fields where the local geology permits them and can often be constrained by leveraging the data availability (wells are often drilled at the periphery of oil fields to determine the extent of producible oil), and by extrapolating characteristics (such as general rock properties, residual oil saturation, oil water contact) from the properties of a well constrained oil field. Greenfield ROZs were identified in several wells. The lack of well data in greenfield areas makes the presence and boundaries of prospects within these fairways difficult to constrain, so estimates were made by using the lower limit of the area, thickness, and saturation for these prospects.

In general, oil migrates upwards through faults and laterally up structural dip. In the Illinois Basin, the hydrocarbon kitchen is in the deepest part of the basin in the southernmost part of the state. In general, the greatest concentration of ROZ prospects is in the northern part of the fairway. This may be the result up-dip migration to the north coupled with northward groundwater flow driven by the uplift of the Pascola Arch at the southwestern margin of the Illinois Basin during the Cretaceous Period (e.g. Bethke, 1986; Bethke and Marshak, 1990). Thick fluvial Cypress Sandstone extends to the

southwestern part of the state where it outcrops. The southernmost ROZ prospects in the fairway are found in southern Hamilton and Franklin Counties (**Figure 6.23**), 56.3 to 80.5 km (35 to 50 mi) northeast of the outcrop area. Well data is exceedingly limited in this area and the Cypress becomes progressively shallower, limiting its utility as a CO_2-EOR and storage resource, but the few wells that were analyzed in this area did not indicate oil saturation (**Figure 6.10**).

Based on the volumetric analyses presented here, 27 identified Cypress Sandstone ROZ prospects have approximately 290.8 million m^3 (1.8 billion barrels) of oil in place (S_{OR} = 23%). Applying two unique development strategies derived from reservoir simulation of the depleted main pay zone and ROZ in the Cypress Sandstone at Noble Field, 31.1 million m^3 (196 million barrels) of oil was calculated to be recoverable using the 80-acre blanket WAG flood (which favors EOR performance and is carbon positive) whereas 21.3 million m^3 (144 million barrels) of oil is estimated to be recoverable using the 40-acre high CO_2 injection rate flood (which favors storage performance and results in net carbon negative oil production). Storage of CO_2 associated with EOR in these ROZ prospects alone, not accounting for associated main pay zones or underlying brine formation, is estimated to be up to 10.4 billion tonnes if the latter development strategy is used in which CO_2 storage is prioritized.

Because ROZs represent areas that once hosted high oil saturations that have been swept away over geologic time, a discussion on the displaced oil is necessary. The Cypress Sandstone is truncated in the subsurface along its northern and western termini by younger Pennsylvanian strata along an angular unconformity, whereas the southern and eastern boundaries are exposed in outcrop. Given the presumed northward migration of oil within the Cypress, two possibilities emerge for the displaced oil: (1) oil migrated northward into up-dip Cypress strata that were subsequently eroded in the geologic past, and (2) oil migrated into Pennsylvanian strata in incised valleys and along faults in drape folded strata along the La Salle Anticline. These two possibilities are not mutually exclusive and both likely occurred. The former contention is supported by the fact that the Cumberland ROZ prospect, a greenfield, has a 21.6 m(71 ft) thick oil column and exists near the northeastern erosional boundary of the Cypress Sandstone. Continued up-dip oil migration to the northeast would have likely been eventually met with a stratigraphic pinch out of the Cypress sandstone which would have the natural location for oil to accumulate. The latter contention is supported by the pattern of Pennsylvanian oil production in the Illinois Basin. The most significant area of Pennsylvanian oil production occurs along the La Salle Anticline where deep valleys at the systemic unconformity juxtapose porous and permeable Pennsylvanian sandstone with thick fluvial Cypress sandstone. Greb (1988) suggested this model to explain the occurrence of oil generally within Pennsylvanian incised valley fill deposits.

7. Conclusions

A prospective ROZ resource has been identified within the thick, fluvial facies of the Cypress Sandstone. Based on well log analyses, 27 brownfield and greenfield ROZ prospects have been defined with 290.8 million m^3 (1.8 billion barrels) of oil in place (assuming a S_{OR} of 23%). Residual oil saturation (S_{OR}) values range from 14 to 35% and the thickness of ROZs in the prospects varies from 2.7 to 21.6 m (9 to 71 ft) thick.

Characterization of the geology of the Cypress Sandstone showed that it consists of multistory fluvial sandstone. At the regional scale, thick Cypress Sandstone porosity is 15% to 21% and horizontal and vertical permeability up to approximately 0.98 μm^2 (1,000 mD). Where multiple sandstone stories amalgamate (e.g. in Noble Field), they create thick, relatively widespread sandstone bodies that have characteristics (e.g. high lateral and vertical permeability, limited compartmentalization, and large pore volumes) favorable for CO_2 storage.

A well log analysis methodology was developed to identify the producing oil-water contact and the oil-water contact, respectively using a combination of established techniques (SW, BVW, MHI, RWA) to identify and characterize ROZs. At the Noble Field, the methodology identified a ROZ (approximately 6.1 m thick interval of 25% residual oil saturation) beneath the MPZ and was validated by comparing oil water contacts to newly collected pulsed neutron logs and historical information (such as oil shows and perforation depths).

The choice of specific development strategies depends on the goals of the project (prioritizing EOR performance vs. storage performance and NCNO) and geologic setting (brownfield vs greenfield), and company's business strategies (economic metrics). As such, this research highlighted three example development strategies for Noble Field:

- EOR, CO_2 storage, and economic metrics with NCNO: 80-acre, MPZ and ROZ injection, continuous high injection rate strategy
- EOR and economic metrics from the MPZ only but has net carbon positive oil production: 80-acre, MPZ only, WAG strategy
- CO_2 storage and economic metrics with NCNO: 40-acre, ROZ only, continuous high injection rate strategy

For the ROZ prospects identified, 31.1 million m^3 (196 million barrels) of oil is estimated to be recoverable using the 80-acre blanket WAG development strategy (which favors EOR and economic metrics, but is carbon positive) whereas 21.3 million m^3 (144 million barrels) of oil is estimated to be recoverable using the 40-acre high CO_2 injection rate development strategy (which favors storage and economic metrics and results in net carbon negative oil production). Storage of CO_2 associated with EOR in these ROZ prospects alone, not accounting for associated main pay zones or underlying brine formation, is estimated to be up to 10.4 billion tonnes.

8. Acknowledgements

This project (DE-FE0024431) was funded by the U.S. Department of Energy through the National Energy Technology Laboratory (NETL). Through a university grant program, IHS software (Petra) was used for geologic modeling and Landmark software (Nexus) was used for the reservoir modeling and simulation in this project.

Appendix A – References

Abrams, R. H., 1995, Long-range buoyancy-driven oil migration in the Illinois Basin: Stanford University, 79 p.

Adams, W.W., 1957, Geology of Loudon Oil Field, Fayette and Effingham Counties, Illinois: Report by the Carter Oil Company, St. Elmo, Illinois, 109 p.

Al Adassani, A., B. Bai, 2011, Analysis of EOR projects and updated screening criteria, Journal of Petroleum Science Engineering 79, p. 10—24.

Allen, J.R.L., 1982, Sedimentary Structures: Their Character and Physical Basis, in Developments in Sedimentology, p. 169.

Allen, J.R.L., 1963, Sedimentation to the lee of small underwater sand waves: An experimental study: Journal of Geology, v. 73, p. 95–116.

Allen, J.R.L., 1970, Studies in fluviatile sedimentation: a comparison of fining-upwards cyclothems, with special reference to coarse-member composition and interpretation: Journal of Sedimentary Petrology, v. 40, p. 298–323.

Allen, J.R.L., and Leeder, M.R., 1980, Criteria for the instability of upper-stage plane beds: Sedimentology, p. 209–217.

Ambers, C.P., and Petzold, D.D., 1992, Ephemeral arid exposure during deposition of the Elwren Formation (Chesterian) in Indiana, in Horowitz, A.S. and Dodd, J.R. eds., Chesterian Sections (Late Mississippian) Along Interstate 64 in Southern Indiana, p. 98–145.

Archie, G. E., 1942, The Electrical Resistivity Log as an Aid in Determining Some Reservoir Characteristics: Transactions of the AIME, v. 146, no. 01, p. 54–62, doi:10.2118/942054-G.

Asquith, G., 1985, COMBINING TECHNIQUES: 22-28 p.

Asquith, G., and C. Gibson, 1982, Basic Well Log Analysis for Geologists, AAPG Methods in Exploration

Asquith, G., and D. Krygowski, 2004, Basic Relationships of Well Log Interpretation: Basic Well Log Analysis, AAPG Methods in Exploration, v. 16, p. 1–20.

Baas, J.H., 2004, Conditions for formation of massive turbiditic sandstones by primary depositional processes: v. 166, p. 293–310, doi: 10.1016/j.sedgeo.2004.01.011.

Baas, J.H., and Best, J.L., 2002, Turbulence modulation in clay-rich sediment-laden flows and some implicaitons for sediment deposition: Journal of Sedimentary Research, v. 72, p. 336–340.

Baas, J.H., Best, J.L., Peakall, J., and Wang, M.I., 2009, A phase diagram for turbulent, transitional, and laminar clay suspension flows: Journal of Sedimentary Research, v. 79, p. 162–183, doi: 10.2110/jsr.2009.025.

Bachu, S., 2016, Identification of oil reservoirs suitable for co2-EOR and CO2 storage (CCUS) using reserves databases, with application to Alberta, Canada. International Journal of Greenhouse Gas Control 44, p. 152—165.

Barrows, M. H., and R. M. Cluff, 1984, New Albany Shale Group (Devonian-Mississippian) source rocks and hydrocarbon generation in the Illinois basin, in G. Demaison, and R. J. Murris, eds., Petroleum Geochemistry and Basin Evaluation: Tulsa, Oklahoma, American Association of Petroleum Geologists, p. 111–138.

Beerbower, J. R., 1964, Cyclothems and cyclic depositional mechanisms in alluvial plain sedimentation, in D.F. Merriam, ed., Symposium on cyclic sedimentation: Kansas Geological Survey, p. 31–42.

Bell, A. H., 1938, Oil and gas development in Illinois in 1937: Urbana, IL, Illinois State Geological Survey, 20 p.

Bell, A.H., 1939, The new Centralia Oil Field: Illinois State Geological Survey, Circular 55, 4 p.

Van den Berg, J.H., Boersma, J.R., and van Gelder, A., 2007, Diagnostic sedimentary structures of the fluvial-tidal transition zone – Evidence from deposits of the Rhine and Meuse: Netherlands Journal of Geosciences, p. 287–306.

Best, J.L., 2005, The fluid dynamics of river dunes: a review and some future research directions: Journal of Geophysical Research: Earth Surface, v. 110, p. 1–21, doi: 10.1029/2004JF000218.

Best, J.L., Ashworth, P.J., Bristow, C.S., and Roden, J., 2003, Three-dimensional sedimentary architecture of a large, mid-channel sand braid bar, Jamuna River, Bangladesh: Journal of Sedimentary Research==, v. 74, p. 516–530.

Best, J.L., and Bridge, J., 1992, The morphology and dynamics of low amplitude bedwaves upon upper stage plane beds and the preservation of planar laminae: Sedimentology, p. 737–752.

Best, J.L., and Kostaschuk, R., 2002, An experimental study of turbulent flow over a low-angle dune: Journal of Geophysical Research, v. 107, p. 18–1–18–9, doi: 10.1029/2000JC000294.

Bethke, C.M; Geochemical and Biogeochemical Reaction Modeling. New York: Oxford University Press; 2008.

Bethke, C., J. Reed, and D. Oltz, 1991, Long-range petroleum migration in the Illinois Basin: AAPG Bulletin, v. 75, no. 5, p. 925–945.

Bhattacharya, J.P., and Tye, R.S., 2004, Searching for modern Ferron analogs and application to subsurface interpretation, in Chidsey, T. C., J., Adams, R.D., and Morris, T.H. eds., The Fluvial-Deltaic Ferron Sandstone: Regional to Wellbore Analog for Fluvial_Deltaic Reservoir Modeling, American Association of Petroleum Geologists, Studies in Geology, p. 38–57.

Bhattacharyya, A., 1993, Proterozoic braided ephemeral fluvial deposits: an example from the Dhandraul Sandstone Formation of the Kaimur Group, Son Valley, central India: v. 84, p. 101–114.

Bhattacharyya, P., Bhattacharya, J.P., and Khan, S.D., 2015, Paleo-channel reconstruction and grain size variability in fl uvial deposits, Ferron Sandstone, Notom Delta, Hanksville , Utah: Sedimentary Geology, v. 325, p. 17–25, doi: 10.1016/j.sedgeo.2015.05.001.

Blatchley, R. S., 1913, The Oil Fields of Crawford and Lawrence Counties: Urbana, IL, Illinois State Geological Survey, Bulletin, 442 p.

Blunt, M., F.J. Fayers, and F.M. Orr Jr, 1993, Carbon dioxide in enhanced oil recovery: Energy Conversion and Management, v. 34, no. 9–11, p. 1197—1204.

Bradley, R.W., and Venditti, J.G., 2017, Reevaluating dune scaling relations: Earth-Science Reviews, v. 165, p. 356–376, doi: 10.1016/j.earscirev.2016.11.004.

Bragg, J. R., W.W. Gale, W.A. McElhannon, O.W. Davenport, M.D. Petrichuk, and T.L. Ashcraft, 1982, Loudon Surfactant Flood Pilot Test: Paper SPE-10862-MS presented at the SPE Enhanced Oil Recovery Symposium, Tulsa, Oklahoma, April 4–7.

Braile, L. W., W. J. Hinze, G. R. Keller, E. G. Lidiak, and J. L. Sexton, 1986, Tectonic development of the New Madrid rift complex, Mississippi embayment, North America: Tectonophysics, v. 131, no. 1–2, p. 1–21, doi:10.1016/0040-1951(86)90265-9.

Bridge, J.S., and Best, J.L., 1988, Flow, sediment transport and bedform dynamics over the transition from dunes to upper stage plane beds: Sedimentology, v. 35, p. 753–764.

Bridge, J., and R. Tye, 2000, Interpreting the dimensions of ancient fluvial channel bars, channels, and channel belts from wireline-logs and cores: AAPG bulletin.

Bristow, C.S., 1993, Sedimentary structures exposed in bar tops in the Brahmaputra River , Bangladesh, in Best, J.L. and Bristow, C.S. eds., Braided Rivers, Geological Society of London, p. 277–289.

Brock, W. R., and L. A. Bryan, 1989, Summary Results of CO2 EOR Field Tests, 1972-1987: Low Permeability Reservoirs Symposium, doi:10.2118/18977-MS.

Brownfield, R.L., 1954, Structural history of the Centralia area: Illinois State Geological Survey, Report of Investigations, 31 p.

Burton-Kelly, M. E., N. W. Dotzenrod, I. K. Foele, A. J. Gorz, S. C. Ayash, and W. D. Peck, 2014, IDENTIFICATION OF RESIDUAL OIL ZONES IN THE WILLISTON AND POWDER RIVER BASINS: LITERATURE REVIEW SUMMARY Deliverable 5.

Burton-Kelly, M. E., N. W. Dotzenrod, I. K. Feole, W. D. Peck, and S. C. Ayash, 2017, High-level Screening for Williston Basin Residual Oil Zones Using Location-independent Data: Energy Procedia, v. 114, no. November 2016, p. 3518–3527, doi:10.1016/j.egypro.2017.03.1481.

Cachine, J. M., 2003, Reservoir characterization of the Cypress Sandstone at Centralia Field, Clinton County, Illinois: University of Illinois at Urbana-Champaign, senior thesis.

Cecil, C. B., 1990, Paleoclimate controls on stratigraphic repetition of chemical and siliciclastic rocks: Geology, v. 18, p. 533–536. doi: 10.1130/0091-7613(1990)018<0533:PCOSRO>2.3.CO;2.

Chang, M. M., N. L. Maerefat, L. Tomutsa, and M. M. Honarpour, 1988, Evaluation and Comparison of Residual Oil Saturation Determination Techniques: SPE Formation Evaluation, doi:10.2118/14887-PA.

Chapin, M.A., Brandon, N.W., Ugueto, G., and Govert, A., 2014, Sedimentology and reservoir characterization of the Upper Cretaceous Lance and Upper Mesaverde intervals from core data in Pinedale Field, Wyoming, in Longman, M., Kneller, S., Meyer, T., and Chapin, M. eds., Pinedale Field: Case study of a giant tight gas sandstone reservoir: AAPG Memoirs, v. 107, p. 175–245, doi: 10.1306/13511891M1071510.

Chapman, J. J., 1953, Sand distribution in the Cypress Formation, Clay County and vicinity, Illinois: University of Illinois at Urbana-Champaign, Ph.D. Thesis, 47 p.

Chen, B., H. Huang, Y. Zhang, L. Wang, S. Ren, A. Huang and P. Sun, 2013. An Improved Predicting Model for Minimum Miscibility Pressure (MMP) of CO2 and Crude Oil, Journal of Oil and Gas Technology, 35(2), 126-130.

Cisneros, J., and Best, J., 2016, Low-angle dunes in big rivers: morphology, occurrence and speculations on their origin, in Landeghem, K.J.., Garlan, T., and Baas, J.. eds., Marine and River Dune Dynamics Conference 5, Caernarfon, United Kingdom, Bangor University and SHOM, p. 37–40, http://maridv.bangor.ac.uk/documents/Book_abstracts_MARIDV_2016_000.pdf.

Clavier, C., G. Coates, and J. Dumanoir, 1984, Theoretical and Experimental Bases for the Dual-Water Model for Interpretation of Shaly Sands: Society of Petroleum Engineers Journal, v. 24, no. 02, p. 153–168, doi:10.2118/6859-PA.

Cluff, R. M., and Z. Lasemi, 1980, Paleochannel across Louden Anticline, Fayette County, Illinois: Illinois Institute of Natural Resources, Illinois Petroleum 119, p. 21.

Cluff, R. M., and A. P. Byrnes, 1991, Lopatin Analyses of Maturation and Petroleum Generation in the Illinois Basin, in M. W. Leighton, D. R. Kolata, D. F. Oltz, and J. J. Eidel, eds., Interior Cratonic Basins: American Association of Petroleum Geologists, p. 425–454.

Cole, R.D. and Nelson, W.J., 1995, Stratigraphic Framework and Environments of Deposition of the Cypress Formation in the Outcrop Belt of Southern Illinois. Illinois State Geological Survey. 47 p.

Cotter, E., and Graham, J.R., 1991, Coastal plain sedimentation in the late Devonian of southern Ireland; hummocky cross-stratification in fluvial deposits? Sedimentary Geology, v. 72, p. 201–224.

Craig, L., C. Connor, and A. Armstrong, 1979, Paleotectonic investigations of the Mississippian System in the United States.

Craig, L.C., and Varnes, K.L., 1979, History of the Mississippian System - an interpretive summary, in L. C. Craig, C. W. Conner, et al., E. ed., Paleotectonic investigations of the Mississippian in the United States - part II, interpretive summary and special features of the MIssissippian System: U.S. Geological Survey Professional Paper 1010, United States Geological Survey, p. 371–406.

Demir, I., 1995, Formation Water Chemistry and Modeling of Fluid-Rock Interaction for Improved Oil Recovery in Aux Vases and Cypress Formations, Illinois Basin.

Devera, J. A., W. J. Nelson, and R. D. Norby, 2011, Middle Devonian Series through Mississippian System, in D. R. Kolata, and C. Nimz, eds., Geology of Illinois: Illinois State Geological Survey, p. 167–186.

Dickey, P.A. and Andresen K.H., 1946, “Selection of Pressure Water Flooding Various Reservoirs”, Drilling and Production Practice, American Petroleum Institute.

DOE, 2012, 2012 United States Carbon Utilization and Storage Atlas: 130 p.

Driese, S.G., and Ober, E.G., 2005, Paleopedologic and paleohydrologic records of precipitation seasonality from Early Pennsylvanian “underclay” paleosols, U.S.A.: Journal of Sedimentary Research, v. 75, p. 977–1010.

Easton, W.H., 1943, Subsurface structure and oil possibilities of parts of Edwards, Richland, and Wabash Counties, Illinois: Illinois State Geological Survey, Illinois Petroleum 46, 13 p.

Ebanks, W.J., 1987, Geology in enhanced oil recovery, in Tillman, R.W. and Weber, K.J. eds., Reservoir Sedimentology, SEPM (Society for Sedimentary Geology), p. 1–14.

Ebanks, W.J.J., Scheihing, M.H., and Atkinson, C.D., 1992, Flow units for reservoir characterization: Part 6 geological methods, in Morton-Thompson, D. and Woods, A.M. eds., Development Geology Reference Manual, American Association of Petroleum Geologists, p. 282–285.

Englemann, H., 1863, On the Lower Carboniferous System as Developed in Southern Illinois: Transactions of the Academy of Science of St. Louis, v. 2, no. 1, p. 188-190

Fielding, C.R., 2008, Sedimentology and Stratigraphy of Large River Deposits: Recognition in the Ancient Record, and Distinction from “Incised Valley Fills”: Large Rivers: Geomorphology and Management, p. 97–113, doi: 10.1002/9780470723722.ch7.

Fielding, C.R., 2006, Upper flow regime sheets , lenses and scour fills : Extending the range of architectural elements for fluvial sediment bodies: Sedimentary Geology, v. 190, p. 227–240, doi: 10.1016/j.sedgeo.2006.05.009.

Fituri, H. S., 1987, Study of Selected Sandstone Reservoirs in the Indiana Portion of the Griffin Consolidated Field that lies above New Harmony: Indiana University, M.S. Thesis, 167 p.

Flemming, B.W., 2000, The role of grain size, water depth and flow velocity as scaling factors controlling the size of subaqueous dunes, in Trentensaux, A. and Garlan, T. eds., Marine Sandwave Dynamics, International Workshop, University of Lille 1, France, p. 55–61.

Fox, M.E., 1957, Waterflood operations, Loudon Pool, Illinois: Paper SPE-938-G presented at the Fall Meeting of the Society of Petroleum Engineers of AIME, Dallas, Texas, October 6–9.

Frailey, S. M., I. G. Krapac, J. R. Damico, R. T. Okwen, and R. W. McKaskle, 2012, CO2 Storage and Enhanced Oil Recovery: Bald Unit Test Site , Mumford Hills Oil Field, Posey County, Indiana: 172 p.

Fredsøe, J., 1981, Unsteady flow in straight alluvials streams. Part 2. Transition from dunes to plane bed: Journal of Fluid Mechanics, v. 102, p. 431–453.

Galeazzi, C.P., Almeida, R.P., Mazoca, C.E.M., Best, J.L., Freitas, B.T., Ianniruberto, M., Cisneros, J., and Tamura, L.N., 2018, The significance of superimposed dunes in the Amazon River: Implications for how large rivers are identified in the rock record: Sedimentology, doi: 10.1111/sed.12471.

George, C.J., and Stiles, L.H., 1978, Improved techniques for evaluating carbonate waterfloods in West Texas: Journal of Petroleum Technology, v. 30, p. 1547–1554.

Greb, S. F., 1988, Hydrocarbon production from the sub-Pennsylvanian paleovalleys of western Kentucky.

Grigsby, N. P. and S. M. Frailey, in prep, Methodology for Using Well Logs to Identify Residual Oil Zones in Siliciclastic Formations: An Example from Noble Field

Grube, J. P., 1992, Reservoir Characterization and Improved Oil Recovery from Multiple Bar Sandstones, Cypress Formation, Tamaroa and Tamaroa South Fields, Perry County, Illinois: Illinois State Geological Survey, Illinois Petroleum 138, 49 p.

Grube, J.P., and Frankie, W.T., 1999, Reservoir characterization and application improved oil recovery from the Cypress Formation (Mississippian) at Richview Field, Washington County, Illinois: Illinois State Geological Survey, Illinois Petroleum 155, 39 p.

Harouaka, A., B. Trentham, and S. Melzer, 2013, Long overlooked residual oil zones (ROZ's) are brought to the limelight, in Society of Petroleum Engineers - SPE Canadian Unconventional Resources Conference 2013 - Unconventional Becoming Conventional: Lessons Learned and New Innovations: Society of Petroleum Engineers, p. 972–980.

Hendershot, M.L., Venditti, J.G., and Bradley, R.W., 2016, Response of low-angle dunes to variable flow: Sed, v. 63, p. 743–760, doi: 10.1111/sed.12236.

Herbert, C.M., Alexander, J., and Martinez de Alvaro, M.J., 2015, Back-flow ripples in troughs downstream of unit bars: Formation, preservation and value for interpreting flow conditions: Sedimentology, v. 62, p. 1814–1836, doi: 10.1111/sed.12203.

Honarpour, M. M., N. R. Nagarajan, A. Grijalba Cuenca, M. Valle, and K. Adesoye, 2010, Rock-Fluid Characterization for Miscible CO2 Injection: Residual Oil Zone, Seminole Field, Permian Basin, in SPE Annual Technical Conference and Exhibition: Society of Petroleum Engineers, doi:10.2118/133089-MS.

Hill, Bruce, Susan Hovorka, and Steve Melzer. 2013. “Geologic Carbon Storage Through Enhanced Oil Recovery.” *Energy Procedia* 37: 6808—6830. doi:10.1016/j.egypro.2013.06.614.

Hjellbakk, A., 1997, Facies and fluvial architecture of a high-energy braided river: the Upper Proterozoic Seglodden Member, Varanger Peninsula, northern Norway: Sedimentary Geology, v. 114, p. 131–161.

Horn, B.L.D., Goldberg, K., and Schultz, C.L., 2018, Interpretation of massive sandstones in ephemeral fluvial settings: A case study from the Upper Candelária Sequence (Upper Triassic, Paraná Basin, Brazil): Journal of South American Earth Sciences, v. 81, p. 108–121.

Howard, R. H., 1991, Hydrocarbon Reservoir Distribution in the Illinois Basin, in M. W. Leighton, D. R. Kolata, D. F. Oltz, and J. J. Eidel, eds., Interior Cratonic Basins: American Association of Petroleum Geologists, p. 299–327.

Howell, K.J., 2017, Sedimentology of multistorey fluvial sandstones of the Mississippian Cypress Formation, Illinois Basin, USA: MS Thesis, University of Illinois, 138 p.

Howell, K. J., N. D. Webb, J. L. Best, and E. W. Prokocki, *in prep*, The Sedimentology of a Large Fine-Grained Carboniferous River: Facies, Palaeohydraulics, and Implications for Reservoir Heterogeneity: Sedimentology.

Hubbert, M. K., 1953, Entrapment of Petroleum Under Hydrodynamic Conditions: AAPG Bulletin, v. 37, no. 8, p. 1954–2026.

Huff, B. G., and B. Seyler, 2010, Oil and Gas Geology, in D. R. Kolata, and C. Nimz, eds., Geology of Illinois: Illinois State Geological Survey, p. 283–298.

Hunter, R.E., 1985, Subaqueous Sand-Flow Cross Strata: Journal of Sedimentary Petrology, v. 55, p. 886–894.

Interstate Oil Compact Commission (IOCC), 1952. Fluid Injection Questionnaire, 1952—1981. Illinois Secondary Recovery and Pressure Maintenance Study Committee. In cooperation with Illinois State Geological Survey.

Jamali, A., and A. Ettehadtavakkol, 2017, CO2storage in Residual Oil Zones: Field-scale modeling and assessment: International Journal of Greenhouse Gas Control, v. 56, p. 102–115, doi:10.1016/j.ijggc.2016.10.005.

Jarrell, P. M., Fox, C. E., Stein, M. H., and Webb, S. L. 2002. Practical Aspects of CO_2 Flooding, SPE Monograph Series, vol. 22. Richardson, Texas: Society of Petroleum Engineers.

Jopling, A. V., 1965, Laboratory study of the distribution of grain sizes in cross-bedded deposits, in Middleton, E.G. ed., Primary Sedimentary Structures and Their Hydrodynamic Interpretation, Spec. Publication No. 12, Oklahoma, U.S.A., Society of Economic Paleontologist and Mineralogists, p. 53–65.

Juho, L., 2015, Storing CO 2 through Enhanced Oil Recovery Combining EOR with CO 2 storage (EOR+) for profit.

Kahmann, J.A., and Driese, S.G., 2008, Paleopedology and geochemistry of Late Mississippian (Chesterian) Pennington Formation paleosols at Pound Gap, Kentucky, USA: Implications for high-

frequency climate variations: Palaeogeography, Palaeoclimatology, Palaeoecology, v. 259, p. 357–381, doi: 10.1016/j.palaeo.2007.09.022.

Kamari A., N. Mohammad, L. Sahranavard, A.H. Mohammadi, 2014, Efficient screening of enhanced oil recovery methods and predictive economic analysis. Neural comput & Applic 25: p. 815—824.

Kehlenbach, R.W.J., 1969, Distribution and depositional environment of the Mississippian Cypress Formation in Southern Illinois: Southern Illinois University, M.S. Thesis, 54 p.

Kirk, M., 1983, Bar development in a fluvial sandstone (Westphalian "A"), Scotland: Sedimentology, v. 30, p. 727–742.

Kleinhans, M.G., 2004, Sorting in grain flows at the lee side of dunes: Earth-Science Reviews, v. 65, p. 75–102, doi: 10.1016/S0012-8252(03)00081-3.

Knepp, R., S. Frailey, J. Grube, B. Seyler, D. Garner, C. Korose, B. Huff, J. Damico, and S. Rittenhouse, 2009, CO2 sequestration and enhanced oil recovery potential in Illinois Basin oil reservoirs, in M. Grobe, J. C. Pashin, and R. L. Dodge, eds., Carbon dioxide sequestration in geological media—State of the science: AAPG Studies in Geology 59, p. 61 – 86.

Kolata, D. R., and W. J. Nelson, 1991, Tectonic History of the Illinois Basin, in M. W. Leighton, D. R. Kolata, D. F. Oltz, and J. J. Eidel, eds., Interior Cratonic Basins: American Association of Petroleum Geologists, p. 263–285.

Koottungal. L., 2014, 2014 worldwide EOR survey. Special report. Oil & Gas Journal

Koperna, G. J., and V. A. Kuuskraa, 2006, TECHNICAL OIL RECOVERY POTENTIAL FROM RESIDUAL OIL ZONES: PERMIAN BASIN Prepared for Advanced Resources International.

Kostaschuk, R., 2000, A field study of turbulence and sediment dynamics over subaqueous dunes with flow separation: Sedimentology, v. 47, p. 519–531, doi: 10.1046/j.1365-3091.2000.00303.x.

Kostaschuk, R.A., 2005, Sediment transport mechanics and dune morphology: River, Coastal and Estuarine Morphodynamics: RCEM 2005, Taylor & Francis, London, p. 795–803.

Kostaschuk, R., Best, J.L., Parsons, D.R., Lane, S.N., Hardy, R.J., and Orfeo, O., 2008, Suspended sediment transport over a dune: Marine and River Dune Dynamics, p. 197–201.

Kostaschuk, R., and Villard, P., 1996, Flow and sediment transport over large subaqueous dunes: Fraser River, Canada: Sedimentology, v. 45, p. 849–863, doi: 10.1111/j.1365-3091.1996.tb01506.x.

Kovscek, A. R., and M. D. Cakici, 2005, "Geologic Storage of Carbon Dioxide and Enhanced Oil Recovery. II. Cooptimization of Storage and Recovery." *Energy Conversion and Management* 46: 1941—1956. doi:10.1016/j.enconman.2004.09.009.

Kuuskraa, V. A., M. L. Godec, and P. Dipietro, 2013, CO2utilization from "next generation" CO2enhanced oil recovery technology, *in* Energy Procedia: doi:10.1016/j.egypro.2013.06.618.

Kuuskraa, V., and M. Wallace, 2014, TECHNOLOGY CO2-EOR set for growth as new CO2 supplies emerge: Oil & Gas Journal, v. 112, no. 5, p. 92–92.

Lake, L.W., A. Yang, P. Zhong, 2014, Listening to the Data: An Analysis of the Oil and Gas Journal Database. SPE-169056-MS

Lamar, J. E., 1925, Geology and mineral resources of the Carbondale Quadrangle: Illinois State Geological Survey Bulletin 48, 172 p.

LeClair, S.F., 2011, Interpreting fluvial hydromorphology from the rock record: Large-river peak flows leave no clear signature: SEPM Special Publication, v. 97, p. 113–123.

Leclair, S.F., and Bridge, J.S., 2001, Quantitative interpretation of sedimentary structures formed by river dunes: Journal of Sedimentary Research, v. 71, p. 713–716, doi: 10.1306/2dc40962-0e47-11d7-8643000102c1865d.

Leach, A., C. F. Mason, and K. van t. Veld, 2011, Co-optimization of enhanced oil recovery and carbon sequestration: Resource and Energy Economics, doi:10.1016/j.reseneeco.2010.11.002.

Lee, L.K., 1939, Geology of basin fields in southeastern Illinois: AAPG Bulletin, v. 23, no. 10, p. 1493–1506.

Leetaru, H. E. (1990). Application of old electric logs in the analysis of Aux Vases Sandstone (Mississippian) reservoirs in Illinois (IP 134). Urbana, IL: Illinois State Geological Survey.

Lewan, M. D., M. E. Henry, D. K. Higley, and J. K. Pitman, 2002, Material-balance assessment of the New Albany-Chesterian petroleum system of the Illinois basin: AAPG Bulletin, v. 86, no. 5, p. 745–777

Long, D.G.F., 1977, Proterozoic stream deposits: some problems of recognition and interpretation of ancient sandy fluvial systems, in Miall, A.D. ed., Fluvial Sedimentology, Canadian Society of Petroleum Geologists, v. Mem. 5, p. 313–341.

Lowe, D.R., 1988, Suspended-load fallout rate as an independent variable in the analysis of current structures: Sedimentology, v. 35, p. 765–776.

Ma, H., Nittrouer, J.A., Naito, K., Fu, X., Zhang, Y., Moodie, A.J., Wang, Y., Wu, B., and Parker, G., 2017, The exceptional sediment load of fine-grained dispersal systems: example of the Yellow River, China: Science Advances, v. 3, p. 1–8, doi: 10.1126/sciadv.1603114.

Magoon, L. B., and W. G. Dow, 1994, The Petroleum System: Chapter 1: Part I. Introduction, in The Petroleum System--From Source to Trap: AAPG Special Volumes, p. 3–24.

Malott, C. A., 1919, The" American Bottoms" Region of Eastern Greene County, Indiana--: A Type Unit in Southern Indiana Physiography: Indiana University Studies, v. 6, no. 40, p. 61.

Martin, C.A.L., and Turner, B.R., 1998, Origins of massive-type sandstones in braided river systems: Earth-Science Reviews, v. 44, p. 15–38.

McBride, E.F., Shepherd, R.G., and Crawley, R.A., 1975, Origin of parallel near-horizontal laminae by migration of bed forms in a small flume: Journal of Sedimentary Petrology, v. 45, p. 132–139.

McKaskle, R. W., Beitler, C. M., Vance, A. E., & Frailey, S. M., 2017, General large-scale carbon dioxide enhanced oil recovery facility design for the Illinois basin. Champaign, Ill.: Illinois State Geological Survey, Prairie Research Institute.

McLean, S.R., Wolfe, S.R., and Nelson, J.M., 1999, Spatially averaged flow over a wavy boundary revisited: Journal of Geophysical Research: Oceans, v. 104, p. 15743–15753, doi: 10.1029/1999JC900116.

Meents, W. F., A. H. Bell, O. W. Rees, and W. G. Tilbury, 1952, Meents Et Al 1983.Pdf.

Melzer, S., 2010, OPTIMIZATION OF CO 2 STORAGE IN CO 2 ENHANCED OIL RECOVERY PROJECTS.

Melzer, L. S., 2006, Stranded Oil in the Residual Oil Zone: 35 p.

Melzer, L. S., G. J. Koperna, and V. A. Kuuskraa, 2006, The origin and resource potential of residual oil zones, in Proceedings - SPE Annual Technical Conference and Exhibition: p. 3507–3511.

MGSC, 2005, An Assessment of Geological Carbon Sequestration Options in the Illinois Basin: 478 p.

Midwest Geological Sequestration Consortium (MGSC), 2005, An assessment of geological carbon sequestration options in the Illinois Basin: DOE Contract DE-FC26-03NT41994 (Issued December 31, 2005).

National Energy Technology Laboratory (NETL), 2010, Geologic storage formation classification: understanding its importance and impacts on CCS opportunities in the United States. US Department of Energy, DOE/NETL 2010/1420.

National Energy Technology Laboratory (NETL), 2012, Carbon sequestration atlas of the United States and Canada, fourth edition, US Department of Energy.

Naqshband, S., Hoitink, A.J.F., McElroy, B., Hurther, D., and Hulscher, S.J.M.H., 2017, A sharp view on river dune transition to upper stage plane bed: Geophysical Research Letters, p. 11,437–11,444, doi: 10.1002/2017GL075906.

Naqshband, S., Ribberink, J.S., and Hulscher, S.J.M.H., 2014, Using both free surface effect and sediment transport mode parameters in defining the morphology of river dunes and their evolution to upper stage plane beds: Journal of Hydraulic Engineering, v. 140, p. 1–6.

Nelson, W. J., 1991, Structural Styles of the Illinois Basin, in M. W. Leighton, D. R. Kolata, D. F. Oltz, and J. J. Eidel, eds., Interior Cratonic Basins: American Association of Petroleum Geologists, p. 209–243.

Nelson, W.J., 1995, Structural features in Illinois: Illinois State Geological Survey, Bulletin 100, 144 p.

Nelson, W.J., L.B. Smith, J.D. Treworgy, L.C Furer, and B.D. Keith, 2002, Sequence stratigraphy of the lower Chesterian (Mississippian) strata of the Illinois Basin: Illinois State Geological Survey, Bulletin 107, 70 p.

Nexus reservoir simulation, 2017. https://www.landmark.solutions/Nexus-Reservoir-Simulation, accessed on 10/31/2017.

Nio, S.D., and Yang, C.S., 1991, Diagnostic attributes of clastic tidal deposits: A review: Clastic Tidal Sedimentology: CSPG Special Publications, p. 3–27.

Nuñez-López, V., R. Gil-Egui, A. Gonzalez-Nicolas, and S. Hovorka, 2017, Carbon Balance of CO2-EOR for NCNO Classification: Energy Procedia, v. 114, no. August, p. 6597–6603, doi:10.1016/j.egypro.2017.03.1803.

Okwen, R., F. Yang, and S. Frailey, 2014, Effect of geologic depositional environment on CO_2 storage efficiency: Energy Procedia, v. 63, p. 5247–5257.

Oltz, D.F., 1994, Improved and enhanced oil recovery in Illinois through reservoir characterization: Department of Energy, Final Report, p. 403.

Orton, G.J., and Reading, H.G., 1993, Variability of deltaic processes in terms of sediment supply, with particular emphasis on grain size: Sedimentology, v. 40, p. 475–512.

Palandri, J.L. and Y.K. Kharaka, 2004. A Compilation of Rate Parameters of Water-mineral Interaction Kinetics for Application to Geochemical Modeling, U.S. Geological Survey Open File Report 2004-1068, 64 p.

Pathak, P., K. P. Babcock, and R. J. Wachtman, 2012, Residual Oil Saturation Determination for EOR Projects in Means Field, a Mature West Texas Carbonate Field.

Peng, D. Y., & Robinson, D. B. (1976). A new two-constant equation of state. Industrial & Engineering Chemistry Fundamentals, 15(1), 59-64.

Phillips, S. H., 1954, Subsurface Studies of the Cypress Formation, Richland County Area, Illinois: University of Illinois at Urbana-Champaign, MS Thesis, 18 p.

Pitman, J. K., M. Henry, and B. Seyler, 1998, Reservoir Quality and Diagenetic Evolution of Upper Mississippian Rocks in the Illinois Basin: Influence of a Regional Hydrothermal Fluid-Flow Event During Late Diagenesis: US Geological Survey Professional Paper 1597, p. 24.

Poeter, E.P., Hill, M.C., 1998, Documentation of Ucode, A Computer Code for Universal Inverse Modeling. U.S.G.S. WATER-RESOURCES INVESTIGATIONS REPORT 98-4080; 116 p.

Pryor, W. A., and E. G. Sable, 1974, Carboniferous of the Eastern Interior Basin, in Garrett Briggs, ed., Carboniferous of the Southeastern United States: Geological Society of America, p. 281–314.

Sandrea, R., D. Dharod, 2016, Approach screens reservoir candidates for EOR. Oil & Gas Journal April 4., 2016 p. 48—52.

Scotese, C. R., and W. S. McKerrow, 1990, Revised World maps and introduction: Geological Society, London, Memoirs, v. 12, no. 1, p. 1–21, doi:10.1144/GSL.MEM.1990.012.01.01.

Siever, R., 1954, Petrology and Sedimentation of Upper Chester Sandstones: Urbana, IL, Illinois State Geological Survey, 208–219 p.

Seyler, B., J.P. Grube, and D.G. Morse, 2000, The Cypress Sandstone in Illinois: Workshop report for the Petroleum Technology Transfer Council Cypress Sandstone Workshop, Mt. Vernon, Illinois, April 5, 157 p.

Seyler, B., and R. M. Cluff, 1991, Petroleum Traps in the Illinois Basin, in M. W. Leighton, D. R. Kolata, D. F. Oltz, and J. J. Eidel, eds., Interior Cratonic Basins: American Association of Petroleum Geologists, p. 361–401.

Smith, L. B. J., and J. F. Read, 2001, Discrimination of local and global effects on Upper Mississippian stratigraphy, Illinois Basin, U.S.A: Journal of Sedimentary Research, v. 71, no. 6, p. 985–1002, doi:10.1306/040501710985.

Sullivan, D. M., 1972, Subsurface stratigraphy of the West Baden Group in Indiana: Bloomington, Indiana, Indiana Geological Survey, 31 p.

Swann, D. H., 1963, Classification of Genevievian and Chesterian (Late Mississippian) Rocks of Illinois: Urbana, IL, Illinois State Geological Survey, 91 p.

Swann, D. H., 1964, Late Mississippian Rhythmic Sediments of Mississippi Valley: AAPG Bulletin, v. 48, no. 5, p. 637–658.

Teklu, T. W., J. S. Brown, H. Kazemi, R. M. Graves, and A. M. AlSumaiti, 2013, Residual Oil Saturation Determination - Case Studies in Sandstone and Carbonate Reservoirs, *in* EAGE Annual Conference & Exhibition incorporating SPE Europec: doi:10.2118/164825-MS.

Trentham, R., and S. Melzer, 2015, Identifying and developing technology for enabling small producers to pursue the residual oil zone (ROZ) fairways in the Permian Basin San Andres. Final Report.

Trentham, R., and L. S. Melzer, 2016, A Cookbook Approach to Exploring for , and Evaluating , Residual Oil Zones in the San Andres Formation of the Permian Basin, in Southwest Section AAPG Annual Convention

Treworgy, J., and R. Norby, 1989, Overview of the Mississippian in the Illinois basin, in Carboniferous Geology of the Eastern United States: Washington, D. C., American Geophysical Union, p. 1–17, doi:10.1029/FT143p0001.

Udegbunam, E.O., D.S. Beaty, and J.P. Fagan, Jr., 1993, Strategies for improved oil recovery from Aux Vases reservoirs in McCreery and McCullum waterflood units, Dale Consolidated Field, Franklin County, Illinois: Illinois State Geological Survey, Illinois Petroleum 1993, 39 p.

US EIA, 2013, U.S. Energy Information Administration (US EIA). 2013. Annual Energy Outlook. http://www.eia.gov/forecasts/archive/aeo13/

Valenti, N. P., R. M. Valenti, and L. F. Koederitz, 2002, A Unified Theory on Residual Oil Saturation and Irreducible Water Saturation: SPE Technical Conference, v. SPE 77545.

Wasson, T., 1938, Recent oil discoveries in southeastern Illinois: AAPG Bulletin, v. 22, no. 1, p. 71–78.

Waxman, M. H., and L. J. M. Smits, 1968, Electrical Conductivities in Oil-Bearing Shaly Sands: Society of Petroleum Engineers Journal, v. 8, no. 02, p. 107–122, doi:10.2118/1863-A.

Webb, N. D., and N. P. Grigsby, *in press*, Assessing the Cypress Sandstone for CO_2-Enhanced Oil Recovery and Carbon Storage: Part I - Reservoir Characterization of Noble Oil Field, Western Richland County, Illinois: Urbana, IL, Illinois State Geological Survey, circular, 59 p.

West, L. M., 2014, A regional assessment of residual oil zones in the Permian Basin and their potential for carbon dioxide capture usage and storage, *in* Energy Procedia: doi:10.1016/j.egypro.2014.11.824.

Willman, H. B., E. Atherton, T. C. Buschbach, C. Collinson, J. C. Frye, M. E. Hopkins, J. A. Lineback, and J. A. Simon, 1975, Handbook of Illinois Stratigraphy: Urbana, IL, Illinois State Geological Survey, Bulletin, 261 p.

Witherspoon, P. A., and E. G. Jackson, 1955, Summary of Water Flood Operations in Illinois Oil Pools During 1954: Urbana, IL, Illinois State Geological Survey, 63 p.

Worthen, A. H., G. C. Broadhead, E. T. Cox, O. St. John, and F. B. Meek, 1875, Geological Survey of Illinois Volume VI: Geology and Palaeontology: Geological Survey of Illinois, 531 p.

Xu, J., and B. G. Huff, 1995, The Cypress Sandstone (Mississippian) Reservoir and Its Recovery Potential at Xenia East Oil Field, Clay County, Illinois, 147: Illinois State Geological Survey, Illinois Petroleum, 47 p.

Xu, T., Sonnenthal, E., Spycher, N., and Pruess, K., 2004. TOUGHREACT User's Guide: A Simulation Program for Non-isothermal Multiphase Reactive Geochemical Transport in Variably Saturated Geologic Media, LBNL-55460, Lawrence Berkeley National Laboratory, Berkeley, CA. 192 p.

Yang, C., and H. Qing, 2016, Possible occurrences of transition zones and residual oil zones below oil-water contacts in mature oil fields, southeast Saskatchewan: doi:10.1190/INT-2016-0008.1.

Yellig, W. F., & Metcalfe, R. S. (1980, January 1). Determination and Prediction of CO2 Minimum Miscibility Pressures (includes associated paper 8876). Society of Petroleum Engineers. doi:10.2118/7477-PA.

Zhang, H., Hou, D., and Li, K., 2015. An improved CO_2-Crude oil minimum miscibility pressure correlation. Journal of Chemistry, Volume 2015, Article ID 175940, 10 pages.

Appendix B – Cypress Cores

API	Core#	Farm Name	Farm#	Top	Bot	Cypress Thickness	Field	Lat	Long
120270161200	14424	Centralia Flood Unit	209-W	1202	1381	179	Centralia	38.543464	-89.155423
120270084000	14334	Hanseman, Wm.	3	1201	1375	174	Centralia	38.547989	-89.148659
121812094100	13619	Lyerla	CB-2	324	439	115	Union Co	37.584763	-89.364836
121013125200	15443	Griggs, J. T. A/C 1	107	1434	1520	86	Lawrence	38.740441	-87.762187
120292361900	13959	Seaman, J. H./AOR	15	1738	1821	83	Mattoon	39.438013	-88.396245
120512572400	14888	Heckert, M. B.	902	1476	1553	77	Loudon	39.035172	-88.894789
120512582900	14219	Griffith, M.J.	502	1522	1593	71	Loudon	39.010712	-88.902766
121590139100	835	Montgomery "B"	2	2575	2645	70	Noble	38.724963	-88.222638
121012760800	14231	Baltzell, Oliver	33	1294	1363	69	Lawrence	38.754824	-87.785391
121013178800	15457	Griggs, J. T. A/C 1	131	1413	1478	65	Lawrence	38.739864	-87.763089
121012836200	14204	Boyd, Isaac (Baltzall)	MI-10	1298	1354	56	Lawrence	38.759727	-87.786585
121012910300	14235	Boyd, Isaac (Boyd-Baltzell)	MI-18	1300	1356	56	Lawrence	38.759684	-87.786858
121010669700	Barn	King, J.R. AC1	QQ-9	1536	1592	56	Lawrence	38.716355	-87.782632
121010745800	14068	George W. Cooper	28	1343	1398	55	Lawrence	38.769430	-87.794291
121012836300	14019	Boyd Isaac	MI-11	1300	1355	55	Lawrence	38.759789	-87.786915
121012910400	14237	Boyd, Isaac (Boyd-Baltzall)	MI-19	1300	1354	54	Lawrence	38.759744	-87.786803
120510270700	14425	Louden S. Unit Wtrfld	38	1556	1609	53	Loudon	39.019666	-88.879273
121012836400	14205	Boyd, Isaac (Baltzall)	MI-12	1302	1355	53	Lawrence	38.759902	-87.786694
121012773400	14067	Baltzall, Oliver	MI-2	1375	1428	53	Lawrence	38.753800	-87.789270

121012910500	14236	Boyd, Isaac (Boyd-Baltzell)	MI-20	1300	1351	51	Lawrence	38.759771	-87.786775
121010717200	Barn	King, P. AC3	KM-4	1488	1533	45	Lawrence	38.742200	-87.793870
121012762300	14018	Baltzell, Oliver	QS-25	1286	1329	43	Lawrence	38.753184	-87.783347
121012821000	14124	Baltzall, Oliver	PC-1	1346	1387	42	Lawrence	38.748900	-87.788400
120510122300	14407	Louden N. Unit Wtrfld	28-W	1544	1585	41	Loudon	39.036961	-88.882744
120270214500	14347	Criley, Earl C.	6	1192	1233	41	Centralia	38.561459	-89.164053
121013190400	15455	King, P. A/C 1 & 2	176	1316	1356	40	Lawrence	38.777705	-87.791925
120472418300	14023	Judge	3-A	2896	2935	39	Parkersburg	38.562130	-88.025132
121013125300	15436	Griggs, J. T. A/C 1	108	1392	1431	39	Lawrence	38.740386	-87.765682
120270098700	14344	Criley, E. C.	7	1190	1229	39	Centralia	38.563279	-89.164002
121010717300	14216	King, Perry A/C 3	KM-1	1510	1549	39	Lawrence	38.743100	-87.795020
120510121300	14406	Louden N. Unit Wtrfld	21-W	1556	1594	38	Loudon	39.038760	-88.873602
121010717500	Barn	King, P. AC3	KM-3	1512	1550	38	Lawrence	38.742200	-87.795020
121010719300	Barn	King, P. AC3	19	1496	1533	37	Lawrence	38.742700	-87.794440
120270118800		Centralia Unit Water Flood	30-W	1200	1235	35	Centralia	38.565436	-89.173254
120270063800	14345	Criley, E. C.	7-A	1185	1220	35	Centralia	38.563417	-89.163998
121010717400	Barn	King, P. AC3	KM-2	1493	1526	33	Lawrence	38.743100	-87.793880
121013125400	15437	Griggs, J.T. A/C 1	109	1424	1457	33	Lawrence	38.742259	-87.765799
120270117300	14400	Centralia Flood Unit	174-W	1207	1239	32	Centralia	38.542028	-89.147015
121013191300	15456	Fyfee, C. H.	27	1400	1432	32	Lawrence	38.744761	-87.783215
120270084100	14335	Hanseman, Wm.	4	1310	1342	32	Centralia	38.551696	-89.150514

121592606400	15658	Montgomery, C. T. "B"	34	2576	2606	30	Noble	38.727821	-88.217885
120510123000	14396	Louden N. Unit Wtrfld	27-W	1523	1553	30	Loudon	39.036957	-88.885006
121852808300	14949	Grayville, City of	3	2660	2690	30	Grayville	38.258715	-87.989688
120472448400	14938	Grayville, City of	10	2719	2748	29	Grayville	38.261219	-87.993897
120270069500	14348	Criley, E. C.	9	1190	1219	29	Centralia	38.561579	-89.166401
121592608300	15659	Coen, John O.	120	2583	2611	28	Noble	38.727132	-88.214030
120512569900	14217	Ripley, Lewis	26	1544	1572	28	Loudon	39.026467	-88.893538
121010023800	2159	Joe Kesl Jr et al	2	1512	1540	28	Lawrence	38.848962	-87.803281
121010707800	14543	Wm Cooper	8	1555	1581	26	Lawrence	38.721549	-87.752296
121010739900	14201	Leighty, T. F.	VV-6	1618	1644	26	Lawrence	38.656068	-87.691343
120270068500	14340	Koelmel, R.	4-A	1189	1214	25	Centralia	38.548631	-89.159635
120270068400	14339	Koelmel, R.	4	1195	1219	24	Centralia	38.548648	-89.159895
121652585700	14900	Moore	5	2582	2602	20	Harco	37.814028	-88.623014
121852807500	14871	Grayville, City of	4	2673	2693	20	Grayville	38.262348	-87.990077
120270118100	14398	Centralia Flood Unit	166-W	1203	1223	20	Centralia	38.544870	-89.157702
121850416600	14415	Mt. Carmel Flood Unit	2-W	2094	2114	20	Mt. Carmel	38.429398	-87.787919
121013190200	15461	Vandermark, L.A.	31	1598	1618	20	Lawrence	38.655182	-87.725096
121852807200	14810	Grayville, City of	2	2650	2670	20	Grayville	38.260527	-87.990112
120270215400	14349	Criley, E. C.	19	1196	1216	20	Centralia	38.561696	-89.168718
121013125500	15041	Griggs, J. T. A/C 1	112	1459	1478	19	Lawrence	38.739465	-87.762299
120270215500	14350	Criley, E. C.	20	1197	1215	18	Centralia	38.558021	-89.166499

120492487700	15401	Schultz	5	2551	2567	16	Sailor Springs	38.966368	-88.405675
120252884900	15406	Moseley	1-C	2645	2661	16	Clay City	38.605556	-88.322866
120492464200	14706	Kluthe	1-A	2533	2549	16	Sailor Springs	38.973700	-88.406852
120492304500	13987	Habbe, John	5	2535	2550	15	Sailor Springs	38.920517	-88.436574
120492304600	13983	Habbe, John	6	2550	2565	15	Sailor Springs	38.924140	-88.431780
120270032700	14353	Criley - Felton	1	1208	1223	15	Centralia	38.555845	-89.159621
120270068600	14341	Lippert, F. W.	1	1190	1205	15	Centralia	38.555582	-89.154893
120270070500	14352	Dunbar, J. E.	1-B	1244	1259	15	Centralia	38.545838	-89.176252
120270084700	14342	Criley, Earl C.	2	1175	1190	15	Centralia	38.557904	-89.164186
120270098600	14343	Criley, E. C.	5	1195	1210	15	Centralia	38.563161	-89.161682
120492487800	15402	Schultz	6	2538	2552	14	Sailor Springs	38.968220	-88.408026
120270117400	14408	Centralia Flood Unit	181-W	1215	1229	14	Centralia	38.540950	-89.153193
121933298900	N/A	Lamar	7	2719	2733	14	Phillipstown	38.165701	-88.033094
120250055300	2101	Mart	1	2563	2575	12	Kenner West	38.688358	-88.615047
120250248300	2103	Colclasure	3	2601	2613	12	Kenner West	38.686536	-88.615070
121852808900	14954	Grayville, City of	8	2684	2696	12	Grayville	38.262343	-87.992388
120250313900	909	J. H. Smith	1	2612	2624	12	Clay City	38.651679	-88.323509
120270215600	14351	Criley, E. C.	21	1210	1222	12	Centralia	38.561816	-89.171034
120510135700	14427	Homan	B-21	1600	1610	10	Loudon	39.014131	-88.881845
121850416800	14416	Mt. Carmel Water Flood Unit	15	2064	2074	10	Mt. Carmel	38.434462	-87.785052
120270084800	14346	Criley, Earl C.	3	1195	1205	10	Centralia	38.559640	-89.164121

121010031700	575	Robert Hoh	1	1824	1832	8	Allendale	38.585587	-87.702415
121013125100	15042	Griggs, J. T. A/C 1	106	1414	1422	8	Lawrence	38.740421	-87.763453
120550135700	14404	West Frankfort Wtrfld Unit	1-SWD	2507	2514	7	W. Frankfort	37.916545	-88.927551
121850192700	14426	Hein, P. F.	11	2043	2045	2	Mt. Carmel	38.425590	-87.784166
121510010800	46	Abner Field	1				Pope Co	37.367874	-88.586593
121512030600	12218	Ditterline, Milo	1				Pope Co	37.309263	-88.668851
121512030700	12217	Ditterline, Milo	2				Pope Co	37.308491	-88.643986
120333802500	N/A	Legg	5	1450			Main	38.867818	-87.782375
121812190900	15660	Tripp	1	26	186	160	Union Co	37.444086	-89.135978
120650139200	14402	Rural Hill Flood	5-S	2859	2966	107	Dale	37.988228	-88.603496
120650139400	14401	Rural Hill Flood	2-S	2953	3054	101	Dale	38.002244	-88.583854
121190035100	146	Mine 2	4	258	337	79	Madison Co	38.728182	-89.993279
121012783100	14238	Boyd, Isaac	MO-1	1336	1390	54	Lawrence	38.757700	-87.788980
121012783200	14206	Baltzell Oliver	MI-2C	1360	1413	53	Lawrence	38.753800	-87.789239
121012892800	14200	Boyd, Isaac (Baltzall)	MI-16	1291	1344	53	Lawrence	38.759900	-87.787640
121012892900	14211	Boyd, Isaac (Boyd-Baltzell Unit)	MI-17	1295	1348	53	Lawrence	38.759850	-87.787390
120650135600	14403	Rural Hill Flood	4-S	2831	2880	49	Dale	37.992723	-88.617112
121592648800	15661	Long	2	2629	2649	20	Noble	38.668979	-88.250383
121592648800	15661	Long	2	2720	2760	40	Noble	38.668979	-88.250383

Appendix C – List of Abbreviations

API – American petroleum institute
ATV – acoustic televiewer
BBL – barrels of crude oil
BHP – bottom hole pressure
BOPD – barrels of oil per day
BPR – back-pressure regulator
BVW – bulk volume water
CapEx – capital expenses
CB – carbon balance of oil produced
CEPL – porosity loss due to cementation
CL – cathodoluminescence
CMI – compact micro imager
COPL – compactional porosity loss
CO_2 – carbon dioxide
CO_2-EOR – carbon dioxide-enhanced oil recovery
DPHI – density porosity (log)
EOR – enhanced oil recovery
EOS – equation of state
GIS – geographic information system
GR – gamma ray (log)
HCPV – hydrocarbon pore volume
IGV – intergranular volume
ILB – Illinois Basin
ILOIL – Illinois Oil and Gas Online
IRR – internal rate of return
ISGS – Illinois State Geological Survey
LST – lowstand systems tract
Ma – mega-annum; one million years
mD – average permeability
MDL – method detection limit
MGSC – Midwest Geological Sequestration Consortium
MHI – movable hydrocarbon index
MMBO – million barrels of oil
MMP – minimum miscibility pressure
MPZ – main pay zone
MROZ – main residual oil zone
NCNO – net carbon negative oil
NPHI – neutron porosity (log)
NPV – net present value
NSP – normalized SP
OWC – oil water contact
PNL – pulsed neutron log
POTA – potassium
POWC – producing oil water contact
PRE – pattern realignment and expansion
PSI – pounds per square inch

PVT – pressure-volume-temperature
RES – resistivity log
RHO – density log
ROZ – residual oil zone
RST – Reservoir Saturation Tools
SAG – soak-alternating-gas
SEM – scanning electron microscope
SP – spontaneous potential
SPE – society of professional engineers
TDS – total dissolved solids
THOR – thorium
TST – transgressive systems tract
XRD – x-ray diffraction
URAN - uranium
UV – ultraviolet
WAG – water alternating gas